The effect of the mode of applied breakage on coal yield

W Potgieter

22160582

Dissertation submitted in fulfilment of the requirements for the degree Master of Engineering in Chemical Engineering at the Potchefstroom Campus of the North-West University

Supervisor: Prof QP Campbell

Co-supervisor: Prof M le Roux

May 2017

It all starts here ™

NORTH-WEST UNIVERSITY
YUNIBESITI YA BOKONE-BOPHIRIMA
NOORDWES-UNIVERSITEIT

OVERVIEW OF DOCUMENT

This document presents the research dissertation entitled: **"The effect of the mode of applied breakage on coal yield"**, completed at the North-West University, Potchefstroom Campus.

General information of the author:

Author:	Wilmeri Potgieter
Student number:	22160582
Highest qualification:	Bachelor of Engineering in Chemical Engineering
Institution:	North-West University, Potchefstroom Campus
Curriculum code:	I103P
Year obtained:	2014

Project title:	The effect of the mode of applied breakage on coal yield
Degree:	Master of Engineering in Chemical Engineering
Institution:	North-West University, Potchefstroom Campus
Curriculum code:	I871P
Principal supervisor:	Prof. Q.P. Campbell
Co-supervisor:	Prof. M. le Roux

DECLARATION

I, Wilmeri Potgieter, hereby declare that the dissertation entitled: **"The effect of the mode of applied breakage on coal yield"**, submitted in fulfilment of the requirements for the degree Master of Engineering in Chemical Engineering, has been done by me individually and has not been submitted before by either myself or another individual at any institution in whole or in part. All informative sources used are fully referenced in the bibliography at the end of this document.

Signed at Potchefstroom.

.....

Wilmeri Potgieter

Student number: 22160582

ABSTRACT

Some coal resources, for example, those in Southern Africa such as the Waterberg and Mozambique Coalfields, have a highly interlayered morphological structure consisting of coal macerals along with mineral matter. The latter is incombustible, and becomes altered during combustion remaining as an undesirable ash by-product. It therefore lowers the economic value by reducing the calorific (heating) value of the coal. Furthermore, coal processing plants experience low yields due to the large quantities of mineral matter. Yields can be improved by liberating the valuable components of coal from the mineral matter. It is of economic importance to maximize the amount of valuable coal recovered from raw coal; since different coal value fractions are intermingled and cannot be used directly as mined.

Size reduction of coal particles may, however, be required to increase the liberation of different coal quality fractions from the mineral material. This would enable the separation of the undesirable incombustible material from the valuable coal after mining, in order to produce a low ash value coal product. Size reduction of coal leads to the generation of fine coal. Not only has fine coal higher moisture retention than coarse coal, but processing of fine coal is also generally more expensive; and less efficient. Despite these difficulties in fine coal processing, crushing of certain coal sources to smaller particle sizes prior to processing may be required to attain higher degrees of liberation, resulting in an increase in the plant yield. Since it is unlikely to eliminate all fines in comminution processes, a balance between sufficient liberation of coal to attain a certain yield, and the formation of excessive fines must be achieved.

The intention of this study was to investigate the liberation of coal to attain a certain yield; and to determine the breakage modes, or combination of breakage modes, that will be best suited to optimize liberation at the coarsest possible coal particle size, whilst keeping fines formation to a minimum. The yield with respect to liberation for a market specification for a low ash product was investigated, with a view to achieving the optimal liberation size. Run-of-mine (ROM) coal from the Moatize Coalfield in Mozambique was chosen because of its highly layered morphological structure consisting of coal seams interlayered with mineral matter. Coal breakage modes investigated were:

i) Impact breakage followed by attrition breakage, and
ii) Compressive breakage followed by attrition breakage.

Compressive breakage was performed by applying a compressive force from a garden roller (80 kg weight) to break the coal sample of approximately 6 kg to certain top sizes. The chosen top sizes were 6.7 mm and 13.2 mm, and were based on the required sizes for industrial application, and also to minimize fines generation. These top sizes were obtained by pushing a

garden roller over a single layer (to prevent inter-particle breakage) of multiple particles located within a steel frame. A drop weight impact rig was used to perform impact breakage according to the SANS 401:2010. Top sizes for impact breakage were similar than that for compressive breakage. After the initial breakage mode, compressive breakage or impact breakage, some samples were also subjected to attrition breakage. Attritioning was performed in a tumbling mill at residence times of 1, 2 and 5 minutes respectively. The tumbling mill was rotated at 20 revolutions per minute (rpm) (30 % of its critical speed), ensuring that only cascading motion occurred to prevent further impact breakage. The coal yield improvement attained by the various combinations of breakage modes, and the washability properties, were investigated by a float-sink analysis. A particle size analysis was performed before and after the breakage to evaluate the particle sizes formed due to breakage. Other analyses performed were the proximate analysis, free swelling index, and calorific value determination, performed according to the relevant standards.

Focus was set on material with a relative density (RD) of lower than 1.4. This is because of the relatively “clean” coal, consisting mainly of liberated coal macerals, at these relative densities (RD<1.4). Results obtained during this research study have indicated that impact breakage as well as compressive breakage to a top size of 13.2 mm had an insignificant effect on the coal yield, compared to the yield of the raw coal prior to any testing. Both impact breakage and compressive breakage to a top size of 6.7 mm resulted in a coal yield enhancement. Particularly, the coal yield was substantially increased by impact breakage to a top size of 6.7 mm. It was concluded that impact breakage resulted in a greater coal yield enhancement of material with the RD<1.4, compared to compressive breakage. Impact breakage thus resulted in a larger proportion of liberated coal with the RD<1.4. Attrition breakage additional to impact breakage, i.e. impact breakage followed by attritioning, to a top size of 6.7 mm resulted in an even further increase in the coal yield. This is because impact breakage to a smaller top size of 6.7 mm exposed more coal macerals than breakage to a top size of 13.2 mm. Exposed coal macerals were then chipped off from the mineral matter during attrition breakage resulting in a higher amount of material with RD<1.4. Attrition breakage additional to breakage to a top size of 13.2 mm did not show any noticeable effect on the coal yield.

A particle size of 4.75 mm was investigated to be an optimum liberation size. It was seen that the cumulative yield of liberated material (at RD<1.4) was an optimum for this particle size. A particle size of 2 mm resulted in a lower cumulative yield of material with the RD<1.4. This was because of the high value vitrinite that was liberated first from the gangue, where after finely disseminated mineral matter began to liberated, leading to a reverse effect of the increase in the cumulative yield at a particle size of 4.75 mm. Breakage to a smaller top size of 2 mm will therefore not result in a significant coal yield increase. Sufficient liberation for the coal used during this study was

defined as the largest particles size with the maximum allowable ash yield obtained to produce a product as required by market specifications. The maximum allowable ash yield was defined as 10 %, since this is the maximum ash yield allowed for coal to be suitable for coking purposes. The largest particle size with a maximum ash yield of 10 % was 4.75 mm, which indicated a yield of 50 %. A hypothetical target ash yield of 10 % was investigated by using Microsoft Excel's FORECAST function to predict the overall cumulative yield that can be obtained, and also to estimate the required relative density for separation to obtain the hypothetical ash yield. Impact breakage to a top size of 6.7 mm followed by attritioning for 1 minute resulted in a cumulative yield of 61 % compared to that of the raw coal which was 26 %.

It was concluded that the most effective combination of breakage modes applied to optimize the coal yield was impact breakage to a top size of 6.7 mm followed by attrition breakage for 1 minute. The residence time for attritioning must be a minimum to minimize fines generation.

Key terms: Coal yield, compressive breakage, impact breakage, attritioning, liberation

DEDICATION

Dedicated to:

My mother, Sonia Potgieter…

Thank you for the encouragement and support throughout my studies.

Byrone Malay, my love…

Thank you for the support and believing in me.

Toffie, Rambo, and Einsteinie…

You paved the road to my heart with paw prints.

ACKNOWLEDGEMENTS

First, I would like to thank God for giving me the opportunity and strength to complete this research study.

"So do not fear, for I am with you; do not be dismayed, for I am your God. I will strengthen you and help you; I will uphold you with my righteous right hand."
Isaiah 41:10

I would like to show gratitude by thanking the following individuals for guidance, motivation, support, and assistance during the course of this research study:

- Prof. Q.P. Campbell (principal supervisor) and Prof. M. Le Roux (co-supervisor) for their guidance, advice and assistance.
- SAMMRI (South African Minerals to Metals Research Institute), NRF (SARChI) Chair in Coal Research, DTS (Department: Science and Technology), and SACPS (The Southern African Coal Processing Society) for the financial support given during the course of this project.
- Mr. David West for arranging a coal sample for experimentation.
- Dr. David Powell for proofreading and advice.
- Dr. Japie Viljoen for guidance and advice.
- Mr. Sarel Naude and Mr. J.W. Hoffman for their assistance with the experiments.
- All the personnel, especially Mrs. Rene Bekker, at the School of Chemical and Minerals Engineering.
- All the workshop personnel, particularly Mr. Adrian Brock, for helping with equipment construction.

TABLE OF CONTENTS

OVERVIEW OF DOCUMENT ..... **I**

DECLARATION ..... **II**

ABSTRACT ..... **III**

DEDICATION ..... **VI**

ACKNOWLEDGEMENTS ..... **VII**

TABLE OF CONTENTS ..... **VIII**

LIST OF FIGURES ..... **XII**

LIST OF TABLES ..... **XVI**

NOMENCLATURE ..... **XVII**

CHAPTER 1 INTRODUCTION **1**

1.1 Background and Motivation **1**

1.2 Objectives **7**

1.3 Scope of investigation **8**

CHAPTER 2 LITERATURE SURVEY **9**

2.1 Coal **9**

2.1.1 Macerals 12

2.1.2 Lithotypes 14

2.1.3 Mineral matter associated with coal 16

2.1.4 Properties of coal affecting its breakage behaviour 19

2.1.4.1 Macerals 20

2.1.4.2 Coal rank 21

2.1.4.3 Cleats and micro-structure of coal 21

2.1.4.4 Lithotypes 23

2.1.4.5 Mechanical properties 24

2.1.5 Proximate analysis 25

2.2 The Mozambique Coalfields 25

2.2.1 Basin stratigraphy 26

2.2.2 Coal qualities 28

2.2.3 Challenges associated with the exploitation of the Mozambique Coalfields 29

2.3 Size reduction 29

2.3.1 Breakage process and related energy 30

2.3.2 Size reduction modes 33

2.3.2.1 Impact drop breakage 34

2.3.2.2 Compression breakage 35

2.3.2.3 Attrition breakage 35

2.3.2.4 Combination of breakage modes 36

2.3.3 Size reduction equipment 36

2.3.3.1 Examples of breakage equipment used for various breakage modes 37

2.4 Liberation 41

2.4.1 Float-sink (densimetric) analysis 43

2.5 Preventing the production of excessive fines 45

CHAPTER 3 EXPERIMENTAL PROCEDURES 47

3.1 Materials 47

3.1.1 Coal 47

3.1.2 Chemicals 51

3.2 Equipment 51

3.3 Experimental overview 53

3.4 Experimental procedure 54

3.4.1.1 Sample preparation 54

3.4.1.2 Experimental procedure 55

3.5 Sampling procedure 60

3.6 Analytical methods 60

3.6.1 Particle size distribution analysis 60

3.6.2 Densimetric (float-sink) analysis 61

3.6.3 Other analytical methods 65

CHAPTER 4 RESULTS AND DISCUSSION 67

4.1 Repeatability and experimental error 67

4.2 Coal properties 69

4.2.1 Proximate analysis 70

4.2.1.1 Ash yield 70

4.2.1.2 Inherent moisture 72

4.2.2 Free swelling index 73

4.2.3 Calorific value 75

4.3 Impact breakage 76

4.3.1 Top size 76

4.3.2 Effect of attrition breakage additional to impact breakage 79

4.4 Compressive breakage 81

4.4.1 Top size 81

4.4.2 Effect of additional attrition 84

4.5 Ash yield 85

4.6 Liberation 91

4.7 Washability 97

CHAPTER 5 INDUSTRIAL APPLICATION 102

CHAPTER 6 CONCLUSIONS AND RECOMMENDATIONS 108

6.1 Conclusions 108

6.2 Recommendations 111

6.3 Contribution to the discipline 112

BIBLIOGRAPHY 113

APPENDIX A: EXPERIMENTAL 122

APPENDIX B: RAW EXPERIMENTAL DATA 125

APPENDIX C: PROCESSED DATA 148

APPENDIX D: CALCULATIONS 282

LIST OF FIGURES

Figure 1.1: Global coal consumption by sector for 2013 (adapted from International Monetary Fund, 2016). 2

Figure 1.2: South African coal market distribution for 2013 (adapted from XMP Consulting CC, 2014). 2

Figure 1.3: Representation of coal breakage and liberation for the ideal case. 6

Figure 1.4: Scope of the investigation. 8

Figure 2.1: The formation of coal in terms of its grade, rank and type (adapted from Falcon & Snyman, 1986). 10

Figure 2.2: Relation between the organic and inorganic matter of coal before and after material is combusted: (a) before any combustion of material, (b) after any combustion of material; (c) contents in coal substance and mineral matter (adapted from Oki et al., 2004). 17

Figure 2.3: The effect of various types of mineral matter on washability (adapted from Falcon & Snyman, 1986). 19

Figure 2.4: An example of the effect of beneficiation of two types of bituminous coals from the Witbank Basin on the distribution of the main constituents (adapted from Falcon & Snyman, 1986). 21

Figure 2.5: Butt and face cleats in coal (adapted from Scholtès et al., 2001). 22

Figure 2.6: Compressive or tensile stresses causing strain of a crystal lattice (adapted from Singh et al., 2014; Usaini et al., 2014; Wills & Napier-Munn, 2006:109). 31

Figure 2.7: Concentration of stress at the crack tip (adapted from Usaini et al., 2014; Wills & Napier-Munn, 2006:109). 32

Figure 2.8: The disintegration of brittle particles due to compressive (F_s) and tensile forces (F_r) (adapted from Drzymala, 2007:127). 32

Figure 2.9: Fracturing of a particle when crushed (adapted from Directorate-General for Energy, 1990:6-10). 35

Figure 2.10: Illustration of impact breakage by a hammer mill. 37

Figure 2.11: Illustration of compressive breakage by double roll crushers. 38

Figure 2.12: Grinding action between particles (adapted from King, 1999; Sankar Prasath & Venkatesh, 2014)..... 38

Figure 2.13: Motion of particles in tumbling mill (Wills & Napier-Munn, 2006:143; King, 1999)..... 40

Figure 2.14: Liberation of mineral and gangue (Usaini et al., 2014). 41

Figure 2.15: Cross-sections of ore particles before and after communition (adapted from Usaini et al., 2014; Wills & Napier-Munn, 2006:15). 42

Figure 2.16: Float and sink analysis (Drzymala, 2007:195). 44

Figure 3.1: Moatize coal sample. 48

Figure 3.2: Micro-focus x-ray tomography scans of Moatize coal. 48

Figure 3.3: Size by washability graph for raw coal. 50

Figure 3.4: Cone and quartering of Moatize coal. 54

Figure 3.5: Lawn roller used for compressive breakage. 56

Figure 3.6: Drop-weight impact rig. 57

Figure 3.7: Tumbling mill. 58

Figure 3.8: Normalized milling curve for Moatize coal (particle sizes 0.0-9.5 mm) 59

Figure 3.9: Normalized milling curve for Moatize coal (particle sizes 9.5-53.0 mm) 59

Figure 3.10: Industrial sieves used for particle size distribution. 60

Figure 3.11: Test sieves 61

Figure 3.12: Densimetric analysis using a zinc chloride solution. 63

Figure 3.13: Float-sink analysis procedure when $ZnCl_2$ was used. 63

Figure 3.14: Rotary splitter 64

Figure 3.15: Densimetric analysis using organic liquids. 65

Figure 4.1: Physical appearance of particles 1.0-6.7 mm. 69

Figure 4.2: Physical appearance of particles 0.0-1.0 mm. 69

Figure 4.3: Ash yield for each relative density interval expressed on a dry basis. 71

Figure 4.4: The inherent moisture of Moatize coal expressed on an air dry basis. 72

Figure 4.5: Free swelling index results. 73

Figure 4.6: Calorific value results. 75

Figure 4.7: Size by washability graph for impact breakage to a top size of 13.2 mm with no additional attrition breakage. 77

Figure 4.8: Size by washability graph for impact breakage to a top size of 6.7 mm with no additional attrition breakage. 77

Figure 4.9: Size by washability graph for impact breakage to a top size of 13.2 mm followed by additional attrition breakage for 5 minutes. 79

Figure 4.10: Size by washability graph for impact breakage to a top size of 6.7 mm followed by additional attrition breakage for 5 minutes. 80

Figure 4.11: Size by washability graph for compressive breakage to a top size of 13.2 mm with no additional attrition breakage. 81

Figure 4.12: Size by washability graph for compressive breakage to a top size of 6.7 mm with no additional attrition breakage. 82

Figure 4.13: Size by washability graph for compressive breakage to a top size of 13.2 mm followed by additional attrition breakage for 5 minutes. 84

Figure 4.14: Size by washability graph for compressive breakage to a top size of 6.7 mm followed by additional attrition breakage for 5 minutes. 85

Figure 4.15: Ash curve for impact breakage to a top size of 13.2 mm. 86

Figure 4.16: Ash curve for impact breakage to a top size of 6.7 mm. 87

Figure 4.17: Ash curve for compressive breakage to a top size of 6.7 mm. 88

Figure 4.18: Float ash per particle size for impact breakage to a top size of 6.7 mm followed by attrition breakage for 1 minute. 89

Figure 4.19: Ash curve for impact breakage to a top size of 6.7 mm followed by attrition breakage for 1 minute. 90

Figure 4.20: Size by washability graph for impact breakage to a top size of 13.2 mm with no additional attrition breakage. 92

Figure 4.21: Liberation curve for impact breakage. 93

Figure 4.22: Liberation curve for compressive breakage. 94

Figure 4.23: Cumulative fractional yield of liberated coal macerals (with RD<1.4) within the particle size interval of 0-4.75 mm. 96

Figure 4.24: Densimetric curve for impact breakage to a top size of 13.2 mm. 97

Figure 4.25: Densimetric curve for impact breakage to a top size of 6.7 mm. 98

Figure 4.26: Densimetric curve for compressive breakage to a top size of 13.2 mm. 99

Figure 4.27: Densimetric curve for compressive breakage to a top size of 6.7 mm. 100

Figure 4.28: Densimetric curve for impact breakage to a top size of 6.7 mm followed by attrition breakage for 1 minute. 101

Figure 5.1: Hypothetical density wash of raw coal. 104

Figure 5.2: Hypothetical density wash of coal subjected to impact breakage to a top size of 6.7 mm with additional attrition breakage for 1 minute. 105

Figure 5.3: Industrial application. 106

LIST OF TABLES

Table 1.1: South African local and international coal prices for 2015 (adapted from Campbell, 2016)..... 3

Table 2.1: Summary of the types of coal along with some properties of each (adapted from Falcon & Falcon, 1987; Falcon & Snyman, 1986; Speight, 2005:2-3; 42)..... 11

Table 2.2: Swelling index of South African coal (adapted from Horsfall, 1980). 12

Table 2.3: Characteristics of the maceral groups (adapted from Falcon & Falcon, 1987; Falcon & Snyman, 1986)..... 13

Table 2.4: Minerals present in coal before any combustion of material and ash yield after combustion (adapted from Oki et al., 2004)..... 17

Table 2.5: The Moatize basin coal stratigraphy and coal quality (Hatton & Fardell, 2012). 27

Table 2.6: Quality of various Moatize coal seams (Lakshminarayana, 2015)..... 28

Table 3.1: Relative densities of materials used for densimetric analysis..... 51

Table 3.2: Apparatus..... 51

Table 3.3: Experimental overview of multiple particle breakage..... 53

Table 3.4: Proximate analysis procedure..... 66

Table 5.1: Required relative density for washing and yield obtained for a target ash yield of 10 %..... 103

NOMENCLATURE

Abbreviation	Description
β_g	Volumetric thermal expansion coefficient of the glass the hydrometer was manufactured of.
$C_{T'}$	Correction factor
ε_L	Degree of liberation
ρ	Actual density
A	Ash (on a dry basis, unless otherwise stated)
CTL	Coal-to-liquid
CV	Calorific value
d	Maximum diameter of grinding media
D	Mill internal diameter
FSI	Free swelling index
GCV	Gross calorific value
ID	Inner diameter
i.e.	Id est (Latin abbreviation for “that is”)
ISO	International Organization for Standardization
M	Moisture (on an air dry basis)
n	Total amount of data points
PSD	Particle size distribution
r	Repeatability limit
ROM	Run-of-mine
S	Standard deviation
SACPS	The Southern African Coal Processing Society
SACRM	South African Coal Roadmap
SAIMM	The Southern African Institute of Mining and Metallurgy
SANS	South African National Standard
TBE	1,1,2,2-tetrabromoethane
TCE	Tetrachloroethylene
VM	Volatile matter (on a dry basis, unless otherwise stated)
WCI	World Coal Institute
WEC	World Energy Council
$\tilde{x}$	Average value
x_i	Experimental data point
$ZnCl_2$	Zinc chloride

Measurement	Description
°C	Degrees Celsius
Ash yield	The term “ash yield” was used instead of “ash content” throughout this study. This is because “ash yield” refers to the ash content remaining after combustion of coal.
$\boldsymbol{C}$	Critical speed
cm	Centimetre
g/cm^3	Gramm per cubic centimetre
g/ml	Gramm per millilitre
kg	kilogram
m	metre
MJ/kg	Mega-joule per kilogram
ml	Millilitre
mm	Millimetres
Mt	Million tonnes
$\boldsymbol{R}$	Measured density at the temperature, T_0
R	South African Rand
RD	Relative density
rpm	Revolutions per minute
R m	Million South African Rand
R/t	South African Rand per tonne
$\boldsymbol{T'}$	Measured temperature
$\boldsymbol{T_0}$	Temperature at which hydrometer is calibrated at.

1

CHAPTER 1 INTRODUCTION

This chapter gives an overview of the investigation undertaken to study the effects of the extent and mode of applied breakage on coal yield. A brief discussion regarding the background and motivation for the research study done are given in Section 1.1, emphasizing the importance of optimizing coal yield while limiting the formation of excessive fines. The objectives are specified in Section 1.2, and the scope of the investigation is given in Section 1.3.

1.1 Background and Motivation

Coal accounts for about 40 % of the global electricity production making it the largest source of energy worldwide (WCI, 2005; WEC, 2013), South Africa depends on coal for over 90 % of its electricity (Jeffrey, 2005; WCI, 2005), making coal the primary energy producing fuel in South Africa (Hancox & Götz, 2014; Jeffrey, 2005; Wagner & Tlotleng, 2012). Figure 1.1 and Figure 1.2 respectively summarizes the global coal consumption and specifically the South African coal consumption for 2013. It is clearly shown that coal consumption is dominated by the electricity generation sector. Although nuclear, and renewable energy sources, were noted to increasingly contribute to the South African energy grid, coal will remain the main energy resource in the foreseeable future because of the wide-spread coal deposits, its abundance, and affordability (Hancox & Götz, 2014; Jeffrey, 2005; Subramoney, 2009). Approximately 75 % of South African coal produced are used locally, mainly by South Africa's electricity provider, Eskom (Pooe & Mathu, 2011), and by Sasol for coal-to-liquid-fuel (CTL) production (Pooe & Mathu, 2011; WEC, 2013). The iron and steel industry also consumed large amounts of coal, whilst the residential consumption of coal is relatively small (WEC, 2013).

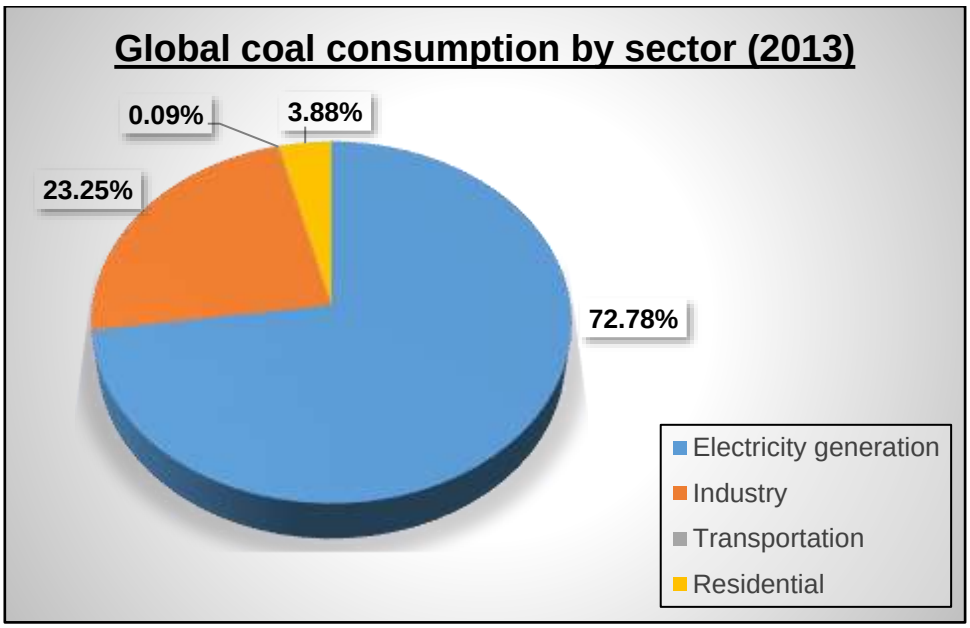

Figure 1.1: Global coal consumption by sector for 2013 (adapted from International Monetary Fund, 2016).

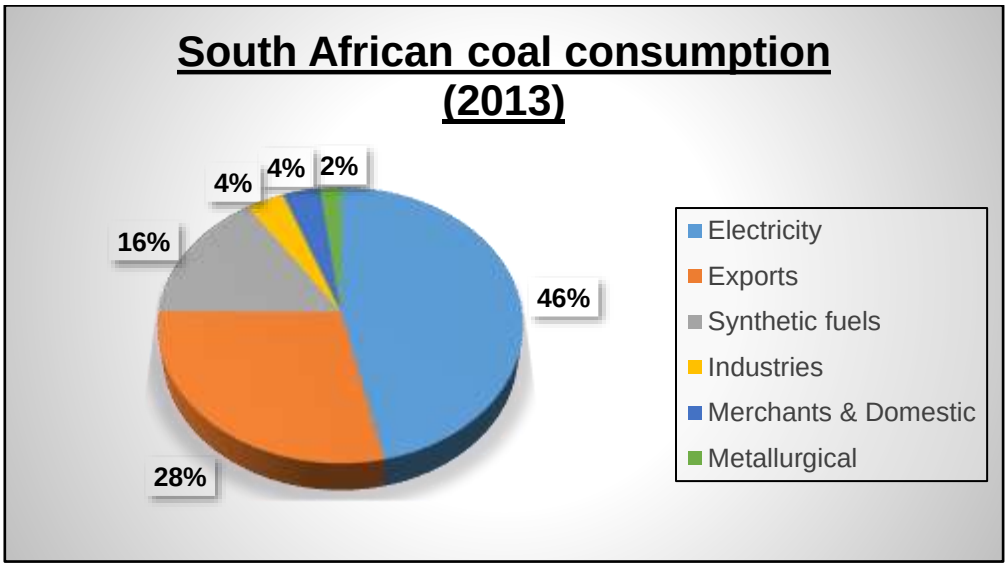

Figure 1.2: South African coal market distribution for 2013 (adapted from XMP Consulting CC, 2014).

Recoverable coal reserves worldwide were projected in 2008 at 411 billion tonnes (Pooe & Mathu, 2011), while the economically recoverable coal reserves of South Africa were estimated at between 15-55 billion tonnes (Eberhard, 2011; Pooe & Mathu, 2011; WEC, 2013) of which 96 % are bituminous coal, 2 % are metallurgical coal, and 2 % are anthracite (Eberhard, 2011). It is estimated that these reserves may only last for the next 130 to 150 years at the current coal consumption rate (Pooe & Mathu, 2011). South Africa is facing a tremendous problem with coal supply, as coal reserves in South Africa are approaching exhaustion (Hartnady, 2010; Jeffrey, 2005), because of the increasing demand for energy due to South Africa's growing economy. Moreover, the population increased in the recent years, resulting in a steady rise in coal

consumption (Hartnady, 2010; Subramoney *et al*., 2009; Weining *et al*., 2013). This is due to higher coal requirements for energy generation, and industrial production activities (Hartnady, 2010; Weining *et al*., 2013). The demand for steel production is increasing due to the rapid urbanization worldwide. Steel is used for, amongst others, food production, water delivery, expansion of telecommunication systems, and transport networks (WCI, 2007). Metallurgical coal, is essential for the manufacturing of steel, which is an alloy of carbon and iron (WCI, 2007). The loss of production accompanying coal reserves exhaustion will lead to economic growth problems (Hartnady, 2010). Not only are the coal resources being depleted, but the quality (grade) of the remaining in situ coal reserves are also decreasing (SACPS, 2015:41; Wagner & Tlotleng, 2012). As the high quality reserves are depleted it is becoming necessary to mine low grade coal to meet the country's increasing energy demand. In many cases, due to the stratigraphy of the seams, it is impractical to mine selectively, and it is required to beneficiate the coal in order to supply a quality product (Wagner & Tlotleng, 2012).

South African exports mainly thermal (steam) coal (Kumba Resources, 2016; SACRM, 2011), together with a negligible amount of coking and metallurgical coal (SACRM, 2011). These are exported mainly to Asia and Europe (WEC, 2013), and sold at a much higher price than that achieved locally (Eberhard, 2011). As tabulated in Table 1.1, South African thermal export coal reached a price of R768/tonne, and export coking coal prices varied between R1072 and R1910 per tonne depending on the export location (Campbell, 2016). The export price of coal was therefore approximately three times the local price of coal, and significantly beneficial for the South African economy (Hancox & Götz, 2014; SACRM, 2011). Coking coal is also more valuable than steam coal since the local price for coking coal was R650/tonne in 2015, and was twice that of the local price for thermal coal, which realised prices of between R225-315/tonne (Campbell, 2016).

Table 1.1: South African local and international coal prices for 2015 (adapted from Campbell, 2016).

Commodity	Local sales (R/t)	Export sales (R/t)
Eskom (Large Companies)	225	
Eskom (Junior Miners)	315	
Thermal Export (at Richard's Bay Coal Terminal)		768
Coking (Waterberg Semi Soft Coking Coal)	650	
Hard Coking Coal (Australia)		1072
Hard Coking Coal (China and England)		1910

Since South African coal reserves are mainly bituminous coal, and therefore the industry is dominated by production of steam coal (Eberhard, 2011) for either local or export purposes. By applying suitable beneficiation processes to reduce the mineral matter content, the lower grade coals can be upgraded in terms of their calorific value, and the mine can realize up to a threefold increase in revenue by exporting the coal, rather than supplying into the local market. The quality requirements of metallurgical coal are both stricter, and have specific requirements, compared to those set for thermal coal (Kumba Resources, 2016). Currently the only operating source of metallurgical coal, in the form of semi-soft coking coal, is from Exxaro's Grootegeluk Coal Mine (Powell, 2016). Southern African coking and thermal coal reserves which have the potential to be of economic value include the Limpopo (Tuli) Coalfield (Hancox & Götz, 2014), and the Mozambique coalfields (Hatton & Fardell, 2012). Although South Africa is one of the largest hard coal producers and exporters according to Eberhard (2011), less than 0.5 Mt of saleable coking coal per annum is produced in South Africa, due to the low yield of this product produced by Grootegeluk (Powell, 2016). Therefore coal resources containing coking coal, such as the Limpopo (Tuli) Coalfield, may be a valuable resource in the future (Jeffrey, 2005). It was estimated that this resource contained some 349-517 Mt recoverable in situ bituminous coal of which, after washing, can produce between 125 Mt to 243 Mt of metallurgical coal (Jeffrey, 2005).

Emerging coal markets worldwide for example, coal to liquid (CTL) processes, and the use of coal in fuel cells, require coal products of different quality specifications compared to that of the traditional electricity generation and coking coal markets (O'Brien *et al*., 2011). South African coals with low mineral matter content are exported (Wagner & Tlotleng, 2012), whilst mineral rich middlings, and low quality thermal coals are used for local electricity generation (Wagner & Tlotleng, 2012; WEC, 2013), and synfuels productions (Eberhard, 2011). The quality of coal used by Eskom for power generation has a calorific value (CV) ranging between 15 MJ/kg and 20 MJ/kg (Eberhard, 2011; SAIMM, 2016; Subramoney *et al*., 2009), with a 29.5 % ash yield and 0.8 % sulphur content (Eberhard, 2011). Sasol's CTL plants consume coal with high ash yield of around 35 %, and with a CV of less than 21 MJ/kg (Eberhard, 2011). The higher quality exported South African thermal coal typically has a CV between 24.7-27.0 MJ/kg, net as received (Eberhard, 2011; SAIMM, 2016), and with sulphur content of 0.6-0.7 % (Eberhard, 2011). The term "ash yield" was used instead of "ash content" throughout this study. This is because "ash yield" refers to the ash content remaining after combustion of coal. The ash yield is therefore related to the mineral matter occurring originally in the coal before combustion (Speight, 2005:55). The mineral matter proportion in coal can be calculated by the Parr formula as shown by Equation 1-1, where A refers to the ash percentage in the coal, and S to the total sulphur content in the coal (Speight, 2005:55).

$$Mineral\ matter\ (\%\ w/w) = 1.08A + 0.55S \qquad \textbf{1-1}$$

The quality of coal used by Eskom has been deteriorating over the years since the higher grade coals are reserved by coal suppliers for the more profitable export market (Eberhard, 2011). South African coals typically have a low sulphur content (WEC, 2013), and generally high mineral matter content. Therefore they usually require washing in a beneficiation plant, to reduce the mineral matter (de Korte, 2010; Eberhard, 2011; WEC, 2013) to meet the export calorific value specification (de Korte, 2010), and to ensure that the ash yield does not exceed 15 %. The beneficiation plant at these qualities typically gives a product yield of the order of 65 % (Eberhard, 2011). The only local semi-soft coking coal plant produces a yield of approximately 10 % at an ash yield of 10 %, and a 30 % volatile matter (de Korte, 2010). Due to the challenging washing characteristics of South African coal, washed coal with 12-15 % ash is permissible (de Korte, 2010). Coal properties, and mineral inclusions within coal particles, must be well known in order to recognise coals that are suitable to produce coal products with qualities as required by the markets as economically possible (O'Brien *et al*., 2011). Hence the mineral, and maceral, associations in individual coal particles must be clearly understood as they influence the utilization performance, and washability (density distribution) properties. The latter is used as an indicator which beneficiation processes to employ to economically produce a low ash coal product according to market requirements (O'Brien *et al*., 2011).

Coal seams, for example, those in Southern Africa such as the Waterberg and Mozambique Coalfields, are interlayered with mineral matter. The latter is incombustible, and does not burn when ignited, but becomes altered during combustion and remains as an undesirable ash by-product. It therefore lowers the economic value (Ito *et al*., 2009; SACPS, 2015:20; Weining *et al.,* 2013) by reducing the calorific (heating) value of the coal (SACPS, 2015:20; Wagner & Tlotleng, 2012). It is of economic importance to maximize the amount of valuable coal recovered from raw coal; since different coal value fractions are intermingled and cannot be used directly as mined (Wagner & Tlotleng, 2012). Size reduction of coal particles may, however, be required to increase the liberation of different coal quality fractions from the mineral material (Ito *et al*., 2009; O'Brien *et al*., 2011; Weining *et al.,* 2013). This would enable the separation of the undesirable incombustible material from the valuable coal after mining (Ito *et al*., 2009; SACPS, 2015:20; Weining *et al.,* 2013), in order to produce a low ash value coal product (O'Brien *et al*., 2011). Figure 1.3 gives a simplistic representation of coal breakage and liberation, showing only two idealized fractions: coal (black) and minerals (white). A raw particle as indicated in Figure 1.3(a) needs to be subjected to some breakage mechanism and, as an example, compressive breakage is illustrated in Figure 1.3(b). Breakage processes generally result in liberated coal particles as can be seen in Figure 1.3(c) (Weining *et al.,* 2013), after which the different particle fractions can be separated from each other by a variety of methods. Again, this representation is idealized, and liberation is seldom complete.

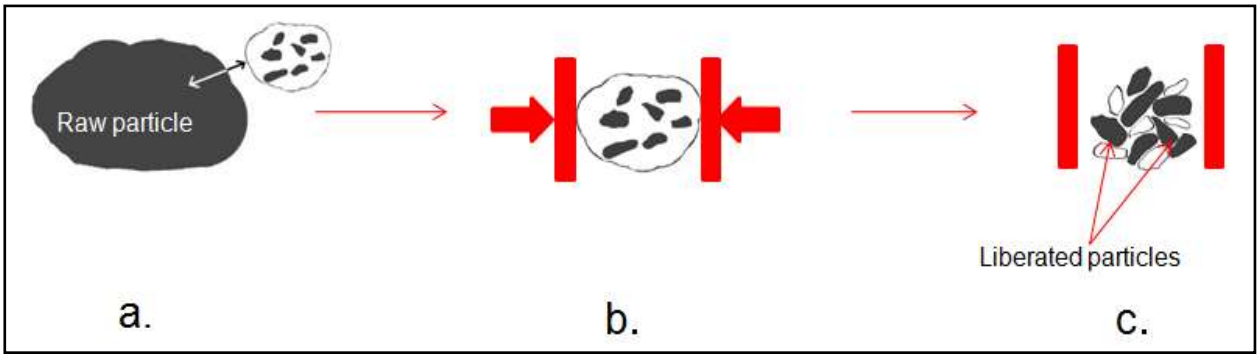

Figure 1.3: Representation of coal breakage and liberation for the ideal case.

Size reduction of coal leads to the generation of fine coal which must be limited since processing, drying and handling operations are difficult when fines (-0.5 mm) are present (Weining *et al.,* 2013). Not only has fine coal higher moisture retention than coarse coal, but processing of fine coal is also generally more expensive; and less efficient, and therefore coal must be processed at the coarsest possible particle size (O'Brien *et al*., 2011). Despite these difficulties in fine coal processing, crushing of certain coal sources to smaller particle sizes prior to processing may be required to attain higher degrees of liberation. This generally results in an increase in the plant yield (O' Brien *et al*., 2011), by liberation of values from the middlings. Middlings are defined as partially liberated coal fractions which still contain mineral matter after size reduction (Holuszko & Grieve, 1990) Comminution (size reduction) processes must therefore be controlled, and optimized, to ensure that adequate liberation takes place, but also that the particle sizes are suitable for utilization (Weining *et al.,* 2013). It is important that the mineral and maceral composition of the parent coal and daughter particles formed from crushing are known and understood to optimize liberation (O' Brien *et al*., 2011). Knowledge of particle breakage will aid in the optimization of liberation, whilst limiting the generation/production of coal fines. Since it is unlikely to eliminate all fines in comminution processes, a balance between sufficient liberation of coal to attain a certain yield, and the formation of excessive fines must be achieved.

Crushing and comminution processes are generally expensive, both in terms of capital expenditure and operational costs, and therefore an appropriate circuit is required to achieve the best liberation size to allow for maximization of the plant yield. Moreover, a higher value product, and optimum plant yield, can be produced from the run-of-mine coal once it has been liberated from the waste rock or gangue minerals. The higher value product achieved should offset the costs associated with the comminution/crushing section of the plant. If well designed the production of fines will be minimized.

Therefore the intention of this study was to investigate:

1. Liberation of coal to attain a certain yield; and

2. Determine the different breakage modes, or combination of breakage modes, that will be best suitable to optimize liberation at the coarsest possible coal particle size, whilst keeping fines formation to a minimum.

The yield with respect to liberation for a market specification for a low ash product was investigated, with a view to achieving the optimal liberation size. Coal as mined, which was run-of-mine (ROM) coal, was used for this study to investigate the effect of the mode of breakage on coal containing fines. It is important to note that when referring to liberation throughout this study, it implies the release, and separation, of entrapped coal particles from mineral inclusions with the intention of increasing the coal yield when washing it to the desired ash specification.

1.2 Objectives

The primary objective of this investigation was to study the effect of various breakage modes, or combinations, of breakage modes on coal yield. Coal from the Moatize Coalfield in Mozambique was chosen because of its highly layered morphological structure consisting of coal seams interlayered with mineral matter. Coal breakage modes to be investigated were:

1. Impact breakage followed by attrition breakage; and,

2. Compressive breakage followed by attrition breakage.

The specific objectives of the conducted research study were as follows:

1. To evaluate the above mentioned combinations of breakage modes to determine the most effective method for optimizing coal yield, and to achieve sufficient liberation whilst limiting excessive fines formation.

2. Determination of the coal yield improvement when a specified combination of breakage modes are implemented.

3. To study the effect of attrition breakage additional to compressive breakage and impact breakage on coal yield.

4. Determination of the optimum liberation size for the coal used in this investigation.

5. To study the advantages of improving liberation processes of current coal resources.

6. Sufficient liberation for the coal used during this study must also be defined; that is to determine the largest particles size with the maximum allowable ash yield obtained to produce a product as required by market specifications.

1.3 Scope of investigation

This dissertation is divided into six chapters. Figure 1.4 presents an outline of the scope of this investigation.

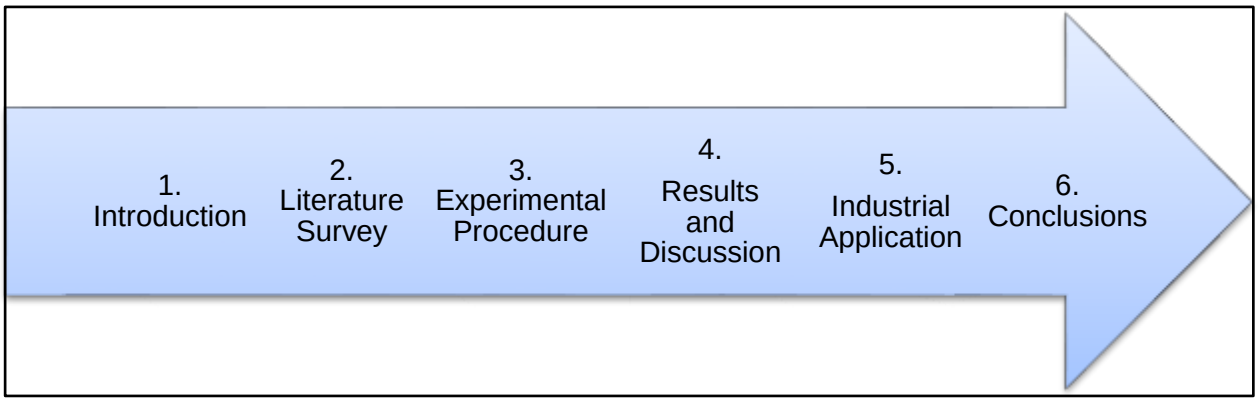

Figure 1.4: Scope of the investigation

- **Chapter 1:** This chapter gives an introductory overview of the research study conducted. The motivation for this study along with some background information regarding the importance of this investigation, coal breakage and liberation is briefly discussed. The objectives made are specified and an outline of the dissertation is given.

- **Chapter 2:** A complete literature survey is conducted where relevant theory concerning this investigation are covered in detail.

- **Chapter 3:** The experimental procedures, including materials and apparatus used during this investigation were explained in detail.

- **Chapter 4:** The results found from the experiments conducted accompanied by a discussion of the outcomes were given.

- **Chapter 5:** The potential for employing this research study outcomes in industrial processes are considered in this chapter.

- **Chapter 6:** This chapter provides a summary of the conclusions made from the results obtained. Shortcomings of the research are also discussed, and recommendations on how to improve future research studies similar to this investigation are given.

2

CHAPTER 2 LITERATURE SURVEY

Chapter 2 contains a review of published literature relevant to this investigation. Section 2.1 gives a brief overview of coal in general, and some specific coal characteristics are discussed. The Mozambique Coalfields will be the only coalfield that will be discussed (Section 2.2), since coal from this coalfield will be used during this research study. The Moatize Coalfield in Mozambique was chosen because of its highly layered morphological structure consisting of coal seams interlayered with mineral matter. Size reduction of coal is discussed in Section 2.3, whilst Section 2.4 contains a discussion of the implementation of breakage for the purpose of liberation of coal from mineral material, along with an explanation of the float and sink analysis used to separate particles according to density. The production of fines is discussed in Section 2.5, and some practical process measures for the minimization of fines generation are suggested.

2.1 Coal

Coal is a sedimentary rock comprising of combustible carbonaceous material and incombustible mineral material (Directorate-General for Energy, 1990:2; Khandelwal & Singh, 2010; SACPS, 2015:13) that formed from accumulated plant remains during coalification. Coalification is a metamorphosis process of peat swamp, under high temperature, and high pressure conditions, to various levels of maturation over time (Falcon & Snyman, 1986). Peat, which is an unconsolidated product formed by the decomposition of vegetation occurring in swampy conditions, is the first step in the coalification process (SACPS, 2015:16), and is followed by the progressive levels of maturation. Maturation is termed the rank of coal, and maturity increases as the peat changes from peat to lignite (also known as brown coal), sub-bituminous coal, and bituminous coal, and anthracite respectively (Falcon & Snyman, 1986). As the material overlaying the lignite increases with time, the pressure and temperature increase cause changes in the material resulting in the formation of bituminous coal (Falcon & Snyman, 1986; SACPS, 2015:13) as illustrated in Figure 2.1. The main parameters used to describe coal are rank, type, and grade, where:

1. type denotes the petrographic composition of coal with regard to its maceral content,
2. rank to the degree of coalification or maturity (O'Brien *et al*., 2011; Vasconcelos, 1999), and,

3. grade to the inorganic matter content or ash yield (Falcon & Snyman, 1986; O'Brien *et al*., 2011; SACPS, 2015:13; Vasconcelos, 1999).

The type of coal is associated with the organic matter composition of the coal, and differs according to the plant material from which the coal was formed (Falcon & Snyman, 1986; SACPS, 2015:13). Coal types found in the coalfields around the world thus vary since the deposition of material, and time of formation, vary (SACPS, 2015:13). The coal rank increases with an increase in the carbon content; thus lignite has the least carbon whereas anthracite has the most carbon (Pinheiro & Cook, 2005). Table 2.1 gives a summary of the main rank classifications of coal along with a short description of the coal properties and its primary use.

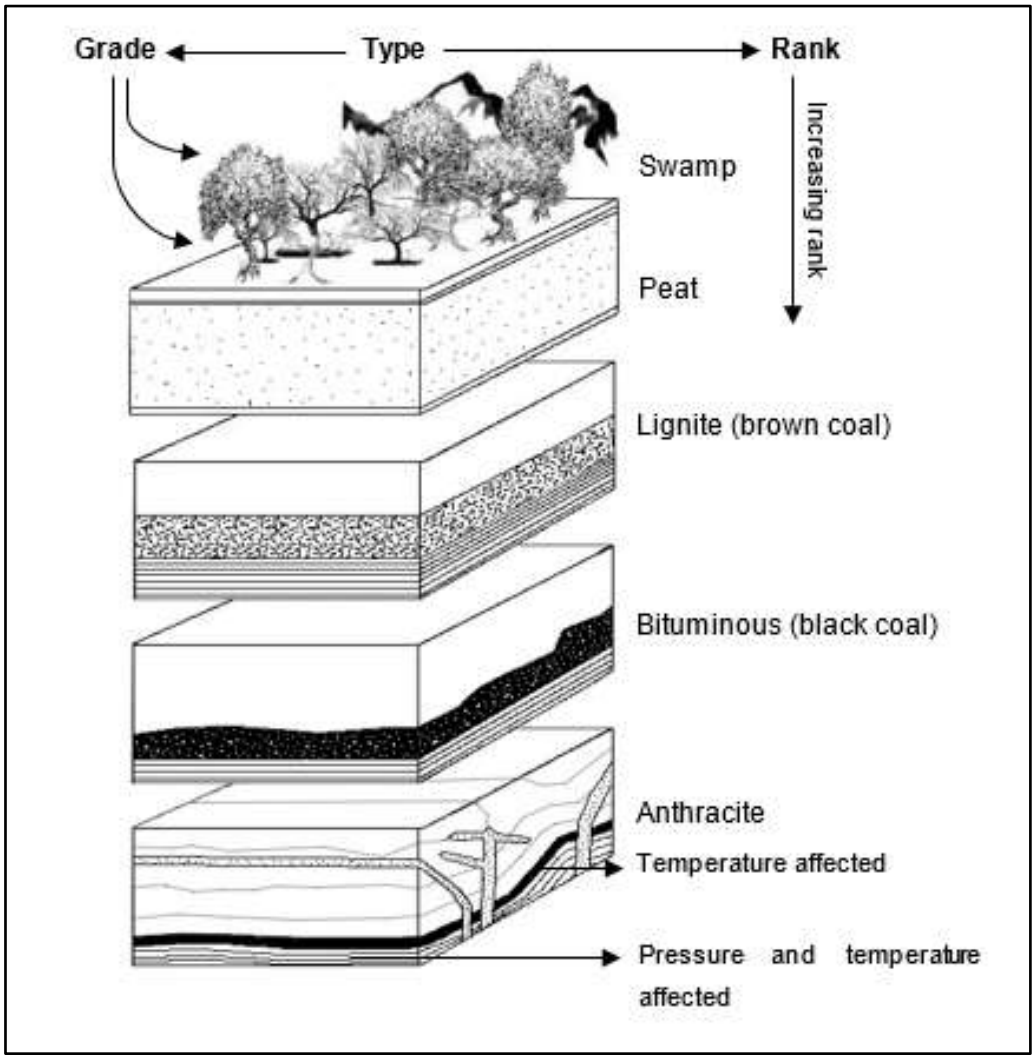

Figure 2.1: The formation of coal in terms of its grade, rank and type (adapted from Falcon & Snyman, 1986).

Table 2.1: Summary of the types of coal along with some properties of each (adapted from Falcon & Falcon, 1987; Falcon & Snyman, 1986; Speight, 2005:2-3; 42).

Type of coal	Rank	Vitrinite reflectance (%)	Description	Relative density (RD)	Primary use
Anthracite (or hard coal)	High	2.0-10.0	Hard, brittle, black	1.35-1.70	Commercial and residential space heating, metallurgical reductants
Bituminous coal	Medium	0.5-2.0	Dense, dark brown to black bands of dull and bright material	1.28-1.35	Steam-electric power generation, manufacturing of coke
Subbituminous coal	Low	0.4-0.5	Varies from soft, dull, dark brown to bright, hard, black	1.35-1.40	Steam-electric power generation
Lignite (or brown coal)	Low	0.3-0.4	Brown-black	1.40-1.45	Steam-electric power generation

Coals can be classified as coking and non-coking (thermal or steam) coal by referring to their coking properties (Speight, 2005:18). They are respectively used in among the manufacturing of iron and steel (Rosenfeld, 2012; Speight, 2005:199), and for electricity generation (Hanlon, 2013; Rosenfeld, 2012). The free swelling index (FSI), which is the increase in coal volume when heated according to conditions as specified in the standard procedure (ISO 501:2003), provides an indication of the coal coking characteristics (Speight, 2005:147). Gas formed during thermal decomposition of coals becomes trapped, and is responsible for the swelling of the coal (Speight, 2005:147). The FSI of bituminous coals usually increases as the coal rank increases (Speight, 2005:147). Table 2.2 indicates the consumption of coal according to its free swelling index. Southern African coking coals typically have a FSI greater than 8 (Powell, 2016). Some macerals, which are the microscopic constituents of coal formed from the remains of plant material, are responsible for the coking properties of coal (Falcon & Snyman, 1986), and will be discussed in Section 2.1.1. Coking coals are thus the coals that are able to soften and swell before solidifying (Kruger, 2013) throughout a carbonization process, where coal is slowly heated up to a specific temperature range (Falcon & Snyman, 1986; Kruger, 2013) between 350°C and 550°C (Kruger, 2013), during which some coal constituents will remain inert whilst others will become soft and porous, to form an ultimately hard product namely coke (Falcon & Snyman, 1986).

Table 2.2: Swelling index of South African coal (adapted from Horsfall, 1980).

Coal consumer	Swelling index
General trade and power generation	0-1
Blend coking coal	2-4
Straight coking coal	4.5-8.5
Low-ash export coal	>2.5

Properties of coking coals include an ash yield of 1-10 %, and volatile matter content of 18-45 % (Kruger, 2013). Mineral matter, especially sulphur and phosphorus, must be as low as possible in coal to be suitable for coking purposes (Falcon & Snyman, 1986). This is because the presence of these mineral matter affects the strength of the coke product (Falcon & Snyman, 1986). Coal that does not comply with these strict quality specifications, and that cannot be used for pulverised fuel injection, are generally sold as thermal coal (O'Brien *et al*., 2011).

Coking coal is more valuable than non-coking coal (Hanlon, 2013), and thus offers the highest market price (O'Brien *et al*., 2011) as discussed in Chapter 1. The occurrence of the type of coal in coal seams, and the value of the product coal, influences the feasibility of a mine (Hanlon, 2013). Thus, the price difference and the proportions of thermal and coking coal produced by a mine effect the viability of a mine, for example, a higher coking coal production will increase the revenue of the mine, and should also be able to bear the production and transport costs (Rosenfeld, 2012). The price difference between coals with different qualities that can be sold into various markets influences the beneficiation and processing methods employed. Mines consequently use beneficiation/processing techniques that result in maximizing the production of the higher value coal products (O'Brien *et al*., 2011).

2.1.1 Macerals

The smallest recognisable organic component of coal are macerals (Holuszko & Mastalerz, 2014; SACPS, 2015:19), which evolved from the remaining material of degraded plant matter during the coalification process of coal (Falcon & Snyman, 1986). Vitrinite, liptinite (formerly known as exinite), and inertinite are the main maceral groups (Falcon & Falcon, 1987; Falcon & Snyman, 1986; Khandelwal & Singh, 2010; O' Brien *et al*., 2011), each group possessing its unique physical and chemical properties associated with their rank or maturity (Falcon & Snyman, 1986; Khandelwal & Singh, 2010). The properties of coal are determined by the proportion of each maceral present (Lakshminarayana, 2015; SACPS, 2015:19). Vitrinite has coking properties at certain ranks, and is thus responsible for the coking properties of coal, whereas liptinite is mostly volatized during the carbonization process, and does not contribute to the formation of coke (Falcon & Snyman, 1986). The most suitable coal for the purpose of coke production is a

vitrinite - rich, medium bituminous coal rank, because of the high swelling characteristics, as well as good plasticity of vitrinite, which leads to the formation of a strong porous structure (Falcon & Snyman, 1986).

The inorganic mineral components, and the organic material (macerals), that coal comprises of (Falcon & Falcon, 1987; Ward & French, 2004) can be identified and distinguished by coal petrography (Falcon & Falcon, 1987; Falcon & Snyman, 1986; Khandelwal & Singh, 2010; O' Brien *et al*., 2011; SACPS; 2015:67). Furthermore, the reflectance of the vitrinite is used to determine the rank of the coal (Falcon & Falcon, 1987; O' Brien *et al*., 2011; SACPS, 2015:20). Maceral groups are distinguished by among others their texture, shape and greyness under incident reflected light (Khandelwal & Singh, 2010; O'Brien *et al*., 2011; Pan *et al.,* 2013). The carbon content is directly associated with the amount of reflected light from the surface of the vitrinite, where a higher carbon content will result in higher reflectance (Falcon & Snyman, 1986); thus the reflectance of vitrinite increases with an increase in rank (O'Brien *et al*., 2011). Table 2.3 summarizes the material from which each maceral group originated, as well as the reflectance of each maceral group, in terms of its colour when under incident light, the rank, and the percentage of light reflected.

Table 2.3: Characteristics of the maceral groups (adapted from Falcon & Falcon, 1987; Falcon & Snyman, 1986).

Maceral group	Plant origin	Rank	Reflectance description	Reflected light (%)
Vitrinite	Cell wall material of woody trunks, stems, detrital organic matter, branches. Anaerobic decomposition	Low to medium rank bituminous	Dark-medium grey	0.5-1.6
		High rank bituminous	Pale grey	1.6-2.0
		Anthracite	White	2.0-10.0
Liptinite	Spores, cuticles, accumulation of algae	Low rank	Black-brown	0.0-0.5
		Bituminous	Dark grey	0.5-0.9
		Medium rank bituminous	Light grey	1.1-1.6
		High rank bituminous and anthracite	Light grey to white shadows	1.6-10.0
Inertinite	Same plant material as vitrinite, but originated in aerobic oxidizing conditions	Low rank bituminous	Medium grey	0.7-1.6
		Medium rank bituminous to anthracite	Pale grey to white or yellow-white	1.6-10.0

Not only have each of the maceral groups different densities, but the densities are also different from the mineral matter content occurring in coal. Coal can therefore be separated by gravity separation from the ash-forming components after breakage of the raw mined material is done to "free" the coal particles (O' Brien *et al*., 2011). Coal grains consisting of large amounts of liptinite often contain more mineral matter while having the same density as coal with high inertinite and a low mineral content, because liptinite is less dense relative to inertinite (O' Brien *et al*., 2011). It is therefore easier to obtain low mineral matter products from coal containing no liptinite compared to low-rank liptinite rich coal. Thus, variations in maceral densities influence the ash yield of the coal (O' Brien *et al*., 2011). Again, it is important to note that the term "ash yield" was used instead of "ash content" throughout this study. This is because ash yield refers to the ash content remaining after combustion of coal. The ash yield therefore are related to the mineral matter content in the coal before combustion, as shown in Equation 1-1 in Section 1.1. The densities of the three groups of macerals can be summarized as follows:

- **Vitrinite:** The density of vitrinite varies with coal rank; high volatile bituminous coal has a relative density (RD) of 1.30, a minimum RD of 1.27 occurs in the medium volatile bituminous range while that of anthracites are up to 1.80 (Falcon & Snyman, 1986).

- **Liptinite:** The RD of liptinite varies between 1.18-1.25 making this maceral group the lightest relative to the other groups. The density changes according to an increase in rank in bituminous coals (Falcon & Snyman, 1986).

- **Inertinite:** The RD of inertinite ranges from 1.35-1.70 and have insignificant change with increasing coal rank (Falcon & Snyman, 1986).

2.1.2 Lithotypes

Lithotypes are the macroscopic bands or layers of coal occurring parallel to the bedding plane of a given seam (SACPS, 2015:18), and are visible to the naked eye (Falcon & Falcon, 1987; Falcon & Snyman, 1986). Lithotypes are divided into sapropelic coal lithotypes which are dull, non-banded with a granular surface, and contain finely dispersed mineral matter, and humic coal lithotypes containing layers of varying brightness, and are banded (Falcon & Snyman, 1986). Humic coal lithotypes refer to plant material that have accumulated in situ near the original peat swamp during coalification, whereas sapropelic coal lithotypes refer to the accumulation of organic matter in open water deposits (Falcon & Falcon, 1987). Humic coal lithotypes namely vitrain, clarain, durain and fusain are also referred to as dull and bright bands (Falcon & Falcon, 1987; Falcon & Snyman, 1986). Coal seams are classified into lithotypes according to the extent of bright vitrain bands present within the attrital matrix which can, consequently, be either bright or dull depending on the material composition (Esterle *et al*., 2002). Coal seams consists of

heterogeneous mixtures of these dull and bright bands, as well as stone and minerals, each of which have various seam thicknesses, composition and fracture density (Esterle *et al*., 2002). The development of diverse lithotypes can be ascribed to the different environmental conditions during the time of deposition (Falcon & Snyman, 1986) influencing the lithotype composition. This is mainly determined by the coal maceral composition, and the proportion of mineral material present (Holuszko & Grieve, 1990).

The properties of the lithotypes are as follows:

- **Vitrain** (bright coal) is black, brittle and shiny. It breaks into cubic blocks with relatively smooth surfaces (Falcon & Falcon, 1987; Falcon & Snyman, 1986; SACPS, 2015:19). The main constituent, vitrinite, is responsible for the coking characteristics of vitrain (SACPS, 2015:19).

- **Durain** (dull coal) can be classified into black and grey durain. Black durain does not shine and is rare in South African coals, while grey durain consists of vitrinite and fusian-like material. Durain is dull when the amount of vitrinite is low (SACPS, 2015:19), yet a few thin bright bands may occur in between the dull bands. This lithotype is relatively tough and fracturing is uneven (Falcon & Snyman, 1986). Coals from South Africa are mainly combinations of grey durain and vitrain, varying from vitrain rich coal (bright coal) to pure durain (dull coal) (SACPS, 2015:19).

- **Clarian** (banded bright coal) consists of thin bands of altering black durain and vitrian (SACPS, 2015:19). Bright coal bands are interlayered with thin dull coal bands (Falcon & Snyman, 1986).

- **Fusain** (fibrous coal) occurs as discrete flat portions, rather than continuous bands, and is relatively soft (Falcon & Snyman, 1986; SACPS, 2015:19).

The properties of the various lithotypes will influence the breakage and liberation of coal. Durain is the hardest and toughest among the lithotypes, and tends to occur in the largest size fractions, vitrain is brittle and occurs as fines, whilst fusain is friable and occurs as dust unless mineral material is present (Holuszko & Grieve, 1990). Clarain is relatively resistant to breakage compared to vitrain, and its hardness relies on either the liptinite band thickness or the inherent mineral material (Holuszko & Grieve, 1990). The density of lithotypes differ, with vitrain and fusain having the lowest densities of respectively 1.30-1.40 and 1.00-1.25, compared to durain and clarain with the highest densities of 1.50-1.70 and 1.30-1.50 respectively (Falcon & Falcon, 1987; Holuszko & Grieve, 1990). It is therefore expected that the liberation process, and washability characteristics, of coal will be influenced by the lithotype composition due to the difference in lithotype properties (Holuszko & Grieve, 1990). An increase in the vitrain content will, for example,

have good washability properties since it will give a high concentration of the lighter particles, leading to low-ash vitrinite particles (Holuszko & Grieve, 1990).

2.1.3 Mineral matter associated with coal

Mineral matter distribution varies from one coal seam to another (Speight, 2005:92) as it is, like macerals, a product of the geological processes related to peat accumulation and maturation (Ward & French, 2004). Minerals are sedimentary rocks which can be interbedded between coal seams (for example shales and sandstones), or occur as mineral grains within the organic coal matrix (for example clays, quartz and carbonates) (Falcon & Falcon, 1987). Minerals present in coal differ in chemical composition and physical characteristics (Falcon & Snyman, 1986), and generally occur as either separate inorganic particles or minerals enclosed in the cleat network to fill the area (Viljoen *et al*., 2015; Ward, 2002). Extrinsic mineral matter is derived from any inorganic material associated with the coal seam, for example, the floor or the roof of the coal seam (Speight, 2005:35), and may also occur as separate partings within the seam (Falcon & Snyman, 1986; O' Brien *et al*., 2011). Extrinsic mineral matter can be divided into syngenetic (primary) and epigenetic (secondary) (Falcon & Snyman, 1986). Syngenetic refers to mineral material that accumulated during peat accumulation, whilst epigenetic refers to mineral matter that deposited by the percolation of water in fractures and pores in coal seams long after peat accumulation occurred (Falcon & Snyman, 1986; Holuszko & Grieve, 1990; Ward, 2002; Ward & French, 2004). Mineral matter in coal includes three fundamental constituents, namely (Ward & French, 2004):

- Discrete inorganic crystalline or non-crystalline particles which are the true mineral particles;
- Dissolved salts and inorganic materials in the coal's inherent pore water, and
- Inorganic materials intimately associated with the organic coal matrix.

Mineral matter occurs as a solid material in coal that is generally inert to combustion, and is only altered during combustion to form ash, as illustrated in Figure 2.2 (Ito *et al.*, 2009; SACPS, 2015:20; Ward, 2002). Ash is undesirable as it causes problems during coal utilization including slagging, fly ash pollution, corrosion during combustion (Speight, 2005:94; Ward, 2002), and reduces the calorific (heating) value of coal (SACPS, 2015:20). A distinction must be made between a coal's ash and mineral matter: mineral matter is the inorganic material occurring in coal, whilst ash is the non-combustible residue of mineral matter. The composition and structure of the ash differs thus from the mineral matter (Ward & French, 2004). The weight of minerals decrease in some cases due to decomposition and dehydration, whilst the weight of others do not change during the combustion process as presented in Table 2.4 (Oki *et al*., 2004). When

coal contains high amounts of mineral matter, the combusted coal yields large quantities of ash. Table 2.4 lists some of the minerals present in a certain coal prior to combustion, along with the remaining ash yield (Oki *et al*., 2004).

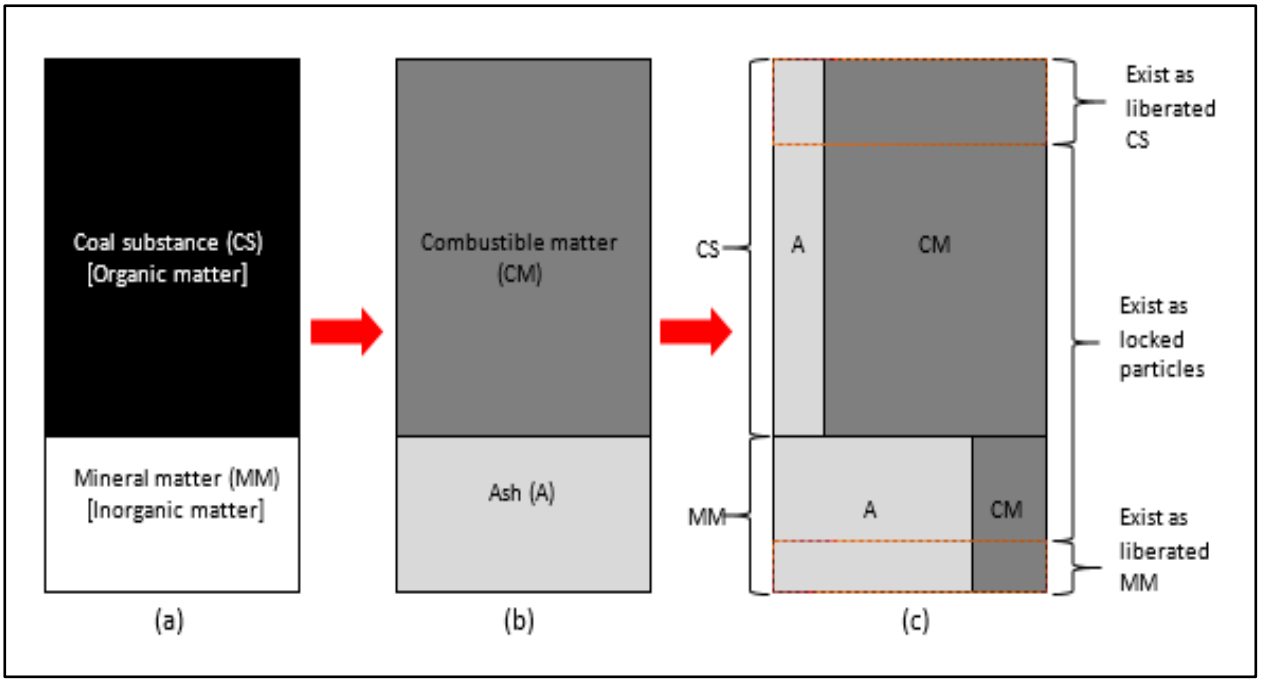

Figure 2.2: Relation between the organic and inorganic matter of coal before and after material is combusted: (a) before any combustion of material, (b) after any combustion of material; (c) contents in coal substance and mineral matter (adapted from Oki *et al*., 2004).

Table 2.4: Minerals present in coal before any combustion of material and ash yield after combustion (adapted from Oki *et al*., 2004).

Mineral groups	Relative Density	Mineral present in coal prior to combustion	Ash component after combustion	Ash yield (%)
High ash-low density	2.61	Kaolinite ($Al_2Si_2O_5(OH)_4$)	Metakaolinite ($Al_2Si_2O_7$)	93.5
	2.65	Quartz (SiO_2)	Quartz (SiO_2)	100.0
	2.75[a]	Illite	(Amorphous)	95.5
High ash-high density	3.90	Anatase (TiO_2)	Anatase (TiO_2)	100.0
Low ash-low density	2.71	Calcite ($CaCO_3$)	Lime (CaO)	56.0
	2.94	Dolomite ($CaMg(CO_3)_2$)	CaO·MgO	60.9
Low ash-high density	3.94	Siderite ($FeCO_3$)	Hematite (Fe_2O_3)	69.0
	5.03[b]	Pyrite/Marcasite (FeS_2)	Hematite (Fe_2O_3)	66.7

[a]Typical density; [b]Average density

Properties of some minerals are as follows:

- **Clay:** The RD of pure clay is 2.4 and it is the most abundant mineral found in South African coal (Falcon & Snyman, 1986).

- **Quartz:** This mineral occurs commonly in small quantities as isolated grains and has a RD of 2.65 if pure (Falcon & Snyman, 1986).

- **Carbonate:** This mineral occurs as nodules and cell fillings of calcite and dolomite and has a RD of 2.85 if pure (Falcon & Snyman, 1986).

- **Pyrite and iron sulphides:** These minerals also occur in Southern African coal in relative small amounts. Pyrite in its pure form has a RD of 5 (Falcon & Snyman, 1986).

The occurrence of mineral matter within coal particles are responsible for the wide range of washability distributions, since the density of coal components are low relative to mineral components (O'Brien *et al*., 2011). Pure coal has a RD of 1.20-1.40 whilst mineral matter have RD's varying between 2.0 and 5.0 depending on the mineralogy (Speight, 2005:94). Composite particles, consisting of varying amounts of macerals and minerals, exhibit intermediate RD values (O'Brien *et al*., 2011). The washability, and the ash yield of coal, depends on the mineral matter associations with the coal macerals (Falcon & Snyman, 1986). The washability, or density distribution, characteristics are determined by float and sink analysis (O'Brien *et al*., 2011). This will be described in Section 2.4.1. The relationship between the mineral matter within a particle, and the RD of a particle, is the basis of most coal beneficiation processes currently used to produce clean coal (O'Brien *et al*., 2011).

As can be seen from Figure 2.3(a), syngenetic minerals occurring as fine particles will produce reasonably equal amounts of high-density discards, middlings and light-density coal when separated by gravity separation (Holuszko & Grieve, 1990). Liberation of the mineral material in this situation can only be attained by fine grinding. Syngenetic minerals that are coarser, reveal better washability characteristics. This is due to the higher degree of liberation of the coarse particles from the coal (Holuszko & Grieve, 1990) as illustrated in Figure 2.3(b). Epigenetic minerals can be removed from the carbonaceous fraction of the coal with relative ease by crushing and washing (Holuszko & Grieve, 1990; Speight, 2005:35). They also produce very little middlings, since this material is not scattered throughout the particle, but occurs mainly in pores and fractures as shown in Figure 2.3(c). Epigenetic minerals, for example quartz, pyrite and calcite, are easily removed by crushing and washing at relative densities of less than 1.80 (Falcon & Snyman, 1986).

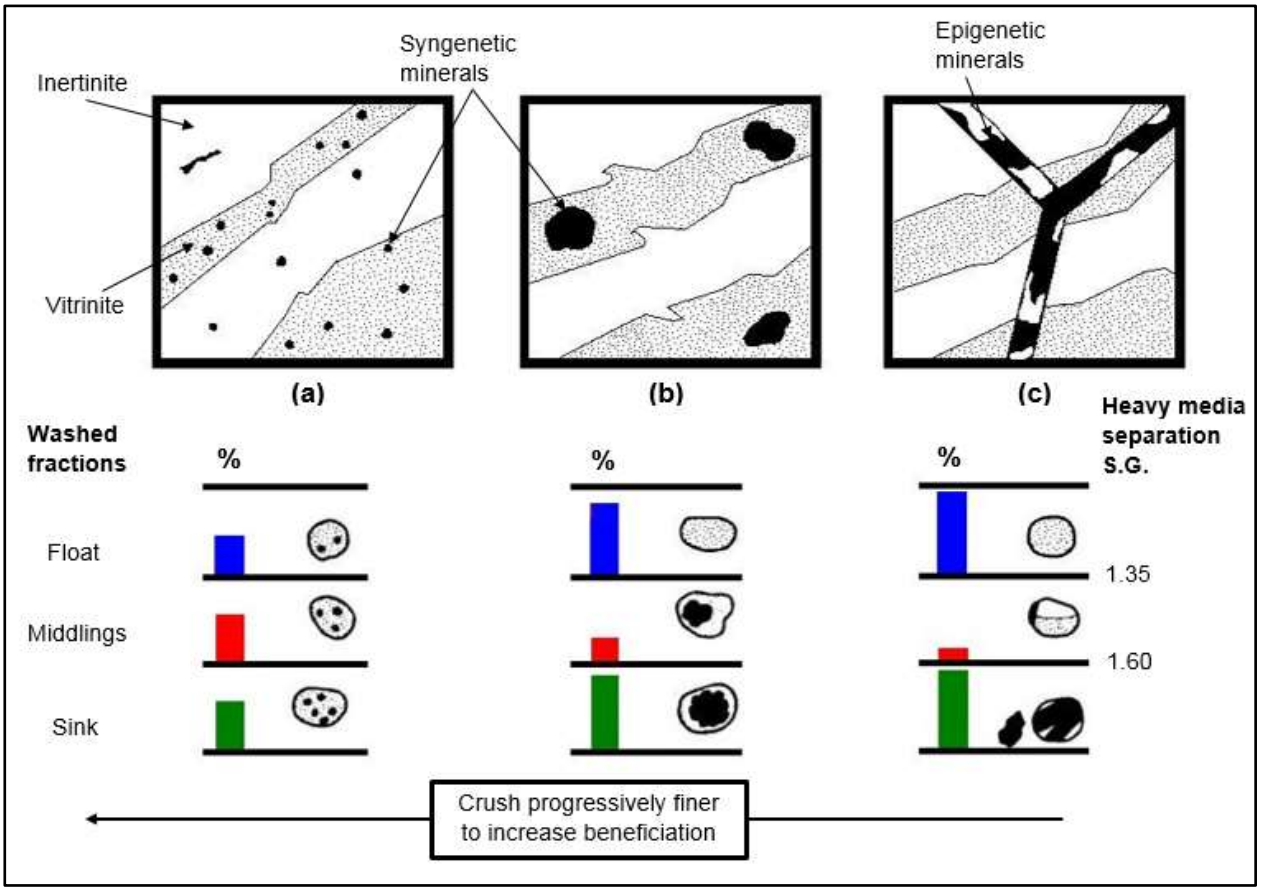

Figure 2.3: The effect of various types of mineral matter on washability (adapted from Falcon & Snyman, 1986).

The breakage characteristics of coal is affected by the presence of mineral matter in coal (Falcon & Snyman, 1986; Shi, 2014), since coal particles of higher density contain larger amounts of mineral matter, making the particle more difficult to break (Shi, 2014). Also, soft minerals are generally eroded from hard minerals during inter-particle grinding, and concentrate in the finer particle size ranges (Singh *et al*., 2014). Minerals present within any given coal need to be known in order to identify the most effective beneficiation route for that coal, and whether it is economically suitable for the intended coal market (O' Brien *et al.,* 2011). Particles with a small amount of mineral inclusions can be easily upgraded by some size reduction to liberate coal from the minerals. Particles with significant mineral inclusions would have to be crushed or milled to very fine sizes for significant liberation to occur, due to these mineral inclusions are very small (O'Brien *et al*., 2011).

2.1.4 Properties of coal affecting its breakage behaviour

The progeny (daughter particles) formed during coal breakage are affected by internal and external factors. Examples of internal factors include the maceral composition of the coal, cleats in coal particles and the initial particle size. External factors are mostly the force intensity, orientation of force relative to the coal bedding plane, and the force application time (Esterle *et*

al., 2002). The form of breakage force applied also influences size reduction. The force intensity affects coal breakage in the sense that a finer progeny can be attained by impacting with a harder surface, or applying higher breakage energy (Sushant & Archana, 2013). The influence of some coal properties on breakage and liberation will be discussed in this section.

2.1.4.1 Macerals

The maceral groups differ in hardness, and will consequently affect the breakage of coal, depending on the proportion of each maceral occurring in the coal (Falcon & Snyman, 1986). Fracturing and breakage of vitrinite-rich coal, results in high amounts of small particles, with sizes of 1 mm or less due to this maceral being very brittle. It tends to fracture angularly, because it contains high concentrations of shrinkage cracks and cleats (Falcon & Snyman, 1986). Liptinite has a high tensile strength, and is relative tough compared to the other macerals. The inertinite group macerals, apart from fusinite, also have high strength. Fusinite on the other hand is very friable, resulting in fine particles and dust during breakage (Falcon & Snyman, 1986). Figure 2.4 illustrates how the maceral content can influence beneficiation of coal. It can be seen from this figure that vitrinite-rich coal produce a large quantity of low mineral matter coal with a relative density of less than 1.30 and middlings with relative density of 1.30-1.50, whilst inertinite-rich coal produce mostly particles with relative density of higher than 1.50.

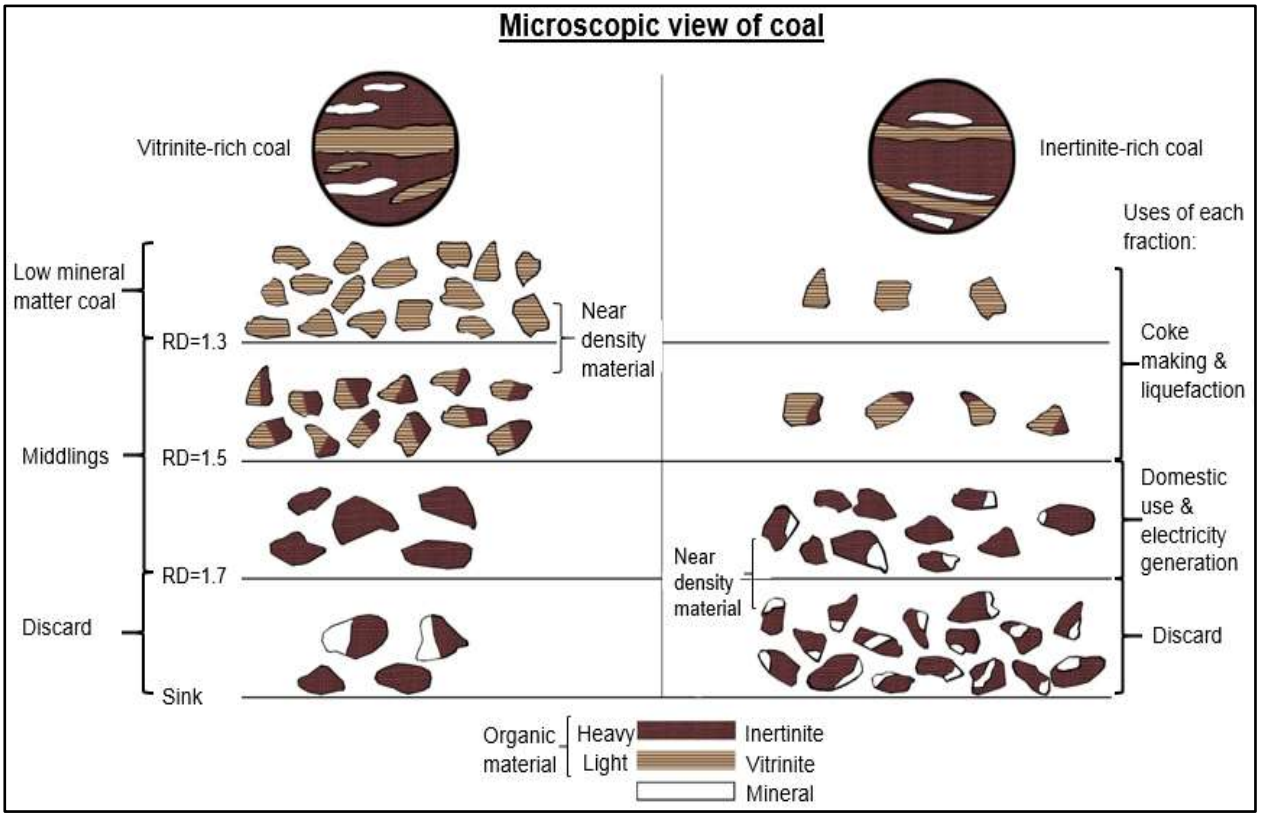

Figure 2.4: An example of the effect of beneficiation of two types of bituminous coals from the Witbank Basin on the distribution of the main constituents (adapted from Falcon & Snyman, 1986).

2.1.4.2 Coal rank

As the carbon content of coal and the vitrinite reflectance, thus coal rank, increase, the porosity of coal, which will be discussed in Section 2.1.4.3, decreases. This influences the behaviour of coal during breakage and handling (Laubach *et al.,* 1998; Speight, 2005:118). Breakage of coal is influenced by coal rank, for example, low rank coals are generally soft and break easily due to their porous and less compact structure (SACPS, 2015:18). The uniaxial compressive strength increases with an increase in coal rank, which can be ascribed to less pore volume within the coal structure (Pan *et al.,* 2013; Scholtès *et al*., 2001). The strength of coal therefore decreases as the cleats within the coal particle increase (Jankovic *et al*., 2000; Scholtès *et al*., 2001). Coals containing large amounts of mineral matter are likely to have larger cleat spacing than coals with low mineral matter content (Laubach *et al.,* 1998).

2.1.4.3 Cleats and micro-structure of coal

Coal is a porous substance containing both micropores and macropores (Levine *et al*., 1982; Pan *et al.,* 2013), which have size ranges of about 0.01 μm, and greater than 0.03 μm respectively (Speight, 2005:119). Macropores are generally predominant in coals with a lower carbon content, whilst micropores are predominant in coals with higher carbon content (Speight, 2005:119).

Cleats, however, are opening-mode fractures (Scholtès *et al*., 2001) with aperture size of 0.1 mm and less at surface conditions. The width of in situ cleats are typically between 0.001-20 mm, whereas wider fractures occur when the cleats are filled with mineral matter (Laubach *et al.,* 1998). These opening-mode fractures form a network which is distributed spatially throughout a coal particle (Scholtès *et al*., 2001), and is responsible for the porosity and the permeability of coal beds (Laubach *et al.,* 1998). The cleat networks may be either organized or chaotic configurations, depending on the coalification process, and can be divided into face cleats, and also butt cleats with an orthogonal structure as indicated in Figure 2.5 (Scholtès *et al*., 2001). The extensional cracks vertical on the area of least compressive stress during the formation process, are known as the face cleats, which are also the main system of cleats. Butt cleats refer to the cross-system of cleats perpendicular to the face cleats, and are formed during the relaxation of the compressive stress (Laubach *et al.,* 1998; Scholtès *et al*., 2001; Speight, 2005:165). The length of the butt cleats are limited, as it depends on the spacing between the face cleats (Laubach *et al.,* 1998). Cleats generally occur perpendicular to bedding planes of coal; thus the cleats are vertical (Laubach *et al*., 1998; Scholtès *et al*., 2001; Speight, 2005:165), giving the coal seam a blocky appearance as illustrated in Figure 2.5 (Laubach *et al.,* 1998).

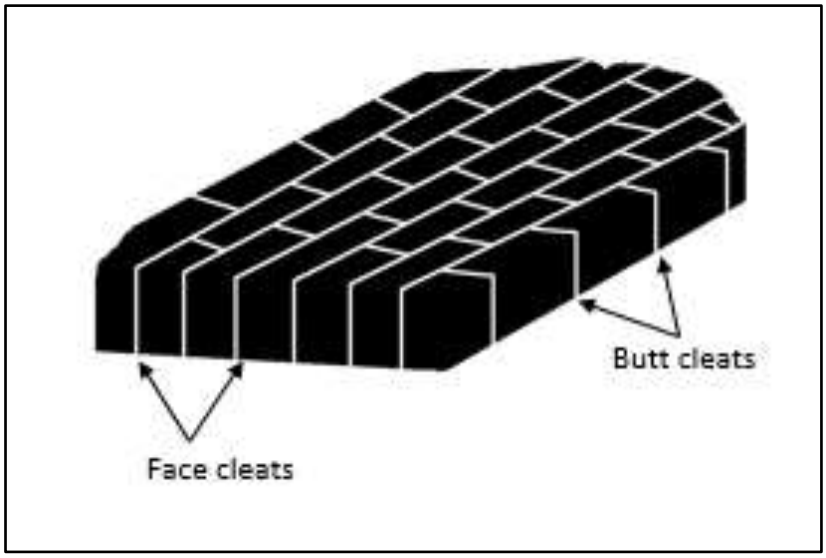

Figure 2.5: Butt and face cleats in coal (adapted from Scholtès *et al*., 2001).

Stress induced perpendicular to pre-existing face cleats cause the formation, and propagation, of parallel fractures (Laubach *et al.,* 1998). When stress is induced parallel to the face cleats, the propagation of secondary fractures at a right angle to the pre-existing face cleats is promoted. The occurrence and frequency of cleats therefore affects the breakage and liberation of coal (Laubach *et al.,* 1998).

A study done by Singh *et al.* (2014), revealed that micropore characteristics influence the fracturing of coal because internal cracks make coal brittle, affecting the breakage behaviour

(Directorate-General for Energy, 1990:2). The specific breakage rate tend to increase with an increase in particle size (Jankovic *et al*., 2000; King, 1999). The crack density in larger particles is much higher than that in smaller particles; thus larger particles have a tendency to be weaker and less difficult to break than smaller particles (Shi, 2014). This is because of the decreasing strength of larger particles containing higher density of microflaws, and the greater possibility that a larger particle will contain a flaw that will lead to fracture under stress conditions (King, 1999).

Fracturing of materials consisting of a single-phase, is primarily controlled by crack initiation, whilst fracturing of multiphase materials is controlled by crack propagation (Singh *et al*., 2014). Fractures in coal can either be cleats, which are the naturally occurring opening mode fractures in coal particles, or fractures induced by comminution (Singh *et al*., 2014). During comminution of coal, the fracture patterns in the particle are primarily directed by the mineral matter in the coal, and the pore network throughout the coal particle. There exists a significant difference in the hardness of coal macerals, and the mineral matter associated with coal, as previously stated. Fractures occurring at the interface between the organic and the inorganic material differs from those occurring in organic only material (Singh *et al*., 2014).

2.1.4.4 Lithotypes

Bright and dull coal, which is vitrain and durain rich respectively, as discussed in Section 2.1.2, are the main components of bituminous coal. Dull coal lithotypes normally have larger cleat spacing than bright coal lithotypes (Laubach *et al.,* 1998; Scholtès *et al*., 2001). Cleat spacing has a significant effect on coal breakage as discussed in Section 2.1.4.3.

Different coal lithotypes with the same vitrinite content exhibit different grindability behaviour, depending on whether the layer is banded or non-banded bright coal, as well as the thickness of the band (Esterle *et al*., 2002). Dull coal requires more energy for breakage to occur than bright coal, as it has a higher inherent strength than bright coal, which is relatively friable (Esterle *et al*., 2002). Because of the friability of bright coals and banded coal lithotypes, these coals break into finer particle sizes. Consequently, the finer coal particles in the progeny will have high concentrations of bright coal which is vitrinite-rich (Esterle *et al*., 2002). Coarser progeny fractions contain dull coal and stones, with an exception when the stones present contain shales and soft claystones. The thickness and the geological distribution of the lithotypes influence the mined coal particle size; thus the feed to process units, and for that reason influence the particle size distribution of the daughter particles formed during communition (Esterle *et al*., 2002).

2.1.4.5 Mechanical properties

- Friability

The friability of coal depends on the strength, toughness, and fracture characteristics of coal, and refers to the ability of coal to withstand size reduction, as well as the tendency to break during handling and transportation (Speight, 2005:159). Friable coals yield larger amounts of smaller particles and less coarse particles; therefore the surface area of friable coals are easily increased (Speight, 2005:159).

- Hardness

Coal hardness refers to the ability of coal to endure external mechanical forces (Xie, 2015:32), such as penetration at the cutting point (Falcon & Falcon, 1987). The scratch hardness, also known as the Mohs hardness, of coal generally varies between 1 and 4. Coals with low or medium coalification, such as lignite has a low scratch hardness between 2.0 and 2.5, whilst coal with a high degree of coalification, such as anthracite, has a high scratch hardness of almost 4 (Xie, 2015:32). However, coal hardness is influenced by its composition in the sense that the hardness of macerals and lithotypes is highly variable. The inertinite maceral group has the greatest hardness, followed by vitrinite, and liptinite with the lowest hardness (Falcon & Falcon, 1987). Another factor affecting the hardness and toughness of materials, is a moisture content of more than 5 %, which consequently influences the breakage of the material (Sushant & Archana, 2013). The hardness of coal is also affected by the presence of mineral matter, for example, anthracite has a hardness of about six times that of soft coal, and pyrite has a hardness of 20 times that of soft coal (Speight, 2005:158).

- Mechanical strength

Coal's ability to resist compaction, crushing and compression are referred to as the compressive strength (Falcon & Falcon, 1987). Coal strength varies depending on the conditions, for example, the strength of a coal within a seam experiencing pressure caused by overburden pressure on the coal in the seam, and that of an unrestricted lump of coal in a laboratory are different (Falcon & Falcon, 1987). The strength of coal is affected by factors including the following (Falcon & Falcon, 1987):

Mineral content: Syngenetic mineral matter that is well distributed throughout the coal matrix increases the coal strength (Falcon & Falcon, 1987; Xie, 2015:30).

Lithotype composition: Durain has the highest mechanical strength, followed by vitrain and fusain has the lowest mechanical strength (Xie, 2015:30).

Degree of coalification: The compressive strength of coal varies with the rank of coal (Speight, 2005:111) where low-rank and high-rank coals have greater mechanical strength than medium rank coals (Xie, 2015:30).

Weathering: The mechanical strength are reduced when coal was subjected to weathering (Xie, 2015:30).

Size: The compressive strength of a sample decreases as the particle size increases (Falcon & Falcon, 1987).

Orientation and number of existing cracks: An increase in cleats reduces the compressive strength of coal (Falcon & Falcon, 1987).

2.1.5 Proximate analysis

The South African National Standard (SANS 17246:2011) procedure is widely used for determining the proximate analysis of coal to evaluate the composition of coal (Khandelwal & Singh, 2010). The volatile matter (VM), moisture content (M) and ash yield (A) are determined by laboratory experiments, whilst the fixed carbon (C) is calculated by the following equation (Khandelwal & Singh, 2010; SACPS, 2015:62; SANS 17246:2011; Speigth, 2005:41):

$$Fixed\ carbon\ (C) = 100 - (M + A + VM) \qquad \textbf{2-1}$$

The moisture is the inherent moisture of the particular analysis sample, which is the moisture remaining in the sample after air drying, and not that of the bulk material (SACPS, 2015:62; Speigth, 2005:42). Ash denotes the remains of the mineral matter existing in the coal that was altered during combustion (Speigth, 2005:41). Volatile matter is the coal constituents that can be driven off in the form of gases or condensable liquids at elevated temperatures. Fixed carbon is the remainder of the material after subtraction of the other components (SACPS, 2015:62).

2.2 The Mozambique Coalfields

The recent interest of large amounts of coal in Mozambique has caused an exponential growth of the Mozambique mining industry (Vasconcelos *et al.,* 2014). Exploration of these coal resources has the potential to be of economic importance (Hatton & Fardell, 2012). Mining companies in Mozambique plan to use the lower grade thermal coal fraction for electricity generation, whilst the coking coal fraction will be exported (Hanlon, 2013; Rosenfeld, 2012). Washed coal products from the Moatize coal basin with a RD up to 1.45 will be used for the production of coking coal, whereas coal with RD ranging between 1.45-1.60 and 1.60-1.90 will be used for export thermal coal, and in-house thermal coal respectively (Vasconcelos *et al.,* 2014).

Coking coal from Mozambique compares well with the coking coals occurring in the Limpopo Province of South Africa (Lakshminarayana, 2015).

2.2.1 Basin stratigraphy

Through the deposition of the Karoo Supergroup coal bearing strata, tectonic activity led to a truncated sequence of sedimentary lithologies, during which inter-banded mudstone and coal layers have accumulated to form so-called “coal zones” (Hatton & Fardell, 2012). This is similar to the formation of the Limpopo Coalfields, which also occurs as layers within coal zones formed during tectonic activity (Hatton & Fardell, 2012). Coal zones in the Mozambique Coalfield are uninterrupted over wide regions, and are recognisable within the coal basin, whilst discrete coal seams are not as continuous. Coal in the region therefore has a low calorific value (CV), and high mineral matter content, with low yield of high quality coal products (Hatton & Fardell, 2012).

The stratigraphy of the Lower Karoo basins can be classified in ascending order as Vuzi, Moatize and Matinde Formations (Lakshminarayana, 2015; Vasconcelos *et al.,* 2014). The Vuzi Formation is 60-140m thick, and contains coal with a high mineral matter content. The Matinde Formation contains a number of coal seams interlayered with fine to coarse sandstones (Vasconcelos *et al.,* 2014). The Moatize Formation has a thickness of 320-400m (Lakshminarayana, 2015), and is a deposit of both thermal and coking coal (Hatton & Fardell, 2012; Vasconcelos *et al.,* 2014). The geological structure of the Moatize basin consists of coal and sediment layers (Hatton & Fardell, 2012; Vasconcelos *et al.,* 2014). The Moatize Coalfield is therefore categorized according to the seam morphology as ‘thick interbedded coal seam’-type, or Barcode type deposit, due to the cyclic layered patterns of mudstone, carbonaceous mudstone, and thin bands of coal. The seam morphology is similar to that of the Limpopo Coalfield (GEMECS (Pty) Ltd, 2010; Lakshminarayana, 2015). The coal occurring in the Moatize Coalfield is medium rank bituminous coal that is rich in vitrinite, and has a medium to high volatile matter content (Lakshminarayana, 2015). The Moatize Coalfield has six coal seams (Vasconcelos *et al.,* 2014), as presented in Table 2.5, along with their thicknesses and lithology, from top to bottom (Hatton & Fardell, 2012; Lakshminarayana, 2015; Vasconcelos *et al.,* 2014).

Table 2.5: The Moatize basin coal stratigraphy and coal quality (Hatton & Fardell, 2012).

Name of coal seam	Thickness* (m)	Lithology (composition)
André	2	Coal
	27	Sandstones with carbonaceous shales
Grande Falésia	12	Coal
	18	Sandstones and mudstones
		Coal
Intermédia	22	Carbonaceous shales
		Coal
	30	Mudstones
		Coal
Bananeiras	27	Carbonaceous shales
		Coal
	14	Sandstones and mudstones
	34	Mudstones siltstones
Chipanga	36	Coal
	56	Mudstones
Sousa Pinto	14	Coal
	16	Siltstones, sandstones and tillites

*It should be noted that the coal seam thicknesses are highly variable within a certain coalfield, and therefore the coal seam thicknesses should only be used as an overall guide (Hancox & Götz, 2014).

The thickest seam in the Moatize Coal Basin is the Chipanga seam, and is therefore the main seam used for exploitation (Hatton & Fardell, 2012; Vasconcelos *et al.,* 2014). This coal seam contains thick alternations of siltstones, carbonaceous siltstones and coal (Vasconcelos *et al.,* 2014). The top part of the Upper Chipanga contains large amounts of phosphorus making it unsuitable for coke production, whilst the Middle Chipanga contains thick carbonaceous siltstone and siltstone intercalations resulting in relative low yields when washability tests were conducted (Vasconcelos *et al.,* 2014). The Lower Chipanga revealed the highest potential for the exploitation of coking coal as the coal from the Lower Chipanga contains more than 90 % bright coal, low mineral matter content, and a low phosphorus content varying between 0.004 % and 0.085 % (Vasconcelos *et al.,* 2014).

2.2.2 Coal qualities

Coal occurring in the Moatize Coalfield is bituminous, vitrain rich and bright with a relatively high ash yield of 28-55 % (Lakshminarayana, 2015). These coals are comparable to the Tuli coal reserves in South Africa (Hatton & Fardell, 2012). The coking coal product yield after washing of Moatize coal is 25-30 %, with a high vitrinite content of 80 %, and volatile matter of 31-33 % (Lakshminarayana, 2015). Moatize coking coal has a low inertinite content of 17 % (Lakshminarayana, 2015). The volatile matter content of Mozambique coals are normally moderate to low varying between 20-30 % on a dry ash free basis, but the occurrence of dolerite intrusions tends to lower the volatile content further (Hatton & Fardell, 2012). The average quality of raw Mozambique coal was determined by Lakshminarayana (2015). A total of 12 137 samples were used to obtain these average values. The average values obtained, on an air-dried basis, were (Lakshminarayana, 2015):

- Moisture (M): 1.4 %
- Ash (A): 44.0 %
- Volatile matter (VM): 25.0 %
- Fixed carbon (FC): 29.6 %
- Gross Calorific Value (GCV): 20.19 MJ/kg
- Free swelling index (FSI): 1 to 7

The quality of the various Moatize coal seams, was determined by Lakshminarayana (2015) and is presented in Table 2.6, on an air-dried basis.

Table 2.6: Quality of various Moatize coal seams (Lakshminarayana, 2015).

Coal seam	Thickness (m)	A%	M%	VM%	FC%	GCV (MJ/kg)*
Andre	10-30	51.0	3.5	24.0	21.5	13.18
Grande Falesia	108-249	54.0	2.7	20.0	23.3	13.17
Intermedia	5-9	49.0	2.6	23.0	25.4	14.86
Bananeiras	10-45	48.0	2.2	21.0	28.8	15.90
Chipanga	25-35	42.0	1.6	23.0	33.4	18.41
Sousa Pinto	2-21	40.0	1.3	23.7	35.0	19.37

* Gross Calorific Value

2.2.3 Challenges associated with the exploitation of the Mozambique Coalfields

Although the Mozambique coalfields are linked to the Richards Bay Coal Terminal via railway for coal export (Pooe & Mathu, 2011), exploitation of these coalfields are limited due to the lack of railway infrastructure for the transportation of coal and other associated infrastructure issues. Coal transport by means of trucks are not viable as this transport method is expensive (Hanlon, 2013; Rosenfeld, 2012). Another problem is the lack of skilled and qualified people in Mozambique to deal with the mining and production of coal (Hanlon, 2013). Even though the sedimentation is very complex making exploitation, and exploration, challenging (Hatton & Fardell, 2012), selective mining can be used to overcome difficulties with the exploitation of coal seams of the Barcode type such as those occurring in Mozambique (Lakshminarayana, 2015).

2.3 Size reduction

Size reduction, also termed comminution, is a procedure where large solid units (coal for the purpose of this study) are reduced in size to produce smaller units (Sahoo, 2006; Sushant & Archana, 2013). Comminution forms an important part of coal beneficiation as it is necessary to exploit and utilize low-grade coal (Drzymala, 2007:144; Singh *et al*., 2014) to satisfy the current energy demand (Drzymala, 2007:144). Beneficiation of low-grade coal also requires large amounts of energy for crushing, since liberation of the valuable coal from gangue material is needed (Singh *et al*., 2014). Reasons for performing comminution include:

- the liberation of mineral matter that is intergrown with the organic coal matrix,
- for effective coal utilization during combustion (Shi & Zuo, 2014),
- to improve handling (Raju *et al*., 2013; Sushant & Archana, 2013), and
- to separate valuable particles from gangue (Drzymala, 2007:124; Jankovic *et al.*, 2000; Raju *et al*., 2013; Surowiak, 2013; Wills & Napier-Munn, 2006:108) in order to provide a product that meets certain criteria and to improve the quality of the product (Ajaka & Akinbinu, 2011; Davis & Dawson, 1989; Raju *et al*., 2013).

Selective comminution is executed with the purpose of liberation, whilst non-selective comminution is performed for size reduction (Drzymala, 2007:143), and also to produce coal with a specified particle size according to the market requirements (SACPS, 2015:89). The intention of breakage during this study was to increase the coal yield, after washing, by liberating the mineral matter from the coal.

Physical separation, as well as various comminution methods, are used to remove minerals from coal before commercial utilization to improve the economic value of the coal (Ito *et al.*, 2009).

Because the mineral components and coal are aggregated at a grain size level, the grains firstly need to be liberated from each other, by means of size reduction of the run of mine coal, to be able to “unlock” the valuable coal particles before the minerals can be separated according to each type present (Ajaka & Akinbinu, 2011; Wills & Napier-Munn, 2006:108). Comminution of middlings, which are particles of gangue with coal trapped inside, will aid in releasing the trapped coal (Wills & Napier-Munn, 2006:14). As the particle size is decreased by comminution, mineral matter liberation from coal is increased (O’ Brien *et al*., 2011; Surowiak, 2013) to produce a product with a low mineral matter content (O’ Brien *et al*., 2011). Separation of some coals from ash forming components is difficult, and therefore fine grinding must be employed, but leads to the formation of large quantities of fines (Ito *et al.*, 2009), which significantly increases the cost of beneficiation, increase the moisture content, and makes handling difficult (Ito *et al.*, 2009; Viljoen *et al.,* 2015). In order to acquire a balance between coal breakage to achieve sufficient liberation and the generation of unnecessary fines, it is important to clearly understand coal breakage (Esterle *et al*., 2002; Viljoen *et al*., 2015; Weining *et al.,* 2013).

Mined particles are subjected to breakage, after which individual particles can consist of pure maceral components, or mineral matter, whilst other particles are comprised of minerals and macerals in varying amounts to form composite particles (O’Brien *et al*., 2011). The fraction of particles exiting the breakage process, either as pure or composite particles, depends on the coal properties and the particle size (O’Brien *et al*., 2011). It is expected that size reduction of particles will cause liberation, and hence increase the yield of coal products (O’Brien *et al*., 2011). However, the degree of liberation achieved from crushing and grinding is coal specific, and hence the yield of clean coal products is also coal specific (O’Brien *et al*., 2011). Crushing of run-of-mine coal particles having different sizes and relative densities will cause the amount of material in a certain density class to change, altering the coal washability characteristics, the coal quality and the efficiency of the separation process (Mohanta *et al*., 2016).

2.3.1 Breakage process and related energy

Minerals are crystalline substances with a structure consisting of atoms ordered in three-dimensional arrangements (Usaini *et al*., 2014; Wills & Napier-Munn, 2006:109), as determined by the types and size of the chemical and physical bonds connecting the atoms (Usaini *et al*., 2014). These inter-atomic bonds can be broken by applying compressive force to the particle, as indicated in Figure 2.6, resulting in tensile failure - that is to say if all failures occur due to tensile stress (Singh *et al*., 2014; Usaini *et al*., 2014; Wills & Napier-Munn, 2006:109). The physical bonding in coal is between the non-crystalline carbon material and the crystalline mineral matter (Singh *et al*., 2014). These crystalline and non-crystalline phases result in uneven distribution of stress during loading, which leads to breakage of the atomic bonds at specific stress levels and crack lengths (Singh *et al*., 2014).

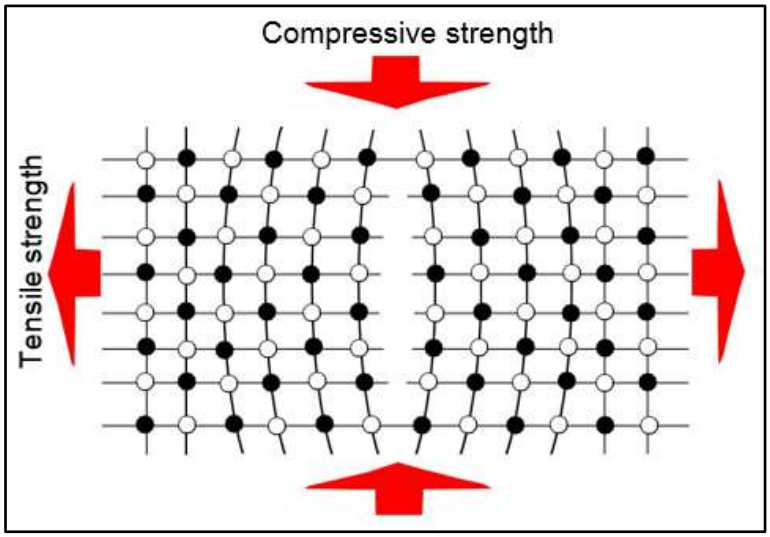

Figure 2.6: Compressive or tensile stresses causing strain of a crystal lattice (adapted from Singh *et al*., 2014; Usaini *et al*., 2014; Wills & Napier-Munn, 2006:109).

Stress applied to the material distributes according to the properties of the material, and will tend to accumulate in areas where cracks or flaws are present in the particle (Wills & Napier-Munn, 2006:109). A crack can withstand only a certain amount of stress, and when the stress increases up to a critical value at the crack tip (see Figure 2.7 for illustration), it is sufficient to break the inter-atomic bonds at the crack tip (Usaini *et al*., 2014). Increased stress at the tip of a crack will cause rupturing of inter-atomic bonds, and propagation of the crack leading to breakage of the particle (Singh *et al*., 2014; Wills & Napier-Munn, 2006:109). Breakage of these bonds will lead to an increase in crack length, and hence an increase in the stress concentration at the crack tip, resulting in rapid propagation of the crack causing fracturing throughout the matrix (Usaini *et al*., 2014). Microcracks act as stress concentration points in particles, and these cracks will propagate when the applied stress exceeds the tensile stress the particle is able to withstand (Singh *et al*., 2014). The stress increase at these sites is directly proportional to the square root of the length of the crack that occurs perpendicularly to the applied stress direction (Usaini *et al*., 2014). Propagation of fractures usually stops at mineral interfaces, or it gets diverted due to the difference in hardness (Singh *et al*., 2014). Thus, even though the load can be applied uniformly, the internal stress will not be uniformly distributed since it will be affected not only by the mechanical properties of the dispersed minerals present, but also by the presence of flaws and cracks in the matrix, that will serve as sites for stress concentration to occur (Usaini *et al*., 2014).

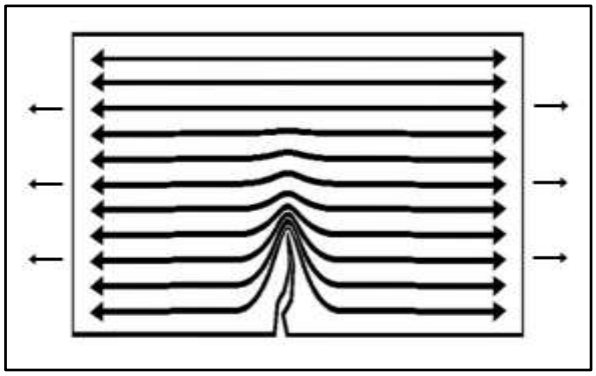

Figure 2.7: Concentration of stress at the crack tip (adapted from Usaini *et al*., 2014; Wills & Napier-Munn, 2006:109).

In cases when the load force (F) applied is less than the critical force (F_{cr}) that the particle can withstand, the particle is able to endure the force leading to deformation of the particle, as illustrated in Figure 2.8, and no breakage will occur. Bonds between the atoms in the particle stretch due to stress, and results in tensile forces (F_r) occurring within the particle. An increase in the load force will cause stress to exceed the adhesion forces keeping the atoms within the particles close, and will result in breakage of the particle as illustrated in Figure 2.8 (Drzymala, 2007:127). A particle will thus fracture whenever the applied stress to the particle is above the particles' fracture strength. Energy equivalent to the bonds holding a particle together must be applied to perform size reduction and to increase the surface area (Sushant & Archana, 2013).

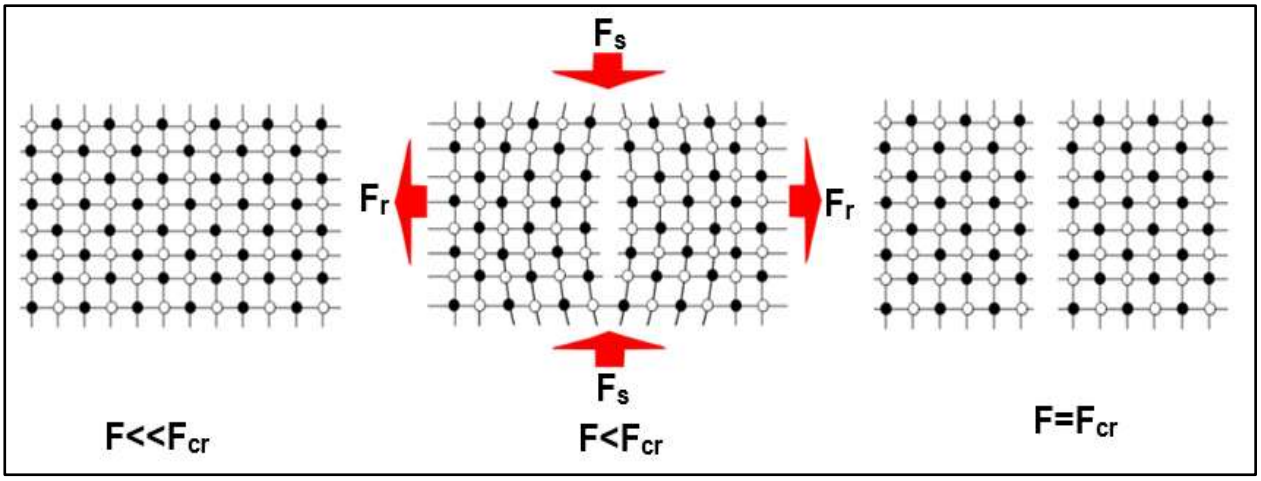

Figure 2.8: The disintegration of brittle particles due to compressive (F_s) and tensile forces (F_r) (adapted from Drzymala, 2007:127).

The level of stressing energy applied to perform particle breakage must be an optimum between the extremes of excessive high level of stressing energy which will break the particle finer than the size required, and very low stressing energy which is insufficient for breakage to occur, causing energy losses in the form of heat energy (Tavares, 2004). Material with different densities, and different sizes, require different breakage energy, for example, mineral particles are generally

denser than coal particles, and require more breakage energy than the less dense coal particles (Shi & Zuo, 2014). The energy that is needed for breakage is directly related to the surface area of the newly formed progeny. Therefore, a higher input energy is needed for the breakage of a smaller particle to attain the same breakage relative to a larger particle (Esterle *et al*., 2002; Jankovic *et al.,* 2000). This behaviour can be ascribed to fewer fractures found within smaller coal particles, which is true for both bright (vitrain) and dull (durain) lithotypes (Esterle *et al*., 2002; Scholtès *et al*., 2001). Separation of the stones and lithotypes during breakage is promoted by the weak boundaries between these substances (Esterle *et al*., 2002). When preferential breakage occurs at the boundary between a mineral and a coal substance, the liberation is of a high degree and the resulting comminution product will be coarse. This enhances the physical separation of the mineral from the coal, and reduces the processing cost associated (Ito *et al.*, 2009).

2.3.2 Size reduction modes

Comminution processes can either be mechanical comminution for instance crushing, cutting, and breaking, which is accomplished by applying external forces to the particle, or chemical comminution including bioleaching and dissolution, which relies on the leaching of certain particles (Drzymala, 2007:124). Various breakage modes including attritioning, impact, and crushing (Weining *et al.,* 2013; Wills & Napier-Munn, 2006:109), result in one of three types of fracture, namely tensile, compressive or shear fracture, and can be used for coal middlings liberation (Wills & Napier-Munn, 2006:109). Other comminution methods, for example, the use of chemicals, ultrasonic treatment, and electrical disintegration, are applicable for liberation. These techniques are not currently feasible for commercial application, due to the high costs associated with these methods (Ito *et al.*, 2009). Crushing equipment generally employ combinations of the above mentioned coal breakage methods, that is tensile, compressive or shear failure (SACPS, 2015:90). The chosen mode, or modes, implemented to attain breakage depend on the characteristics of the material, and the level of stress required for size reduction (Hogg, 1999). The main modes used for the breakage of brittle solids can be classified arbitrarily as attritioning, and massive fracture, due to the applied stress exceeding the critical stress the particle is able to withstand, resulting in disintegration of a particle into smaller particles (Hogg, 1999).

Comminution is done as a sequence of processes involving crushing and grinding (Raju *et al*., 2013; Usaini *et al*., 2014), with crushing as the first comminution stage (Usaini *et al*., 2014; Wills & Napier-Munn, 2006:149). This is to both reduce the particle size, and to liberate precious minerals from gangue (Wills & Napier-Munn, 2006:118). Crushing is usually followed by grinding, if it is required, to obtain very small particles (Wills & Napier-Munn, 2006:149), especially if the valuable mineral and gangue mineral must be substantially separated as discrete particles (Usaini *et al*., 2014). Crushing is attained by either compressing or impacting of the ore against solid

surfaces with a controlled motion, whereas grinding refers to abrasion or impact breakage of the ore, by the free motion of the particles in rotating cylindrical vessels (tumbling mills), which may contain a suitable grinding media (Raju *et al*., 2013; Usaini *et al*., 2014; Wills & Napier-Munn, 2006:108). Large particles are generally reduced in size by crushing, whilst smaller particles are milled (Sahoo, 2006). Abrasion is performed by applying low energy forces, resulting in smaller particles tearing off a larger solid, whilst shattering results in a relative large quantity of smaller particles due to a stronger (higher) energy force (Drzymala, 2007:125).

2.3.2.1 Impact drop breakage

Impact breakage refers to the direct immediate impingement of an object in motion against another object, which may also be in motion or stationary (SACPS, 2015:90). The two types of impact breakage are:

- gravity impact which is coal that is dropped onto a solid surface, such as a steel plate, and,
- dynamic impact when both objects are in motion for example coal dropped in front of a hammer that is moving (SACPS, 2015:91).

Gravity impact is generally employed for the separation of two materials of which the relative friability is different. In this mechanism the material that is more friable will be broken, whilst the other material that is less friable will remain unbroken (SACPS, 2015:91). The materials can then be separated by means of screening.

Dynamic impact is recommended when breakage along the natural cleavage lines of ores is required to free and liberate undesired inclusions (SACPS, 2015:91). Double impact breakage is the breaking of a particle between two relative hard surfaces, which can be either a drop weight test with a falling weight coming into contact with a stationary particle on a hard surface, or pendulum breakage. The latter is useful in providing information regarding energy requirements for breakage (Sahoo, 2006). This breakage method causes coal particles to crack from the surface of impact, therefore following different patterns throughout the particle depending on the particles' characteristics (Sahoo, 2006). The effect of impact energy is the formation of daughter particles with different particle size distributions (Esterle *et al*., 2002). Some particles will not break during the first impact breakage, depending on the energy required for particle fracture and the impact energy applied, whilst some particles will break to form particles remaining in the top size category. Single particles must lose 10% or more of its initial weight to be considered as broken (Tavares, 2004).

2.3.2.2 Compression breakage

Compression breakage is achieved by squeezing the material between two crushing surfaces of which either one, or both, of these surfaces is doing the work. It is recommended to use compression for size reduction of hard and abrasive materials, non-sticky materials, and when fines must be minimized (SACPS, 2015:91). The product resulting from compression will either be coarse due to the induced tensile breakdown, or fine because of the compressive breakdown at the force contact areas as seen in Figure 2.9. The quantity of fines generated can be minimized by reducing the force contact area (Wills & Napier-Munn, 2006:110). A study done by Özer & Whiten (2012), using compression breakage of a cylindrical particle bed, showed that an increase in the energy applied to the bed resulted in a finer particle size distribution (PSD) of the progeny.

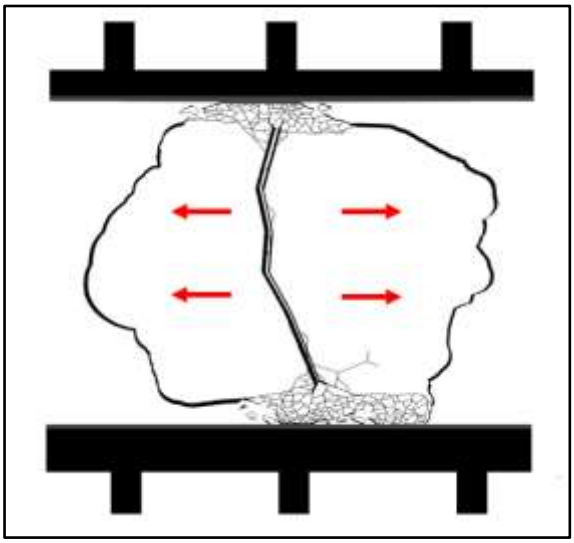

Figure 2.9: Fracturing of a particle when crushed (adapted from Directorate-General for Energy, 1990:6-10).

2.3.2.3 Attrition breakage

During attrition breakage, the parent particle experiences slow, constant loss of mass, to produce very small fragments relative to the parent particle. This is due to smaller stresses being applied that only exceed the critical point at the edges of the particles. The parent particle retains its original identity (Hogg, 1999). The modes of breakage occurring during attritioning, are

- fracturing along weak pre-existing fractures, leading to a fast-breaking material fraction, and,
- abrasion or chipping resulting in a slow-breaking fraction (Davis & Dawson, 1989), where most of the size reduction are accomplished by the latter (Davis & Dawson, 1989).

Two types of breakage occur during attrition breakage by means of a tumbling test, namely surface and volume breakage, each corresponding to a certain breakage rate (Sahoo & Roach, 2005). Volume breakage refers to complete breakage, or fracturing, along a weak plane within the particle to produce a relative smaller progeny, whilst surface breakage denotes the wear of a particles' surface by chipping and abrasion resulting in rounding of the particle (Sahoo & Roach, 2005). According to a study done by Sahoo & Roach (2005) on South Blackwater coal from Australia, the initial breakage rate during attritioning within a tumbling mill, is due to volume breakage and mainly occurred within the first 4 minutes of attritioning. Thereafter the rate of volume breakage decreased due to stabilization, and then surface breakage dominated up to 20 minutes. This was ascribed to the probability that larger particles would contain larger pre-existing cracks making it more susceptible to attrition breakage during tumbling (Sahoo & Roach, 2005).

Under-grinding of particles will result in coarse product that has a low degree of liberation, and will give a poor yield. However, care must be taken to ensure that over-grinding does not occur, since this will increase the energy consumption, and ultimately result in higher amounts of undesired fines (Wills & Napier-Munn, 2006:146). Although attritioning uses more energy, and causes wear to equipment and liners, it is suitable for size reduction of less abrasive materials such as coal in the case that large proportions of fines are required (SACPS, 2015:91).

2.3.2.4 Combination of breakage modes

Generally two or more breakage modes occur simultaneously during the handling and transportation of coal. According to Sahoo (2006), the major comminution mechanism during handling is compressive stresses, while slight attritioning or abrasion of the particle also occurs, due to particles rubbing against one another. When massive fracture is performed alone as a comminution process, the process requires multiple distinct breakage events done in a series, and the specific rate of breakage is related to the frequency of the breakage events (Hogg, 1999). It is expected that practical comminution systems include a combination of massive fracture and attritioning (Hogg, 1999).

2.3.3 Size reduction equipment

Various types of comminution equipment have been developed for the purpose of size reduction of different materials with specific characteristics (Sushant & Archana, 2013). Not only do the characteristics, especially the hardness of the material to be treated, play a vital role in the choice of comminution equipment (Sushant & Archana, 2013), but also the initial coal particle size and the desired final product size (SACPS, 2015:92). Coal comminution equipment is designed for the size reduction of large particles to smaller particles in the least number of steps possible (SACPS, 2015:90). Size reduction can be carried out through numerous primary, secondary and

tertiary stages, where primary and secondary crushing stages generally require different size reduction equipment, whilst grinding can be done at the various stages by using the same equipment, although with a decrease in the efficiency as the particle sizes become smaller (Ajaka & Akinbinu, 2011). Coal is not usually subjected to grinding.

The difference between size reduction equipment is the breakage modes, for example, the main breakage mechanism in a ring mill is compression, impact breakage in a hammer mill, and attritioning in fluid energy mills, while some mill types include a combination of the modes of breakage (Directorate-General for Energy, 1990:6). Mills with similar breakage modes may have different efficiencies, since the particles are subjected to different forces and velocities (Directorate-General for Energy, 1990:6). An example is that it is not known what the difference in coal breakage is in cases when impact breakage is applied by multiple small force low impact velocities compared to a single application of large force at high impact velocity (Directorate-General for Energy, 1990:6).

2.3.3.1 Examples of breakage equipment used for various breakage modes

- Impact

The hammer mill consists of round hammers mounted on a rotating shaft to induce a swinging motion, as illustrated in Figure 2.10. Coal breakage occurs when the material enters the crusher by falling, and also when the hammers thrust the material against the breaker plate (SACPS, 2015:103).

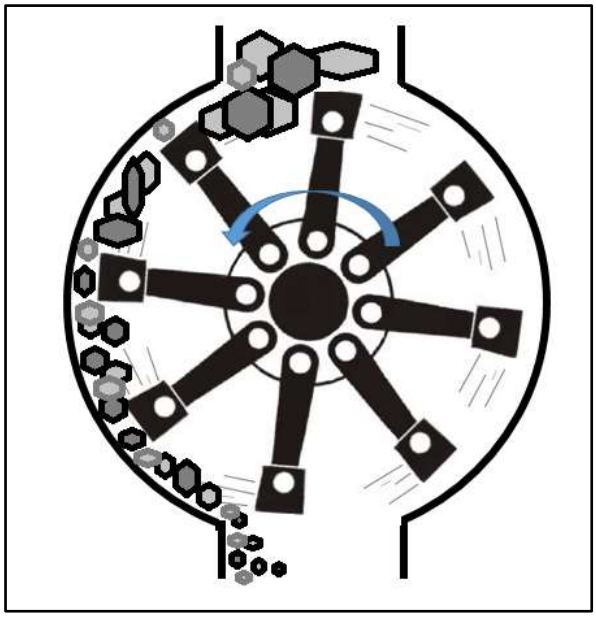

Figure 2.10: Illustration of impact breakage by a hammer mill.

- Compression

A roller mill consists of two cylindrical metal rollers which are mounted horizontal to one another, and are rotated along the longitudinal axis to compress the material (Sushant & Archana, 2013), as illustrated in Figure 2.11. Double roll crushers compress material between the rollers, during which few fines are generated (SACPS, 2015:98), whilst single roll crushers consists of a heavyweight frame with a crushing roll mounted inside containing an immobile breaker plate (SACPS, 2015:102).

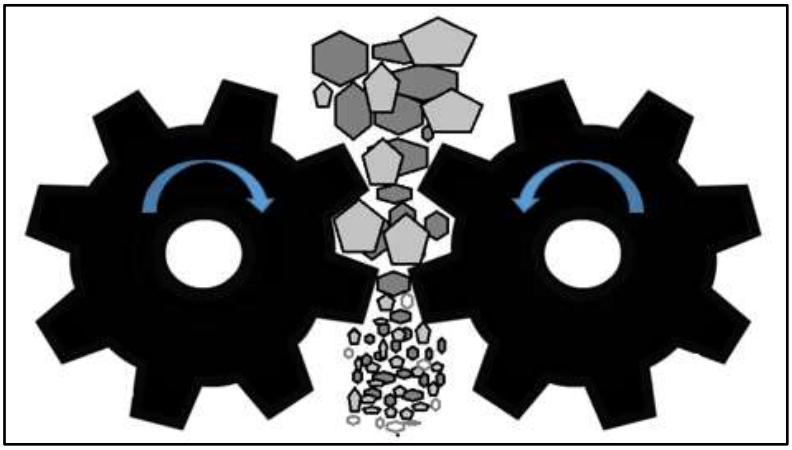

Figure 2.11: Illustration of compressive breakage by double roll crushers.

- Attritioning

Attritioning is generally performed in tumbling mills consisting of cylindrical shells with a wearing liner on the inside (Wills & Napier-Munn, 2006:149) and is rotated along the horizontal axis (Directorate-General for Energy, 1990:11; Sushant & Archana, 2013; Wills & Napier-Munn, 2006:149). Attritioning mills consist mainly of a tank and a motor, making it relative inexpensive to construct (Davis & Dawson, 1989). The hollow inside of the mill may contain grinding media, occupying not more than 50% of the container volume (Directorate-General for Energy, 1990:11; Sushant & Archana, 2013; Wills & Napier-Munn, 2006:143), which can be either balls, rods, or only lumps of the feed material, that can tumble freely as the container rotates (Directorate-General for Energy, 1990:11; Wills & Napier-Munn, 2006:143). The movement of particles inside the mill cause a grinding action as illustrated in Figure 2.12 (King, 1999).

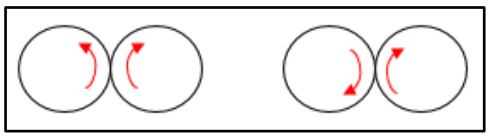

Figure 2.12: Grinding action between particles (adapted from King, 1999; Sankar Prasath & Venkatesh, 2014).

The breakage of particles inside the mill can be either impact breakage during collision, or it can be attritioning due to rolling of the particles (King, 1999), which correlates respectively with cataracting, and cascading movement of the particles from the dead zone to the toe of the tumbling mill (Wills & Napier-Munn, 2006:147). Combinations of these breakage modes might also occur (King, 1999). The nature of movement occurring inside the mill is dependent on the rotating speed of the mill (Wills & Napier-Munn, 2006:147). The rotation of the mill causes the particles inside to lift along the side of the mill, as illustrated in Figure 2.13 (Wills & Napier-Munn, 2006:143), until dynamic equilibrium is achieved (Wills & Napier-Munn, 2006:147). During dynamic equilibrium, there is a balance between the centrifugal force, and the weight of the material within the mill, when rotation is at the critical speed (Directorate-General for Energy, 1990:12). Some of the material will not fall from the inner wall of the mill but will be carried around as the mill rotates. This is called "centrifuging" (Directorate-General for Energy, 1990:12). The speed at which the gravitational force is equal to the centrifugal force is called the critical speed, C (Sankar Prasath & Venkatesh, 2014), and can be calculated by Equation 2-2 in revolutions/minute (Directorate-General for Energy, 1990:12; King, 1999):

$$C = \frac{42.2}{(D-d)^{0.5}} \qquad \textbf{2-2}$$

Where d is the maximum diameter of grinding media, and D is the mill internal diameter, both in metres. The rotation speed is approximately 75-80% of the critical speed to prevent centrifuging (cataracting), and to attain maximum grinding with low energy consumption (Directorate-General for Energy, 1990:12). The attritioning process is influenced by two factors: the relative velocities of particles, and the frequency of collisions between particles (Davis & Dawson, 1989).

Cascading motion: Relatively low rotation speeds, and smooth inside liners, will cause the particles to roll down to the toe area of the mill, as illustrated in Figure 2.13 (Wills & Napier-Munn, 2006:148), since they do not have sufficient energy to be lifted high along the mill wall (Directorate-General for Energy, 1990:12). The mill must be run at such a speed so that the descending grinding media land on the toe of the charge. This prevents impact on the inner liner and causes wearing of the liner (Directorate-General for Energy, 1990:12). During cascading motion, abrasion and compression between the processed material and grinding media occurs throughout the descent (Directorate-General for Energy, 1990:12), leading to the formation of fine particles (Wills & Napier-Munn, 2006:148). When the internal surface of the cylindrical mill is fitted with liners, cascading motion will occur at a lower critical speed (Directorate-General for Energy, 1990:13).

Cataracting motion: Cataracting motion occurs when the rotation speed is increased to the "critical" speed. The grinding media and processed material are carried higher up in the mill shell (Directorate-General for Energy, 1990:12) because of the centrifugal force exceeding the gravitational force (Sankar Prasath & Venkatesh, 2014). The contents of the mill are lifted along the side of the mill during rotation and then fall to the bottom as described in Figure 2.13 (Directorate-General for Energy, 1990:12). High rotating speeds will cause the particles to move in these parabolic trajectories (Wills & Napier-Munn, 2006:148). Impact comminution will occur during the cataracting movement to form coarser particles (Wills & Napier-Munn, 2006:148).

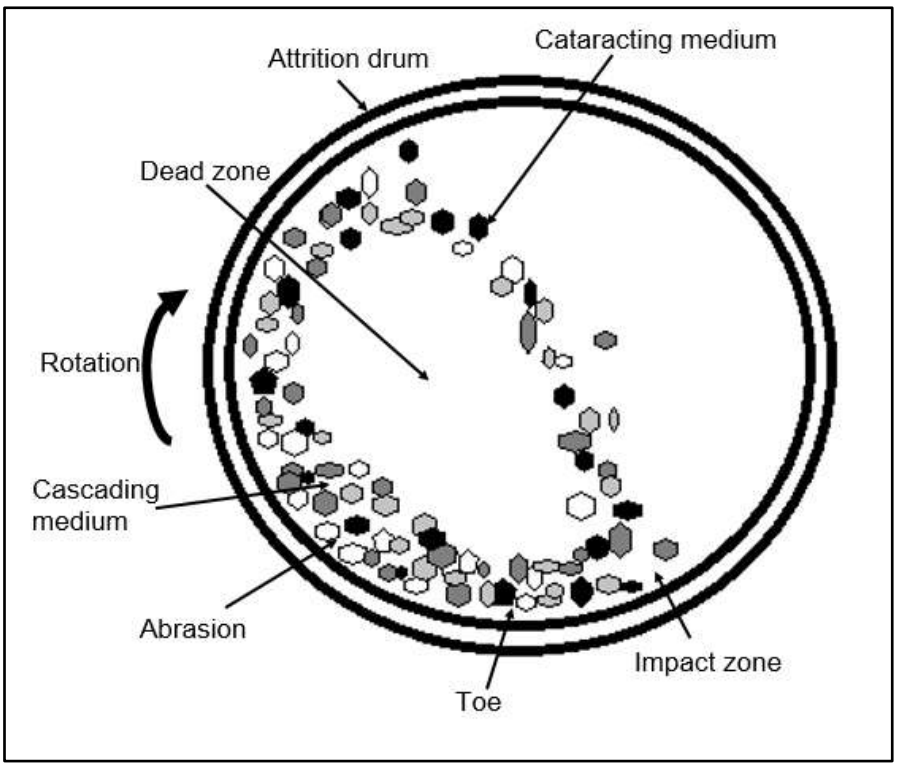

Figure 2.13: Motion of particles in tumbling mill (Wills & Napier-Munn, 2006:143; King, 1999).

The size reduction occurring in tumbling mills are mostly dependent on the motion in the mill, size and quantity of particles, and the probability of particles coming into contact with the grinding medium (Wills &Napier-Munn, 2006:147). Large amounts of energy are needed for attritioning, since the applied energy needs to be separated along particles present (Hogg, 1999), and fines formation during grinding is problematic (Drzymala, 2007:126; Jankovic *et al*., 2000). The residence time for sufficient grinding is acquired experimentally (SACPS, 2015:104). According to Raju *et al*. (2013), the newly formed surface area will increase as the grinding time increases, and hence the energy consumption also increases.

2.4 Liberation

Valuable mineral material are generally highly distributed and intimately associated with gangue minerals, and must firstly be unlocked (released), or liberated by means of comminution before it can be separated from the gangue minerals (Usaini *et al*., 2014). It is preferential to liberate the valuable minerals from the gangue minerals at the coarsest particle size possible as this will reduce fines production, as well as save energy during further succeeding separation stages (Usaini *et al*., 2014). Figure 2.14 illustrates liberation by referring to a lump of ore of which the size has been reduced to a number of identical volume cubes with a size smaller than the observed valuable mineral grain size. Each cube represents a particle produced by size reduction, and contains either or both valuable mineral (black) and gangue (white). None of the particles have been completely liberated. However the bulk of the gangue material present in the original ore has been liberated from the minor valuable mineral (Usaini *et al*., 2014). Complete liberation of valuable minerals from gangue is rarely achieved, and fine grinding is required to attain the necessary degree of liberation (Jankovic *et al*., 2000; Wills & Napier-Munn, 2006:14). Further liberation can be attained by additional comminution. The particles containing "locked" mineral together with gangue are referred to as middlings (Usaini *et al*., 2014). Liberation by means of size reduction is done to separate the mineral matter from the coal at the coarsest particle size possible (Weining *et al.,* 2013; Wills & Napier-Munn, 2006:14) to increase the amount of coal recovered from coal middlings (Weining *et al.,* 2013); thus increasing the coal yield.

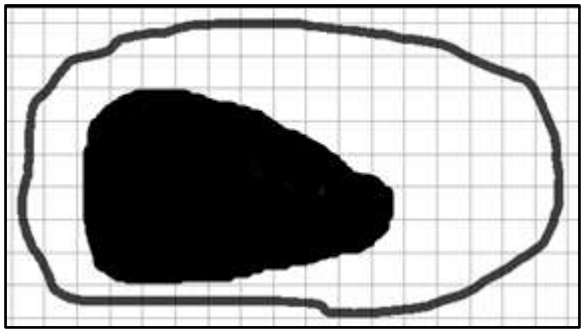

Figure 2.14: Liberation of mineral and gangue (Usaini *et al*., 2014).

Breakage of coal particles leads to either single components of pure minerals or macerals, while other particles are composites with varying amounts of minerals and macerals present (O' Brien *et al*., 2011). A cross-section of a particle is given in Figure 2.15 to demonstrate the problem associated with liberation. The regions (X) resemble the valuable mineral of interest and regions (XX) are small particles of valuable mineral trapped between gangue. The products of comminution varies from completely liberated particles, to particles associated with gangue as illustrated in Figure 2.15 (Usaini *et al*., 2014; Wills & Napier-Munn, 2006:15). Particle 1 is mineral-rich and highly concentrated, whilst Particle 4 is considered as tailings because of the low valuable mineral content that is difficult to recover. Particles 2 and 3 are middlings and require further

breakage or grinding to liberate the mineral matter from the gangue (Usaini *et al*., 2014; Wills & Napier-Munn, 2006:15). The products of comminution can therefore be divided into three types of particles namely, fully liberated coal particles, particles containing both coal substance and mineral matter, and liberated mineral matter (Oki *et al*., 2004). The combustible coal matter needs to be recovered from the incombustible mineral matter as explained in Section 2.1.3 by referring to Figure 2.2. Complete liberation of the desired mineral particles is rarely achieved even when the ore is milled to obtain grain size particles (Usaini *et al*., 2014).

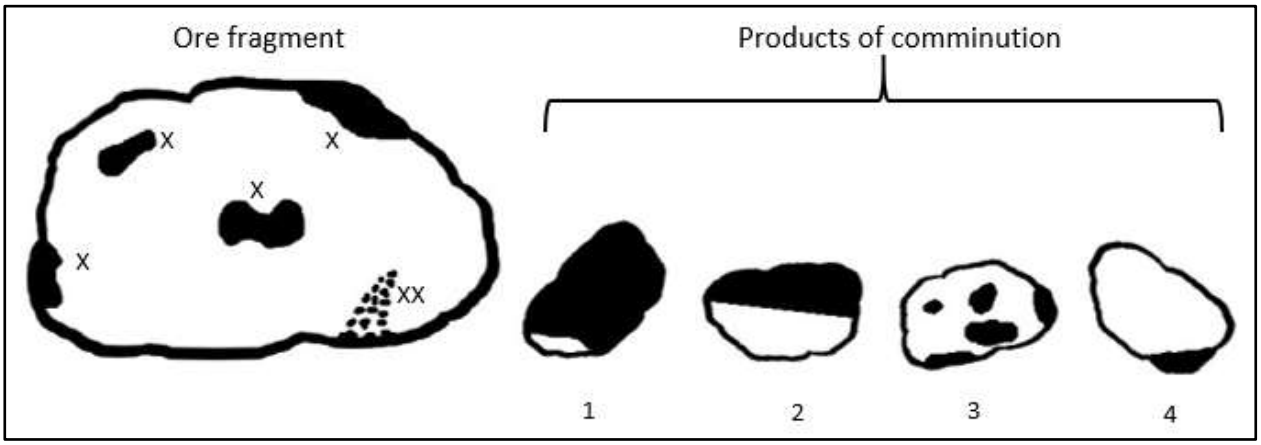

Figure 2.15: Cross-sections of ore particles before and after communition (adapted from Usaini *et al*., 2014; Wills & Napier-Munn, 2006:15).

The degree of liberation gives an indication of the mineral percentage that occurs as liberated particles in the ore relative to the total content (Usaini *et al*., 2014; Wills & Napier-Munn, 2006:14). A high degree of liberation can be achieved in cases where the boundaries between the mineral matter and gangue material are weak (Wills & Napier-Munn, 2006:14). A low degree of liberation is attained when breakage during comminution occurs across the various constituents because of strong adhesion forces between minerals and gangue (Usaini *et al*., 2014). A low degree of liberation leads to a large middlings production, and can be avoided by directing the breaking force towards the boundaries between minerals and gangue. This ensures that breakage occurs along the boundaries to separate minerals without the formation of too much middlings, enhancing the overall degree of liberation (Usaini *et al*., 2014; Wills & Napier-Munn, 2006:14). The degree to which liberation occurs is coal specific; likewise the yield obtained in the plant is also specific to the coal. The yield of pure components can be increased by further size reduction of the material (O' Brien *et al*., 2011). The degree of liberation (ε_L) is either the yield of a certain constituent, or the recovery of free particles of a certain component in the liberation product, and can be determined by Equation 2-3 (Drzymala, 2007:143).

$$\varepsilon_L = \frac{mass\ of\ free\ particles\ of\ considered\ constituent}{mass\ of\ considered\ constituent\ in\ feed} \times 100\% \qquad \textbf{2-3}$$

The closer the liberation index of coal is to 1, the better the likelihood that the washability of the coal will be able to produce a clean coal with low mineral matter present. The liberation of mineral matter from coal macerals increases with a decrease in particle size (King & Birtek, 1990). The liberation particle size of a particular ore is important during process design, as this affects the capital and operating costs, and gives an indication of the target screen size (Usaini *et al*., 2014). Sufficient liberation can be correlated to the quality and particle size of coal required by the market (Weining *et al.,* 2013; Wills & Napier-Munn, 2006:14). Examination of certain coal particles on a microscopic scale revealed that sufficient liberation may not occur until the particles are finer than 20 µm (Jankovic *et al*., 2000).

2.4.1 Float-sink (densimetric) analysis

Various coal upgrading methods depend on gravity or dense medium separation processes as there is a substantial difference in the specific gravity of the organic matter of coal (macerals), and that of the mineral matter present (Holuszko & Grieve, 1990; Oki *et al*., 2004). Coal is therefore washed according to relative densities to meet the requirements specified in terms of the ash yield by the consumer (SACPS, 2015:77). Washability analyses are employed to determine the amount and quality of coal that can be recovered at a certain specific gravity, or to determine the separation gravity required to recover an anticipated coal quality (Holuszko & Grieve, 1990). The particle density distribution of coal, also known as the coal washability, is important for equipment and plant design, as well as evaluating plant efficiency. Float-sink tests used to determine coal washability (Callen *et al*., 2002) are conducted according to the relevant South African National Standard (SANS 7936:2010).

The separation of coal into different relative density (RD) fractions is performed, according to the abovementioned standard, by the immersion of a coal sample consecutively into a series of liquids with relative densities varying between the RD of pure coal and the RD of the impurities present in the coal (SACPS 2015:70). Some particles will float, while others will sink in the liquid depending on the particles' density (Drzymala, 2007:101). The range of relative densities used for the float-sink analysis of coal varies according to the purpose of the analysis (SACPS, 2015:71). Zinc chloride ($ZnCl_2$) solutions with a relative density range between 1.30-1.80 can be used for coal analyses, since pure coal has a density varying between 1.17 g/cm^3 and 1.35 g/cm^3, while the minerals present in coals have densities ranging from 1.80 g/cm^3 to 5.20 g/cm^3 (Drzymala, 2007:195). Middlings will have a relative density between these values (O' Brien *et al*., 2011). The analysed material is, usually, firstly immersed in the liquid with the lowest density, that is the lowest $ZnCl_2$ concentration (Drzymala, 2007:195). All the material present in the sample with a RD lower than 1.30 will float on the surface of the liquid, whilst the material with the RD higher than 1.30 sinks to the bottom of the container. This sinks fraction is then removed, rinsed and is then immersed into another container with the next higher density (1.40 g/cm^3), as

illustrated in Figure 2.16 (Drzymala, 2007:196). Particles that float on the liquid with density of 1.40 g/cm^3 will have a density between 1.30 g/cm^3 and 1.40 g/cm^3. The method is repeated until at the highest density as illustrated in Figure 2.16 (Drzymala, 2007:196). The fractions that float and those that sink, are then analysed for the quality parameters of interest (Drzymala, 2007:101). When $ZnCl_2$ solutions are used for the float-sink analyses, separate relative density fractions must be rinsed with water immediately after separation, where after the respective relative density fractions must be air-dried. Zinc chloride solutions must be disposed of according to legislation as it creates environmental problems and are highly corrosive (SACPS, 2015:72). It is not known whether the use of $ZnCl_2$ solutions for the float and sink analysis, weakens the coal structure to such a nature that it affects the liberation of coal from mineral matter. Research regarding this matter should be done.

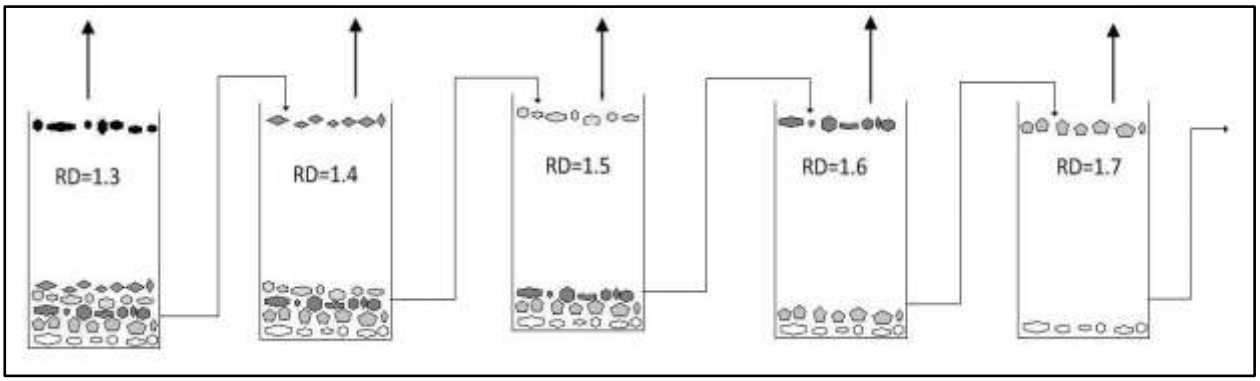

Figure 2.16: Float and sink analysis (Drzymala, 2007:195).

The minimum time required for separation of large coal particles is typically two minutes, but more time is required as the particles decrease in size. The time necessary for complete separation of the floats and sinks depends on the viscosity of the separation liquid used, the proportion of near density particles (particles within ±0.1 of the separation RD), and the size of the particles to be separated (SACPS, 2015:72). Agitation by means of stirring is used to enhance the separation of particles larger than 0.5 mm (SACPS, 2015:72), however, stirring will slow the separation of particles smaller than 0.5 mm (SACPS, 2015:72).

The separating medium used for float-sink testing can also be a mixture of dense organic liquids, for example, tetrachloroethylene (RD of 1.62), white spirits (RD of 0.79), and tetrabromoethane (RD of 2.97), which are mixed to produce solutions with different relative densities (Callen *et al*., 2002). These liquids are accompanied by environmental and health concerns as they release organic vapours, and air extractions systems must be used in the laboratory (Callen *et al*., 2002). The float-sink tests are done in a similar process as explained previously, by adding the coal sample to the solution starting with the lowest RD (Callen *et al*., 2002).

The material occurring in the different relative density intervals is expressed by means of cumulated distribution curves or washability curves (Drzymala, 2007:196; Holuszko & Grieve, 1990). Washability curves are characterized by the yield at a certain density of separation as well as the ash yield (Holuszko & Grieve, 1990), and are used to identify the mineral matter spread throughout coal particles (O' Brien *et al*., 2011). The ash yield of the discards can be used to evaluate the efficiency of the liberation and washing process. When the ash yield of the discards are not significant higher than the ash yield of the feed material, it indicates that valuable material is being lost to the discards, and therefore either the liberation is insufficient, and/or the washing process is inefficient (Holuszko & Grieve, 1990).

2.5 Preventing the production of excessive fines

Coal fines are usually defined as those particles smaller than 0.5 mm (SACPS, 2015:225), and are mostly formed during mining, transportation, conveying, stockpiling and comminution (Viljoen *et al.,* 2015). Drying, retreatment, and handling of coal fines formed during size reduction processes are difficult (Weining *et al.,* 2013), since fines have higher moisture retention, which makes them build up in chutes and transfer points, and are more expensive to process than coarse coal. The plant feed coal must therefore be processed at the coarsest possible particle size (O'Brien *et al*., 2011). The quality of coal is negatively influenced by the presence of fines retaining higher moisture, and it will only be viable to include fine coal in the export coal product if its total moisture content is below 15 %, and it is upgraded to a calorific value of about 28 MJ/kg (de Korte, 2010). Due to the difficult and time consuming dewatering process of fines, high amounts of fine coal are discarded (Esterle *et al*., 2002; Le Roux *et al*., 2012; Viljoen *et al.,* 2015). Despite the difficulties in fine coal processing, crushing of coal to smaller particle sizes may be required to attain higher degrees of liberation resulting in coal yield increase depending upon the coal source (O' Brien *et al*., 2011). Coal particles with mineral matter distributed throughout the particle can be upgraded by means of size reduction, but when high mineral distributions are present, it requires fine crushing of the coal (O' Brien *et al*., 2011), leading to high amounts of fines generated. When higher degrees of size reduction are accomplished, more fines are generated (SACPS, 2015:92). Since it is unlikely to eliminate all fines generated in the comminution processes, a balance between sufficient liberation of coal to attain a certain yield, and the formation of excessive fines must be achieved. Although fines are undesired during most size reduction operations, a crusher that generates no fines has yet to be invented. However, some size reduction equipment does produce less fines than others (SACPS, 2015:92). Comminution processes must therefore be controlled to ensure that particle sizes are large enough to be suitable for utilization, and fines formation during size reduction processes must be limited (Weining *et al.,* 2013), as they increase downstream beneficiation costs, and lead to

economic losses. Fines generation in the plant environment can be reduced and limited by the following:

- Screening out the desired particle sizes before re-crushing of the oversize material (SACPS, 2015:92).
- Removing the undersize material before crushing (SACPS, 2015:92) and removal of fines prior to crushing to increase the plant throughput capacity, and reduce the wear to equipment (SACPS, 2015:93).
- Crushing the material to a slightly greater particle size than the desired top size. The required particle sizes can be screened out, whilst oversize material can be re-crushed (SACPS, 2015:105).
- Minimizing the travel path of material through the size reduction process. The crushing circuit must be short, in terms of length, with the least possible sharp alterations in direction (SACPS, 2015:105).

3

CHAPTER 3 EXPERIMENTAL PROCEDURES

The experimental procedure including all materials and equipment used for this research study are explained in this chapter. Methods used for coal sample analysis including densimetric analysis, proximate analysis, calorific value, swelling index, and particle size distribution analysis will be described in detail. All samples were handled with care during the experimental procedures to keep the formation of fines and the breakage of particles due to handling a minimum, as this will influence the margin of error. It is important to note that during this study it was assumed that the coal properties, specifically the ash yield, at a relative density interval is independent of the particle size. This assumption was made since it is impossible to analyse all individual samples due to the cost and time, and will be tested and verified in further projects. Sample mass loss during the experimental procedure might have occurred, but was kept a minimum.

It is important to note that the term “ash yield” was used instead of “ash content” throughout this study. This is because “ash yield” refers to the ash content remaining after combustion of coal. The ash yield are related to mineral matter content in the coal before combustion, as given in Equation 1-1.

3.1 Materials

3.1.1 Coal

Run-of-mine coal samples from the Chipanga Seam in the Moatize Coalfield in Mozambique were obtained. This coalfield was chosen, because of its highly layered structure consisting of coal seams interlayered with mineral matter, as seen from Figure 3.1 and Figure 3.2. Figure 3.2 presents a micro-focus x-ray tomography scan of a Moatize coal particle. The parallel layered structure of the coal particle can be clearly seen. The coal samples were mixed uniformly, in order to ensure repeatability of experiments, to achieve accurate experimental results according to ISO 5725:1994 titled “Accuracy (trueness and precision) of measurement methods and results”.

Figure 3.1: Moatize coal sample.

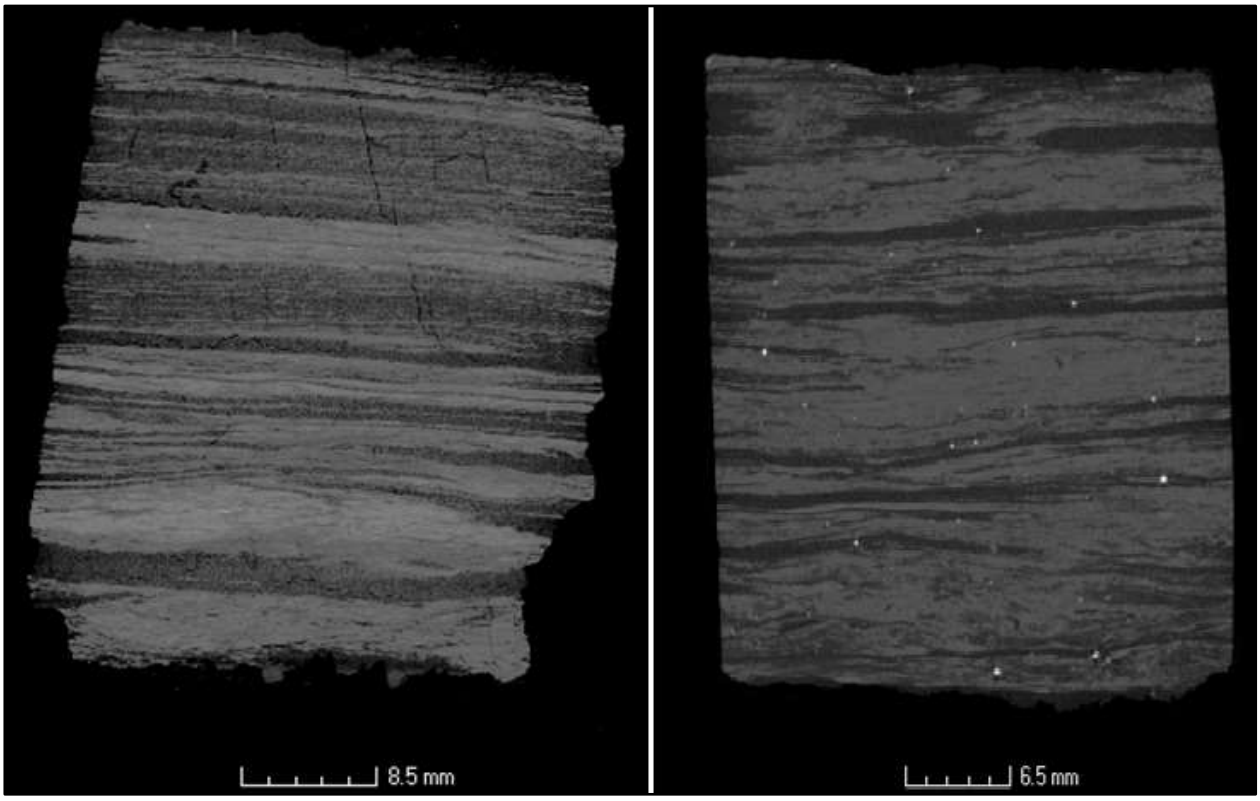

Figure 3.2: Micro-focus x-ray tomography scans of Moatize coal.

The properties of the raw run-of-mine coal used for experimental procedures will be described, as the experimental results obtained will be compared to these properties. The size by washability graph for raw Moatize coal, prior to testing is given in Figure 3.3 to illustrate the mass percentage of material distributed according to both particle size and relative density. This curve was obtained

by particle size distribution (PSD) and densimetric analysis which will be described in Section 3.6. The reason the mass distribution percentage on the y-axis is up to 20 %, is for easy comparison with figures discussed in Chapter 4, and for ease of readability.

There is a bi-modal distribution (showing two peaks of high amounts of material) in the 13.2-19.0 mm and the 37.5-53.0 mm size fractions, as well as in the relative density fractions as shown in Figure 3.3. This can be ascribed to the amount of mineral matter occurring in the larger particle sizes, and the amount of macerals in smaller particle size ranges. The ROM coal was already subjected to some breakage during mining and transportation, and resulted in liberation of some coal. It can be seen from Figure 3.3 that particles with a relative density of 1.8 and higher are mostly larger particles with sizes of 13.2-75.0 mm. These particles are high in mineral matter content, and may contain only small grains of coal. As explained in Section 2.1.3, pure coal has a RD of 1.2-1.4, whilst mineral matter has RD's varying between 2.0 and 5.0 depending on the mineralogy (Speight, 2005:94). Composite particles consisting of varying amounts of macerals and minerals exhibit intermediate RD values (O'Brien *et al*., 2011). The intermediate relative density ranges 1.4-1.7 also contain particles with sizes of 13.2-75.0 mm. These particles are composites, or middlings, consisting of different quantities of coal macerals as well as mineral matter. In order to increase the yield of coal, the mineral matter and coal need to be separated. Size reduction of these particles is necessary to "free" or liberate the coal particles from the included minerals. It was expected that size reduction will increase the yield of material with relative densities of 1.4 and lower. As seen from Figure 3.3, particles with relative densities of 1.4 and lower, are almost "pure" coal, mainly occurring in the particle size interval of 0.0-6.7 mm. These particles are already liberated during mining and transportation procedures. Particles with relative densities of 1.4 and lower consist of almost pure coal macerals, and therefore do not need any liberation.

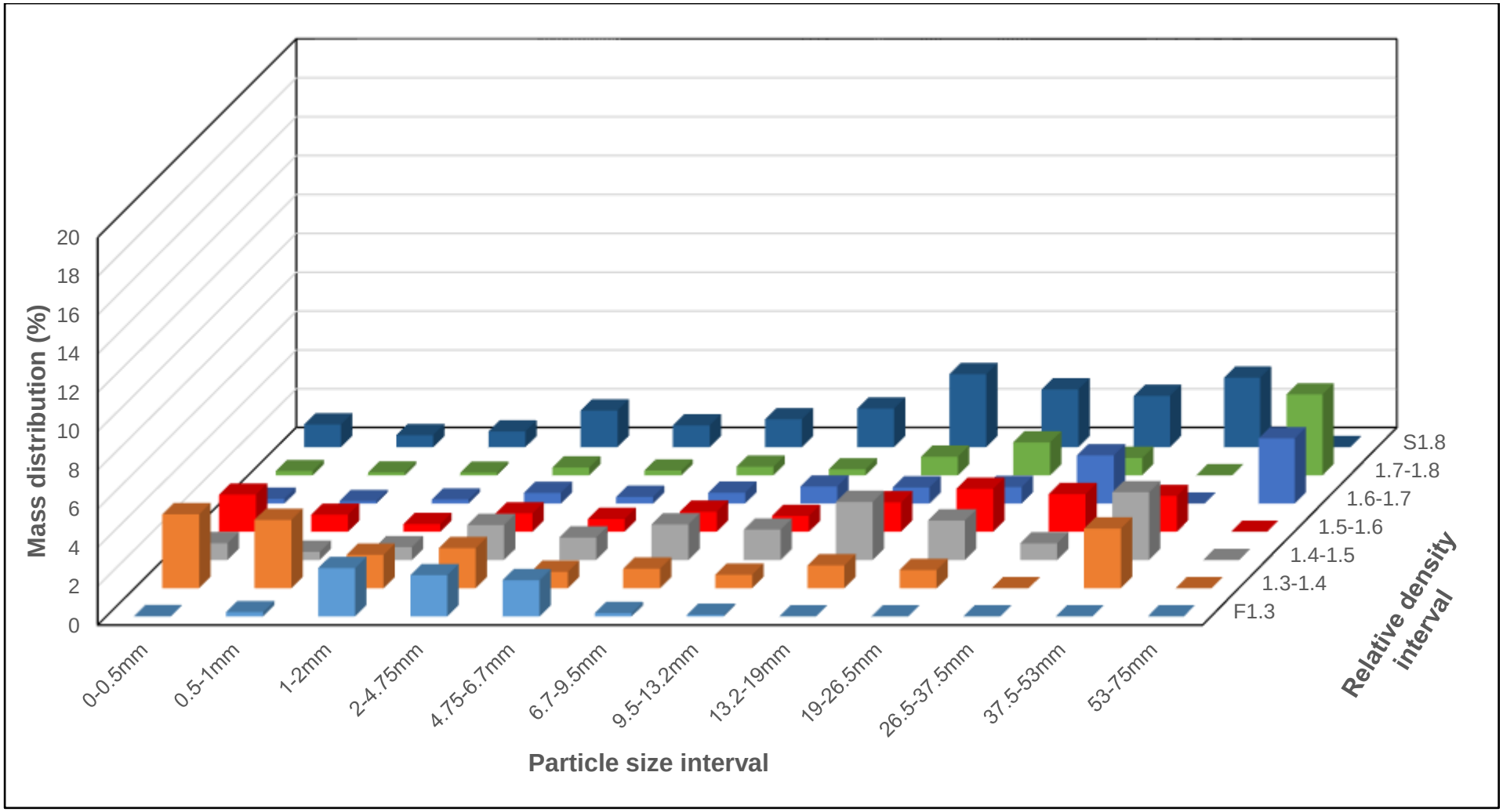

Figure 3.3: Size by washability graph for raw coal.

3.1.2 Chemicals

The chemicals used to conduct the densimetric analysis according to SANS 7936:2010/ISO 7936:1992 were zinc chloride ($ZnCl_2$) and demineralized water, while the organic liquids used were tetrachloroethylene (TCE), 1,1,2,2-tetrabromoethane (TBE) and white spirits. Relative densities of these chemicals are tabulated in Table 3.1

Table 3.1: Relative densities of materials used for densimetric analysis.

Material	Zinc chloride	Demineralized water	TCE	TBE	White spirits
Relative density at 20°C	2.907	1.00	1.62	2.97	0.785

3.2 Equipment

The apparatus used for experimentation, along with a description of the equipment, and its purpose are listed in Table 3.2. Pictures of some of the equipment listed can be found in Appendix A.

Table 3.2: Apparatus

Apparatus	Description/Model	Purpose
100 litre container	Blue 100 litre container	Contain bulk $ZnCl_2$ solution.
Aluminium containers	Silver aluminium containers	Contain coal samples subjected to organic liquids during float and sink analysis.
Beakers	1 litre glass beakers	Container for organic liquids.
Buchner filter funnel	500 ml glass filter funnel	Contained filter paper during filtration.
Ventilation chamber	See Figure 3.15	Extraction of toxic gasses during densimetric analysis using organic liquids.
Funnel	11.0 cm household funnel	Used to transfer coal particles into separation funnels.
Drop weight impact rig	See Figure 3.6	Used for impact breakage of coal particles.
Electronic scale	Sartorius® AG GÖTTINGEN Model number: EA60EDE - L	Used for weight measurements up to 60.0 kg.
Electronic scale	Sartorius® AG GÖTTINGEN Model number: PMA7500	Used for weight measurements up to 7.5 kg.
Lawn roller	Lawn roller with mass of 80 kg. See Figure 3.5	Compressive breakage of multiple particles.

Hand sieve	Hand sieve with aperture size of 0.5 mm.	Collection of floating material during densimetric analysis.
Hydrometer	Glass hydrometer with a density range of 0.7-2.0 g/ml.	Determination of relative densities of solutions.
Measuring cylinder	250 ml glass measuring cylinder.	Contain organic liquids during determination of relative densities and temperatures.
Paint brush	40 mm wide paint brush.	Used during sieving to ensure that particles do not stick to one another, and to carefully transfer particles from sieves to containers.
Plastic containers	2 litre and 500 ml plastic containers.	To contain samples for air-drying of material after subjected to $ZnCl_2$ during float and sink analysis.
Riffle splitter	See Figure A.2	Used for splitting of coal samples.
Rotary splitter	SMC Rotary Sample Splitter See Figure 3.14	Used for splitting of coal samples.
Separation funnels	1 litre and 2 litre glass separation funnels	Used for densimetric analysis by using organic liquids.
Shovel	Steel shovel	Used during the cone and quatering of the bulk coal sample.
Sieves	Labotec® stainless steel test sieves and industrial sieves.	Determination of particle size distribution.
Stainless steel bucket	Cylindric stainless steel frame (lenght of 40 cm and ID of 20 cm) with a mesh aperture size of 1 mm. See Figure 3.13	To contain coal samples during densimetric analysis when using $ZnCl_2$.
Steel frame	Steel plate with width of 0.5 m and lenght of 2 m containing square tubing (12.7 mm) and flat bar (6 mm) on the side. See Figure 3.5	To contain coal sample during compressive breakage and to limit the formation of fines.
Stopwatch	Tempo TEMP-250-M03 S13/2	Measuring of time intervals used during attrition breakage of samples.
Thermometer	Glass thermometer with temperature range of 0-100°C.	Measuring of temperature.
Tumbling mill	Cylindrical blue Perspex drum (length of 0.5 m and ID of 0.385 m) equipped with opening lid. See Figure 3.7	Used for attrition breakage of multiple particles.

Ziplock bags	Plastic resealable bags.	Used as sample bags to contain samples avoiding moisture loss or absorption.
$ZnCl_2$ containers	25 litre white plastic drums with lids.	To contain $ZnCl_2$ solution during float-sink analysis.

3.3 Experimental overview

Multiple particle breakage experiments were performed to investigate the influence of the mode of applied breakage on coal yield. The multiple particle breakage experimental runs are summarized in Table 3.3, where the first column indicates the mode of breakage applied, the second column the top size for breakage, and the third column the residence time for attrition breakage following the initial type of breakage. The last column indicated the number of experiments conducted for that particular combination of breakage modes. The top sizes were chosen based on the required sizes for industrial application, and to minimize fines generation. Duplicate experimental runs conformed to ISO 5725:1994 standards for repeatability.

Table 3.3: Experimental overview of multiple particle breakage.

Form of breakage	Top size	Attritioning residence time	Experimental runs
Impact	6.7 mm	0 minutes	3
		1 minute	1
		2 minutes	1
		5 minutes	1
	13.2 mm	0 minutes	3
		1 minute	1
		2 minutes	1
		5 minutes	1
Compressive	6.7 mm	0 minutes	3
		1 minute	1
		2 minutes	1
		5 minutes	1
	13.2 mm	0 minutes	3
		1 minute	1
		2 minutes	1
		5 minutes	1

3.4 Experimental procedure

3.4.1.1 Sample preparation

The bulk coal sample was divided into samples of approximately 6 kg each, by using the cone and quartering method according to SANS 18283:2007/ISO 18283: 2006. This method is suitable for dividing large samples of coal into smaller samples, and is performed by mixing all the material thoroughly by using a shovel, forming a conical heap with radially uniform segregation of the coal particles as shown in Figure 3.4(a). This conical heap is then divided into quarters with approximately the same mass, where after opposite quarters, that is quarters 1 and 3 or quarters 2 and 4, as illustrated in Figure 3.4(b), were mixed again to form a new conical heap. This was repeated until the opposite quarters had the desired mass, which was in this case 6 kg. The mass of coal used for each subsequent multiple particle breakage experimental run mentioned in Section 3.3 needed to be 6 kg or more, since this mass of material is required to perform the densimetric analysis (ISO 13909-2:2001; ISO 13909-4:2001; Zhu, 2014). The required amount of material was obtained by using ISO 13909:2001, titled “Hard coal and coke – Mechanical sampling”. The initial particle size distribution of each 6 kg coal sample was determined by screening into the various particle size intervals with a top size of 75 mm. The PSD analysis was done according to ISO 1953:1994, by employing Labotec® test sieves with a $\sqrt{2}$ aperture size interval. Screening was done manually to prevent breakage of the particles, and the formation of fines, as far possible. After the initial particle size distribution of each sample was obtained, the samples were subjected to either compressive or impact breakage as described in the following section.

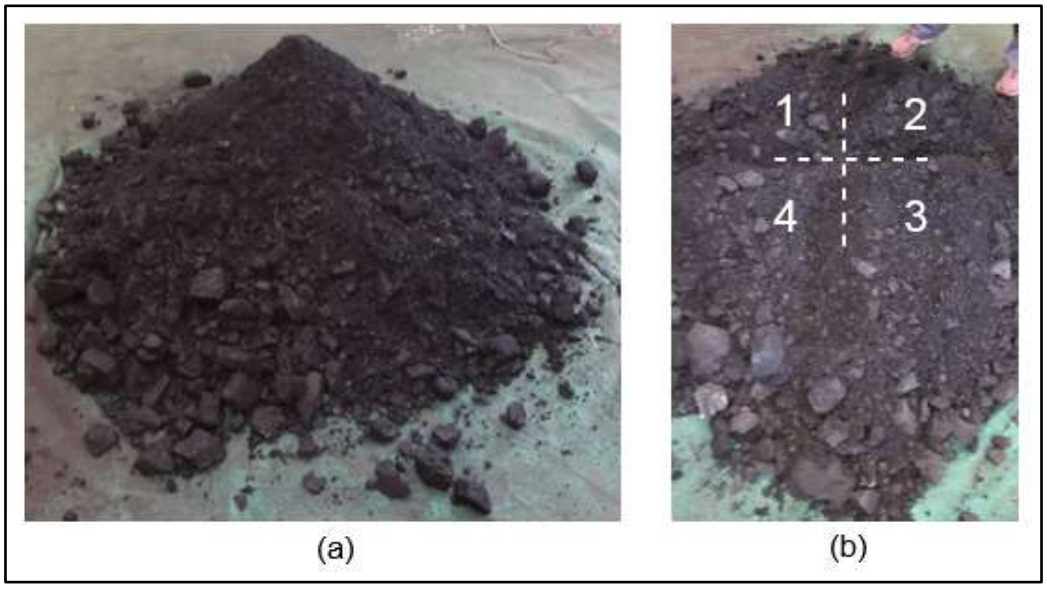

Figure 3.4: Cone and quartering of Moatize coal.

It should be noted that although the mass of 6 kg is an absolute minimum increment mass and not optimal for the float and sink analysis, this mass was chosen because of the time consuming float and sink procedure as well as the high costs associated with the process. The total coal sample size required for the float and sink analysis is the product of the minimum increment mass and the number of increments necessary to obtain the desired precision level. The required sample mass for float and sink testing of raw coal with topsize of 75 mm would be 50-100 kg, or greater.

3.4.1.2 Experimental procedure

Steps performed during the experimental procedure are summarized in flow diagrams that are illustrated in Appendix A (Figure A.3 and Figure A.4). Impact, compressive and attrition breakage will be described in detail.

- Compressive breakage

Compressive breakage of each 6 kg coal sample was conducted by placing particles within steel frames (length of 2.0 m and width of 0.5 m) with height of 6.0 mm and 12.7 mm respectively. Again, these top sizes were chosen based on the required sizes for industrial application, and to minimize fines generation. Breakage was thus done to top sizes of 6.7 mm and 13.2 mm. The orientation of the particles placed within the steel frame was random, and particles were placed in a single layer in the steel frame to prevent inter-particle breakage and cushioning effects. A lawn roller, as seen in Figure 3.5, with mass of 80 kg, was pulled over the steel frame containing the coal sample to compress the particles resulting in breakage. The particles were screened after breakage using a sieve with an aperture size of 6.7 mm or 13.2 mm, depending on the top size to which breakage was done. Particles larger than this size (oversize material) were again placed within the steel frame, and compressive breakage using the lawn roller, was repeated until all particles passed through either the 6.7 mm or 13.2 mm screen.

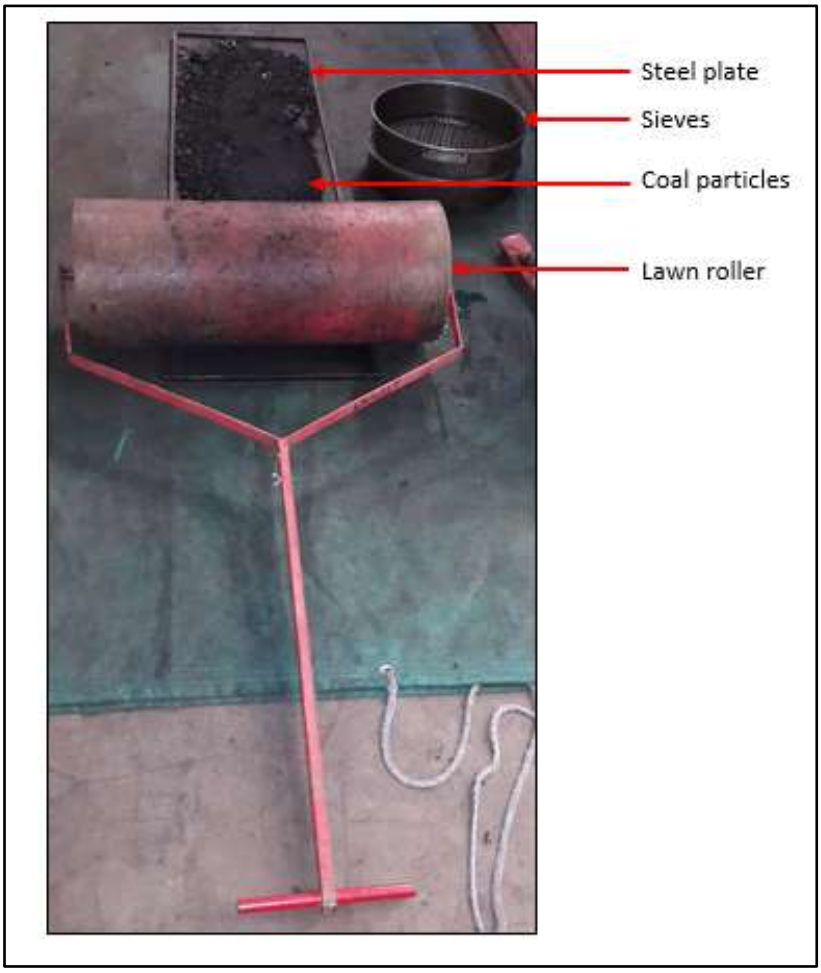

Figure 3.5: Lawn roller used for compressive breakage.

- Impact breakage

Multiple particle impact breakage of each 6 kg coal sample was performed according to the SANS 401:2010 for “Standard test method of drop shatter test for coal”, by using a locally manufactured drop-weight impact rig (see Figure 3.6). The coal sample was placed within a single layer, again to prevent inter-particle breakage and cushioning effects, at the bottom of the drop-weight impact rig, together with either square tube spacers of 12.7 mm, or flat bar spacers of 6.0 mm, depending on the required top size of the experimental run performed. Spacers were used to minimize fines, and to ensure the desired top size. The steel plate, with a mass of 14.65 kg, was secured at the top of the rig by means of a safety pin as a safety precaution. After the coal sample was placed at the bottom of the rig, the steel plate was released from a height of 1.83 m to allow for optimum breakage. The steel plate was directed by a steel pipe to ensure a uniform impact force was applied to the particles. The orientation of the particles relative to the coal bedding plane was random. Removable steel sides at the bottom formed an enclosure, and ensured minimal particle loss during impact of the steel plate with the coal. They were also safety precaution, since the impact resulted in splattering of the particles. Again, the coal sample was screened to the top size using sieves with either 6.7 mm or 13.2 mm aperture size depending on

the experimental run conducted as explained for compressive breakage. Particles larger than the required top size (oversize material) were again subjected to impact breakage, and repeated until all particles passed through the screen.

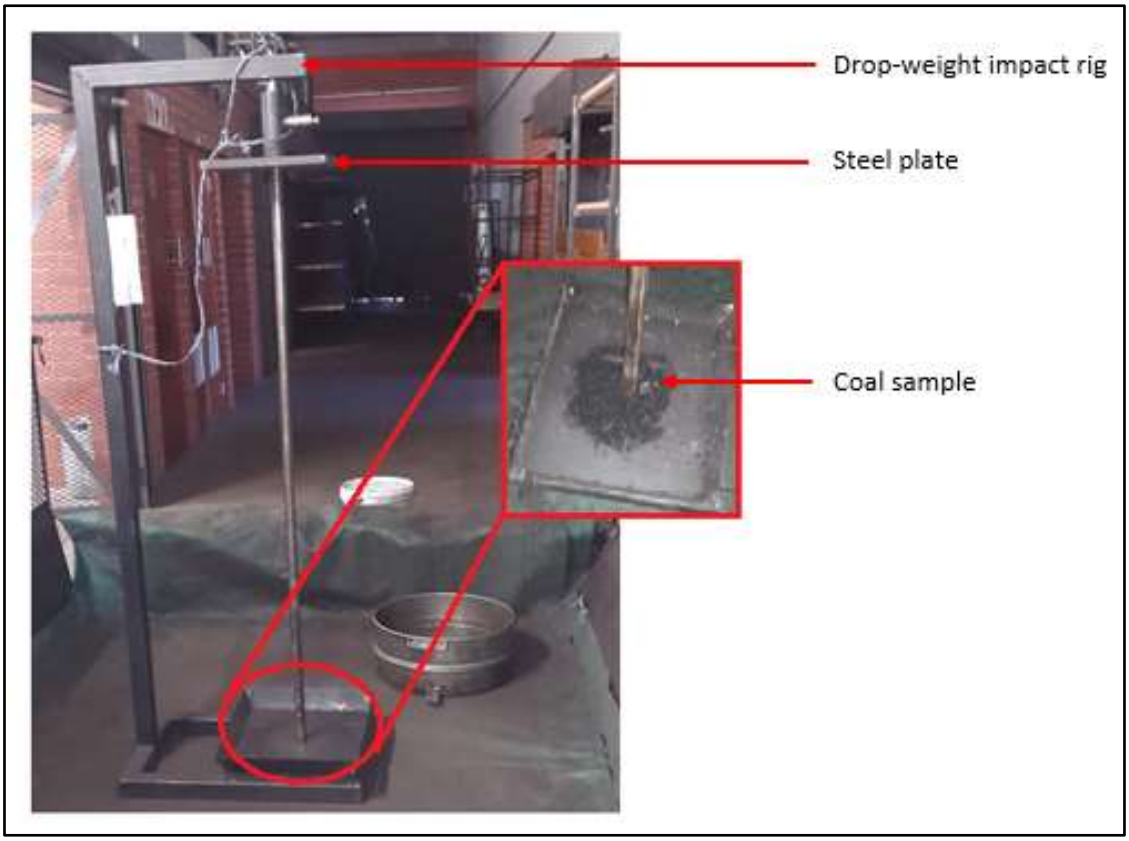

Figure 3.6: Drop-weight impact rig.

- Attrition breakage

Some experimental runs were performed by applying only impact or compressive breakage, without any additional attrition breakage, whilst others involved subjecting the sample to attritioning after the initial breakage mode was applied as indicated in Table 3.3, and in the experimental flow diagrams depicted in Figure A.3 and Figure A.4 in Appendix A. This was done to evaluate the effect of attrition breakage in addition to impact or compressive breakage upon the coal yield. It was expected that the coal particles were released and exposed during the initial breakage modes, and that additional attritioning would cause wear at the particle surface to chip off the exposed coal from the mineral matter. After the initial breakage mode, the intermediate particle size distribution of each sample was done according to the relevant standard, ISO 1953:1994, prior to additional attrition breakage.

Attrition breakage was performed using a tumbling mill (see Figure 3.7), fabricated from Perspex with an internal diameter of 0.385 m and length of 0.5 m, containing no milling media (for example steel rods or balls). Attrition breakage of particles was thus accomplished autogenously, that is

only by the particles contacting against one another, and against the tumbling mill wall. A small opening at the back end of the drum, allowed a decrease in pressure that might build up during attrition, to prevent a dust explosion or explosion of the drum. The total coal sample of about 6 kg was inserted into the tumbling mill, the lid was sealed to the mill using bolts to prevent the loss of material. The mill was put in a horizontal position on the rollers, driven by a motor and gearbox, responsible for the rotation along the cylindrical axis of the mill. The rotation of the mill took place within a steel cage ensuring a safe environment during operation.

The rotation of the mill had to be at such a speed that only a cascading motion (as discussed in Chapter 2.3.3.1) occurred to prevent the particles from breaking further due to impact. The critical speed of the tumbling mill was calculated according to Equation 2-2 to be 68 revolutions/minute (rpm), but to ensure that only cascading motion occurred, the actual rotation speed was significantly reduced to 20 rpm, which equated to 30 % of the calculated critical speed.

Figure 3.7: Tumbling mill.

The attritioning residence times were determined by developing a milling curve. A Moatize coal sample of 6 kg was firstly screened to evaluate the initial (residence time of 0 minutes) particle size distribution (PSD) according to ISO 1953:1994, after which the sample was placed in the tumbling mill. The mill was rotated at the above mentioned speed for 1 minute, where after the sample was carefully removed from the mill to minimize breakage due to handling. A PSD analysis of the sample was performed to compare the difference in particle sizes after subjecting them to attritioning for 1 minute. The same coal sample was again placed within the tumbling mill and attritioned for a further 1 minute. Again, the sample was removed from the mill and the PSD determined. This process was repeated to obtain the PSD at times of 1, 2, 5, 10 and 20 minutes respectively, to give an indication of the difference in particle sizes for various residence times. The data was used to construct a milling curve to determine when steady state is reached, and which residence times will be best suitable to use during experimental procedures. Two separate curves were constructed for ease of readability, firstly Figure 3.8 for particle sizes 0.0-9.5 mm, and secondly Figure 3.9 for particle sizes of 9.5-53.0 mm.

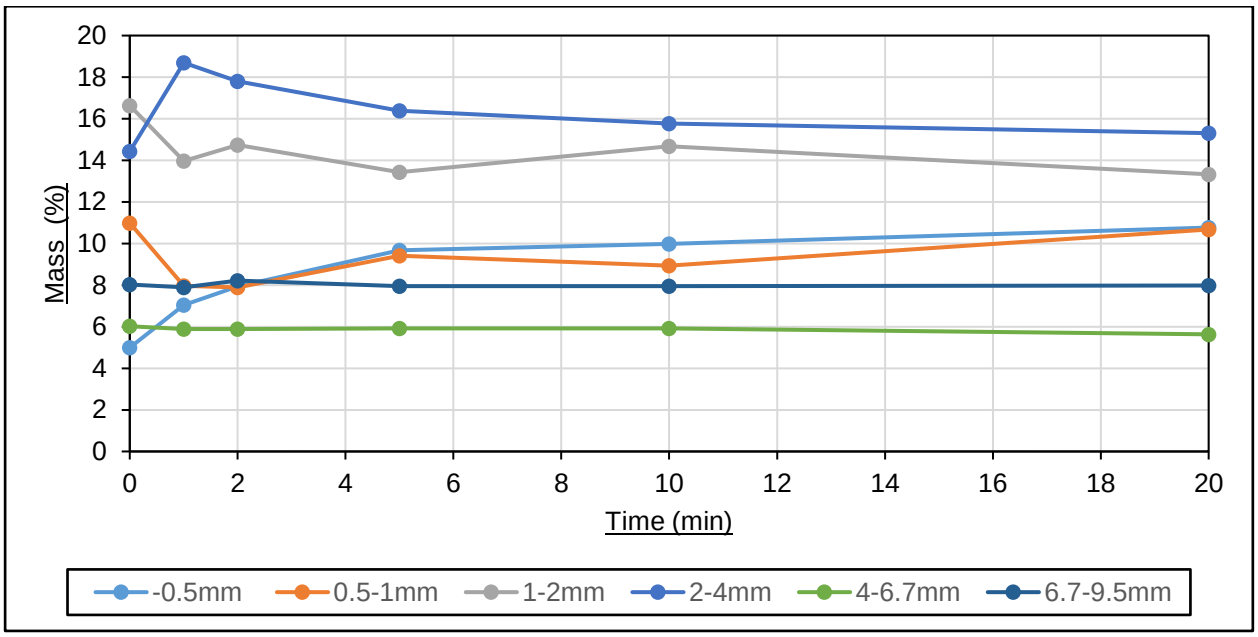

Figure 3.8: Normalized milling curve for Moatize coal (particle sizes 0.0-9.5 mm)

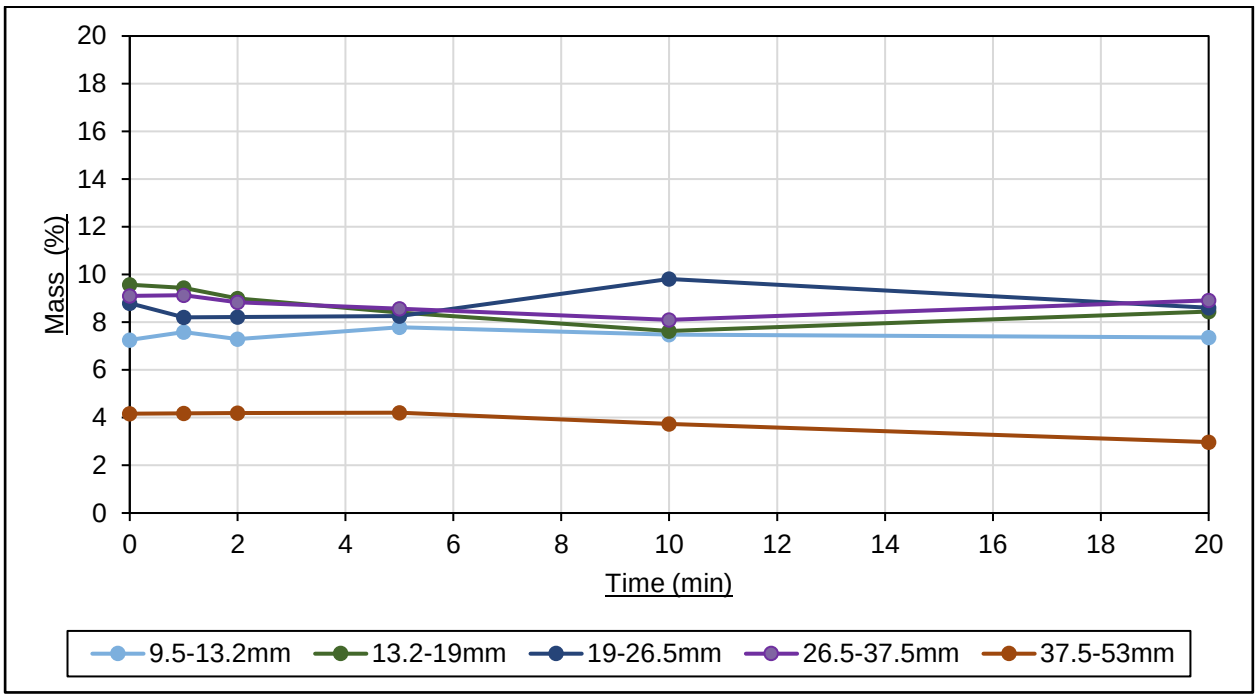

Figure 3.9: Normalized milling curve for Moatize coal (particle sizes 9.5-53.0 mm)

It can be seen from these milling curves that attrition breakage mostly occurred during the first 5 minutes, thereafter a steady state was reached, and no further breakage occurred as indicated by the flattening of the graphs. These results correspond to the study done by Sahoo & Roach (2005) as described in Section 2.3.2.3. The sample residence times were therefore selected to be 1, 2 and 5 minutes depending on the experimental run conducted.

3.5 Sampling procedure

Due to different samples that were used for the various analysis, the sampling procedure used for each analysis will be described before the analysis is explained as in the following section.

3.6 Analytical methods

Analyses that were performed throughout the experimental procedure were particle size distribution, proximate analysis, calorific value determination, and free swelling index. These were then correlated to the relative density of the sample as determined by the densimetric analysis.

3.6.1 Particle size distribution analysis

The particle size distribution analysis was performed according to the standard, ISO 1953:1994, by employing Labotec® sieves with a $\sqrt{2}$ aperture size interval. Industrial sieves were used to determine the initial and intermediate particle size distributions (as indicated in Figure A.3 and Figure A.4 in Appendix A) of each sample using the total mass of each sample for particle sizes larger than 4.75 mm. Sieving was done manually by using a paint brush, no sieve shaker was employed to minimize further fracturing and breakage of particles during analysis; since the movement of a sieve shaker could lead to unwanted breakage. The total mass of particles smaller than 4.75 mm within each sample was divided into two sub-samples by using a riffle splitter according to the manual sampling standard, ISO 18283:2006. The sub-sample was divided again by the riffle splitter; the total mass was now divided into quarters. A quarter of the total mass of material with particle sizes smaller than 4.75 mm within each sample was used for the particle size distribution. This was then recalculated back to the total mass. This was done due to the difficulty in sieving such a large mass of coal at these small sizes without using a sieve shaker. Test sieves, as illustrated in Figure 3.11, were used to determine the PSD of these samples. The final particle size distribution analysis, which was done after the float-sink analysis, was done by using the total mass of material within each density interval sample. During the PSD analysis of each sample, the mass of material remaining on each screen was weighted to determine the mass percentage at each particle size interval.

Figure 3.10: Industrial sieves used for particle size distribution.

Figure 3.11: Test sieves

3.6.2 Densimetric (float-sink) analysis

A densimetric (float-sink) analysis was performed according to the SANS 7936:2010 standard, on each sample of 6 kg to evaluate the relative density distribution of the particles present within the sample. The relative densities of the particles were then correlated to the ash yield, as determined by the proximate analysis described in Section 3.6.3. The ash yield gives an indication of the mineral matter present within the coal samples as discussed in Section 2.1.3, and can thus be used to determine the mineral matter content at each relative density interval. The densimetric analysis was done in two stages, particles of sizes smaller than 1 mm were screened out for densimetric analysis using organic liquids, whilst the densimetric analysis of particles larger than 1 mm was done by using zinc chloride solutions with different relative densities. The reason for this was that zinc chloride and demineralized water are relatively inexpensive compared to the organic liquids. Due to the limited resources, and funding available for this project, is was decided to use the organic liquids only for float and sink tests on particles smaller than 1 mm, as this fraction will only need a small quantity of the expensive organic liquids. Another reason why the densimetric analysis of particles with sizes specific smaller than 1 mm was done by using organic liquids, was that these particle sizes washed through the mesh of the stainless steel buckets used for the float-sink tests with zinc chloride.

Densimetric analysis using zinc chloride:

A bulk dense medium solution consisting of solid zinc chloride (with RD of 2.907), and demineralized water (RD of 1.0), with a relative density of 2.00 was prepared in a 100 litre container by adding the solid $ZnCl_2$ to the demineralized water and stirring. This solution was diluted in 25 L containers to give a range of relative densities from 1.30 to 1.80 in increments of 0.10. A hydrometer and thermometer were used to determine the relative density of each solution. Relative density corrections with regards to the solution temperature and the meniscus correction were made. Temperature corrections were made according to Equations 3-1 and 3-2, where the

correction factor, $C_{T'}$ was calculated by Equation 3-1, where R is the measured density at the temperature, T_0, which the hydrometer is calibrated at, in this case 20°C, and β_g is the volumetric thermal expansion coefficient of the glass the hydrometer was manufactured of, that is $26\times 10^{-6}/°C$. The temperature of the solution as measured by the thermometer is given by T' (Wright *et al*., 2008).

$$C_{T'} = -R\beta_g(T' - T_0) \qquad \textbf{3-1}$$

The actual density of the solution, ρ, is then calculated according to Equation 3-2, where the correction factor is added to measured density at temperature T' (Wright *et al*., 2008).

$$\rho = R + C_{T'} \qquad \textbf{3-2}$$

The coal sample containing particles larger than 1 mm was inserted into the stainless steel buckets as shown in Figure 3.13(d) with a mesh aperture size of 1 mm. The stainless steel bucket containing the sample was carefully placed inside the lightest density (relative density of 1.30) $ZnCl_2$ solution in the 25 L container as illustrated in Figure 3.13(a). Time was allowed for particles to either float or sink. Floats were collected using a hand sieve (Figure 3.13(b)) and were rinsed with demineralized water (Figure 3.13(c)) to ensure that particles are free of $ZnCl_2$. Floating material at a relative density of 1.30 had a relative density less than 1.30, whilst the sinks at a RD of 1.30 had a RD higher than 1.30. After all floats were collected, the solution containing the coal was gently stirred to release material that might be trapped underneath the sinks material, and time was allowed for particles to either float or sink. Floats were again removed, and the process was repeated until no floats were present. The stainless steel bucket containing the coal sample sinks was removed from the $ZnCl_2$ solution with RD of 1.30 (Figure 3.13(d)) and then placed in the $ZnCl_2$ solution with RD of 1.40. The process was repeated until the highest solution density of 1.80 was reached. Again floating material at a relative density of 1.40 thus had a relative density between 1.30 and 1.40 while sinks at a RD of 1.40 had a RD higher than 1.40. Figure 2.16 in Section 2.4.1 gives an indication of the flow diagram used for the +1 mm float and sink tests.

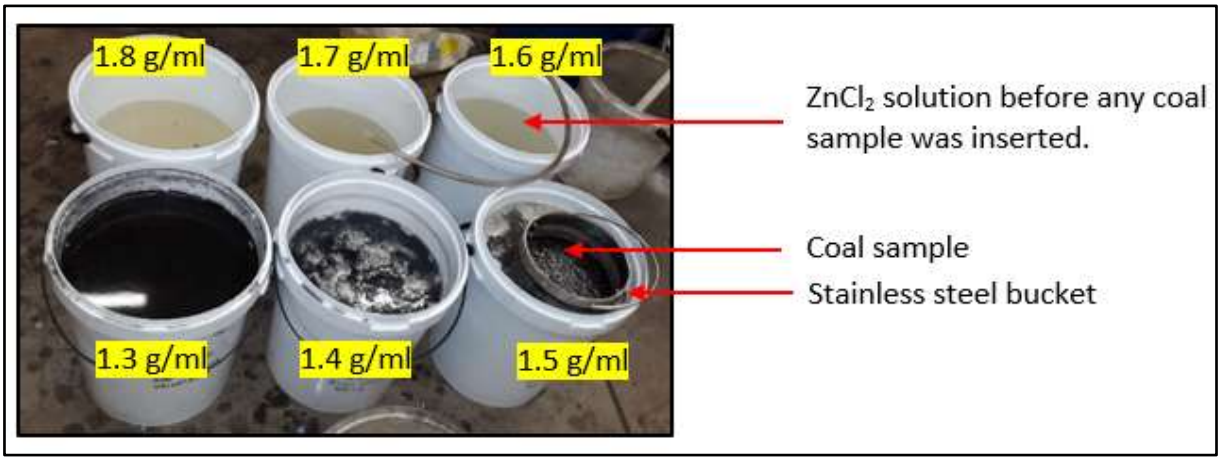

Figure 3.12: Densimetric analysis using a zinc chloride solution.

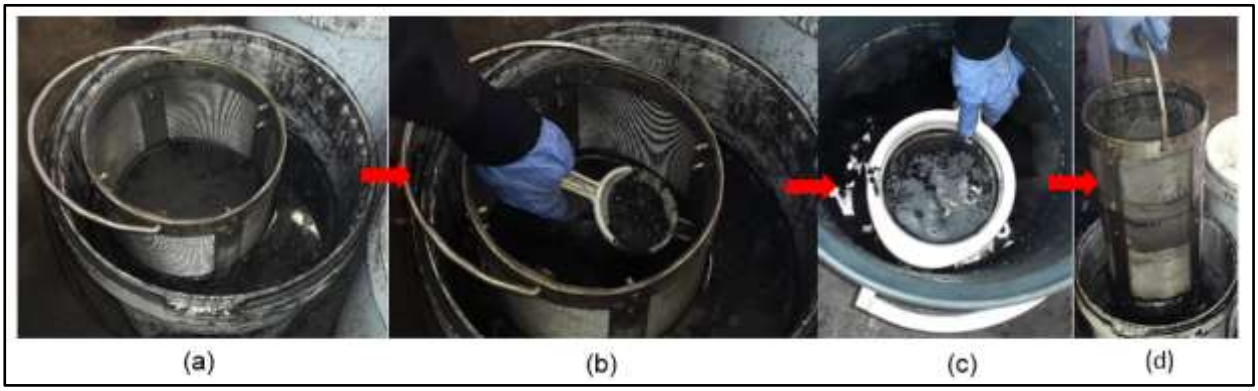

Figure 3.13: Float-sink analysis procedure when $ZnCl_2$ was used.

Densimetric analysis using organic liquids:

The coal sample of particles smaller than 1 mm was divided in half by using a rotary splitter to obtain a smaller quantity of material according to the manual sampling standard, ISO 18283:2006. This was done because of the limited funding, time available, and also due to the high cost of the organic liquids used for the float-sink tests. The sample was placed in the conical square bucket (see Figure 3.14) and the machine was switched on. The vibration of the machine caused particles to move down the chute into 6 sub-sample buckets. This type of splitting ensured a particle size distribution representative of the whole initial sample. To obtain half of the initial sample, either buckets 1, 3 and 5 or buckets 2, 4 and 6 were mixed together, and was used for the densimetric analysis using organic liquids.

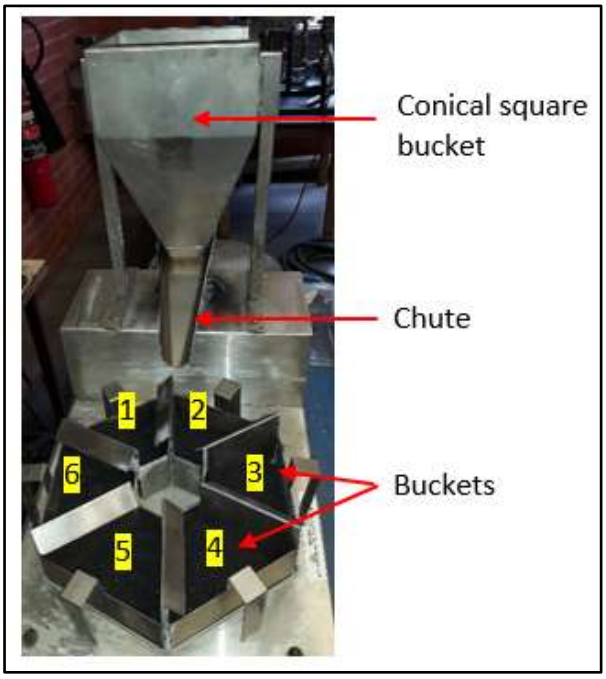

Figure 3.14: Rotary splitter

Organic solutions of white spirits (RD of 0.785) and tetrachloroethylene (RD of 1.62) were prepared to obtain relative densities of 1.30 to 1.60 with increments of 0.10, while solutions of tetrachloroethylene and tetrabromoethane (RD of 2.97) were prepared to obtain relative densities of 1.70 and 1.80. These solutions were prepared in separation funnels held by a stand as shown in Figure 3.15 within a ventilation chamber as a safety precaution. Again, a hydrometer and thermometer was used to determine the relative density of each solution, and relative density corrections with regarding to the solution temperature, and the meniscus correction made. The coal sample containing particles with sizes smaller than 1 mm was inserted by means of a household funnel into the separation funnel holding the lightest solution with relative density of 1.30. Again time was allowed for particles to either float or sink. After separation of the particles occurred, all sinks were drained from the separation funnel, and then the floats were collected. Filter paper and Buchner funnels were used to recover the organic liquid from the coal particles in order to reuse the organic liquids. The floats were rinsed with white spirits, to ensure that particles are free of TBE and TCE. The sinks were inserted into the next separation funnel containing the solution with relative density of 1.40 for which the process was repeated until the highest solution density of 1.80 was reached.

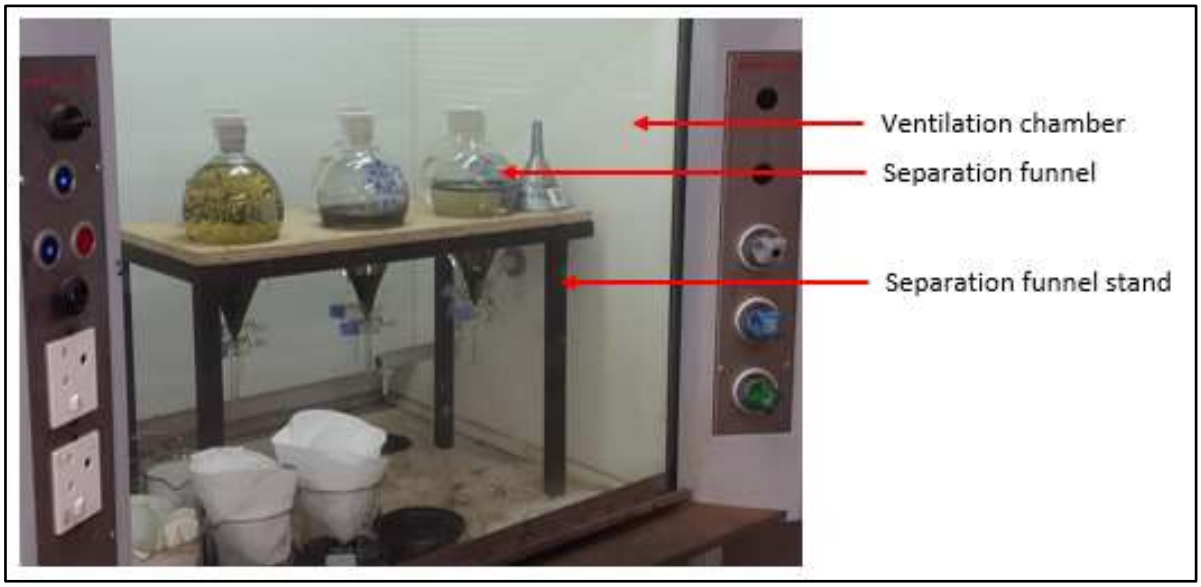

Figure 3.15: Densimetric analysis using organic liquids.

Collected samples within each density interval were placed in suitable containers; aluminium containers were used for samples subjected to organic liquids, as it is a solvent for plastic, and plastic containers were used for samples collected from the highly corrosive $ZnCl_2$ solution. These samples were air-dried in a controlled conditioned environment at a temperature of 22±0.1 °C, and 40 % relative humidity, in order to reach equilibrium moisture to ensure that the moisture basis of each sample was similar.

3.6.3 Other analytical methods

During this study it was assumed that the coal properties, specifically the ash yield, at any given relative density interval was independent of the particle size. This assumption was made since it is impossible to analyse all individual samples due to both the cost and time, and it will be tested and verified in further projects. The experimental run with the breakage mode as impact breakage to a top size of 12.7 mm with no attrition, along with two repetitions was separated by the densimetric analysis described in Section 3.6.2 to obtain samples at the various density intervals. The samples of each density interval were mixed uniformly to provide enough sample to conduct proximate analysis, calorific value analysis and the free swelling index analysis. These analyses were outsourced, and performed by ALS Laboratory Group in Witbank. The standard methods used for each analysis are tabulated in Table 3.4.

Table 3.4: Proximate analysis procedure

Coal property	Standard
Inherent moisture	ISO 11722:2013
Volatile matter	ISO 562:2010
Ash content	ISO 1171:2010
Fixed carbon	Calculated by difference, Equation 2-1.
Calorific value	ISO 1928:2009
Free swelling index/Crucible swelling number	ISO 501:2003

4

CHAPTER 4 RESULTS AND DISCUSSION

This chapter presents results obtained through experimental procedures, and focusses on interpreting these results to achieve the objectives stated in the introduction chapter, Section 1.2. It is important to note that during this study it was assumed that the coal properties, specifically the ash yield, at any given relative density interval, were independent of the particle size. This assumption was made since it is impossible to analyse all individual samples due to the cost and time, and will be tested and verified in further projects. Sample mass loss might have occurred during the experimental procedure, but mass loss was kept to a minimum as far possible. It must be noted that the small sample mass (6 kg) used, might have resulted in potential clouding of the results and trends due to the sample variability.

Graphs and data used for explanation of the experimental results obtained are provided in this chapter. Raw data and processed data are included in Appendix B and Appendix C respectively. Equations used for calculations can be obtained from Appendix D.

4.1 Repeatability and experimental error

The repeatability and accuracy of experimental results are affected by amongst others: the equipment used, measuring instruments, sampling methods, and sample mass. The analyses themselves are relative accurate and reproducible, but variations, or errors, in the sample analytical results might occur, due to the variations in the samples used or the methodology applied during experimentation. The word repeatability refers to a number of experiments done at the same test conditions, and the same parameters to avoid inaccurate results. These are also done to evaluate the effectiveness of the equipment used during experimental procedures. The number of repeats for each breakage experiment are summarized in Section 3.3. Repeats were also done for the proximate analysis, calorific value, and free swelling index determination.

Inaccurate data, and experimental errors were minimized by the following:

- Repeats of experiments for all modes of breakage.
- Weight scales with three decimals to ensure accurate weight measurements.
- Hydrometer readings were corrected for temperature affects, and meniscus corrections were made.

- The sample mass used for densimetric analysis had to be 6000±100 g to prevent inaccurate relative density and particle size distribution results. These minimum mass amounts were received from ALS Witlab, and also conform to ISO 13909:2001, titled "Hard coal and coke – Mechanical sampling.
- All experimental procedures had to adhere SABS/ISO standards.
- Attention was given to significant numbers.

Presenting accurate results was ensured by using the average, standard deviation, and experimental error calculations. All calculations were made within the 95 % confidence interval. Average values ($\tilde{x}$), and standard deviations (S), were determined by Equation 4-1 and Equation 4-2, where x_i is the experimental data point and n the total amount of data points used for the calculation.

$$\tilde{x} = \frac{\sum_1^n x_i}{n} \qquad \textbf{4-1}$$

$$S = \sqrt{(\frac{1}{n-1})\sum_1^n (x_i - \tilde{x})^2} \qquad \textbf{4-2}$$

Error bars with a 95 % confidence interval were calculated by Equation 4-3.

$$Error = 1.96\times(\frac{S}{\sqrt{n}}) \qquad \textbf{4-3}$$

The experimental errors were included in applicable data graphs by using error bars. Repeatability and experimental error data are given in Appendix C. Take note that the standard deviation and experimental errors are given as percentage points implying that it is the percentage difference between experimental data points. Therefore each data point can increase or decrease with the amount as calculated.

The standard deviation for the calorific value (S<3.0) and free swelling index (S<4.0) was good. The experimental error for a 95 % confidence range for the calorific value ($Error$<4.0) and free swelling index ($Error$<5.0) was also good. All standard deviation and experimental error data, including that for the proximate analysis, can be found in Appendix B (Table B.1 and Table B.2) and Appendix C (Table C.207 to Table C.215).

The acceptability of these experimental results, as obtained under repeatability conditions, was checked by using the standard SANS 5725-6:2009. The repeatability limit (r) was calculated by Equation 4-4, where S denotes the standard deviation.

$$r = 2.8 \times S \quad \text{4-4}$$

The proximate analysis, free swelling index and calorific value determination was done only once for the particle size interval of 0.0-1.0 mm, and also only once for the particle size range of 1.0-13.2 mm due to the limited funding available. The absolute difference between the values, x_1 and x_2, as obtained for each particle size interval was calculated. The acceptability of the results was checked according to Equation 4-5. If the absolute difference between the values x_1 and x_2, was smaller than or equal to the calculated repeatability limit, the result was acceptable. If not, two further results were necessary to perform this acceptability check again (SANS 5725-6:2009).

$$|x_1 - x_2| \leq r \quad \text{4-5}$$

The acceptability of the results is summarized in Table C.216 to Table C.218 in Appendix C.

4.2 Coal properties

The physical appearance of the coal samples, for example, brightness, and shape was investigated visually. Figure 4.1 and Figure 4.2 show the progeny (daughter particles) formed due to compression breakage to a top size of 6.7 mm. The shape of the particles are mostly angular and flaky. The relative density samples, F1.3 (material that floated at RD=1.30) and S1.3F1.4 (material that sank at RD=1.30 but floated at RD=1.40), are bright and shiny, and therefore vitrinite-rich. Material in the relative density fraction of S1.8, the material that sank at RD=1.80, have a dark appearance and are dull. The occurrence of bright and dull coal gives an indication of intergranular fracturing and breakage according to the layered structure of the coal.

Figure 4.1: Physical appearance of particles 1.0-6.7 mm.

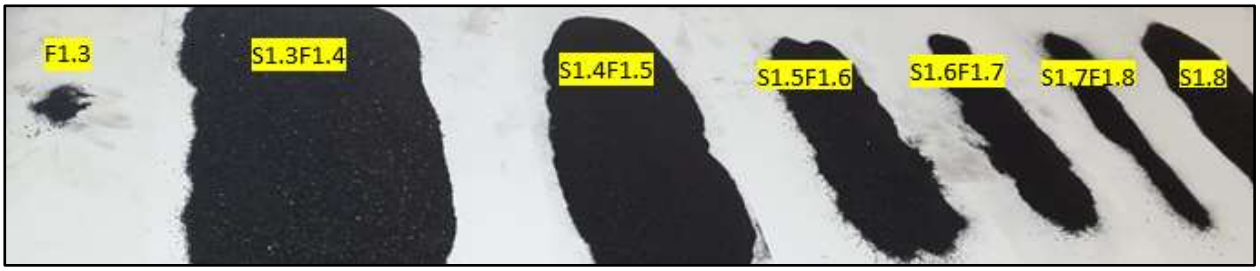

Figure 4.2: Physical appearance of particles 0.0-1.0 mm.

Information obtained visually was restricted. Other analysis, for example the proximate analysis, would give a better indication of the coal properties. The proximate analysis, free swelling index and calorific value determination was done only once for particle sizes smaller than 1 mm, and also only once for particles larger than 1 mm due to the limited funding available. Particles smaller than 1 mm thus refers to the particle size interval of 0.0-1.0 mm while particles larger than 1 mm is within the particle size range of 1.0-13.2 mm. The sampling method used was explained in Section 3.6.3. It was assumed that the mineral- and maceral abundances remained constant in all particle size intervals. It is accepted that this assumption is unlikely to be valid, but this had to be done in the absence of any other supporting data. There might be some variation in the calorific value and the ash yield for a given relative density fraction, because of the change in particle sizes due to the nature of the coal macerals and the mineral matter.

4.2.1 Proximate analysis

Proximate analysis results indicating the coal properties, namely, inherent moisture, ash, volatile matter, and fixed carbon can be seen in Appendix B. Table B.1 and Table B.2 give these properties for particles in the 0.0-1.0 mm and 1.0-13.2 mm size fractions respectively. The inherent moisture and ash will be discussed in detail since these properties is of importance for this study.

4.2.1.1 Ash yield

It is important to note that the term “ash yield” was used instead of “ash content” throughout this study. This is because “ash yield” refers to the non-combustible residue of mineral matter content. The ash yield can, therefore, be related to the mineral matter content in the coal before combustion, as explained previously in Section 2.1.3. During this study, the ash yield will be used to evaluate the amount of mineral matter present in the coal at each relative density interval.

Figure 4.3 shows the ash yield obtained during the proximate analysis for each relative density interval. Error bars are used to indicate the experimental error for a 95 % confidence range.

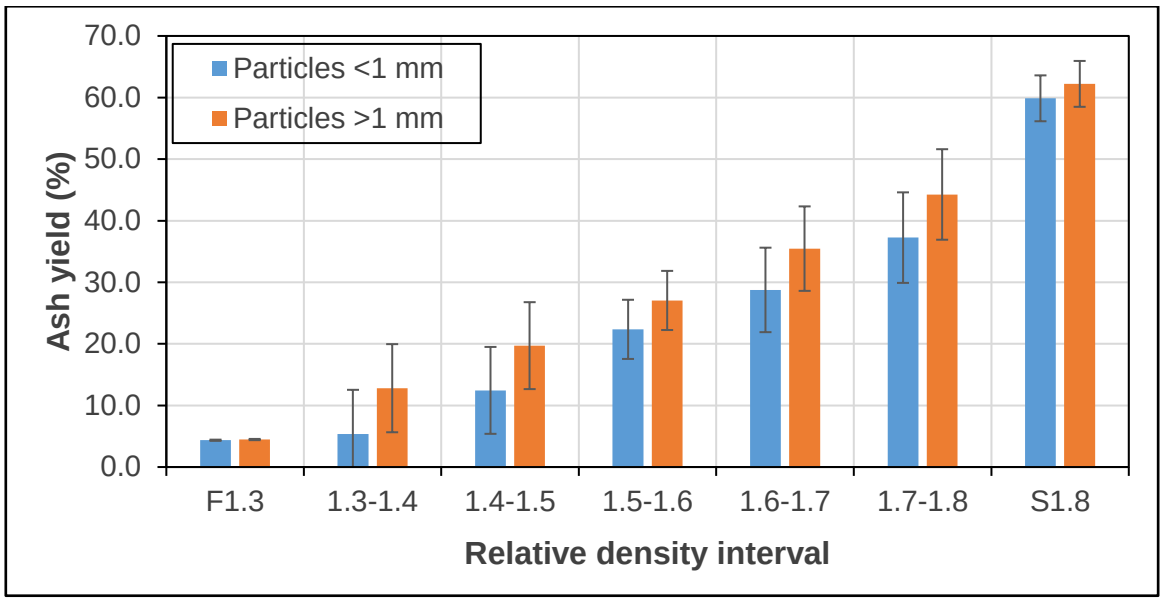

Figure 4.3: Ash yield for each relative density interval expressed on a dry basis.

It was observed that the ash yield increased with increasing relative density (RD). It can consequently be assumed that the mineral matter content of the coal increased with increasing RD. This was expected, since pure coal has a relative density of 1.2-1.4, whilst that of mineral matter varies from 2.0 to approximately 5.0 (Speight, 2005:94). Particles with a relative density of less than 1.4 are thus almost pure coal macerals, and may contain very low mineral matter content, while particles with RDs of higher than 1.8 are mainly minerals although they may contain very small grains of coal macerals. The relative densities in between these values, that is from RD=1.4 to RD=1.8, indicate the ash yield of composite particles, or middlings, containing both coal macerals and mineral matter. The mineral matter fraction of the composites increases as the relative density increases, for example, the relative density interval 1.6-1.7 contains a higher amount of mineral matter and less coal macerals, than the relative density interval of 1.5-1.6. Particles smaller than 1 mm had slightly less ash yields than that for particles larger than 1 mm, but the error bars still overlapped with the ash yield obtained for particles larger than 1 mm.

During a study done by Lakshminarayana (2015), an ash yield of 40-54 % for the Moatize coal seams was observed. When comparing these values to those illustrated in Figure 4.3, it can be seen that only the relative densities higher than 1.7 reached an ash yield of 40 % and higher. Relative density intervals between 1.3-1.7 had an ash yield of less than 40 %, which can be ascribed to the fact that the ash analysis during this study was done on a coal sample that had already been subjected to size reduction as described in Section 3.6, and was not done on a raw coal sample as done by Lakshminarayana (2015). Liberation of the coal macerals from the mineral matter had thus occurred during size reduction of a raw coal sample leading to a very high ash yield at relative densities higher than 1.8.

4.2.1.2 Inherent moisture

Figure 4.4 presents the inherent moisture results of Moatize coal as determined during the proximate analysis. Inherent moisture refers to the retained moisture within pores in the coal particle after all surface moisture has been removed (Falcon & Ham, 1988). Error bars are included according to a 95 % confidence range.

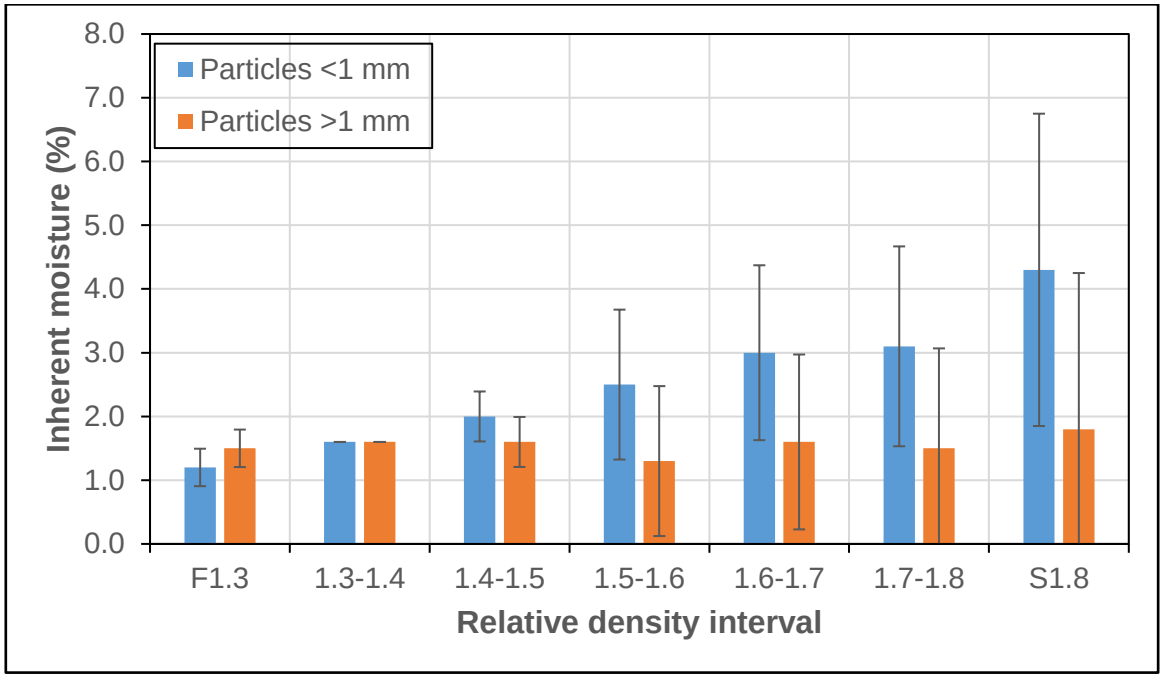

Figure 4.4: The inherent moisture of Moatize coal expressed on an air dry basis.

It can be seen from Figure 4.4 that the inherent moisture varies between 1.2 % and 4.3 %. These values correlate well with the inherent moisture varying between 1.3 % and 3.5 % as found during a study done by Lakshminarayana (2015). The coal qualities for each seam of the Moatize coalfield are summarized in Table 2.6 in Section 2.2.2.

It was also noted that particles smaller than 1 mm had an increase in inherent moisture with an increase in relative density, while particles larger than 1 mm had a consistent inherent moisture regardless of the relative density interval. The increase in inherent moisture, with the increase in relative density, for particles smaller than 1 mm can either be because of the type of mineral matter, or the type of coal macerals, present in the fraction smaller than 1 mm. Inertinite macerals have a higher macroporosity than vitrinite macerals, and therefore may contain higher inherent moisture within the pores (Campbell *et al*., 2013). Inertinite tends to comprise of more oxygen functional groups than vitrinite. Due to the oxygen functional groups, there are more hydrophilic sites present in the inertinite (Campbell *et al*., 2013). Unfortunately, the Moatize coal consist of minor amounts (<5.0 %) of inertinite (Dorland, 2016). The properties of the minerals present in the material may also affect the inherent moisture. Clay minerals, for example, possess high

proportions of moisture within their crystalline structure (Falcon & Ham, 1988). The presence of clay minerals may also result in an increased moisture adsorption (Campbell *et al*., 2013). Mineral moisture refers to moisture that forms part of the crystal structure of hydrous silicates, for example, clay minerals (Mahapatra, 2015).

When comparing Figure 4.4 with Figure 4.3, it can be seen that although the particles smaller than 1 mm have higher inherent moistures than particles larger than 1 mm, the particles smaller than 1 mm have lower ash yields than that for particles larger than 1 mm. The possibility that the presence of mineral matter in the size fractions smaller than 1 mm was responsible for the increase the inherent moisture can therefore be eliminated. If it was due to the presence of mineral matter, the ash yield would have reflected it by having a higher ash yield for the particles smaller than 1 mm compared to that for the particles larger than 1 mm. The particles smaller than 1 mm are thus liberated macerals.

4.2.2 Free swelling index

The free swelling index gives an indication of the expandability of coal, and the potential of the coal to be used for the production of coking coal (Falcon & Ham, 1988). Figure 4.5 summarizes the free swelling index for each relative density interval. Error bars are included according to a 95 % confidence range. Again as abovementioned, particles smaller than 1 mm refers to the particle size interval of 0.0-1.0 mm while particles larger than 1 mm is within the particle size range of 1.0-13.2 mm.

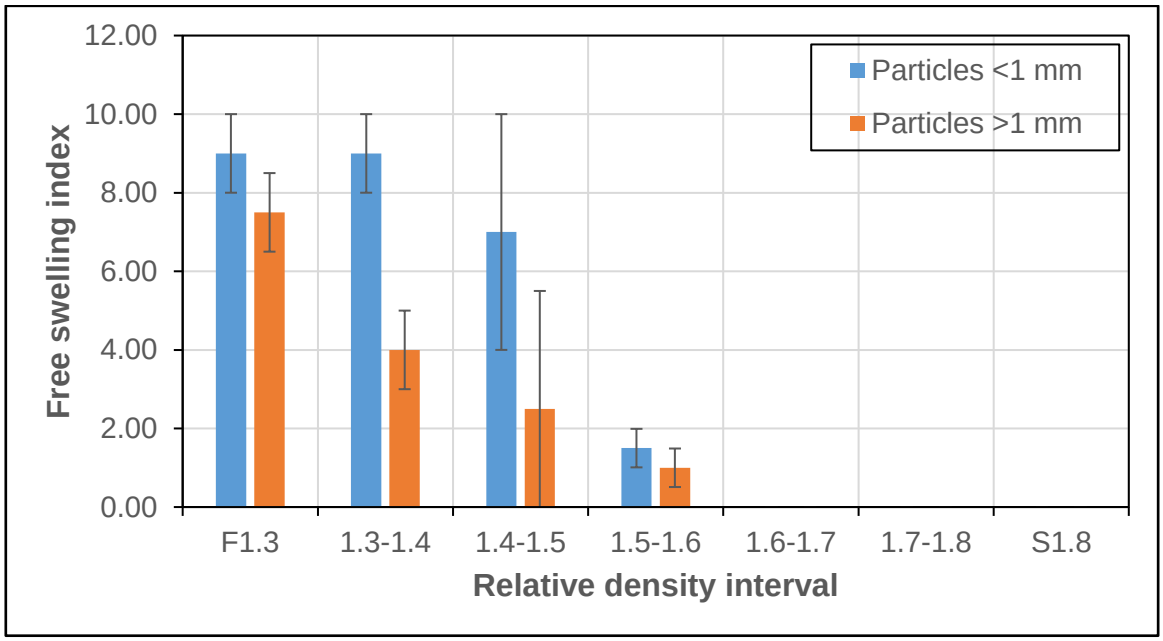

Figure 4.5: Free swelling index results.

As seen in Figure 4.5, relative density intervals of 1.6 and greater had a free swelling index of 0 (zero) meaning that these material are non-coking. This graph was compared with Figure 4.3 presenting the ash yield at each relative density interval. High ash yields, thus high amounts of mineral matter content, at the relative densities of 1.6 and greater were observed. The reason for a free swelling index of 0 at these densities can be ascribed to the large amounts of mineral matter present, as reflected by the high ash yields at relative densities of 1.6 and greater.

Figure 4.5 illustrates that the free swelling index increases with a decrease in relative densities from 1.6 and lower. Southern African coking coals typically have a free swelling index greater than 8, and a free swelling index of greater than 2.5 indicates blend coking coals (Powell, 2016). These free swelling index values were kept in mind when evaluating Figure 4.5. The material with particles sizes smaller than 1 mm, and occurring within the relative density range of less than 1.4, have a free swelling index of 9.0; demonstrating that this fraction are strongly coking coals, and of very high value. Material within the same relative density range (RD of less than 1.4), but with particle sizes larger than 1 mm also had a relative high free swelling index varying between 4.0 and 7.5, thereby suggesting fair to good coking properties.

The relative density ranges of 1.3-1.6 contain composite particles of coal macerals and mineral matter. Higher amounts of mineral matter will lower the free swelling index of coal, for example, the relative density range of 1.5-1.6 contain coal macerals responsible for the free swelling index, but also contain a high ash yield as illustrated in Figure 4.3, thus the high mineral matter content causes the free swelling index to be lower. Whereas the relative density interval of 1.3-1.4 has a very high free swelling index, indicating that material in this density interval consist mainly of coal macerals, and may contain only small grains of minerals. The reason for the large error bands can be ascribed to the presence of two relatively “pure” sources of material i.e. macerals and mineral matter. It might also be because of sampling errors or analytical errors.

It can also be seen that particles smaller than 1 mm have a much higher free swelling index than particles larger than 1 mm; thus confirming the theory in Section 4.2.1 that the particles smaller than 1 mm are liberated macerals.

From the free swelling index data, it can be seen that Moatize coal, specifically from the Chipanga Seam, exhibits very good coking characteristics, and may be suitable for coking purposes, if the high value coal can be liberated from the mineral matter. It must be kept in mind that the ash yield must be 10% or less to be suitable for coking purposes (Falcon & Snyman, 1986; Kruger, 2013).

4.2.3 Calorific value

Figure 4.6 indicates the calorific value obtained for material from each relative density interval. The calorific value is a measure of the “heat energy” the coal is able to produce (Falcon & Ham, 1988). Again, particles smaller than 1 mm refers to the particle size interval of 0.0-1.0 mm, while particles larger than 1 mm are within the particle size range of 1.0-13.2 mm.

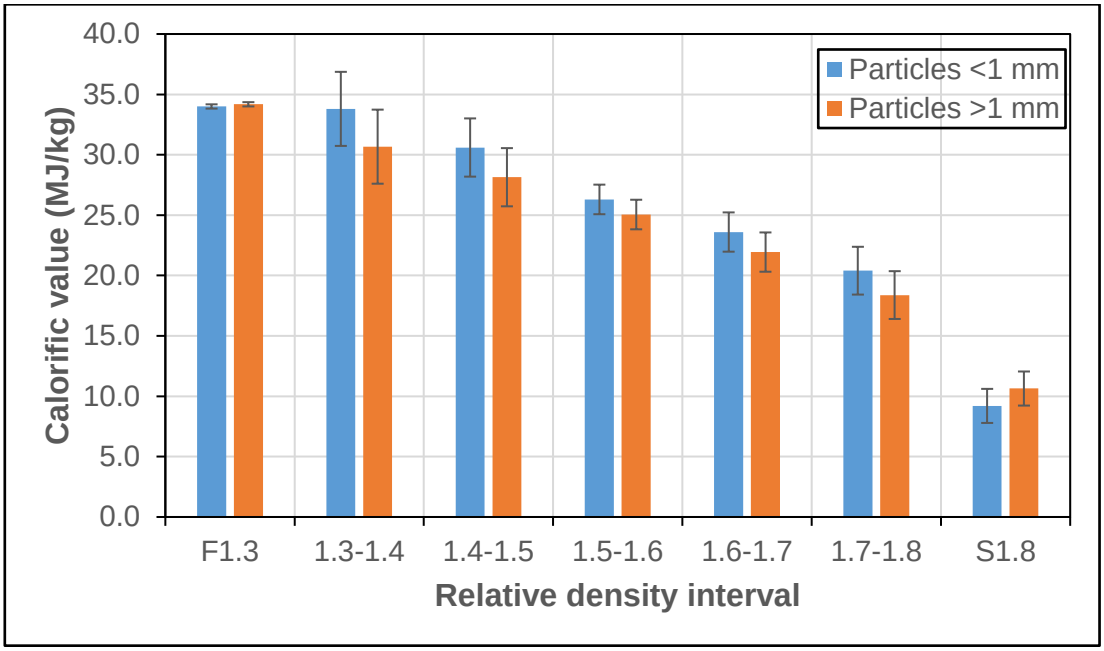

Figure 4.6: Calorific value results.

The calorific value of the material increases as the relative density of the material decreases as illustrated in Figure 4.6. This can be correlated to Figure 4.3 representing the ash yield at each relative density interval, which shows an inverse relationship with respect to the relative density, *i.e.* the ash yield, and thus the mineral matter, increases with an increase in the relative density. For most Southern African coals, the calorific value decreases with an increase in the ash yield or mineral matter content. This was expected since mineral matter lowers the calorific or heating value of coal as it is incombustible. Higher amounts of mineral matter are present at higher relative density intervals causing the calorific value to be lower.

The particles smaller than 1 mm have higher calorific values than that for particles larger than 1 mm. This can again be ascribed to liberated coal macerals. Coal fines are generated during the size reduction processes, but these fines will be of a high quality. Figure 4.6 also shows that very little differences between the two size ranges existed, as was noted with the ash and free swelling index results.

4.3 Impact breakage

Impact breakage was performed by varying the top size of particles as well as varying the residence time for attritioning. Various curves were constructed from the experimental data obtained, and will be used to explain the effect of the two different top sizes, and three residence times for attritioning on the particle size distribution, relative density intervals, and liberation of coal from mineral matter.

4.3.1 Top size

Impact breakage was performed to top sizes of 13.2 mm and 6.7 mm as explained in Section 3. These top sizes were chosen based on the required sizes for industrial application, and to minimize fines generation. The top sizes will be compared by means of graphs to evaluate the effect of the top sizes on the liberation of coal from mineral matter and the coal yield enhancement.

Figure 4.7 is the size by washability graph for impact breakage to a top size of 13.2 mm with no additional attritioning while Figure 4.8 is the size by washability graph for impact breakage to a top size of 6.7 mm with no additional attritioning. It presents the mass distribution of the whole sample as a percentage according to its relative density and particle size distributions. The reason for the mass distribution percentage of 20.0 % on the y-axis was to enable easy comparison of the size by washability graphs with one another as well as with the size by washability graph of the raw coal, Figure 3.3. Although the top particle size on the x-axis of Figure 4.8 should be 6.7 mm, it was decided to keep the particle sizes similar to that of Figure 4.7 for ease of readability and comparison.

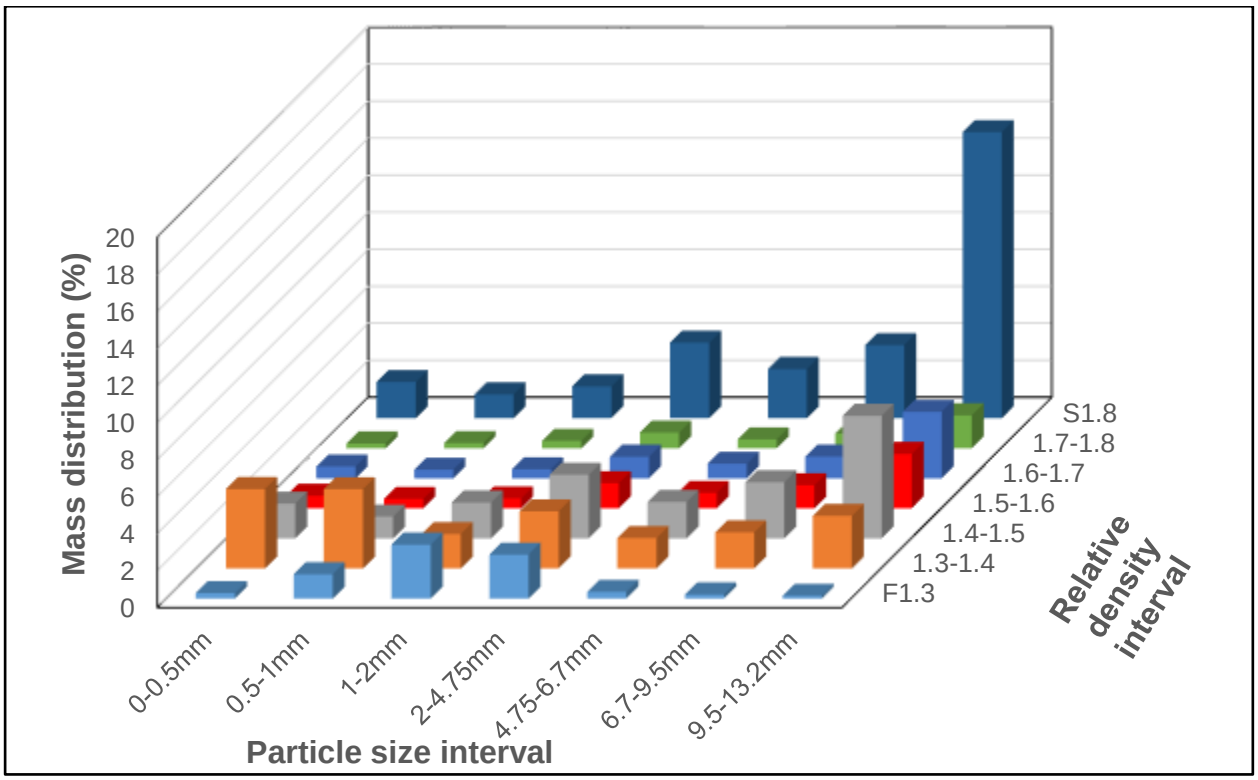

Figure 4.7: Size by washability graph for impact breakage to a top size of 13.2 mm with no additional attrition breakage.

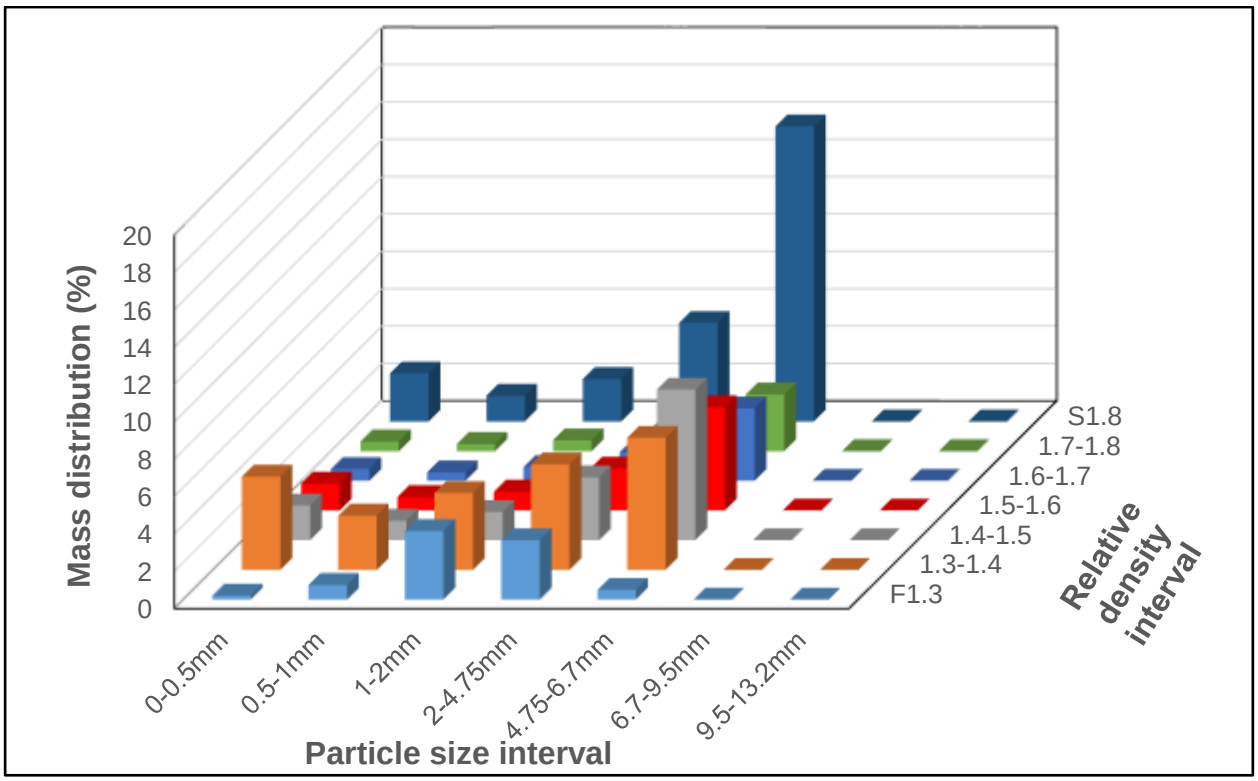

Figure 4.8: Size by washability graph for impact breakage to a top size of 6.7 mm with no additional attrition breakage.

This study focuses on the material with a relative density of 1.4 or less because of the relatively “clean” coal at these densities. Material occurring in this relative density range (RD<1.4) are already liberated coal macerals, and are almost pure coal macerals, but may contain very small grains of mineral matter. The material occurring in the relative density interval F1.3, that is material with a relative density lower than 1.3, will be discussed first. When comparing the material at a relative density of less than 1.3 in Figure 4.7 and Figure 4.8, it was observed that this material mainly occurred in the particle size range of 1.0-4.75 mm. The mass distribution percentage of material with a relative density less than 1.3 showed a slight increase in breakage to a top size of 6.7 mm when compared to the top size of 13.2 mm. This material is liberated coal macerals, as discussed in Sections 4.2.2 and 4.2.3. The mass distribution percentages of impact breakage to these top sizes are a little higher than that for the raw coal as given in Figure 3.3.

Next the relative density interval of 1.3-1.4 for each top size will be compared. Material occurring in this relative density interval is more or less evenly distributed throughout the particle sizes with slight peaks at some particle size intervals. When comparing Figure 4.7 and Figure 4.8, it was observed that breakage to a top size of 6.7 mm resulted in a relative higher yield of material with relative density of 1.4 and less, than breakage to a top size of 13.2 mm. This can be ascribed to the exposure and liberation of vitrinite-rich material when breakage is done to a smaller top size (6.7 mm).

Middlings, or composite material, containing coal macerals as well as mineral matter occur in the relative density ranges of 1.4-1.8. It can be seen from Figure 4.7 and Figure 4.8 that this material mainly occurs in the larger particle size ranges. A large amount of middlings (RD varying between 1.4 and 1.8) with particle sizes 6.7-13.2 mm are still present after breakage to a top size of 13.2 mm. When further reduced to a top size of 6.7 mm, more coal macerals may have been liberated from the mineral matter, resulting in a yield increase for material in the relative density range lower than 1.4.

When comparing Figure 4.7 and Figure 4.8, it can be seen in both graphs that the material with a relative density of greater than 1.8, that is S1.8 fraction, mainly occurs within the larger particle size ranges regardless of the top size of breakage. For the breakage to a top size of 13.2 mm this material occurred within the particle size interval of 9.5-13.2 mm, while for a breakage to a top size of 6.7 mm it occurred in the 4.75-6.7 mm particle size range. It is important to bear in mind that the ash yield for each relative density range can be correlated to the mineral matter present in the material as explained in Section 4.2.1. It was seen that the ash yield, or mineral matter, increases as the relative density of the material increase. The material with a relative density greater than 1.8 can thus be referred to as mainly mineral matter. Minerals are usually more difficult to break than coal (Shi, 2014) leading to relatively large particles formed, and is thus responsible for the high amount of material at a particle size interval of 9.5-13.2 mm and at relative

density greater than 1.8. Material with a relative density greater than 1.8 will have very high mineral matter content and low coal maceral content. This can either be upgraded by beneficiation processes to recover small grains of coal macerals that might be present, or it can be considered to be discarded.

4.3.2 Effect of attrition breakage additional to impact breakage

Attrition breakage additional to impact breakage was performed in some cases. Residence times in the unit used for the attrition breakage was either 1, 2 or 5 minutes. It was expected that different residence times for attrition breakage would result in different degrees of liberation of coal from mineral matter. Attrition breakage additional to the initial breakage mode would ensure further liberation by chipping off the vitrinite-rich material exposed by the initial breakage mode. The effect of attrition breakage on the mass distribution according to relative density and particle size distribution was investigated. Figure 4.9 displays the size by washability graph for impact breakage to a top size of 13.2 mm followed by attritioning for a residence time of 5 minutes.

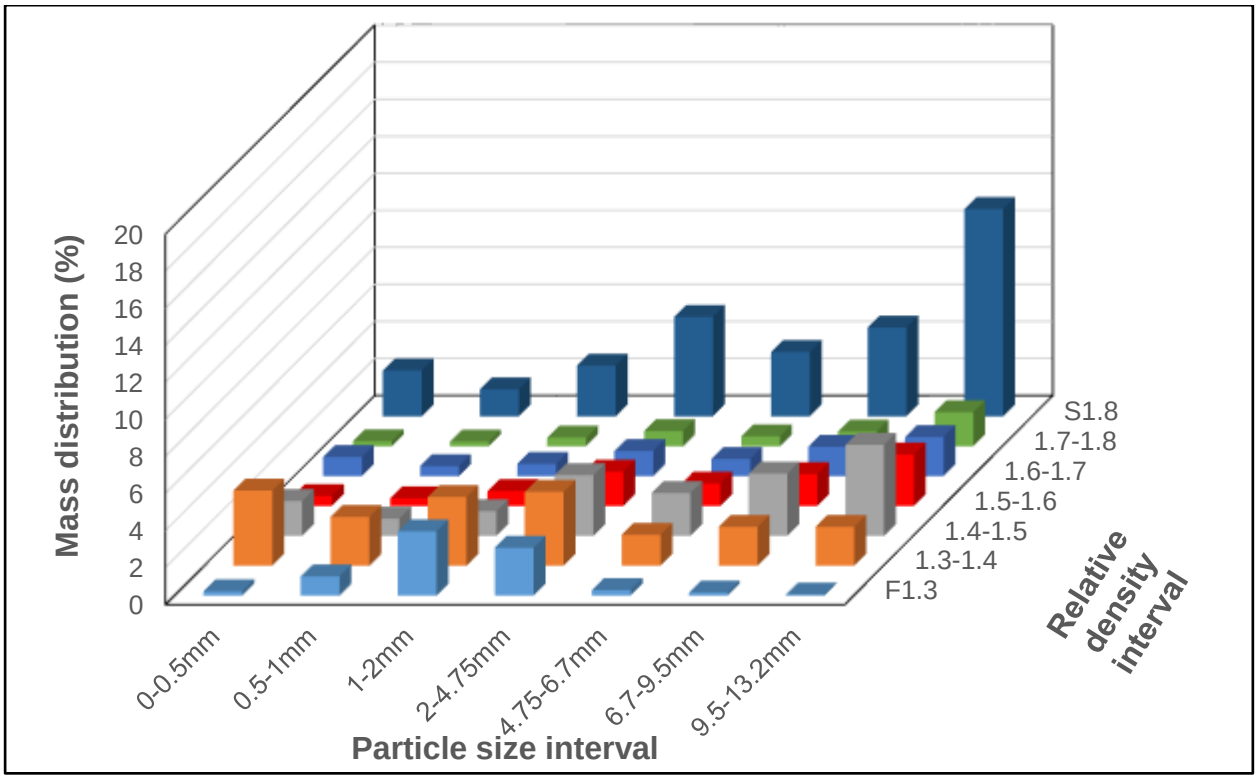

Figure 4.9: Size by washability graph for impact breakage to a top size of 13.2 mm followed by additional attrition breakage for 5 minutes.

When comparing Figure 4.9 with Figure 4.7, showing impact breakage to a top size of 13.2 mm with no attritioning, it was seen that attrition breakage for a residence time of 5 minutes had no fundamental effect on the mass distribution according to its density and particle sizes. Size by washability graphs for impact breakage to a top size of 13.2 mm followed by attritioning for

1 minute and 2 minutes can be obtained from Appendix C. These graphs also showed similar results as for impact breakage to a top size of 13.2 mm with 5 minutes attritioning.

Figure 4.10 shows the size by washability graph for impact breakage to a top size of 6.7 mm followed by attrition breakage for a residence time of 5 minutes.

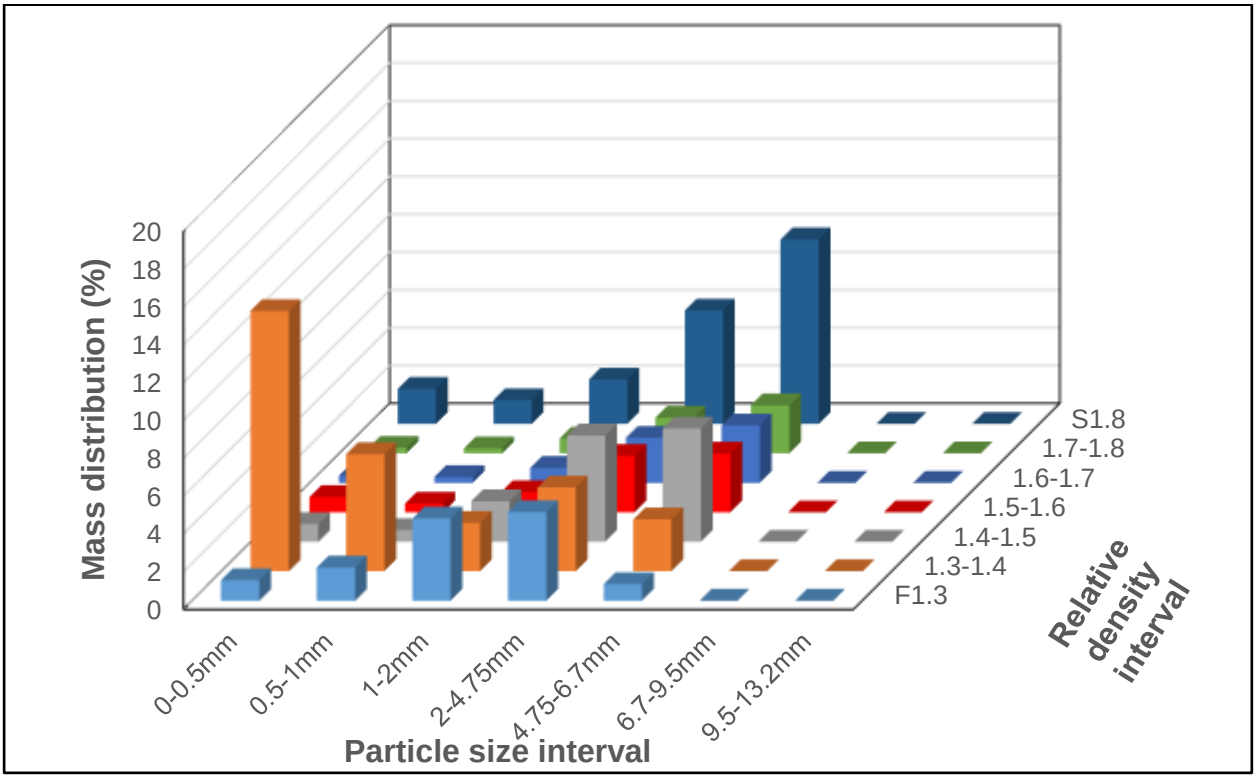

Figure 4.10: Size by washability graph for impact breakage to a top size of 6.7 mm followed by additional attrition breakage for 5 minutes.

Although attrition breakage after impact breakage of 13.2 mm had no noticeable effect on the mass distribution of the material according to its relative density and particle sizes, this was however, not the case for attritioning after impact breakage to a top size of 6.7 mm. When comparing Figure 4.10 with Figure 4.8, showing the mass distribution of impact breakage to a top size of 6.7 mm without attrition breakage, it can be seen that the mass distribution was altered by the attrition breakage. An increase in mass in the relative density ranges F1.3 and 1.3-1.4 was observed after attritioning was performed. This is because breakage to the smaller top size of 6.7 mm exposed more of the coal macerals, which was then further released or liberated during attrition breakage after the initial impact breakage. Exposure of the coal macerals on the outer layer of the particles might have occurred during breakage to a top size of 6.7 mm. This might have increased liberation of the brittle vitrinite-rich fraction when attritioning was performed. Breakage to a top size of 13.2 mm was too coarse to expose all coal macerals entrapped between mineral materials. Size by washability graphs for attritioning residence times of 1 minute and 2 minutes can be obtained from Appendix C. These curves had similar results as Figure 4.10.

4.4 Compressive breakage

Compressive breakage was performed to similar top sizes (6.7 mm and 13.2 mm) as for impact breakage. Attrition breakage at different residence times (1, 2 and 5 minutes) was also performed in addition to compressive breakage in some cases. As for impact breakage, the effect of these variables on coal liberation and yield improvement will be discussed.

4.4.1 Top size

Figure 4.11 and Figure 4.12 give the size by washability graphs for compressive breakage to top sizes of 13.2 mm and 6.7 mm, respectively. These experimental runs had no additional attrition breakage following the initial compressive breakage. The size by washability graphs show the mass percentage of the whole sample as distributed according to its relative density and particle size distribution. The mass distribution percentage (y-axis) will once again reach 20 % for ease of readability and easy comparison with other graphs. Although the top size for breakage of Figure 4.12 was 6.7 mm, the sizes on the x-axis will be up to 13.2 mm as for Figure 4.11 for easy comparison.

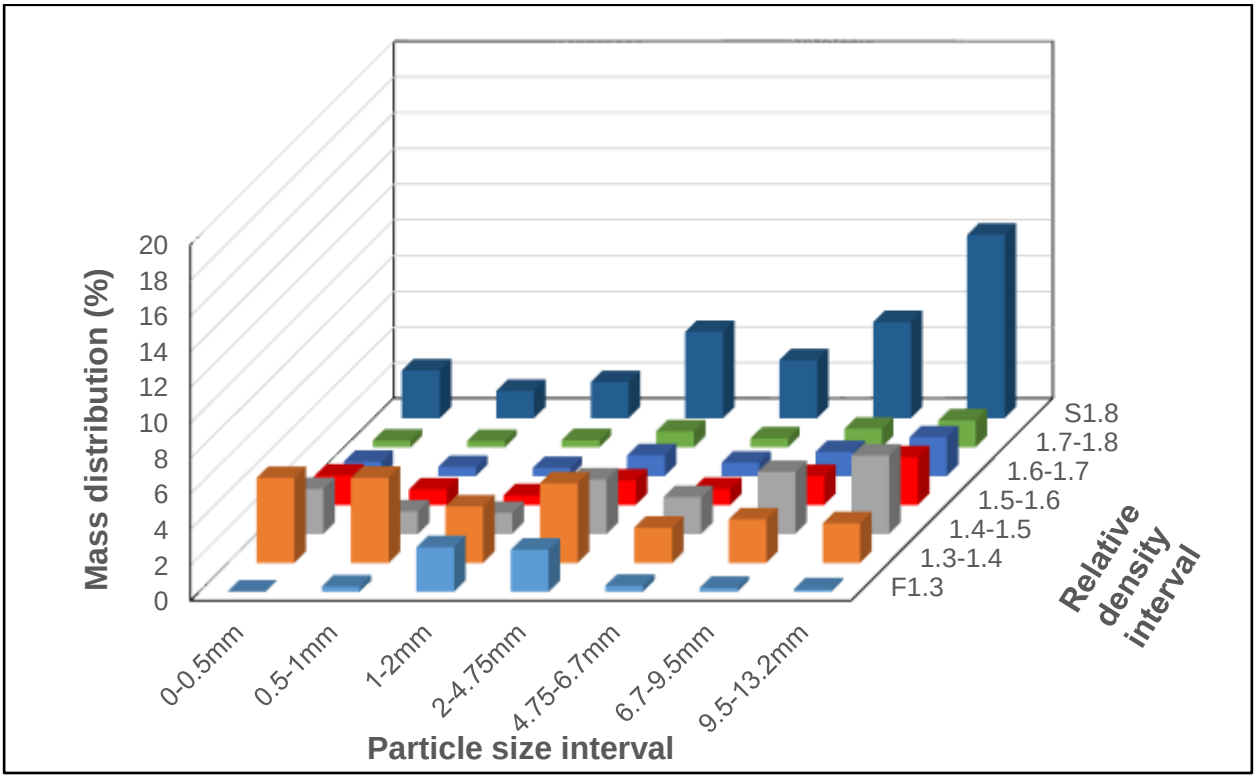

Figure 4.11: Size by washability graph for compressive breakage to a top size of 13.2 mm with no additional attrition breakage.

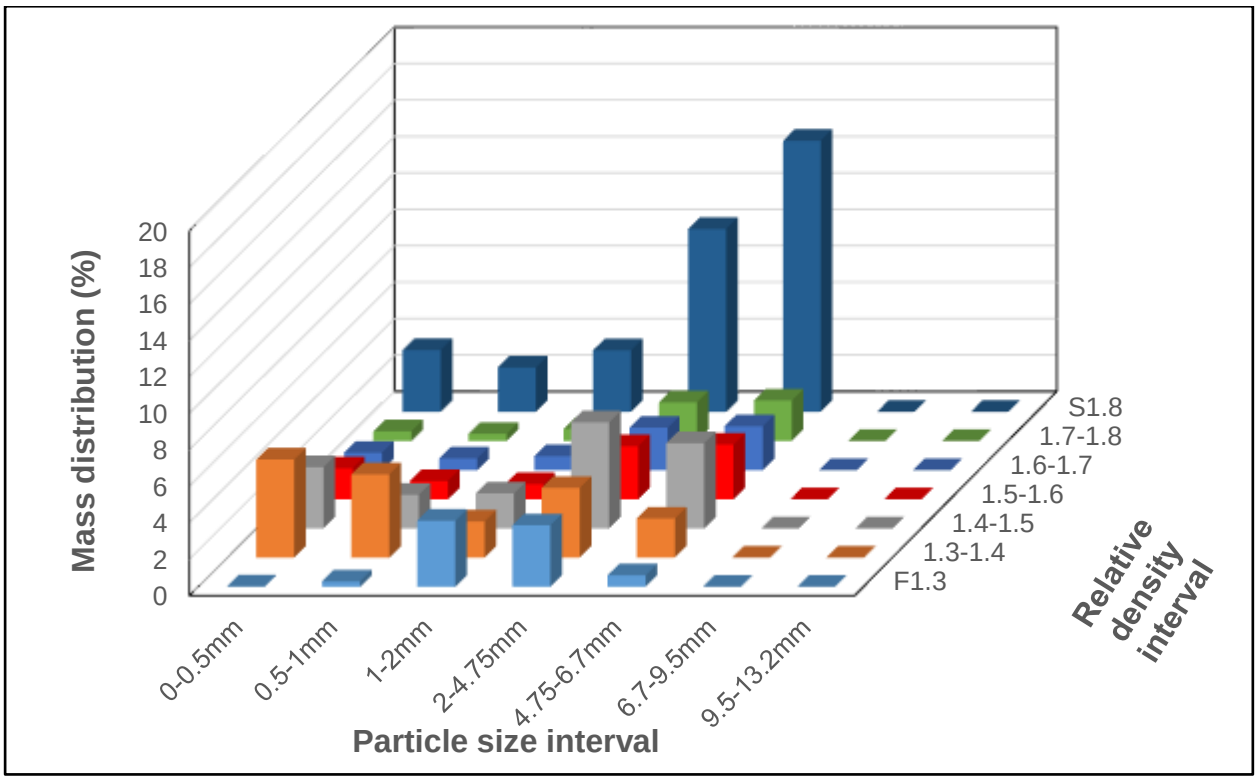

Figure 4.12: Size by washability graph for compressive breakage to a top size of 6.7 mm with no additional attrition breakage.

As explained in Section 4.3, focus was set on the material with relative density of 1.4 and lower due to the “clean” coal at these relative densities. Material with relative density of less than 1.3 will firstly be discussed followed by material in the relative density range of 1.3-1.4. As for impact breakage, material with a relative density of less than 1.3 mainly occurred in the particle size range of 1.0-4.75 mm. When comparing the amount of material in this relative density range, it can be seen that there was a slight increase in the amount of material by breakage to a top size of 6.7 mm compared to a top size of 13.2 mm. Therefore, compressive breakage to a smaller top size of 6.7 mm resulted in a higher amount of liberated coal macerals than that for a top size of 13.2 mm. Compressive breakage to a top size of 13.2 mm had no increase in the amount of material occurring in the relative density interval of 1.3 and lower compared to that of raw coal as given in Figure 3.3.

Material in the relative density range of 1.3-1.4 is more or less equally distributed among the particle size intervals with slight peaks in some particle size ranges, as was observed for impact breakage. When comparing the material with relative density of 1.3-1.4 in Figure 4.11 with Figure 3.3 (Size by washability graph for raw coal), it was observed that there was a small increase in the amount of material in each particle size range when compressive breakage was applied to a top size of 13.2 mm. Breakage to a top size of 6.7 mm resulted in an greater increase in the material occurring in the relative density range of 1.3-1.4, compared to the top size of 13.2 mm. Therefore compressive breakage to a smaller top size of 6.7 mm resulted in higher yield of

material in the relative density range of 1.4 and lower. However, this increase was not as great as that for impact breakage to a top size of 6.7 mm.

Composite particles with relative densities of 1.4-1.8 mainly occurred in the larger particle size ranges as for impact breakage. The yield of “clean” coal with relative density of 1.4 and lower can be enhanced by further size reduction of these composites to liberate more coal from the mineral matter. As illustrated in Figure 4.11 and Figure 4.12, material with relative density greater than 1.8 occurred in the larger particle size intervals of either 9.5-13.2 mm or 4.75-6.7 mm depending on the breakage top size. Again, a similar observation was made for impact breakage. As explained in Section 4.3.1, it can be said that these material are mostly mineral matter due to the high relative density. Mineral matter is harder to break or crack, and it was expected that this would occur in the coarser particle size ranges.

When comparing impact breakage and compressive breakage, with no additional attrition breakage, it was observed that compressive breakage generated more fines (-0.5 mm) than impact breakage. This can be ascribed to the compressive forces that were applied directly to the surface of the particles as explained in Section 2.3.2.2.

4.4.2 Effect of additional attrition

Attrition breakage additional to compressive breakage was done for residence times of 1, 2 or 5 minutes. Figure 4.13 indicates the mass distribution as a percentage according to relative density and particle size for compressive breakage to a top size of 13.2 mm followed by attrition breakage for 5 minutes.

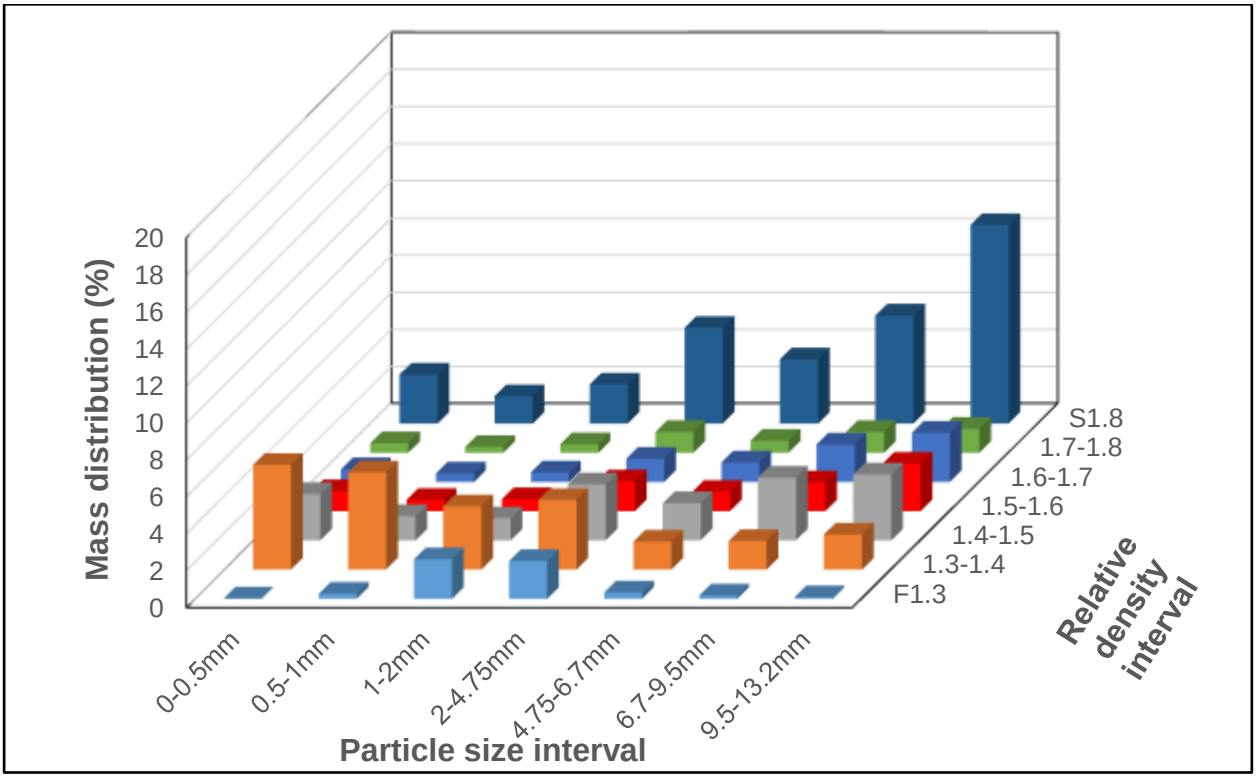

Figure 4.13: Size by washability graph for compressive breakage to a top size of 13.2 mm followed by additional attrition breakage for 5 minutes.

To see the effect of attrition breakage additional to compressive breakage to a top size of 13.2 mm, Figure 4.13 can be compared with Figure 4.11 showing compressive breakage to a top size of 13.2 mm with no attrition breakage. It can be concluded that attritioning following compressive breakage to a top size of 13.2 mm had an insignificant effect on the mass distribution of the material. Size by washability graphs for attritioning times of 1 and 2 minutes also had no effect on the size by washability mass distribution and can be seen in Appendix C.

The effect of attrition additional to compressive breakage to a top size of 6.7 mm will be evaluated by comparing Figure 4.14 with Figure 4.12 showing the mass distribution of material subjected to compressive breakage to a top size of 6.7 mm with no attrition breakage.

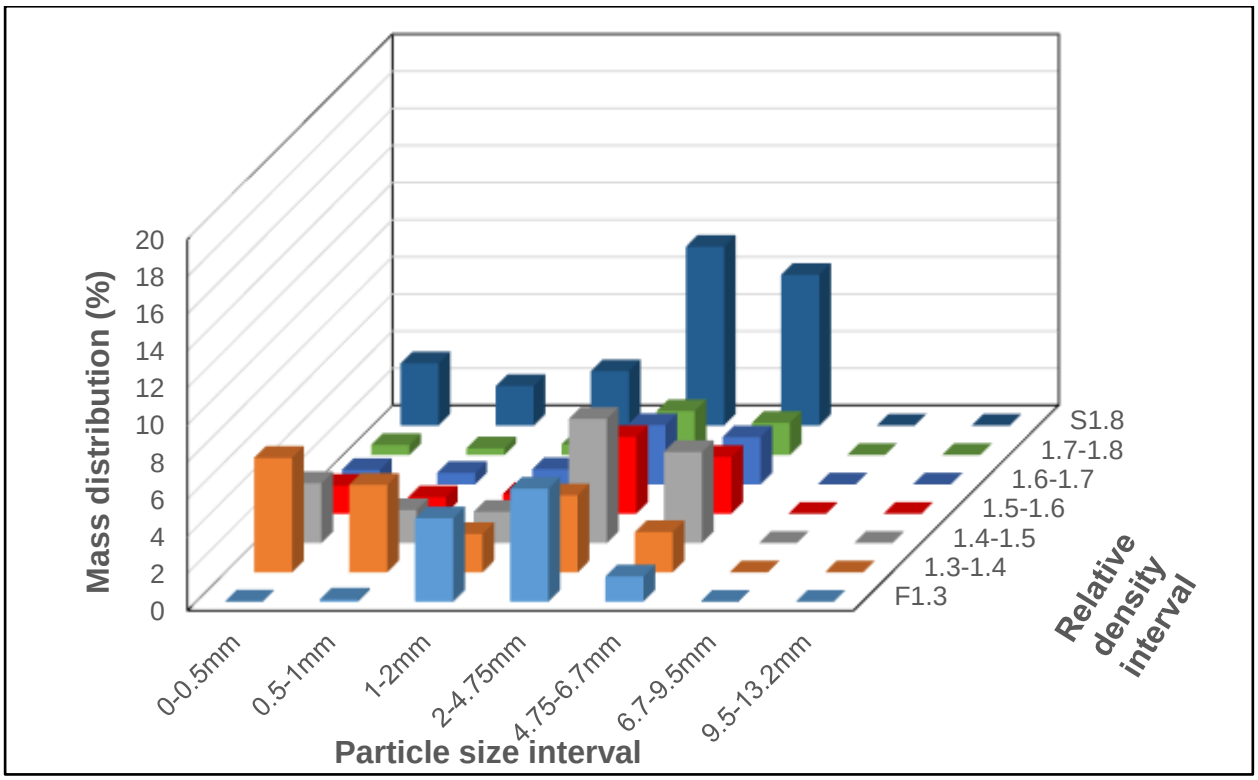

Figure 4.14: Size by washability graph for compressive breakage to a top size of 6.7 mm followed by additional attrition breakage for 5 minutes.

Material with a relative density greater than 1.8 showed a decrease in the particle size range of 4.75-6.7 mm while material with relative density lower than 1.3 and particle sizes of 2-4.75 mm slightly increased. Again, this can be attributed to the exposure of coal macerals on the outer layer of the particles after compressive breakage. Attritioning therefore resulted in an increase in liberation by chipping off the exposed material. There was no noticeable difference in the other relative density ranges. Size by washability graphs presenting the effect of attritioning for 1 minute and 2 minutes gave similar results and are included in Appendix C.

4.5 Ash yield

As discussed in Section 2.1.3, the formation of the undesirable ash by-product during coal combustion is accompanied by various problems including decreasing the calorific value of the coal (SACPS, 2015:20; Wagner & Tlotleng, 2012), and problems during coal utilization for example slagging (Speight, 2005:94; Ward, 2002). Since the ash remaining after combustion can be related to the mineral matter content of the coal prior to combustion, the emerging coal markets worldwide require coal with the lowest mineral matter content possible. However, some coal markets utilize low quality thermal coal, for example thermal coal with ash yield of 29.5 % is used for electricity generation (Eberhard, 2011), whilst others require that the ash yield does not exceed a certain amount. An example of the latter is that the ash yield may not exceed 10 % to be suitable

for the production of coking coal (Kruger, 2013). Ash yield can therefore also be used as an indicator to what coal value fractions are suitable for the current coal market.

The ash yield attained by applying each combination of breakage modes will be discussed. Ash curves were constructed by presenting the cumulative floats mass yield, and the associated cumulative float ash yield. These curves are shown for each breakage top size along with the attritioning following the initial breakage mode (namely impact and compressive). The ash curve for the raw coal prior to any testing was also included in each graph to compare the yield increase due to breakage. It must be noted that the ash curves for the raw coal were presented as for the whole sample and not a specific size fraction. It is important to note that the term “ash yield” was used instead of “ash content” throughout this study. This is because “ash yield” refers to the ash content remaining after combustion of coal. The ash yield and mineral matter content are related, according to Equation 1-1 as given in Section 1.1.

Impact breakage as well as compressive breakage to a top size of 13.2 mm displayed similar results, and did not reveal any increase in the cumulative float mass yield compared to the cumulative floats mass yield for the raw coal prior to testing. Figure 4.15 shows the ash curve for impact breakage to a top size of 13.2 mm, whilst that of compressive breakage to a top size of 13.2 mm can be obtained in Appendix C (Figure C.88).

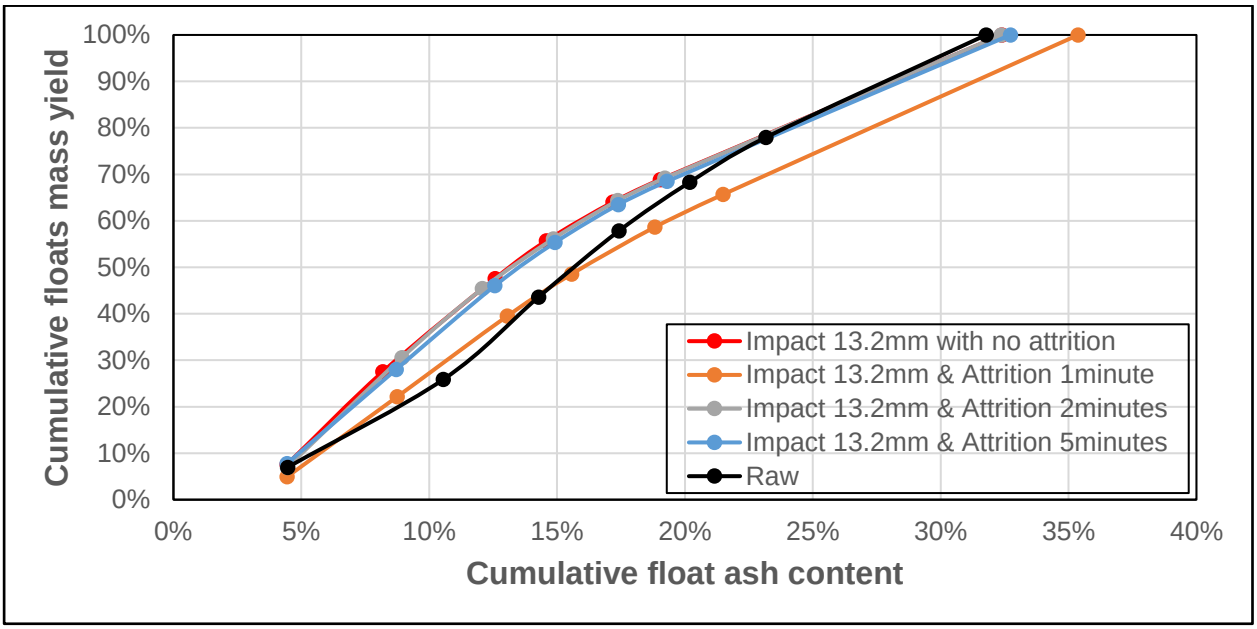

Figure 4.15: Ash curve for impact breakage to a top size of 13.2 mm.

Figure 4.16 shows the ash curve for impact breakage to a top size of 6.7 mm.

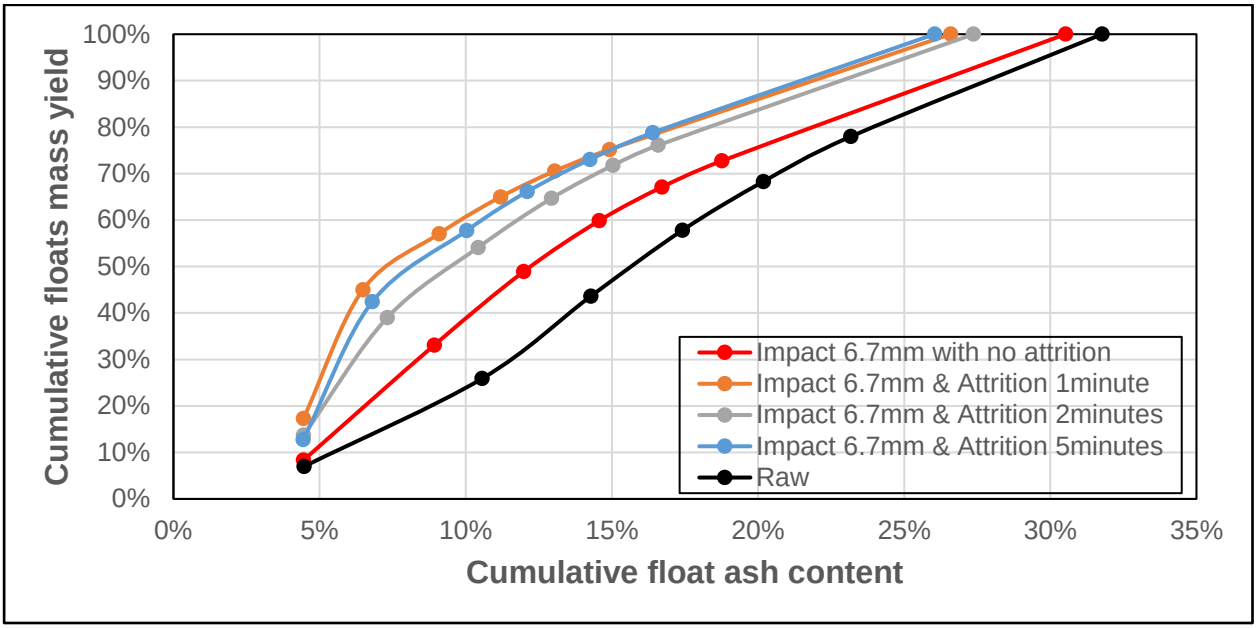

Figure 4.16: Ash curve for impact breakage to a top size of 6.7 mm.

When comparing Figure 4.15 with Figure 4.16, it can be seen that breakage to a top size of 6.7 mm resulted in an increase in the cumulative floats mass yield at a lower cumulative float ash yield. Therefore a higher cumulative floats mass yield can be obtained containing a lower ash yield. This can again be ascribed to the exposure and liberation of vitrinite-rich material when breakage is done to a smaller top size (6.7 mm). The cumulative floats mass yield attained by impact breakage to a top size of 6.7 mm followed by attritioning at the various residence times, also showed a substantial increase compared to that for raw coal, as well as for impact breakage to a top size of 6.7 mm with no additional attrition breakage. For example, at a cumulative float ash of 10 %, the cumulative floats mass yield for raw coal was 26 %, while that for impact breakage to 6.7 mm with no attrition breakage was 39 %, and that for impact breakage to 6.7 mm with attrition breakage for 1 minute is 61 %. It can therefore be concluded that impact breakage to a top size of 6.7 mm resulted in an increase in the cumulative floats mass yield with a cumulative float ash of 10 %, compared to that for the raw coal. Additional attrition breakage resulted in an even further increase in the cumulative floats mass yield. This is because breakage to the smaller top size of 6.7 mm exposed more of the coal macerals, which was then further released or liberated during attrition breakage after the initial impact breakage.

Figure 4.17 presents the ash curve for compressive breakage to a top size of 6.7 mm.

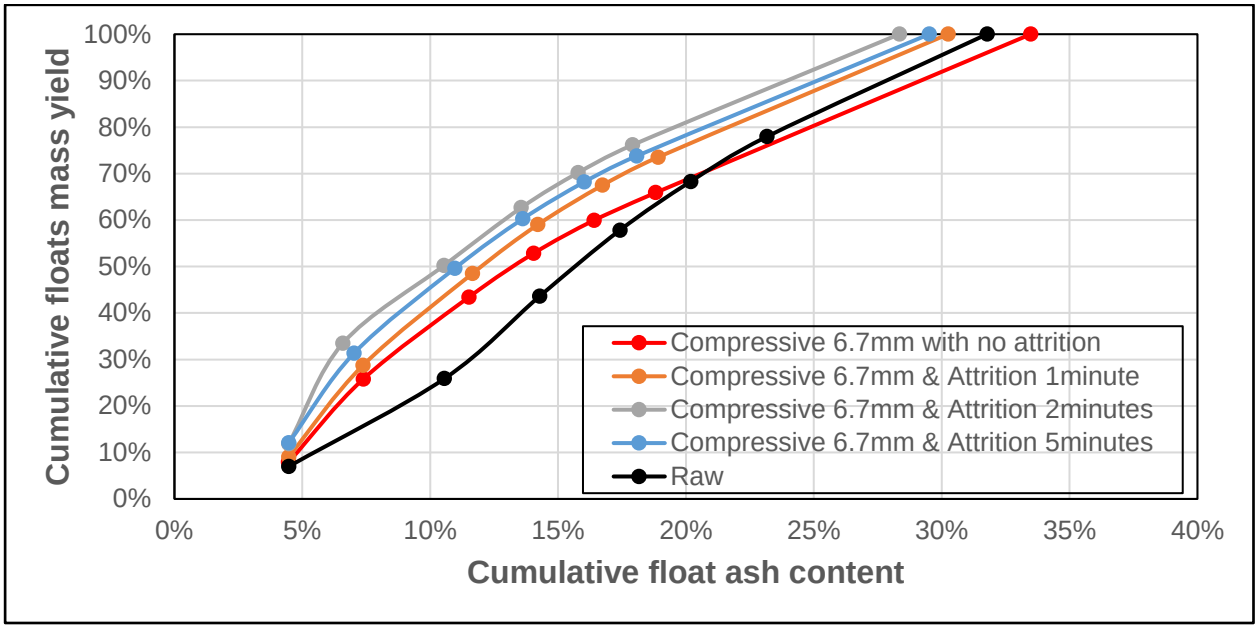

Figure 4.17: Ash curve for compressive breakage to a top size of 6.7 mm.

It can be seen from Figure 4.17, that compressive breakage to a top size of 6.7 mm followed by attrition breakage, also resulted in an increase in the cumulative floats mass yield compared to that of the raw coal. The increase is, however, not as substantial as that for impact breakage to a top size of 6.7 mm followed by attrition breakage. The highest cumulative floats mass yield attained at a cumulative float ash yield of 10 %, for compressive breakage to a top size of 6.7 mm was 49 %, for the sample subjected to 2 minutes of attritioning. This was much lower than for impact breakage followed by 1 minute of attritioning, which gave a yield of 60 %. Impact breakage to a top size of 6.7 mm thus resulted in a much higher cumulative floats mass yield compared to compressive breakage.

Coal markets do not only require that the ash yield may not exceed a certain amount to be suitable for the various industrial processes, but it also require that the coal feed is at the coarsest particle size possible. Drying, retreatment, and handling of coal fines (-0.5 mm) formed during size reduction processes are difficult (Weining *et al.,* 2013), since fines have higher moisture retention, which makes them build up in chutes and transfer points, and are more expensive to process than coarse coal. The plant feed coal must therefore be processed at the coarsest possible particle size (O'Brien *et al*., 2011). Comminution processes must be controlled to ensure that particle sizes are large enough to be suitable for utilization, and fines formation during size reduction processes must be limited (Weining *et al.,* 2013), as they increase downstream beneficiation costs, and lead to economic losses.

Figure 4.18 presents the float ash per particle size for the experimental test conditions of impact breakage to a top size of 6.7 mm followed by attrition breakage for 1 minute. This graph gives an indication of the cumulative floats mass yield attained for a specific cumulative float ash yield, at each particle size range.

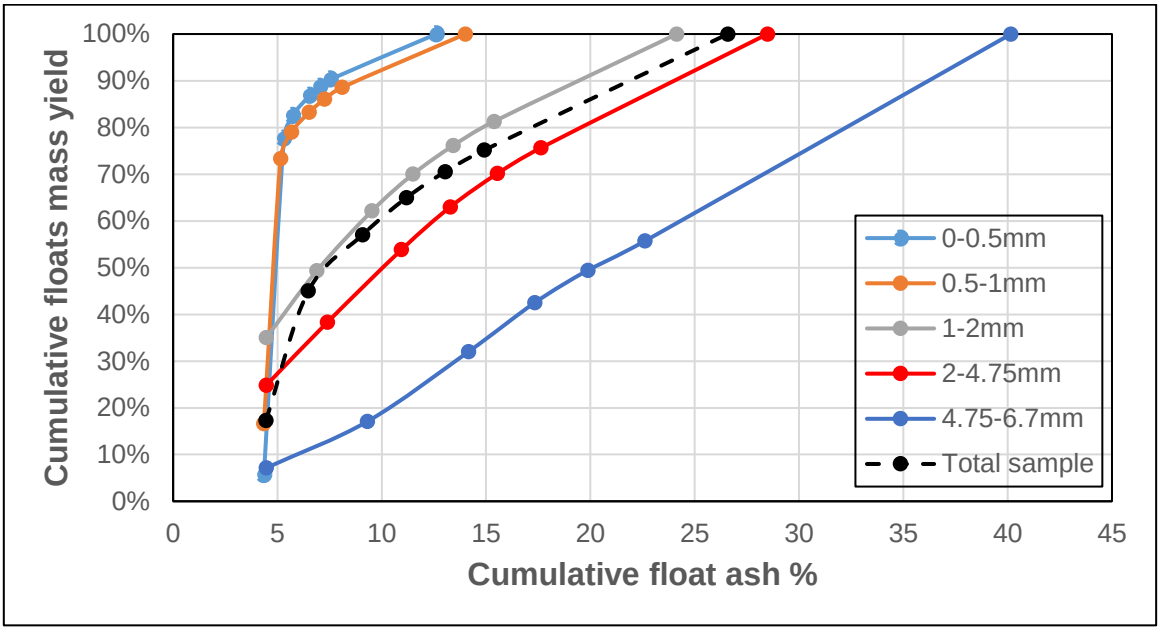

Figure 4.18: Float ash per particle size for impact breakage to a top size of 6.7 mm followed by attrition breakage for 1 minute.

Again, a hypothetical ash yield of 10 % will be used to compare the outcomes of the various particle size intervals as shown in Figure 4.18. The cumulative floats mass yield, for a cumulative float ash of 10 %, was over 90 % for two of the particles size ranges, 0.0-0.5 mm and 0.5-1.0 mm respectively. The particle size range of 1.0-2.0 mm showed a 64 % cumulative floats mass yield, whilst that for 2.0-4.75mm and 4.75-6.7 mm were 50 % and 18 %, respectively. It can be concluded that as the particle sizes increase, the cumulative floats mass yield at an ash yield of 10 % decrease. This observation can be ascribed to the brittle vitrinite-rich material that are more susceptible to breakage, resulting in smaller particle sizes. The cumulative floats mass yield will therefore be higher at smaller particle size ranges. Liberation of coal macerals increase as the particle size decrease, as would be expected. The cumulative floats mass yield for the particle size range of 4.75-6.7 mm is relative low compared to the other particle size ranges. As discussed in Section 4.3.1, this particle size fraction contained high amounts of mineral matter leading to high ash yield. Mineral matter is more difficult to break (Shi, 2014) leading to relative large particles formed, and is responsible for high ash yield at the particle size range of 4.75-6.7 mm. Further size reduction of this particle size interval might improve liberation of coal from mineral matter, resulting in an increase in the cumulative floats mass yield at a cumulative float ash of 10 %. Size reduction will however result in a higher amount of fines generation; but these fines will be of high quality. Whether size reduction will be performed to increase the cumulative float

yield even further depends on the size requirements for the industrial process the coal will be used in.

Another possible solution, instead of crushing the particle size fraction of 4.75-6.7 mm further, is to screen the coal at a particle size of 4.75 mm. This will ensure that the cumulative floats mass yield and the relative low cumulative float ash yield of the particles smaller than 4.75 mm is not lowered by the presence of material larger than 4.75 mm. Figure 4.19 presents the ash curve for impact breakage to a top size of 6.7 mm followed by attrition breakage for 1 minute. This curve was used to compare the cumulative floats mass yield of particles smaller than 4.75 mm and those larger than 4.75 mm. The cumulative float mass yield does not add up the 100 %. This is because the particle sizes are presented separately. Together, the particles smaller than 4.75 mm, and those larger than 4.75 mm will add to 100 %.

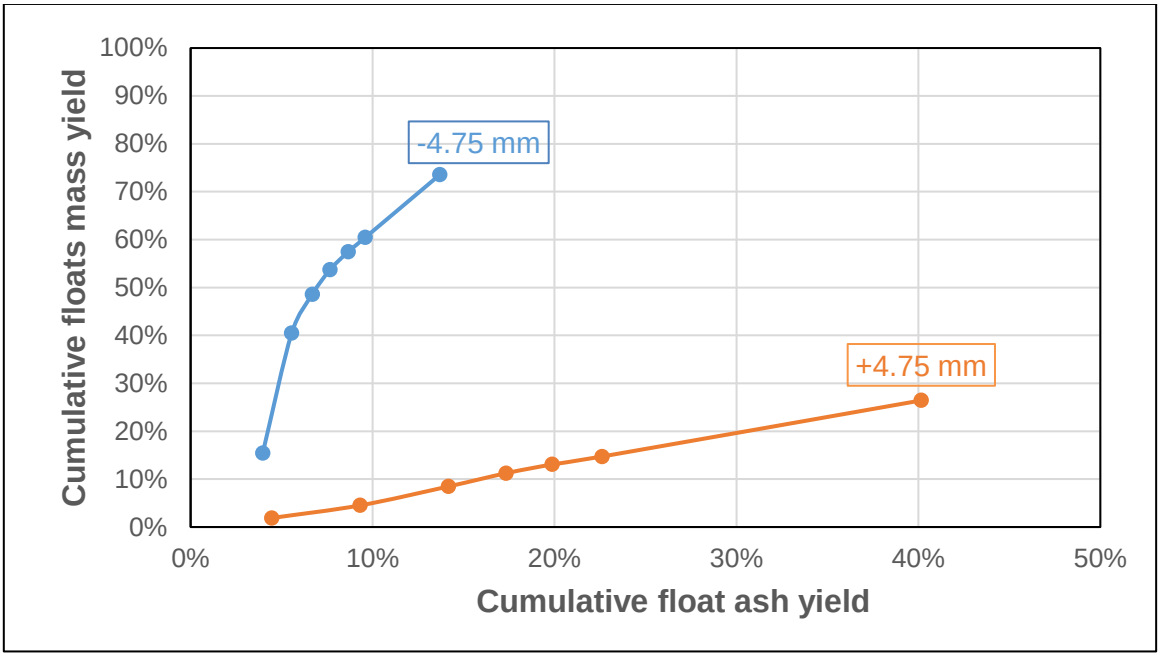

Figure 4.19: Ash curve for impact breakage to a top size of 6.7 mm followed by attrition breakage for 1 minute.

As given in Figure 4.19, the cumulative floats mass yield of particles smaller than 4.75 mm was 73.6 % with a cumulative float ash yield of 13.7 %. The cumulative floats mass yield of particles larger than 4.75 mm was 26.4 % with a cumulative float ash yield of 40.2 %. Not only was the cumulative float mass yield of the particles smaller than 4.75 mm higher than the larger particles, but the cumulative ash yield was also much lower. This corresponds with Figure 4.18, showing that the particle size fraction of 4.75-6.7 mm has a relatively high cumulative float ash yield compared to the other particle size ranges.

4.6 Liberation

Liberated material was defined as material with a relative density of 1.4 and lower. This relative density was chosen because of the relative density of “pure” coal being 1.2-1.4 while mineral matter has a relative density varying between 2.0 and 5.0 (Speight, 2005:94). Particular interest was thus in the relative density range up to 1.4, as these density fractions were mainly liberated coal macerals.

A liberation curve was constructed to evaluate the yield of material with relative density of 1.4 and lower attained by each combination of breakage modes. This was done by cumulatively adding the mass of material with relative density of less than 1.3, as well as material in the relative density range of 1.3-1.4 at each particle size, and then dividing it by the total mass of the whole sample. Figure 4.20 can be used to illustrate the calculation followed to obtain the liberation curve. For example, the sum of the mass of material with relative density less than 1.3 (F1.3) and material with a relative density of 1.3-1.4 for the particle size range 0.0-0.5 mm was calculated. It is indicated on the graph below by a red parallelogram. Please note that Figure 4.20 gives the mass distribution as a percentage. For this calculation the actual mass was used and not the mass percentage. The calculated mass amount was then divided by the mass of all material in the sample. This was done cumulatively at each particle size interval until the size interval of 9.5-13.2 mm was reached.

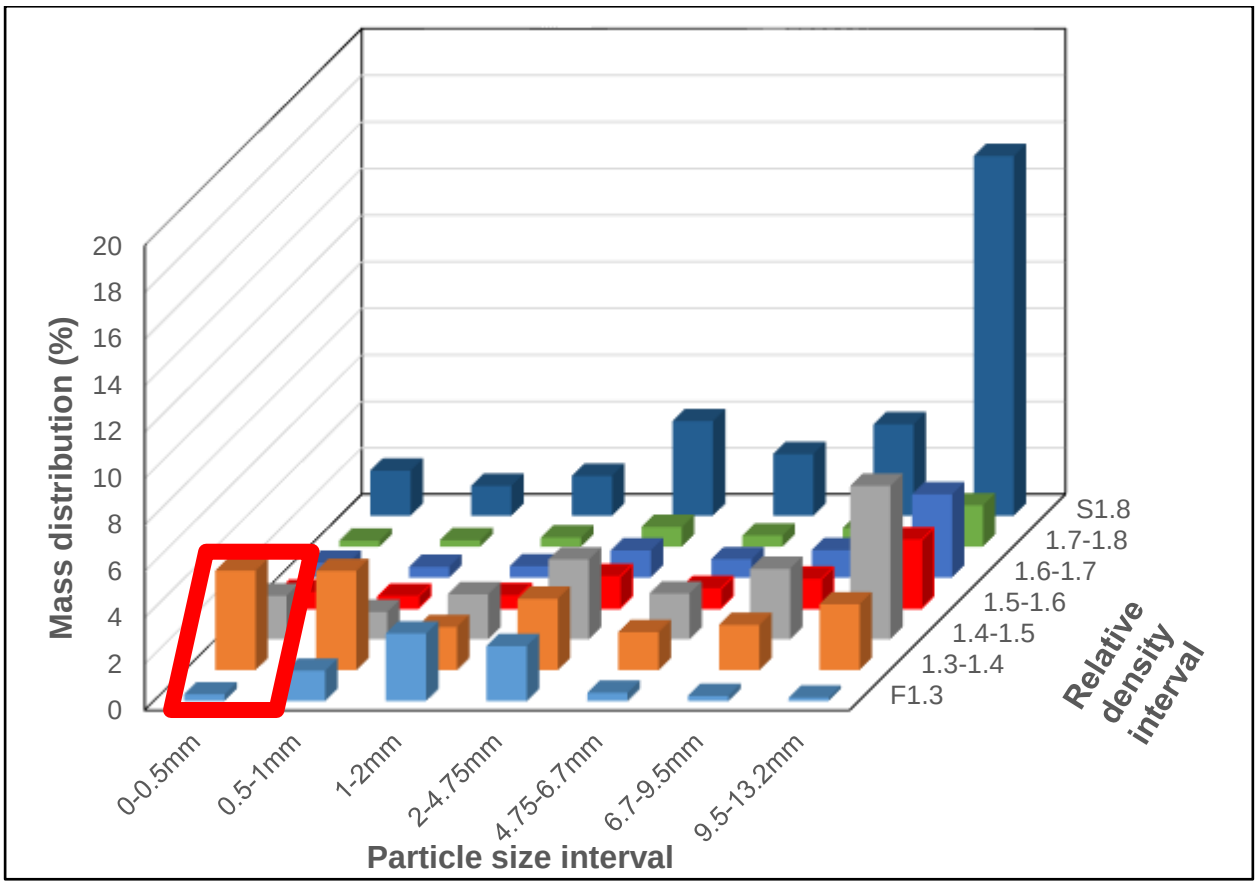

Figure 4.20: Size by washability graph for impact breakage to a top size of 13.2 mm with no additional attrition breakage.

Figure 4.21 and Figure 4.22 respectively presents the liberation curve for impact and compressive breakage.

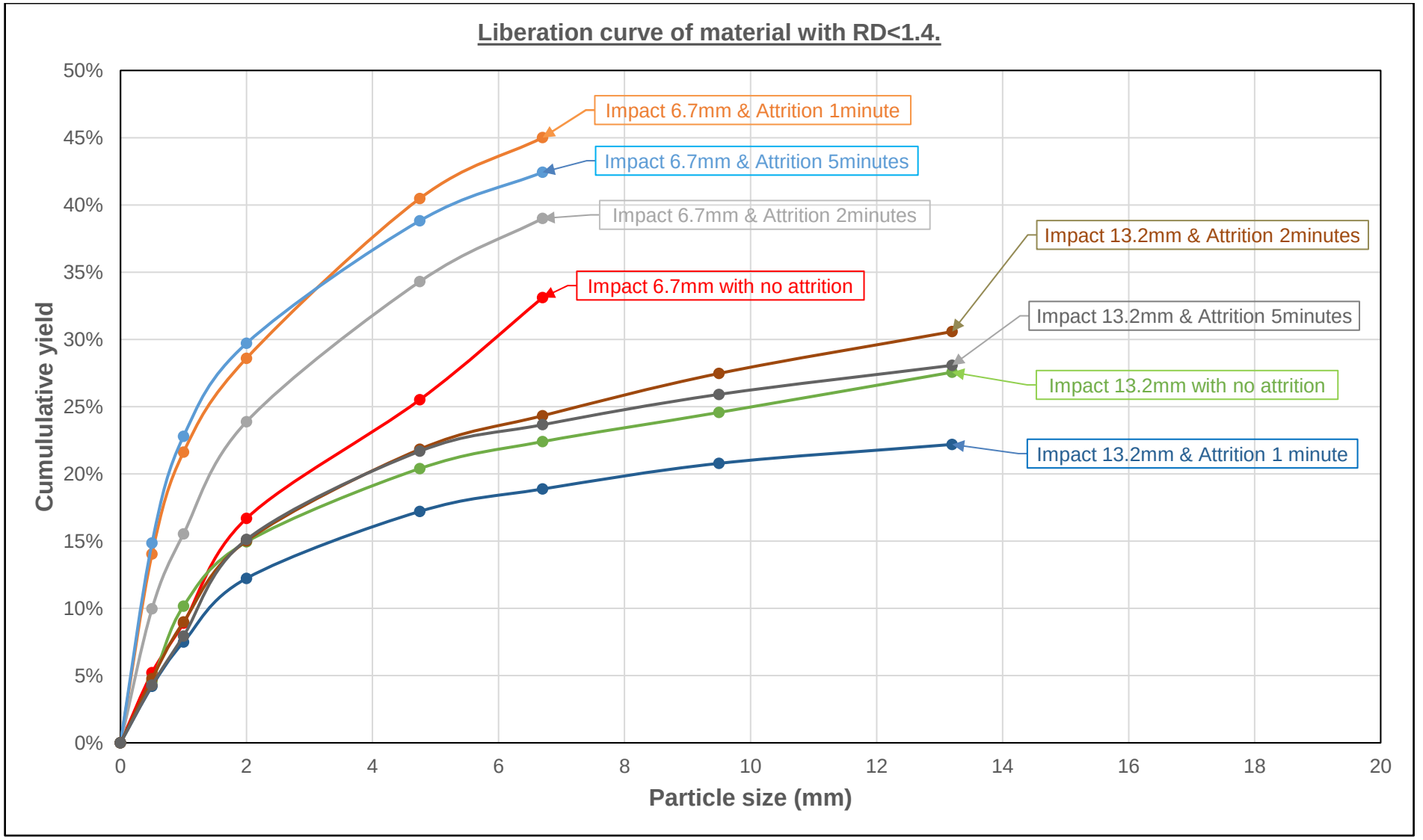

Figure 4.21: Liberation curve for impact breakage.

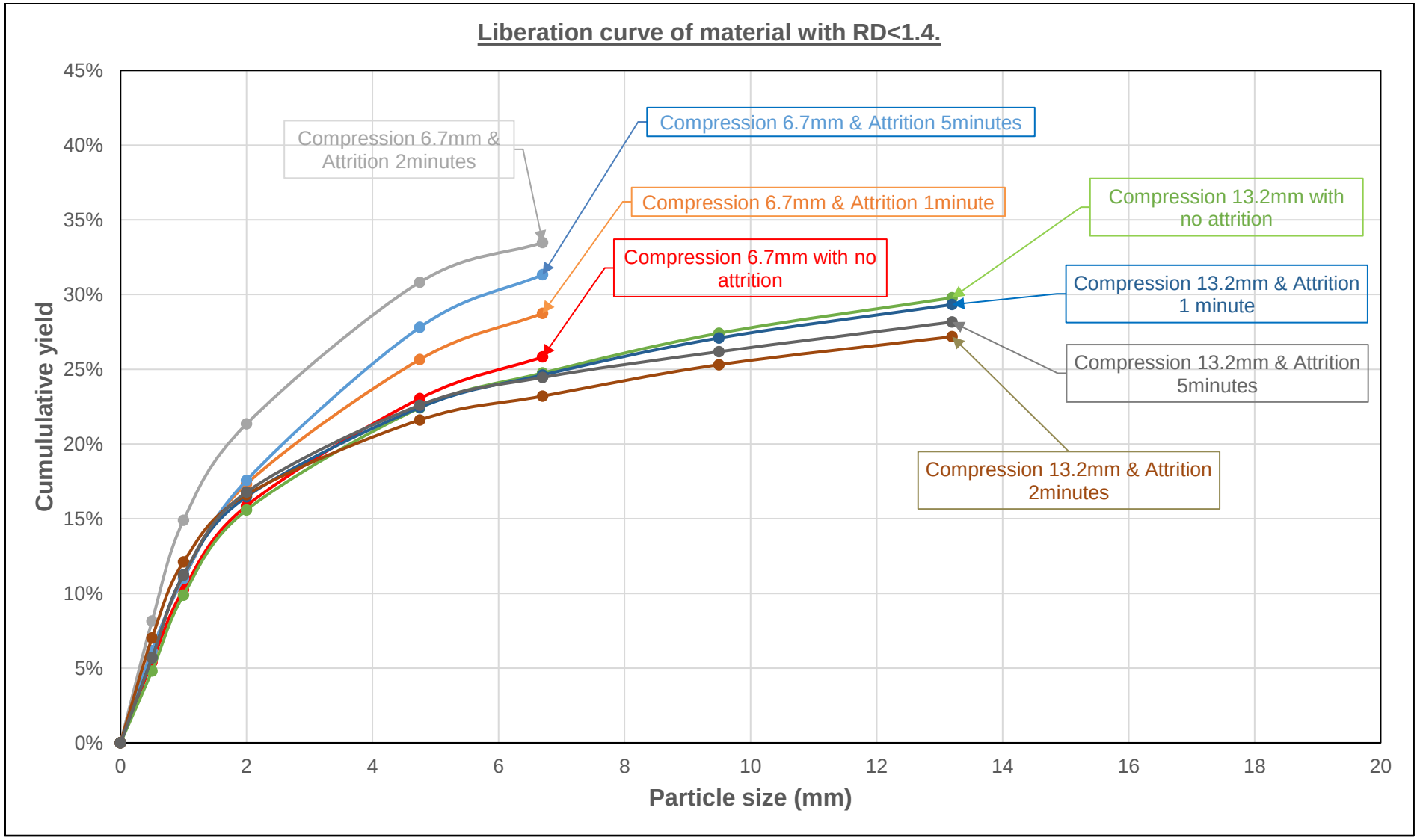

Figure 4.22: Liberation curve for compressive breakage.

When comparing Figure 4.21 and Figure 4.22, it was observed that breakage, impact as well as compressive, to a top size of 13.2 mm revealed similar results in terms of the cumulative yield of material with a relative density of 1.4 and lower. Once again, these graphs highlighted that attrition breakage additional to breakage to a top size of 13.2 mm had an insignificant effect on the cumulative yield of material with a relative density of 1.4 and lower. Breakage to a top size of 13.2 mm was too coarse to expose all coal macerals entrapped between mineral materials.

Figure 4.21 and Figure 4.22 show that the yield of the liberated coal fraction (RD<1.4) was higher for breakage, impact as well as compressive, to a top size of 6.7 mm than for breakage to a top size of 13.2 mm. Additional attrition breakage also had a substantial effect on the cumulative yield of the liberated coal fraction when breakage was performed to a top size of 6.7 mm. Again, this observation can be ascribed to breakage to a top size of 6.7 mm exposing more of the coal macerals which was then further released during attrition breakage following impact breakage. Impact breakage to a top size of 6.7 mm resulted in a higher cumulative yield of the liberated coal fraction, than that for compressive breakage to a top size of 6.7 mm. When comparing Figure 4.21 and Figure 4.22, it can be seen that impact breakage to 6.7 mm followed by attritioning resulted in a cumulative yield (of the liberated coal fraction) of 39-45 %, compared to that for compressive breakage to 6.7 mm followed by attritioning was 29-33 %. The cumulative yield of the liberated coal fraction was thus highest for the breakage combination of impact breakage to a top size of 6.7 mm followed by attrition breakage.

The cumulative fractional yield of the liberated coal particles (with RD of 1.4 and lower) at a specific particle size interval (0-4.75 mm), as attained by the various breakage modes are compared by using Figure 4.23. The cumulative fractional yield for the particle size range of 0.0-2.0 mm is presented in Figure C.90 in Appendix C. The breakage mode and top size for breakage are indicated above the columns in these figures, with the same colour as the columns, while the residence times for attrition breakage are indicated on the x-axis. This is because of the lengthy naming convention of the various experimental test conditions, and for ease of readability.

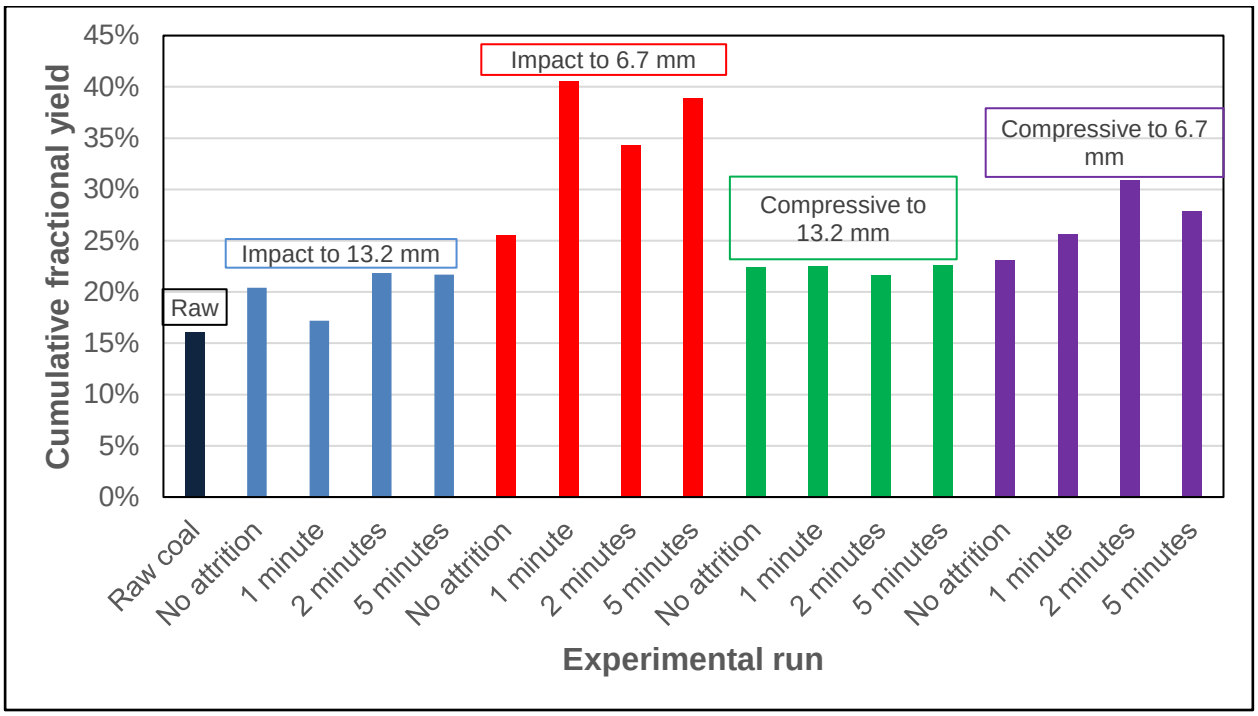

Figure 4.23: Cumulative fractional yield of liberated coal macerals (with RD<1.4) within the particle size interval of 0-4.75 mm.

When comparing the cumulative fractional yield of the liberated coal macerals at a particle size interval of 0.0-4.75 mm, by using Figure 4.23, it can again be seen that results for breakage, impact as well as compressive, to a top size of 13.2 mm resulted in only a slight increase in the cumulative fractional yield compared to that of the raw coal, prior to testing. Breakage to a top size of 6.7 mm resulted in a relatively higher cumulative fractional yield compared to that of the raw coal. Attrition breakage following the initial breakage mode (impact or compressive) to a top size of 6.7 mm, resulted in an even higher cumulative fractional yield of the liberated coal macerals, especially in the case of impact breakage to a top size of 6.7 mm. Impact breakage to a top size of 6.7 mm followed by attrition breakage for 1 minute resulted in a cumulative fractional yield of up to 40 % for the 0.0-4.75 mm particle size range. It might be expected that 5 minutes attritioning after impact breakage to a top size of 6.7 mm, would have resulted in the highest cumulative fractional yield. It must be kept in mind that different samples were used for the different experimental conditions, therefore sampling split errors might have occurred. The cumulative fractional yield (with RD<1.4) for the particle size range of 0.0-2.0 mm (Figure C.90) indicated a lower cumulative fractional yield than the particle size range of 0.0-4.75 mm. This was because of the high value vitrinite that was liberated first from the gangue, where after finely disseminated mineral matter began to liberated, leading to a reverse effect of the increase in the cumulative yield at a particle size of 4.75 mm. Breakage to a smaller top size of 2 mm will therefore not result in a significant coal yield increase.

4.7 Washability

Densimetric curves were used to investigate the washability of the coal samples after subjected them to the various test conditions. These curves indicate the cumulative float mass yield of each sample at the different relative densities used during this study. As can be seen from Figure 4.24, the total floats mass yields do not add up to 100 %. The reason for this is that the material sinking at a relative density of 1.8, that is material with very high mineral matter content, were not included in the densimetric curve.

Figure 4.24 gives the washability of material subjected to impact breakage to a top size of 13.2 mm. Cases where the initial impact breakage was followed by attrition for various residence times were also included in the graph. The densimetric curve obtained for coal as is, or raw coal, will also be given to compare whether the yield was increased by the applied mode of breakage. It must be noted that the raw coal washability was presented as for the whole sample and not a specific size fraction.

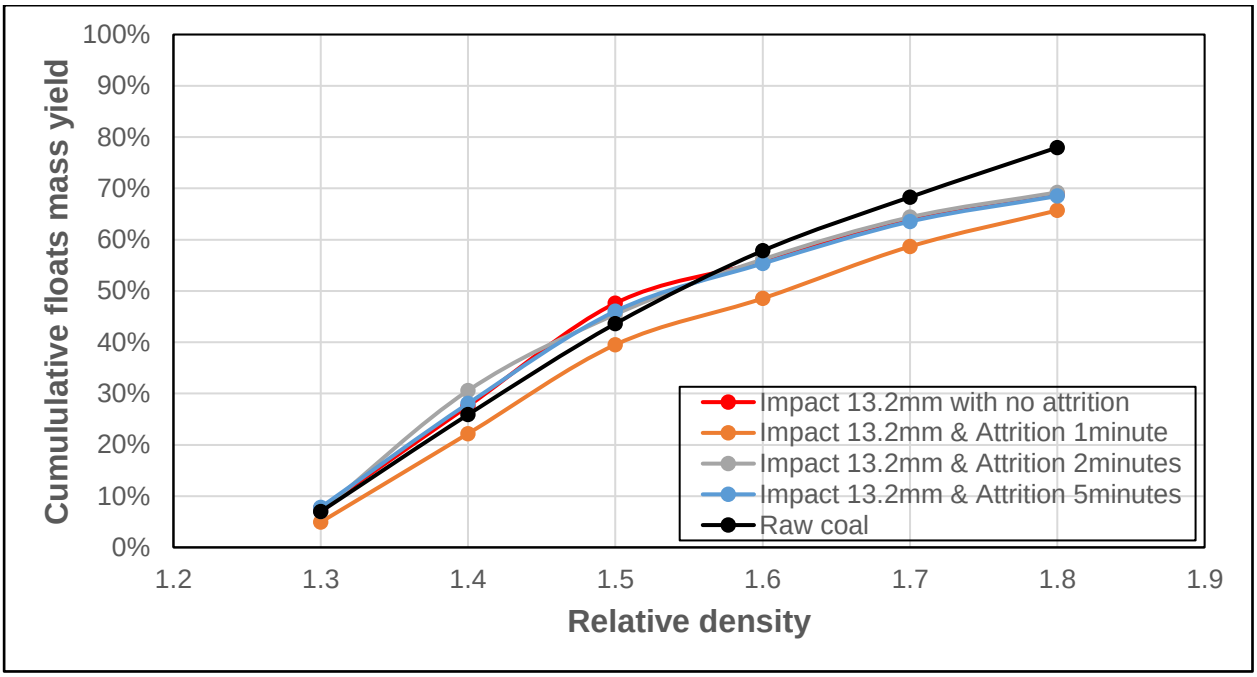

Figure 4.24: Densimetric curve for impact breakage to a top size of 13.2 mm.

As illustrated in Figure 4.24, impact breakage to a top size of 13.2 mm did not show an increase in the cumulative floats mass yield compared to that of raw coal, prior to any testing. Attrition breakage additional to impact breakage had no effect on the floats mass yield attained, regardless of the residence time used for attrition. This confirms the statement made in Section 4.3.2 that attrition breakage additional to impact breakage to a top size of 13.2 mm had an insignificant effect on the yield. Impact breakage to a top size of 13.2 mm followed by attrition for 1 minute was considered to be an outlier. It was seen that the cumulative floats mass yield of the raw coal

was higher than that for crushing, at relative densities of 1.6 to 1.8. The cumulative floats mass yield was increased, between relative densities of 1.3 to 1.6, and then slightly decreased, between relative densities of 1.6 to 1.8. This was because of the liberated coal fraction (RD<1.4) that was liberated first from the gangue, where after finely disseminated mineral matter began to liberated, leading to a reverse effect of the increase in the cumulative yield.

The next densimetric graph, Figure 4.25, gives the washability for impact breakage to a top size of 6.7 mm as well as for cases when additional attritioning was performed.

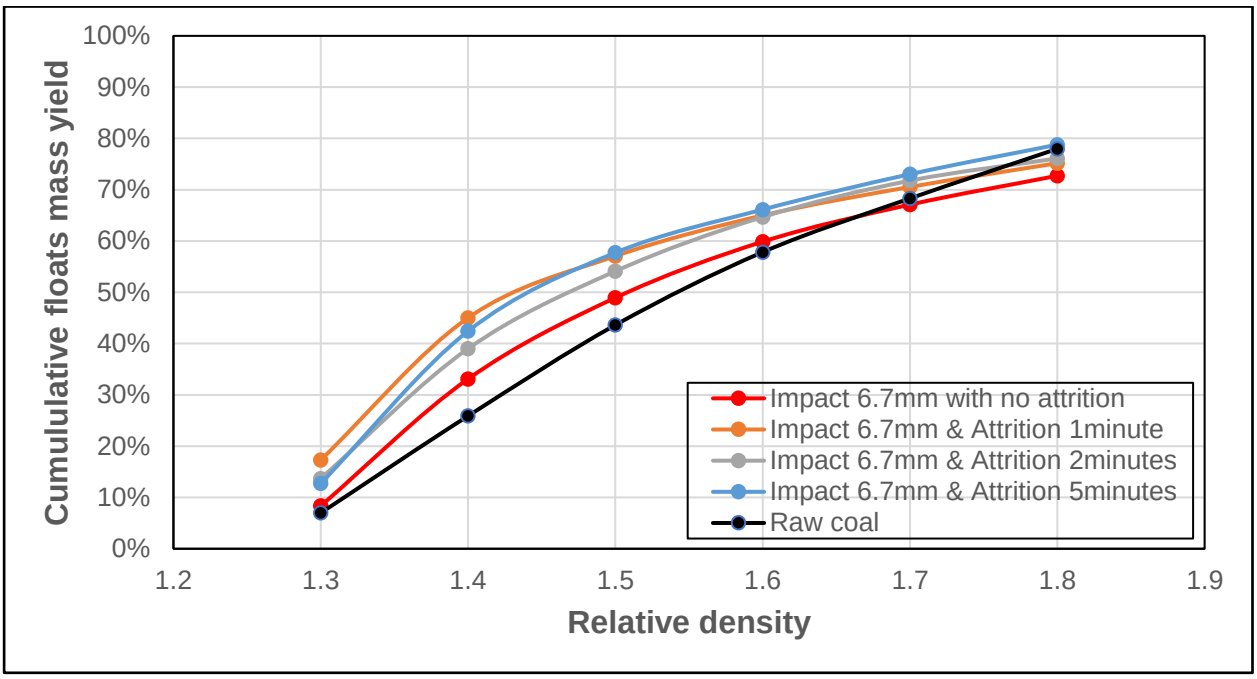

Figure 4.25: Densimetric curve for impact breakage to a top size of 6.7 mm.

Although attrition additional to impact breakage to a top size of 13.2 mm had no effect on the floats mass yield, Figure 4.25 shows that this was not the case for impact breakage to a top size of 6.7 mm. Again, this confirms the effect of attrition breakage additional to impact breakage of a top size of 6.7 mm as described in Section 4.3.2. Impact breakage to a top size of 6.7 mm resulted in exposure of vitrinite-rich material. The brittle vitrinite-rich material was chipped from the exposed surface during attritioning. This resulted in an increase in the amount of material with a density of 1.4 and less; the yield of coal was thus increased. When comparing the curves showing attrition breakage additional to impact breakage to a top size of 6.7 mm, it can be seen that there was a 5-10 % yield increase after attritioning was performed. The cumulative floats mass yield at a relative density of 1.4 for the raw coal prior to any testing was 26 %. Impact breakage to a top size of 6.7 mm resulted in a cumulative floats mass yield of 33 % at a relative density of 1.4, while that for the case of additional attritioning was up to 45 %. Not only does this graph show that attrition breakage further increase the floats mass yield when impact breakage to a top size of 6.7 mm was done, but it also shows that a higher floats mass yield was attained by impact

breakage to a top size of 6.7 mm instead of a top size of 13.2 mm. As seen from Figure 4.25, the cumulative floats mass yield for all experimental conditions, at a relative density of 1.8, were very similar. This might be because of sample preparation errors.

Figure 4.26 presents the densimetric curve for compressive breakage to a top size of 13.2 mm as well as the results when additional attrition breakage was performed.

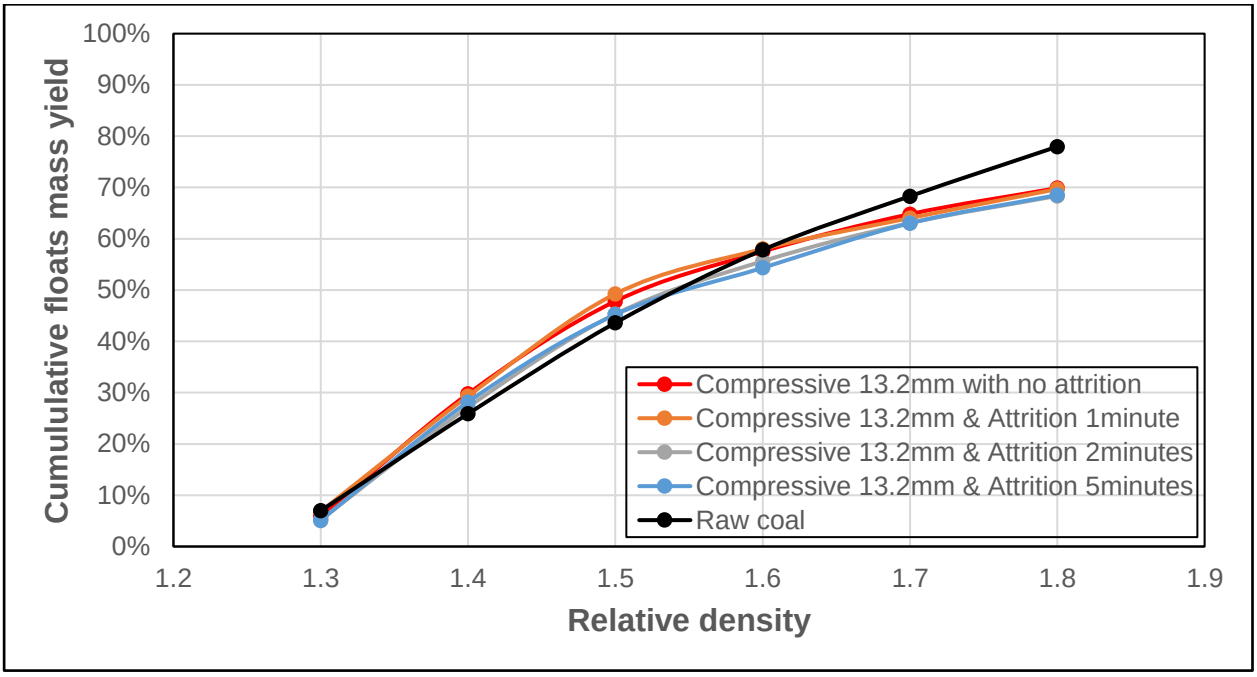

Figure 4.26: Densimetric curve for compressive breakage to a top size of 13.2 mm.

The cumulative floats mass yield attained for compressive breakage to a top size of 13.2 mm with no attrition was 29 % at a relative density of 1.4. As seen from Figure 4.26, not only was the yield of raw coal not significantly increased by compressive breakage to a top size of 13.2 mm, but the yield was also not enhanced by additional attritioning. This again confirms that attrition breakage additional to compressive breakage to a top size of 13.2 mm had no effect on liberating coal macerals as explained in Section 4.4.2. When comparing results for impact breakage (Figure 4.24) and compressive breakage (Figure 4.26) to a top size of 13.2 mm, it can be seen that results in terms of the floats mass yields attained are similar for both breakage modes. Again, it was seen that the cumulative floats mass yield of the raw coal was higher than that for crushing, at relative densities of 1.6 to 1.8. The cumulative floats mass yield was increased, between relative densities of 1.3 to 1.6, and then slightly decreased, between relative densities of 1.6 to 1.8. As for impact breakage to a top size of 13.2 mm, this was because of the liberated coal fraction (RD<1.4) that was liberated first from the gangue, where after finely disseminated mineral matter began to liberated, leading to a reverse effect of the increase in the cumulative yield. As seen from Figure 4.26, the cumulative floats mass yield for the raw coal at a relative density of 1.8 was 10 % higher

than that for the compressive breakage to a top size of 13.2 mm. This might be because of sampling split or experimental errors.

Figure 4.27 indicates the cumulative floats mass yield for compressive breakage to a top size of 6.7 mm.

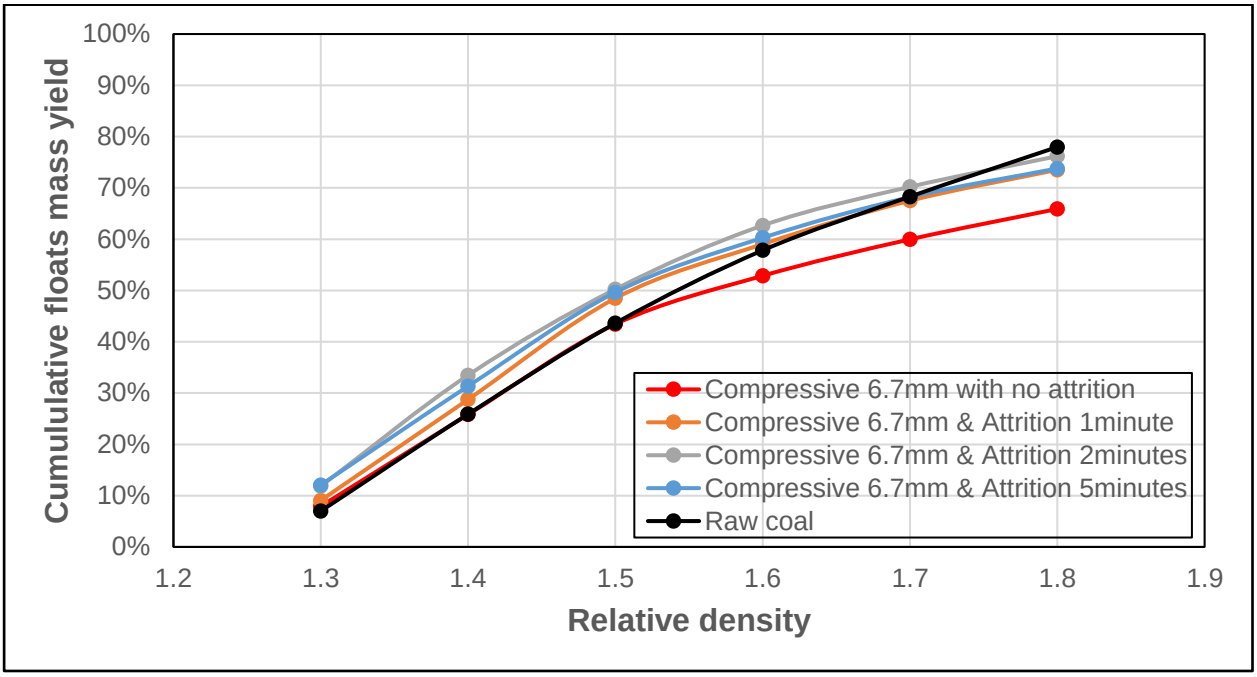

Figure 4.27: Densimetric curve for compressive breakage to a top size of 6.7 mm.

Attrition breakage additional to compressive breakage to a top size of 6.7 mm had a noticeable effect on the cumulative floats mass yield. As seen from Figure 4.27, there was a slight increase in the amount of floats mass yield at each relative density, though this was not as much as the increase in floats mass yield produced by the results for impact breakage to a top size of 6.7 mm followed by attrition breakage. It was seen that the cumulative floats mass yield of the raw coal was higher than that for compressive breakage to a top size of 6.7 mm with no attritioning, at relative densities of 1.6 to 1.8. This might be because of sampling split or experimental errors.

By comparing all the test conditions including top size, applied breakage mode and attrition residence time, it can be concluded that impact breakage to a top size of 6.7 mm followed by attrition breakage for 1 minutes resulted in the greatest increase in cumulative floats mass yield.

Figure 4.28 presents the densimetric curve for impact breakage to a top size of 6.7 mm followed by attrition breakage for a residence time 1 minute. Only two size fractions are shown: particles smaller than 4.75 mm, and particles larger than 4.75 mm.

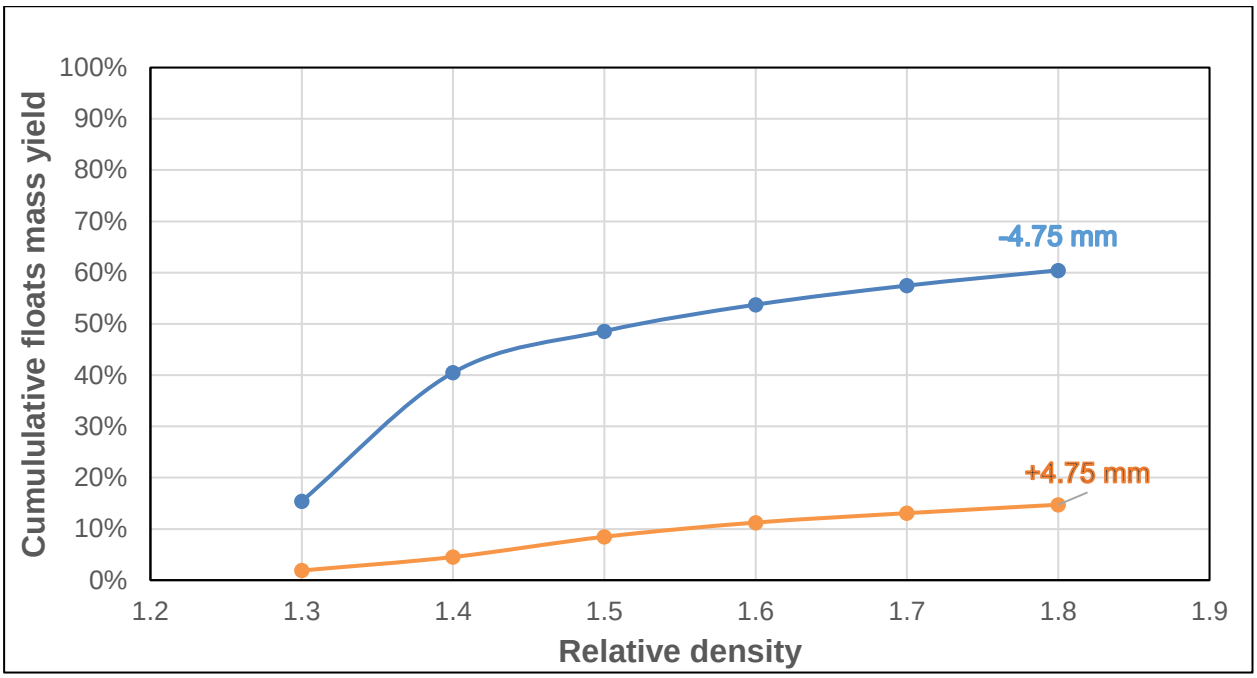

Figure 4.28: Densimetric curve for impact breakage to a top size of 6.7 mm followed by attrition breakage for 1 minute.

Figure 4.28 was used to compare the cumulative floats mass yield at the various relative densities, for the mentioned sizes. It can be seen that the cumulative floats mass yield of particles smaller than 4.75 mm was greater than that for particles larger than 4.75 mm, at all relative densities. The cumulative floats mass yield at a relative density of 1.4 for particles smaller than 4.75 mm was 40.5 %, while that for particle larger than 4.75 mm was only 4.5 %. As discussed in Section 4.5, the particles larger than 4.75 mm also have higher ash yield than those smaller than 4.75 mm. Figure 4.28 therefore supports the suggestion regarding screening at a particle size topsize of 4.75 mm.

5

CHAPTER 5 INDUSTRIAL APPLICATION

Industrial processes require coal of different quality specifications, for example, Eskom utilizes low grade thermal coal for power generation. These coal usually have a calorific value of 15-20 MJ/kg (Eberhard, 2011; SAIMM, 2016; Subramoney *et al*., 2009), a 29.5 % ash yield and 0.8 % sulphur content (Eberhard, 2011). Sasols' coal to liquid (CTL) plants consume coal with high ash yield of around 35 %, and with a calorific value (CV) of less than 21 MJ/kg (Eberhard, 2011). The quality of South African thermal export coal has to be of higher quality. These coal typically must have a calorific value of 24.7-28.0 MJ/kg (de Korte, 2010; Eberhard, 2011; SAIMM, 2016), and a sulphur content of 0.6-0.7 % (Eberhard, 2011) to be suitable for export purposes.

The various coal quality fractions, as required by these and other coal markets, can be obtained by washing at different relative densities. Run-of-mine coal needs to be subjected to some form of size reduction prior to washing. This is because the high quality coal fractions are mostly intermingled with mineral matter. The mineral matter needs to be reduced in order to upgrade the quality of the coal, i.e. increase the CV, and reduce the ash yield and sulphur content. Therefore, coal fractions firstly needs to be liberated from the mineral matter to increase the coal yield attained by "washing" in order to meet the calorific value specification, and to ensure that the ash yield does not exceed the permissible amount.

Washing and size reduction of coal needs to be optimized to ensure maximum recovery of high value coal. These processes need to be fully understood in order to apply the breakage mode or combination of breakage modes that will result in the maximum recovery of the high value coal fraction. Washing of coal needs to be done at certain relative densities that will provide an ash yield and calorific value as specified by the consumer. The relative density required for washing, and the cumulative yield that can be obtained for the specified ash yield is of importance. The washing process (plant) needs to be designed accordingly to optimize the coal yield.

A hypothetical target ash yield of 10 % was investigated. This ash yield was only used as a guideline, although a hypothetical ash yield of 10 % is a little low for Moatize coal. The cumulative float yield, and the cumulative float ash at each specific relative density was used to investigate the outcomes. Microsoft Excel's FORECAST function was used to predict the overall cumulative yield that can be obtained, and to estimate the required relative density for separation to obtain the hypothetical ash yield. This was done for all experimental test conditions. The results obtained

are summarized in Table 5.1. The absolute increase in yield compared to the yield of raw coal was calculated by subtracting the cumulative yield of the raw coal from the cumulative yield of a given run. The percentage yield increase was calculated by using Equation D-2.

Table 5.1: Required relative density for washing and yield obtained for a target ash yield of 10 %.

Experimental conditions	For a target ash yield of 10%		Absolute increase in yield compared to the raw coal	% yield increase compared to the raw coal
	RD required	Cumulative Yield		
Raw coal/Base run	1.39	24.2%	-	-
Impact 13.2mm No attrition	1.44	35.8%	11.6	47.9%
Impact 13.2mm Attrition 1min	1.43	27.2%	3.0	12.4%
Impact 13.2mmAttrition 2min	1.43	35.6%	11.4	47.1%
Impact 13.2mm Attrition 5min	1.43	34.1%	9.9	40.9%
Compression 13.2mm No attrition	1.43	36.0%	11.8	48.8%
Compression 13.2mm Attrition 1min	1.45	38.5%	14.3	59.1%
Compression 13.2mm Attrition 2min	1.45	36.4%	12.2	50.4%
Compression 13.2mm Attrition 5min	1.44	35.6%	11.4	47.1%
Impact 6.7mm No attrition	1.44	38.7%	14.5	59.9%
Impact 6.7mm Attrition 1min	1.54	60.5%	36.3	150.0%
Impact 6.7mmAttrition 2min	1.49	52.1%	27.9	115.3%
Impact 6.7mm Attrition 5min	1.50	57.6%	33.4	138.0%
Compression 6.7mm No attrition	1.46	37.0%	12.8	52.9%
Compression 6.7mm Attrition 1min	1.46	40.9%	16.7	69.0%
Compression 6.7mm Attrition 2min	1.49	47.9%	23.7	97.9%
Compression 6.7mm Attrition 5min	1.48	45.2%	21.0	86.8%

As shown in Table 5.1, raw coal, that is run-of-mine coal prior to any testing, will result in a cumulative float yield of 24.2 % when washing is performed at a relative density of 1.39 in order to reach the specified target ash yield of 10 %. When comparing the cumulative yield for each of the test conditions to that of the raw coal, it can be seen that the yield was improved by all combinations of breakage modes. Breakage to a smaller top size of 6.7 mm resulted in an overall higher increase in the cumulative yield, compared to breakage to a top size of 13.2 mm. Furthermore, impact breakage to a top size of 6.7 mm followed by attrition breakage at the various residence times resulted in an absolute yield increase of 25 % and more, for a target ash of 10 %. The required relative density to obtain this yield at the test conditions (impact breakage to a top size of 6.7 mm followed by attritioning) was 1.50-1.54. Therefore, according to these results, impact breakage to a top size of 6.7 mm followed by attritioning attained the optimum cumulative float yield for the specified target ash yield of 10 %.

Equipment and chemicals required for dense medium separation during washing operations, i.e. full scale processing plants, are relatively expensive. It might be therefore more economical to separate coal according to particle sizes by means of screening ahead of washing. For screening to be a practical method, the cumulative yield that can be obtained for a certain particle size needs to be known. Again, Microsoft Excel's FORECAST function was used to predict the cumulative yield that can be obtained for each specific particle size range when washing is done at the predicted relative density as tabulated in Table 5.1. This was done by using the estimated relative density for separation to obtain the hypothetical ash yield of 10 %. In other words, this will give an indication of how much the cumulative yield at each particle size will be when coal is washed at the predicted relative density to attain a hypothetical ash yield of 10 %.

Figure 5.1 shows the hypothetical density wash of the raw coal. The cumulative particle size distribution for the feed material, as well as for the product floats after subjected to washing at a relative density of 1.39 (as indicated in Table 5.1) are shown. The cumulative floats mass yield (at the relative density of 1.39) at a particle size, for example, 4.75 mm will be 62.0 %.

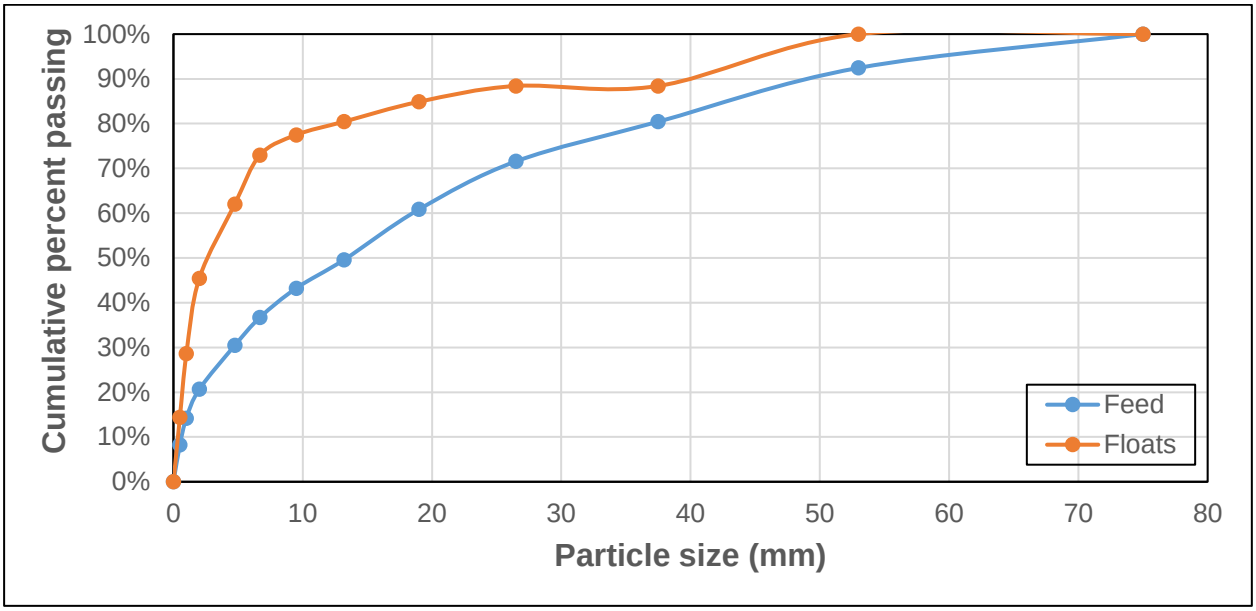

Figure 5.1: Hypothetical density wash of raw coal.

Figure 5.2 shows the hypothetical density wash of coal subjected to impact breakage to a top size of 6.7 mm with additional attrition breakage for 1 minute.

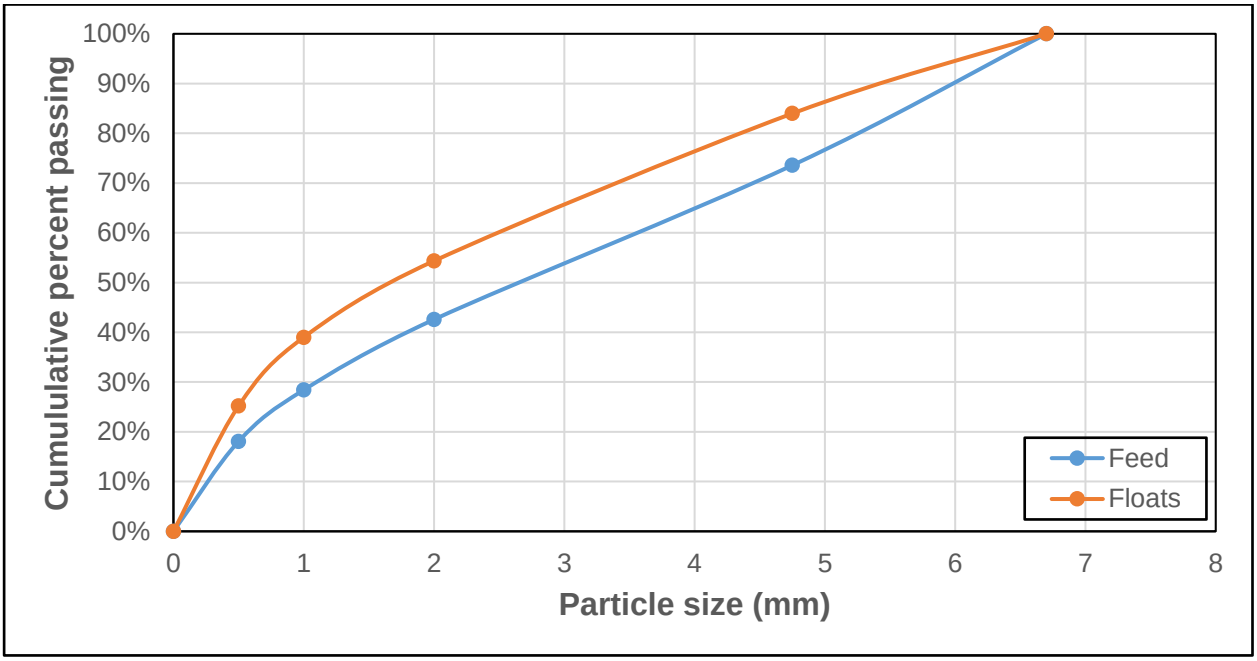

Figure 5.2: Hypothetical density wash of coal subjected to impact breakage to a top size of 6.7 mm with additional attrition breakage for 1 minute.

It is shown that the cumulative floats mass yield (at the relative density of 1.54) at a particle size, for example, 4.75 mm will be 84.0 %. The increase in cumulative floats mass yield are substantial compared to that of raw coal. These hypothetical wash curves give an indication of what the cumulative floats yield of material with a specific density will be, when screening at a certain particle size is performed.

These results can be applied to industrial processes to increase the coal yield. Figure 5.3 gives a suggestion, by means of a flow diagram, of how the breakage modes can be implemented for industrial processes.

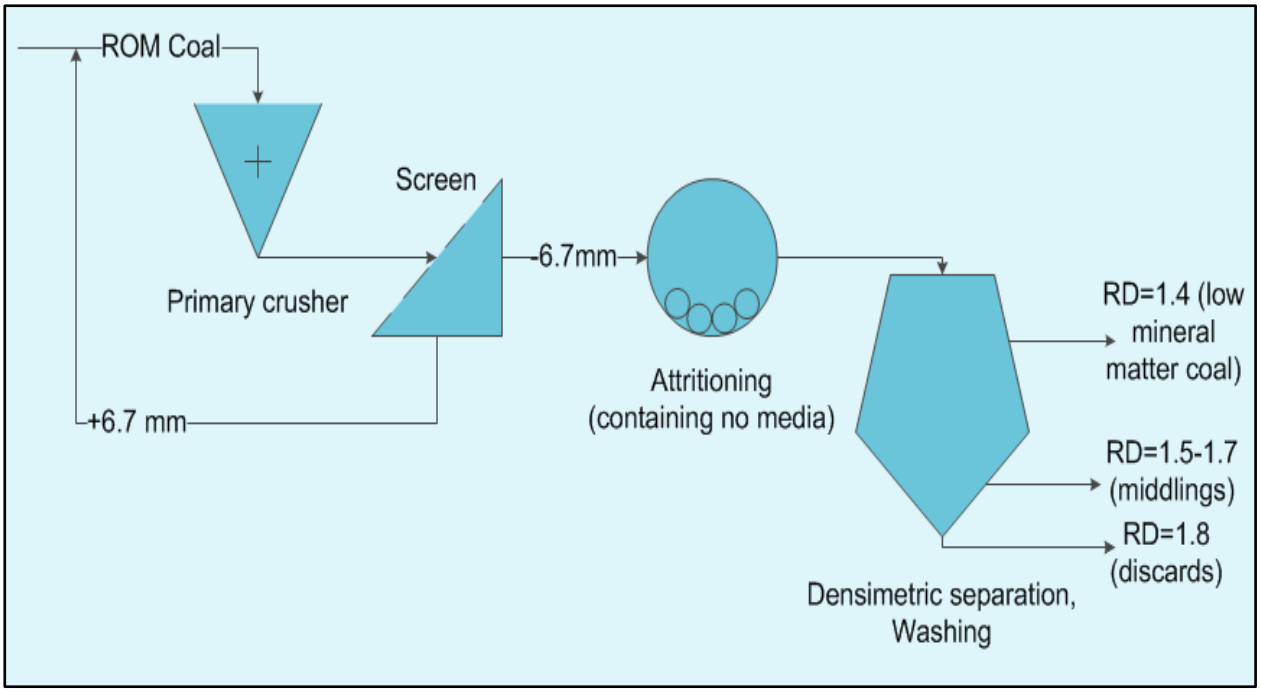

Figure 5.3: Industrial application.

It is suggested that run-of-mine coal are fed to a primary crusher, preferably one that uses impact breakage as the main breakage mode. The reason impact breakage is preferred, is that results obtained during this study have shown that impact breakage resulted in a higher yield of liberated coal macerals (material with a relative density of 1.4 and lower). Another reason why impact breakage is preferred to compressive breakage is that compressive breakage resulted in a larger quantity of fines generation. As discussed in Section 4.4, the fines generation during compressive breakage can be ascribed to the compressive forces that were applied directly to the surface of the particles.

Screening of the products from the primary crusher can be performed to any desired top size. For the instance of this study, a screening size of 6.7 mm was chosen, because of the experimental results obtained during this study showing that the yield of liberated coal macerals are significantly increased when breakage to a top size of 6.7 mm was performed. These results are discussed in Chapter 4. Screening of undersize material can also minimize fines generation. Oversize material (+6.7 mm) can be recycled back to the primary crusher, or it can be used as thermal coal. Results have shown that material with sizes larger than 6.7 mm mainly occur in the middlings density fractions, and therefore can be used as thermal coal. Attritioning of undersize material (-6.7 mm) can then be performed at a residence time of not more than 5 minutes. Attritioning is performed to chip off all coal macerals exposed during the primary breakage stage. The residence time for

attritioning must be minimum practically possible to prevent the generation of undesirable fines. Attritioning must also be accomplished autogenously, that is only by the particles contacting against one another and against the tumbling mill wall, since media (for example steel balls or rods) will cause even more undesirable fines generation. Material can be separated according to relative density after attritioning. Material occurring in the different relative density fractions can then be used for the various markets, the lower density fractions being used for coking coal and the middlings for a power station feed. It should be kept in mind that the discussed results are the theoretical washability yield and do not take into account the plant inefficiencies. These results will differ in practise, since the efficiency of the separation deteriorates as the particle size decreases. In practice, a density based separation process needs to be applied to the coarse material, while flotation and water based density separations will be required for fines.

6

CHAPTER 6 CONCLUSIONS AND RECOMMENDATIONS

This chapter presents the conclusions that were made according to the results obtained and will be discussed in this chapter. Thereafter, some recommendations on how to improve future research studies similar to this investigation to enhance the body of knowledge in the subject area will be suggested. The chapter concludes with a section detailing the contribution to the discipline, which lists the various papers presented during the course of the study.

6.1 Conclusions

Conclusions that were made during this study can relate to the specific objectives as stated in Section 1.2. The specific objectives of this research study will again be given along with the conclusions made:

1. To evaluate the combinations of breakage modes to determine the most effective method for optimizing coal yield, and to achieve sufficient liberation whilst limiting excessive fines formation.

Results of impact breakage and compressive breakage to the top sizes of 6.7 mm and 13.2 mm were investigated, as well as the cases where the initial breakage mode was followed by additional breakage using autogenous attritioning at different residence times. These results have shown that impact breakage and compressive breakage to a top size of 13.2 mm had an insignificant effect on the coal yield compared to the coal yield of raw coal prior to testing. Results for breakage, impact as well as compressive, to a top size of 6.7 mm showed an increase in the coal yield compared to that of the raw coal. Specifically, impact breakage to a top size of 6.7 mm had shown a substantial increase in the coal yield. Attrition breakage additional to impact breakage resulted in an even further increase in the coal yield. It can therefore be concluded that the most effective combinations of breakage modes applied to optimize the coal yield are impact breakage to a top size of 6.7 mm followed by attritioning for 1 minute. The residence time for attritioning must be a minimum to keep fines generation as low possible.

2. Determination of the coal yield improvement when a specified combination of breakage modes are implemented.

This study focused on the material with relative density of 1.4 and less because of the relative "clean" coal at these densities. Material occurring in this relative density range (RD<1.4) are already liberated coal macerals. Therefore, the yield of this material attained for each of the various test conditions was compared. When comparing the size by washability graphs for impact breakage and compressive breakage to both top sizes of 6.7 mm and 13.2 mm, it can be concluded that impact breakage resulted in a higher mass percentage (yield) of material with relative density of 1.4 and lower, regardless of the top size. Specifically, the yield was significantly increased by impact breakage to a top size of 6.7 mm. Impact breakage thus resulted in a higher amount of liberated coal with relative density of 1.4 and less. Impact breakage to 6.7 mm followed by attritioning resulted in a cumulative yield (of the liberated coal fraction with RD<1.4) of 39-45 %, while that for compressive breakage to 6.7 mm with additional attrition breakage was 29-33 %. The yield improvement of the liberated coal fraction was thus highest for the breakage combination of impact breakage to a top size of 6.7 mm followed by attrition breakage.

3. To study the effect of attrition breakage additional to compressive breakage and impact breakage on coal yield.

Attrition breakage additional to compressive and impact breakage to a top size of 13.2 mm had no fundamental effect on the coal yield. The only noticeable effect of additional attrition breakage was seen in the results for impact breakage to a top size of 6.7 mm. It was expected that this might be due to impact breakage to a smaller top size of 6.7 mm exposing more coal macerals than breakage to a top size of 13.2 mm. Exposed coal macerals were then chipped off from the mineral matter during attritioning resulting in a higher amount of material with relative density of lower than 1.4. Densimetric curves showed that attrition breakage additional to impact breakage to a top size of 6.7 mm resulted in a 5-10 % yield increase at each relative density fraction. The cumulative floats mass yield at a relative density of 1.4 for the raw coal prior to any testing was 26 %. Impact breakage to a top size of 6.7 mm resulted in a cumulative floats mass yield of 33 % at a relative density of 1.4, while that for the case of additional attritioning was up to 45 %.

4. Determination of the optimum liberation size for the coal used in this investigation.

The cumulative floats mass yield, for a cumulative float ash of 10 %, was over 90 % for the two particles size ranges, 0.0-0.5 mm and 0.5-1.0 mm respectively. The particle size range of 1.0-2.0 mm showed a 64 % cumulative floats mass yield, whilst that for 2.0-4.75mm and 4.75-6.7 mm were 50 % and 18 %, respectively. It can be concluded that as the particle sizes increase, the cumulative floats mass yield at an ash yield of 10 % decreases. This observation

can be ascribed to the brittle vitrinite-rich material that are more susceptible to breakage, resulting in smaller particle sizes. The 4.75-6.7 mm size fraction showed a very low yield compared to the other size fractions. A particle size of 4.75 mm was investigated to be an optimum liberation size. The cumulative fractional yield (with RD<1.4) for the particle size range of 0.0-2.0 mm indicated a lower cumulative fractional yield than the particle size range of 0.0-4.75 mm. This was because of the high value vitrinite that was liberated first from the gangue, where after finely disseminated mineral matter began to liberated, leading to a reverse effect of the increase in the cumulative yield at a particle size of 4.75 mm. Breakage to a smaller top size of 2 mm will therefore not result in a significant coal yield increase.

5. To study the advantages of improving liberation processes of current coal resources.

Current coal resources are being depleted, and the quality (grade) of the remaining in situ coal reserves are also decreasing. This requires the upgrading of low value coal to meet the increasing energy and various other industrial demands. Liberation of coal from mineral matter is not only important for the high energy demand, but the economy also benefits from it. Upgraded coal can be sold as coking coal if the coal meets the strict requirements to be suitable for coking purposes. Coking coal is sold at a higher price internationally than that locally. Other advantages of improving liberation of coal from mineral matter include a decrease in undesired ash yield for the various industrial processes utilizing coal.

6. Sufficient liberation for the coal used during this study must also be defined; that is to determine the largest particles size with the maximum allowable ash yield obtained to produce a product as required by market specifications.

The maximum allowable ash yield was defined as 10 %, since this is the maximum ash yield allowed for coal to be suitable for coking purposes. The cumulative floats mass yield (for impact breakage to a top size followed by attritioning for 1 minute), for a cumulative float ash of 10 %, was over 90 % for the particles size ranges of 0.0-0.5 mm and 0.5-1.0 mm. The particle size range of 1.0-2.0 mm showed a 64 % cumulative floats mass yield, whilst that for 2.0-4.75mm was 50 %. Although smaller particle size ranges showed a higher coal yield, a particle size of 4.75 mm also indicated a relative high coal yield. Therefore, the largest particle size with a maximum ash yield of 10 % was 4.75, which indicated a yield of 50 %.

6.2 Recommendations

Recommendations on how to improve future research studies similar to this investigation, and areas that potentially need further research are as follow:

- It is recommended that this study should be repeated by similar experimental procedures, but by using coal particles larger than 0.5 mm instead of using coal as mined. The presence or absence of fines (-0.5 mm) will influence the outcome of the study. For the case of coal containing no fines, the results will be significant different.
- A smaller top size, for example 4.75 mm, should be considered. As the particle size decreases, the liberation of coal from mineral matter increases, resulting in a coal yield increase. Possible practical and economic problems related to the breakage of material to a smaller top size must be considered first. Breakage to a smaller top size will cause an increase in fines generation.
- It is recommended that the direction (orientation) of the breakage force applied relative to the coal bedding plane should be altered. According to Viljoen *et al*. (2015), the direction (along or across the coal bedding plane) of the breakage force applied has a significant effect on the breakage and fracturing of the coal particles. Yet this is impractical for industrial purposes.
- A breakage mode that exposes the vitrinite on the outer layers of the particle are recommended. Attritioning following the primary breakage mode can then better chip off the vitrinite increasing the coal yield.
- It is highly recommended that a study on the petrography of Moatize coal should be done. This will give a better indication of the optimum size for liberation and the mineral matter/coal macerals associations present in the coal.
- It is also recommended to do mineral characterization on Moatize coal, as well as determination of the hardgrove grindability index. This will give an indication of the specific mineral matter composition and an indication of the material hardness.
- Larger sample masses should be used for future studies, especially for the float and sink analysis, as this will give more accurate results. Due to the small subsample mass (6 kg), significant sample variation might have occurred, hiding some underlying trends.
- Liberation mainly occurs at particle sizes smaller than 37.5 mm. Sample sizes can therefore me reduced by screening out the +37.5 mm particles and hand knapping before dividing the sample into subsamples, as this will not affect liberation.

6.3 Contribution to the discipline

This research study indicated that the most effective combination of breakage modes applied to optimize the coal yield was impact breakage to a top size of 6.7 mm followed by attrition breakage for 1 minute. It was concluded that the optimum liberation size was 4.75 mm. As discussed in Section 4.6, breakage to a smaller top size of 2 mm will not result in a significant coal yield increase.

Outputs from this research study are detailed the following conference proceedings:

- Potgieter, W., Campbell, Q.P. & Le Roux, M. 2015. The effect of the breakage mechanism on coal liberation. Paper presented at 20th Southern African Conference on Research in Coal Science and Technology: Latest Research at Universities and R&D Organizations, Potchefstroom, South Africa, 25 November 2015.
- Potgieter, W., Campbell, Q.P. & Le Roux, M. 2015. The effect of the breakage mechanism on coal liberation. Paper presented at the 6th National Student Colloquium, Braamfontein, Johannesburg, South Africa, 30 June 2015.
- Potgieter, W., Campbell, Q.P. & Le Roux, M. 2015. The effect of the breakage mechanism on coal liberation. Paper presented at SAMMRI Workshop, Newlands, Cape Town, South Africa, 03 November 2015.
- Campbell, Q.P., Potgieter, W. & Le Roux, M. 2016. The effect of the mode of applied breakage on coal yield. Paper presented at SAMMRI Workshop, Newlands, Cape Town, South Africa, 31 October 2016.

BIBLIOGRAPHY

Ajaka, E.O. & Akinbinu, V.A. 2011. Design, fabrication and performance analysis of a planetary roll mill for fine graining. *ARPN Journal of Engineering and Applied Science*, 6(4):75-90.

ASTM (American Society for Testing and Materials). 2014. Hard coal – Standard Test Method for Sulfur in the Analysis Sample of Coal and Coke Using High-Temperature Tube Furnace Combustion. United States: ASTM International. (ASTM D4239-14e1).

Callen, A.M., Pratten, S.J., Belcher, B.D. Lambert, N. & Galvin, K.P. 2010. An Alternative Method for Float-Sink Analysis of Fine Coal Samples using Water Fluidization. *Coal Preparation*, 22:293-310.

Campbell, Q.P. 2016. Product prices [E-mail]. 2 June 2016, Potchefstroom.

Campbell, Q.P., Barnardo, M.D. & Bunt, J.R. 2013. Moisture adsorption and desorption characteristics of some South African coals. *The Journal of The Southern Africa Institute of Mining and Metallurgy*, 113:803-807.

Davis, S.B. & Dawson, M.F. 1989. A laboratory study of attrition grinding. *Journal of The South African Institute of Mining and Metallurgy*, 89(8):231-241.

De Korte, G.J. 2001. Beneficiation of Weathered Coal. http://www.coaltech.co.za/chamber%20databases%5Ccoaltech%5CCom_DocMan.nsf/0/D1887A4A1676BCD142257436002B53EC/$File/Oxidised%20Coal%20Report.pdf. Date of access: 25 October 2016.

Directorate-General for Energy. 1990. Coal breakage characteristics in various forms of comminution equipment. Luxembourg: Commission of the European Communities. http://www.bookshop.europa.eu/es/coal-breakage-characteristics-in-various-forms-of-comminution-equipment.-report-pbCDNA12362/downloads/CD-NA-12-362-EN-C/CDNA12362ENC_001.pdf;pgid=y8dIS7GUWMdSR0EAlMEUUsWb0000UnZZGQV9?FileName=CDNA12362ENC_001.pdf&SKU=CDNA12362ENC_PDF&CatalogueNumber=CD-NA-12-362-EN-C. Date of access: 25 October 2016.

Dorland, H. 2016. Visual description of Moatize coal. [E-mail]. 26 August 2016, Potchefstroom.

Drzymala, J. 2007. Mineral Processing. 1st Ed. Wroclaw: University of Technology.

Eberhard, A. 2011. The future of South African coal: Market, investment, and policy challenges. https://pesd.fsi.stanford.edu/sites/default/files/WP_100_Eberhard_Future_of_South_African_Coal.pdf. Date of access: 25 October 2016.

Esterle, J.S., Kolatschek, Y. & O'Brien, G. 2002. Relationship between in situ coal stratigraphy and particle size and composition after breakage in bituminous coals. *International Journal of Coal Geology*, 49(2002):195-214.

Falcon, L.M. & Falcon, R.M.S. 1987. The petrographic composition of Southern African coals in relation to friability, hardness, and abrasive indices. *Journal of the South African Institute of Mining and Metallurgy*, 87(10):323-336.

Falcon, R. & Ham, A.J. 1988. The characteristics of Southern African coals. *Journal of the South African Institute of Mining and Metallurgy*, 88(5):145-161.

Falcon, R.M.S. & Snyman, C.P. 1986. An introduction to coal petrography: Atlas of petrographic constituents in the bituminous coals of Southern Africa. Johannesburg, South Africa: The Geological Society of South Africa.

GEMECS (Pty) Ltd. 2010. Limpopo Coal Project Coal Resource CPR. http://www.universalcoal.com/wp-content/sharelink/20101209-independent-competent-persons-report----limpopo-87548883349868851.pdf. Date of access: 25 October 2016.

Hancox, P.J. & Götz, A.E. 2014. South Africa's coalfields – A 2014 perspective. *International Journal of Coal Geology*, 132(2014):170-254.

Hanlon, J. 2013. Mozambique to become one of biggest coal & gas producers. *Mozambique political process bulletin,* 53(2013):1-12.

Hartnady, C.J.H. 2010. South Africa's diminishing coal reserves. *South African Journal of Science*, 106(9/10):1-5.

Hatton, W. & Fardell, A. 2012. New discoveries of coal in Mozambique - Development of the coal resource estimation methodology for International Resource Reporting Standards. *International Journal of Coal Geology*, 89(2012):2-12.

Hogg, R. 1999. Breakage mechanisms and mill performance in ultrafine grinding. *Powder Technology,* 105(1999):135-140.

Holuszko, M.E. & Grieve, D.A. 1990. Washability characteristics of British Columbia Coals. *Geological Fieldwork,* 1991(1):371-379.

Holuszko, M.E. & Mastalerz, M.D. 2014. Coal Macerals Chemistry and its Implications for Selectivity in Coal Floatability. *International Journal of Coal Preparation and Utilization*, 35(2):99-110.

Horsfall, D.W. 1980. A general review of coal preparation in South Africa. *Journal of the South African Institute of Mining and Metallurgy*, 1980(80):257-268.

International Monetary Fund. 2016. Commodity Special Feature from World Economic Outlook. https://www.imf.org/external/pubs/ft/weo/2016/01/pdf/SF_Commod.pdf. Date of access: 25 October 2016.

ISO (International Organization for Standardization). 1992. Hard coal – Determination and presentation of float and sink characteristics – General directions for apparatus and procedures. Pretoria: SABS Standards Division. (ISO 7936).

ISO (International Organization for Standardization). 1994. Hard coal – Size analysis by sieving. Pretoria: SABS Standards Division. (ISO 1953).

ISO (International Organization for Standardization). 1994. Accuracy (trueness and precision) of measurement methods and results. Pretoria: SABS Standards Division. (ISO 5725).

ISO (International Organization for Standardization). 1997. Solid mineral fuels – Determination of ash content. Pretoria: Standards South Africa. (ISO 1171).

ISO (International Organization for Standardization). 1998. Hard coal and coke – Determination of volatile matter. Pretoria: Standards South Africa. (ISO 562).

ISO (International Organization for Standardization). 2001. Hard coal and coke – Mechanical sampling. Pretoria: SABS Standards Division. (ISO 13909).

ISO (International Organization for Standardization). 2003. Hard coal – Determination of the crucible swelling number. Pretoria: SABS Standards Division. (ISO 501).

ISO (International Organization for Standardization). 2006. Hard coal and coke – Manual sampling. Pretoria: Standards South Africa. (ISO 18283).

ISO (International Organization for Standardization). 2009. Solid mineral fuels – Determination of gross calorific value by the bomb calorimetric method, and calculation of net calorific value. Pretoria: SABS Standards Division. (ISO 1928).

Ito, M., Owada, S., Nishimura, T. & Ota, T. 2009. Experimental study of coal liberation: Electrical disintegration versus roll-crusher comminution. *International Journal of Mineral Processing*, 92(2009):7-14.

Jankovic, A., Valery, W. & La Rosa, D. 2000. Fine grinding in the Australian mining industry. http://www.metso.com/miningandconstruction/mct_service.nsf/WebWID/WTB-120106-22576-A45AE/$File/043.pdf. Date of access: 25 October 2016.

Jeffrey, L.S. 2005. Characterization of the coal resources of South Africa. *The Journal of The South African Institute of Mining and Metallurgy*, 105(2):95-102.

Khandelwal, M. & Singh, T.N. 2010. Prediction of macerals contents of Indian coals from proximate and ultimate analyses using artificial neural networks. *Fuel,* 89(2010):1101-1109.

King, R.P. 1999. Technical notes 8 Grinding. http://www.mineraltech.com/MODSIM/ModsimTraining/Module6/Grinding.pdf. Date of access: 25 October 2016.

King, R.P. & Birtek, N. 1990. The washability of fine South African coals. *Journal of the South African Institute of Mining and Metallurgy,* 90(11):289-301.

Kruger, H. 2013. Coking coal. http://www.fossilfuel.co.za/conferences/2013/CoalCokeCarbon/Day-One/02-Hannes-Kruger_Coking-Coal.pdf. Date of access: 25 October 2016.

Kumba Resources, 2016. Macro-economics and commodity prices. http://www.exxaro.com/pdf/icpr/ef/me/coal_analysis.htm. Date of access: 25 October 2016.

Lakshminarayana, G. 2015. Geology of Barcode type coking coal seams, Mecondezi sub-basin, Moatize Coalfield, Mozambique. *International Journal of Coal Geology*, 146(2015):1-13.

Laubach, S.E., Marrett, R.A., Olson, J.E. & Scott, A.R. 1998. Characteristics and origins of coal cleat: A review. *International Journal of Coal Geology,* 35(1998): 175-207.

Le Roux, M., Campbell, Q.P. & Smit, W. 2012. Large-scale design and testing of an improved fine coal dewatering system. *The Journal of the Southern African Institute of Mining and Metallurgy,* 112:673-676.

Levine, D.G., Schlosberg, R.H. & Silbernagel, B.G. 1982. Understanding the Chemistry and Physics of Coal Structure (A Review). *Proceedings of the National Academy of Sciences of the United States of America*, 79(10):3365-3370.

Mahapatra, D. 2015. A Review on Steam Coal Analysis – Moisture. American International Journal of Research in Science, Technology, Engineering and Mathematics, pp143-152.

Mohanta, S., Sahoo, B., Behera, I.D. & Pradhan, S. 2015. Effect of crushing on near-gravity material distribution in different size fractions of an Indian non-coking coal. *The Journal of The South African Institute of Mining and Metallurgy*, 116(2):209-213.

O' Brien, G., Firth, B. & Adair, B. 2011. The application of the coal grain analysis method to coal liberation studies. *International Journal of Coal Preparation and Utilization*, 31(2011):96-111.

Oki, T., Yotsumoto, H. & Owada, S. 2004. Calculation of degree of mineral matter liberation in coal from sink-float separation data. *Minerals Engineering*, 17(2004):39-51.

Özer, C.E. & Whiten, W.J. 2012. A multi-component appearance function for the breakage of coal. *International Journal of Mineral Processing*, 104-105(2012):37-44.

Pan, J., Meng, Z., Hou, Q., Ju, Y. & Cao, Y. 2013. Coal strength and Young's modulus related to coal rank, compressional velocity and maceral composition. *Journal of Structural Geology*, 54(2013):129-135.

Pinheiro, H.J. & Cook, A.C. 2005. Cutting out the complexities of coal classification. *ISO Focus*, 2(6):20-24.

Pooe, D. & Mathu, K. 2011. The South African Coal Mining Industry: A need for a more efficient and collaborative supply chain. *Journal of Transport and Supply Chain Management*, 5(1):316-336.

Powell, D. 2016. Coal beneficiation [personal communication]. 7 October 2016, Potchefstroom.

Raju, C.A.I., Satyanandam, K , Sravanthi, D.V.S., Hussain Reddy, P. & Rao, P.J. 2013. Studies on Batch Grinding of Bauxite Ore in Ball Mill. *International Journal of Engineering and Innovative Technology*, 2(11):140-147.

Rosenfeld, D. 2012. The coal mining sector in Mozambique: A simple mode of predicting government revenue. http://www.iese.ac.mz/lib/publication/III_Conf2012/IESE_IIIConf_Paper19.pdf. Date of access: 25 October 2016.

Sahoo, R. 2006. Review: An investigation of single particle breakage tests for coal handling system of the Gladstone Port. *Powder Technology*, 161(2006):158-167.

Sahoo, R. & Roach, D. 2005. Quantification of the lump coal breakage during handling operation at the Gladstone Port. *Chemical Engineering and Processing*, 44(2005):797-804.

Sankar Prasath, D. & Venkatesh, N. 2014. Design and analysis of ball mill inlet chute for roller press circuit in cement industry. International Journal of Research in Engineering and Technology, 3(11):205-212.

SANS (South African National Standards). 1994. Hard coal – Size analysis by sieving. Pretoria: SABS Standards Division. (SANS 1953).

SANS (South African National Standards). 2005. Solid minerals fuels – Determination of moisture in the general analysis test sample by drying in nitrogen. Pretoria: SABS Standards Division. (SANS 11722).

SANS (South African National Standards). 2009. Accuracy (trueness and precision) of measurement methods and results. Part 6: Use in practice of accuracy values. Pretoria: SABS Standards Division. (SANS 5725).

SANS (South African National Standards). 2011. Coal – Proximate analysis. Pretoria: SABS Standards Division. (SANS 17246).

SANS (South African National Standards). 2007. Hard coal and coke – Manual sampling. Pretoria: SABS Standards Division. (SANS 18283).

SANS (South African National Standards). 2010. Hard coal – Determination and presentation of float and sink characteristics – General directions for apparatus and procedures. Pretoria: SABS Standards Division. (SANS 7936).

SANS (South African National Standards). 2010. Standard test method of drop shatter test for coal. Pretoria: SABS Standards Division. (SANS 401).

Scholtès, L., Donzé, F. & Khanal, M. 2001. Scale effects on strength of geomaterials, case study: coal. *Journal of the Mechanics and Physics of Solids*, 59(5):1131-1146.

Shi, F. 2014. Coal breakage characterization – Part 2: Multi-component breakage modelling. *Fuel*, 117(2014):1156-1162.

Shi, F. & Zuo, W., 2014. Coal breakage characterization – Part 1: Breakage testing with the JKFBC. *Fuel*, 117(2014):1148-1155.

Singh, V., Venugopal, R., Banerjee, P.K. & Saxena, V.K. 2014. Effect of morphology on breakage and liberation characteristics of minerals and coal. *Minerals and Metallurgical Processing*, 31(4):186-192.

Speight, J.G. 2005. Handbook of Coal Analysis. 1st ed. New Jersey: John Wiley & Sons, Inc.

Subramoney, J., van Wyk, J., Dithupe, M., Molapo, A., Mahlangu, N. & Morumudi, R. 2009. Digest of South African energy statistics 2009. http://www.energy.gov.za/files/media/explained/2009%20Digest%20PDF%20version.pdf. Date of access: 25 October 2016.

Surowiak, A. 2013. Assessment of Coal Mineral Matter Liberation Efficiency Index. http://www.potopk.republika.pl/Full_text/im_2013_z2_a28.pdf. Date of access: 25 October 2016.

Sushant, S. & Archana, K. 2013. Methods of size reduction and factors affecting size reduction in pharmaceutics. *International Research Journal of Pharmacy*, 4(8):57-64.

Tavares, L.M. 2004. Optimum routes for particle breakage by impact. *Powder Technology*, 142(2004):81-91.

The South African Coal Roadmap. 2011. Overview of the South African coal value chain. http://www.sanedi.org.za/wp-content/uploads/2016/02/sacrm_overview.pdf. Date of access: 25 October 2016.

The Southern African Coal Processing Society. 2015. Coal Preparation in Southern Africa. 5th ed. South Africa: The Southern African Coal Processing Society.

The Southern African Institute of Mining and Metallurgy. 2013. Coal – Balance between supplies to Eskom and exports. http://www.saimm.co.za/journal-presidents-corner/323-coal-balance-between-supplies-to-eskom-and-exports. Date of access: 25 October 2016.

Usaini, M.N.S., Ali, M. & Usman, H.A. 2014. Determination of liberation size of Akiri copper ore, Nasarawa state, north-central Nigeria. *International Journal of Engineering Development and Research*, 2(2):1444-1452.

Vasconcelos, L. 1999. The petrographic composition of world coals. Statistical results obtained from a literature survey with reference to coal type (maceral composition). *International Journal of Coal Geology*, 40(1999):27-58.

Vasconcelos, L., Chafy, A. & Xerinda, L. 2014. Determination of the limit of oxidation in zones of sub-outcropping Chipanga Coal Seam, Moatize Coal Basin, Mozambique. *Journal of African Earth Sciences*, 99(2014):554-567.

Viljoen, J., Campbell, Q.P., Le Roux, M. & De Beer, F. 2015. An Analysis of the Slow Compression Breakage of Coal Using Microfocus X-Ray Computed Tomography. *International Journal of Coal Preparation and Utilization*, 35(2015):1-13.

Wagner, N.J. & Tlotleng, M.T. 2012. Distribution of selected trace elements in density fractionated Waterberg coals from South Africa. *International Journal of Coal Geology*, 94(2012):225-237.

Ward, C.R. 2002. Analysis and significance of mineral matter in coal seams. *International Journal of Coal Geology,* 50(2002):135-168.

Ward, C.R. & French, D. 2004. Analysis and Significance of Mineral Matter in Coal. Paper presented at the Twenty-first Annual Meeting of The Society for Organic Petrology, Sydney, Australia, 27 September. https://pubs.usgs.gov/of/2004/1283/tsop_volume.pdf. Date of access: 25 October 2016.

Weining, X., Yaqun, H., Xiangnan, Z.,Linhan, G., Yajun, H., Haifeng, W. 2013. Liberation characteristics of coal middlings comminuted by jaw crusher and ball mill. *International Journal of Mining Science and Technology*, 23(2013):669-674.

Wills, B.A. & Napier-Napier-Munn, T.J. 2006. Wills' Mineral Processing Technology. 7th ed. Queensland: Elsevier Science & Technology Books.

World Coal Institute. 2005. The Coal Resource: A Comprehensive Overview of Coal. http://www.worldcoal.org/file_validate.php?file=coal_resource_overview_of_coal_report(03_06_2009).pdf. Date of access: 25 October 2016.

World Energy Council. 2013. World Energy Resources: Coal. https://www.worldenergy.org/wp-content/uploads/2013/10/WER_2013_1_Coal.pdf. Date of access: 25 October 2016.

Wright, J.D., Bean, V.E. & Aguilera, J. 2008. NIST Calibration Services for Hydrometers. https://www.nist.gov/sites/default/files/documulents/calibrations/sp250-78.pdf. Date of access: 19 September 2016.

Xie, K.C. 2015. Structure and Reactivity of Coal. 1st ed. London: Springer-Verlag Berlin Heidelberg.

XMP Consulting CC. 2014. The South African Coal industry. Paper presented at the Coaltrans Conferences, Dubai, 25 November. http://www.fossilfuel.co.za/presentations/2014/The_SA_Coal_Industry_Middle_East_Coaltrans-2014.pdf. Date of access: 25 October 2016.

Zhu, Q. 2014. Coal sampling and analysis standards. https://www.usea.org/sites/default/files/042014_Coal%20sampling%20and%20analysis%20standards_ccc235.pdf. Date of access: 13 October 2016.

APPENDIX A: EXPERIMENTAL

Figure A. 1: Belt sander

Figure A. 2: Riffle splitter

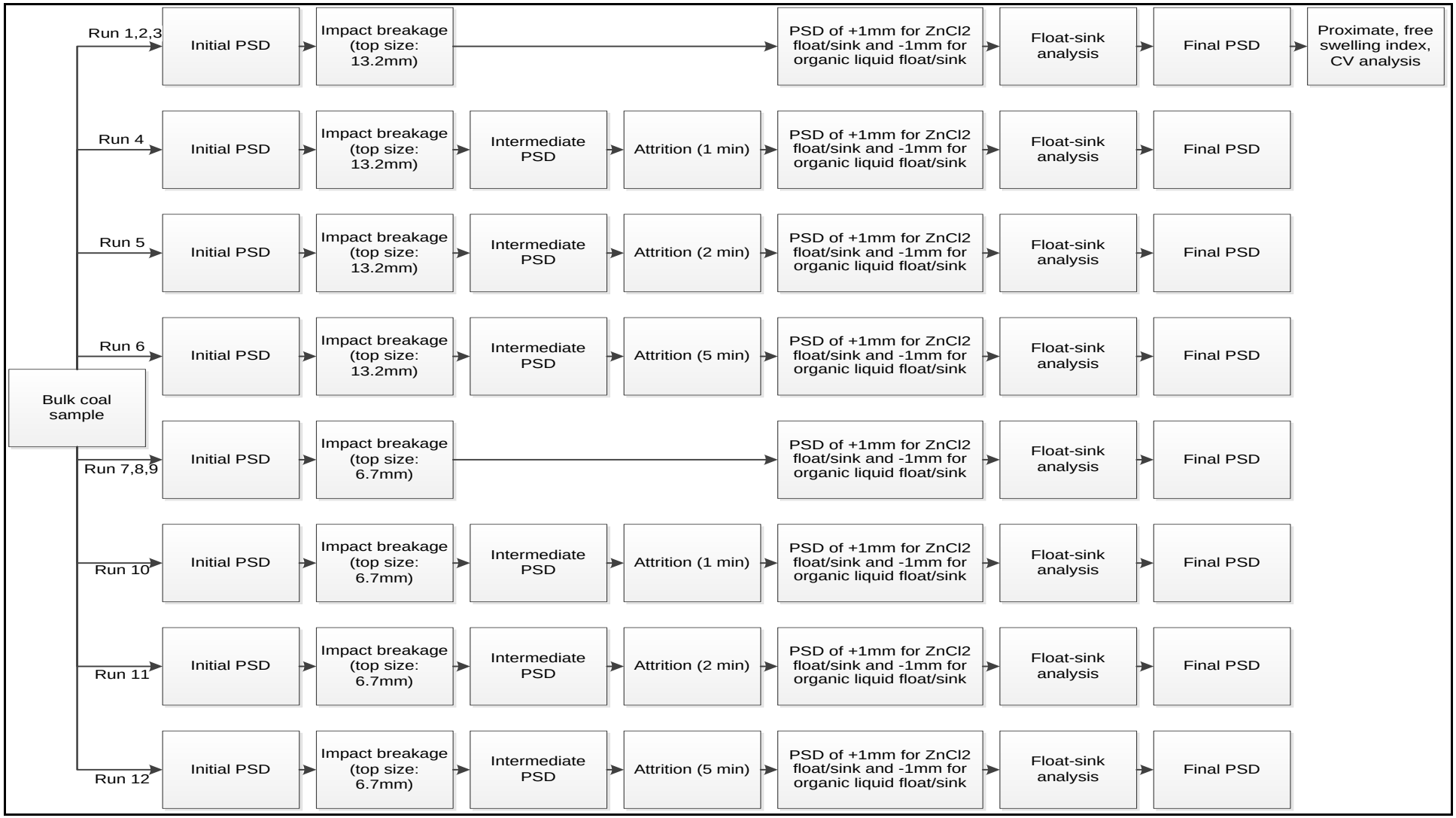

Figure A. 3: Flow diagram of steps performed during impact breakage.

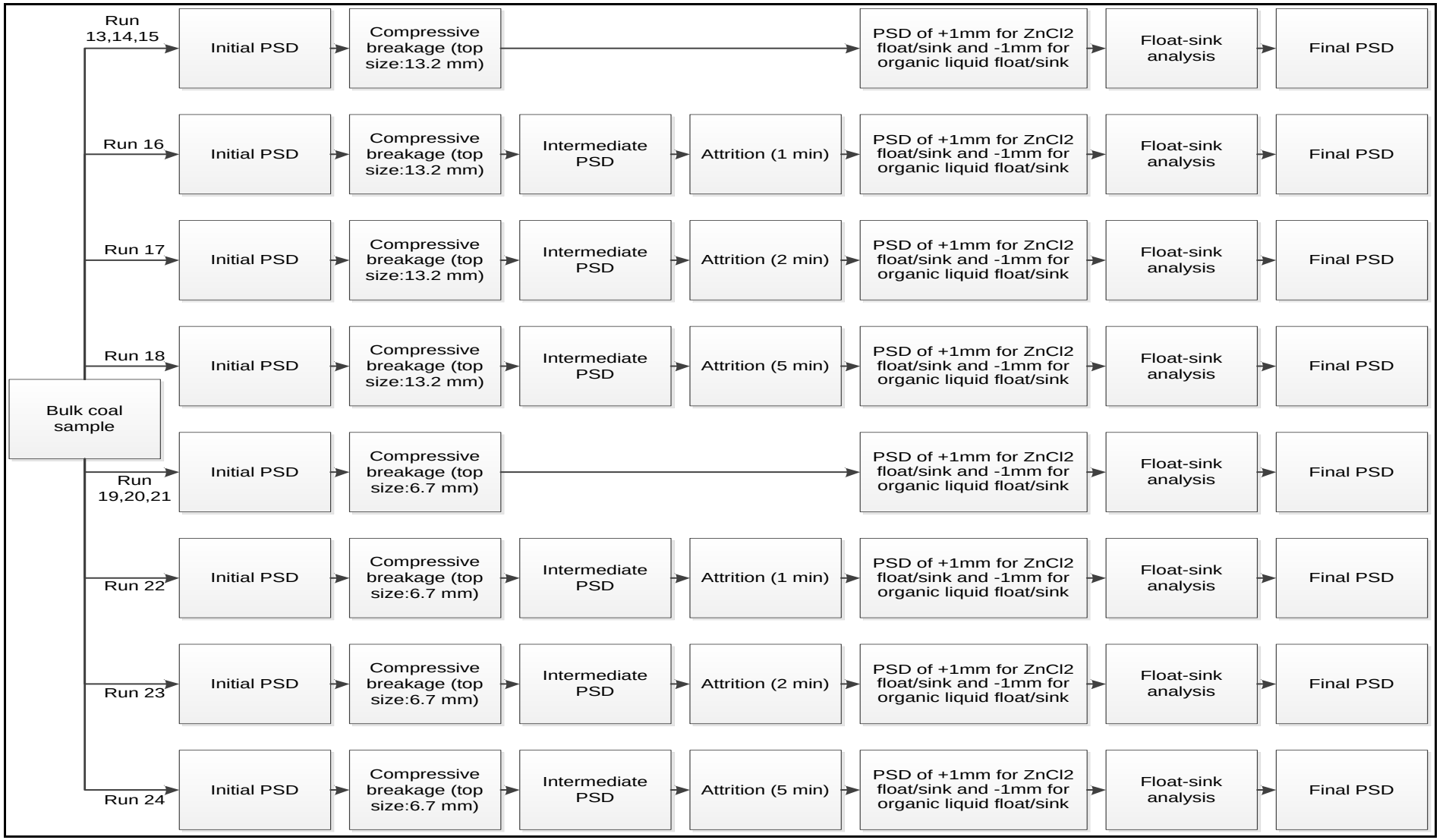

Figure A. 4: Flow diagram of steps done during compressive breakage.

APPENDIX B: RAW EXPERIMENTAL DATA

Appendix B gives all raw experimental data. The abbreviation “Attr” was used to indicate attrition breakage, and “Comp” refers to compressive breakage. These abbreviations were used to indicate the experimental conditions and to shorten the lengthy naming convention of the various experimental test conditions.

Proximate analysis, calorific value and free swelling index analysis

Table B. 1 and Table B. 2 give the raw data for the proximate analysis, calorific value and free swelling index determination.

Table B. 1: Proximate analysis, calorific value analysis and free swelling index analysis results for particle sizes 0.0-1.0 mm (Air dry basis).

	Inherent moisture (%)	Ash (%)	Volatile matter (%)	Fixed Carbon (%)	Calorific value (MJ/kg)	Total sulphur (%)	Free swelling index
Sample Name	ISO 11722: 2013	ISO 1171:2010	ISO 562:2010	By difference (Equation 2.1)	ISO 1928:2009	ASTM D4239-14e1	ISO 501: 2003
F1.3	1.20	4.30	22.60	71.90	34.00	1.44	9.00
1.3-1.4	1.60	5.30	21.50	71.60	33.80	1.22	9.00
1.4-1.5	2.00	12.20	19.70	66.10	30.60	1.31	7.00
1.5-1.6	2.50	21.80	18.50	57.20	26.30	1.46	1.50
1.6-1.7	3.00	27.90	17.30	51.80	23.60	1.56	0.00
1.7-1.8	3.10	36.10	16.70	44.10	20.40	1.56	0.00
S1.8	4.30	57.30	23.80	14.60	9.20	4.24	0.00

Table B. 2: Proximate analysis, calorific value analysis and free swelling index analysis results for particle sizes 1.0-13.2 mm (Air dry basis).

	Inherent moisture (%)	Ash (%)	Volatile matter (%)	Fixed Carbon (%)	Calorific value (MJ/kg)	Total sulphur (%)	Free swelling index
Sample Name	ISO 11722: 2013	ISO 1171:2010	ISO 562:2010	By difference (Equation 2.1)	ISO 1928:2009	ASTM D4239-14e1	ISO 501: 2003
F1.3	1.50	4.40	18.90	75.20	34.18	0.98	7.50
1.3-1.4	1.60	12.60	17.20	68.60	30.67	0.90	4.00
1.4-1.5	1.60	19.40	16.20	62.80	28.14	0.90	2.50
1.5-1.6	1.30	26.70	15.30	56.70	25.05	0.82	1.00
1.6-1.7	1.60	34.90	14.10	49.40	21.94	0.80	0.00
1.7-1.8	1.50	43.60	12.90	42.00	18.38	0.86	0.00
S1.8	1.80	61.10	12.70	24.40	10.64	1.70	0.00

Initial particle size distributions:

Table B. 3 to Table B. 7 presents the initial PSD for the experiments conducted. The initial PSD was the PSD done before any breakage occurred.

Table B. 3: Initial particle size distribution for raw ROM coal.

Particle size (mm)	Sieve mass (g)	Run 28- Base run (raw coal) (g)
53-75	4780	5260
37.5-53	3590	4340
26.5-37.5	3400	3960
19-26.5	3500	4160
13.2-19	3330	4030
9.5-13.2	3380	3850
6.7-9.5	3510	3920
4.75-6.7	3590	3890
0-4.75	3040	4970
Mass after riffle splitter	-	505.5
2-4.75	511.6	562.6
1-2	360.6	501.8
0.5-1	315.3	474.0
0-0.5	464.5	501.7

Table B. 4: Initial particle size distribution for impact breakage to a top size of 13.2 mm.

Particle size (mm)	Sieve mass (g)	Run 1-Impact13.2mm, Attr0min (g)	Run 2-Impact13.2mm Attr0min (g)	Run 3-Impact13.2mm, Attr0min (g)	Run 4-Impact13.2mm, Attr1min (g)	Run 5-Impact13.2mm, Attr2min (g)	Run 6-Impact13.2mm, Attr5min (g)
53-75	4990	4990	4990	4990	5440	4990	4990
37.5-53	3600	4840	5170	4080	4910	5040	4550
26.5-37.5	3400	4230	3970	4210	4400	4220	3930
19-26.5	3490	4160	4110	4190	4300	4090	4090
13.2-19	3330	4060	4120	4090	3950	3920	4020
9.5-13.2	3380	3830	3900	3920	3790	3880	4010
6.7-9.5	3520	3990	3940	4030	3860	3950	4000
4.75-6.7	3600	3870	3870	3930	3800	3870	3940
0-4.75	3040	4820	4860	5120	4330	4820	5130
Mass after riffle splitter	-	465.9	523.4	545.2	668.3	469.9	527.1
2-4.75	511.3	702.0	717.8	720.5	775.8	698.6	750.3
1-2	359.9	549.9	547.3	600.7	664.2	558.0	596.9
0.5-1	315.2	384.6	427.2	392.3	387.9	387.0	357.4
0-0.5	464.5	478.8	479.1	479.8	488.3	474.5	470.1

Table B. 5: Initial particle size distributions for impact breakage to a top size of 6.7 mm.

Particle size (mm)	Sieve mass (g)	Run 7-Impact6.7mm, Attr0min (g)	Run 8-Impact6.7mm Attr0min (g)	Run 9-Impact6.7mm, Attr0min (g)	Run 10-Impact6.7mm, Attr1min (g)	Run 11-Impact6.7mm, Attr2min (g)	Run 12-Impact6.7mm, Attr5min (g)
53-75	4990	4990	5530	4990	4990	5500	5500
37.5-53	3600	4240	4150	4810	4830	4380	4240
26.5-37.5	3400	4020	3820	4500	3770	4190	4230
19-26.5	3490	4150	4640	4360	3950	4230	3990
13.2-19	3330	4040	4030	3990	3880	3880	3890
9.5-13.2	3380	3970	3870	3900	3810	3800	3970
6.7-9.5	3520	4050	3980	3930	3990	3910	3890
4.75-6.7	3600	3950	3930	3910	3940	3870	3890
0-4.75	3040	5200	5100	5130	5490	4800	4960
Mass after riffle splitter	-	550.7	564.2	551.2	566.3	430.3	525.2
2-4.75	511.3	737.1	744.8	703.8	707.6	657.5	692.6
1-2	359.9	618.1	598.5	516.5	534.2	486.3	534.2
0.5-1	315.2	374.9	391.1	460	463.6	422.3	449.2
0-0.5	464.5	468.6	474.8	520.6	509.2	513.9	496.8

Table B. 6: Initial particle size distributions for compressive breakage to a top size of 13.2 mm.

Particle size (mm)	Sieve mass (g)	Run 13-Comp13.2mm, Attr0min (g)	Run 14-Comp13.2mm Attr0min (g)	Run 15-Comp13.2mm, Attr0min (g)	Run 16-Comp13.2mm, Attr1min (g)	Run 17-Comp13.2mm, Attr2min (g)	Run 18-Comp13.2mm, Attr5min (g)
53-75	4790	4790	5350	4940	5000	4790	5090
37.5-53	3600	4000	3830	4000	4650	4370	4200
26.5-37.5	3400	4390	4060	3810	3890	4410	3760
19-26.5	3490	4330	4150	4000	4130	4170	4130
13.2-19	3330	4080	4070	4020	3930	4020	3870
9.5-13.2	3390	3950	3930	3980	3850	3850	3870
6.7-9.5	3520	4070	4030	4160	3990	3980	4050
4.75-6.7	3600	3870	3980	4020	3920	3920	3940
0-4.75	3040	5040	5120	5560	5090	5010	5300
Mass after riffle splitter	-	472.5	599.6	804.5	419.6	501.7	649.5
2-4.75	511.2	709.6	778.3	856.9	706.4	718.3	805.4
1-2	360.0	576.9	631.7	748.3	548.0	602.9	656.2
0.5-1	315.1	365.7	371.0	382.3	351.1	365.4	374.1
0-0.5	464.6	469.6	468.5	467.6	465.6	466.3	465.7

Table B. 7: Initial particle size distributions for compressive breakage to a top size of 6.7 mm.

Particle size (mm)	Sieve mass (g)	Run 19-Comp6.7mm, Attr0min (g)	Run 20-Comp6.7mm Attr0min (g)	Run 21-Comp6.7mm, Attr0min (g)	Run 22-Comp6.7mm, Attr1min (g)	Run 23-Comp6.7mm, Attr2min (g)	Run 24-Comp6.7mm, Attr5min (g)
53-75	4780	6730	5950	4780	5230	5490	5170
37.5-53	3600	3960	4060	4370	4430	4070	3950
26.5-37.5	3400	4030	4120	4040	3870	4040	3980
19-26.5	3490	3950	3990	4060	4100	4110	4290
13.2-19	3330	3750	3950	4090	3990	3780	3990
9.5-13.2	3380	3740	3760	3880	3840	3790	3900
6.7-9.5	3520	3860	3910	4060	4000	3940	4030
4.75-6.7	3600	3840	3840	3970	3880	3890	3900
0-4.75	3040	4580	4740	5340	5030	5210	5220
Mass after riffle splitter	-	388.7	560.6	485.5	507.1	595.5	470.4
2-4.75	511.6	667.3	734.7	715.7	726.5	725.4	683.4
1-2	360.6	531.3	621.8	591.9	568.6	553.4	501.9
0.5-1	315.3	376.5	389.8	365.2	395.2	477.6	437.4
0-0.5	464.5	466.6	466.6	465.4	467.9	490.2	498.8

Intermediate particle size distributions:

Table B. 8 to Table B. 11 presents the intermediate PSD, i.e. the PSD after the first breakage event, compressive or impact, and before any attrition breakage.

Table B. 8: Intermediate particle size distributions for impact breakage to a top size of 13.2 mm.

Particle size (mm)	Sieve mass (g)	Run 1-Impact13.2mm, Attr0min (g)	Run 2-Impact13.2mm Attr0min (g)	Run 3-Impact13.2mm, Attr0min (g)	Run 4-Impact13.2mm, Attr1min (g)	Run 5-Impact13.2mm, Attr2min (g)	Run 6-Impact13.2mm, Attr5min (g)
53-75	4990	No intermediate PSD since no attrition done			4990	4990	4990
37.5-53	3600				3600	3600	3600
26.5-37.5	3400				3400	3400	3400
19-26.5	3490				3490	3490	3490
13.2-19	3330				3330	3330	3330
9.5-13.2	3380				5190	5420	5150
6.7-9.5	3520				4610	4430	4430
4.75-6.7	3600				4160	4080	4120
0-4.75	3040				5980	5960	6100
Mass after riffle splitter	-				738.6	720.9	693.3
2-4.75	511.3				802.3	778.4	763.6
1-2	359.9				517.2	543.4	563.5
0.5-1	315.2				462.7	461.5	483.3
0-0.5	417.5				558.3	541.3	486.5

Table B. 9: Intermediate particle size distributions for impact breakage to a top size of 6.7 mm.

Particle size (mm)	Sieve mass (g)	Run 7-Impact6.7mm, Attr0min (g)	Run 8-Impact6.7mm Attr0min (g)	Run 9-Impact6.7mm, Attr0min (g)	Run 10-Impact6.7mm, Attr1min (g)	Run 11-Impact6.7mm, Attr2min (g)	Run 12-Impact6.7mm, Attr5min (g)
53-75	4980	No intermediate PSD since no attrition done			4980	4980	4980
37.5-53	3600				3600	3600	3600
26.5-37.5	3400				3400	3400	3400
19-26.5	3490				3490	3490	3490
13.2-19	3330				3330	3330	3330
9.5-13.2	3380				3380	3380	3380
6.7-9.5	3520				3520	3520	3520
4.75-6.7	3600				5240	5520	5540
0-4.75	3040				7630	7260	7290
Mass after riffle splitter	-				533.1	828.9	561.0
2-4.75	511.2				718.7	844.6	724.0
1-2	360.1				475.6	551.3	481.8
0.5-1	315.2				413.8	472.9	428.2
0-0.5	417.5				528.8	563.0	531.1

Table B. 10: Intermediate particle size distributions for compressive breakage to a top size of 13.2 mm.

Particle size (mm)	Sieve mass (g)	Run 13-Comp13.2mm, Attr0min (g)	Run 14-Comp13.2mm Attr0min (g)	Run 15-Comp13.2mm, Attr0min (g)	Run 16-Comp13.2mm, Attr1min (g)	Run 17-Comp13.2mm, Attr2min (g)	Run 18-Comp13.2mm, Attr5min (g)
53-75	4790	No intermediate PSD since no attrition done			4790	4790	4790
37.5-53	3600				3600	3600	3600
26.5-37.5	3400				3400	3400	3400
19-26.5	3500				3500	3500	3500
13.2-19	3330				3330	3330	3330
9.5-13.2	3380				5150	5270	5130
6.7-9.5	3520				4580	4560	4490
4.75-6.7	3600				4070	4110	4100
0-4.75	3040				5940	5890	6010
Mass after riffle splitter	-				882.8	593.1	835.1
2-4.75	511.5				869.0	740.1	855.0
1-2	360.2				583.1	509.7	608.7
0.5-1	315.3				526.6	464.8	502.2
0-0.5	417.5				505.1	481.2	471.7

Table B. 11: Intermediate particle size distributions for compressive breakage to a top size of 6.7 mm.

Particle size (mm)	Sieve mass (g)	Run 19-Comp6.7mm, Attr0min (g)	Run 20-Comp6.7mm Attr0min (g)	Run 21-Comp6.7mm, Attr0min (g)	Run 22-Comp6.7mm, Attr1min (g)	Run 23-Comp6.7mm, Attr2min (g)	Run 24-Comp6.7mm, Attr5min (g)
53-75	4790	No intermediate PSD since no attrition done			4790	4790	4790
37.5-53	3600				3600	3600	3600
26.5-37.5	3400				3400	3400	3400
19-26.5	3500				3500	3500	3500
13.2-19	3330				3330	3330	3330
9.5-13.2	3380				3380	3380	3380
6.7-9.5	3520				3520	3520	3520
4.75-6.7	3600				5390	5050	5180
0-4.75	3040				7390	7700	7690
Mass after riffle splitter	-				628.7	991.2	893.2
2-4.75	511.5				807.0	960.9	915.2
1-2	360.2				503.2	572.0	549.9
0.5-1	315.3				447.1	500.9	476.5
0-0.5	417.5				473.0	559.3	552.5

Final particle size distribution:

Table B. 12 to Table B. 16 presents the final PSD. This is the PSD after all breakage events and after the float-sink analysis was done.

Table B. 12: Final particle size distribution for raw ROM coal.

Particle size (mm)	Run 28- Base run (raw coal) (g)
53-75	462.40
37.5-53	735.70
26.5-37.5	541.50
19-26.5	655.80
13.2-19	688.80
9.5-13.2	389.90
6.7-9.5	398.90
4.75-6.7	383.70
2-4.75	600.50
1-2	395.30
0.5-1	364.23
0-0.5	505.07

Table B. 13: Final particle size distributions for impact breakage to a top size of 13.2 mm.

Particle size (mm)	Run 1- Impact13.2mm, Attr0min (g)	Run 2- Impact13.2mm Attr0min (g)	Run 3- Impact13.2mm, Attr0min (g)	Run 4- Impact13.2mm, Attr1min (g)	Run 5- Impact13.2mm, Attr2min (g)	Run 6- Impact13.2mm, Attr5min (g)
9.5-13.2	1926.50	2381.00	1884.90	1477.30	1781.50	1501.40
6.7-9.5	806.60	757.30	734.00	1118.90	864.10	870.70
4.75-6.7	551.20	519.90	550.30	717.80	608.90	626.90
2-4.75	1043.90	947.40	1042.80	1150.20	1058.70	1156.30
1-2	621.50	552.20	654.30	619.80	647.50	790.50
0.5-1	731.73	572.82	421.79	418.28	435.48	436.75
0-0.5	596.17	688.58	567.61	630.62	617.52	630.62

Table B. 14: Final particle size distributions for impact breakage to a top size of 6.7 mm.

Particle size (mm)	Run 7-Impact6.7mm, Attr0min (g)	Run 8-Impact6.7mm Attr0min (g)	Run 9-Impact6.7mm, Attr0min (g)	Run 10-Impact6.7mm, Attr1min (g)	Run 11-Impact6.7mm, Attr2min (g)	Run 12-Impact6.7mm, Attr5min (g)
4.75-6.7	2557.60	2524.10	2928.20	1711.20	1539.90	1714.80
2-4.75	1302.60	1303.90	1470.20	2005.10	1651.10	1710.90
1-2	859.90	806.90	870.20	916.70	911.40	858.20
0.5-1	448.74	383.35	563.01	668.37	584.62	664.39
0-0.5	499.16	541.85	1189.49	1168.93	1065.28	1168.93

Table B. 15: Final particle size distributions for compressive breakage to a top size of 13.2 mm.

Particle size (mm)	Run 13-Comp13.2mm, Attr0min (g)	Run 14-Comp13.2mm Attr0min (g)	Run 15-Comp13.2mm, Attr0min (g)	Run 16-Comp13.2mm, Attr1min (g)	Run 17-Comp13.2mm, Attr2min (g)	Run 18-Comp13.2mm, Attr5min (g)
9.5-13.2	1218.10	1413.30	1330.50	1413.90	1497.80	1372.10
6.7-9.5	749.80	977.00	906.00	986.30	1033.90	944.00
4.75-6.7	426.70	633.90	598.60	601.60	601.80	607.60
2-4.75	816.60	1125.90	1137.10	1042.90	1029.80	1083.90
1-2	447.90	625.00	671.60	587.90	575.80	632.10
0.5-1	500.25	511.45	615.25	583.77	574.76	582.85
0-0.5	650.35	740.05	787.85	790.63	980.44	790.63

Table B. 16: Final particle size distributions for compressive breakage to a top size of 6.7 mm.

Particle size (mm)	Run 19-Comp6mm, Attr0min (g)	Run 20-Comp6mm Attr0min (g)	Run 21-Comp6mm, Attr0min (g)	Run 22-Comp6mm, Attr1min (g)	Run 23-Comp6mm, Attr2min (g)	Run 24-Comp6mm, Attr5min (g)
4.75-6.7	1634.10	2041.60	1828.10	1511.50	1394.10	1427.00
2-4.75	2011.50	1701.90	1870.30	2038.50	2111.70	2167.20
1-2	831.40	741.70	843.90	873.20	838.40	814.70
0.5-1	687.16	647.99	715.14	635.39	734.22	634.08
0-0.5	940.84	895.41	978.36	931.21	1046.28	931.21

Samples mass for float-sink analysis

Table B. 17 to Table B. 21 presents the total mass of the particles with size 0.0-1.0 mm in the sample, as well as the mass used for the float-sink analysis after the sample is split by using a rotary splitter.

Table B. 17: Mass of -1 mm particles for float-sink analysis (raw ROM coal).

Particle size (mm)	Sieve mass (g)	Run 28- Base run (raw coal)
0-1	3040	3860
Mass after rotary splitter	-	398.1
Mass % of 0-1 mm total mass	-	49%

Table B. 18: Mass of -1 mm particles for float-sink analysis (impact breakage to a top size of 13.2 mm).

Particle size (mm)	Sieve mass (g)	Run 1- Impact13.2mm, Attr0min (g)	Run 2- Impact13.2mm Attr0min (g)	Run 3- Impact13.2mm, Attr0min (g)	Run 4- Impact13.2mm, Attr1min (g)	Run 5- Impact13.2mm, Attr2min (g)	Run 6- Impact13.2mm, Attr5min (g)
0-1	3040	4254.2	4230	3860	3970	3930	3630
Mass after rotary splitter	-	579.4	551.2	377.2	533.9	351.9	272.32
Mass % of 0-1 mm total mass	-	48%	46%	46%	57%	40%	46%

Table B. 19: Mass of -1 mm particles for float-sink analysis (impact breakage to a top size of 6.7 mm).

Particle size (mm)	Sieve mass (g)	Run 7- Impact6.7mm, Attr0min (g)	Run 8- Impact6.7mm Attr0min (g)	Run 9- Impact6.7mm, Attr0min (g)	Run 10- Impact6.7mm, Attr1min (g)	Run 11- Impact6.7mm, Attr2min (g)	Run 12- Impact6.7mm, Attr5min (g)
0-1	3040	3750	3810	4670	4760	4530	4710
Mass after rotary splitter	-	349.4	371.5	1026.1	664.9	382.3	859.0
Mass % of 0-1 mm total mass	-	49%	48%	63%	39%	26%	51%

Table B. 20: Mass of -1 mm particles for float-sink analysis (compressive breakage to a top size of 13.2 mm).

Particle size (mm)	Sieve mass (g)	Run 13-Comp13.2mm, Attr0min (g)	Run 14-Comp13.2mm Attr0min (g)	Run 15-Comp13.2mm, Attr0min (g)	Run 16-Comp13.2mm, Attr1min (g)	Run 17-Comp13.2mm, Attr2min (g)	Run 18-Comp13.2mm, Attr5min (g)
0-1	3040	4110	4160	4370	4350	4320	4290
Mass after rotary splitter	-	533.3	577.2	668.1	616.2	559.0	629.8
Mass % of 0-1 mm total mass	-	50%	52%	50%	47%	44%	50%

Table B. 21: Mass of -1 mm particles for float-sink analysis (compressive breakage to a top size of 6.7 mm).

Particle size (mm)	Sieve mass (g)	Run 19-Comp6mm, Attr0min (g)	Run 20-Comp6mm Attr0min (g)	Run 21-Comp6mm, Attr0min (g)	Run 22-Comp6mm, Attr1min (g)	Run 23-Comp6mm, Attr2min (g)	Run 24-Comp6mm, Attr5min (g)
0-1	3040	4600	4520	4640	4530	4780	4830
Mass after rotary splitter	-	845.3	741.4	701.8	748.2	876.6	903.5
Mass % of 0-1 mm total mass	-	54%	50%	44%	50%	50%	50%

Sample mass after float-sink analysis:

Table B. 22 to Table B. 46 presents the raw mass data for all experimental conditions according to the relative density and particle size distribution.

Table B. 22: Raw data for raw ROM coal

Particle size (mm)	Sieve mass (g)	Sample mass + sieve mass at RD interval (g)						
		F1.3	S1.3F1.4	S1.4F1.5	S1.5F1.6	S1.6F1.7	S1.7F1.8	S1.8
53-75	4780.0	4780.0	4780.0	4780.0	4780.0	4986.6	5035.8	4780.0
37.5- 53	3590.0	3590.0	3778.3	3804.5	3703.4	3590.0	3590.0	3809.5
26.5-37.5	3400.0	3400.0	3400.0	3452.5	3519.3	3552.6	3454.9	3562.2
19-26.5	709.6	709.6	766.9	834.7	845.2	761.4	813.4	891.8
13.2-19	606.3	606.3	678.4	790.2	699.4	656.9	664.9	836.8
9.5-13.2	573.8	578.6	616.9	670.2	624.3	627.9	592.8	695.8
6.7-9.5	530.0	540.5	592.0	642.9	593.4	564.2	557.7	618.2
4.75-6.7	462.8	577.1	514.9	533.8	503.1	484.5	478.3	531.6
2-4.75	394.0	524.1	520.9	504.8	452.1	427.8	418.8	510.0
1-2	360.5	513.8	466.7	400.9	384.8	373.2	369.2	410.2
0.5-1	315.3	328.8	331.2	320.3	318.0	316.6	315.7	322.7
0-0.5	464.5	464.7	465.7	464.9	464.7	464.6	464.7	465.3
For float sink analysis done in organic solution								
0.5-1	315.3	315.3	412.5	325.3	340.2	318.5	319.7	330.0
0-0.5	464.4	464.5	577.3	490.0	521.3	471.9	470.8	498.7

Table B. 23: Raw data for impact breakage to a top size of 13.2 mm with no attrition (Run 1).

Particle size (mm)	Sieve mass (g)	Sample mass + sieve mass at RD interval (g)						
		F1.3	S1.3F1.4	S1.4F1.5	S1.5F1.6	S1.6F1.7	S1.7F1.8	S1.8
9.5-13.2	573.7	579.8	723.8	830.8	827.7	878.0	663.6	1438.7
6.7-9.5	530.2	554.8	653.7	655.5	678.5	616.9	578.6	780.0
4.75-6.7	462.7	498.6	541.0	551.9	550.7	523.5	499.4	625.0
2-4.75	395.3	611.4	555.4	538.0	524.1	482.8	449.1	650.2
1-2	360.8	618.6	445.2	421.4	407.1	397.9	383.6	473.3
0.5-1	315.3	339.1	332.9	328.2	324.7	322.6	321.0	331.8
0-0.5	464.5	471.6	470.2	468.0	465.7	465.1	464.6	466.8
For float-sink analysis done in organic solution								
0.5-1	315.3	321.4	489.3	362.7	334.1	328.1	325.0	351.2
0-0.5	464.5	464.9	563.0	534.5	490.5	479.3	473.2	520.8

Table B. 24: Raw data for impact breakage to a top size of 13.2 mm with no attrition (Run 2).

Particle size (mm)	Sieve mass (g)	Sample mass + sieve mass at RD interval (g)						
		F1.3	S1.3F1.4	S1.4F1.5	S1.5F1.6	S1.6F1.7	S1.7F1.8	S1.8
9.5-13.2	573.7	575.0	775.9	1184.9	650.5	806.0	684.8	1719.8
6.7-9.5	530.2	535.0	656.0	783.0	540.8	598.3	575.0	780.6
4.75-6.7	462.7	469.7	563.9	626.3	479.6	504.3	487.5	627.5
2-4.75	395.3	446.8	567.7	718.8	434.2	458.4	446.0	642.6
1-2	360.8	429.2	458.5	587.4	378.1	386.3	383.7	454.6
0.5-1	315.3	322.6	327.0	329.1	321.3	321.9	322.0	330.4
0-0.5	464.5	464.6	465.5	465.7	464.6	464.6	464.7	466.0
For float-sink analysis done in organic solution								
0.5-1	319.0	374.9	411.7	342.7	328.1	331.7	322.6	355.5
0-0.5	464.5	482.2	604.7	511.7	479.9	488.2	471.6	530.2

Table B. 25: Raw data for impact breakage to a top size of 13.2 mm with no attrition (Run 3).

Particle size (mm)	Sieve mass (g)	Sample mass + sieve mass at RD interval (g)						
		F1.3	S1.3F1.4	S1.4F1.5	S1.5F1.6	S1.6F1.7	S1.7F1.8	S1.8
9.5-13.2	573.7	594.5	747.7	933.9	787.5	703.8	702.1	1431.3
6.7-9.5	530.2	541.8	642.7	715.6	603.0	594.5	585.4	762.4
4.75-6.7	462.7	486.8	587.9	574.5	513.7	506.1	490.4	629.8
2-4.75	395.3	568.3	634.8	566.9	480.2	461.3	448.4	650.0
1-2	360.8	573.9	524.4	433.8	397.0	388.5	388.5	473.8
0.5-1	315.3	388.3	354.6	327.4	322.3	320.4	320.7	334.1
0-0.5	464.5	470.1	466.5	464.7	464.5	464.7	464.7	465.0
For float-sink analysis done in organic solution								
0.5-1	317.3	319.8	391.0	330.8	323.4	322.5	320.0	333.7
0-0.5	464.6	465.4	592.7	508.2	481.6	480.8	471.3	509.3

Table B. 26: Raw data for impact breakage to a top size of 13.2 mm with 1 minute attrition breakage (Run 4).

Particle size (mm)	Sieve mass (g)	Sample mass + sieve mass at RD interval (g)						
		F1.3	S1.3F1.4	S1.4F1.5	S1.5F1.6	S1.6F1.7	S1.7F1.8	S1.8
9.5-13.2	573.7	578.8	654.8	833.5	732.4	741.5	707.8	1244.4
6.7-9.5	530.2	537.2	640.3	746.7	652.5	649.7	614.8	989.1
4.75-6.7	462.7	476.5	551.0	599.8	542.4	541.4	524.7	720.9
2-4.75	395.3	483.9	612.0	596.1	491.1	505.9	480.3	748.0
1-2	360.8	491.7	520.8	440.0	400.5	410.0	395.4	487.0
0.5-1	315.3	342.2	342.0	328.4	324.1	323.4	321.8	337.6
0-0.5	464.5	465.9	464.8	464.8	465.0	464.8	464.7	468.0
For float-sink analysis done in organic solution								
0.5-1	315.2	324.6	390.8	339.6	324.7	329.3	320.2	352.8
0-0.5	464.5	471.8	604.1	529.3	482.8	500.0	473.6	548.2

Table B. 27: Raw data for impact breakage to a top size of 13.2 mm with 2 minutes attrition breakage (Run 5).

Particle size (mm)	Sieve mass (g)	Sample mass + sieve mass at RD interval (g)						
		F1.3	S1.3F1.4	S1.4F1.5	S1.5F1.6	S1.6F1.7	S1.7F1.8	S1.8
9.5-13.2	573.7	578.5	755.9	853.1	817.9	744.5	697.6	1349.9
6.7-9.5	530.2	538.6	710.9	689.5	642.2	614.6	577.8	801.9
4.75-6.7	462.7	479.1	596.3	562.8	535.6	518.0	491.8	664.2
2-4.75	395.3	556.2	643.8	543.2	500.3	477.9	440.7	663.7
1-2	360.8	537.1	547.8	426.1	409.0	394.6	383.7	474.8
0.5-1	315.3	346.6	360.3	330.8	326.9	323.0	323.1	347.1
0-0.5	464.5	466.1	466.0	464.7	464.9	464.8	465.0	472.3
For float-sink analysis done in organic solution								
0.5-1	315.6	322.1	379.2	327.1	320.6	321.8	317.5	333.5
0-0.5	464.8	466.0	575.7	502.7	479.8	482.2	468.7	517.8

Table B. 28: Raw data for impact breakage to a top size of 13.2 mm with 5 minutes attrition breakage (Run 6).

Particle size (mm)	Sieve mass (g)	Sample mass + sieve mass at RD interval (g)						
		F1.3	S1.3F1.4	S1.4F1.5	S1.5F1.6	S1.6F1.7	S1.7F1.8	S1.8
9.5-13.2	573.7	577.0	700.2	869.0	740.5	699.7	684.5	1246.4
6.7-9.5	530.2	539.6	656.5	732.0	633.0	625.3	577.5	818.2
4.75-6.7	462.7	480.6	563.4	601.6	535.4	518.4	495.0	671.4
2-4.75	395.3	550.5	634.9	592.5	506.4	476.3	444.7	718.1
1-2	360.8	569.0	583.9	440.8	408.8	399.6	388.6	525.4
0.5-1	315.3	368.6	341.8	337.6	332.8	328.9	327.2	360.6
0-0.5	464.5	466.1	465.2	465.5	465.3	464.9	465.2	471.2
For float-sink analysis done in organic solution								
0.5-1	315.4	319.3	361.1	325.4	320.5	318.4	318.0	328.8
0-0.5	464.6	465.4	554.3	495.3	480.3	472.2	471.1	502.2

Table B. 29: Raw data for impact breakage to a top size of 6.7 mm with no attrition breakage (Run 7).

Particle size (mm)	Sieve mass (g)	Sample mass + sieve mass at RD interval (g)						
		F1.3	S1.3F1.4	S1.4F1.5	S1.5F1.6	S1.6F1.7	S1.7F1.8	S1.8
4.75-6.7	463.1	490.3	721.3	1046.5	845.7	675.6	687.7	1332.2
2-4.75	394.2	515.0	654.7	663.5	559.1	493.8	477.0	698.9
1-2	360.6	542.9	599.2	500.4	433.6	404.0	403.4	500.6
0.5-1	315.3	340.6	377.6	355.6	338.5	328.4	329.5	361.3
0-0.5	464.6	465.6	468.1	466.1	465.6	464.9	464.8	470.6
For float-sink analysis done in organic solution								
0.5-1	315.4	319.5	372.8	327.6	325.4	320.5	320.2	332.2
0-0.5	464.5	467.6	573.6	502.8	490.1	476.9	475.3	504.2

Table B. 30: Raw data for impact breakage to a top size of 6.7 mm with no attrition breakage (Run 8).

Particle size (mm)	Sieve mass (g)	Sample mass + sieve mass at RD interval (g)						
		F1.3	S1.3F1.4	S1.4F1.5	S1.5F1.6	S1.6F1.7	S1.7F1.8	S1.8
4.75-6.7	463.1	488.4	993.4	852.8	736.2	694.2	610.3	1390.5
2-4.75	394.2	646.9	805.2	539.5	497.1	471.3	449.7	653.6
1-2	360.6	556.8	689.5	420.8	406.3	404.8	390.7	462.2
0.5-1	315.3	342.4	348.7	336.8	331.1	330.4	326.3	339.5
0-0.5	464.6	465.5	465.1	466.4	465.4	465.2	465.0	466.7
For float-sink analysis done in organic solution								
0.5-1	315.2	316.7	372.9	339.8	322.5	318.9	318.3	330.8
0-0.5	464.4	465.9	565.2	534.2	489.2	471.5	474.6	508.2

Table B. 31: Raw data for impact breakage to a top size of 6.7 mm with no attrition breakage (Run 9).

Particle size (mm)	Sieve mass (g)	Sample mass + sieve mass at RD interval (g)						
		F1.3	S1.3F1.4	S1.4F1.5	S1.5F1.6	S1.6F1.7	S1.7F1.8	S1.8
4.75-6.7	463.1	506.2	965.2	960.8	815.9	728.0	643.5	1550.3
2-4.75	394.2	600.7	752.9	592.8	535.9	495.2	459.5	792.6
1-2	360.6	652.5	545.4	436.7	425.4	407.6	392.7	534.1
0.5-1	315.3	338.0	337.6	329.6	326.8	324.3	323.6	343.2
0-0.5	464.6	464.7	465.3	465.9	465.0	464.9	465.2	467.7
For float-sink analysis done in organic solution								
0.5-1	315.4	350.3	426.6	339.2	344.2	331.9	327.5	369.5
0-0.5	464.5	482.0	764.0	535.0	563.0	511.1	496.6	644.5

Table B. 32: Raw data for impact breakage to a top size of 6.7 mm with 1 minute attrition breakage (Run 10).

Particle size (mm)	Sieve mass (g)	Sample mass + sieve mass at RD interval (g)						
		F1.3	S1.3F1.4	S1.4F1.5	S1.5F1.6	S1.6F1.7	S1.7F1.8	S1.8
4.75-6.7	463.1	585.6	633.4	719.0	642.5	581.4	570.0	1221.0
2-4.75	394.2	892.4	664.9	704.5	578.1	537.5	505.0	882.1
1-2	360.6	681.3	491.8	478.5	432.5	416.7	407.8	532.3
0.5-1	315.3	339.5	328.4	327.7	325.7	324.1	323.3	350.6
0-0.5	464.6	465.0	464.9	464.7	464.7	464.6	464.7	468.7
For float-sink analysis done in organic solution								
0.5-1	315.4	349.0	456.8	325.3	322.3	319.3	318.8	331.3
0-0.5	464.5	490.1	789.8	486.5	483.6	473.3	471.4	506.7

Table B. 33: Raw data for impact breakage to a top size of 6.7 mm with 2 minutes attrition breakage (Run 11).

Particle size (mm)	Sieve mass (g)	Sample mass + sieve mass at RD interval (g)						
		F1.3	S1.3F1.4	S1.4F1.5	S1.5F1.6	S1.6F1.7	S1.7F1.8	S1.8
4.75-6.7	463.1	527.1	669.5	771.1	663.7	611.5	543.7	995.0
2-4.75	394.2	678.4	709.2	691.4	570.4	527.2	461.0	772.9
1-2	360.6	679.3	521.8	473.6	428.1	409.2	391.6	532.0
0.5-1	315.3	362.2	332.0	333.1	327.8	327.5	323.5	353.0
0-0.5	464.6	466.7	464.9	465.1	464.8	465.2	464.8	468.6
For float-sink analysis done in organic solution								
0.5-1	315.2	324.4	372.0	324.7	325.4	319.8	319.8	331.3
0-0.5	464.2	473.5	601.3	488.7	492.6	476.5	475.6	512.5

Table B. 34: Raw data for impact breakage to a top size of 6.7 mm with 5 minutes attrition breakage (Run 12).

Particle size (mm)	Sieve mass (g)	Sample mass + sieve mass at RD interval (g)						
		F1.3	S1.3F1.4	S1.4F1.5	S1.5F1.6	S1.6F1.7	S1.7F1.8	S1.8
4.75-6.7	463.1	516.4	630.6	828.7	652.5	649.3	618.6	1060.4
2-4.75	394.2	680.7	665.1	737.8	576.5	539.9	509.2	761.1
1-2	360.6	626.7	517.5	491.8	425.2	408.8	408.3	504.1
0.5-1	315.3	336.7	340.1	337.5	327.2	324.2	325.1	346.4
0-0.5	464.6	465.2	465.3	465.7	464.8	464.5	465.1	467.1
For float-sink analysis done in organic solution								
0.5-1	315.3	359.4	420.2	340.0	343.6	327.1	326.6	348.6
0-0.5	464.5	512.1	721.2	527.2	550.9	493.7	483.6	563.4

Table B. 35: Raw data for compressive breakage to a top size of 13.2 mm with no attrition breakage (Run 13).

Particle size (mm)	Sieve mass (g)	Sample mass + sieve mass at RD interval (g)						
		F1.3	S1.3F1.4	S1.4F1.5	S1.5F1.6	S1.6F1.7	S1.7F1.8	S1.8
9.5-13.2	573.5	586.0	733.0	810.4	700.5	698.5	653.1	1051.1
6.7-9.5	530.3	542.5	658.0	704.1	611.3	598.0	599.1	748.9
4.75-6.7	463.1	481.2	553.8	555.9	504.0	499.3	487.8	586.4
2-4.75	394.2	540.8	575.6	528.6	457.6	453.1	437.8	582.5
1-2	360.6	512.8	463.0	409.6	384.7	383.1	377.7	441.2
0.5-1	315.3	332.1	332.6	325.1	322.7	322.1	321.8	326.2
0-0.5	464.6	465.3	465.8	464.9	464.8	464.6	464.6	467.3
For float-sink analysis done in organic solution								
0.5-1	315.2	315.9	437.5	335.6	340.2	322.2	323.1	343.6
0-0.5	464.4	464.8	604.4	502.0	523.7	478.0	475.5	524.0

Table B. 36: Raw data for compressive breakage to a top size of 13.2 mm with no attrition breakage (Run 14).

Particle size (mm)	Sieve mass (g)	Sample mass + sieve mass at RD interval (g)						
		F1.3	S1.3F1.4	S1.4F1.5	S1.5F1.6	S1.6F1.7	S1.7F1.8	S1.8
9.5-13.2	573.5	579.6	688.0	840.8	728.7	694.4	661.0	1235.3
6.7-9.5	530.3	540.4	676.4	720.0	611.3	616.9	594.0	930.1
4.75-6.7	463.1	481.4	582.3	578.6	518.2	509.1	495.4	710.6
2-4.75	394.2	514.1	666.0	576.3	476.8	464.1	447.4	740.6
1-2	360.6	486.0	551.9	436.9	394.3	386.8	386.6	506.7
0.5-1	315.3	333.5	351.9	333.4	326.3	324.3	324.0	339.4
0-0.5	464.6	464.9	465.4	465.7	465.7	464.8	464.7	466.8
For float-sink analysis done in organic solution								
0.5-1	315.2	315.3	417.1	342.5	327.7	326.5	320.6	355.5
0-0.5	464.4	464.6	588.2	548.5	497.7	492.0	474.5	563.7

Table B. 37: Raw data for compressive breakage to a top size of 13.2 mm with no attrition breakage (Run 15).

Particle size (mm)	Sieve mass (g)	Sample mass + sieve mass at RD interval (g)						
		F1.3	S1.3F1.4	S1.4F1.5	S1.5F1.6	S1.6F1.7	S1.7F1.8	S1.8
9.5-13.2	573.4	578.4	675.7	814.7	745.0	696.5	661.5	1172.5
6.7-9.5	530.1	544.9	669.7	755.6	642.7	605.9	572.6	825.3
4.75-6.7	463.1	484.7	587.7	604.1	519.6	508.6	490.4	645.2
2-4.75	393.9	527.8	696.3	595.0	481.2	465.1	448.7	680.3
1-2	360.6	506.5	603.9	436.0	396.2	389.8	385.0	478.4
0.5-1	316.8	328.2	333.3	327.7	321.7	320.5	320.5	333.7
0-0.5	464.5	464.5	464.5	465.8	465.1	464.7	464.7	467.3
For float-sink analysis done in organic solution								
0.5-1	315.3	315.6	464.0	356.3	340.5	331.4	322.2	352.0
0-0.5	464.5	465.3	607.3	558.6	513.2	492.8	474.7	532.8

Table B. 38: Raw data for compressive breakage to a top size of 13.2 mm with 1 minute attrition breakage (Run 16).

Particle size (mm)	Sieve mass (g)	Sample mass + sieve mass at RD interval (g)						
		F1.3	S1.3F1.4	S1.4F1.5	S1.5F1.6	S1.6F1.7	S1.7F1.8	S1.8
9.5-13.2	576.3	582.2	704.6	845.4	700.8	669.2	687.2	1258.6
6.7-9.5	530.5	540.9	669.1	782.5	647.0	608.1	590.1	862.1
4.75-6.7	463.9	487.9	570.6	616.4	525.6	505.9	499.5	643.0
2-4.75	394.0	552.6	594.3	607.5	480.8	450.9	451.9	662.9
1-2	360.4	554.3	480.4	440.3	395.8	383.0	386.0	470.9
0.5-1	315.7	332.5	326.2	326.3	319.9	318.1	318.1	328.1
0-0.5	464.5	465.1	465.6	465.7	464.8	464.7	464.6	466.1
For float-sink analysis done in organic solution								
0.5-1	314.9	315.0	458.6	347.0	330.1	326.7	322.8	350.8
0-0.5	464.0	464.4	623.8	534.7	494.4	483.3	478.7	538.2

Table B. 39: Raw data for compressive breakage to a top size of 13.2 mm with 2 minutes attrition breakage (Run 17).

Particle size (mm)	Sieve mass (g)	Sample mass + sieve mass at RD interval (g)						
		F1.3	S1.3F1.4	S1.4F1.5	S1.5F1.6	S1.6F1.7	S1.7F1.8	S1.8
9.5-13.2	575.1	579.1	689.2	814.7	781.7	707.9	675.5	1275.4
6.7-9.5	530.1	539.9	652.6	757.7	662.6	622.7	592.2	916.9
4.75-6.7	463.3	484.1	543.0	594.6	534.1	519.7	502.8	666.6
2-4.75	393.6	520.4	581.5	587.2	488.6	473.5	450.1	683.7
1-2	359.9	514.7	488.5	443.6	401.0	391.4	383.1	472.8
0.5-1	315.1	325.2	331.3	324.8	321.5	319.6	318.0	334.7
0-0.5	464.5	464.6	564.9	565.0	465.1	464.9	464.8	468.0
For float-sink analysis done in organic solution								
0.5-1	315.0	315.6	442.9	334.8	328.4	327.0	323.1	353.9
0-0.5	464.0	464.8	612.1	511.8	493.2	482.9	476.2	545.3

Table B. 40: Raw data for compressive breakage to a top size of 13.2 mm with 5 minutes attrition breakage (Run 18).

Particle size (mm)	Sieve mass (g)	Sample mass + sieve mass at RD interval (g)						
		F1.3	S1.3F1.4	S1.4F1.5	S1.5F1.6	S1.6F1.7	S1.7F1.8	S1.8
9.5-13.2	573.6	578.9	687.6	788.5	728.0	734.0	651.9	1218.4
6.7-9.5	530.2	540.8	623.2	734.8	624.1	652.3	598.2	882.0
4.75-6.7	463.0	483.2	554.3	584.3	525.6	526.9	501.8	672.5
2-4.75	393.6	516.9	620.4	575.5	490.4	469.5	460.8	705.6
1-2	360.1	488.5	566.3	432.2	399.1	391.5	387.6	487.6
0.5-1	315.2	330.9	335.6	326.5	319.5	320.3	318.8	331.6
0-0.5	464.5	465.2	464.7	464.7	464.6	464.6	464.5	465.0
For float-sink analysis done in organic solution								
0.5-1	315.2	315.4	446.1	346.1	334.7	325.7	323.2	351.2
0-0.5	464.4	464.8	622.3	546.4	505.6	482.6	478.1	544.8

Table B. 41: Raw data for compressive breakage to a top size of 6.7 mm with no attrition breakage (Run 19).

Particle size (mm)	Sieve mass (g)	Sample mass + sieve mass at RD interval (g)						
		F1.3	S1.3F1.4	S1.4F1.5	S1.5F1.6	S1.6F1.7	S1.7F1.8	S1.8
4.75-6.7	463.0	504.1	605.4	752.2	608.7	567.3	599.4	1238.0
2-4.75	394.1	598.2	671.8	779.1	559.2	524.1	544.0	1093.8
1-2	360.6	581.5	495.7	484.2	406.2	406.3	407.0	574.7
0.5-1	315.5	332.2	324.9	327.0	317.8	318.1	318.0	336.1
0-0.5	464.6	465.1	464.6	464.8	464.7	464.7	464.6	466.1
For float-sink analysis done in organic solution								
0.5-1	315.3	315.4	446.9	389.9	349.3	334.2	325.5	382.7
0-0.5	464.5	464.7	618.3	611.5	524.7	494.7	477.8	568.3

Table B. 42: Raw data for compressive breakage to a top size of 6.7 mm with no attrition breakage (Run 20).

Particle size (mm)	Sieve mass (g)	Sample mass + sieve mass at RD interval (g)						
		F1.3	S1.3F1.4	S1.4F1.5	S1.5F1.6	S1.6F1.7	S1.7F1.8	S1.8
4.75-6.7	462.5	501.9	574.0	762.9	675.1	631.4	618.1	1515.7
2-4.75	393.5	585.1	579.2	729.5	571.7	543.2	516.2	931.5
1-2	359.9	558.0	472.9	468.5	408.7	404.9	400.1	547.9
0.5-1	315.1	326.6	326.4	322.1	317.8	318.3	318.2	337.6
0-0.5	464.5	464.9	464.6	464.6	464.6	464.6	464.5	465.8
For float-sink analysis done in organic solution								
0.5-1	315.3	315.4	453.2	355.9	343.1	334.2	323.9	375.3
0-0.5	464.4	464.7	633.1	550.7	515.1	493.9	478.4	562.4

Table B. 43: Raw data for compressive breakage to a top size of 6.7 mm with no attrition breakage (Run 21).

Particle size (mm)	Sieve mass (g)	Sample mass + sieve mass at RD interval (g)						
		F1.3	S1.3F1.4	S1.4F1.5	S1.5F1.6	S1.6F1.7	S1.7F1.8	S1.8
4.75-6.7	462.5	498.2	602.5	731.3	655.0	631.5	579.2	1367.9
2-4.75	393.4	616.6	630.9	740.6	585.1	540.9	509.5	1000.5
1-2	359.9	605.9	476.1	480.5	417.7	410.6	395.5	576.9
0.5-1	315.2	339.4	324.6	327.1	319.9	320.0	317.4	345.5
0-0.5	464.5	465.1	464.7	464.6	464.6	464.6	464.5	469.4
For float-sink analysis done in organic solution								
0.5-1	315.3	315.3	443.2	355.0	339.4	330.3	327.6	371.6
0-0.5	464.5	464.6	625.9	540.2	508.3	490.4	483.9	564.7

Table B. 44: Raw data for compressive breakage to a top size of 6.7 mm with 1 minute attrition breakage (Run 22).

Particle size (mm)	Sieve mass (g)	Sample mass + sieve mass at RD interval (g)						
		F1.3	S1.3F1.4	S1.4F1.5	S1.5F1.6	S1.6F1.7	S1.7F1.8	S1.8
4.75-6.7	547.1	597.2	682.3	887.9	728.1	718.0	667.1	1060.6
2-4.75	511.3	759.5	761.8	911.7	745.2	711.5	653.3	1074.6
1-2	364.9	601.0	507.7	506.3	439.7	417.6	409.8	545.4
0.5-1	457.8	466.3	469.6	471.3	465.0	462.1	461.4	482.3
0-0.5	377.1	377.1	377.2	377.5	377.2	377.2	377.1	379.6
For float-sink analysis done in organic solution								
0.5-1	315.3	315.3	450.8	361.8	338.2	331.5	324.6	367.1
0-0.5	464.5	464.6	649.5	561.3	509.6	487.9	480.7	563.9

Table B. 45: Raw data for compressive breakage to a top size of 6.7 mm with 2 minutes attrition breakage (Run 23).

Particle size (mm)	Sieve mass (g)	Sample mass + sieve mass at RD interval (g)						
		F1.3	S1.3F1.4	S1.4F1.5	S1.5F1.6	S1.6F1.7	S1.7F1.8	S1.8
4.75-6.7	463.0	523.1	565.5	782.3	675.3	614.1	575.0	899.8
2-4.75	393.7	763.5	604.9	795.2	664.9	576.7	537.5	924.9
1-2	359.9	648.2	466.9	487.1	426.9	408.1	402.2	518.3
0.5-1	315.2	322.2	321.6	322.2	318.0	317.0	316.5	327.2
0-0.5	464.3	464.4	464.4	464.5	464.3	464.5	464.6	465.6
For float-sink analysis done in organic solution								
0.5-1	315.3	315.4	516.4	349.1	355.3	330.7	324.5	366.3
0-0.5	464.5	464.6	715.7	517.3	529.4	487.7	488.3	574.5

Table B. 46: Raw data for compressive breakage to a top size of 6.7 mm with 5 minutes attrition breakage (Run 24).

Particle size (mm)	Sieve mass (g)	Sample mass + sieve mass at RD interval (g)						
		F1.3	S1.3F1.4	S1.4F1.5	S1.5F1.6	S1.6F1.7	S1.7F1.8	S1.8
4.75-6.7	463.0	544.3	592.4	756.3	645.3	614.5	566.4	948.8
2-4.75	393.9	757.6	641.6	793.8	640.9	584.3	535.7	970.6
1-2	360.3	628.8	484.1	460.8	424.1	409.5	394.4	535.1
0.5-1	315.7	322.7	320.8	317.6	317.0	316.4	316.3	328.4
0-0.5	464.6	465.0	465.1	464.6	464.6	464.7	464.6	467.6
For float-sink analysis done in organic solution								
0.5-1	315.4	315.5	410.6	419.6	378.7	323.8	330.9	389.6
0-0.5	464.5	464.5	557.7	548.4	626.2	492.2	515.4	589.7

APPENDIX C: PROCESSED DATA

Proximate analysis, calorific value and free swelling index analysis

Table C. 1 and Table C. 2 present the processed data for proximate analysis, calorific value and free swelling index determination. Data on an air dry basis was recalculated according to Equation D- 1 to be on a dry basis.

Table C. 1: Proximate, calorific value and free swelling index analysis results for particle sizes 0.0-1.0 mm expressed on a dry basis.

Sample Name	Ash (%)	Volatile matter (%)	Fixed Carbon (%)	Calorific value (MJ/kg)	Total sulphur (%)	Free swelling index
F1.3	4.35	22.87	72.77	34.00	1.44	9.00
1.3-1.4	5.39	21.85	72.76	33.80	1.22	9.00
1.4-1.5	12.45	20.10	67.45	30.60	1.31	7.00
1.5-1.6	22.36	18.97	58.67	26.30	1.46	1.50
1.6-1.7	28.76	17.84	53.40	23.60	1.56	0.00
1.7-1.8	37.25	17.23	45.51	20.40	1.56	0.00
S1.8	59.87	24.87	15.26	9.20	4.24	0.00

Table C. 2: Proximate, calorific value and free swelling index analysis results for particle sizes 1.0-13.2 mm expressed on a dry basis.

Sample Name	Ash (%)	Volatile matter (%)	Fixed Carbon (%)	Calorific value (MJ/kg)	Total sulphur (%)	Free swelling index
F1.3	4.47	19.19	76.35	34.18	0.98	7.50
1.3-1.4	12.80	17.48	69.72	30.67	0.90	4.00
1.4-1.5	19.72	16.46	63.82	28.14	0.90	2.50
1.5-1.6	27.05	15.50	57.45	25.05	0.82	1.00
1.6-1.7	35.47	14.33	50.20	21.94	0.80	0.00
1.7-1.8	44.26	13.10	42.64	18.38	0.86	0.00
S1.8	62.22	12.93	24.85	10.64	1.70	0.00

Particle size distribution data:

Table C. 3 to Table C. 30 presents data for the calculation of the amount of mass occurring in each particle size range. The mass of the sample along with the sieve mass was measured, and therefore Equation D- 3 needs to be used to determine the sample mass only. Equation D- 4 was used to recalculate the mass of material with particle size smaller than 4.75 mm, as split for the PSD, to be as for the total sample. The final mass was calculated by using Equation D- 5. The mass loss, relative to the initial sample mass, was also included by employing Equation D- 8. The initial, intermediate and final masses was recalculated to be a normalized mass percentage by using Equation D- 9.

Table C. 3: Particle size distribution of raw ROM coal.

Particle size	Mass (g)		Normalized mass	
	Initial	Final	Initial	Final
53-75 mm	480.00	462.40	8.26%	7.55%
37.5-53 mm	750.00	735.70	12.90%	12.02%
26.5-37.5 mm	560.00	541.50	9.64%	8.85%
19-26.5 mm	660.00	655.80	11.36%	10.71%
13.2-19 mm	700.00	688.80	12.04%	11.25%
9.5-13.2 mm	470.00	389.90	8.09%	6.37%
6.7-9.5 mm	410.00	398.90	7.05%	6.52%
4.75-6.7 mm	300.00	383.70	5.16%	6.27%
2-4.75 mm	194.72	600.50	3.35%	9.81%
1-2 mm	539.10	395.30	9.28%	6.46%
0.5-1 mm	605.92	364.23	10.43%	5.95%
0-0.5 mm	142.03	505.07	2.44%	8.25%
Total mass	5811.77	6121.80	100.00%	100.00%
Mass loss	0.00%	-5.33%		

Table C. 4: Particle size distribution of impact breakage to a top size of 13.2 mm with no attrition (Run 1).

Particle size	Mass (g)		Normalized mass	
	Initial	Final	Initial	Final
53-75 mm	0.00	0.00	0.00%	0.00%
37.5-53 mm	1240.00	0.00	19.27%	0.00%
26.5-37.5 mm	830.00	0.00	12.90%	0.00%
19-26.5 mm	670.00	0.00	10.41%	0.00%
13.2-19 mm	730.00	0.00	11.35%	0.00%
9.5-13.2 mm	450.00	1926.50	6.99%	30.69%
6.7-9.5 mm	470.00	806.60	7.30%	12.85%
4.75-6.7 mm	270.00	551.20	4.20%	8.78%
2-4.75 mm	728.58	1043.90	11.32%	16.63%
1-2 mm	725.91	621.50	11.28%	9.90%
0.5-1 mm	265.15	731.73	4.12%	11.66%
0-0.5 mm	54.63	596.17	0.85%	9.50%
Total mass	6434.27	6277.60	100.00%	100.00%
Mass loss	0%	2.43%		

Table C. 5: Particle size distribution of impact breakage to a top size of 13.2 mm with no attrition (Run 2).

Particle size	Mass (g)		Normalized mass	
	Initial	Final	Initial	Final
53-75 mm	0.00	0.00	0.00%	0.00%
37.5-53 mm	1570.00	0.00	23.90%	0.00%
26.5-37.5 mm	570.00	0.00	8.68%	0.00%
19-26.5 mm	620.00	0.00	9.44%	0.00%
13.2-19 mm	790.00	0.00	12.02%	0.00%
9.5-13.2 mm	520.00	2381.00	7.91%	37.09%
6.7-9.5 mm	420.00	757.30	6.39%	11.80%
4.75-6.7 mm	270.00	519.90	4.11%	8.10%
2-4.75 mm	718.06	947.40	10.93%	14.76%
1-2 mm	651.64	552.20	9.92%	8.60%
0.5-1 mm	389.45	572.82	5.93%	8.92%
0-0.5 mm	50.77	688.58	0.77%	10.73%
Total mass	6569.92	6419.20	100.00%	100.00%
Mass loss	0.00%	2.29%		

Table C. 6: Particle size distribution of impact breakage to a top size of 13.2 mm with no attrition (Run 3).

Particle size	Mass (g)		Normalized mass	
	Initial	Final	Initial	Final
53-75 mm	0.00	0.00	0.00%	0.00%
37.5-53 mm	480.00	0.00	7.74%	0.00%
26.5-37.5 mm	810.00	0.00	13.07%	0.00%
19-26.5 mm	700.00	0.00	11.29%	0.00%
13.2-19 mm	760.00	0.00	12.26%	0.00%
9.5-13.2 mm	540.00	1884.90	8.71%	32.19%
6.7-9.5 mm	510.00	734.00	8.23%	12.53%
4.75-6.7 mm	330.00	550.30	5.32%	9.40%
2-4.75 mm	798.12	1042.80	12.87%	17.81%
1-2 mm	918.68	654.30	14.82%	11.17%
0.5-1 mm	294.15	421.79	4.74%	7.20%
0-0.5 mm	58.37	567.61	0.94%	9.69%
Total mass	6199.32	5855.70	100.00%	100.00%
Mass loss	0.00%	5.54%		

Table C. 7: Particle size distribution of impact breakage to a top size of 13.2 mm with no attrition (Run 1-3 average).

Particle size	Mass (g)		Normalized mass	
	Initial	Final	Initial	Final
53-75 mm	0.00	0.00	0.00%	0.00%
37.5-53 mm	1096.67	0.00	17.13%	0.00%
26.5-37.5 mm	736.67	0.00	11.51%	0.00%
19-26.5 mm	663.33	0.00	10.36%	0.00%
13.2-19 mm	760.00	0.00	11.87%	0.00%
9.5-13.2 mm	503.33	2064.13	7.86%	33.38%
6.7-9.5 mm	466.67	765.97	7.29%	12.39%
4.75-6.7 mm	290.00	540.47	4.53%	8.74%
2-4.75 mm	748.25	1011.37	11.69%	16.35%
1-2 mm	765.41	609.33	11.96%	9.85%
0.5-1 mm	316.25	575.45	4.94%	9.31%
0-0.5 mm	54.59	617.45	0.85%	9.98%
Total mass	6401.17	6184.17	100.00%	100.00%
Mass loss	0.00%	3.39%		

Table C. 8: Particle size distribution of impact breakage to a top size of 13.2 mm with 1 minute attritioning (Run 4).

Particle size	Mass (g)			Normalized mass		
	Initial	Intermediate	Final	Initial	Intermediate	Final
53-75 mm	450.00	0.00	0.00	6.51%	0.00%	0.00%
37.5-53 mm	1310.00	0.00	0.00	18.95%	0.00%	0.00%
26.5-37.5 mm	1000.00	0.00	0.00	14.46%	0.00%	0.00%
19-26.5 mm	810.00	0.00	0.00	11.71%	0.00%	0.00%
13.2-19 mm	620.00	0.00	0.00	8.97%	0.00%	0.00%
9.5-13.2 mm	410.00	1810.00	1477.30	5.93%	28.32%	24.09%
6.7-9.5 mm	340.00	1090.00	1118.90	4.92%	17.05%	18.24%
4.75-6.7 mm	200.00	560.00	717.80	2.89%	8.76%	11.70%
2-4.75 mm	728.58	1158.33	1150.20	10.54%	18.12%	18.75%
1-2 mm	725.91	626.13	619.80	10.50%	9.80%	10.11%
0.5-1 mm	265.15	587.12	418.28	3.83%	9.19%	6.82%
0-0.5 mm	54.63	560.45	630.62	0.79%	8.77%	10.28%
Total mass	6914.27	6392.04	6132.9	100.00%	100.00%	100.00%
Mass loss	0.00%	7.55%	11.30%			

Table C. 9: Particle size distribution of impact breakage to a top size of 13.2 mm with 2 minutes attritioning (Run 5).

Particle size	Mass (g)			Normalized mass		
	Initial	Intermediate	Final	Initial	Intermediate	Final
53-75 mm	0.00	0.00	0.00	0.00%	0.00%	0.00%
37.5-53 mm	1440.00	0.00	0.00	22.43%	0.00%	0.00%
26.5-37.5 mm	820.00	0.00	0.00	12.77%	0.00%	0.00%
19-26.5 mm	600.00	0.00	0.00	9.35%	0.00%	0.00%
13.2-19 mm	590.00	0.00	0.00	9.19%	0.00%	0.00%
9.5-13.2 mm	500.00	2040.00	1781.50	7.79%	32.13%	29.62%
6.7-9.5 mm	430.00	910.00	864.10	6.70%	14.33%	14.37%
4.75-6.7 mm	270.00	480.00	608.90	4.21%	7.56%	10.13%
2-4.75 mm	709.50	1081.89	1058.70	11.05%	17.04%	17.60%
1-2 mm	750.41	743.27	647.50	11.69%	11.71%	10.77%
0.5-1 mm	271.98	592.59	435.48	4.24%	9.33%	7.24%
0-0.5 mm	37.88	501.45	617.52	0.59%	7.90%	10.27%
Total mass	6419.77	6349.19	6013.70	100.00%	100.00%	100.00%
Mass loss	0.00%	1.10%	6.33%			

Table C. 10: Particle size distribution of impact breakage to a top size of 13.2 mm with 5 minutes attritioning (Run 6).

Particle size	Mass (g)			Normalized mass		
	Initial	Intermediate	Final	Initial	Intermediate	Final
53-75 mm	0.00	0.00	0.00	0.00%	0.00%	0.00%
37.5-53 mm	950.00	0.00	0.00	15.09%	0.00%	0.00%
26.5-37.5 mm	530.00	0.00	0.00	8.42%	0.00%	0.00%
19-26.5 mm	600.00	0.00	0.00	9.53%	0.00%	0.00%
13.2-19 mm	690.00	0.00	0.00	10.96%	0.00%	0.00%
9.5-13.2 mm	630.00	1770.00	1501.40	10.00%	28.28%	24.97%
6.7-9.5 mm	480.00	910.00	870.70	7.62%	14.54%	14.48%
4.75-6.7 mm	340.00	520.00	626.90	5.40%	8.31%	10.43%
2-4.75 mm	947.66	1113.57	1156.30	15.05%	17.79%	19.23%
1-2 mm	939.73	898.62	790.50	14.92%	14.36%	13.15%
0.5-1 mm	167.33	741.94	436.75	2.66%	11.85%	7.26%
0-0.5 mm	22.20	304.54	630.62	0.35%	4.87%	10.49%
Total mass	6296.92	6258.68	6013.18	100.00%	100.00%	100.00%
Mass loss	0.00%	0.61%	4.51%			

Table C. 11: Particle size distribution of impact breakage to a top size of 6.7 mm with no attritioning (Run 7).

Particle size	Mass (g)		Normalized mass	
	Initial	Final	Initial	Final
53-75 mm	0.00	0.00	0.00%	0.00%
37.5-53 mm	640.00	0.00	10.24%	0.00%
26.5-37.5 mm	620.00	0.00	9.92%	0.00%
19-26.5 mm	660.00	0.00	10.56%	0.00%
13.2-19 mm	710.00	0.00	11.36%	0.00%
9.5-13.2 mm	590.00	0.00	9.44%	0.00%
6.7-9.5 mm	530.00	0.00	8.48%	0.00%
4.75-6.7 mm	350.00	2557.60	5.60%	45.12%
2-4.75 mm	885.65	1302.60	14.17%	22.98%
1-2 mm	1012.73	859.90	16.21%	15.17%
0.5-1 mm	234.16	448.74	3.75%	7.92%
0-0.5 mm	16.08	499.16	0.26%	8.81%
Total mass	6248.63	5668.00	100.00%	100.00%
Mass loss	0.00%	9.29%		

Table C. 12: Particle size distribution of impact breakage to a top size of 6.7 mm with no attritioning (Run 8).

Particle size	Mass (g)		Normalized mass	
	Initial	Final	Initial	Final
53-75 mm	540.00	0.00	8.09%	0.00%
37.5-53 mm	550.00	0.00	8.24%	0.00%
26.5-37.5 mm	420.00	0.00	6.29%	0.00%
19-26.5 mm	1150.00	0.00	17.22%	0.00%
13.2-19 mm	700.00	0.00	10.48%	0.00%
9.5-13.2 mm	490.00	0.00	7.34%	0.00%
6.7-9.5 mm	460.00	0.00	6.89%	0.00%
4.75-6.7 mm	330.00	2524.10	4.94%	45.40%
2-4.75 mm	852.55	1303.90	12.77%	23.45%
1-2 mm	871.17	806.90	13.04%	14.51%
0.5-1 mm	277.13	383.35	4.15%	6.89%
0-0.5 mm	37.61	541.85	0.56%	9.75%
Total mass	6678.46	5560.10	100.00%	100.00%
Mass loss	0.00%	16.75%		

Table C. 13: Particle size distribution of impact breakage to a top size of 6.7 mm with no attritioning (Run 9).

Particle size	Mass (g)		Normalized mass	
	Initial	Final	Initial	Final
53-75 mm	0.00	0.00	0.00%	0.00%
37.5-53 mm	1210.00	0.00	16.89%	0.00%
26.5-37.5 mm	1100.00	0.00	15.35%	0.00%
19-26.5 mm	870.00	0.00	12.14%	0.00%
13.2-19 mm	660.00	0.00	9.21%	0.00%
9.5-13.2 mm	520.00	0.00	7.26%	0.00%
6.7-9.5 mm	410.00	0.00	5.72%	0.00%
4.75-6.7 mm	310.00	2928.20	4.33%	41.71%
2-4.75 mm	729.91	1470.20	10.19%	20.94%
1-2 mm	593.78	870.20	8.29%	12.39%
0.5-1 mm	549.04	563.01	7.66%	8.02%
0-0.5 mm	212.72	1189.49	2.97%	16.94%
Total mass	7165.45	7021.10	100.00%	100.00%
Mass loss	0.00%	2.01%		

Table C. 14: Particle size distribution of impact breakage to a top size of 6.7 mm with no attritioning (Run 7-9 average).

Particle size	Mass (g)		Normalized mass	
	Initial	Final	Initial	Final
53-75 mm	180.00	0.00	2.69%	0.00%
37.5-53 mm	800.00	0.00	11.94%	0.00%
26.5-37.5 mm	713.33	0.00	10.65%	0.00%
19-26.5 mm	893.33	0.00	13.34%	0.00%
13.2-19 mm	690.00	0.00	10.30%	0.00%
9.5-13.2 mm	533.33	0.00	7.96%	0.00%
6.7-9.5 mm	466.67	0.00	6.97%	0.00%
4.75-6.7 mm	330.00	2669.97	4.93%	43.89%
2-4.75 mm	822.70	1358.90	12.28%	22.34%
1-2 mm	825.90	845.67	12.33%	13.90%
0.5-1 mm	353.44	465.03	5.28%	7.64%
0-0.5 mm	88.80	743.50	1.33%	12.22%
Total mass	6697.51	6083.07	100.00%	100.00%
Mass loss	0.00%	9.17%		

Table C. 15: Particle size distribution of impact breakage to a top size of 6.7 mm with 1 minute attritioning (Run 10).

	Mass (g)			Normalized mass		
Particle size	Initial	Intermediate	Final	Initial	Intermediate	Final
53-75 mm	0.00	0.00	0.00	0.00%	0.00%	0.00%
37.5-53 mm	1230.00	0.00	0.00	20.50%	0.00%	0.00%
26.5-37.5 mm	370.00	0.00	0.00	6.17%	0.00%	0.00%
19-26.5 mm	460.00	0.00	0.00	7.67%	0.00%	0.00%
13.2-19 mm	550.00	0.00	0.00	9.17%	0.00%	0.00%
9.5-13.2 mm	430.00	0.00	0.00	7.17%	0.00%	0.00%
6.7-9.5 mm	470.00	0.00	0.00	7.84%	0.00%	0.00%
4.75-6.7 mm	340.00	1640.00	1711.20	5.67%	26.33%	26.45%
2-4.75 mm	885.65	1786.58	2005.10	14.76%	28.68%	30.99%
1-2 mm	1012.73	994.46	916.70	16.88%	15.97%	14.17%
0.5-1 mm	234.16	848.95	668.37	3.90%	13.63%	10.33%
0-0.5 mm	16.08	958.29	1168.93	0.27%	15.39%	18.07%
Total mass	5998.63	6228.28	6470.30	100.00%	100.00%	100.00%
Mass loss	0.00%	-3.83%	-7.86%			

Table C. 16: Particle size distribution of impact breakage to a top size of 6.7 mm with 2 minutes attritioning (Run 11).

	Mass (g)			Normalized mass		
Particle size	Initial	Intermediate	Final	Initial	Intermediate	Final
53-75 mm	510.00	0.00	0.00	8.22%	0.00%	0.00%
37.5-53 mm	780.00	0.00	0.00	12.57%	0.00%	0.00%
26.5-37.5 mm	790.00	0.00	0.00	12.73%	0.00%	0.00%
19-26.5 mm	740.00	0.00	0.00	11.93%	0.00%	0.00%
13.2-19 mm	550.00	0.00	0.00	8.86%	0.00%	0.00%
9.5-13.2 mm	420.00	0.00	0.00	6.77%	0.00%	0.00%
6.7-9.5 mm	390.00	0.00	0.00	6.29%	0.00%	0.00%
4.75-6.7 mm	270.00	1920.00	1539.90	4.35%	31.30%	26.77%
2-4.75 mm	597.98	1697.37	1651.10	9.64%	27.67%	28.70%
1-2 mm	517.00	973.42	911.40	8.33%	15.87%	15.84%
0.5-1 mm	438.06	802.86	584.62	7.06%	13.09%	10.16%
0-0.5 mm	202.05	740.75	1065.28	3.26%	12.08%	18.52%
Total mass	6205.09	6134.40	5752.30	100.00%	100.00%	100.00%
Mass loss	0.00%	1.14%	7.00%			

Table C. 17: Particle size distribution of impact breakage to a top size of 6.7 mm with 5 minutes attritioning (Run 12).

Particle size	Mass (g)			Normalized mass		
	Initial	Intermediate	Final	Initial	Intermediate	Final
53-75 mm	510.00	0.00	0.00	8.23%	0.00%	0.00%
37.5-53 mm	640.00	0.00	0.00	10.33%	0.00%	0.00%
26.5-37.5 mm	830.00	0.00	0.00	13.39%	0.00%	0.00%
19-26.5 mm	500.00	0.00	0.00	8.07%	0.00%	0.00%
13.2-19 mm	560.00	0.00	0.00	9.04%	0.00%	0.00%
9.5-13.2 mm	590.00	0.00	0.00	9.52%	0.00%	0.00%
6.7-9.5 mm	370.00	0.00	0.00	5.97%	0.00%	0.00%
4.75-6.7 mm	290.00	1940.00	1714.80	4.68%	31.34%	28.03%
2-4.75 mm	662.79	1612.12	1710.90	10.69%	26.04%	27.97%
1-2 mm	637.20	921.97	858.20	10.28%	14.89%	14.03%
0.5-1 mm	489.87	856.06	664.39	7.90%	13.83%	10.86%
0-0.5 mm	118.08	860.61	1168.93	1.91%	13.90%	19.11%
Total mass	6197.94	6190.76	6117.22	100.00%	100.00%	100.00%
Mass loss	0.00%	0.12%	1.30%			

Table C. 18: Particle size distribution of compressive breakage to a top size of 13.2 mm with no attritioning (Run 13).

Particle size	Mass (g)		Normalized mass	
	Initial	Final	Initial	Final
53-75 mm	0.00	0.00	0.00%	0.00%
37.5-53 mm	400.00	0.00	6.30%	0.00%
26.5-37.5 mm	990.00	0.00	15.58%	0.00%
19-26.5 mm	840.00	0.00	13.22%	0.00%
13.2-19 mm	750.00	0.00	11.81%	0.00%
9.5-13.2 mm	560.00	1218.10	8.81%	25.33%
6.7-9.5 mm	550.00	749.80	8.66%	15.59%
4.75-6.7 mm	270.00	426.70	4.25%	8.87%
2-4.75 mm	839.79	816.60	13.22%	16.98%
1-2 mm	918.10	447.90	14.45%	9.31%
0.5-1 mm	214.18	500.25	3.37%	10.40%
0-0.5 mm	21.16	650.35	0.33%	13.52%
Total mass	6353.23	4809.70	100.00%	100.00%
Mass loss	0.00%	24.30%		

Table C. 19: Particle size distribution of compressive breakage to a top size of 13.2 mm with no attritioning (Run 14).

Particle size	Mass (g)		Normalized mass	
	Initial	Final	Initial	Final
53-75 mm	560.00	0.00	8.81%	0.00%
37.5-53 mm	230.00	0.00	3.62%	0.00%
26.5-37.5 mm	660.00	0.00	10.38%	0.00%
19-26.5 mm	660.00	0.00	10.38%	0.00%
13.2-19 mm	740.00	0.00	11.64%	0.00%
9.5-13.2 mm	540.00	1413.30	8.50%	23.45%
6.7-9.5 mm	510.00	977.00	8.02%	16.21%
4.75-6.7 mm	380.00	633.90	5.98%	10.52%
2-4.75 mm	926.56	1125.90	14.58%	18.68%
1-2 mm	942.52	625.00	14.83%	10.37%
0.5-1 mm	193.92	511.45	3.05%	8.49%
0-0.5 mm	13.53	740.05	0.21%	12.28%
Total mass	6356.53	6026.60	100.00%	100.00%
Mass loss	0.00%	5.19%		

Table C. 20: Particle size distribution of compressive breakage to a top size of 13.2 mm with no attritioning (Run 15).

Particle size	Mass (g)		Normalized mass	
	Initial	Final	Initial	Final
53-75 mm	150.00	0.00	2.37%	0.00%
37.5-53 mm	400.00	0.00	6.32%	0.00%
26.5-37.5 mm	410.00	0.00	6.48%	0.00%
19-26.5 mm	510.00	0.00	8.06%	0.00%
13.2-19 mm	690.00	0.00	10.90%	0.00%
9.5-13.2 mm	590.00	1330.50	9.32%	22.00%
6.7-9.5 mm	640.00	906.00	10.11%	14.98%
4.75-6.7 mm	420.00	598.60	6.64%	9.90%
2-4.75 mm	1082.86	1137.10	17.11%	18.80%
1-2 mm	1216.30	671.60	19.22%	11.11%
0.5-1 mm	210.50	615.25	3.33%	10.17%
0-0.5 mm	9.40	787.85	0.15%	13.03%
Total mass	6329.06	6046.90	100.00%	100.00%
Mass loss	0.00%	4.46%		

Table C. 21: Particle size distribution of compressive breakage to a top size of 13.2 mm with 1 minute attritioning (Run 16).

	Mass (g)			Normalized mass		
Particle size	Initial	Intermediate	Final	Initial	Intermediate	Final
53-75 mm	210.00	0.00	0.00	3.37%	0.00%	0.00%
37.5-53 mm	1050.00	0.00	0.00	16.85%	0.00%	0.00%
26.5-37.5 mm	490.00	0.00	0.00	7.86%	0.00%	0.00%
19-26.5 mm	640.00	0.00	0.00	10.27%	0.00%	0.00%
13.2-19 mm	600.00	0.00	0.00	9.63%	0.00%	0.00%
9.5-13.2 mm	460.00	1770.00	1413.90	7.38%	28.60%	23.54%
6.7-9.5 mm	470.00	1060.00	986.30	7.54%	17.13%	16.42%
4.75-6.7 mm	320.00	470.00	601.60	5.13%	7.59%	10.01%
2-4.75 mm	839.79	1174.39	1042.90	13.47%	18.98%	17.36%
1-2 mm	918.10	732.23	587.90	14.73%	11.83%	9.79%
0.5-1 mm	214.18	694.12	583.77	3.44%	11.22%	9.72%
0-0.5 mm	21.16	287.77	790.63	0.34%	4.65%	13.16%
Total mass	6233.23	6188.50	6007	100.00%	100.00%	100.00%
Mass loss	0.00%	0.72%	4.00%			

Table C. 22: Particle size distribution of compressive breakage to a top size of 13.2 mm with 2 minutes attritioning (Run 17).

	Mass (g)			Normalized mass		
Particle size	Initial	Intermediate	Final	Initial	Intermediate	Final
53-75 mm	0.00	0.00	0.00	0.00%	0.00%	0.00%
37.5-53 mm	770.00	0.00	0.00	12.10%	0.00%	0.00%
26.5-37.5 mm	1010.00	0.00	0.00	15.88%	0.00%	0.00%
19-26.5 mm	680.00	0.00	0.00	10.69%	0.00%	0.00%
13.2-19 mm	690.00	0.00	0.00	10.85%	0.00%	0.00%
9.5-13.2 mm	460.00	1890.00	1497.80	7.23%	30.09%	23.80%
6.7-9.5 mm	460.00	1040.00	1033.90	7.23%	16.56%	16.43%
4.75-6.7 mm	320.00	510.00	601.80	5.03%	8.12%	9.56%
2-4.75 mm	813.21	1098.48	1029.80	12.78%	17.49%	16.36%
1-2 mm	953.78	718.39	575.80	14.99%	11.44%	9.15%
0.5-1 mm	197.51	718.39	574.76	3.10%	11.44%	9.13%
0-0.5 mm	6.68	306.10	980.44	0.10%	4.87%	15.58%
Total mass	6361.18	6281.35	6294.3	100.00%	100.00%	100.00%
Mass loss	0.00%	1.25%	1.00%			

Table C. 23: Particle size distribution of compressive breakage to a top size of 13.2 mm with 5 minutes attritioning (Run 18).

	Mass (g)			Normalized mass		
Particle size	Initial	Intermediate	Final	Initial	Intermediate	Final
53-75 mm	300.00	0.00	0.00	4.96%	0.00%	0.00%
37.5-53 mm	600.00	0.00	0.00	9.91%	0.00%	0.00%
26.5-37.5 mm	360.00	0.00	0.00	5.95%	0.00%	0.00%
19-26.5 mm	640.00	0.00	0.00	10.57%	0.00%	0.00%
13.2-19 mm	540.00	0.00	0.00	8.92%	0.00%	0.00%
9.5-13.2 mm	480.00	1750.00	1372.10	7.93%	28.30%	22.82%
6.7-9.5 mm	530.00	970.00	944.00	8.76%	15.69%	15.70%
4.75-6.7 mm	340.00	500.00	607.60	5.62%	8.09%	10.10%
2-4.75 mm	1023.70	1221.64	1083.90	16.91%	19.76%	18.03%
1-2 mm	1030.66	883.78	632.10	17.03%	14.29%	10.51%
0.5-1 mm	205.30	664.70	582.85	3.39%	10.75%	9.69%
0-0.5 mm	3.83	192.76	790.63	0.06%	3.12%	13.15%
Total mass	6053.48	6182.89	6013.18	100.00%	100.00%	100.00%
Mass loss	0.00%	-2.14%	1.00%			

Table C. 24: Particle size distribution of compressive breakage to a top size of 6.7 mm with no attritioning (Run 19).

	Mass (g)		Normalized mass	
Particle size	Initial	Final	Initial	Final
53-75 mm	1950.00	0.00	30.93%	0.00%
37.5-53 mm	360.00	0.00	5.71%	0.00%
26.5-37.5 mm	630.00	0.00	9.99%	0.00%
19-26.5 mm	460.00	0.00	7.30%	0.00%
13.2-19 mm	420.00	0.00	6.66%	0.00%
9.5-13.2 mm	360.00	0.00	5.71%	0.00%
6.7-9.5 mm	340.00	0.00	5.39%	0.00%
4.75-6.7 mm	240.00	1634.10	3.81%	26.77%
2-4.75 mm	616.87	2011.50	9.79%	32.95%
1-2 mm	676.30	831.40	10.73%	13.62%
0.5-1 mm	242.47	687.16	3.85%	11.26%
0-0.5 mm	8.32	940.84	0.13%	15.41%
Total mass	6303.96	6105.00	100.00%	100.00%
Mass loss	0.00%	3.16%		

Table C. 25: Particle size distribution of compressive breakage to a top size of 6.7 mm with no attritioning (Run 20).

Particle size	Mass (g)		Normalized mass	
	Initial	Final	Initial	Final
53-75 mm	1170.00	0.00	18.93%	0.00%
37.5-53 mm	460.00	0.00	7.44%	0.00%
26.5-37.5 mm	720.00	0.00	11.65%	0.00%
19-26.5 mm	500.00	0.00	8.09%	0.00%
13.2-19 mm	620.00	0.00	10.03%	0.00%
9.5-13.2 mm	380.00	0.00	6.15%	0.00%
6.7-9.5 mm	390.00	0.00	6.31%	0.00%
4.75-6.7 mm	240.00	2041.60	3.88%	33.87%
2-4.75 mm	676.54	1701.90	10.95%	28.23%
1-2 mm	792.08	741.70	12.81%	12.30%
0.5-1 mm	225.92	647.99	3.66%	10.75%
0-0.5 mm	6.37	895.41	0.10%	14.85%
Total mass	6180.91	6028.60	100.00%	100.00%
Mass loss	0.00%	2.46%		

Table C. 26: Particle size distribution of compressive breakage to a top size of 6.7 mm with no attritioning (Run 21).

Particle size	Mass (g)		Normalized mass	
	Initial	Final	Initial	Final
53-75 mm	0.00	0.00	0.00%	0.00%
37.5-53 mm	770.00	0.00	11.93%	0.00%
26.5-37.5 mm	640.00	0.00	9.92%	0.00%
19-26.5 mm	570.00	0.00	8.83%	0.00%
13.2-19 mm	760.00	0.00	11.78%	0.00%
9.5-13.2 mm	500.00	0.00	7.75%	0.00%
6.7-9.5 mm	540.00	0.00	8.37%	0.00%
4.75-6.7 mm	370.00	1828.10	5.73%	29.32%
2-4.75 mm	966.90	1870.30	14.98%	29.99%
1-2 mm	1095.76	843.90	16.98%	13.53%
0.5-1 mm	236.40	715.14	3.66%	11.47%
0-0.5 mm	4.26	978.36	0.07%	15.69%
Total mass	6453.32	6235.80	100.00%	100.00%
Mass loss	0.00%	3.37%		

Table C. 27: Particle size distribution of compressive breakage to a top size of 6.7 mm with no attritioning (Run 19-21 average).

Particle size	Mass (g)		Normalized mass	
	Initial	Final	Initial	Final
53-75 mm	1040.00	0.00	16.47%	0.00%
37.5-53 mm	530.00	0.00	8.40%	0.00%
26.5-37.5 mm	663.33	0.00	10.51%	0.00%
19-26.5 mm	510.00	0.00	8.08%	0.00%
13.2-19 mm	600.00	0.00	9.50%	0.00%
9.5-13.2 mm	413.33	0.00	6.55%	0.00%
6.7-9.5 mm	423.33	0.00	6.71%	0.00%
4.75-6.7 mm	283.33	1834.60	4.49%	29.96%
2-4.75 mm	753.44	1861.23	11.94%	30.40%
1-2 mm	854.71	805.67	13.54%	13.16%
0.5-1 mm	234.93	683.43	3.72%	11.16%
0-0.5 mm	6.32	938.20	0.10%	15.32%
Total mass	6312.73	6123.13	100.00%	100.00%
Mass loss	0.00%	3.00%		

Table C. 28: Particle size distribution of compressive breakage to a top size of 6.7 mm with 1 minute attritioning (Run 22).

Particle size	Mass (g)			Normalized mass		
	Initial	Intermediate	Final	Initial	Intermediate	Final
53-75 mm	450.00	0.00	0.00	7.78%	0.00%	0.00%
37.5-53 mm	830.00	0.00	0.00	14.35%	0.00%	0.00%
26.5-37.5 mm	470.00	0.00	0.00	8.13%	0.00%	0.00%
19-26.5 mm	610.00	0.00	0.00	10.55%	0.00%	0.00%
13.2-19 mm	660.00	0.00	0.00	11.41%	0.00%	0.00%
9.5-13.2 mm	460.00	0.00	0.00	7.95%	0.00%	0.00%
6.7-9.5 mm	480.00	0.00	0.00	8.30%	0.00%	0.00%
4.75-6.7 mm	280.00	1790.00	1511.50	4.84%	29.25%	25.23%
2-4.75 mm	616.87	2044.58	2038.50	10.67%	33.41%	34.03%
1-2 mm	676.30	989.42	873.20	11.69%	16.17%	14.58%
0.5-1 mm	242.47	911.93	635.39	4.19%	14.90%	10.61%
0-0.5 mm	8.32	384.01	931.21	0.14%	6.27%	15.55%
Total mass	5783.96	6119.93	5989.8	100.00%	100.00%	100.00%
Mass loss	0.00%	-5.81%	-4.00%			

Table C. 29: Particle size distribution of compressive breakage to a top size of 6.7 mm with 2 minutes attritioning (Run 23).

	Mass (g)			Normalized mass		
Particle size	Initial	Intermediate	Final	Initial	Intermediate	Final
53-75 mm	710.00	0.00	0.00	11.49%	0.00%	0.00%
37.5-53 mm	470.00	0.00	0.00	7.61%	0.00%	0.00%
26.5-37.5 mm	640.00	0.00	0.00	10.36%	0.00%	0.00%
19-26.5 mm	620.00	0.00	0.00	10.04%	0.00%	0.00%
13.2-19 mm	450.00	0.00	0.00	7.29%	0.00%	0.00%
9.5-13.2 mm	410.00	0.00	0.00	6.64%	0.00%	0.00%
6.7-9.5 mm	420.00	0.00	0.00	6.80%	0.00%	0.00%
4.75-6.7 mm	290.00	1450.00	1394.10	4.70%	23.78%	22.76%
2-4.75 mm	779.09	2112.80	2111.70	12.61%	34.65%	34.48%
1-2 mm	702.56	995.75	838.40	11.37%	16.33%	13.69%
0.5-1 mm	591.42	872.57	734.22	9.57%	14.31%	11.99%
0-0.5 mm	93.65	666.65	1046.28	1.52%	10.93%	17.08%
Total mass	6176.72	6097.78	6124.7	100.00%	100.00%	100.00%
Mass loss	0.00%	1.28%	1.00%			

Table C. 30: Particle size distribution of compressive breakage to a top size of 6.7 mm with 5 minutes attritioning (Run 24).

	Mass (g)			Normalized mass		
Particle size	Initial	Intermediate	Final	Initial	Intermediate	Final
53-75 mm	390.00	0.00	0.00	6.20%	0.00%	0.00%
37.5-53 mm	350.00	0.00	0.00	5.57%	0.00%	0.00%
26.5-37.5 mm	580.00	0.00	0.00	9.23%	0.00%	0.00%
19-26.5 mm	800.00	0.00	0.00	12.73%	0.00%	0.00%
13.2-19 mm	660.00	0.00	0.00	10.50%	0.00%	0.00%
9.5-13.2 mm	520.00	0.00	0.00	8.27%	0.00%	0.00%
6.7-9.5 mm	510.00	0.00	0.00	8.11%	0.00%	0.00%
4.75-6.7 mm	300.00	1580.00	1427.00	4.77%	25.44%	23.89%
2-4.75 mm	796.18	2101.66	2167.20	12.67%	33.84%	36.28%
1-2 mm	654.83	987.58	814.70	10.42%	15.90%	13.64%
0.5-1 mm	565.85	839.21	634.08	9.00%	13.51%	10.61%
0-0.5 mm	158.96	702.81	931.21	2.53%	11.32%	15.59%
Total mass	6285.83	6211.26	5974.20	100.00%	100.00%	100.00%
Mass loss	0.00%	1.19%	4.96%			

Particle size distribution graphs

Figure C. 1 to Figure C. 17 presents the particle size distribution data given in Table C. 3 to Table C. 30 as graphs. The value on the y-axis representing the mass distribution percentage is up to 50 % in all graphs. This is to easily compare the graphs.

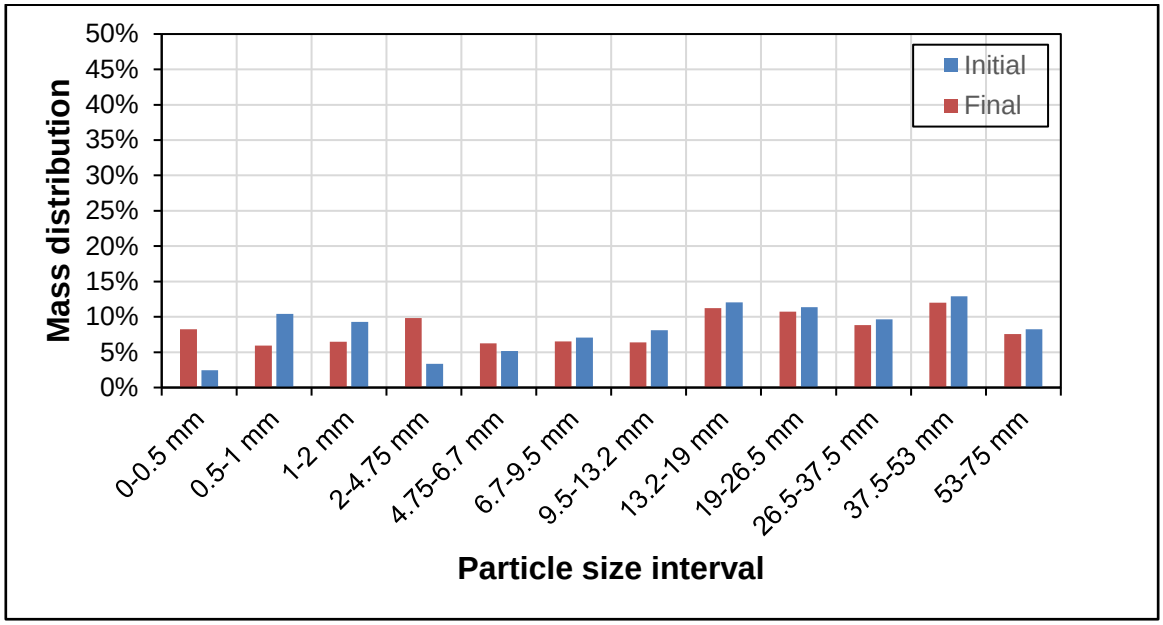

Figure C. 1: Particle size distribution for raw ROM coal.

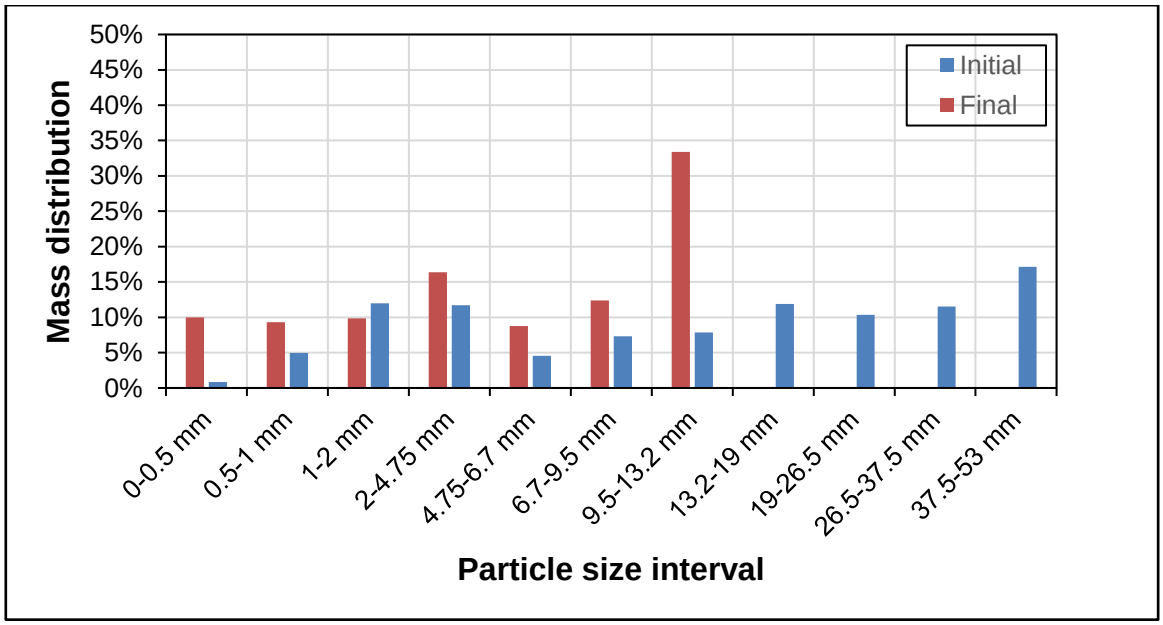

Figure C. 2: Particle size distribution for impact breakage to a top size of 13.2 mm with no attrition breakage (Run 1-3 average).

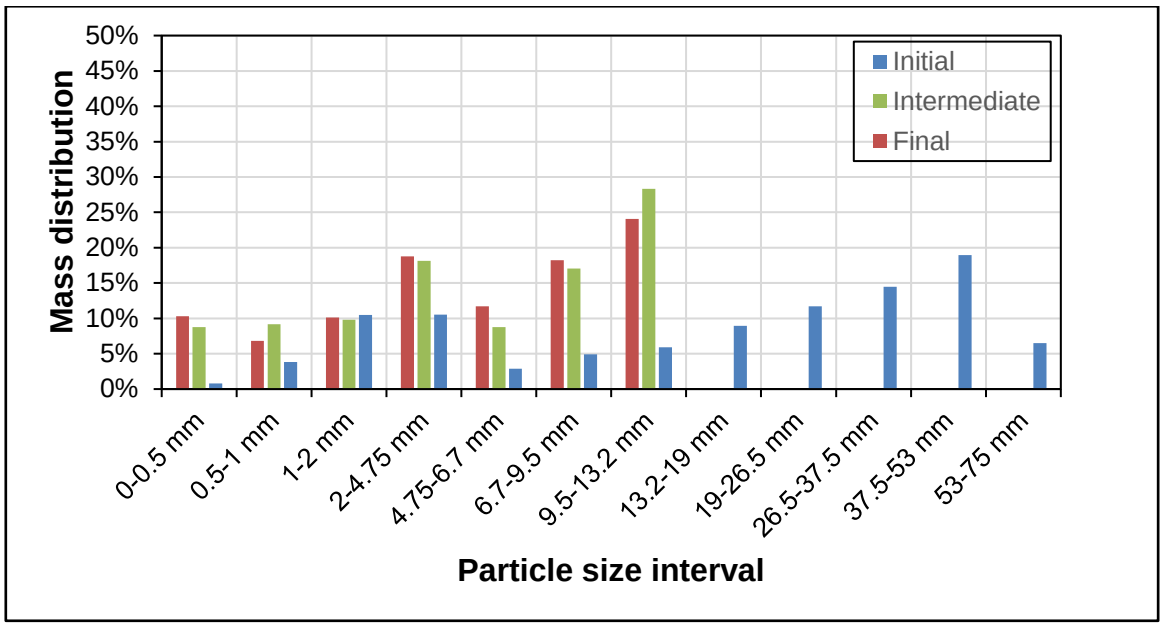

Figure C. 3: Particle size distribution for impact breakage to a top size of 13.2 mm with 1 minute attritioning (Run 4).

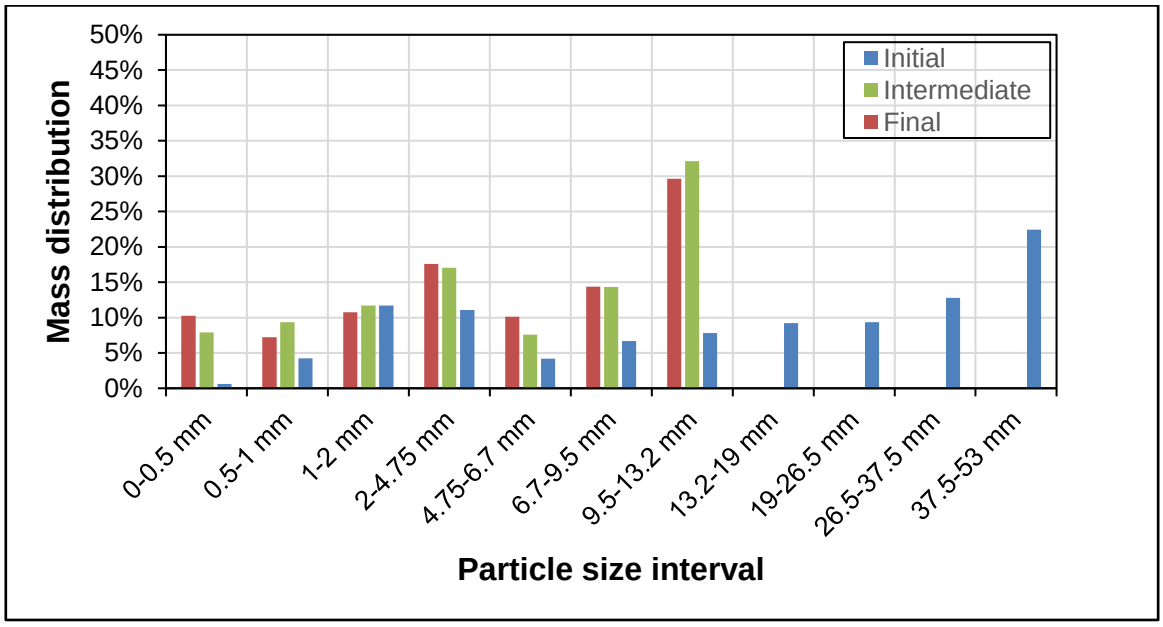

Figure C. 4: Particle size distribution for impact breakage to a top size of 13.2 mm with 2 minutes attritioning (Run 5).

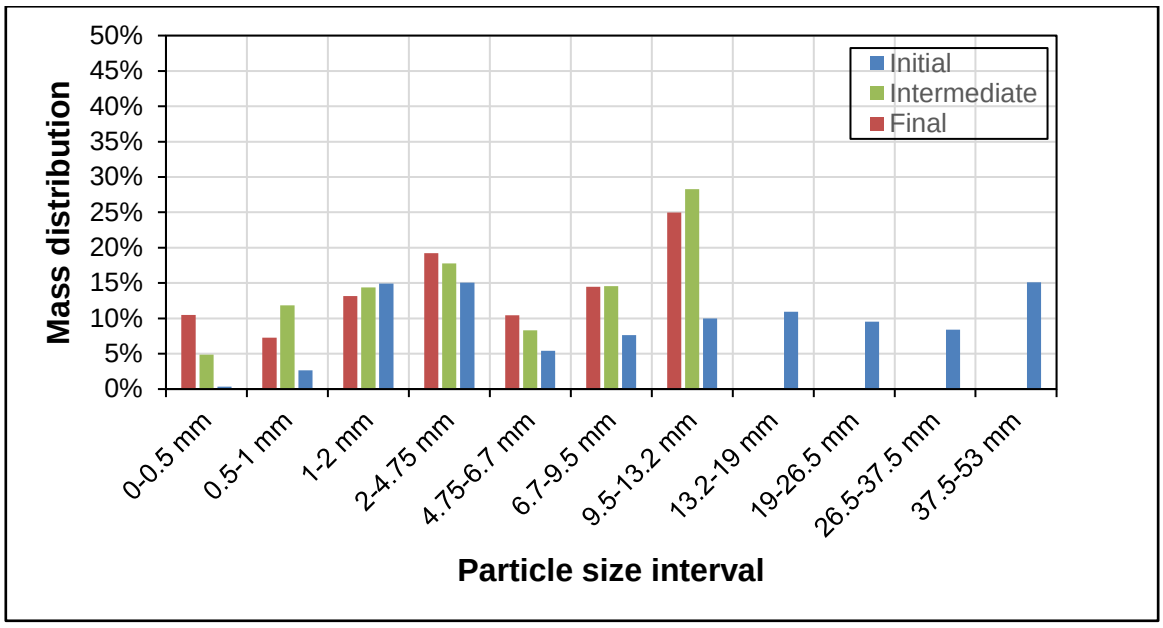

Figure C. 5: Particle size distribution for impact breakage to a top size of 13.2 mm with 5 minutes attritioning (Run 6).

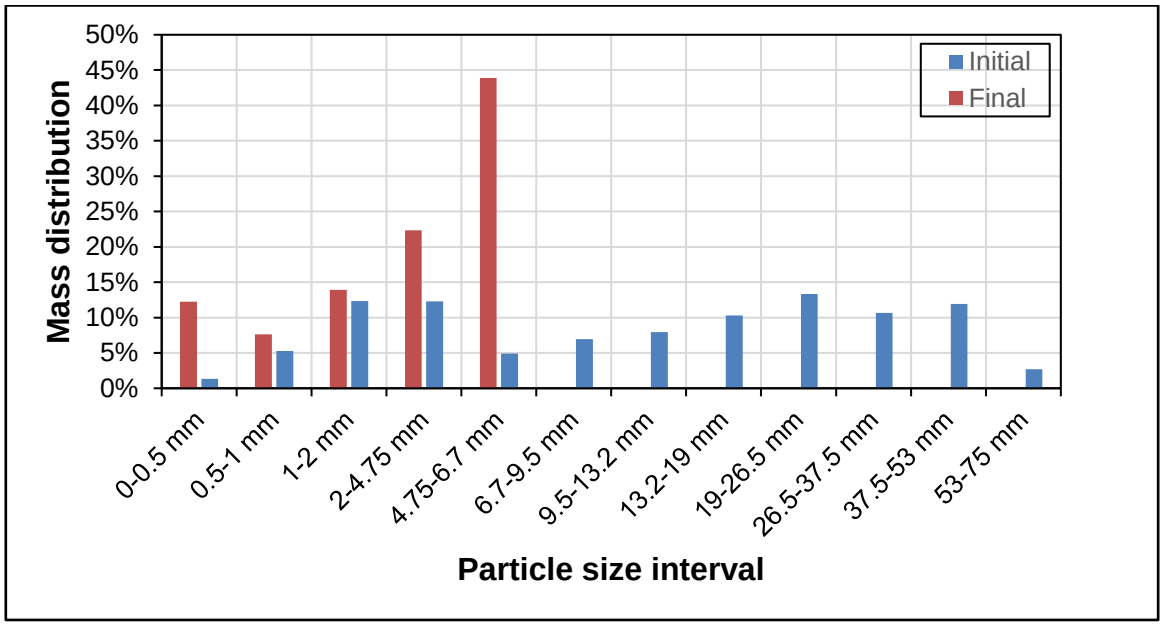

Figure C. 6: Particle size distribution for impact breakage to a top size of 6.7 mm with no attritioning (Run 7-9 average).

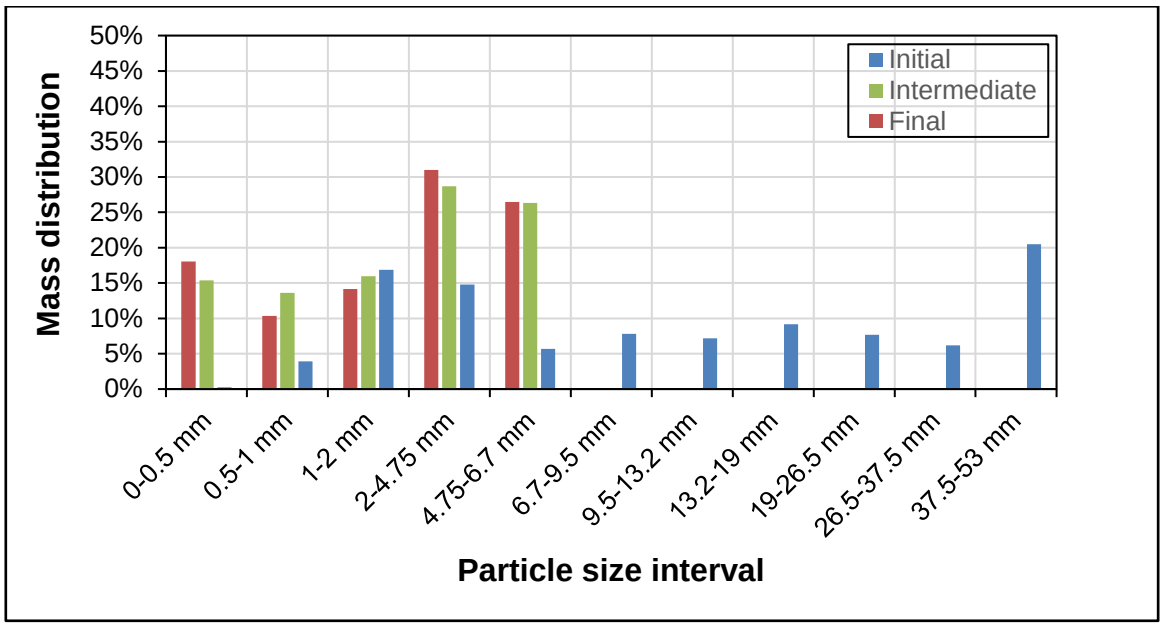

Figure C. 7: Particle size distribution for impact breakage to a top size of 6.7 mm with 1 minute attritioning (Run 10).

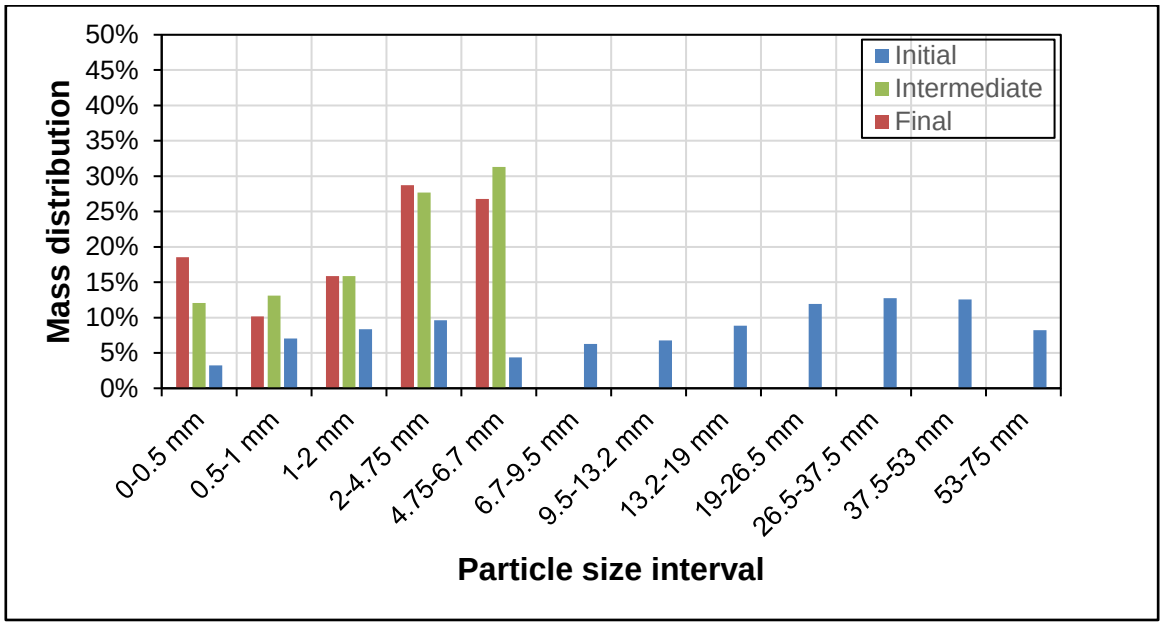

Figure C. 8: Particle size distribution for impact breakage to a top size of 6.7 mm with 2 minutes attritioning (Run 11).

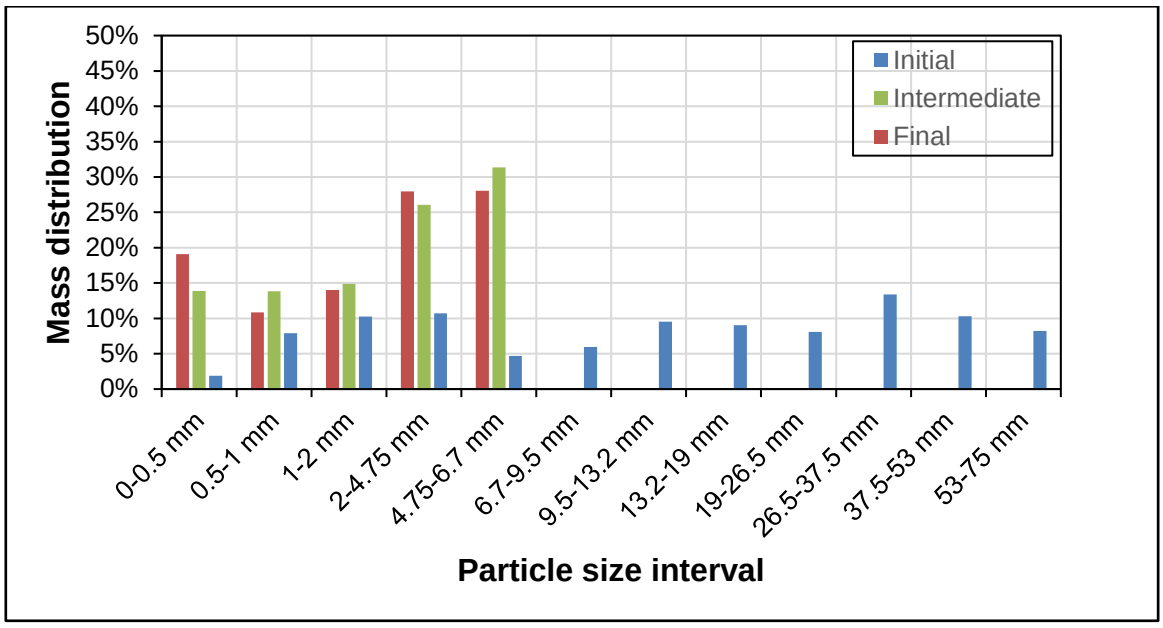

Figure C. 9: Particle size distribution for impact breakage to a top size of 6.7 mm with 5 minutes attritioning (Run 12).

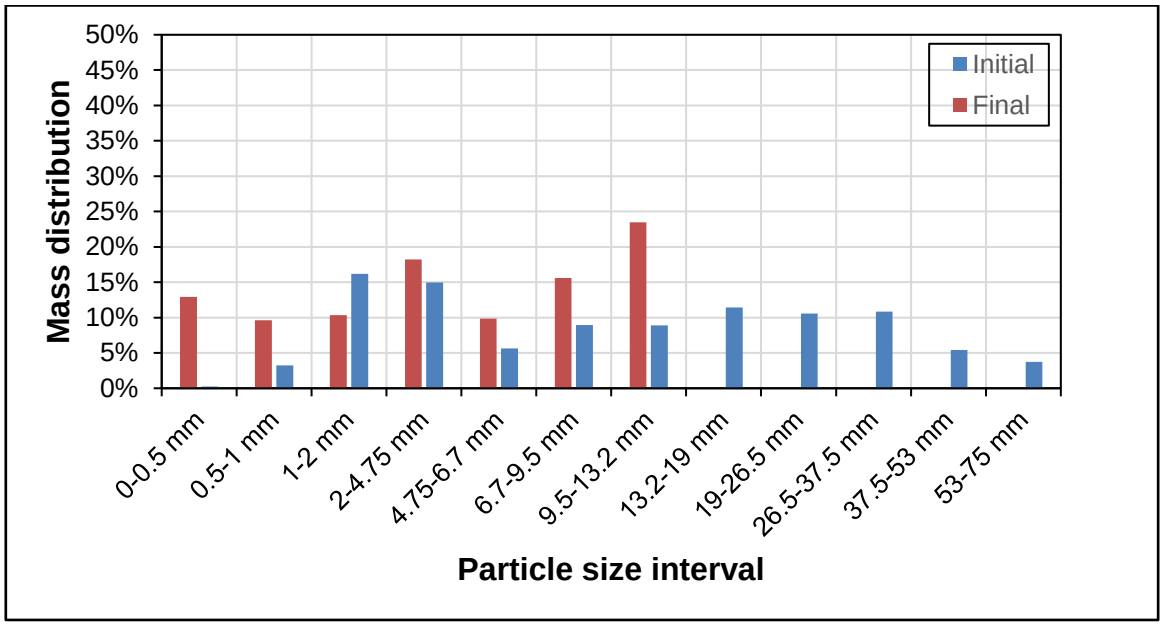

Figure C. 10: Particle size distribution for compressive breakage to a top size of 13.2 mm with no attritioning (Run 13-15 average).

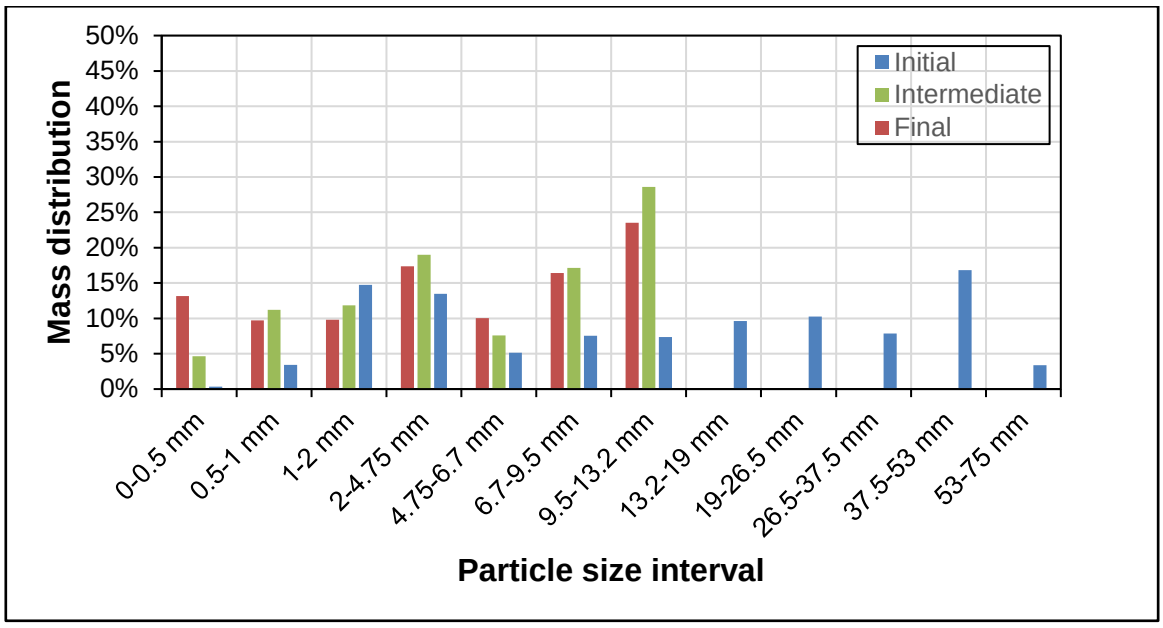

Figure C. 11: Particle size distribution for compressive breakage to a top size of 13.2 mm with 1 minute attritioning (Run 16).

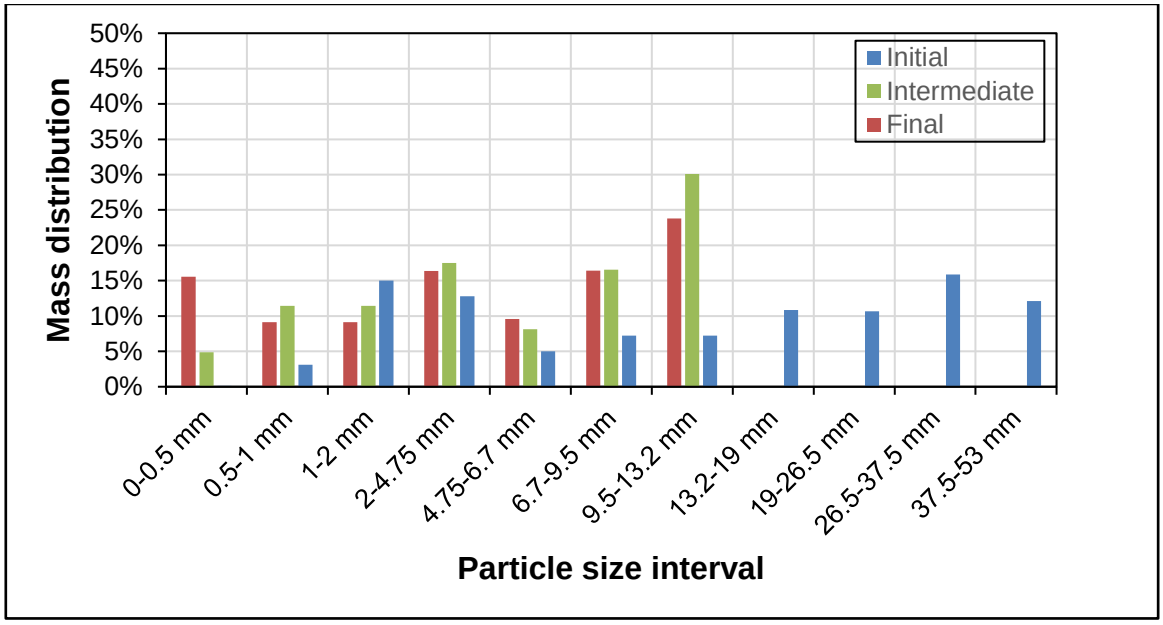

Figure C. 12: Particle size distribution for compressive breakage to a top size of 13.2 mm with 2 minutes attritioning (Run 17).

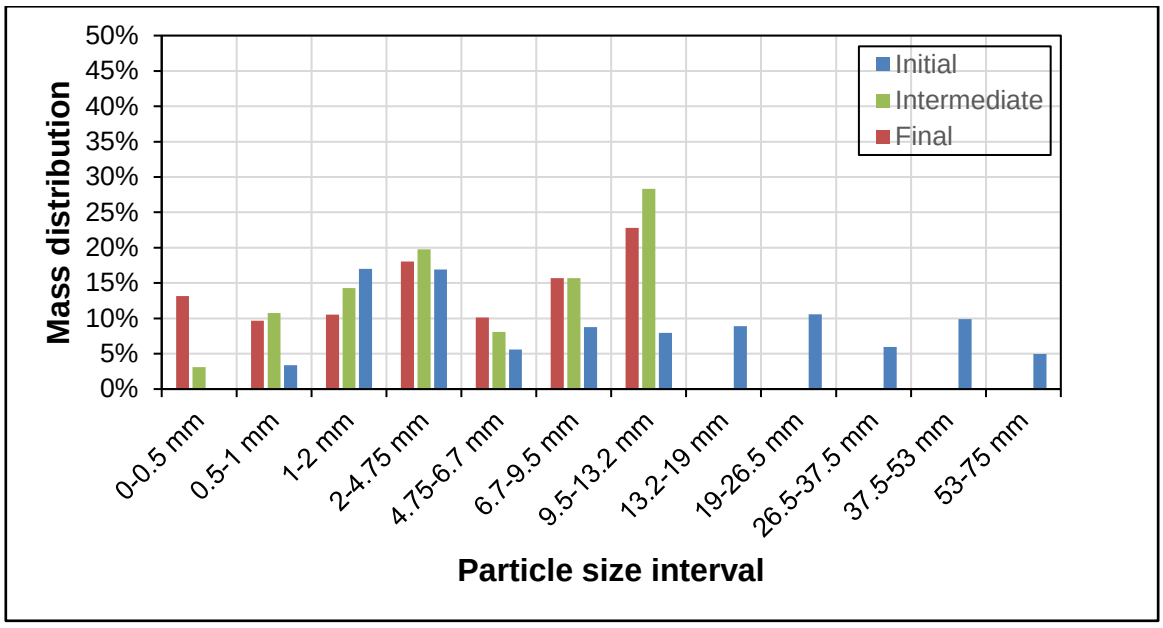

Figure C. 13: Particle size distribution for compressive breakage to a top size of 13.2 mm with 5 minutes attritioning (Run 18).

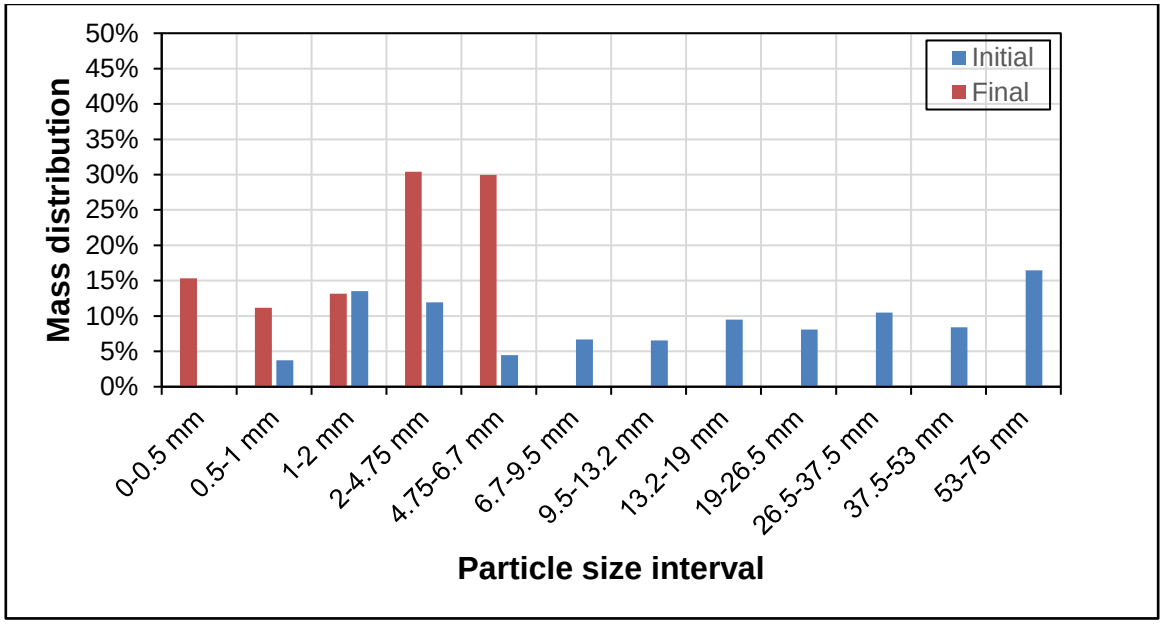

Figure C. 14: Particle size distribution for compressive breakage to a top size of 6.7 mm with no attritioning (Run 19-21 average).

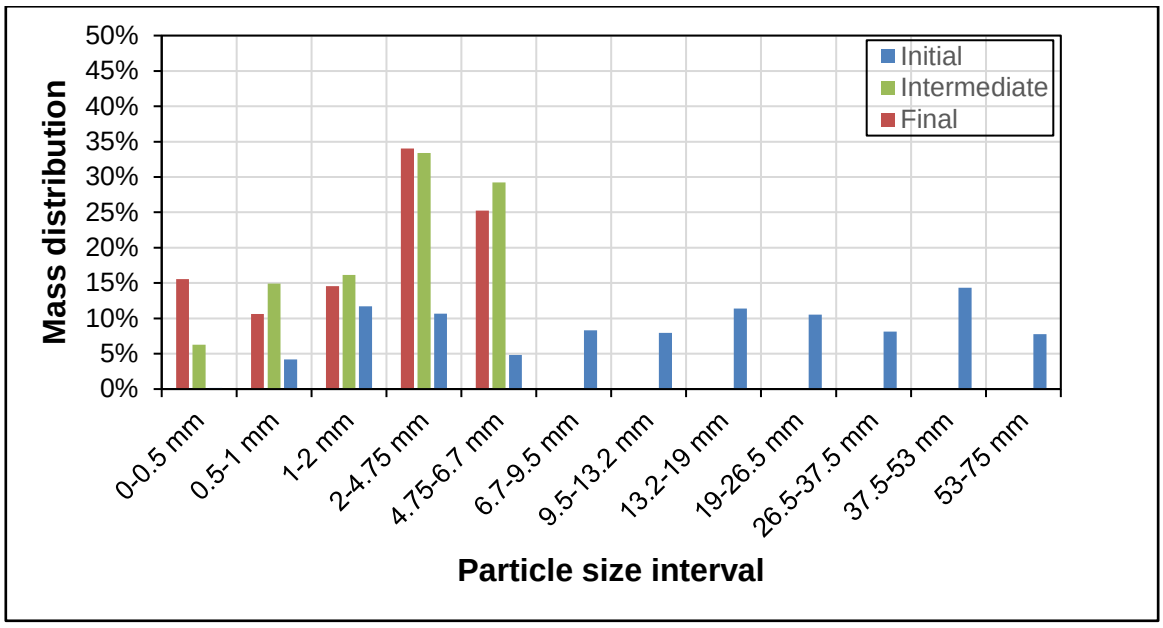

Figure C. 15: Particle size distribution for compressive breakage to a top size of 6.7 mm with 1 minute attritioning (Run 22).

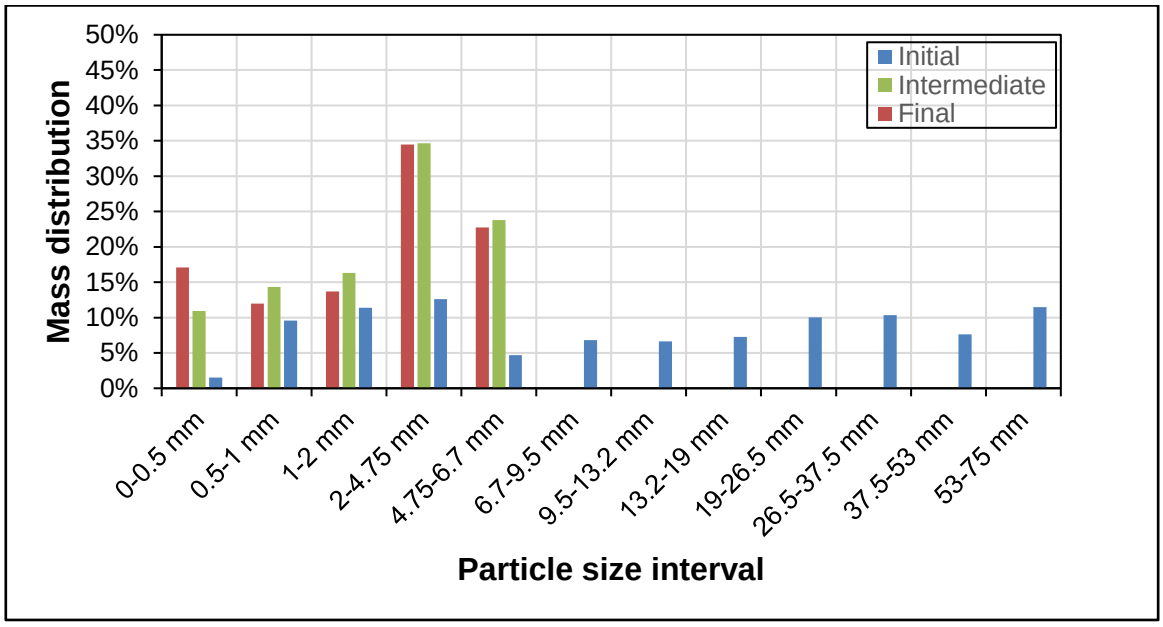

Figure C. 16: Particle size distribution for compressive breakage to a top size of 6.7 mm with 2 minutes attritioning (Run 23).

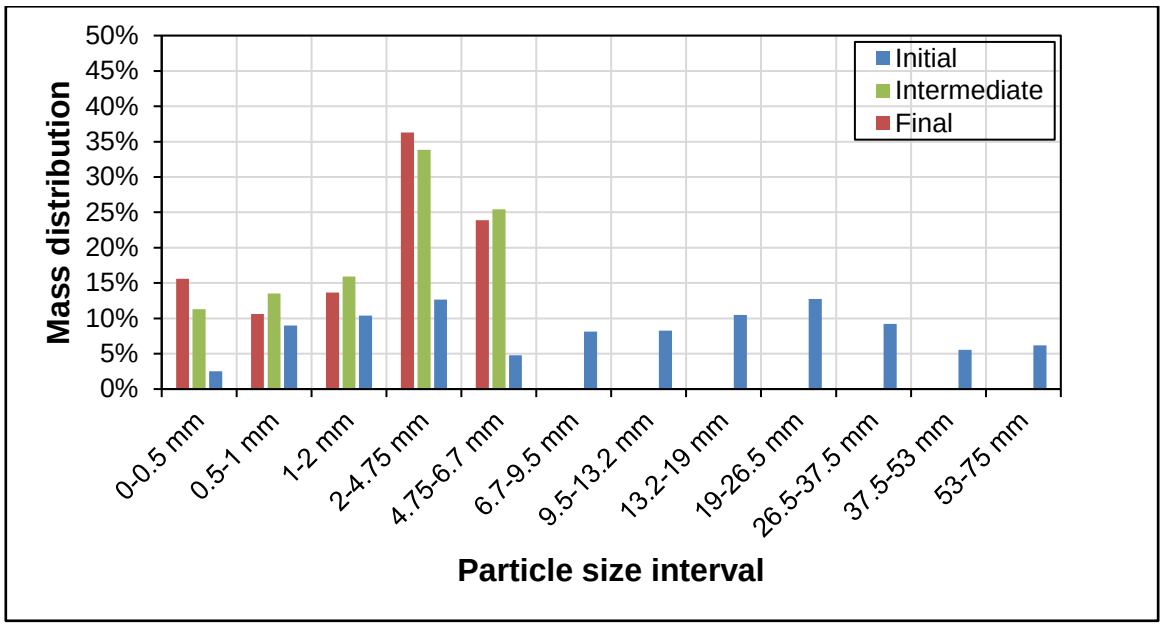

Figure C. 17: Particle size distribution for compressive breakage to a top size of 6.7 mm with 5 minutes attritioning (Run 24).

Partition of sample mass according to relative density and particle size:

The partition data presents the mass distribution of the whole sample according to its relative density and particle size distribution (PSD). Equation D- 10 was used to calculate the mass in each interval, as the sieve mass and sample mass was weigh together. The fractional mass yield occurring in each relative density interval, and particle size interval was calculated to be as a percentage of the total mass according to Equation D- 11. The calculated mass percentage distributions are given in Table C. 31 to Table C. 59.

Table C. 31: Mass percentage distribution for raw ROM coal.

Particle size interval	Relative density interval							Total
	F1.3	1.3-1.4	1.4-1.5	1.5-1.6	1.6-1.7	1.7-1.8	S1.8	
0-0.5mm	0.01	3.82	0.87	1.92	0.25	0.22	1.17	8.26
0.5-1mm	0.22	3.53	0.42	0.88	0.13	0.15	0.62	5.95
1-2mm	2.50	1.73	0.66	0.40	0.21	0.14	0.81	6.45
2-4.75mm	2.13	2.07	1.81	0.95	0.55	0.41	1.89	9.81
4.75-6.7mm	1.87	0.85	1.16	0.66	0.35	0.25	1.12	6.26
6.7-9.5mm	0.17	1.01	1.84	1.04	0.56	0.45	1.44	6.51
9.5-13.2mm	0.08	0.70	1.57	0.82	0.88	0.31	1.99	6.35
13.2-19mm	0.00	1.18	3.00	1.52	0.83	0.96	3.77	11.26
19-26.5mm	0.00	0.94	2.04	2.22	0.85	1.70	2.98	10.73
26.5-37.5mm	0.00	0.00	0.86	1.95	2.49	0.90	2.65	8.85
37.5-53mm	0.00	3.08	3.50	1.85	0.00	0.00	3.59	12.02
53-75mm	0.00	0.00	0.00	0.00	3.37	4.18	0.00	7.55
Total	6.98	18.91	17.73	14.21	10.47	9.67	22.03	100.00

Table C. 32: Mass percentage distribution for impact breakage to a top size of 13.2 mm with no attritioning (Run 1).

Particle size interval	Relative density interval							Total
	F1.3	1.3-1.4	1.4-1.5	1.5-1.6	1.6-1.7	1.7-1.8	S1.8	
0-0.5mm	0.13	3.38	2.39	0.89	0.50	0.29	1.92	9.50
0.5-1mm	0.58	6.09	1.79	0.78	0.54	0.41	1.46	11.65
1-2mm	4.11	1.34	0.97	0.74	0.59	0.36	1.79	9.90
2-4.75mm	3.44	2.55	2.27	2.05	1.39	0.86	4.06	16.62
4.75-6.7mm	0.57	1.25	1.42	1.40	0.97	0.58	2.59	8.78
6.7-9.5mm	0.39	1.97	2.00	2.36	1.38	0.77	3.98	12.85
9.5-13.2mm	0.10	2.39	4.10	4.05	4.85	1.43	13.78	30.70
Total	9.32	18.97	14.94	12.27	10.22	4.70	29.58	100.00

Table C. 33: Mass percentage distribution for impact breakage to a top size of 13.2 mm with no attritioning (Run 2).

Particle size interval	Relative density interval							Total
	F1.3	1.3-1.4	1.4-1.5	1.5-1.6	1.6-1.7	1.7-1.8	S1.8	
0-0.5mm	0.6	4.73	1.61	0.52	0.80	0.24	2.23	10.73
0.5-1mm	1.99	3.30	1.01	0.40	0.53	0.23	1.46	8.92
1-2mm	1.07	1.52	3.53	0.27	0.40	0.36	1.46	8.61
2-4.75mm	0.8	2.69	5.04	0.61	0.98	0.79	3.85	14.76
4.75-6.7mm	0.11	1.58	2.55	0.26	0.65	0.39	2.57	8.11
6.7-9.5mm	0.07	1.96	3.94	0.17	1.06	0.70	3.90	11.80
9.5-13.2mm	0.02	3.15	9.52	1.20	3.62	1.73	17.85	37.09
Total	4.66	18.93	27.20	3.43	8.04	4.44	33.32	100.00

Table C. 34: Mass percentage distribution for impact breakage to a top size of 13.2 mm with no attritioning (Run 3).

Particle size interval	Relative density interval							Total
	F1.3	1.3-1.4	1.4-1.5	1.5-1.6	1.6-1.7	1.7-1.8	S1.8	
0-0.5mm	0.13	4.79	1.62	0.63	0.60	0.25	1.67	9.69
0.5-1mm	1.34	3.41	0.71	0.35	0.28	0.19	0.93	7.21
1-2mm	3.64	2.79	1.25	0.62	0.47	0.47	1.93	11.17
2-4.75mm	2.95	4.09	2.93	1.45	1.13	0.91	4.35	17.81
4.75-6.7mm	0.41	2.14	1.91	0.87	0.74	0.47	2.85	9.39
6.7-9.5mm	0.20	1.92	3.17	1.24	1.10	0.94	3.97	12.54
9.5-13.2mm	0.36	2.97	6.15	3.65	2.22	2.19	14.65	32.19
Total	9.03	22.11	17.74	8.81	6.54	5.42	30.35	100.00

Table C. 35: Mass percentage distribution for impact breakage to a top size of 13.2 mm with no attritioning (Run 1-3 average).

Particle size interval	Relative density interval							Total
	F1.3	1.3-1.4	1.4-1.5	1.5-1.6	1.6-1.7	1.7-1.8	S1.8	
0-0.5mm	0.29	4.29	1.88	0.68	0.64	0.26	1.95	9.99
0.5-1mm	1.31	4.28	1.18	0.51	0.46	0.28	1.29	9.31
1-2mm	2.91	1.86	1.94	0.54	0.49	0.40	1.72	9.86
2-4.75mm	2.37	3.08	3.44	1.36	1.17	0.85	4.08	16.35
4.75-6.7mm	0.36	1.64	1.97	0.84	0.79	0.48	2.66	8.74
6.7-9.5mm	0.22	1.95	3.04	1.25	1.18	0.80	3.95	12.39
9.5-13.2mm	0.15	2.84	6.62	2.94	3.59	1.78	15.46	33.38
Total	7.61	19.94	20.07	8.12	8.32	4.85	31.11	100.00

Table C. 36: Mass percentage distribution for impact breakage to a top size of 13.2 mm with 1 minute attritioning (Run 4).

Particle size interval	Relative density interval							Total
	F1.3	1.3-1.4	1.4-1.5	1.5-1.6	1.6-1.7	1.7-1.8	S1.8	
0-0.5mm	0.23	3.97	1.85	0.53	1.01	0.26	2.43	10.28
0.5-1mm	0.71	2.58	0.91	0.41	0.53	0.25	1.43	6.82
1-2mm	2.13	2.61	1.29	0.65	0.80	0.56	2.06	10.10
2-4.75mm	1.44	3.53	3.27	1.56	1.80	1.39	5.75	18.74
4.75-6.7mm	0.23	1.44	2.24	1.30	1.28	1.01	4.21	11.71
6.7-9.5mm	0.11	1.80	3.53	1.99	1.95	1.38	7.48	18.24
9.5-13.2mm	0.08	1.32	4.24	2.59	2.74	2.19	10.94	24.10
Total	4.93	17.25	17.33	9.03	10.11	7.04	34.30	100.00

Table C. 37: Mass percentage distribution for impact breakage to a top size of 13.2 mm with 2 minutes attritioning (Run 5).

Particle size interval	Relative density interval							Total
	F1.3	1.3-1.4	1.4-1.5	1.5-1.6	1.6-1.7	1.7-1.8	S1.8	
0-0.5mm	0.08	4.69	1.60	0.64	0.74	0.17	2.36	10.28
0.5-1mm	0.79	3.42	0.74	0.40	0.39	0.21	1.28	7.24
1-2mm	2.93	3.11	1.09	0.80	0.56	0.38	1.90	10.77
2-4.75mm	2.68	4.13	2.46	1.75	1.37	0.75	4.46	17.60
4.75-6.7mm	0.27	2.22	1.66	1.21	0.92	0.48	3.35	10.11
6.7-9.5mm	0.14	3.00	2.65	1.86	1.40	0.79	4.52	14.36
9.5-13.2mm	0.08	3.03	4.65	4.06	2.84	2.06	12.91	29.63
Total	6.97	23.6	14.85	10.72	8.22	4.84	30.78	100.00

Table C. 38: Mass percentage distribution for impact breakage to a top size of 13.2 mm with 5 minutes attritioning (Run 6).

Particle size interval	Relative density interval							Total
	F1.3	1.3-1.4	1.4-1.5	1.5-1.6	1.6-1.7	1.7-1.8	S1.8	
0-0.5mm	0.23	4.05	1.88	0.54	1.03	0.27	2.48	10.48
0.5-1mm	1.03	2.63	0.92	0.42	0.54	0.25	1.46	7.25
1-2mm	3.46	3.71	1.33	0.80	0.65	0.46	2.74	13.15
2-4.75mm	2.58	3.98	3.28	1.85	1.35	0.82	5.37	19.23
4.75-6.7mm	0.30	1.67	2.31	1.21	0.93	0.54	3.47	10.43
6.7-9.5mm	0.16	2.10	3.36	1.71	1.58	0.79	4.79	14.49
9.5-13.2mm	0.05	2.10	4.91	2.77	2.10	1.84	11.19	24.96
Total	7.81	20.24	17.99	9.30	8.18	4.97	31.50	100.00

Table C. 39: Mass percentage distribution for impact breakage to a top size of 6.7 mm with no attritioning (Run 7).

Particle size interval	Relative density interval							Total
	F1.3	1.3-1.4	1.4-1.5	1.5-1.6	1.6-1.7	1.7-1.8	S1.8	
0-0.5mm	0.13	3.97	1.4	0.94	0.45	0.39	1.53	8.81
0.5-1mm	0.59	3.16	1.15	0.77	0.41	0.42	1.41	7.91
1-2mm	3.22	4.21	2.47	1.29	0.77	0.76	2.47	15.19
2-4.75mm	2.13	4.6	4.75	2.91	1.76	1.46	5.38	22.99
4.75-6.7mm	0.48	4.56	10.29	6.75	3.75	3.96	15.33	45.12
Total	6.55	20.5	20.06	12.66	7.14	6.99	26.12	100.00

Table C. 40: Mass percentage distribution for impact breakage to a top size of 6.7 mm with no attritioning (Run 8).

Particle size interval	Relative density interval							Total
	F1.3	1.3-1.4	1.4-1.5	1.5-1.6	1.6-1.7	1.7-1.8	S1.8	
0-0.5mm	0.07	3.77	2.63	0.94	0.28	0.39	1.67	9.75
0.5-1mm	0.54	2.75	1.3	0.56	0.41	0.31	1.02	6.89
1-2mm	3.53	5.92	1.08	0.82	0.79	0.54	1.83	14.51
2-4.75mm	4.54	7.39	2.61	1.85	1.39	1.00	4.67	23.45
4.75-6.7mm	0.46	9.54	7.01	4.91	4.16	2.65	16.68	45.41
Total	9.14	29.37	14.63	9.08	7.03	4.89	25.87	100.00

Table C. 41: Mass percentage distribution for impact breakage to a top size of 6.7 mm with no attritioning (Run 9).

Particle size interval	Relative density interval							Total
	F1.3	1.3-1.4	1.4-1.5	1.5-1.6	1.6-1.7	1.7-1.8	S1.8	
0-0.5mm	0.40	6.79	1.61	2.23	1.06	0.73	4.12	16.94
0.5-1mm	1.11	2.83	0.74	0.82	0.50	0.39	1.62	8.01
1-2mm	4.16	2.63	1.08	0.92	0.67	0.46	2.47	12.39
2-4.75mm	2.94	5.11	2.83	2.02	1.44	0.93	5.67	20.94
4.75-6.7mm	0.61	7.15	7.09	5.02	3.77	2.57	15.48	41.69
Total	9.22	24.51	13.35	11.01	7.44	5.08	29.36	100.00

Table C. 42: Mass percentage distribution for impact breakage to a top size of 6.7 mm with no attritioning (Run 7-9 average).

Particle size interval	Relative density interval							Total
	F1.3	1.3-1.4	1.4-1.5	1.5-1.6	1.6-1.7	1.7-1.8	S1.8	
0-0.5mm	0.21	4.99	1.86	1.44	0.63	0.52	2.57	12.22
0.5-1mm	0.78	2.91	1.04	0.72	0.45	0.38	1.37	7.65
1-2mm	3.67	4.12	1.51	1.01	0.74	0.58	2.27	13.90
2-4.75mm	3.18	5.65	3.36	2.24	1.52	1.12	5.27	22.34
4.75-6.7mm	0.52	7.07	8.06	5.53	3.88	3.03	15.8	43.89
Total	8.36	24.74	15.83	10.94	7.22	5.63	27.28	100.00

Table C. 43: Mass percentage distribution for impact breakage to a top size of 6.7 mm with 1 minute attritioning (Run 10).

Particle size interval	Relative density interval							Total
	F1.3	1.3-1.4	1.4-1.5	1.5-1.6	1.6-1.7	1.7-1.8	S1.8	
0-0.5mm	1.03	13.01	0.88	0.77	0.35	0.28	1.75	18.07
0.5-1mm	1.72	5.86	0.59	0.44	0.29	0.26	1.18	10.34
1-2mm	4.96	2.03	1.82	1.11	0.87	0.73	2.65	14.17
2-4.75mm	7.70	4.18	4.80	2.84	2.21	1.71	7.54	30.98
4.75-6.7mm	1.89	2.63	3.95	2.77	1.83	1.65	11.71	26.43
Total	17.3	27.71	12.04	7.93	5.55	4.63	24.83	100.00

Table C. 44: Mass percentage distribution for impact breakage to a top size of 6.7 mm with 2 minutes attritioning (Run 11).

Particle size interval	Relative density interval							Total
	F1.3	1.3-1.4	1.4-1.5	1.5-1.6	1.6-1.7	1.7-1.8	S1.8	
0-0.5mm	0.67	9.29	1.67	1.93	0.84	0.78	3.34	18.52
0.5-1mm	1.44	4.14	0.95	0.91	0.52	0.45	1.75	10.16
1-2mm	5.54	2.80	1.96	1.17	0.84	0.54	2.98	15.83
2-4.75mm	4.94	5.48	5.17	3.06	2.31	1.16	6.58	28.70
4.75-6.7mm	1.11	3.59	5.35	3.49	2.58	1.40	9.25	26.77
Total	13.70	25.30	15.10	10.56	7.09	4.33	23.90	100.00

Table C. 45: Mass percentage distribution for impact breakage to a top size of 6.7 mm with 5 minutes attritioning (Run 12).

Particle size interval	Relative density interval							Total
	F1.3	1.3-1.4	1.4-1.5	1.5-1.6	1.6-1.7	1.7-1.8	S1.8	
0-0.5mm	1.09	13.76	0.93	0.81	0.37	0.29	1.85	19.10
0.5-1mm	1.75	6.19	0.62	0.46	0.31	0.27	1.25	10.85
1-2mm	4.35	2.56	2.14	1.06	0.79	0.78	2.35	14.03
2-4.75mm	4.68	4.43	5.62	2.98	2.38	1.88	6.00	27.97
4.75-6.7mm	0.87	2.74	5.98	3.10	3.04	2.54	9.76	28.03
Total	12.74	29.68	15.29	8.41	6.89	5.76	21.21	100.00

Table C. 46: Mass percentage distribution for compressive breakage to a top size of 13.2 mm with no attritioning (Run 13).

Particle size interval	Relative density interval							Total
	F1.3	1.3-1.4	1.4-1.5	1.5-1.6	1.6-1.7	1.7-1.8	S1.8	
0-0.5mm	0.03	5.87	1.57	2.48	0.57	0.46	2.54	13.52
0.5-1mm	0.38	5.46	1.05	1.20	0.43	0.46	1.41	10.39
1-2mm	3.16	2.13	1.02	0.50	0.47	0.36	1.68	9.32
2-4.75mm	3.05	3.77	2.79	1.32	1.22	0.91	3.92	16.98
4.75-6.7mm	0.38	1.89	1.93	0.85	0.75	0.51	2.56	8.87
6.7-9.5mm	0.25	2.66	3.61	1.68	1.41	1.43	4.54	15.58
9.5-13.2mm	0.26	3.32	4.93	2.64	2.6	1.65	9.93	25.33
Total	7.51	25.10	16.9	10.67	7.45	5.78	26.58	100.00

Table C. 47: Mass percentage distribution for compressive breakage to a top size of 13.2 mm with no attritioning (Run 14).

Particle size interval	Relative density interval							Total
	F1.3	1.3-1.4	1.4-1.5	1.5-1.6	1.6-1.7	1.7-1.8	S1.8	
0-0.5mm	0.01	4.00	2.73	1.09	0.89	0.33	3.23	12.28
0.5-1mm	0.31	3.89	1.18	0.58	0.51	0.32	1.70	8.49
1-2mm	2.08	3.17	1.27	0.56	0.43	0.43	2.42	10.36
2-4.75mm	1.99	4.51	3.02	1.37	1.16	0.88	5.75	18.68
4.75-6.7mm	0.30	1.98	1.92	0.91	0.76	0.54	4.11	10.52
6.7-9.5mm	0.17	2.42	3.15	1.34	1.44	1.06	6.63	16.21
9.5-13.2mm	0.10	1.90	4.44	2.58	2.01	1.45	10.98	23.46
Total	4.96	21.87	17.71	8.43	7.20	5.01	34.82	100.00

Table C. 48: Mass percentage distribution for compressive breakage to a top size of 13.2 mm with no attritioning (Run 15).

Particle size interval	Relative density interval							Total
	F1.3	1.3-1.4	1.4-1.5	1.5-1.6	1.6-1.7	1.7-1.8	S1.8	
0-0.5mm	0.03	4.7	3.12	1.61	0.93	0.34	2.29	13.02
0.5-1mm	0.2	5.17	1.53	0.91	0.59	0.29	1.49	10.18
1-2mm	2.41	4.02	1.25	0.59	0.48	0.40	1.95	11.10
2-4.75mm	2.21	5.00	3.33	1.44	1.18	0.91	4.74	18.81
4.75-6.7mm	0.36	2.06	2.33	0.93	0.75	0.45	3.01	9.89
6.7-9.5mm	0.24	2.31	3.73	1.86	1.25	0.70	4.88	14.97
9.5-13.2mm	0.08	1.69	3.99	2.84	2.04	1.46	9.91	22.01
Total	5.53	24.95	19.28	10.18	7.22	4.55	28.27	100.00

Table C. 49: Mass percentage distribution for compressive breakage to a top size of 13.2 mm with no attritioning (Run 13-15 average).

Particle size interval	Relative density interval							Total
	F1.3	1.3-1.4	1.4-1.5	1.5-1.6	1.6-1.7	1.7-1.8	S1.8	
0-0.5mm	0.02	4.78	2.54	1.67	0.81	0.37	2.70	12.89
0.5-1mm	0.29	4.79	1.27	0.88	0.52	0.35	1.54	9.64
1-2mm	2.51	3.18	1.19	0.55	0.46	0.40	2.04	10.33
2-4.75mm	2.37	4.48	3.07	1.38	1.18	0.90	4.86	18.24
4.75-6.7mm	0.34	1.98	2.07	0.90	0.76	0.50	3.27	9.82
6.7-9.5mm	0.22	2.45	3.49	1.63	1.36	1.04	5.41	15.60
9.5-13.2mm	0.14	2.23	4.42	2.69	2.19	1.51	10.3	23.48
Total	5.89	23.89	18.05	9.70	7.28	5.07	30.12	100.00

Table C. 50: Mass percentage distribution for compressive breakage to a top size of 13.2 mm with 1 minute attritioning (Run 16).

Particle size interval	Relative density interval							Total
	F1.3	1.3-1.4	1.4-1.5	1.5-1.6	1.6-1.7	1.7-1.8	S1.8	
0-0.5mm	0.02	5.67	2.52	1.08	0.69	0.52	2.65	13.15
0.5-1mm	0.28	5.26	1.31	0.61	0.46	0.32	1.48	9.72
1-2mm	3.23	2.00	1.33	0.59	0.38	0.43	1.84	9.80
2-4.75mm	2.64	3.33	3.55	1.44	0.95	0.96	4.48	17.35
4.75-6.7mm	0.40	1.78	2.54	1.03	0.70	0.59	2.98	10.02
6.7-9.5mm	0.17	2.31	4.20	1.94	1.29	0.99	5.52	16.42
9.5-13.2mm	0.10	2.14	4.48	2.07	1.55	1.85	11.36	23.55
Total	6.84	22.49	19.93	8.76	6.02	5.66	30.31	100.00

Table C. 51: Mass percentage distribution for compressive breakage to a top size of 13.2 mm with 2 minutes attritioning (Run 17).

Particle size interval	Relative density interval							Total
	F1.3	1.3-1.4	1.4-1.5	1.5-1.6	1.6-1.7	1.7-1.8	S1.8	
0-0.5mm	0.03	6.98	3.34	1.07	0.69	0.45	3.01	15.57
0.5-1mm	0.18	4.91	0.87	0.59	0.51	0.34	1.73	9.13
1-2mm	2.46	2.04	1.33	0.65	0.50	0.37	1.79	9.14
2-4.75mm	2.01	2.99	3.08	1.51	1.27	0.90	4.61	16.37
4.75-6.7mm	0.33	1.27	2.09	1.12	0.90	0.63	3.23	9.57
6.7-9.5mm	0.16	1.95	3.62	2.11	1.47	0.99	6.15	16.45
9.5-13.2mm	0.06	1.81	3.81	3.28	2.11	1.60	11.13	23.80
Total	5.23	21.95	18.14	10.33	7.45	5.28	31.65	100.00

Table C. 52: Mass percentage distribution for compressive breakage to a top size of 13.2 mm with 5 minutes attritioning (Run 18).

Particle size interval	Relative density interval							Total
	F1.3	1.3-1.4	1.4-1.5	1.5-1.6	1.6-1.7	1.7-1.8	S1.8	
0-0.5mm	0.02	5.67	2.52	1.08	0.69	0.52	2.65	13.15
0.5-1mm	0.27	5.26	1.31	0.61	0.46	0.32	1.48	9.71
1-2mm	2.14	3.43	1.20	0.65	0.52	0.46	2.12	10.52
2-4.75mm	2.05	3.77	3.03	1.61	1.26	1.12	5.19	18.03
4.75-6.7mm	0.34	1.52	2.02	1.04	1.06	0.65	3.48	10.11
6.7-9.5mm	0.18	1.55	3.40	1.56	2.03	1.13	5.85	15.70
9.5-13.2mm	0.09	1.90	3.57	2.57	2.67	1.30	10.72	22.82
Total	5.09	23.1	17.05	9.12	8.69	5.50	31.49	100.00

Table C. 53: Mass percentage distribution for compressive breakage to a top size of 6.7 mm with no attritioning (Run 19).

Particle size interval	Relative density interval							Total
	F1.3	1.3-1.4	1.4-1.5	1.5-1.6	1.6-1.7	1.7-1.8	S1.8	
0-0.5mm	0.01	4.65	4.45	1.82	0.91	0.40	3.16	15.40
0.5-1mm	0.28	4.13	2.44	1.07	0.61	0.35	2.37	11.25
1-2mm	3.62	2.21	2.02	0.75	0.75	0.76	3.51	13.62
2-4.75mm	3.34	4.55	6.31	2.70	2.13	2.46	11.46	32.95
4.75-6.7mm	0.67	2.33	4.74	2.39	1.71	2.23	12.69	26.76
Total	7.92	17.87	19.96	8.73	6.11	6.20	33.19	100.00

Table C. 54: Mass percentage distribution for compressive breakage to a top size of 6.7 mm with no attritioning (Run 20).

Particle size interval	Relative density interval							Total
	F1.3	1.3-1.4	1.4-1.5	1.5-1.6	1.6-1.7	1.7-1.8	S1.8	
0-0.5mm	0.02	5.59	2.86	1.68	0.98	0.46	3.27	14.86
0.5-1mm	0.19	4.75	1.46	0.97	0.68	0.34	2.36	10.75
1-2mm	3.29	1.87	1.80	0.81	0.75	0.67	3.12	12.31
2-4.75mm	3.18	3.08	5.57	2.96	2.48	2.04	8.92	28.23
4.75-6.7mm	0.65	1.85	4.98	3.53	2.80	2.58	17.47	33.86
Total	7.33	17.14	16.67	9.95	7.69	6.09	35.14	100.00

Table C. 55: Mass percentage distribution for compressive breakage to a top size of 6.7 mm with no attritioning (Run 21).

Particle size interval	Relative density interval							Total
	F1.3	1.3-1.4	1.4-1.5	1.5-1.6	1.6-1.7	1.7-1.8	S1.8	
0-0.5mm	0.01	5.90	2.77	1.60	0.95	0.71	3.74	15.68
0.5-1mm	0.39	4.83	1.64	0.96	0.63	0.48	2.54	11.47
1-2mm	3.94	1.86	1.93	0.93	0.81	0.57	3.48	13.52
2-4.75mm	3.58	3.81	5.57	3.07	2.37	1.86	9.74	30.00
4.75-6.7mm	0.57	2.25	4.31	3.09	2.71	1.87	14.52	29.32
Total	8.49	18.65	16.22	9.65	7.47	5.49	34.02	100.00

Table C. 56: Mass percentage distribution for compressive breakage to a top size of 6.7 mm with no attritioning (Run 19-21 average).

Particle size interval	Relative density interval							Total
	F1.3	1.3-1.4	1.4-1.5	1.5-1.6	1.6-1.7	1.7-1.8	S1.8	
0-0.5mm	0.01	5.38	3.36	1.7	0.95	0.53	3.39	15.32
0.5-1mm	0.29	4.57	1.85	1.00	0.64	0.39	2.43	11.17
1-2mm	3.62	1.98	1.92	0.83	0.77	0.67	3.37	13.16
2-4.75mm	3.37	3.82	5.82	2.91	2.33	2.12	10.04	30.41
4.75-6.7mm	0.63	2.14	4.67	3.00	2.41	2.22	14.88	29.95
Total	7.92	17.89	17.62	9.44	7.10	5.93	34.11	100.00

Table C. 57: Mass percentage distribution for compressive breakage to a top size of 6.7 mm with 1 minute attritioning (Run 22).

Particle size interval	Relative density interval							Total
	F1.3	1.3-1.4	1.4-1.5	1.5-1.6	1.6-1.7	1.7-1.8	S1.8	
0-0.5mm	0.00	6.15	3.23	1.50	0.78	0.54	3.35	15.55
0.5-1mm	0.14	4.70	1.77	0.88	0.61	0.37	2.13	10.60
1-2mm	3.94	2.38	2.36	1.25	0.88	0.75	3.01	14.57
2-4.75mm	4.14	4.18	6.68	3.90	3.34	2.37	9.40	34.01
4.75-6.7mm	0.84	2.26	5.69	3.02	2.85	2.00	8.57	25.23
Total	9.06	19.67	19.73	10.55	8.46	6.03	26.46	100.00

Table C. 58: Mass percentage distribution for compressive breakage to a top size of 6.7 mm with 2 minutes attritioning (Run 23).

Particle size interval	Relative density interval							Total
	F1.3	1.3-1.4	1.4-1.5	1.5-1.6	1.6-1.7	1.7-1.8	S1.8	
0-0.5mm	0.00	8.14	1.71	2.10	0.76	0.78	3.59	17.08
0.5-1mm	0.12	6.62	1.21	1.34	0.53	0.32	1.85	11.99
1-2mm	4.71	1.75	2.08	1.09	0.79	0.69	2.59	13.70
2-4.75mm	6.04	3.45	6.56	4.43	2.99	2.35	8.67	34.49
4.75-6.7mm	0.98	1.67	5.21	3.47	2.47	1.83	7.13	22.76
Total	11.85	21.63	16.77	12.43	7.54	5.97	23.83	100.00

Table C. 59: Mass percentage distribution for compressive breakage to a top size of 6.7 mm with 5 minutes attritioning (Run 24).

Particle size interval	Relative density interval							Total
	F1.3	1.3-1.4	1.4-1.5	1.5-1.6	1.6-1.7	1.7-1.8	S1.8	
0-0.5mm	0.00	6.17	3.23	1.51	0.78	0.54	3.36	15.59
0.5-1mm	0.12	4.71	1.78	0.88	0.61	0.37	2.14	10.61
1-2mm	4.49	2.07	1.68	1.07	0.82	0.57	2.93	13.63
2-4.75mm	6.09	4.15	6.69	4.13	3.19	2.37	9.65	36.27
4.75-6.7mm	1.36	2.17	4.91	3.05	2.54	1.73	8.13	23.89
Total	12.06	19.27	18.29	10.64	7.94	5.58	26.21	100.00

Size by washability graphs:

Data from Table C. 31 to Table C. 59 was used to construct the size by washability graphs, Figure C. 18 to Figure C. 37.

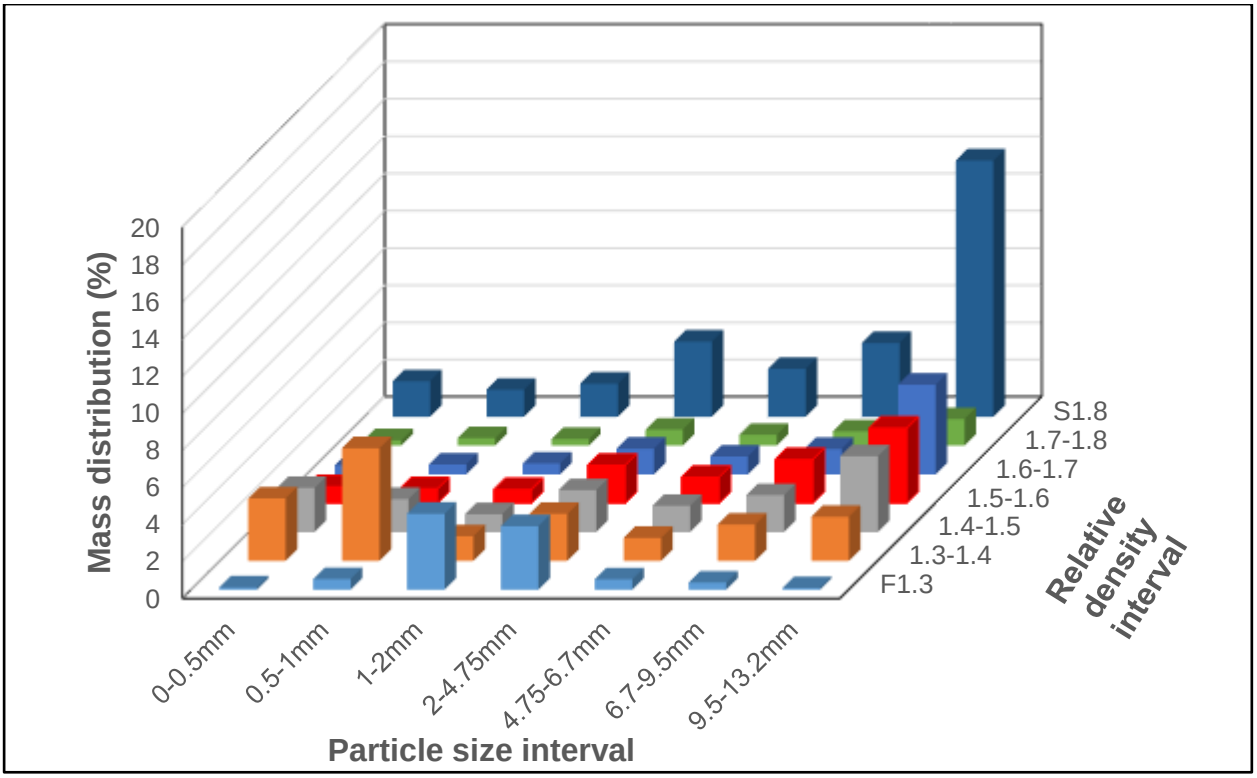

Figure C. 18: Size by washability graph for impact breakage to a top size of 13.2 mm with no additional attrition breakage (Run 1).

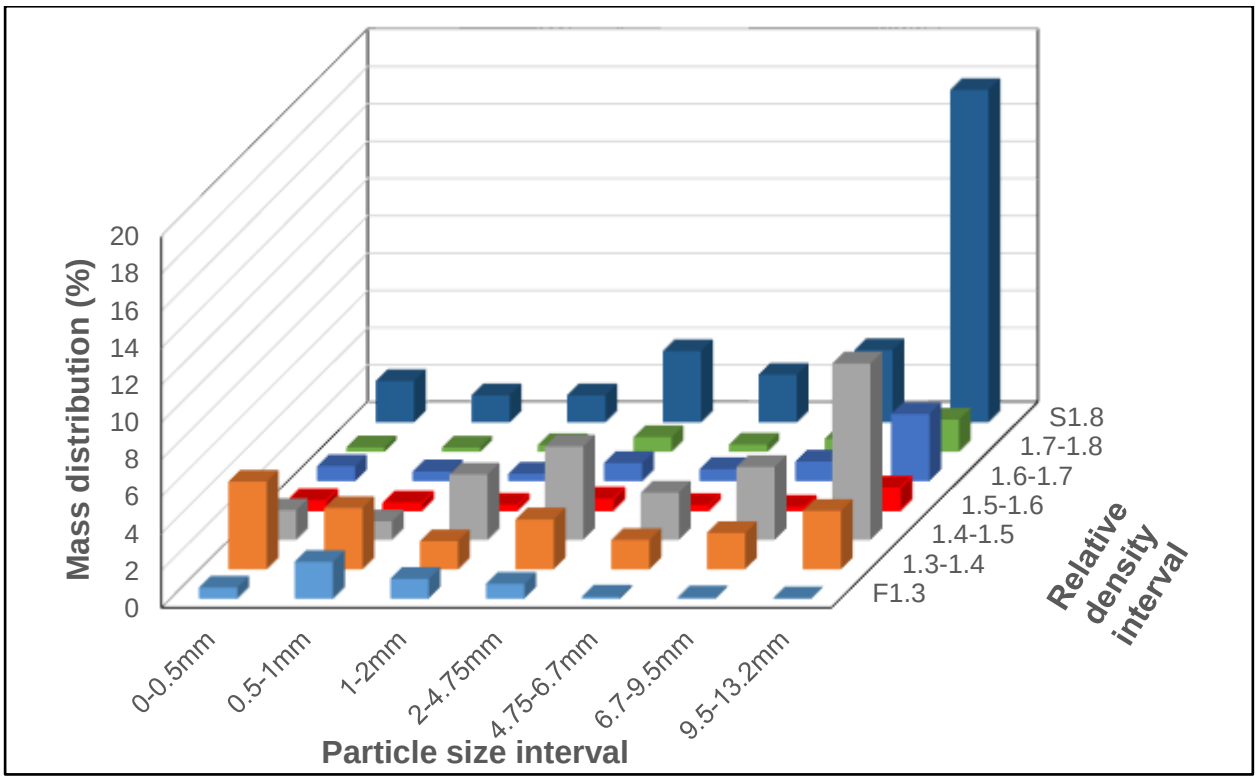

Figure C. 19: Size by washability graph for impact breakage to a top size of 13.2 mm with no additional attrition breakage (Run 2).

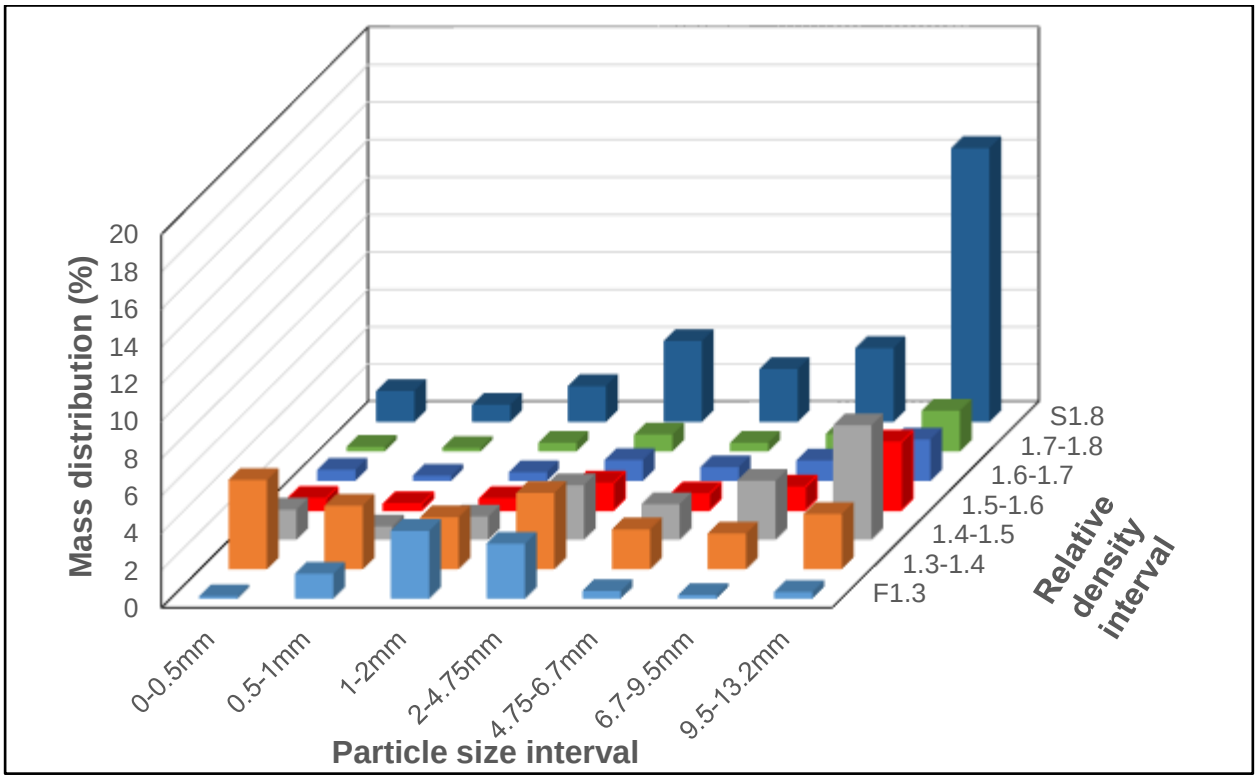

Figure C. 20: Size by washability graph for impact breakage to a top size of 13.2 mm with no additional attrition breakage (Run 3).

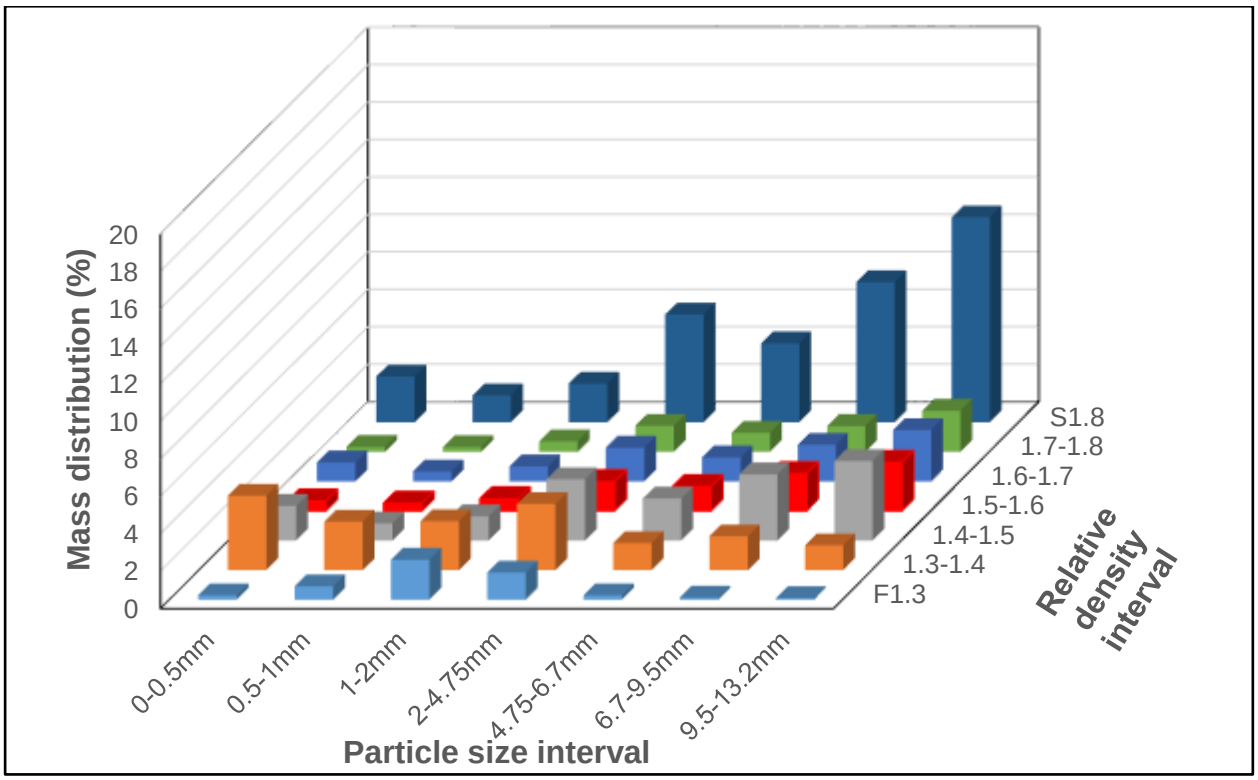

Figure C. 21: Size by washability graph for impact breakage to a top size of 13.2 mm with no 1 minute attritioning (Run 4).

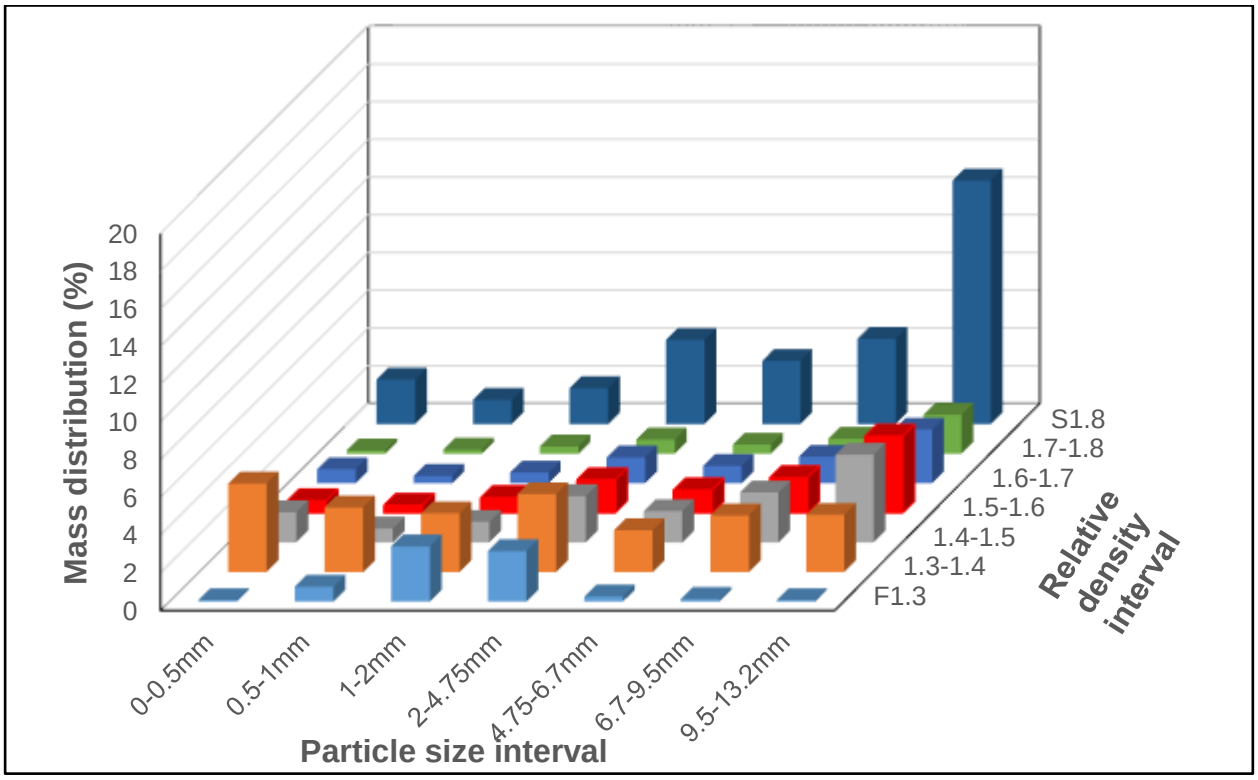

Figure C. 22: Size by washability graph for impact breakage to a top size of 13.2 mm with 2 minutes attritioning (Run 5).

Note that the size by washability graph for impact breakage to a top size of 13.2 mm with 5 minutes attritioning is presented as Figure 4.9.

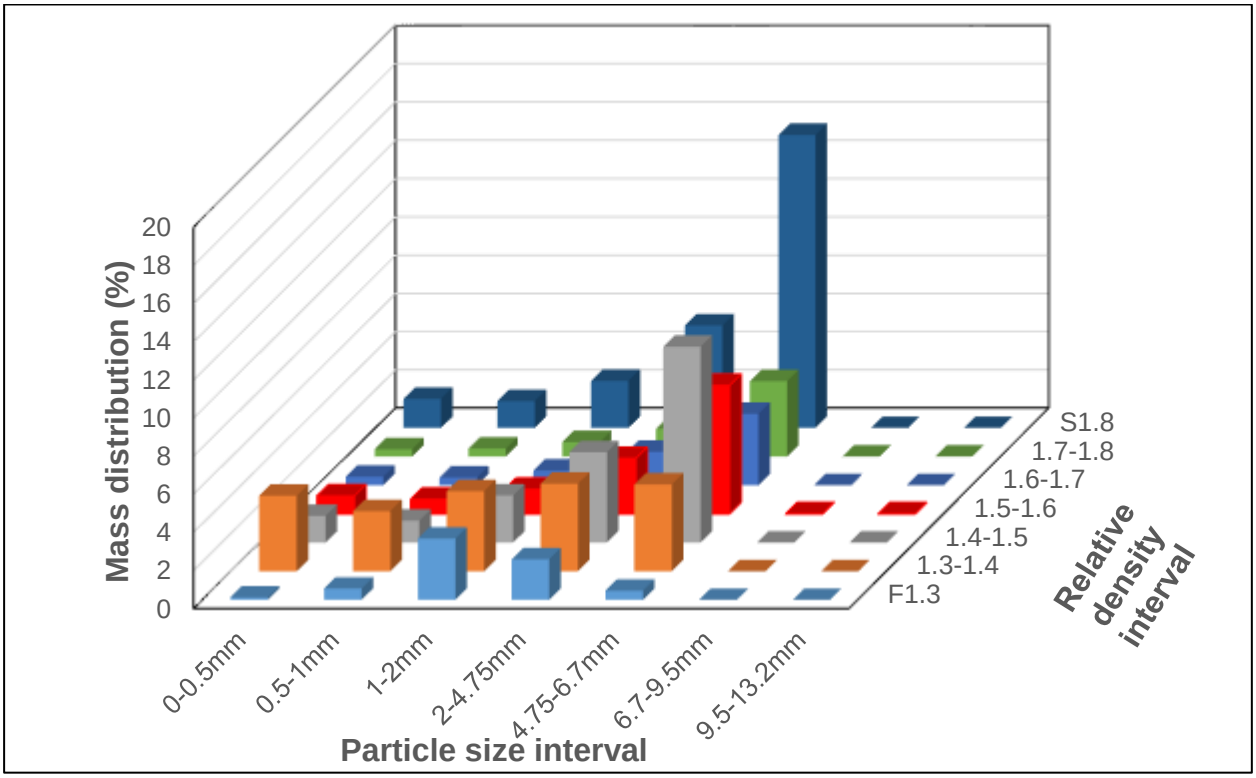

Figure C. 23: Size by washability graph for impact breakage to a top size of 6.7 mm with no attritioning (Run 7).

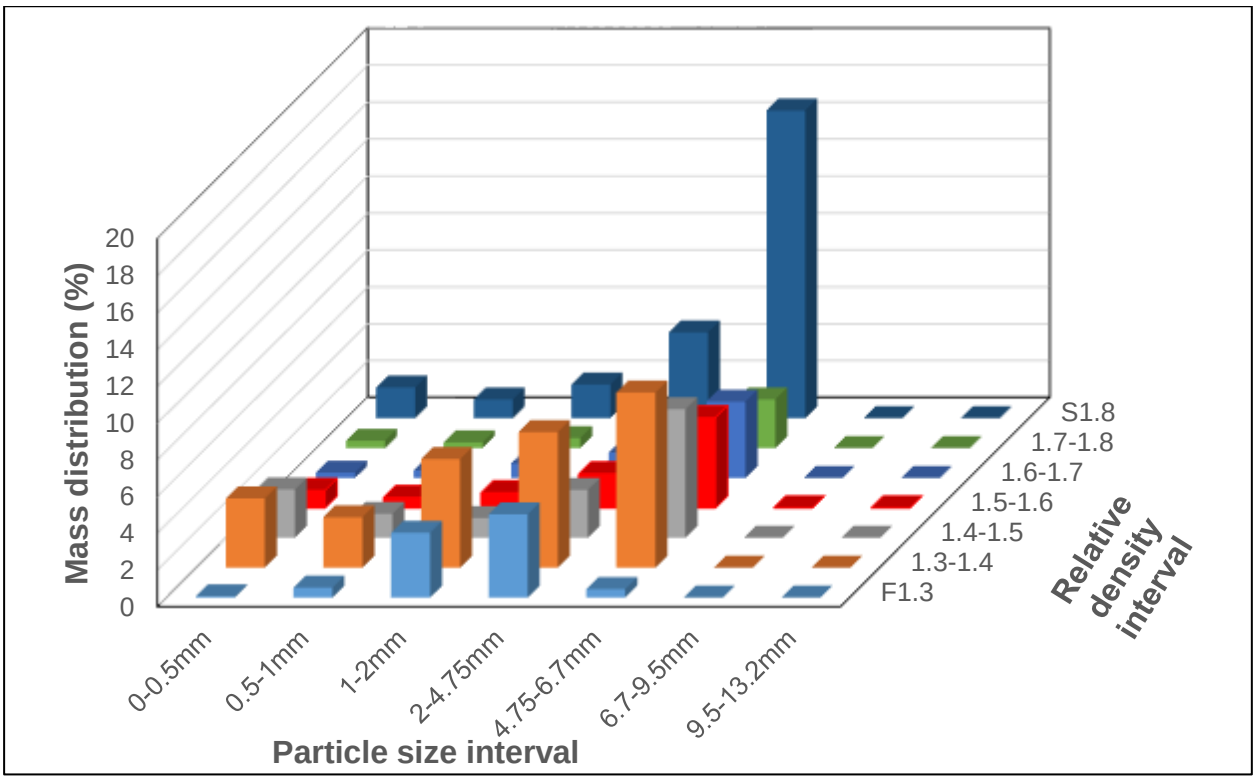

Figure C. 24: Size by washability graph for impact breakage to a top size of 6.7 mm with no attritioning (Run 8).

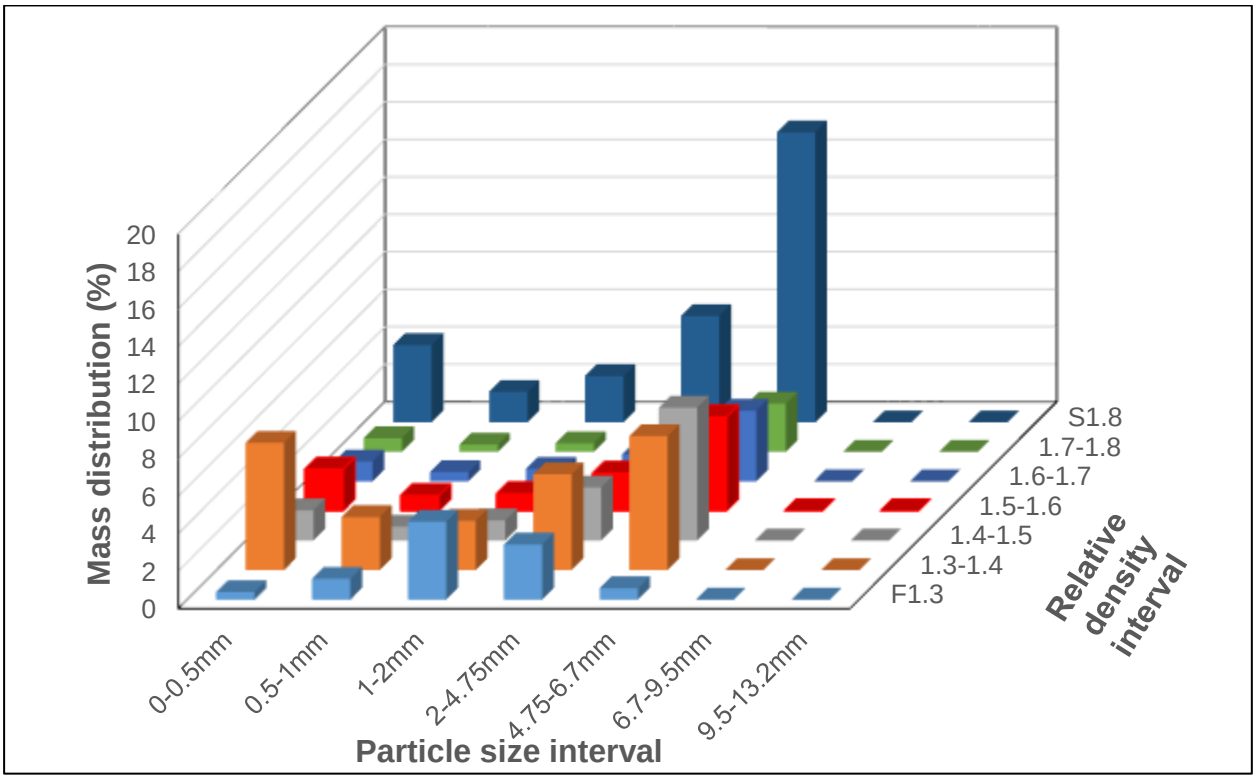

Figure C. 25: Size by washability graph for impact breakage to a top size of 6.7 mm with no attritioning (Run 9).

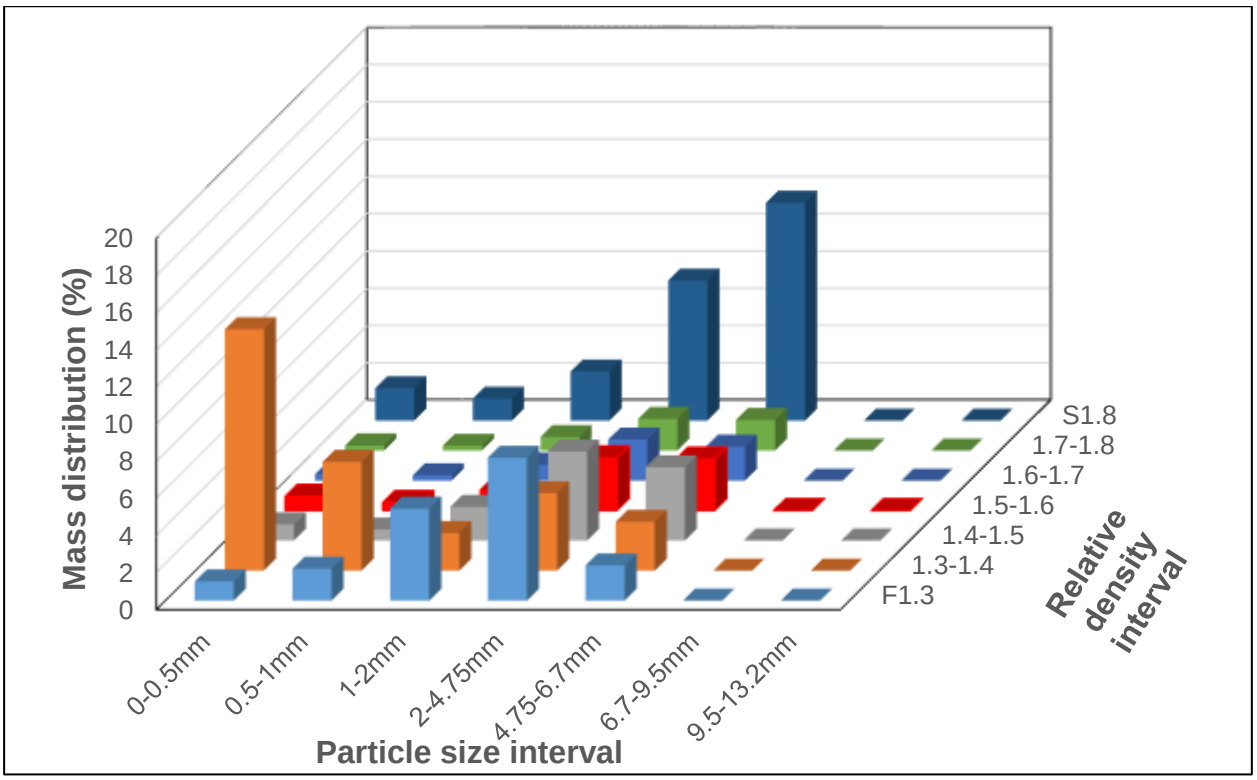

Figure C. 26: Size by washability graph for impact breakage to a top size of 6.7 mm with 1 minute attritioning (Run 10).

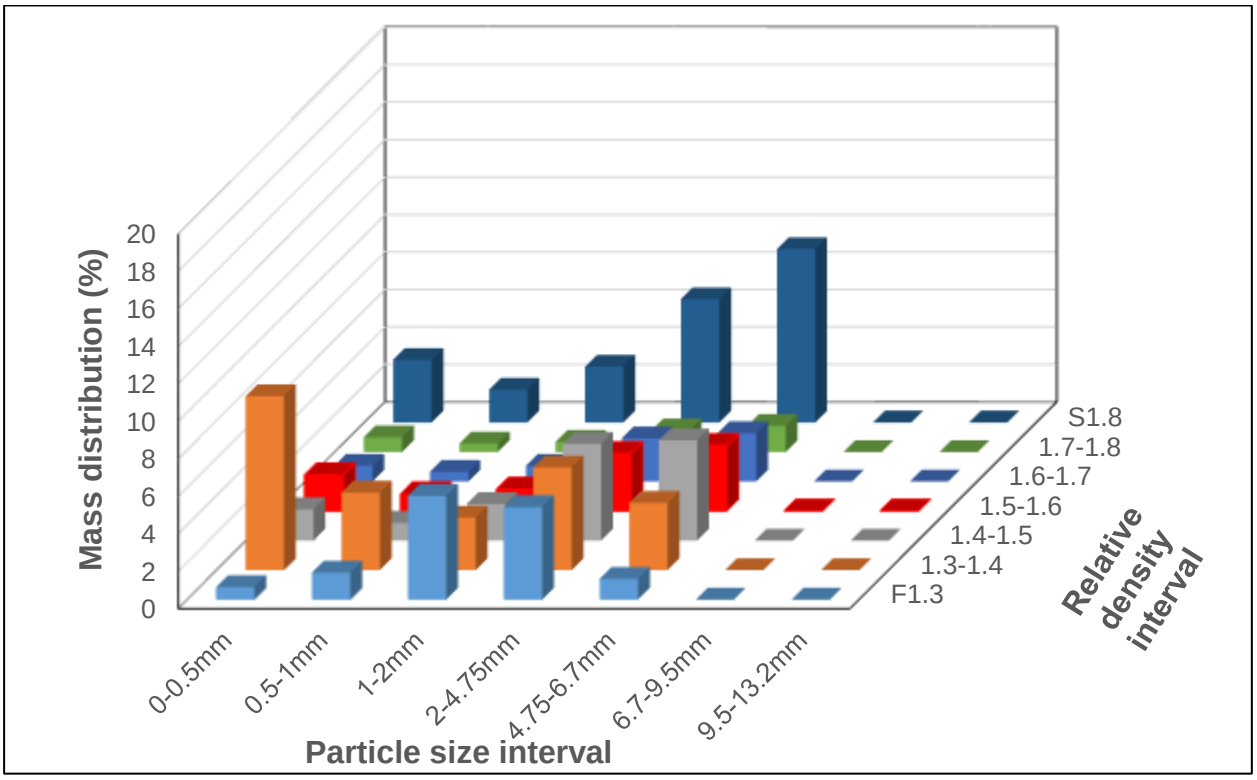

Figure C. 27: Size by washability graph for impact breakage to a top size of 6.7 mm with 2 minutes attritioning (Run 11).

Note that the size by washability graph for impact breakage to a top size of 6.7 mm with 5 minutes attritioning is presented as Figure 4.10.

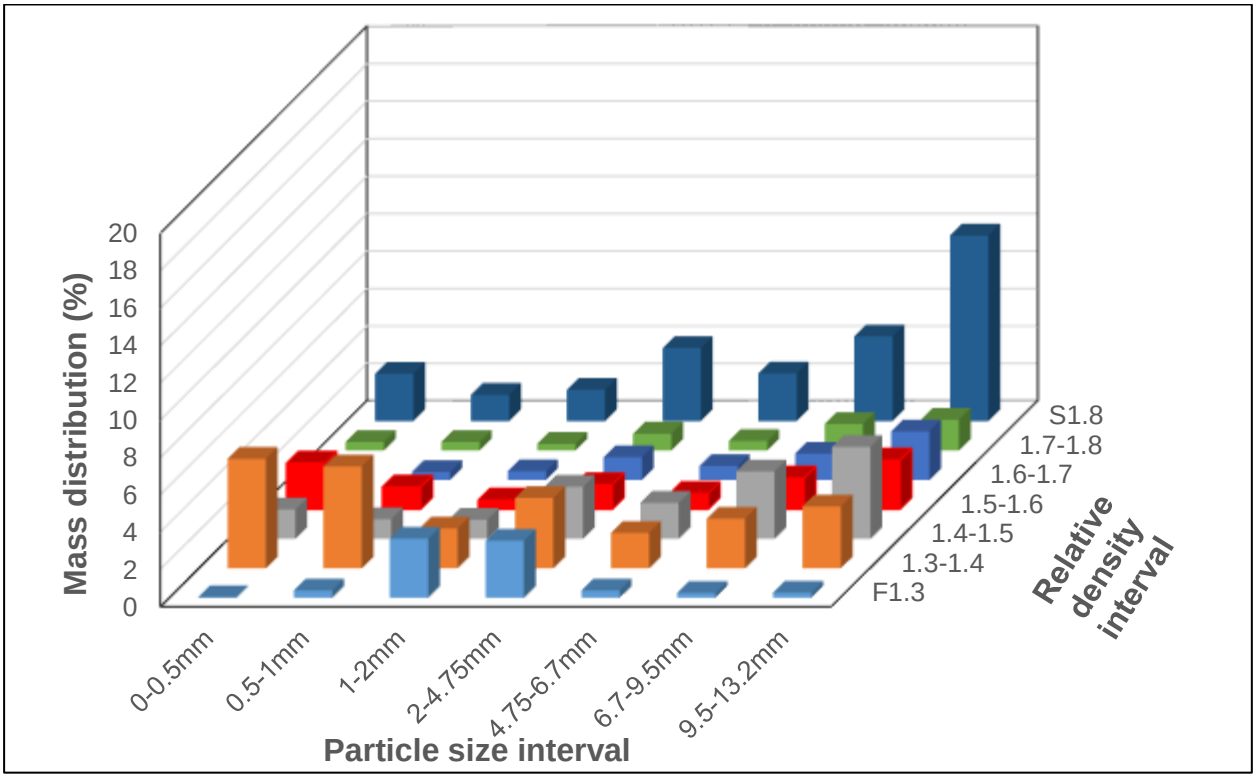

Figure C. 28: Size by washability graph for compressive breakage to a top size of 13.2 mm with no attritioning (Run 13).

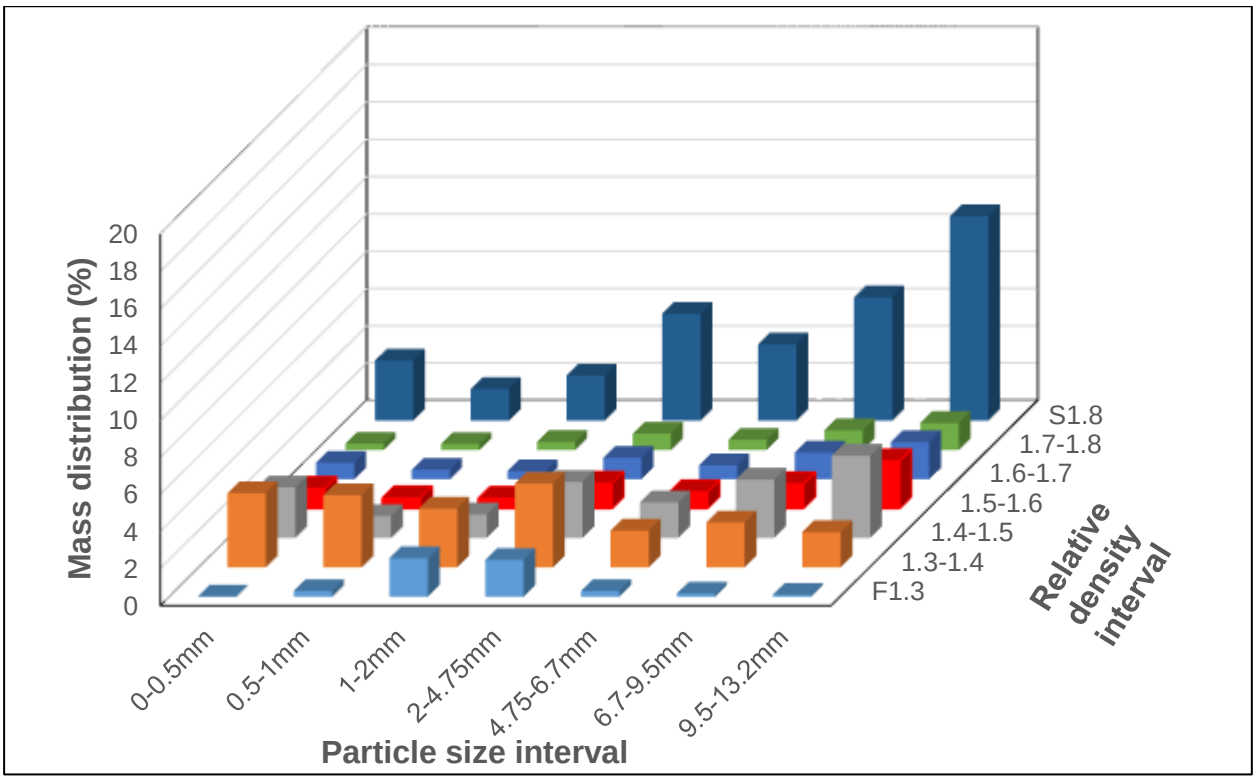

Figure C. 29: Size by washability graph for compressive breakage to a top size of 13.2 mm with no attritioning (Run 14).

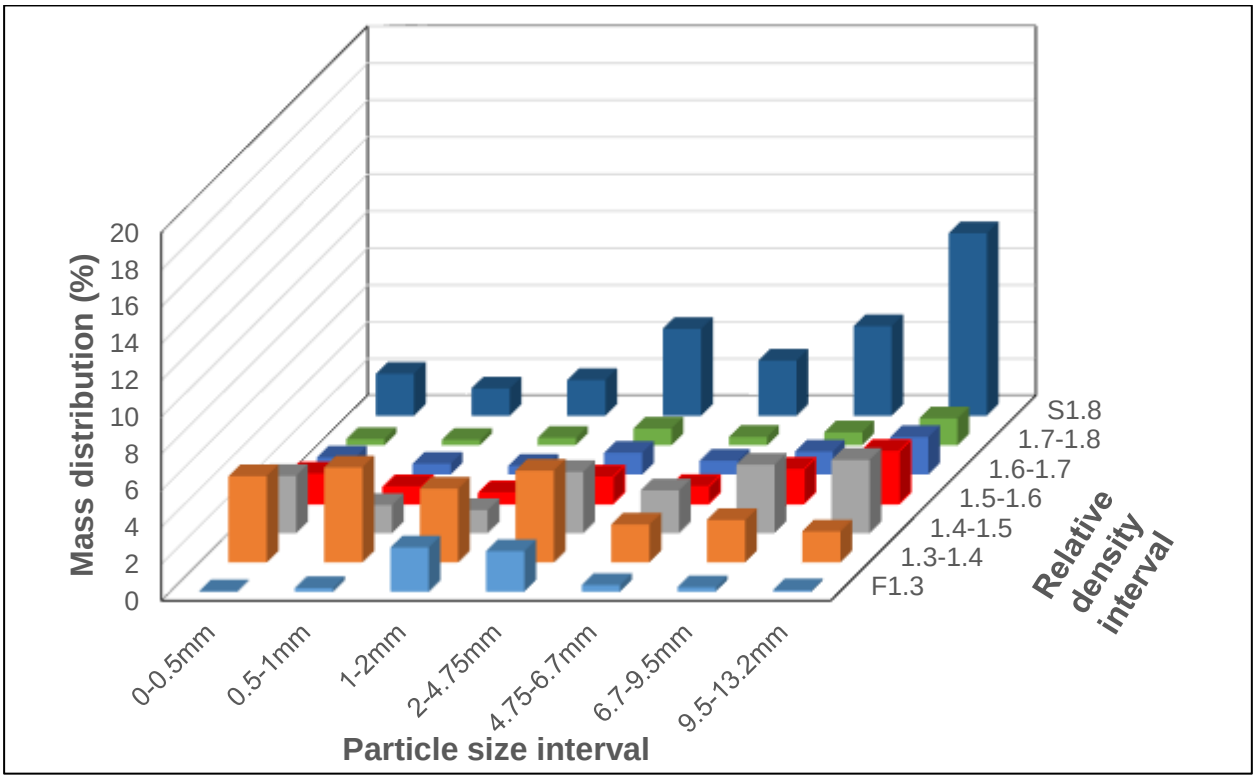

Figure C. 30: Size by washability graph for compressive breakage to a top size of 13.2 mm with no attritioning (Run 15).

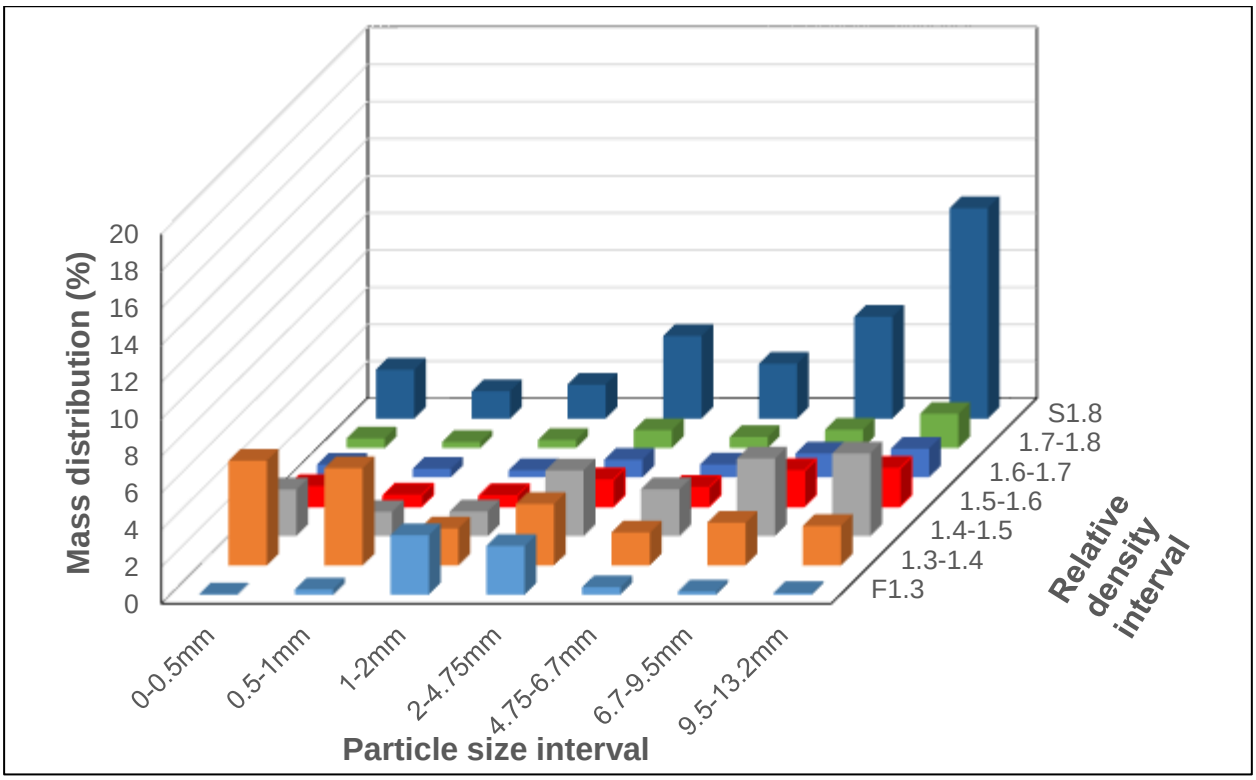

Figure C. 31: Size by washability graph for compressive breakage to a top size of 13.2 mm with 1 minute attritioning (Run 16).

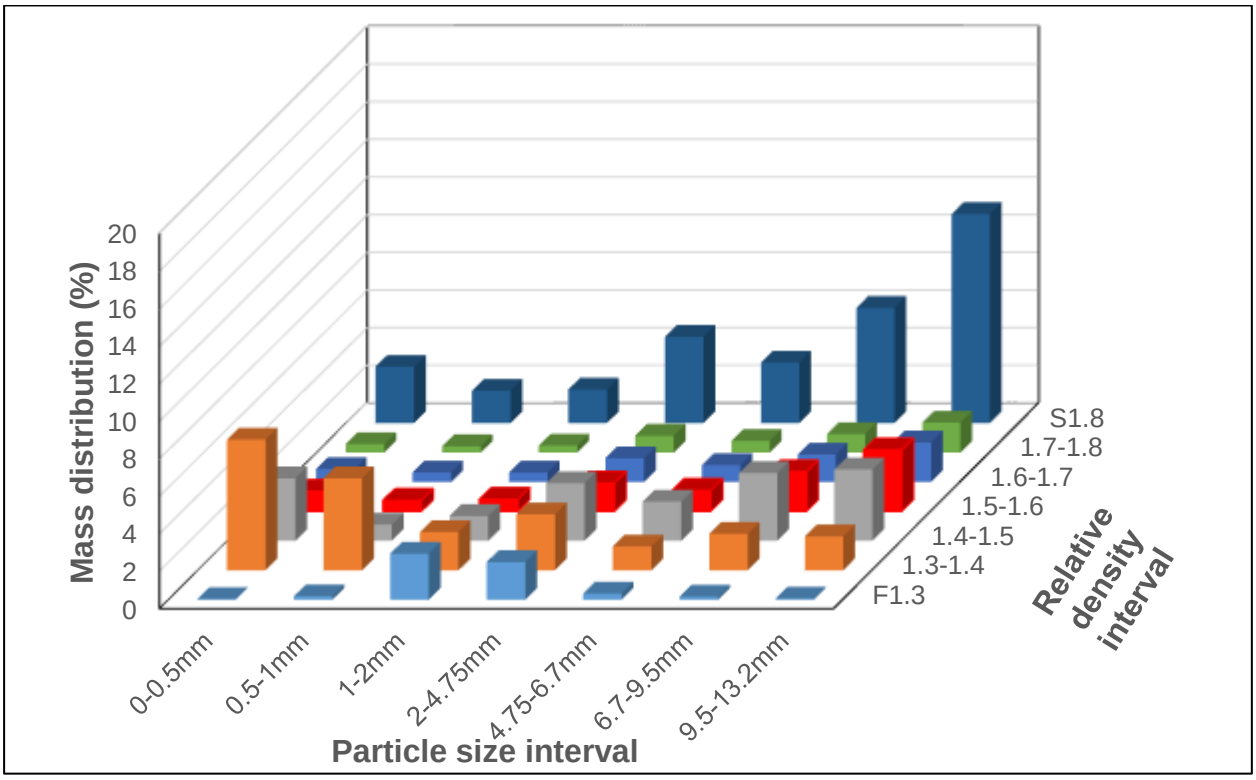

Figure C. 32: Size by washability graph for compressive breakage to a top size of 13.2 mm with 2 minutes attritioning (Run 17).

Note that the size by washability graph for compressive breakage to a top size of 13.2 mm with 5 minutes attritioning is presented as Figure 4.13.

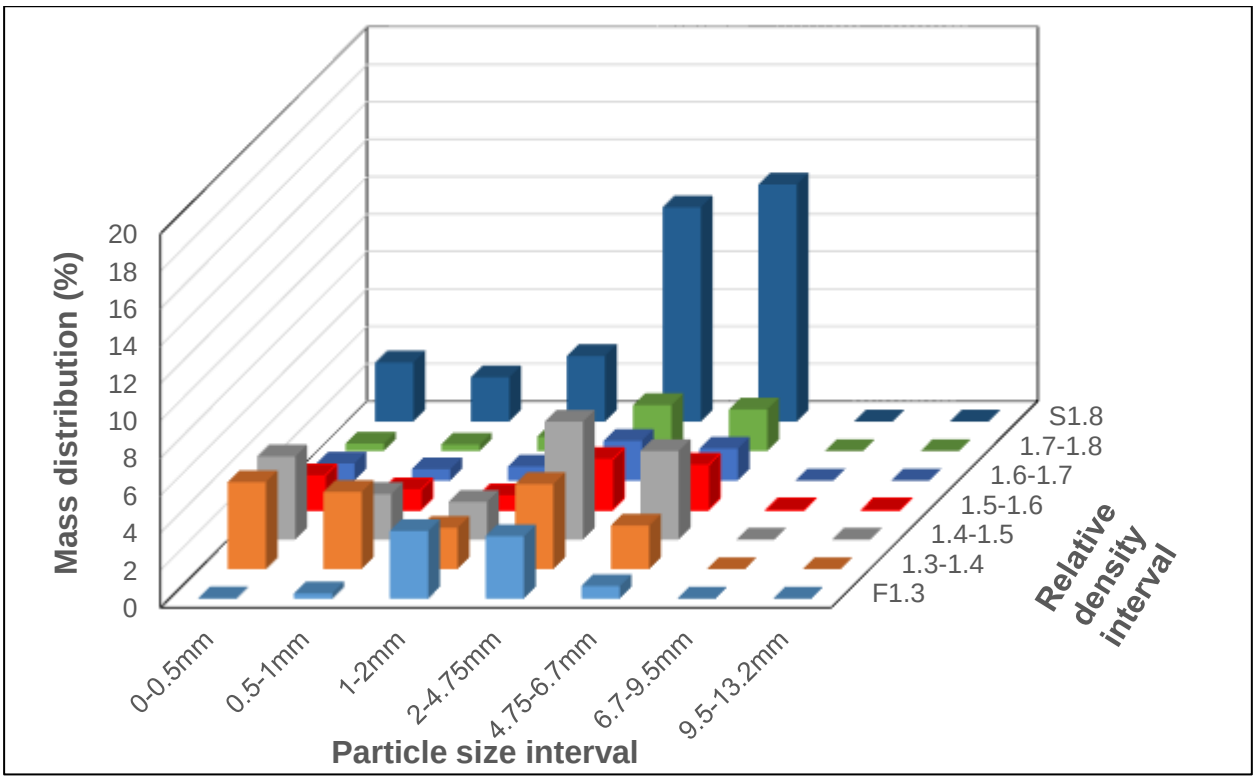

Figure C. 33: Size by washability graph for compressive breakage to a top size of 6.7 mm with no attritioning (Run 19).

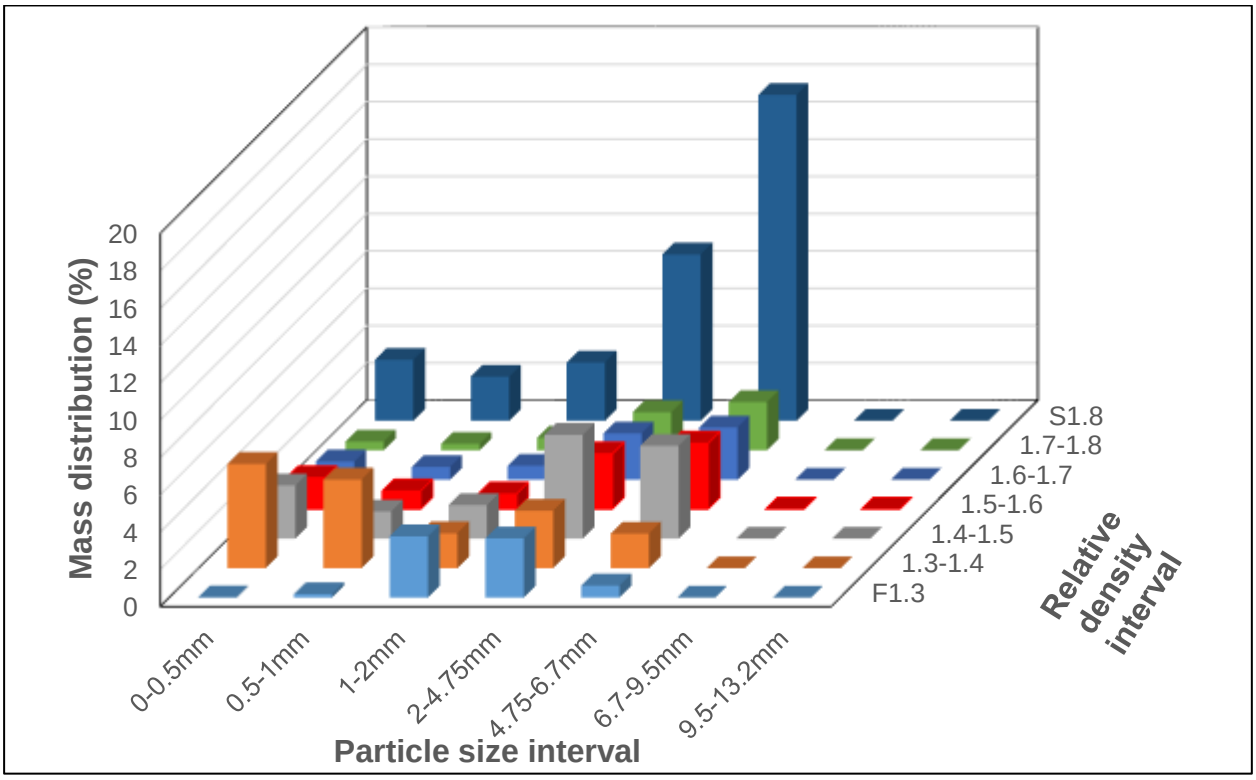

Figure C. 34: Size by washability graph for compressive breakage to a top size of 6.7 mm with no attritioning (Run 20).

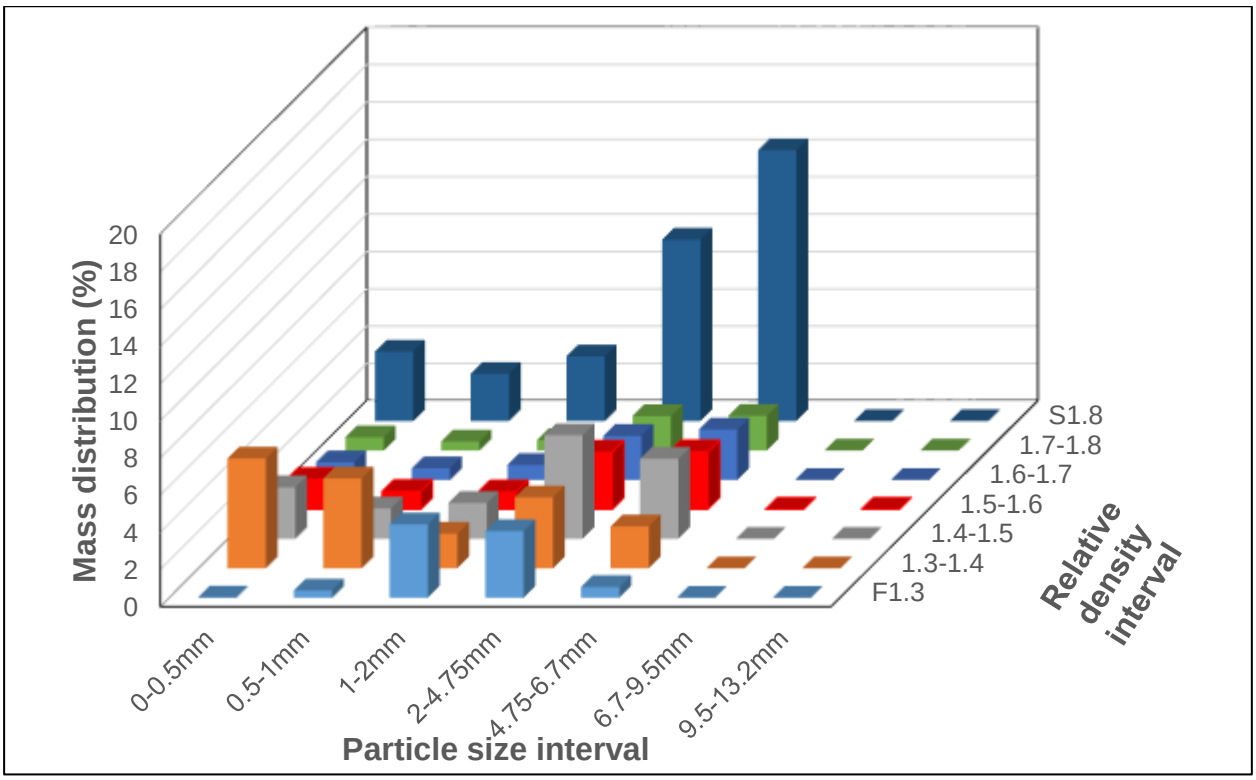

Figure C. 35: Size by washability graph for compressive breakage to a top size of 6.7 mm with no attritioning (Run 21).

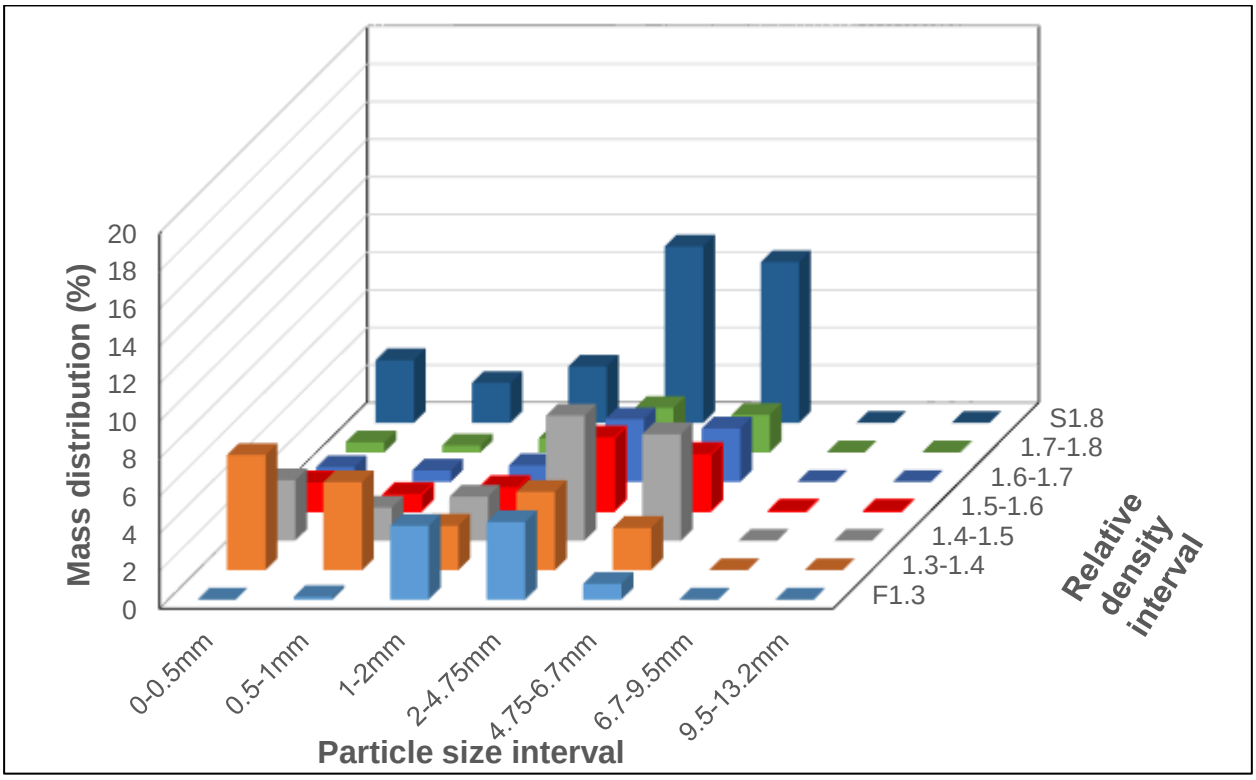

Figure C. 36: Size by washability graph for compressive breakage to a top size of 6.7 mm with 1 minute attritioning (Run 22).

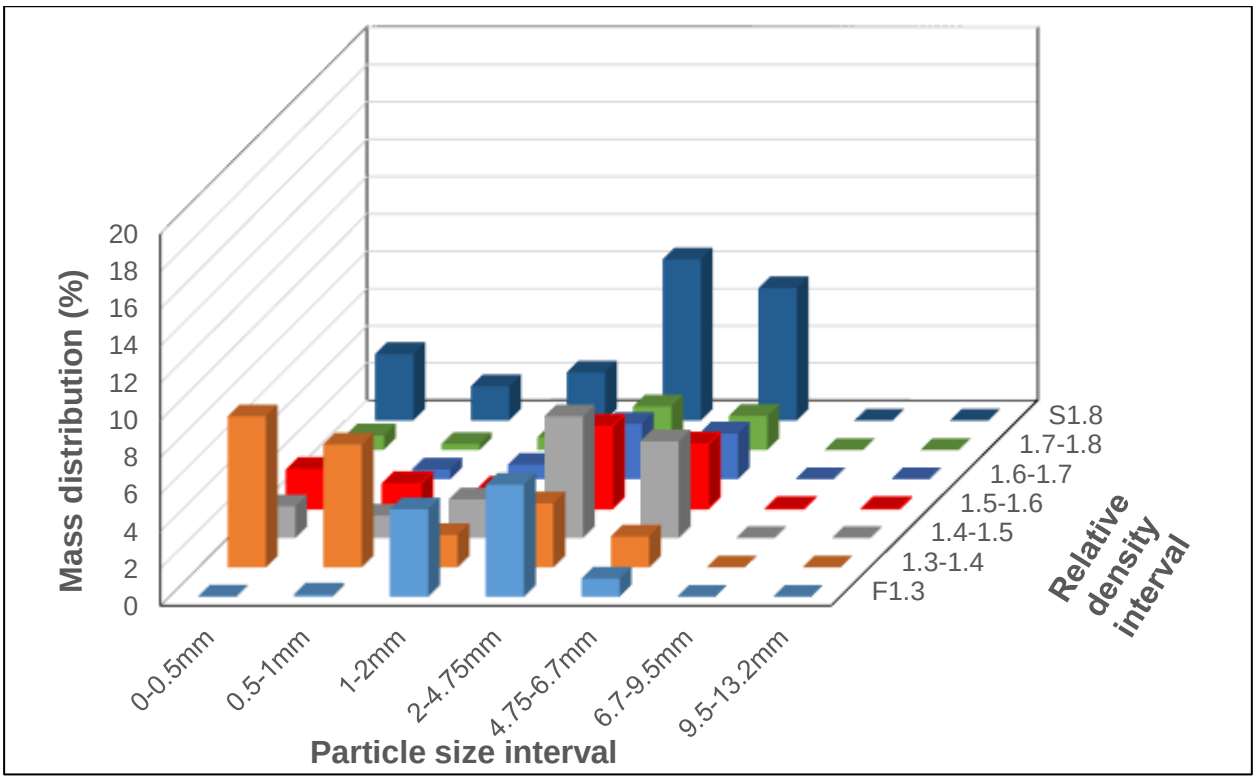

Figure C. 37: Size by washability graph for compressive breakage to a top size of 6.7 mm with 2 minutes attritioning (Run 23).

Note that the size by washability graph for compressive breakage to a top size of 6.7 mm with 5 minutes attritioning is presented as Figure 4.14.

Particle size per density:

The *particle size per density* was calculated for each relative density (RD) interval by cumulatively adding the mass percentage at each particle size interval for a specific RD interval, as a fraction of the total mass at that specific RD interval. Thus the total mass fraction at that specific RD interval added up to 1.

Table C. 60: Particle size per density for raw ROM coal.

	Float yield	Density interval						
		F1.3	1.3-1.4	1.4-1.5	1.5-1.6	1.6-1.7	1.7-1.8	S1.8
Particle size (mm)	0	0.00	0.00	0.00	0.00	0.00	0.00	0.00
	0.5	0.00	0.20	0.05	0.14	0.02	0.02	0.05
	1	0.03	0.39	0.07	0.20	0.04	0.04	0.08
	2	0.39	0.48	0.11	0.23	0.06	0.05	0.12
	4.75	0.70	0.59	0.21	0.29	0.11	0.10	0.20
	6.7	0.96	0.63	0.28	0.34	0.14	0.12	0.25
	9.5	0.99	0.69	0.38	0.41	0.20	0.17	0.32
	13.2	1.00	0.73	0.47	0.47	0.28	0.20	0.41
	19	1.00	0.79	0.64	0.58	0.36	0.30	0.58
	26.5	1.00	0.84	0.75	0.73	0.44	0.47	0.72
	37.5	1.00	0.84	0.80	0.87	0.68	0.57	0.84
	53	1.00	1.00	1.00	1.00	0.68	0.57	1.00
	75	1.00	1.00	1.00	1.00	1.00	1.00	1.00

Table C. 61: Particle size per density for impact breakage to a top size of 13.2 mm with no attritioning (Run 1-3 average).

	Float yield	Density interval						
		F1.3	1.3-1.4	1.4-1.5	1.5-1.6	1.6-1.7	1.7-1.8	S1.8
Particle size (mm)	0	0.00	0.00	0.00	0.00	0.00	0.00	0.00
	0.5	0.04	0.22	0.09	0.08	0.08	0.05	0.06
	1	0.21	0.43	0.15	0.15	0.13	0.11	0.10
	2	0.59	0.52	0.25	0.21	0.19	0.19	0.16
	4.75	0.90	0.68	0.42	0.38	0.33	0.37	0.29
	6.7	0.95	0.76	0.52	0.48	0.43	0.47	0.38
	9.5	0.98	0.86	0.67	0.64	0.57	0.63	0.50
	13.2	1.00	1.00	1.00	1.00	1.00	1.00	1.00

Table C. 62: Particle size per density for impact breakage to a top size of 13.2 mm with 1 minute attritioning (Run 4).

		Density interval						
	Float yield	F1.3	1.3-1.4	1.4-1.5	1.5-1.6	1.6-1.7	1.7-1.8	S1.8
Particle size (mm)	0	0.00	0.00	0.00	0.00	0.00	0.00	0.00
	0.5	0.05	0.23	0.11	0.06	0.10	0.04	0.07
	1	0.19	0.38	0.16	0.10	0.15	0.07	0.11
	2	0.62	0.53	0.23	0.18	0.23	0.15	0.17
	4.75	0.91	0.74	0.42	0.35	0.41	0.35	0.34
	6.7	0.96	0.82	0.55	0.49	0.54	0.49	0.46
	9.5	0.98	0.92	0.76	0.71	0.73	0.69	0.68
	13.2	1.00	1.00	1.00	1.00	1.00	1.00	1.00

Table C. 63: Particle size per density for impact breakage to a top size of 13.2 mm with 2 minutes attritioning (Run 5).

		Density interval						
	Float yield	F1.3	1.3-1.4	1.4-1.5	1.5-1.6	1.6-1.7	1.7-1.8	S1.8
Particle size (mm)	0	0.00	0.00	0.00	0.00	0.00	0.00	0.00
	0.5	0.01	0.20	0.11	0.06	0.09	0.04	0.08
	1	0.12	0.34	0.16	0.10	0.14	0.08	0.12
	2	0.55	0.48	0.23	0.17	0.21	0.16	0.18
	4.75	0.93	0.65	0.40	0.33	0.37	0.31	0.32
	6.7	0.97	0.74	0.51	0.45	0.48	0.41	0.43
	9.5	0.99	0.87	0.69	0.62	0.65	0.57	0.58
	13.2	1.00	1.00	1.00	1.00	1.00	1.00	1.00

Table C. 64: Particle size per density for impact breakage to a top size of 13.2 mm with 5 minutes attritioning (Run 6).

		Density interval						
	Float yield	F1.3	1.3-1.4	1.4-1.5	1.5-1.6	1.6-1.7	1.7-1.8	S1.8
Particle size (mm)	0	0.00	0.00	0.00	0.00	0.00	0.00	0.00
	0.5	0.03	0.20	0.10	0.06	0.13	0.05	0.08
	1	0.16	0.33	0.16	0.10	0.19	0.10	0.13
	2	0.60	0.51	0.23	0.19	0.27	0.20	0.21
	4.75	0.93	0.71	0.41	0.39	0.44	0.36	0.38
	6.7	0.97	0.79	0.54	0.52	0.55	0.47	0.49
	9.5	0.99	0.90	0.73	0.70	0.74	0.63	0.64
	13.2	1.00	1.00	1.00	1.00	1.00	1.00	1.00

Table C. 65: Particle size per density for impact breakage to a top size of 6.7 mm with no attritioning (Run 7-9 average).

		Density interval						
	Float yield	F1.3	1.3-1.4	1.4-1.5	1.5-1.6	1.6-1.7	1.7-1.8	S1.8
Particle size (mm)	0	0.00	0.00	0.00	0.00	0.00	0.00	0.00
	0.5	0.03	0.20	0.12	0.13	0.09	0.09	0.09
	1	0.12	0.32	0.18	0.20	0.15	0.16	0.14
	2	0.56	0.49	0.28	0.29	0.25	0.26	0.23
	4.75	0.94	0.71	0.49	0.49	0.46	0.46	0.42
	6.7	1.00	1.00	1.00	1.00	1.00	1.00	1.00

Table C. 66: Particle size per density for impact breakage to a top size of 6.7 mm with 1 minute attritioning (Run 10).

		Density interval						
	Float yield	F1.3	1.3-1.4	1.4-1.5	1.5-1.6	1.6-1.7	1.7-1.8	S1.8
Particle size (mm)	0	0.00	0.00	0.00	0.00	0.00	0.00	0.00
	0.5	0.06	0.47	0.07	0.10	0.06	0.06	0.07
	1	0.16	0.68	0.12	0.15	0.12	0.12	0.12
	2	0.45	0.75	0.27	0.29	0.27	0.27	0.22
	4.75	0.89	0.91	0.67	0.65	0.67	0.64	0.53
	6.7	1.00	1.00	1.00	1.00	1.00	1.00	1.00

Table C. 67: Particle size per density for impact breakage to a top size of 6.7 mm with 2 minutes attritioning (Run 11).

		Density interval						
	Float yield	F1.3	1.3-1.4	1.4-1.5	1.5-1.6	1.6-1.7	1.7-1.8	S1.8
Particle size (mm)	0	0.00	0.00	0.00	0.00	0.00	0.00	0.00
	0.5	0.05	0.37	0.11	0.18	0.12	0.18	0.14
	1	0.15	0.53	0.17	0.27	0.19	0.28	0.21
	2	0.56	0.64	0.30	0.38	0.31	0.41	0.34
	4.75	0.92	0.86	0.65	0.67	0.64	0.68	0.61
	6.7	1.00	1.00	1.00	1.00	1.00	1.00	1.00

Table C. 68: Particle size per density for impact breakage to a top size of 6.7 mm with 5 minutes attritioning (Run 12).

		Density interval						
	Float yield	F1.3	1.3-1.4	1.4-1.5	1.5-1.6	1.6-1.7	1.7-1.8	S1.8
Particle size (mm)	0	0.00	0.00	0.00	0.00	0.00	0.00	0.00
	0.5	0.09	0.46	0.06	0.10	0.05	0.05	0.09
	1	0.22	0.67	0.10	0.15	0.10	0.10	0.15
	2	0.56	0.76	0.24	0.28	0.21	0.23	0.26
	4.75	0.93	0.91	0.61	0.63	0.56	0.56	0.54
	6.7	1.00	1.00	1.00	1.00	1.00	1.00	1.00

Table C. 69: Particle size per density for compressive breakage to a top size of 13.2 mm with no attritioning (Run 13).

		Density interval						
	Float yield	F1.3	1.3-1.4	1.4-1.5	1.5-1.6	1.6-1.7	1.7-1.8	S1.8
Particle size (mm)	0	0.00	0.00	0.00	0.00	0.00	0.00	0.00
	0.5	0.00	0.23	0.09	0.23	0.08	0.08	0.10
	1	0.05	0.45	0.16	0.34	0.13	0.16	0.15
	2	0.48	0.54	0.22	0.39	0.20	0.22	0.21
	4.75	0.88	0.69	0.38	0.52	0.36	0.38	0.36
	6.7	0.93	0.76	0.49	0.60	0.46	0.47	0.46
	9.5	0.97	0.87	0.71	0.75	0.65	0.71	0.63
	13.2	1.00	1.00	1.00	1.00	1.00	1.00	1.00

Table C. 70: Particle size per density for compressive breakage to a top size of 13.2 mm with no attritioning (Run 14).

		Density interval						
	Float yield	F1.3	1.3-1.4	1.4-1.5	1.5-1.6	1.6-1.7	1.7-1.8	S1.8
Particle size (mm)	0	0.00	0.00	0.00	0.00	0.00	0.00	0.00
	0.5	0.00	0.18	0.15	0.13	0.12	0.07	0.09
	1	0.06	0.36	0.22	0.20	0.19	0.13	0.14
	2	0.48	0.51	0.29	0.26	0.25	0.22	0.21
	4.75	0.89	0.71	0.46	0.43	0.42	0.39	0.38
	6.7	0.95	0.80	0.57	0.53	0.52	0.50	0.49
	9.5	0.98	0.91	0.75	0.69	0.72	0.71	0.68
	13.2	1.00	1.00	1.00	1.00	1.00	1.00	1.00

Table C. 71: Particle size per density for compressive breakage to a top size of 13.2 mm with no attritioning (Run 15).

		Density interval						
	Float yield	F1.3	1.3-1.4	1.4-1.5	1.5-1.6	1.6-1.7	1.7-1.8	S1.8
Particle size (mm)	0	0.00	0.00	0.00	0.00	0.00	0.00	0.00
	0.5	0.01	0.19	0.16	0.16	0.13	0.07	0.08
	1	0.04	0.40	0.24	0.25	0.21	0.14	0.13
	2	0.48	0.56	0.31	0.31	0.28	0.23	0.20
	4.75	0.88	0.76	0.48	0.45	0.44	0.43	0.37
	6.7	0.94	0.84	0.60	0.54	0.54	0.53	0.48
	9.5	0.99	0.93	0.79	0.72	0.72	0.68	0.65
	13.2	1.00	1.00	1.00	1.00	1.00	1.00	1.00

Table C. 72: Particle size per density for compressive breakage to a top size of 13.2 mm with no attritioning (Run 13-15 average).

		Density interval						
	Float yield	F1.3	1.3-1.4	1.4-1.5	1.5-1.6	1.6-1.7	1.7-1.8	S1.8
Particle size (mm)	0	0.00	0.00	0.00	0.00	0.00	0.00	0.00
	0.5	0.00	0.20	0.14	0.17	0.11	0.07	0.09
	1	0.05	0.40	0.21	0.26	0.18	0.14	0.14
	2	0.48	0.53	0.28	0.32	0.25	0.22	0.21
	4.75	0.88	0.72	0.45	0.46	0.41	0.40	0.37
	6.7	0.94	0.80	0.56	0.55	0.51	0.50	0.48
	9.5	0.98	0.91	0.76	0.72	0.70	0.70	0.66
	13.2	1.00	1.00	1.00	1.00	1.00	1.00	1.00

Table C. 73 Particle size per density for compressive breakage to a top size of 13.2 mm with 1 minute attritioning (Run 16).

		Density interval						
	Float yield	F1.3	1.3-1.4	1.4-1.5	1.5-1.6	1.6-1.7	1.7-1.8	S1.8
Particle size (mm)	0	0.00	0.00	0.00	0.00	0.00	0.00	0.00
	0.5	0.00	0.25	0.13	0.12	0.11	0.09	0.09
	1	0.04	0.49	0.19	0.19	0.19	0.15	0.14
	2	0.52	0.57	0.26	0.26	0.25	0.22	0.20
	4.75	0.90	0.72	0.44	0.42	0.41	0.39	0.34
	6.7	0.96	0.80	0.56	0.54	0.53	0.50	0.44
	9.5	0.99	0.90	0.78	0.76	0.74	0.67	0.63
	13.2	1.00	1.00	1.00	1.00	1.00	1.00	1.00

Table C. 74: Particle size per density for compressive breakage to a top size of 13.2 mm with 2 minutes attritioning (Run 17).

		Density interval						
	Float yield	F1.3	1.3-1.4	1.4-1.5	1.5-1.6	1.6-1.7	1.7-1.8	S1.8
Particle size (mm)	0	0.00	0.00	0.00	0.00	0.00	0.00	0.00
	0.5	0.01	0.32	0.18	0.10	0.09	0.09	0.10
	1	0.04	0.54	0.23	0.16	0.16	0.15	0.15
	2	0.51	0.63	0.31	0.22	0.23	0.22	0.21
	4.75	0.89	0.77	0.48	0.37	0.40	0.39	0.35
	6.7	0.96	0.83	0.59	0.48	0.52	0.51	0.45
	9.5	0.99	0.92	0.79	0.68	0.72	0.70	0.65
	13.2	1.00	1.00	1.00	1.00	1.00	1.00	1.00

Table C. 75: Particle size per density for compressive breakage to a top size of 13.2 mm with 5 minutes attritioning (Run 18).

		Density interval						
	Float yield	F1.3	1.3-1.4	1.4-1.5	1.5-1.6	1.6-1.7	1.7-1.8	S1.8
Particle size (mm)	0	0.00	0.00	0.00	0.00	0.00	0.00	0.00
	0.5	0.00	0.25	0.15	0.12	0.08	0.09	0.08
	1	0.06	0.47	0.22	0.19	0.13	0.15	0.13
	2	0.48	0.62	0.30	0.26	0.19	0.24	0.20
	4.75	0.88	0.78	0.47	0.43	0.34	0.44	0.36
	6.7	0.95	0.85	0.59	0.55	0.46	0.56	0.47
	9.5	0.98	0.92	0.79	0.72	0.69	0.76	0.66
	13.2	1.00	1.00	1.00	1.00	1.00	1.00	1.00

Table C. 76: Particle size per density for compressive breakage to a top size of 6.7 mm with no attritioning (Run 19).

		Density interval						
	Float yield	F1.3	1.3-1.4	1.4-1.5	1.5-1.6	1.6-1.7	1.7-1.8	S1.8
Particle size (mm)	0	0.00	0.00	0.00	0.00	0.00	0.00	0.00
	0.5	0.00	0.26	0.22	0.21	0.15	0.06	0.10
	1	0.04	0.49	0.35	0.33	0.25	0.12	0.17
	2	0.49	0.61	0.45	0.42	0.37	0.24	0.27
	4.75	0.92	0.87	0.76	0.73	0.72	0.64	0.62
	6.7	1.00	1.00	1.00	1.00	1.00	1.00	1.00

Table C. 77: Particle size per density for compressive breakage to a top size of 6.7 mm with no attritioning (Run 20).

		Density interval						
	Float yield	F1.3	1.3-1.4	1.4-1.5	1.5-1.6	1.6-1.7	1.7-1.8	S1.8
Particle size (mm)	0	0.00	0.00	0.00	0.00	0.00	0.00	0.00
	0.5	0.00	0.33	0.17	0.17	0.13	0.08	0.09
	1	0.03	0.60	0.26	0.27	0.22	0.13	0.16
	2	0.48	0.71	0.37	0.35	0.31	0.24	0.25
	4.75	0.91	0.89	0.70	0.65	0.64	0.58	0.50
	6.7	1.00	1.00	1.00	1.00	1.00	1.00	1.00

Table C. 78: Particle size per density for compressive breakage to a top size of 6.7 mm with no attritioning (Run 21).

		Density interval						
	Float yield	F1.3	1.3-1.4	1.4-1.5	1.5-1.6	1.6-1.7	1.7-1.8	S1.8
Particle size (mm)	0	0.00	0.00	0.00	0.00	0.00	0.00	0.00
	0.5	0.00	0.32	0.17	0.17	0.13	0.13	0.11
	1	0.05	0.58	0.27	0.27	0.21	0.22	0.18
	2	0.51	0.68	0.39	0.36	0.32	0.32	0.29
	4.75	0.93	0.88	0.73	0.68	0.64	0.66	0.57
	6.7	1.00	1.00	1.00	1.00	1.00	1.00	1.00

Table C. 79: Particle size per density for compressive breakage to a top size of 6.7 mm with no attritioning (Run 19-21 average).

		Density interval						
	Float yield	F1.3	1.3-1.4	1.4-1.5	1.5-1.6	1.6-1.7	1.7-1.8	S1.8
Particle size (mm)	0	0.00	0.00	0.00	0.00	0.00	0.00	0.00
	0.5	0.00	0.30	0.19	0.18	0.13	0.09	0.10
	1	0.04	0.56	0.30	0.29	0.22	0.16	0.17
	2	0.49	0.67	0.40	0.37	0.33	0.27	0.27
	4.75	0.92	0.88	0.73	0.68	0.66	0.63	0.56
	6.7	1.00	1.00	1.00	1.00	1.00	1.00	1.00

Table C. 80: Particle size per density for compressive breakage to a top size of 6.7 mm with 1 minute attritioning (Run 22).

		Density interval						
	Float yield	F1.3	1.3-1.4	1.4-1.5	1.5-1.6	1.6-1.7	1.7-1.8	S1.8
Particle size (mm)	0	0.00	0.00	0.00	0.00	0.00	0.00	0.00
	0.5	0.00	0.31	0.16	0.14	0.09	0.09	0.13
	1	0.02	0.55	0.25	0.23	0.16	0.15	0.21
	2	0.45	0.67	0.37	0.34	0.27	0.28	0.32
	4.75	0.91	0.89	0.71	0.71	0.66	0.67	0.68
	6.7	1.00	1.00	1.00	1.00	1.00	1.00	1.00

Table C. 81: Particle size per density for compressive breakage to a top size of 6.7 mm with 2 minutes attritioning (Run 23).

	Float yield	Density interval						
		F1.3	1.3-1.4	1.4-1.5	1.5-1.6	1.6-1.7	1.7-1.8	S1.8
Particle size (mm)	0	0.00	0.00	0.00	0.00	0.00	0.00	0.00
	0.5	0.00	0.38	0.10	0.17	0.10	0.13	0.15
	1	0.01	0.68	0.17	0.28	0.17	0.18	0.23
	2	0.41	0.76	0.30	0.36	0.28	0.30	0.34
	4.75	0.92	0.92	0.69	0.72	0.67	0.69	0.70
	6.7	1.00	1.00	1.00	1.00	1.00	1.00	1.00

Table C. 82: Particle size per density for compressive breakage to a top size of 6.7 mm with 5 minutes attritioning (Run 24).

	Float yield	Density interval						
		F1.3	1.3-1.4	1.4-1.5	1.5-1.6	1.6-1.7	1.7-1.8	S1.8
Particle size (mm)	0	0.00	0.00	0.00	0.00	0.00	0.00	0.00
	0.5	0.00	0.32	0.18	0.14	0.10	0.10	0.13
	1	0.01	0.56	0.27	0.22	0.18	0.16	0.21
	2	0.38	0.67	0.37	0.33	0.28	0.27	0.32
	4.75	0.89	0.89	0.73	0.71	0.68	0.69	0.69
	6.7	1.00	1.00	1.00	1.00	1.00	1.00	1.00

Figure C. 38 to Figure C. 53 presents the particle size per density data in Table C. 60 to Table C. 82, by graphs.

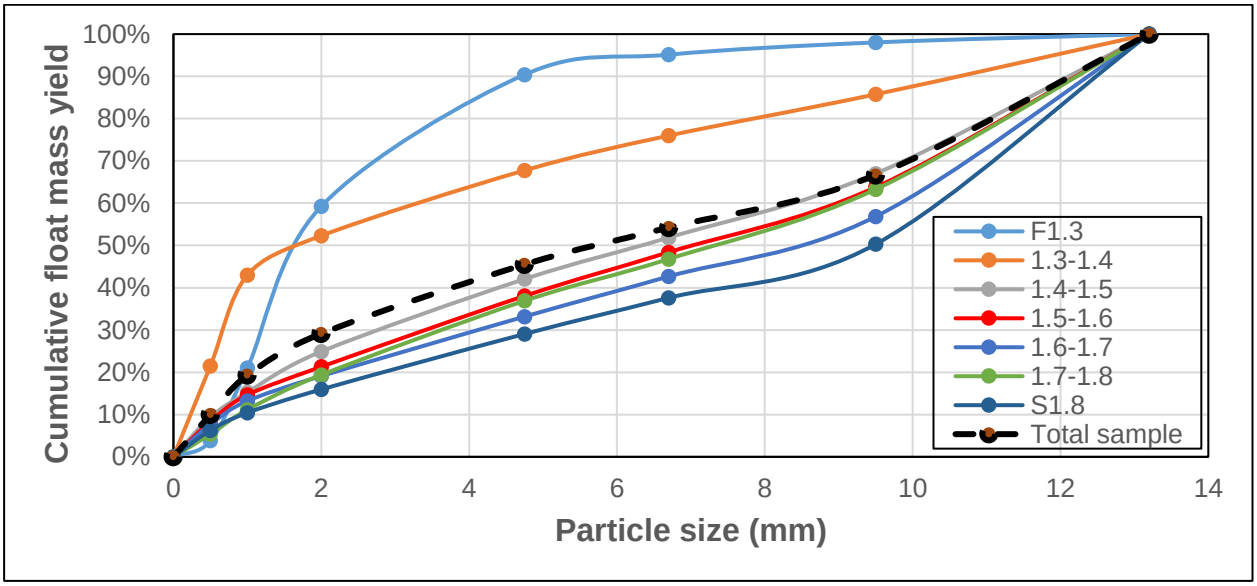

Figure C. 38: Particle size per density graph for impact breakage to a top size of 13.2 mm with no attritioning (Run 1-3 average).

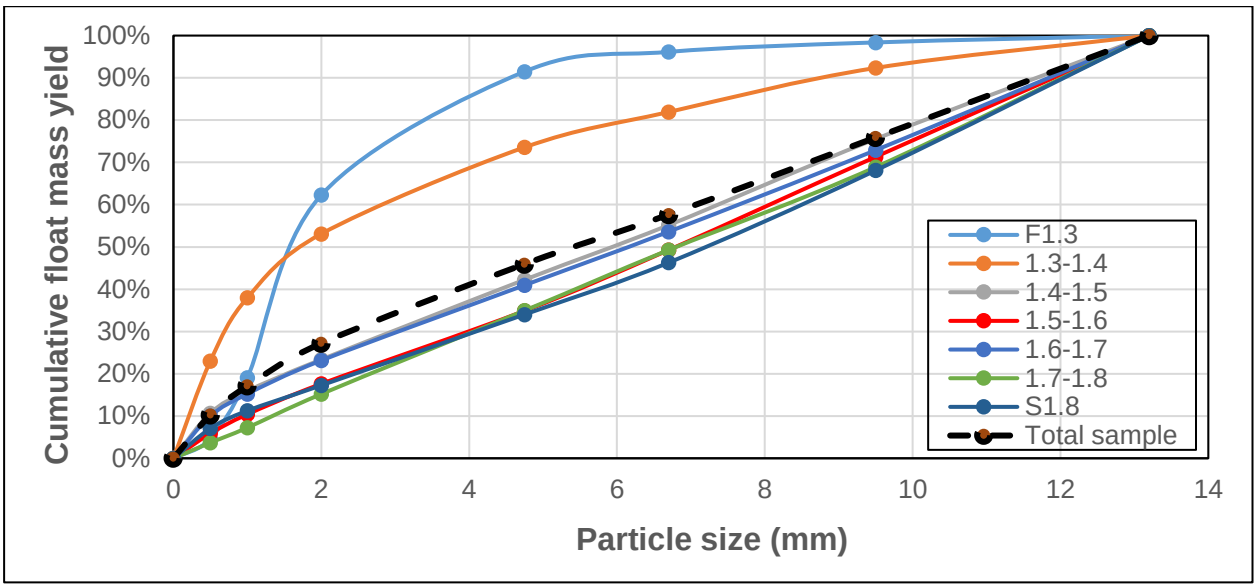

Figure C. 39: Particle size per density graph for impact breakage to a top size of 13.2 mm with 1 minute attritioning (Run 4).

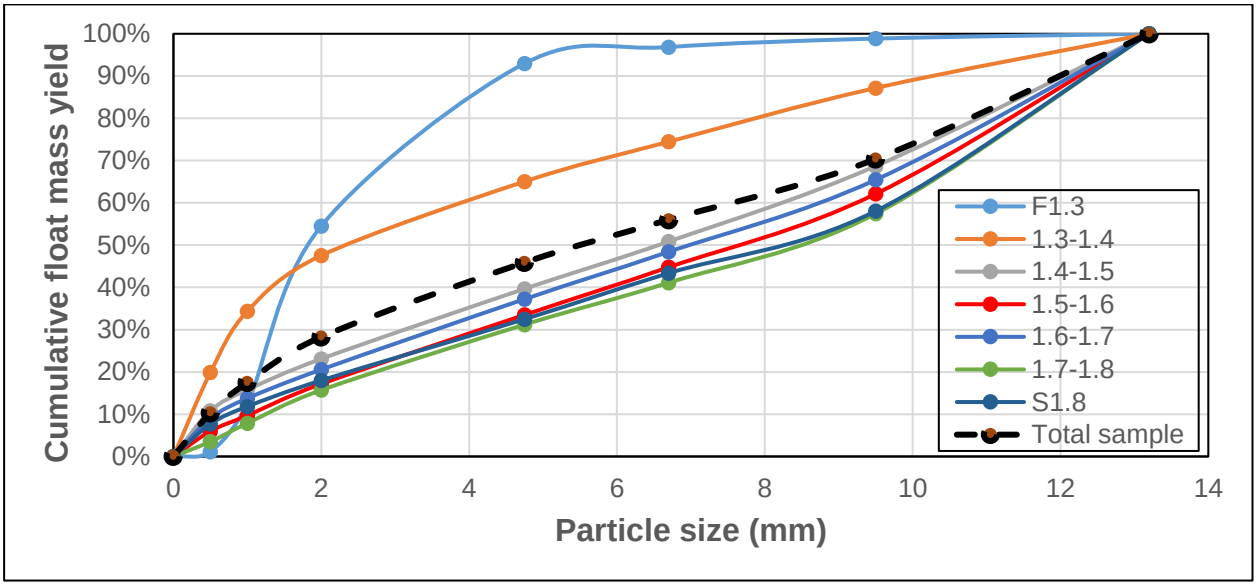

Figure C. 40: Particle size per density graph for impact breakage to a top size of 13.2 mm with 2 minutes attritioning (Run 5).

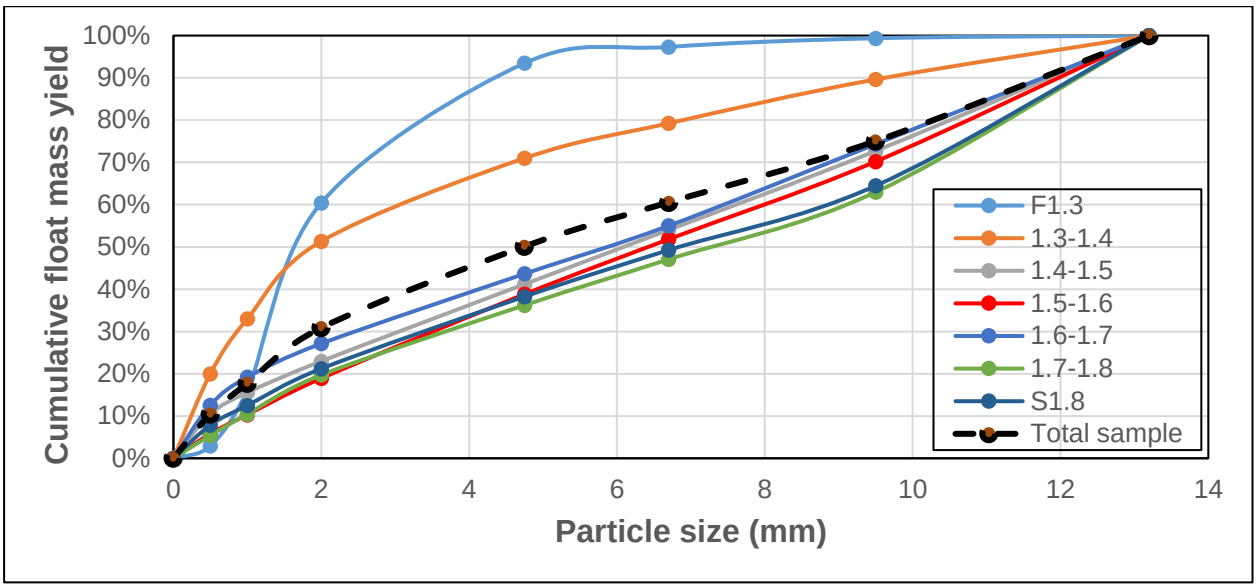

Figure C. 41: Particle size per density graph for impact breakage to a top size of 13.2 mm with 5 minutes attritioning (Run 6).

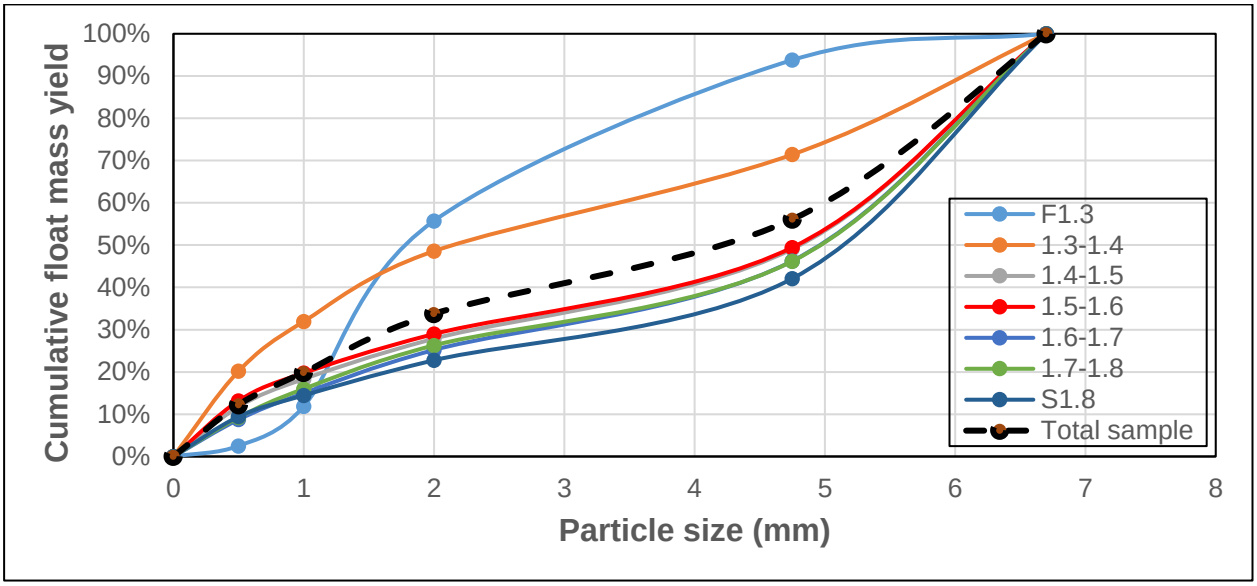

Figure C. 42: Particle size per density graph for impact breakage to a top size of 6.7 mm with no attritioning (Run 7-9).

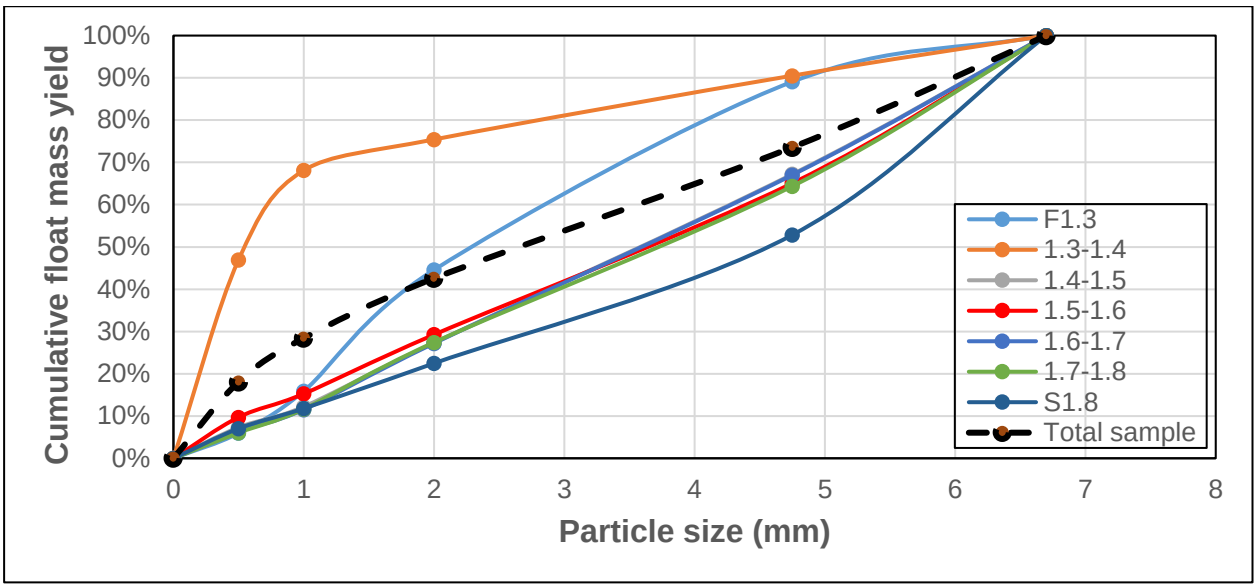

Figure C. 43: Particle size per density graph for impact breakage to a top size of 6.7 mm with 1 minute attritioning (Run 10).

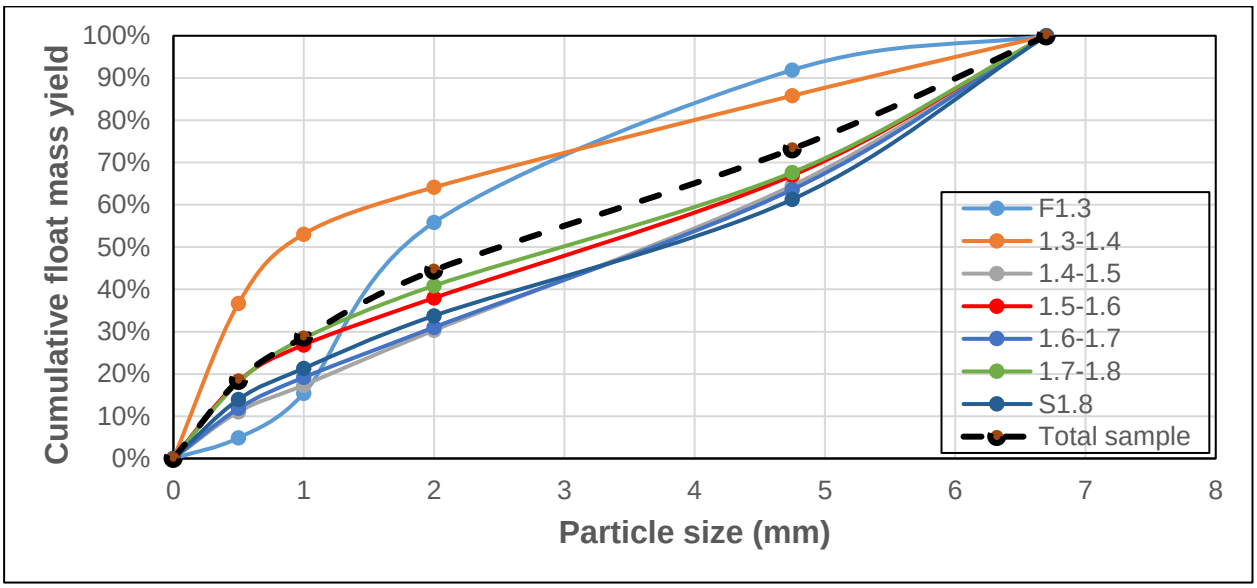

Figure C. 44: Particle size per density graph for impact breakage to a top size of 6.7 mm with 2 minutes attritioning (Run 11).

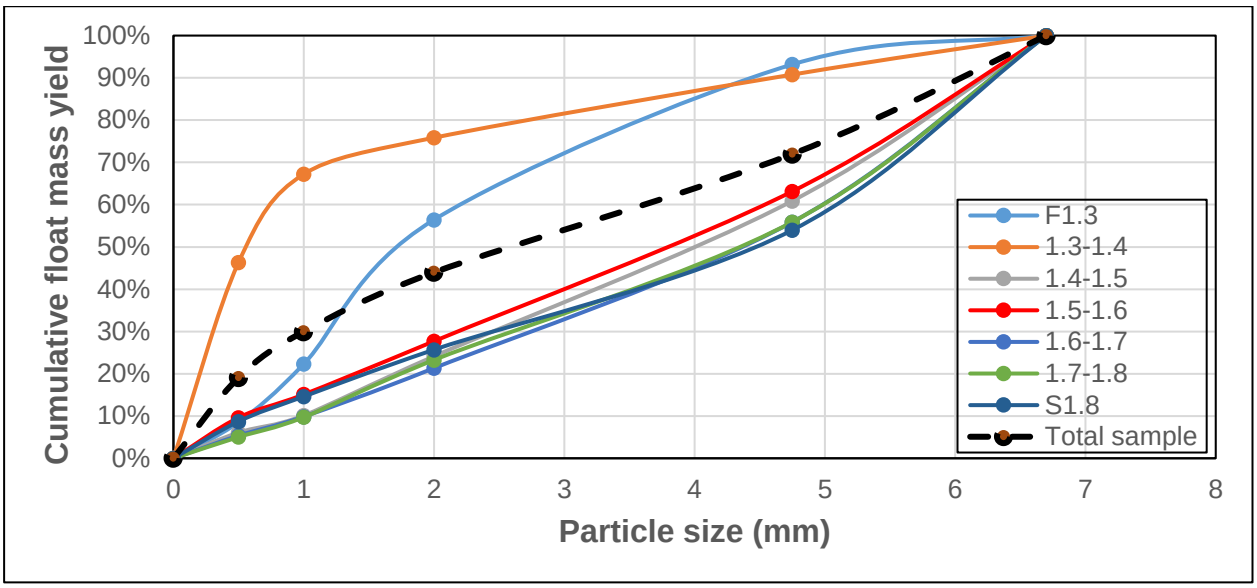

Figure C. 45: Particle size per density graph for impact breakage to a top size of 6.7 mm with 5 minutes attritioning (Run 12).

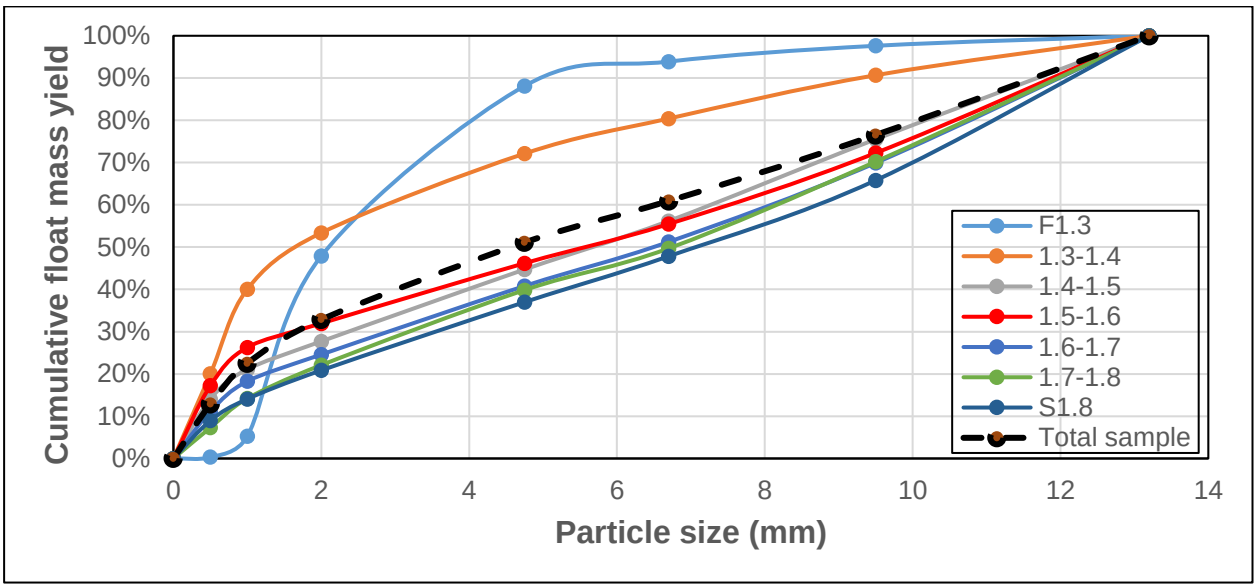

Figure C. 46: Particle size per density graph for compressive breakage to a top size of 13.2 mm with no attritioning (Run 13-15 average).

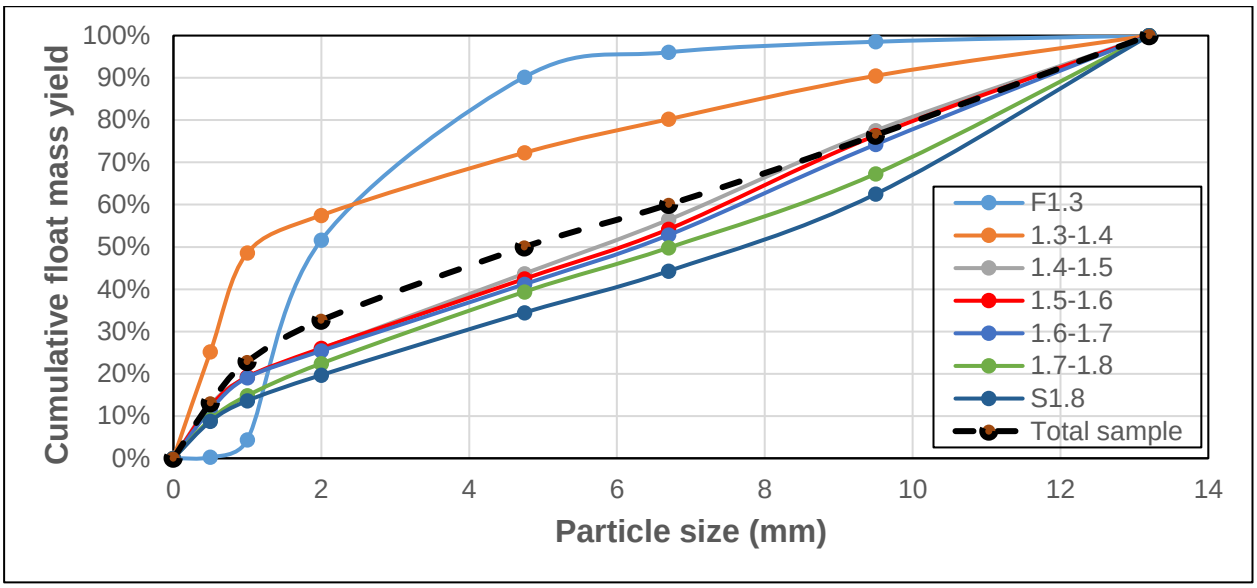

Figure C. 47: Particle size per density graph for compressive breakage to a top size of 13.2 mm with 1 minute attritioning (Run 16).

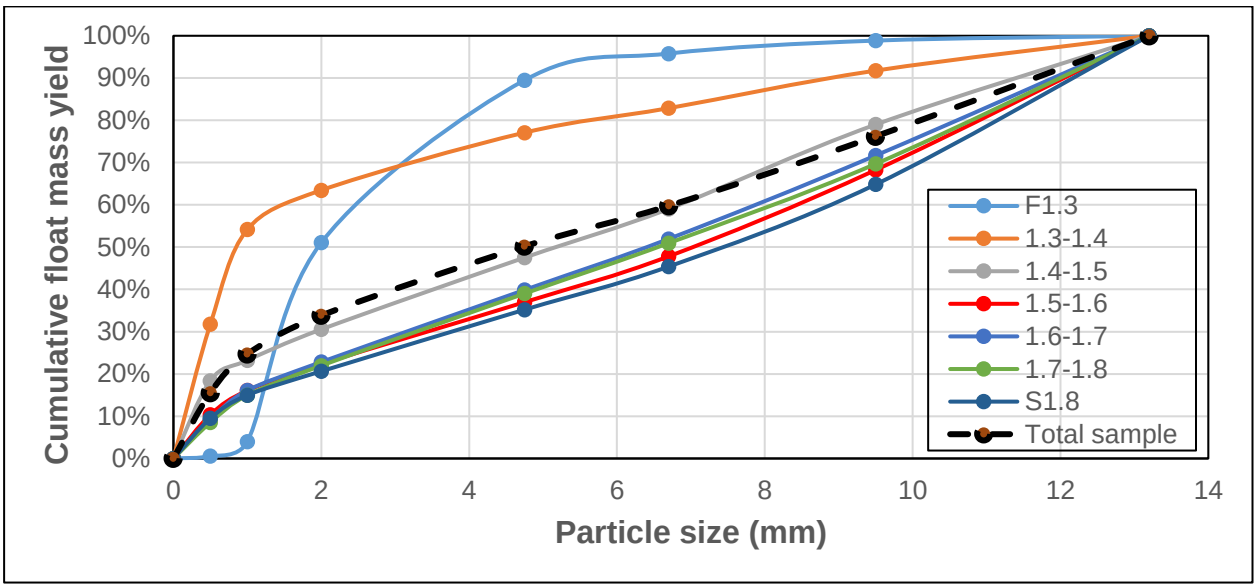

Figure C. 48: Particle size per density graph for compressive breakage to a top size of 13.2 mm with 2 minutes attritioning (Run 17).

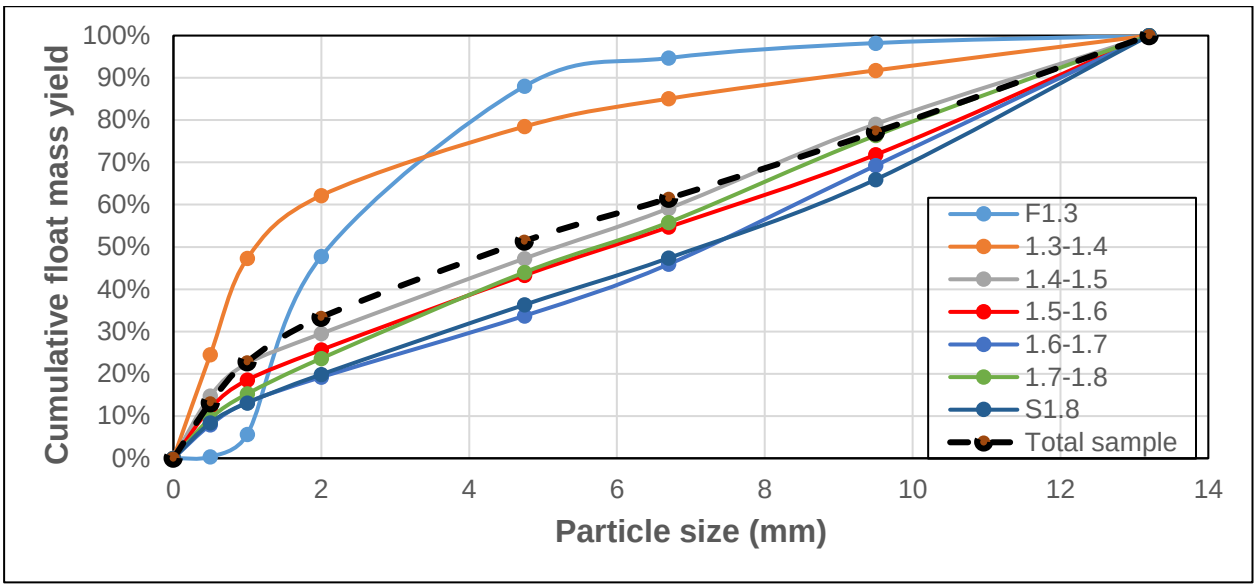

Figure C. 49: Particle size per density graph for compressive breakage to a top size of 13.2 mm with 5 minutes attritioning (Run 18).

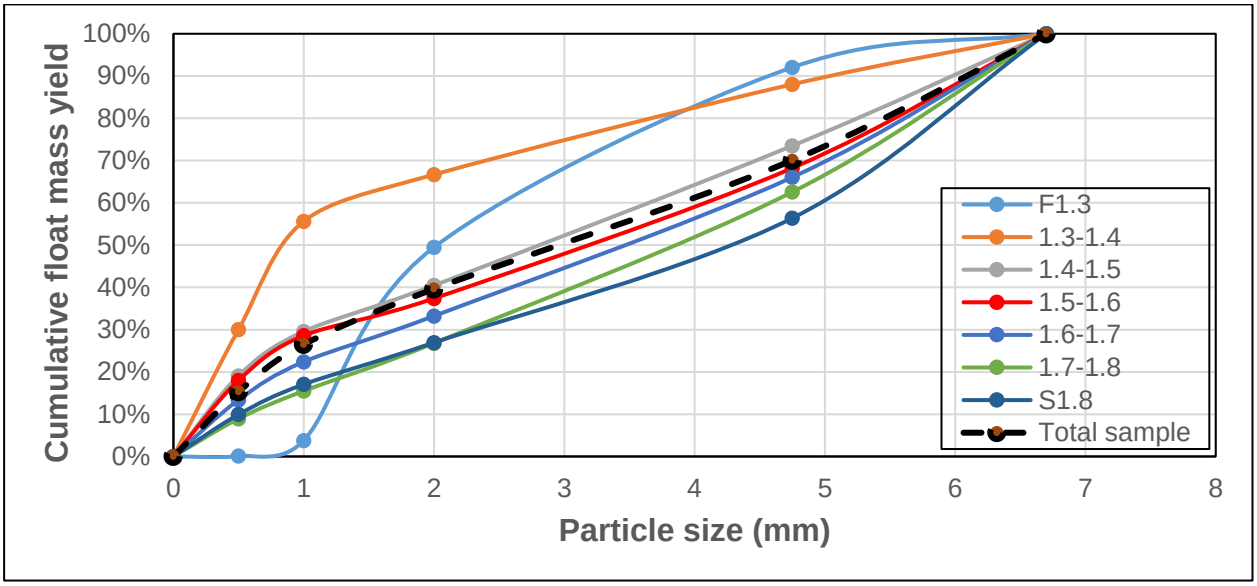

Figure C. 50: Particle size per density graph for compressive breakage to a top size of 6.7 mm with no attritioning (Run 19-21 average).

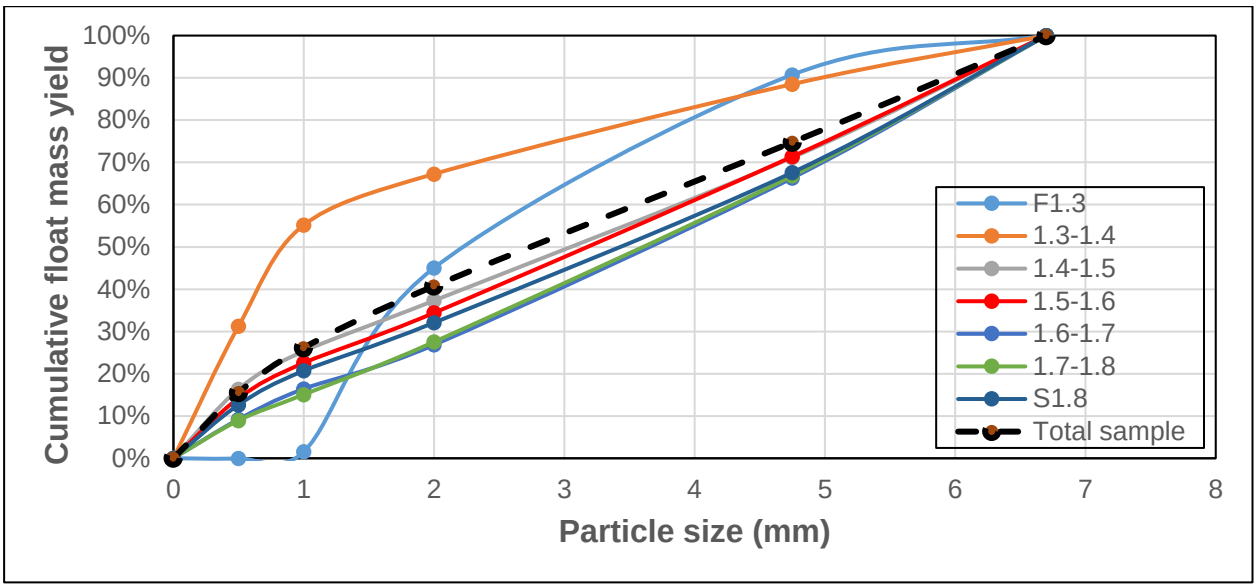

Figure C. 51: Particle size per density graph for compressive breakage to a top size of 6.7 mm with 1 minute attritioning (Run 22).

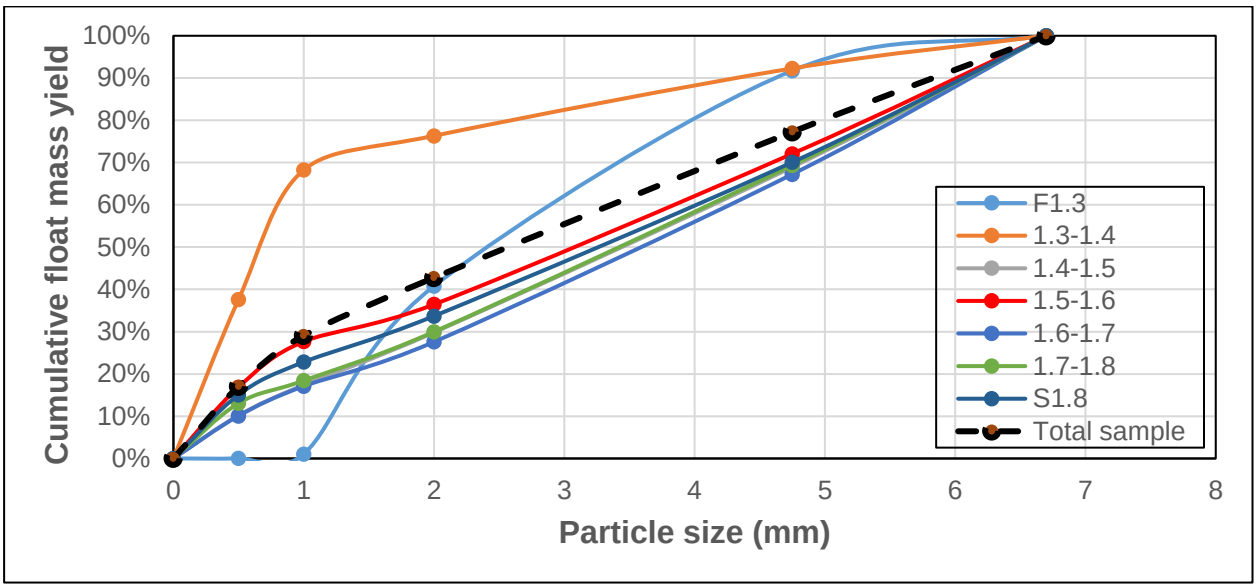

Figure C. 52: Particle size per density graph for compressive breakage to a top size of 6.7 mm with 2 minutes attritioning (Run 23).

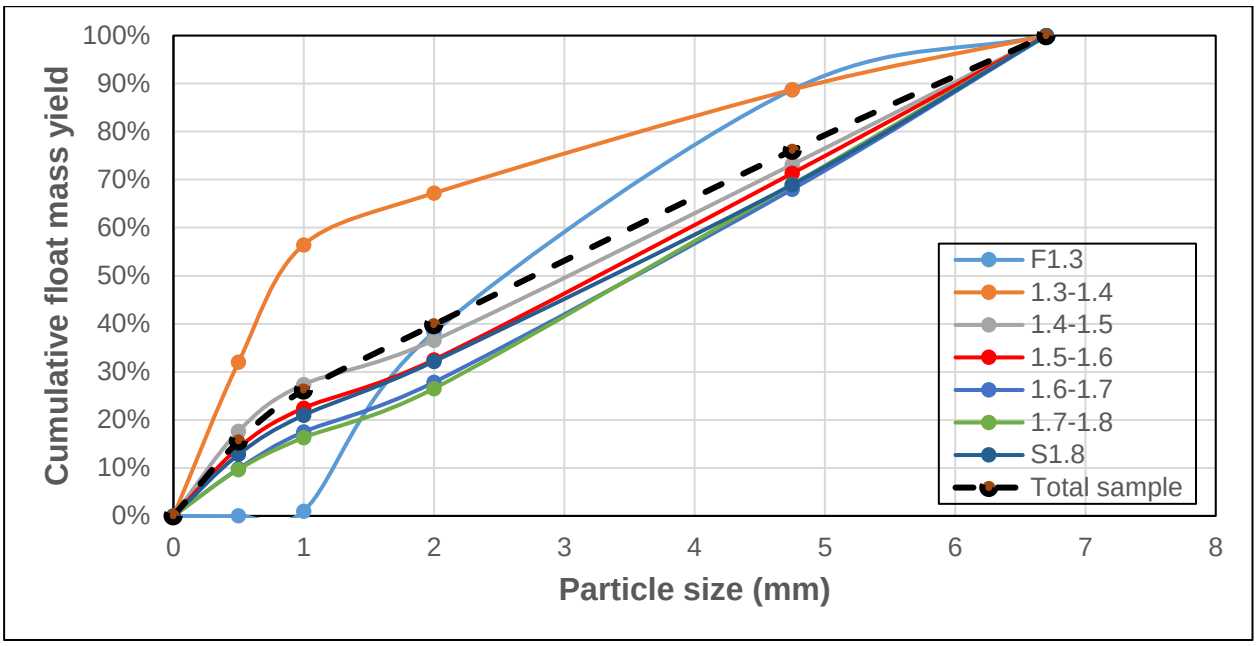

Figure C. 53: Particle size per density graph for compressive breakage to a top size of 6.7 mm with 5 minutes attritioning (Run 24).

Density per particle size:

The *density per particle size*, or float yield, was calculated similar as the particle size per density. The density per particle size for each particle size interval was calculated by cumulatively adding the mass at each RD interval for a specific particle size interval as a fraction of the total mass at that specific particle size interval. Thus the total mass fraction at that specific size interval will add up to 1.

Table C. 83: Density per particle size for raw ROM coal.

		Density interval						
	Float yield	1.3	1.4	1.5	1.6	1.7	1.8	Whole coal
Particle size	0-0.5mm	0.00	0.46	0.57	0.80	0.83	0.86	1.00
	0.5-1mm	0.04	0.63	0.70	0.85	0.87	0.90	1.00
	1-2mm	0.39	0.66	0.76	0.82	0.85	0.87	1.00
	2-4.75mm	0.22	0.43	0.61	0.71	0.77	0.81	1.00
	4.75-6.7mm	0.30	0.43	0.62	0.73	0.78	0.82	1.00
	6.7-9.5mm	0.03	0.18	0.46	0.62	0.71	0.78	1.00
	9.5-13.2mm	0.01	0.12	0.37	0.50	0.64	0.69	1.00
	13.2-19mm	0.00	0.10	0.37	0.51	0.58	0.67	1.00
	19-26.5mm	0.00	0.09	0.28	0.48	0.56	0.72	1.00
	26.5-37.5mm	0.00	0.00	0.10	0.32	0.60	0.70	1.00
	37.5-53mm	0.00	0.26	0.55	0.70	0.70	0.70	1.00
	53-75mm	0.00	0.00	0.00	0.00	0.45	1.00	1.00

Table C. 84: Density per particle size for impact breakage to a top size of 13.2 mm with no attritioning (Run 1-3 average).

		Density interval						
	Float yield	1.3	1.4	1.5	1.6	1.7	1.8	Whole coal
Particle size	0-0.5mm	0.03	0.46	0.65	0.71	0.78	0.80	1.00
	0.5-1mm	0.14	0.60	0.73	0.78	0.83	0.86	1.00
	1-2mm	0.30	0.48	0.68	0.74	0.78	0.83	1.00
	2-4.75mm	0.14	0.33	0.54	0.63	0.70	0.75	1.00
	4.75-6.7mm	0.04	0.23	0.45	0.55	0.64	0.70	1.00
	6.7-9.5mm	0.02	0.18	0.42	0.52	0.62	0.68	1.00
	9.5-13.2mm	0.00	0.09	0.29	0.38	0.48	0.54	1.00

Table C. 85: Density per particle size for impact breakage to a top size of 13.2 mm with 1 minute attritioning (Run 4).

		Density interval						
	Float yield	1.3	1.4	1.5	1.6	1.7	1.8	Whole coal
Particle size	0-0.5mm	0.02	0.41	0.59	0.64	0.74	0.76	1.00
	0.5-1mm	0.10	0.48	0.62	0.68	0.75	0.79	1.00
	1-2mm	0.21	0.47	0.60	0.66	0.74	0.80	1.00
	2-4.75mm	0.08	0.27	0.44	0.52	0.62	0.69	1.00
	4.75-6.7mm	0.02	0.14	0.33	0.44	0.55	0.64	1.00
	6.7-9.5mm	0.01	0.10	0.30	0.41	0.51	0.59	1.00
	9.5-13.2mm	0.00	0.06	0.23	0.34	0.46	0.55	1.00

Table C. 86: Density per particle size for impact breakage to a top size of 13.2 mm with 2 minutes attritioning (Run 5).

		Density interval						
	Float yield	1.3	1.4	1.5	1.6	1.7	1.8	Whole coal
Particle size	0-0.5mm	0.01	0.46	0.62	0.68	0.75	0.77	1.00
	0.5-1mm	0.11	0.58	0.68	0.74	0.79	0.82	1.00
	1-2mm	0.27	0.56	0.66	0.74	0.79	0.82	1.00
	2-4.75mm	0.15	0.39	0.53	0.63	0.70	0.75	1.00
	4.75-6.7mm	0.03	0.25	0.41	0.53	0.62	0.67	1.00
	6.7-9.5mm	0.01	0.22	0.40	0.53	0.63	0.69	1.00
	9.5-13.2mm	0.00	0.10	0.26	0.40	0.49	0.56	1.00

Table C. 87: Density per particle size for impact breakage to a top size of 13.2 mm with 5 minutes attritioning (Run 6).

		Density interval						
	Float yield	1.3	1.4	1.5	1.6	1.7	1.8	Whole coal
Particle size	0-0.5mm	0.02	0.41	0.59	0.64	0.74	0.76	1.00
	0.5-1mm	0.14	0.50	0.63	0.69	0.76	0.80	1.00
	1-2mm	0.26	0.55	0.65	0.71	0.76	0.79	1.00
	2-4.75mm	0.13	0.34	0.51	0.61	0.68	0.72	1.00
	4.75-6.7mm	0.03	0.19	0.41	0.53	0.62	0.67	1.00
	6.7-9.5mm	0.01	0.16	0.39	0.51	0.61	0.67	1.00
	9.5-13.2mm	0.00	0.09	0.28	0.39	0.48	0.55	1.00

Table C. 88: Density per particle size for impact breakage to a top size of 6.7 mm with no attritioning (Run 7-9 average).

		Density interval						
	Float yield	1.3	1.4	1.5	1.6	1.7	1.8	Whole coal
Particle size	0-0.5mm	0.02	0.43	0.58	0.70	0.75	0.79	1.00
	0.5-1mm	0.10	0.48	0.62	0.71	0.77	0.82	1.00
	1-2mm	0.26	0.56	0.67	0.74	0.79	0.84	1.00
	2-4.75mm	0.14	0.40	0.55	0.65	0.71	0.76	1.00
	4.75-6.7mm	0.01	0.17	0.36	0.48	0.57	0.64	1.00

Table C. 89: Density per particle size for impact breakage to a top size of 6.7 mm with 1 minute attritioning (Run 10).

		Density interval						
	Float yield	1.3	1.4	1.5	1.6	1.7	1.8	Whole coal
Particle size	0-0.5mm	0.06	0.78	0.83	0.87	0.89	0.90	1.00
	0.5-1mm	0.17	0.73	0.79	0.83	0.86	0.89	1.00
	1-2mm	0.35	0.49	0.62	0.70	0.76	0.81	1.00
	2-4.75mm	0.25	0.38	0.54	0.63	0.70	0.76	1.00
	4.75-6.7mm	0.07	0.17	0.32	0.43	0.49	0.56	1.00

Table C. 90: Density per particle size for impact breakage to a top size of 6.7 mm with 2 minutes attritioning (Run 11).

		Density interval						
	Float yield	1.3	1.4	1.5	1.6	1.7	1.8	Whole coal
Particle size	0-0.5mm	0.04	0.54	0.63	0.73	0.78	0.82	1.00
	0.5-1mm	0.14	0.55	0.64	0.73	0.78	0.83	1.00
	1-2mm	0.35	0.53	0.65	0.72	0.78	0.81	1.00
	2-4.75mm	0.17	0.36	0.54	0.65	0.73	0.77	1.00
	4.75-6.7mm	0.04	0.18	0.38	0.51	0.60	0.65	1.00

Table C. 91: Density per particle size for impact breakage to a top size of 6.7 mm with 5 minutes attritioning (Run 12).

		Density interval						
	Float yield	1.3	1.4	1.5	1.6	1.7	1.8	Whole coal
Particle size	0-0.5mm	0.06	0.78	0.83	0.87	0.89	0.90	1.00
	0.5-1mm	0.16	0.73	0.79	0.83	0.86	0.88	1.00
	1-2mm	0.31	0.49	0.65	0.72	0.78	0.83	1.00
	2-4.75mm	0.17	0.33	0.53	0.63	0.72	0.79	1.00
	4.75-6.7mm	0.03	0.13	0.34	0.45	0.56	0.65	1.00

Table C. 92: Density per particle size for compressive breakage to a top size of 13.2 mm with no attritioning (Run 13-15 average).

		Density interval						
	Float yield	1.3	1.4	1.5	1.6	1.7	1.8	Whole coal
Particle size	0-0.5mm	0.00	0.37	0.57	0.70	0.76	0.79	1.00
	0.5-1mm	0.03	0.53	0.66	0.75	0.80	0.84	1.00
	1-2mm	0.24	0.55	0.67	0.72	0.76	0.80	1.00
	2-4.75mm	0.13	0.38	0.54	0.62	0.68	0.73	1.00
	4.75-6.7mm	0.03	0.24	0.45	0.54	0.62	0.67	1.00
	6.7-9.5mm	0.01	0.17	0.39	0.50	0.59	0.65	1.00
	9.5-13.2mm	0.01	0.10	0.29	0.40	0.50	0.56	1.00

Table C. 93: Density per particle size for compressive breakage to a top size of 13.2 mm with 1 minute attritioning (Run 16).

		Density interval						
	Float yield	1.3	1.4	1.5	1.6	1.7	1.8	Whole coal
Particle size	0-0.5mm	0.00	0.43	0.62	0.71	0.76	0.80	1.00
	0.5-1mm	0.03	0.57	0.70	0.77	0.81	0.85	1.00
	1-2mm	0.33	0.53	0.67	0.73	0.77	0.81	1.00
	2-4.75mm	0.15	0.34	0.55	0.63	0.69	0.74	1.00
	4.75-6.7mm	0.04	0.22	0.47	0.57	0.64	0.70	1.00
	6.7-9.5mm	0.01	0.15	0.41	0.52	0.60	0.66	1.00
	9.5-13.2mm	0.00	0.10	0.29	0.37	0.44	0.52	1.00

Table C. 94: Density per particle size for compressive breakage to a top size of 13.2 mm with 2 minutes attritioning (Run 17).

		Density interval						
	Float yield	1.3	1.4	1.5	1.6	1.7	1.8	Whole coal
Particle size	0-0.5mm	0.00	0.45	0.66	0.73	0.78	0.81	1.00
	0.5-1mm	0.02	0.56	0.65	0.72	0.77	0.81	1.00
	1-2mm	0.27	0.49	0.64	0.71	0.76	0.80	1.00
	2-4.75mm	0.12	0.31	0.49	0.59	0.66	0.72	1.00
	4.75-6.7mm	0.03	0.17	0.39	0.50	0.60	0.66	1.00
	6.7-9.5mm	0.01	0.13	0.35	0.48	0.57	0.63	1.00
	9.5-13.2mm	0.00	0.08	0.24	0.38	0.47	0.53	1.00

Table C. 95: Density per particle size for compressive breakage to a top size of 13.2 mm with 5 minutes attritioning (Run 18).

		Density interval						
	Float yield	1.3	1.4	1.5	1.6	1.7	1.8	Whole coal
Particle size	0-0.5mm	0.00	0.43	0.62	0.71	0.76	0.80	1.00
	0.5-1mm	0.03	0.57	0.70	0.77	0.81	0.85	1.00
	1-2mm	0.20	0.53	0.64	0.71	0.75	0.80	1.00
	2-4.75mm	0.11	0.32	0.49	0.58	0.65	0.71	1.00
	4.75-6.7mm	0.03	0.18	0.38	0.49	0.59	0.66	1.00
	6.7-9.5mm	0.01	0.11	0.33	0.43	0.56	0.63	1.00
	9.5-13.2mm	0.00	0.09	0.24	0.36	0.47	0.53	1.00

Table C. 96: Density per particle size for compressive breakage to a top size of 6.7 mm with no attritioning (Run 19-21 average).

		Density interval						
	Float yield	1.3	1.4	1.5	1.6	1.7	1.8	Whole coal
Particle size	0-0.5mm	0.00	0.35	0.57	0.68	0.74	0.78	1.00
	0.5-1mm	0.03	0.44	0.60	0.69	0.75	0.78	1.00
	1-2mm	0.28	0.43	0.57	0.63	0.69	0.74	1.00
	2-4.75mm	0.11	0.24	0.43	0.52	0.60	0.67	1.00
	4.75-6.7mm	0.02	0.09	0.25	0.35	0.43	0.50	1.00

Table C. 97: Density per particle size for compressive breakage to a top size of 6.7 mm with 1 minute attritioning (Run 22).

		Density interval						
	Float yield	1.3	1.4	1.5	1.6	1.7	1.8	Whole coal
Particle size	0-0.5mm	0.00	0.40	0.60	0.70	0.75	0.78	1.00
	0.5-1mm	0.01	0.46	0.62	0.71	0.76	0.80	1.00
	1-2mm	0.27	0.43	0.60	0.68	0.74	0.79	1.00
	2-4.75mm	0.12	0.24	0.44	0.56	0.65	0.72	1.00
	4.75-6.7mm	0.03	0.12	0.35	0.47	0.58	0.66	1.00

Table C. 98: Density per particle size for compressive breakage to a top size of 6.7 mm with 2 minutes attritioning (Run 23).

		Density interval						
	Float yield	1.3	1.4	1.5	1.6	1.7	1.8	Whole coal
Particle size	0-0.5mm	0.00	0.48	0.58	0.70	0.74	0.79	1.00
	0.5-1mm	0.01	0.56	0.66	0.77	0.82	0.85	1.00
	1-2mm	0.34	0.47	0.62	0.70	0.76	0.81	1.00
	2-4.75mm	0.18	0.28	0.47	0.59	0.68	0.75	1.00
	4.75-6.7mm	0.04	0.12	0.35	0.50	0.61	0.69	1.00

Table C. 99: Density per particle size for compressive breakage to a top size of 6.7 mm with 5 minutes attritioning (Run 24).

		Density interval						
	Float yield	1.3	1.4	1.5	1.6	1.7	1.8	Whole coal
Particle size	0-0.5mm	0.00	0.40	0.60	0.70	0.75	0.78	1.00
	0.5-1mm	0.01	0.46	0.62	0.71	0.76	0.80	1.00
	1-2mm	0.33	0.48	0.60	0.68	0.74	0.79	1.00
	2-4.75mm	0.17	0.28	0.47	0.58	0.67	0.73	1.00
	4.75-6.7mm	0.06	0.15	0.35	0.48	0.59	0.66	1.00

The above mentioned density per particle size data are presented as graphs in Figure C. 54 to Figure C. 70.

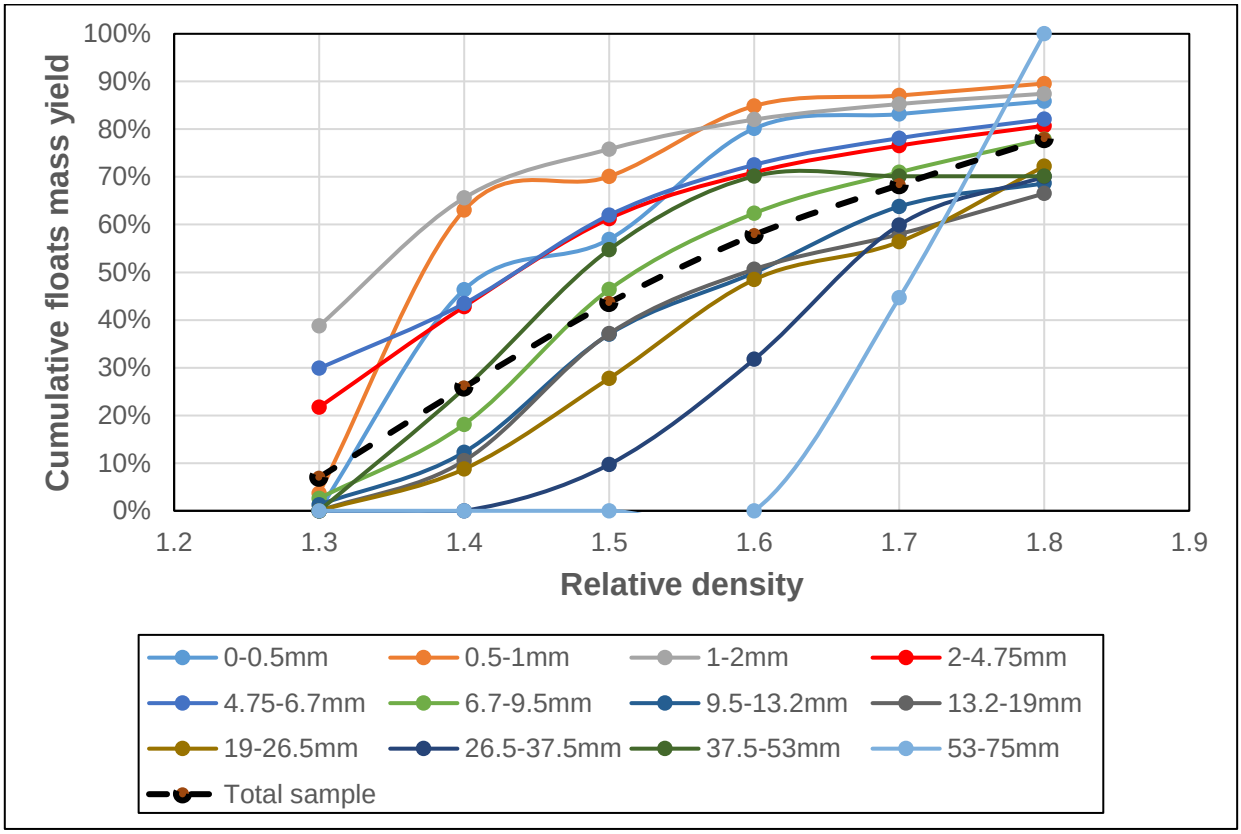

Figure C. 54: Density per particle size graph for raw ROM coal.

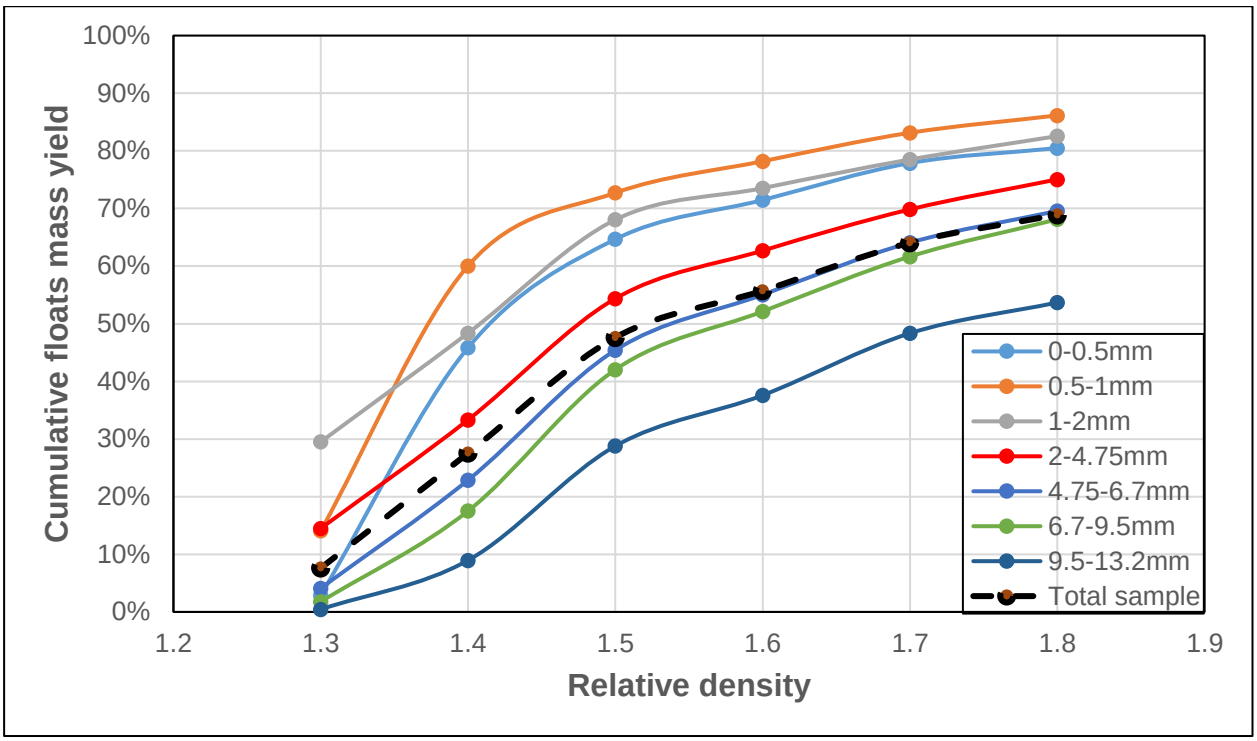

Figure C. 55: Density per particle size graph for impact breakage to a top size of 13.2 mm with no attritioning (Run 1-3 average).

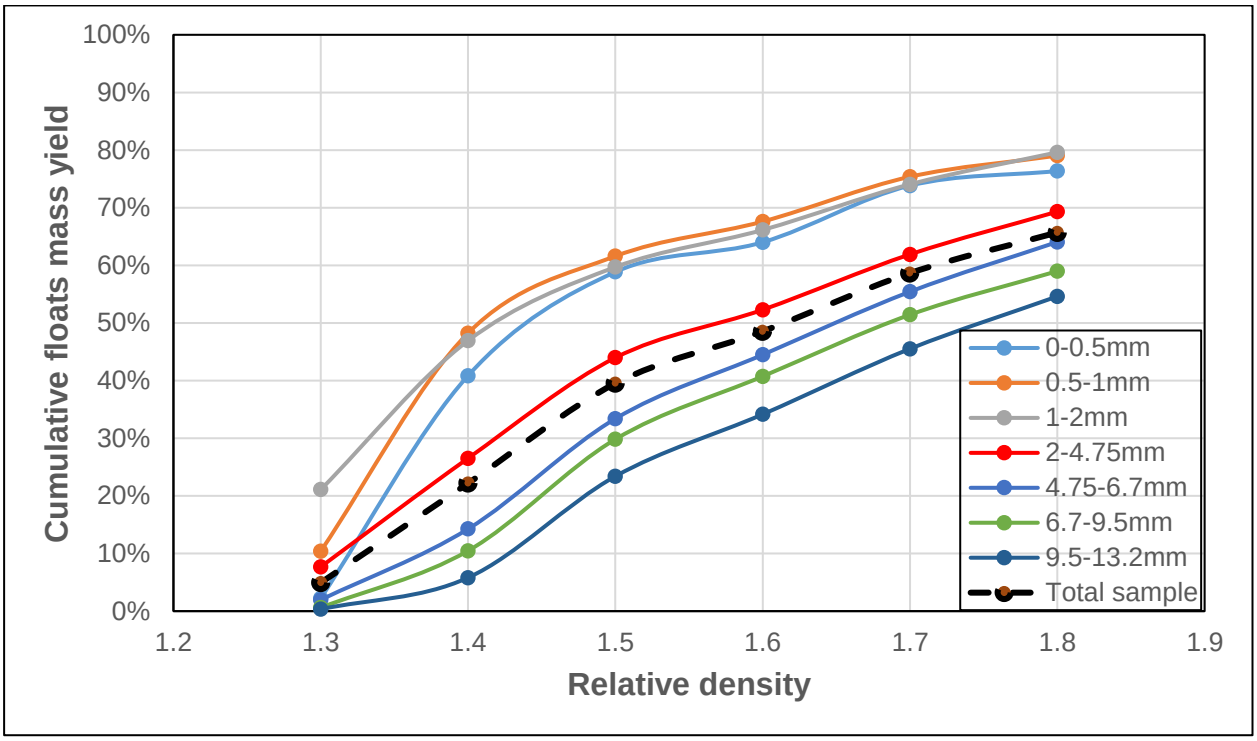

Figure C. 56: Density per particle size graph for impact breakage to a top size of 13.2 mm with 1 minute attritioning (Run 4).

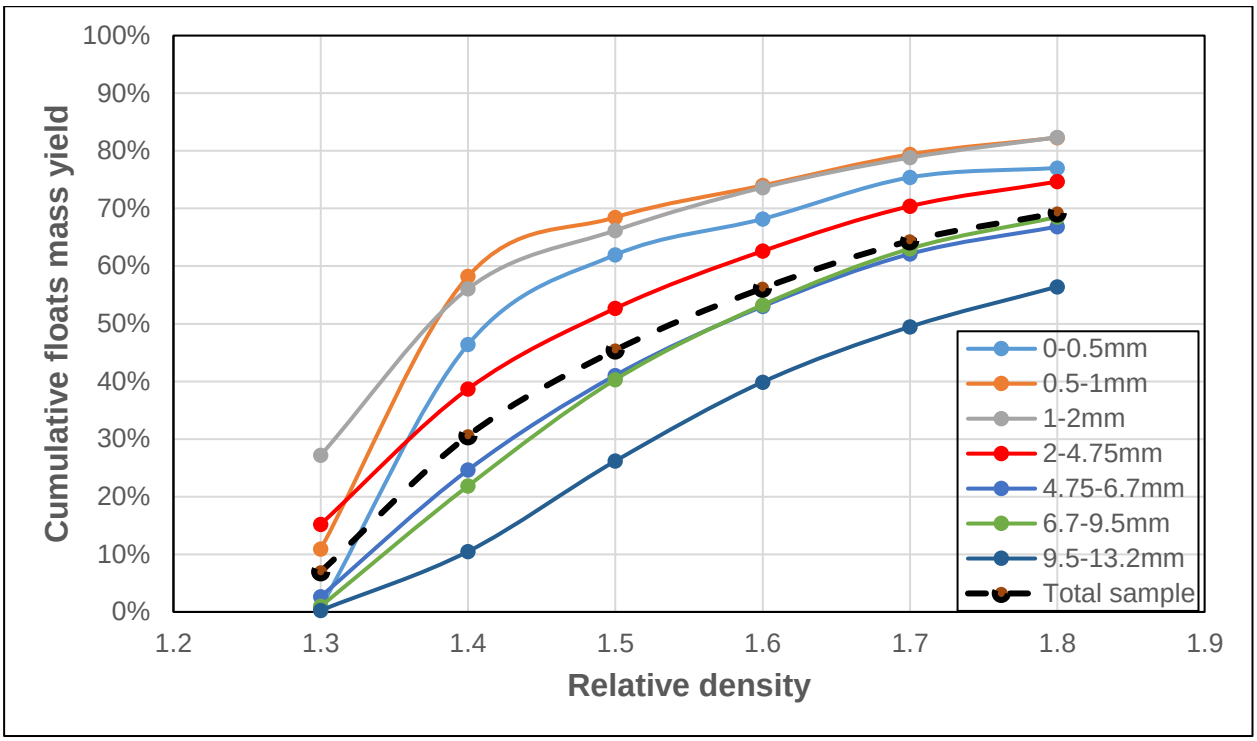

Figure C. 57: Density per particle size graph for impact breakage to a top size of 13.2 mm with 2 minutes attritioning (Run 5).

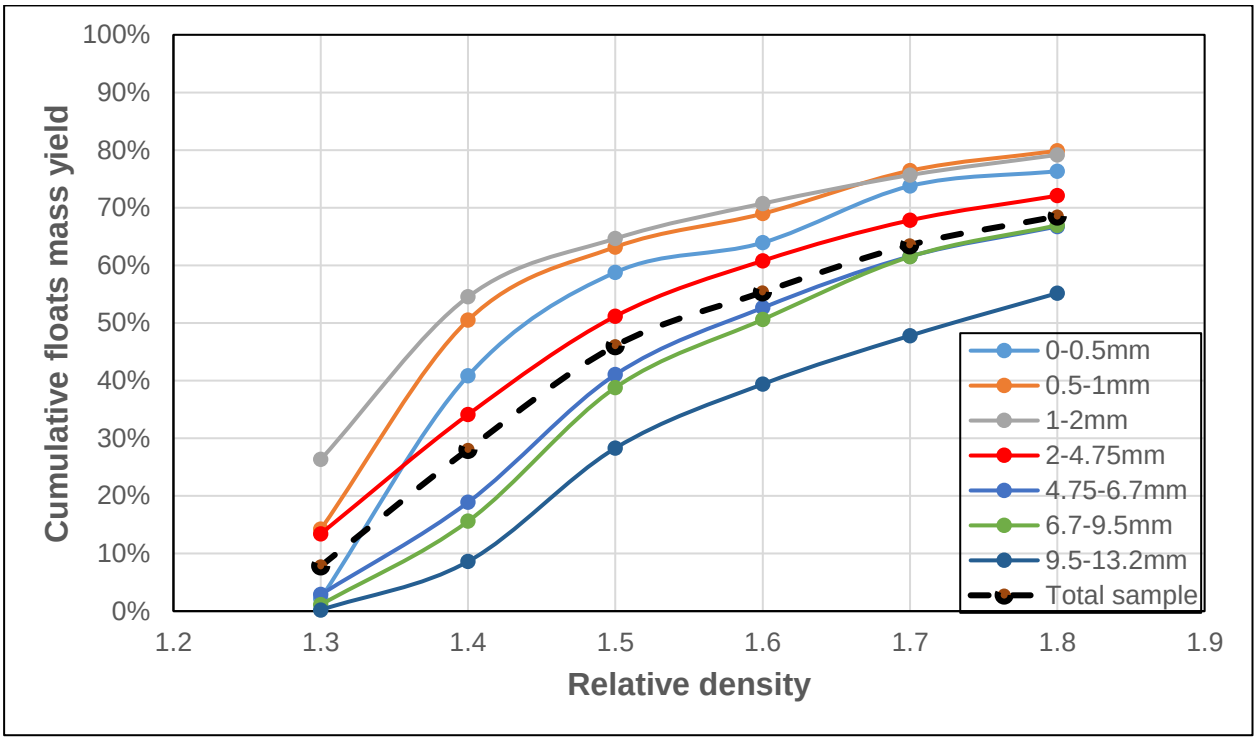

Figure C. 58: Density per particle size graph for impact breakage to a top size of 13.2 mm with 5 minutes attritioning (Run 6).

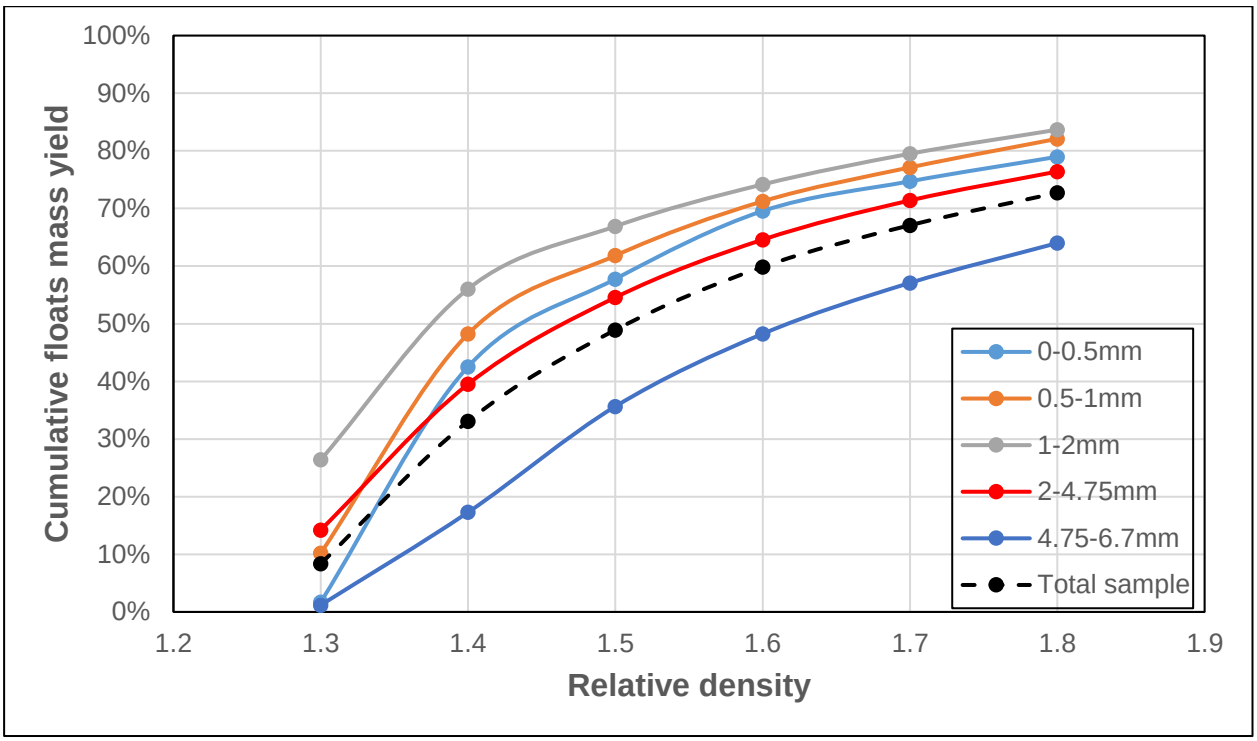

Figure C. 59: Density per particle size graph for impact breakage to a top size of 6.7 mm with no attritioning (Run 7-9 average).

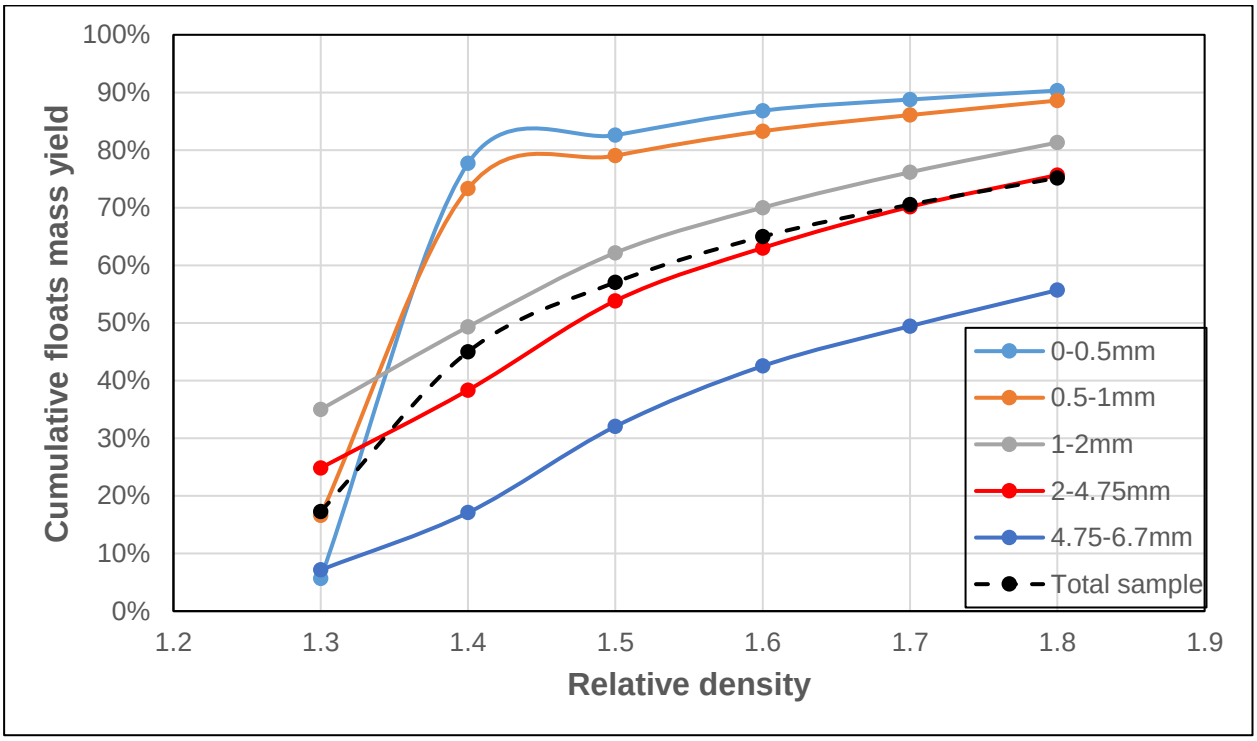

Figure C. 60: Density per particle size graph for impact breakage to a top size of 6.7 mm with 1 minute attritioning (Run 10).

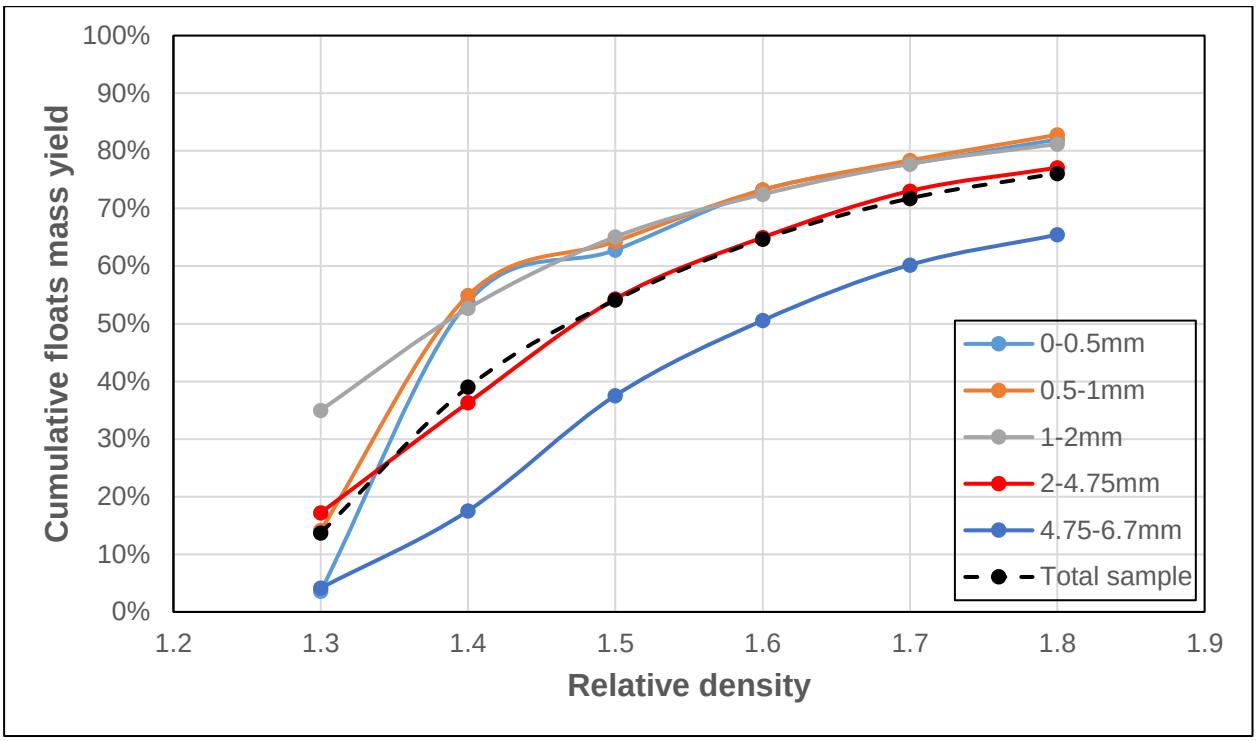

Figure C. 61: Density per particle size graph for impact breakage to a top size of 6.7 mm with 2 minutes attritioning (Run 11).

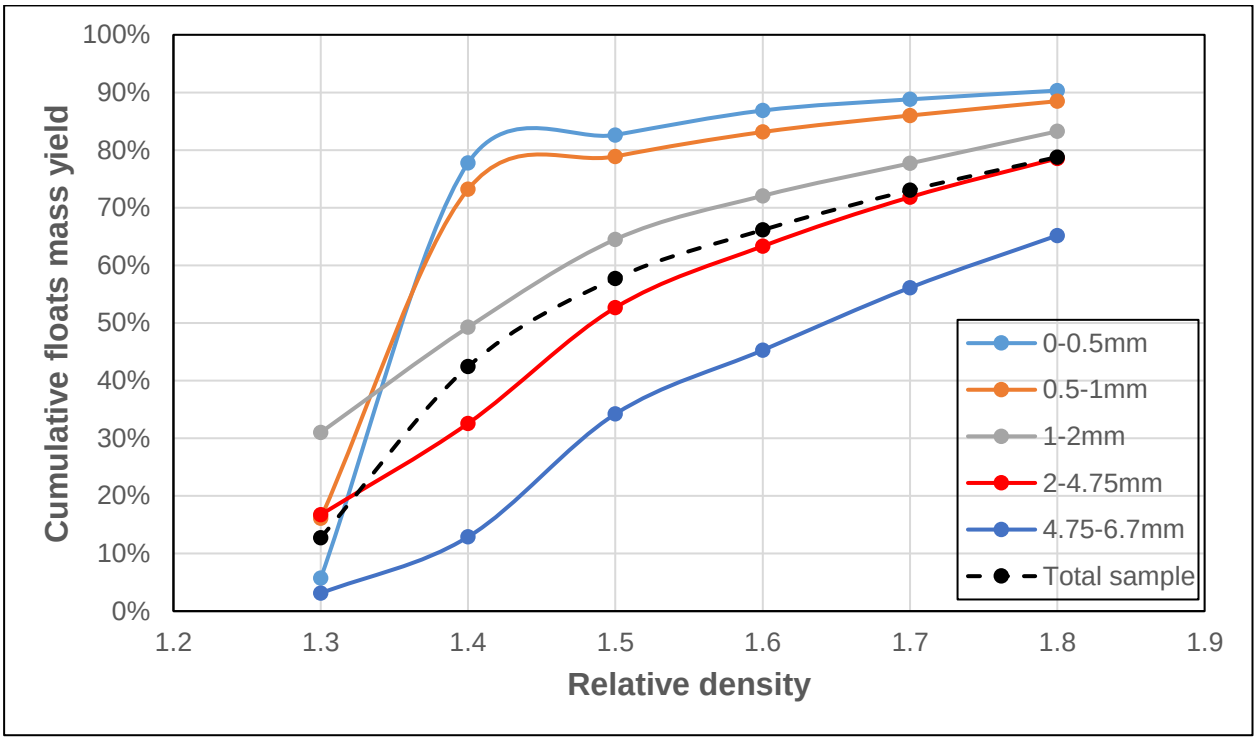

Figure C. 62: Density per particle size graph for impact breakage to a top size of 6.7 mm with 5 minutes attritioning (Run 12).

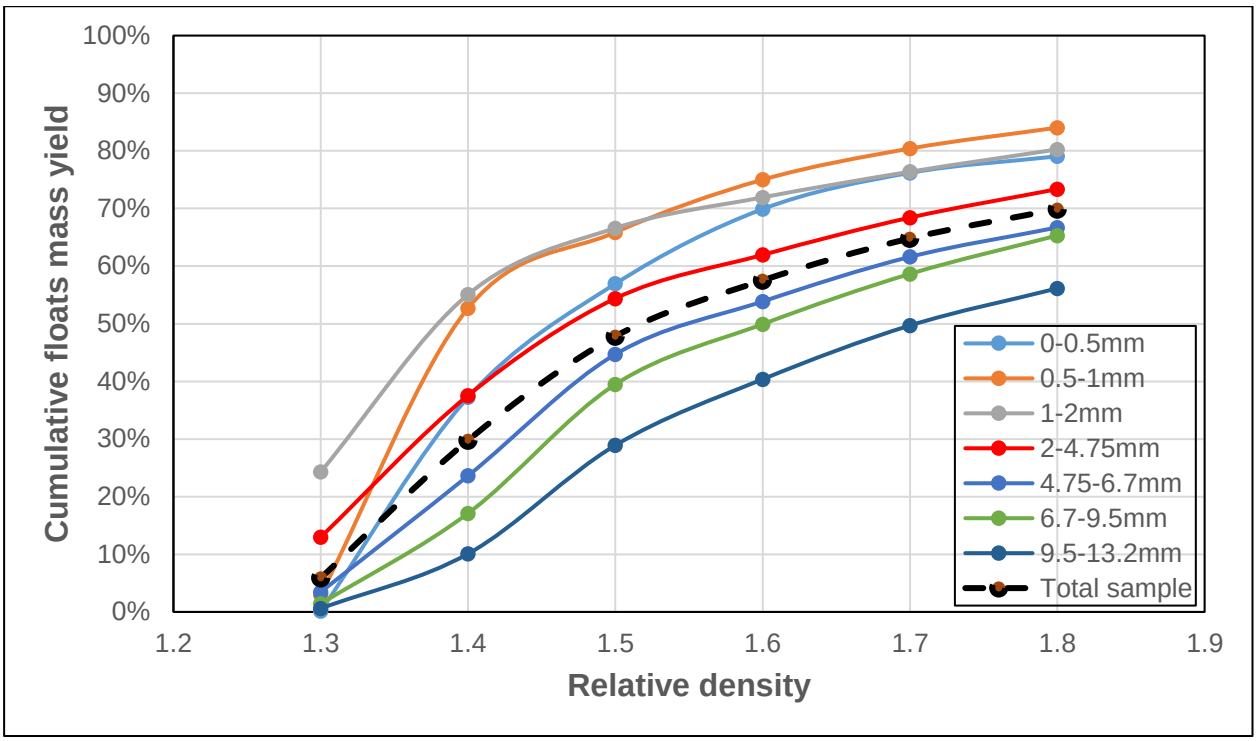

Figure C. 63: Density per particle size graph for compressive breakage to a top size of 13.2 mm with no attritioning (Run 13-15 average).

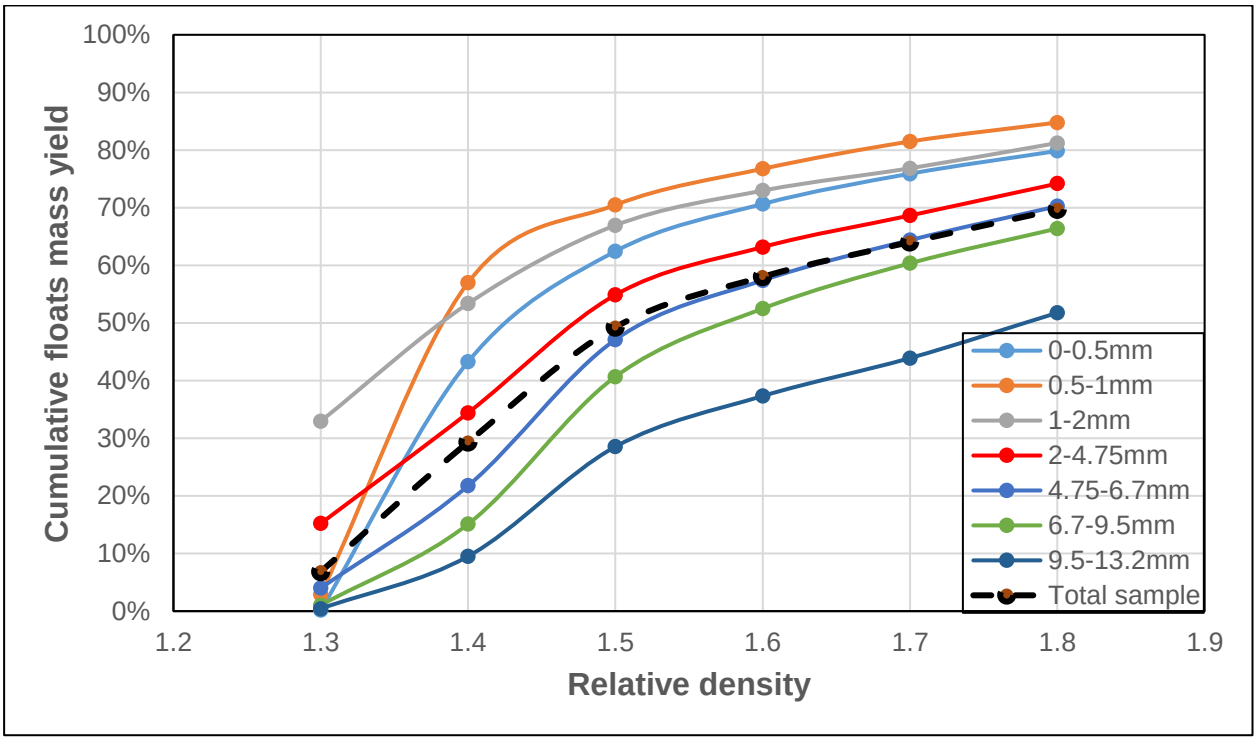

Figure C. 64: Density per particle size graph for compressive breakage to a top size of 13.2 mm with 1 minute attritioning (Run 16).

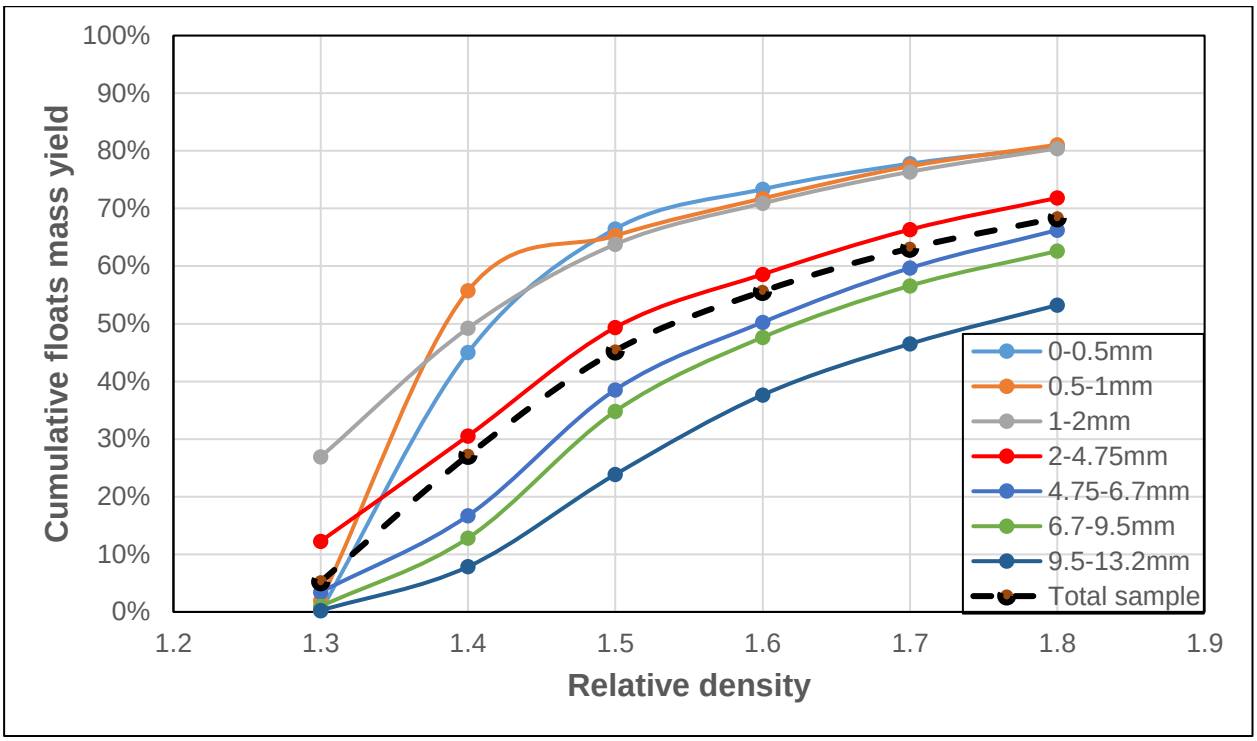

Figure C. 65: Density per particle size graph for compressive breakage to a top size of 13.2 mm with 2 minutes attritioning (Run 17).

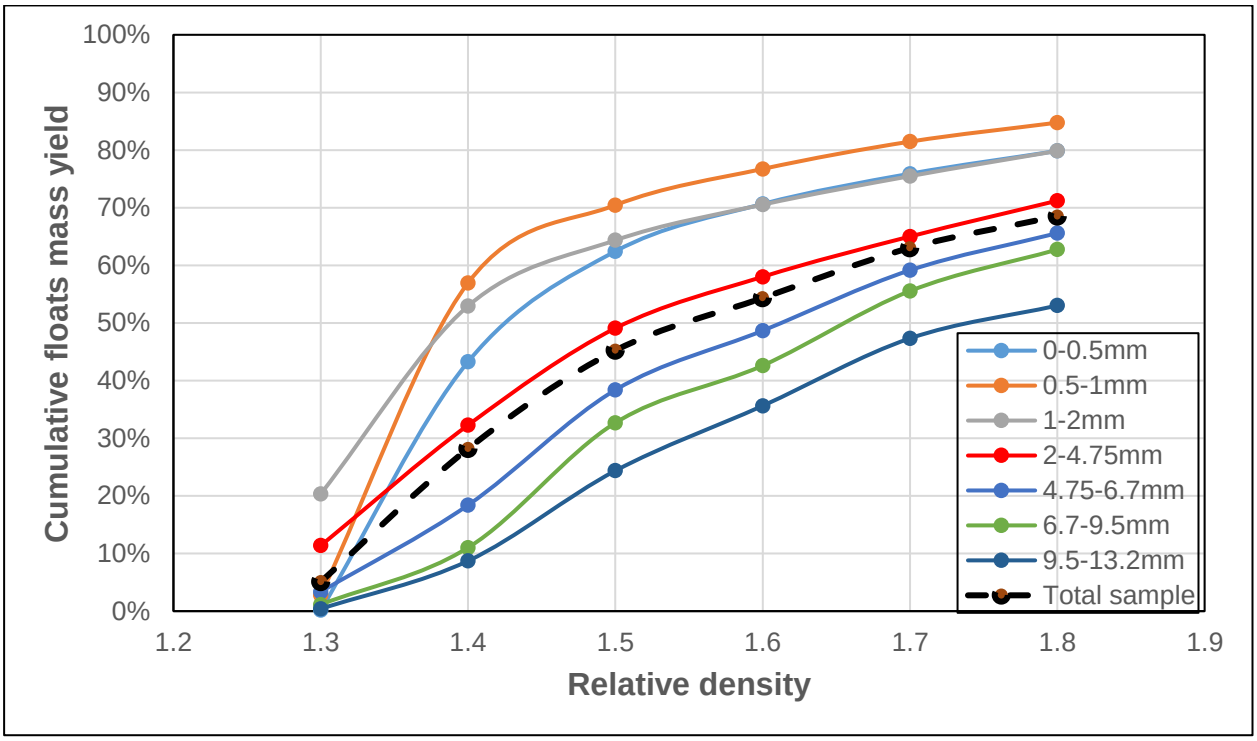

Figure C. 66: Density per particle size graph for compressive breakage to a top size of 13.2 mm with 5 minutes attritioning (Run 18).

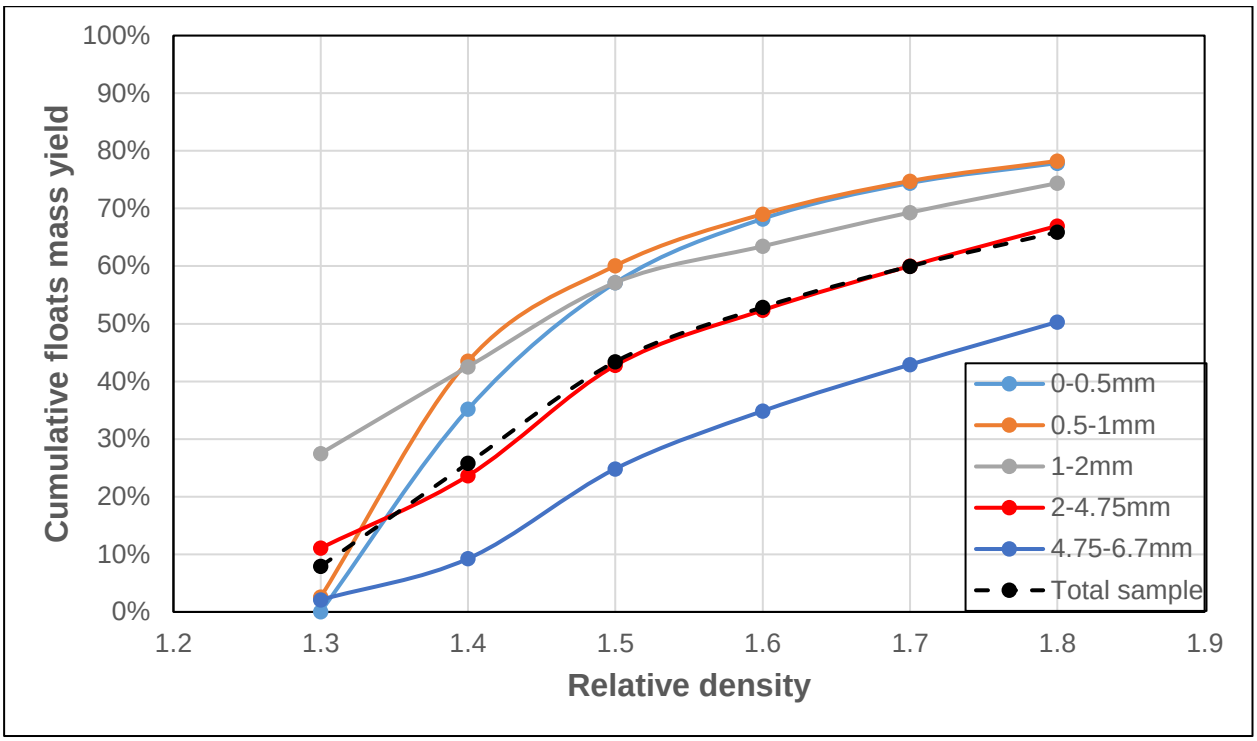

Figure C. 67: Density per particle size graph for compressive breakage to a top size of 6.7 mm with no attritioning (Run 19-21 average).

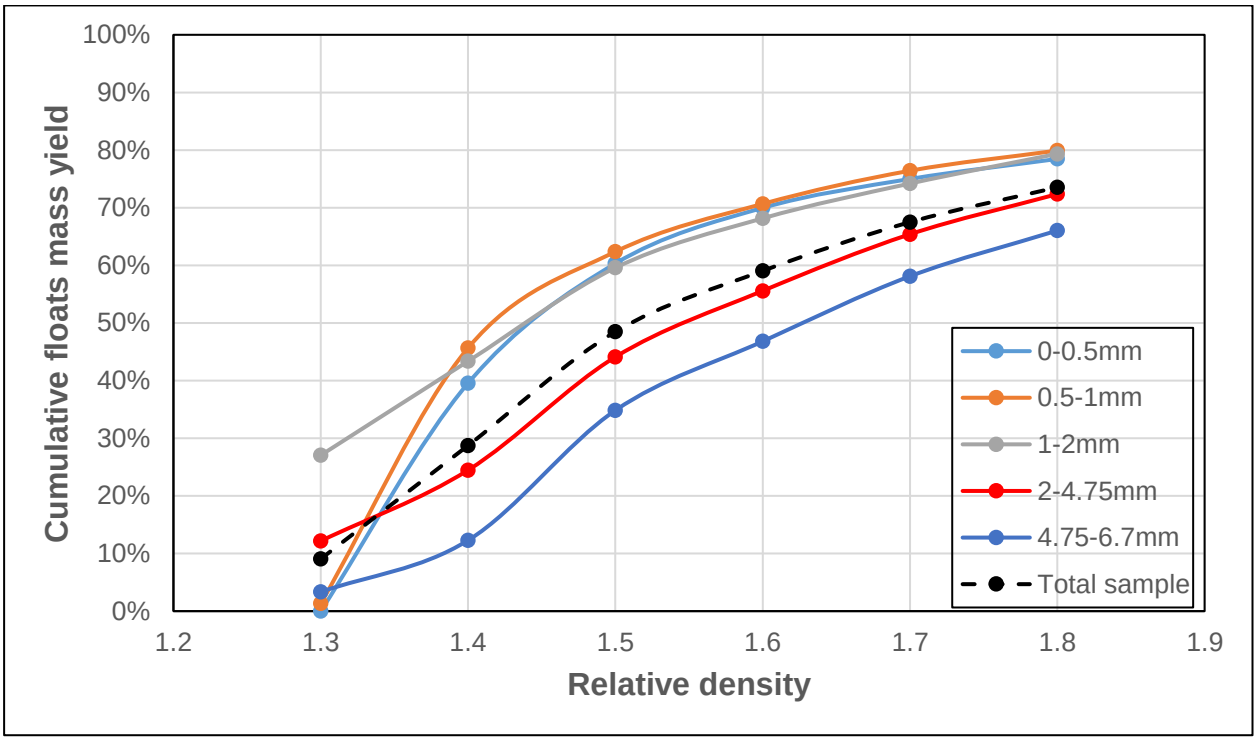

Figure C. 68: Density per particle size graph for compressive breakage to a top size of 6.7 mm with 1 minute attritioning (Run 22).

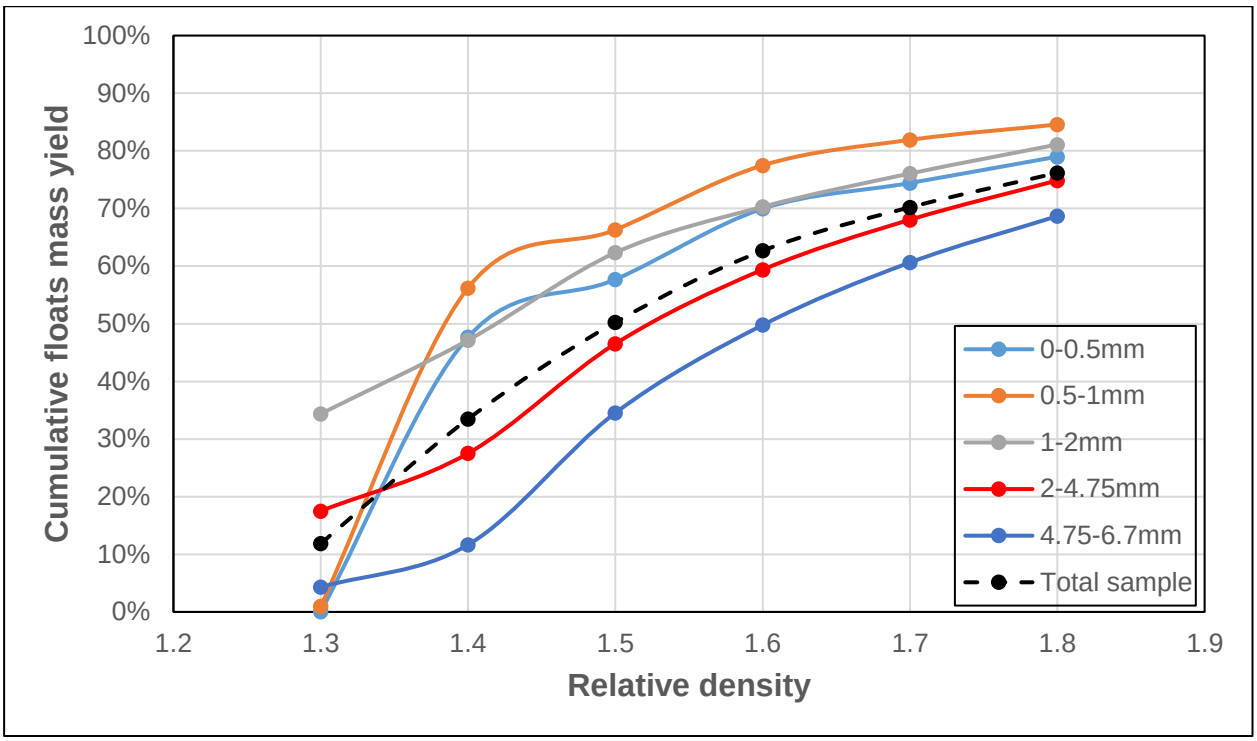

Figure C. 69: Density per particle size graph for compressive breakage to a top size of 6.7 mm with 2 minutes attritioning (Run 23).

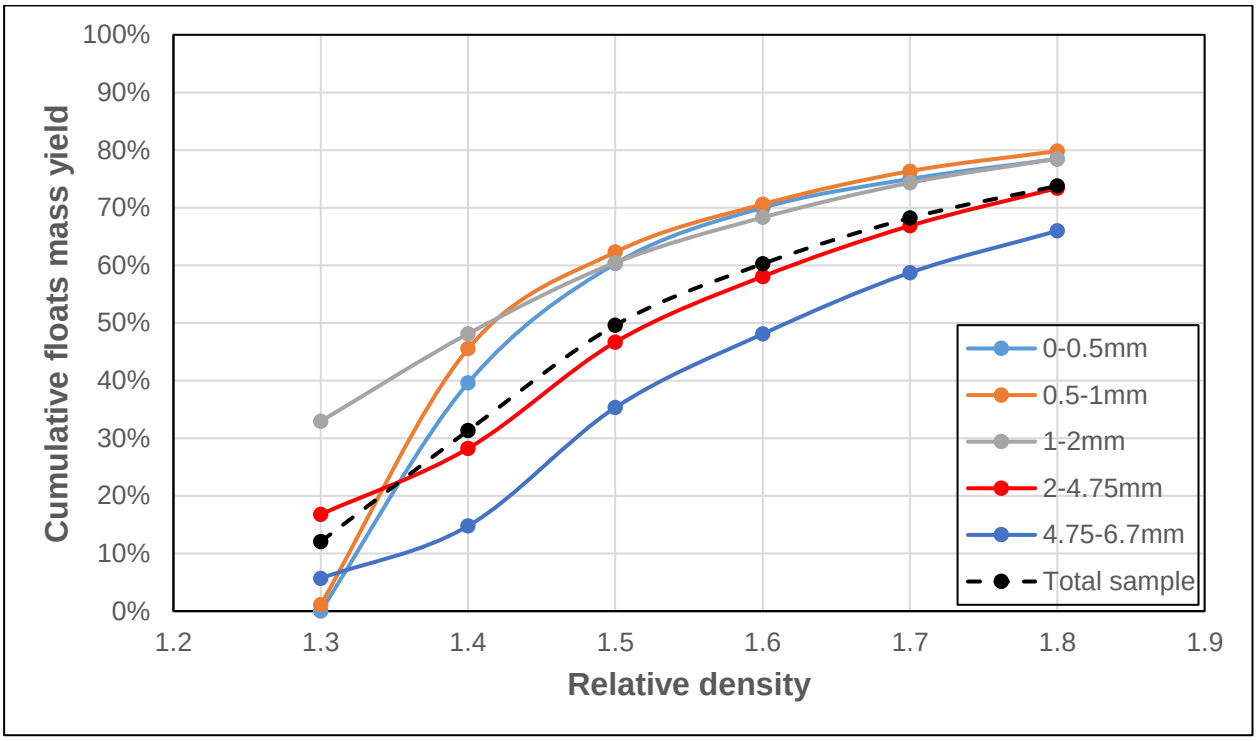

Figure C. 70: Density per particle size graph for compressive breakage to a top size of 6.7 mm with 5 minutes attritioning (Run 24).

Float ash per particle size:

The float ash per particle size was calculated by using Equation D- 12 and Equation D- 13. Results obtained from the calculation are given in Table C. 100 to Table C. 116.

Table C. 100: Float ash per particle size for raw ROM coal.

		Density interval						
	Float ash	1.3	1.4	1.5	1.6	1.7	1.8	Whole coal
Particle size	0-0.5mm	4.35	5.38	6.69	11.24	11.87	12.66	19.35
	0.5-1mm	4.35	5.33	6.04	8.89	9.39	10.17	15.35
	1-2mm	4.47	7.88	9.47	10.80	11.75	12.55	18.79
	2-4.75mm	4.47	8.58	11.93	13.99	15.57	17.05	25.75
	4.75-6.7mm	4.47	7.07	10.85	13.21	14.80	16.23	24.46
	6.7-9.5mm	4.47	11.60	16.55	19.24	21.20	23.25	31.87
	9.5-13.2mm	4.47	11.95	17.14	19.70	23.13	24.63	36.41
	13.2-19mm	4.47	12.80	17.76	20.24	22.18	25.01	37.47
	19-26.5mm	4.47	12.80	17.54	21.60	23.55	28.09	37.57
	26.5-37.5mm	4.47	12.72	19.72	24.81	29.82	31.91	40.99
	37.5-53mm	4.47	12.80	16.48	18.80	18.80	18.80	31.77
	53-75mm	4.47	12.72	13.35	14.48	35.47	40.34	40.34

Table C. 101: Float ash per particle size for impact breakage to 13.2 mm with no attritioning (Run 1-3 average).

		Density interval						
	Float ash	1.3	1.4	1.5	1.6	1.7	1.8	Whole coal
Particle size	0-0.5mm	4.35	5.32	7.40	8.82	10.46	11.33	20.80
	0.5-1mm	4.35	5.14	6.42	7.53	8.80	9.79	16.73
	1-2mm	4.47	7.72	11.19	12.37	13.83	15.33	23.51
	2-4.75mm	4.47	9.18	13.26	15.09	17.17	19.05	29.82
	4.75-6.7mm	4.47	11.30	15.48	17.50	20.03	21.95	34.20
	6.7-9.5mm	4.47	11.96	16.49	18.53	21.15	23.34	35.73
	9.5-13.2mm	4.47	12.39	17.44	19.69	23.20	25.29	42.39
	Overall	4.44	8.19	12.58	14.59	17.18	19.03	32.39

Table C. 102: Float ash per particle size for impact breakage to 13.2 mm with 1 minute attritioning (Run 4).

		Density interval						
	Float ash	1.3	1.4	1.5	1.6	1.7	1.8	Whole coal
Particle size	0-0.5mm	4.35	5.33	7.51	8.70	11.37	12.23	23.49
	0.5-1mm	4.35	5.16	6.74	8.13	10.26	11.51	21.65
	1-2mm	4.47	9.06	11.34	12.87	15.28	17.30	26.46
	2-4.75mm	4.47	10.39	14.09	16.15	19.15	21.84	34.23
	4.75-6.7mm	4.47	11.66	16.27	18.96	22.22	25.19	38.50
	6.7-9.5mm	4.47	12.32	17.12	19.78	23.04	25.76	40.71
	9.5-13.2mm	4.47	12.33	17.88	20.77	24.44	27.74	43.39
	Overall	4.45	8.76	13.06	15.57	18.82	21.49	35.37

Table C. 103: Float ash per particle size for impact breakage to 13.2 mm with 2 minutes attritioning (Run 5).

		Density interval						
	Float ash	1.3	1.4	1.5	1.6	1.7	1.8	Whole coal
Particle size	0-0.5mm	4.35	5.37	7.15	8.54	10.47	11.04	22.25
	0.5-1mm	4.35	5.19	6.28	7.48	8.93	9.93	18.77
	1-2mm	4.47	8.76	10.43	12.11	13.65	14.96	23.30
	2-4.75mm	4.47	9.52	12.23	14.58	16.89	18.45	29.54
	4.75-6.7mm	4.47	11.90	15.03	17.74	20.34	22.04	35.35
	6.7-9.5mm	4.47	12.43	15.77	18.51	21.13	22.99	35.34
	9.5-13.2mm	4.47	12.59	16.86	20.36	23.29	25.87	41.71
	Overall	4.45	8.93	12.08	14.85	17.37	19.21	32.37

Table C. 104: Float ash per particle size for impact breakage to 13.2 mm with 5 minutes attritioning (Run 6).

		Density interval						
	Float ash	1.3	1.4	1.5	1.6	1.7	1.8	Whole coal
Particle size	0-0.5mm	4.35	5.33	7.50	8.70	11.37	12.25	23.52
	0.5-1mm	4.35	5.10	6.57	7.90	9.93	11.11	20.93
	1-2mm	4.47	8.78	10.49	11.92	13.46	14.82	24.69
	2-4.75mm	4.47	9.53	12.92	15.16	17.26	18.86	30.97
	4.75-6.7mm	4.47	11.54	15.95	18.40	20.87	22.68	35.84
	6.7-9.5mm	4.47	12.21	16.70	19.11	22.01	23.83	36.52
	9.5-13.2mm	4.47	12.61	17.55	20.23	22.91	25.76	42.11
	Overall	4.45	8.71	12.57	14.92	17.40	19.30	32.73

Table C. 105: Float ash per particle size for impact breakage to 6.7 mm with no attritioning (Run 7-9 average).

		Density interval						
	Float ash	1.3	1.4	1.5	1.6	1.7	1.8	Whole coal
Particle size	0-0.5mm	4.35	5.34	7.22	9.78	11.09	12.50	22.46
	0.5-1mm	4.35	5.17	6.77	8.83	10.35	11.98	20.55
	1-2mm	4.47	8.88	10.64	12.24	13.80	15.32	22.98
	2-4.75mm	4.47	9.80	12.53	14.79	16.76	18.56	28.86
	4.75-6.7mm	4.47	12.23	16.09	18.95	21.51	23.96	37.73
	Overall	4.45	8.92	11.99	14.57	16.71	18.76	30.52

Table C. 106: Float ash per particle size for impact breakage to 6.7 mm with 1 minute attritioning (Run 10).

		Density interval						
	Float ash	1.3	1.4	1.5	1.6	1.7	1.8	Whole coal
Particle size	0-0.5mm	4.35	5.31	5.73	6.55	7.03	7.55	12.62
	0.5-1mm	4.35	5.15	5.68	6.53	7.26	8.11	14.01
	1-2mm	4.47	6.89	9.54	11.50	13.43	15.38	24.14
	2-4.75mm	4.47	7.40	10.94	13.29	15.54	17.64	28.49
	4.75-6.7mm	4.47	9.32	14.17	17.34	19.88	22.61	40.16
	Overall	4.45	6.48	9.09	11.19	13.04	14.92	26.59

Table C. 107: Float ash per particle size for impact breakage to 6.7 mm with 2 minutes attritioning (Run 11).

		Density interval						
	Float ash	1.3	1.4	1.5	1.6	1.7	1.8	Whole coal
Particle size	0-0.5mm	4.35	5.32	6.34	8.62	9.80	11.21	19.98
	0.5-1mm	4.35	5.12	6.19	8.16	9.51	10.99	19.41
	1-2mm	4.47	7.27	9.64	11.41	13.05	14.36	23.37
	2-4.75mm	4.47	8.85	12.45	14.85	17.12	18.55	28.56
	4.75-6.7mm	4.47	10.84	15.56	18.52	21.24	23.08	36.60
	Overall	4.45	7.32	10.42	12.93	15.03	16.58	27.37

Table C. 108: Float ash per particle size for impact breakage to 6.7 mm with 5 minutes attritioning (Run 12).

		Density interval						
	Float ash	1.3	1.4	1.5	1.6	1.7	1.8	Whole coal
Particle size	0-0.5mm	4.35	5.31	5.73	6.54	7.03	7.54	12.61
	0.5-1mm	4.35	5.16	5.69	6.54	7.28	8.12	14.08
	1-2mm	4.47	7.56	10.43	12.17	13.86	15.89	23.65
	2-4.75mm	4.47	8.52	12.79	15.19	17.59	19.88	28.96
	4.75-6.7mm	4.47	10.80	16.36	18.97	22.16	25.23	38.11
	Overall	4.44	6.80	10.03	12.10	14.25	16.39	26.04

Table C. 109: Float ash per particle size for compressive breakage to 13.2 mm with no attritioning (Run 13-15 average).

		Density interval						
	Float ash	1.3	1.4	1.5	1.6	1.7	1.8	Whole coal
Particle size	0-0.5mm	4.35	5.38	7.83	10.52	12.03	12.94	22.77
	0.5-1mm	4.35	5.33	6.75	8.65	10.00	11.18	18.96
	1-2mm	4.47	9.13	10.96	12.15	13.51	14.99	24.32
	2-4.75mm	4.47	9.92	12.95	14.67	16.64	18.50	30.15
	4.75-6.7mm	4.47	11.58	15.42	17.40	19.67	21.54	35.09
	6.7-9.5mm	4.47	12.12	16.42	18.65	21.15	23.51	36.93
	9.5-13.2mm	4.47	12.31	17.13	19.95	22.86	25.31	41.50
	Overall	4.46	8.77	12.32	14.60	16.80	18.72	31.73

Table C. 110: Float ash per particle size for compressive breakage to 13.2 mm with 1 minute attritioning (Run 16).

		Density interval						
	Float ash	1.3	1.4	1.5	1.6	1.7	1.8	Whole coal
Particle size	0-0.5mm	4.35	5.38	7.55	9.27	10.62	11.94	21.60
	0.5-1mm	4.35	5.33	6.69	7.98	9.18	10.27	17.83
	1-2mm	4.47	7.66	10.10	11.50	12.71	14.41	23.39
	2-4.75mm	4.47	9.12	13.07	14.91	16.55	18.61	29.87
	4.75-6.7mm	4.47	11.27	15.82	17.83	19.74	21.80	33.82
	6.7-9.5mm	4.47	12.23	16.94	19.21	21.33	23.41	36.46
	9.5-13.2mm	4.47	12.43	17.29	19.59	21.97	25.35	43.14
	Overall	4.46	8.09	12.23	14.33	16.20	18.39	31.58

Table C. 111: Float ash per particle size for compressive breakage to 13.2 mm with 2 minutes attritioning (Run 17).

		Density interval						
	Float ash	1.3	1.4	1.5	1.6	1.7	1.8	Whole coal
Particle size	0-0.5mm	4.35	5.38	7.66	9.04	10.16	11.13	20.56
	0.5-1mm	4.35	5.35	6.39	7.82	9.34	10.62	19.95
	1-2mm	4.47	8.25	10.86	12.49	14.13	15.65	24.77
	2-4.75mm	4.47	9.45	13.36	15.52	17.85	19.87	31.80
	4.75-6.7mm	4.47	11.09	15.97	18.55	21.22	23.51	36.57
	6.7-9.5mm	4.47	12.17	16.94	19.66	22.16	24.28	38.46
	9.5-13.2mm	4.47	12.54	17.35	20.90	23.68	26.28	43.09
	Overall	4.46	7.95	11.99	14.64	16.97	19.00	32.56

Table C. 112: Float ash per particle size for compressive breakage to 13.2 mm with 5 minutes attritioning (Run 18).

		Density interval						
	Float ash	1.3	1.4	1.5	1.6	1.7	1.8	Whole coal
Particle size	0-0.5mm	4.35	5.38	7.55	9.27	10.62	11.94	21.60
	0.5-1mm	4.35	5.34	6.70	7.98	9.19	10.28	17.84
	1-2mm	4.47	9.60	11.39	12.77	14.25	15.90	25.23
	2-4.75mm	4.47	9.87	13.24	15.37	17.53	19.86	32.05
	4.75-6.7mm	4.47	11.28	15.67	18.08	21.16	23.43	36.78
	6.7-9.5mm	4.47	11.94	17.09	19.41	23.15	25.57	39.23
	9.5-13.2mm	4.47	12.43	17.11	20.25	24.01	26.19	43.11
	Overall	4.46	8.42	12.06	14.43	17.21	19.29	32.71

Table C. 113: Float ash per particle size for compressive breakage to 6.7 mm with no attritioning (Run 19-21 average).

		Density interval						
	Float ash	1.3	1.4	1.5	1.6	1.7	1.8	Whole coal
Particle size	0-0.5mm	4.35	5.38	8.10	10.42	11.95	13.07	23.43
	0.5-1mm	4.35	5.32	7.29	9.24	10.74	11.92	22.35
	1-2mm	4.47	7.42	10.56	12.20	14.16	16.22	28.00
	2-4.75mm	4.47	8.90	13.74	16.17	18.63	21.30	34.81
	4.75-6.7mm	4.47	10.91	16.44	19.49	22.48	25.69	43.84
	Overall	4.46	7.39	11.52	14.05	16.41	18.82	33.48

Table C. 114: Float ash per particle size for compressive breakage to 6.7 mm with 1 minute attritioning (Run 22).

		Density interval						
	Float ash	1.3	1.4	1.5	1.6	1.7	1.8	Whole coal
Particle size	0-0.5mm	4.35	5.39	7.82	9.82	11.09	12.25	22.51
	0.5-1mm	4.35	5.36	7.26	9.03	10.52	11.68	21.37
	1-2mm	4.47	7.61	10.90	12.93	14.77	16.68	26.09
	2-4.75mm	4.47	8.66	13.58	16.36	19.23	21.64	32.86
	4.75-6.7mm	4.47	10.55	16.48	19.18	22.35	24.98	37.63
	Overall	4.47	7.37	11.65	14.21	16.74	18.91	30.25

Table C. 115: Float ash per particle size for compressive breakage to 6.7 mm with 2 minutes attritioning (Run 23).

		Density interval						
	Float ash	1.3	1.4	1.5	1.6	1.7	1.8	Whole coal
Particle size	0-0.5mm	4.35	5.39	6.61	9.38	10.54	12.08	22.12
	0.5-1mm	4.35	5.37	6.45	8.74	9.82	10.69	18.28
	1-2mm	4.47	6.73	9.89	11.83	13.62	15.53	24.35
	2-4.75mm	4.47	7.50	12.49	15.64	18.17	20.54	31.02
	4.75-6.7mm	4.47	9.72	16.35	19.62	22.46	25.01	36.67
	Overall	4.47	6.58	10.54	13.56	15.79	17.92	28.34

Table C. 116: Float ash per particle size for compressive breakage to 6.7 mm with 5 minutes attritioning (Run 24).

		Density interval						
	Float ash	1.3	1.4	1.5	1.6	1.7	1.8	Whole coal
Particle size	0-0.5mm	4.35	5.39	7.81	9.82	11.09	12.24	22.51
	0.5-1mm	4.35	5.36	7.27	9.04	10.53	11.69	21.41
	1-2mm	4.47	7.10	9.67	11.67	13.59	15.23	25.33
	2-4.75mm	4.47	7.85	12.54	15.38	18.02	20.36	31.50
	4.75-6.7mm	4.47	9.59	15.48	18.55	21.62	24.10	37.07
	Overall	4.47	7.02	10.96	13.62	16.03	18.07	29.52

The cumulative float ash and the according float ash per particle size at each relative density interval were plotted, as given in Figure C. 71 and Figure C. 86.

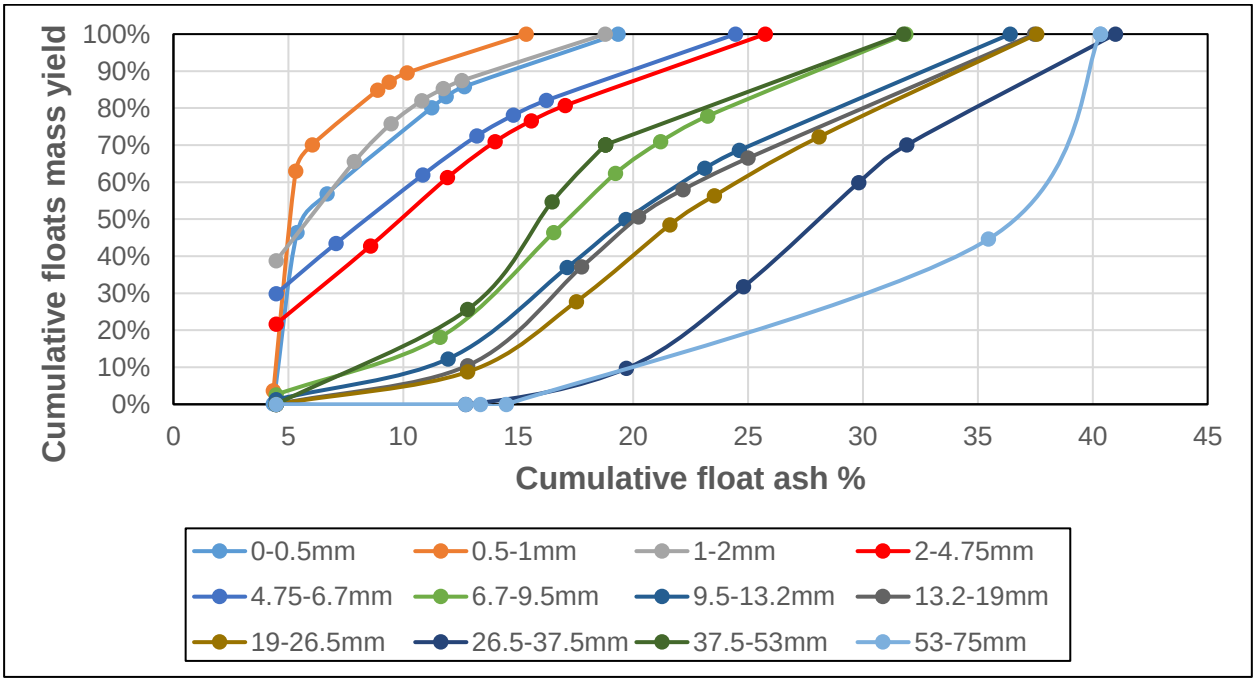

Figure C. 71: Float ash per particle size graph for raw ROM coal.

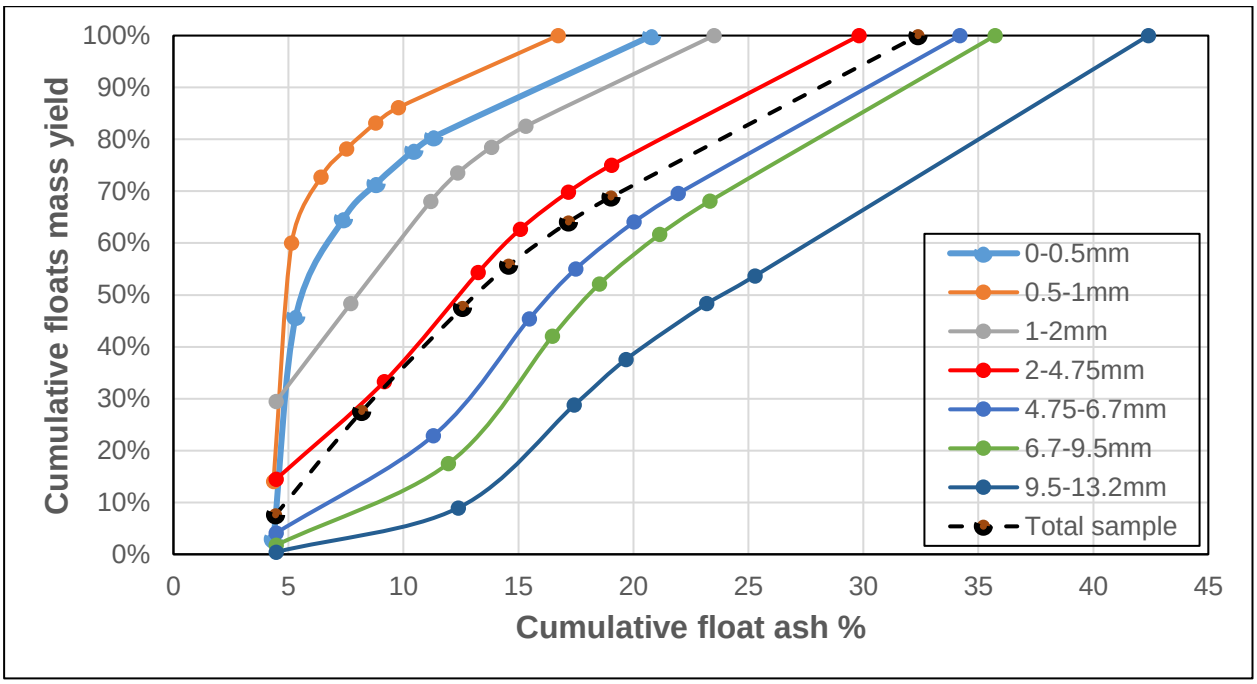

Figure C. 72: Float ash per particle size graph for impact breakage to 13.2 mm with no attritioning (Run 1-3 average).

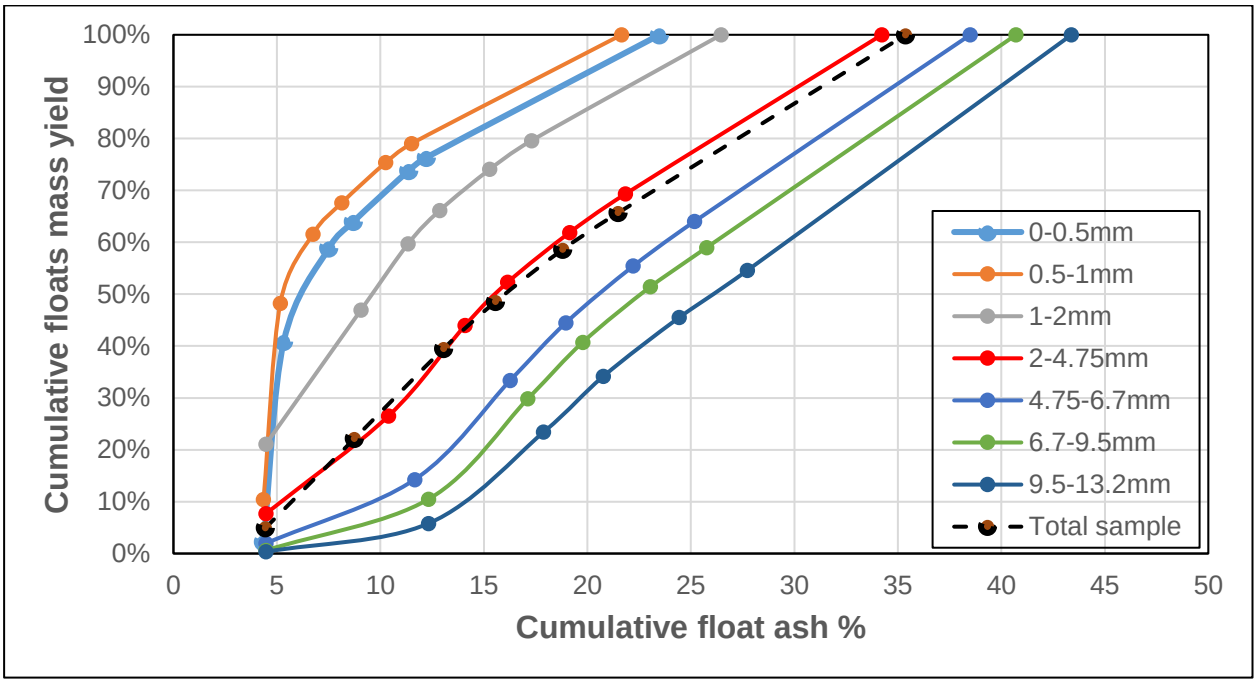

Figure C. 73: Float ash per particle size graph for impact breakage to 13.2 mm with 1 minute attritioning (Run 4).

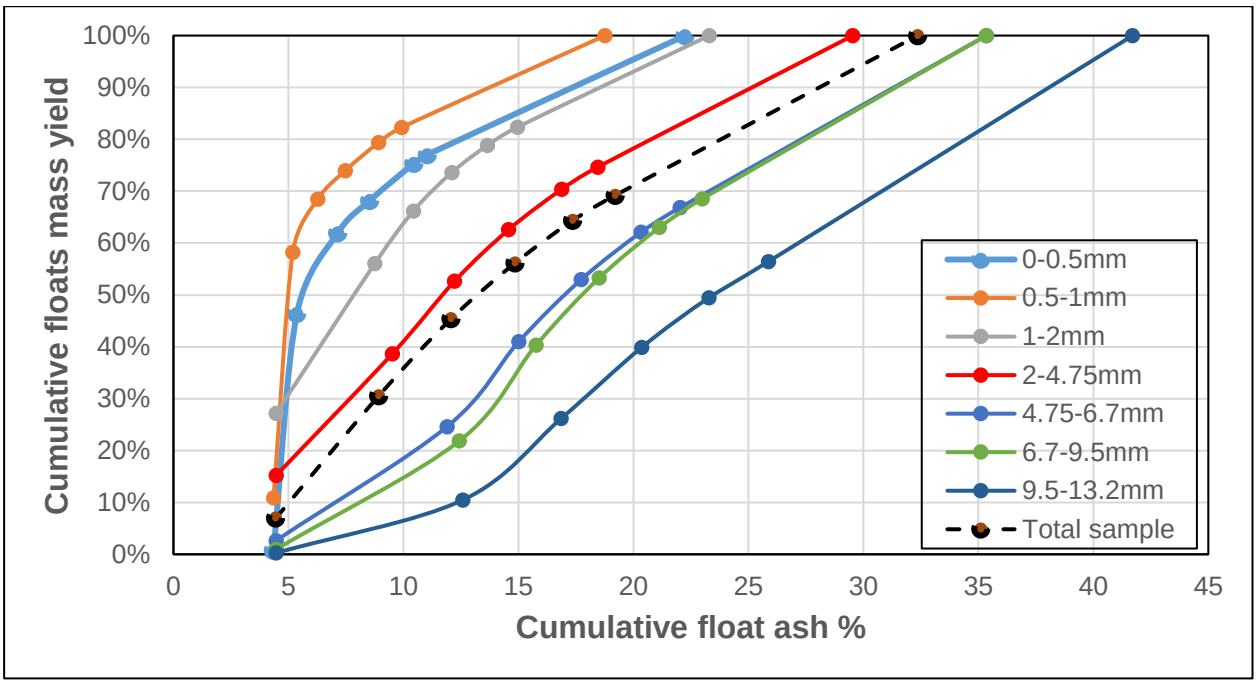

Figure C. 74: Float ash per particle size graph for impact breakage to 13.2 mm with 2 minutes attritioning (Run 5).

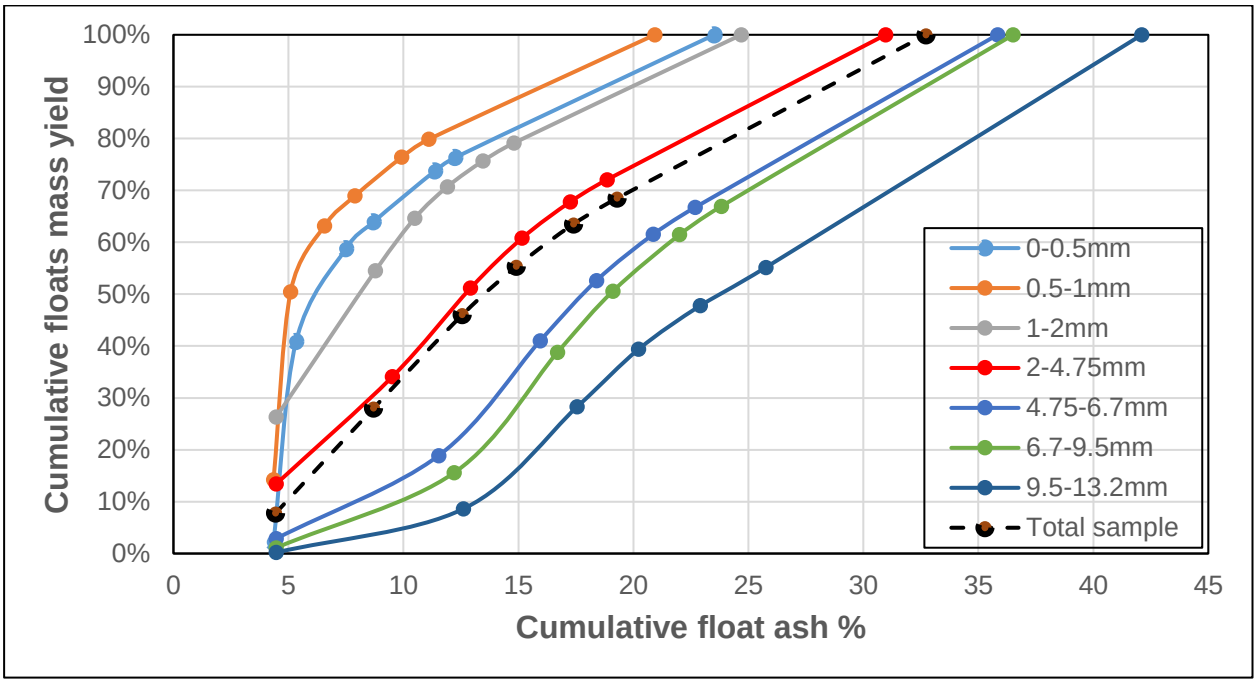

Figure C. 75: Float ash per particle size graph for impact breakage to 13.2 mm with 5 minutes attritioning (Run 6).

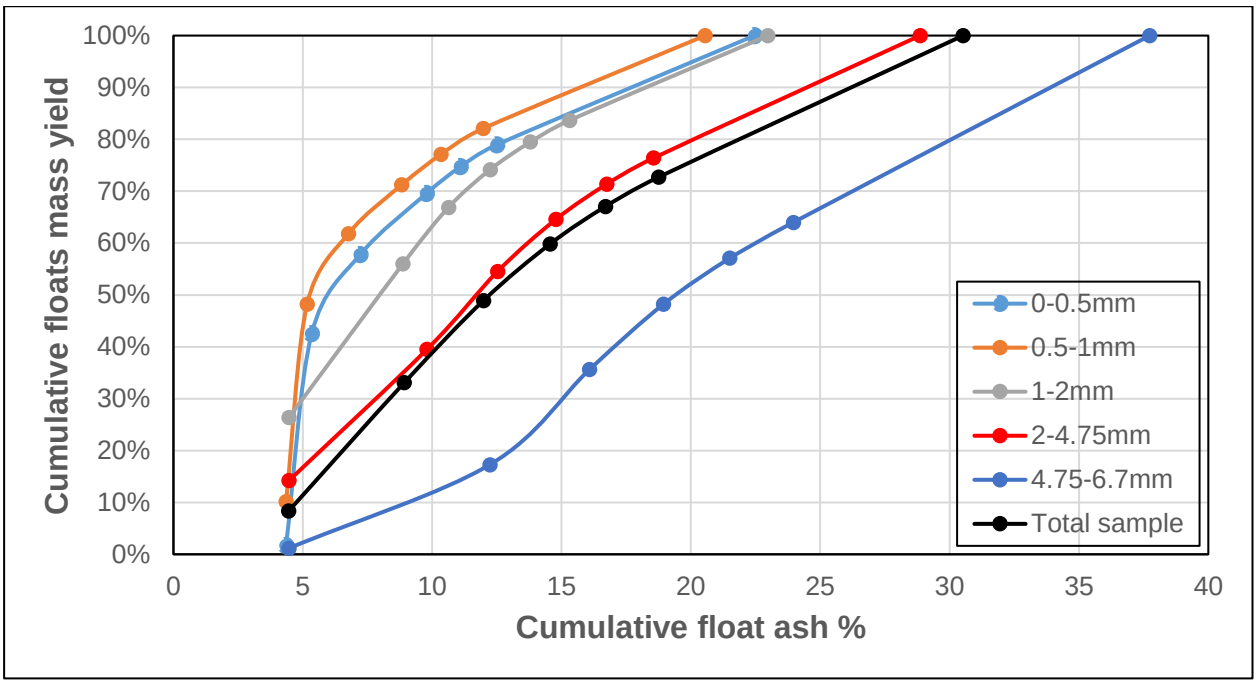

Figure C. 76: Float ash per particle size graph for impact breakage to 6.7 mm with no attritioning (Run 7-9 average).

Note that the float ash per particle size graph for impact breakage to a top size of 6.7 mm with 1 minute attritioning is presented as Figure 4.18.

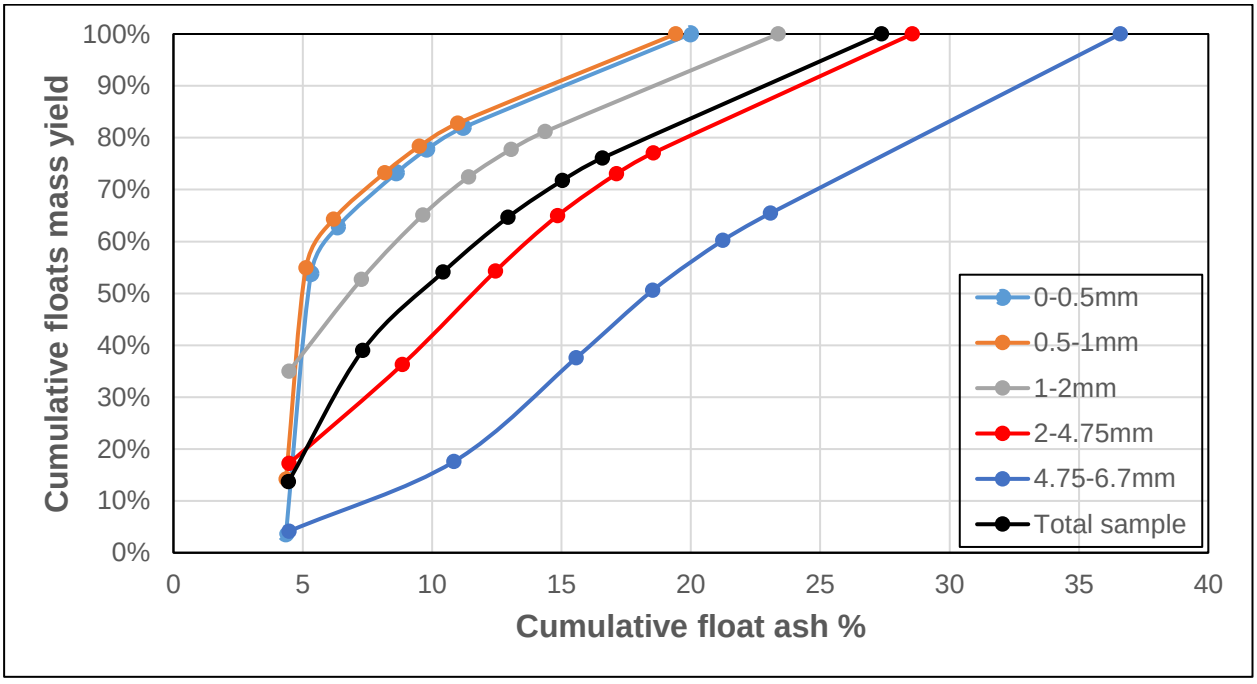

Figure C. 77: Float ash per particle size graph for impact breakage to 6.7 mm with 2 minutes attritioning (Run 11).

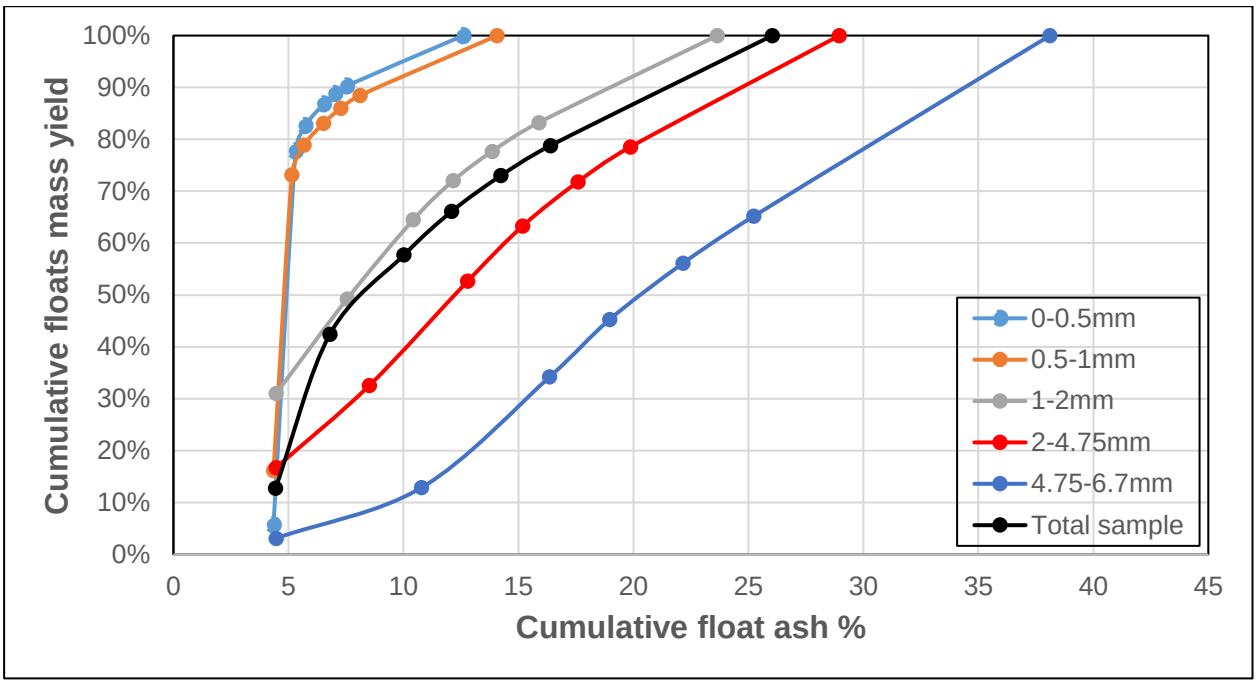

Figure C. 78: Float ash per particle size graph for impact breakage to 6.7 mm with 5 minutes attritioning (Run 12).

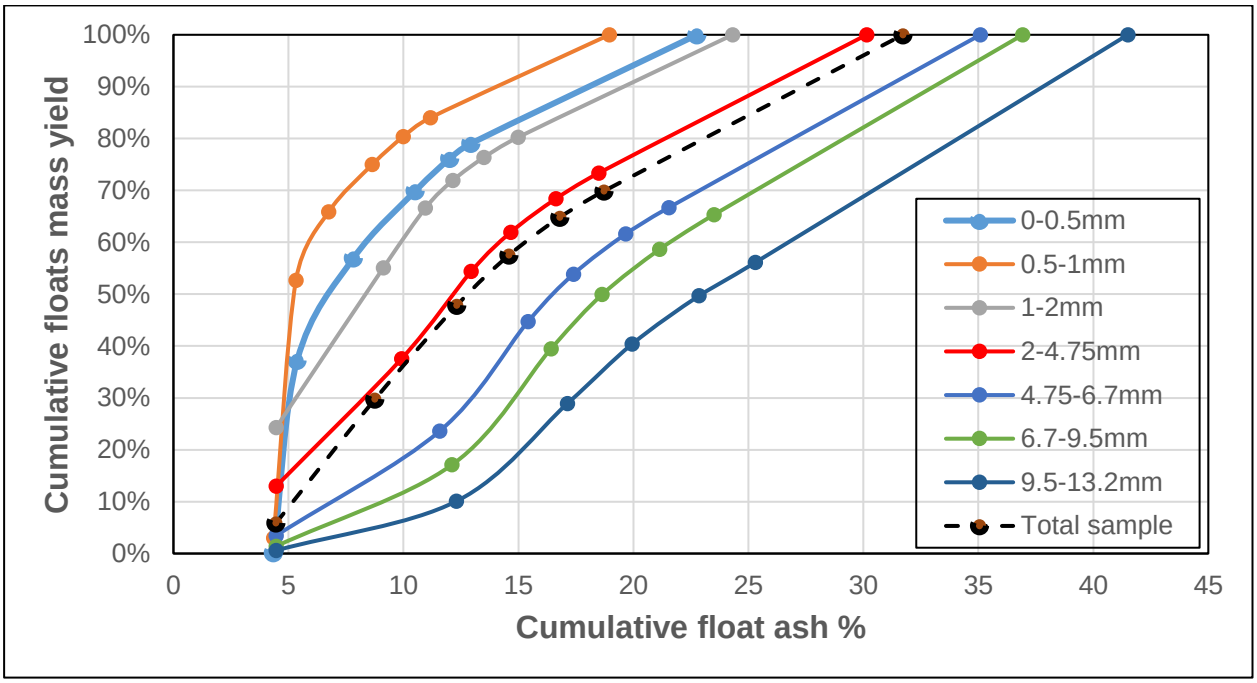

Figure C. 79: Float ash per particle size graph for compressive breakage to 13.2 mm with no attritioning (Run 13-15 average).

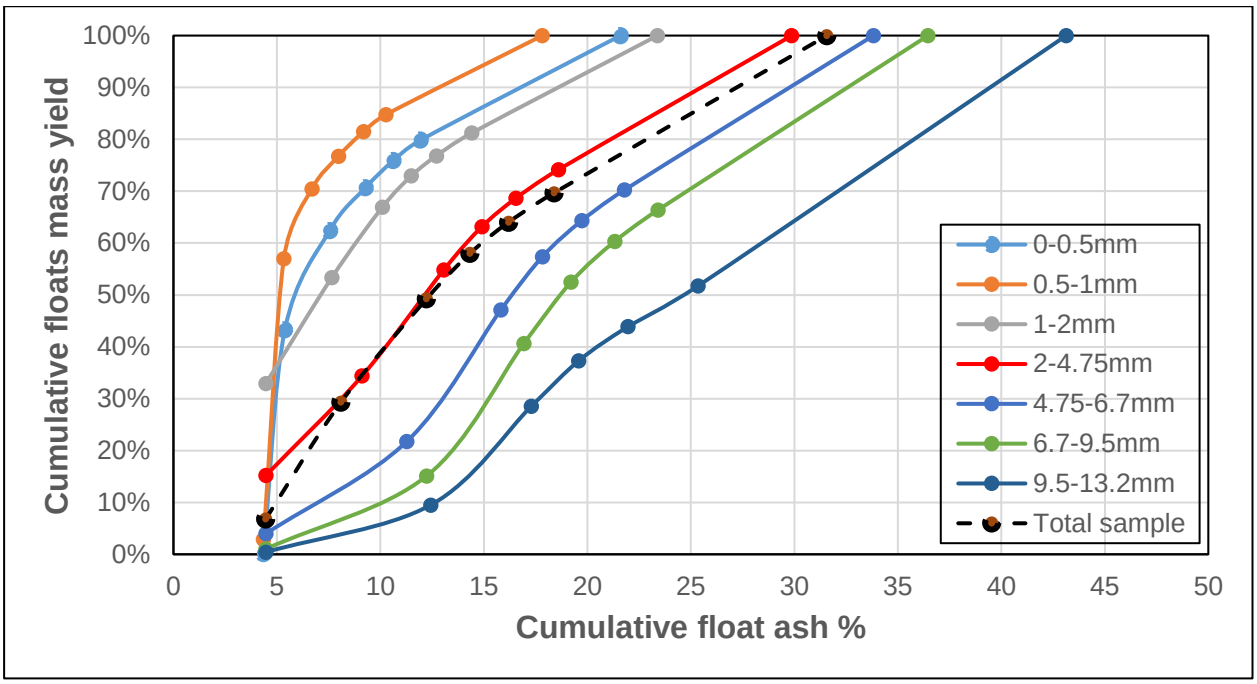

Figure C. 80: Float ash per particle size graph for compressive breakage to 13.2 mm with 1 minute attritioning (Run 16).

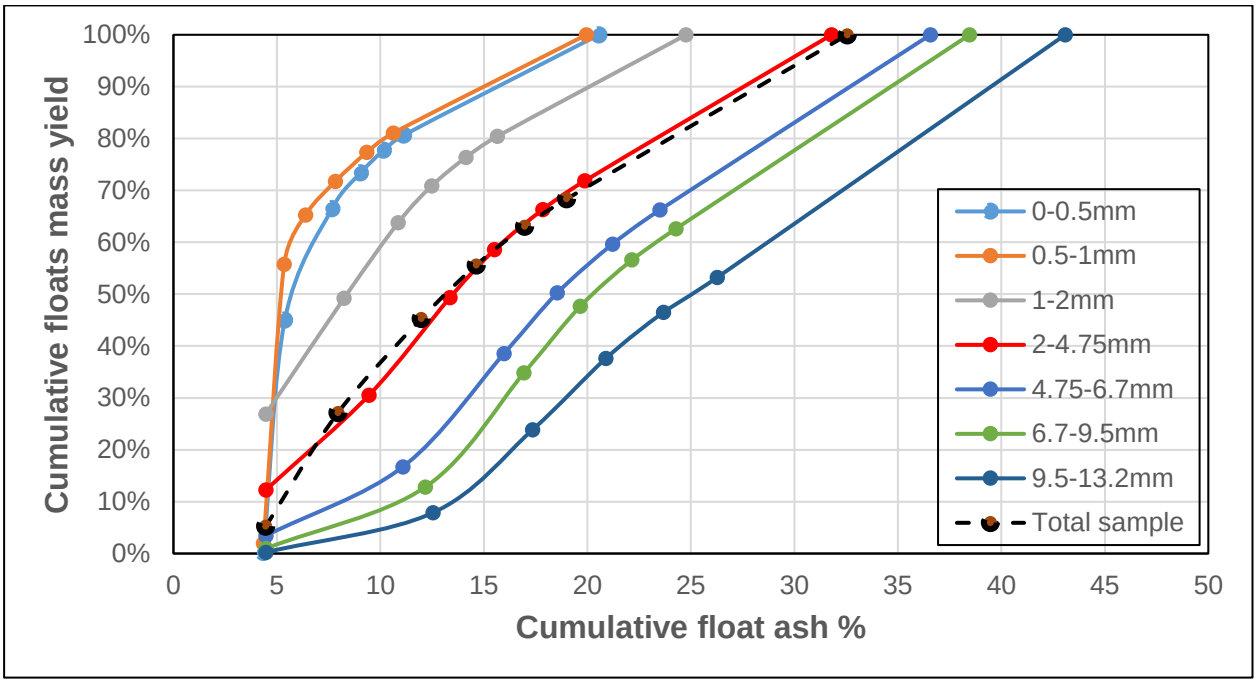

Figure C. 81: Float ash per particle size graph for compressive breakage to 13.2 mm with 2 minutes attritioning (Run 17).

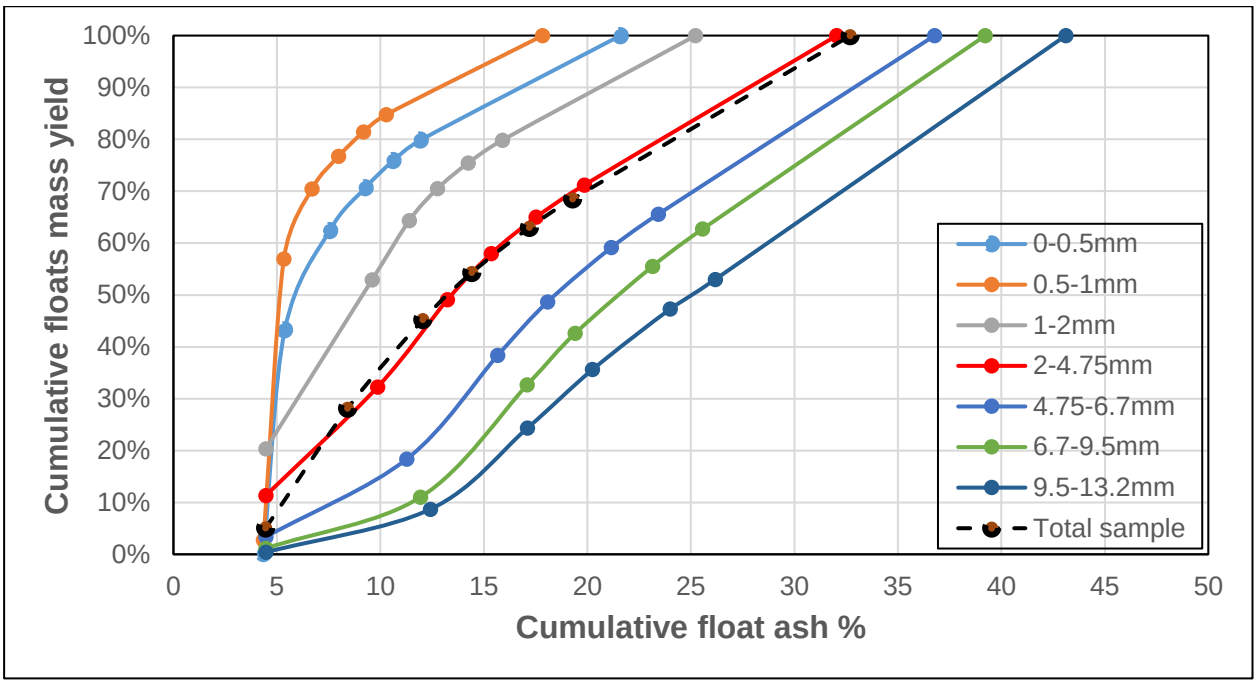

Figure C. 82: Float ash per particle size graph for compressive breakage to 13.2 mm with 5 minutes attritioning (Run 18).

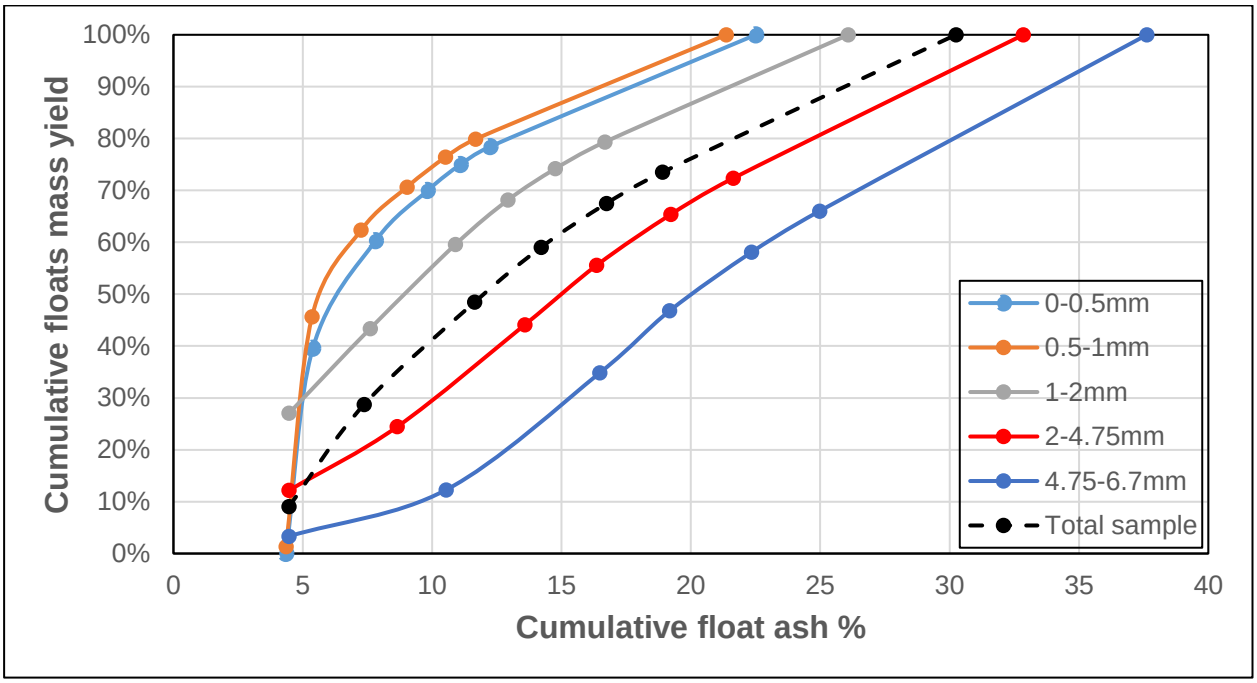

Figure C. 83: Float ash per particle size graph for compressive breakage to 6.7 mm with no attritioning (Run 19-21 average).

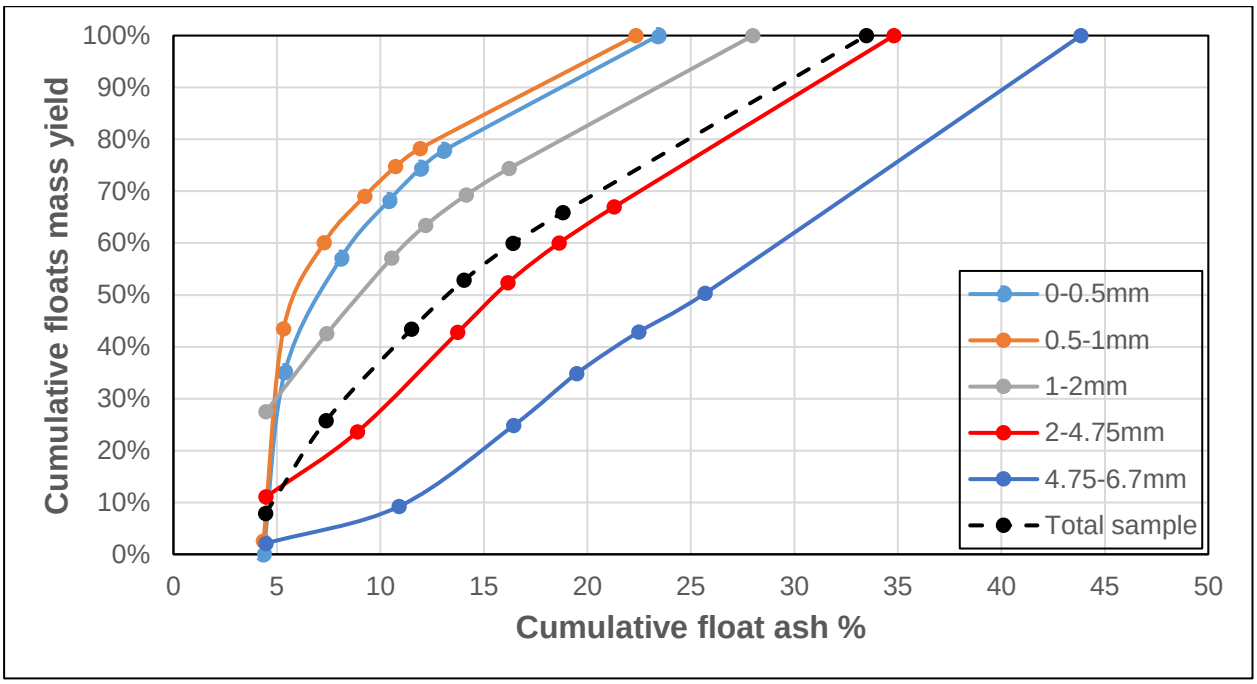

Figure C. 84: Float ash per particle size graph for compressive breakage to 6.7 mm with 1 minute attritioning (Run 22).

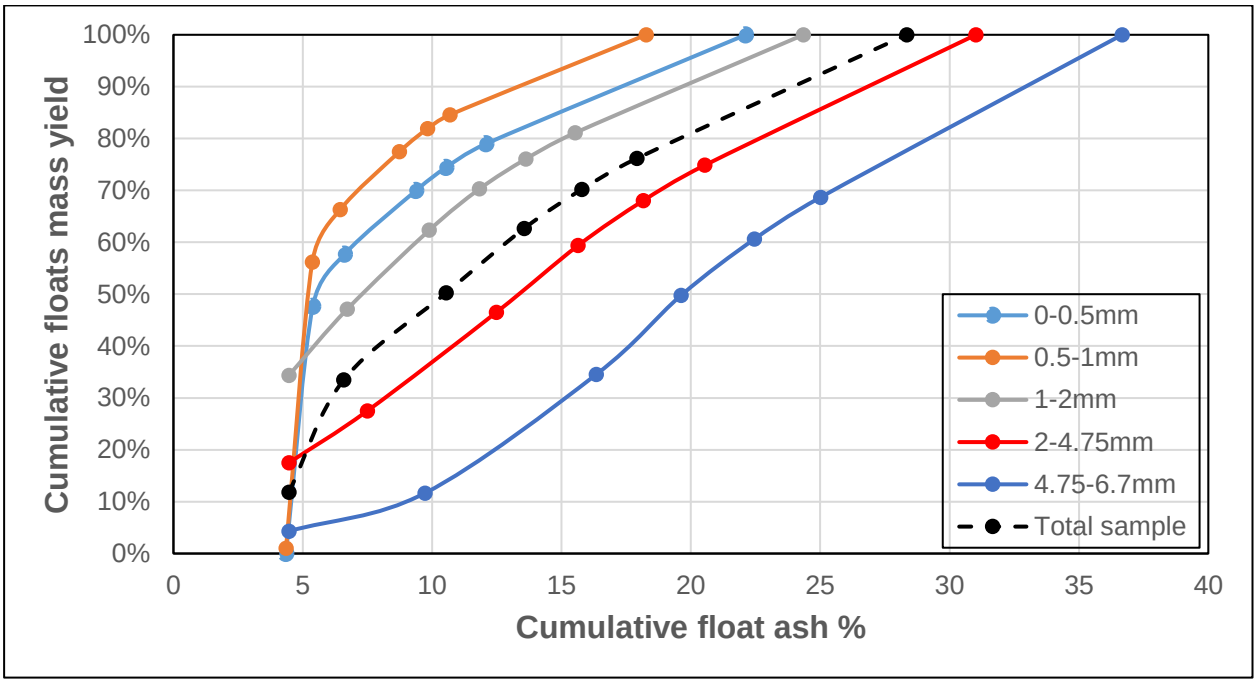

Figure C. 85: Float ash per particle size graph for compressive breakage to 6.7 mm with 2 minutes attritioning (Run 23).

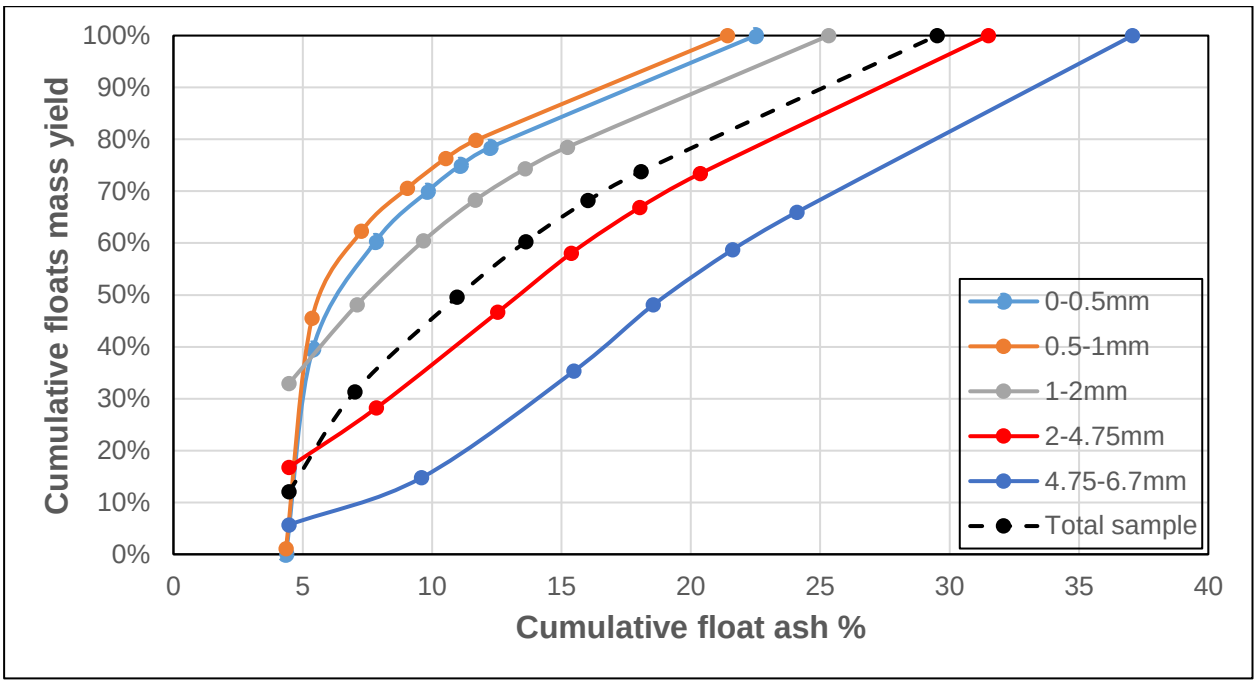

Figure C. 86: Float ash per particle size graph for compressive breakage to 6.7 mm with 5 minutes attritioning (Run 24).

Overall washability:

The overall washability of each sample was analysed by using the float yield and the float ash. The float yield and the float ash for each sample was calculated by using Equation D- 14 and Equation D- 15, and are presented in Table C. 117 to Table C. 133. The cumulative float yield was calculated by cumulatively adding the total fractional mass yield at each RD interval to give a total cumulative float yield of 100% at S1.8.

Table C. 117: Overall washability for raw ROM coal.

	Density interval						
	1.3	1.4	1.5	1.6	1.7	1.8	Whole coal
Float yield	7.0%	25.9%	43.6%	57.8%	68.3%	78.0%	100.0%
Float ash	4.47%	10.56%	14.28%	17.42%	20.18%	23.17%	31.77%

Table C. 118: Overall washability for impact breakage to a top size of 13.2 mm with no attritioning (Run 1-3 average).

	Density interval						
	1.3	1.4	1.5	1.6	1.7	1.8	Whole coal
Float yield	7.6%	27.5%	47.6%	55.7%	64.0%	68.9%	100.0%
Float ash	4.44%	8.19%	12.58%	14.59%	17.18%	19.03%	32.39%

Table C. 119: Overall washability for impact breakage to a top size of 13.2 mm with 1 minute attritioning (Run 4).

	Density interval						
	1.3	1.4	1.5	1.6	1.7	1.8	Whole coal
Float yield	4.9%	22.2%	39.5%	48.5%	58.7%	65.7%	100.0%
Float ash	4.45%	8.76%	13.06%	15.57%	18.82%	21.49%	35.37%

Table C. 120: Overall washability for impact breakage to a top size of 13.2 mm with 2 minutes attritioning (Run 5).

	Density interval						
	1.3	1.4	1.5	1.6	1.7	1.8	Whole coal
Float yield	7.0%	30.6%	45.4%	56.2%	64.4%	69.2%	100.0%
Float ash	4.45%	8.93%	12.08%	14.85%	17.37%	19.21%	32.37%

Table C. 121: Overall washability for impact breakage to a top size of 13.2 mm with 5 minutes attritioning (Run 6).

	Density interval						
	1.3	1.4	1.5	1.6	1.7	1.8	Whole coal
Float yield	7.8%	28.1%	46.0%	55.3%	63.5%	68.5%	100.0%
Float ash	4.45%	8.71%	12.57%	14.92%	17.40%	19.30%	32.73%

Table C. 122: Overall washability for impact breakage to a top size of 6.7 mm with no attritioning (Run 7-9 average).

	Density interval						
	1.3	1.4	1.5	1.6	1.7	1.8	Whole coal
Float yield	8.4%	33.1%	48.9%	59.9%	67.1%	72.7%	100.0%
Float ash	4.45%	8.92%	11.99%	14.57%	16.71%	18.76%	30.52%

Table C. 123: Overall washability for impact breakage to a top size of 6.7 mm with 1 minute attritioning (Run 10).

	Density interval						
	1.3	1.4	1.5	1.6	1.7	1.8	Whole coal
Float yield	17.3%	45.0%	57.1%	65.0%	70.5%	75.2%	100.0%
Float ash	4.45%	6.48%	9.09%	11.19%	13.04%	14.92%	26.59%

Table C. 124: Overall washability for impact breakage to a top size of 6.7 mm with 2 minutes attritioning (Run 11).

	Density interval						
	1.3	1.4	1.5	1.6	1.7	1.8	Whole coal
Float yield	13.7%	39.0%	54.1%	64.7%	71.8%	76.1%	100.0%
Float ash	4.45%	7.32%	10.42%	12.93%	15.03%	16.58%	27.37%

Table C. 125: Overall washability for impact breakage to a top size of 6.7 mm with 5 minutes attritioning (Run 12).

	Density interval						
	1.3	1.4	1.5	1.6	1.7	1.8	Whole coal
Float yield	12.7%	42.4%	57.7%	66.1%	73.0%	78.8%	100.0%
Float ash	4.44%	6.80%	10.03%	12.10%	14.25%	16.39%	26.04%

Table C. 126: Overall washability for compressive breakage to a top size of 13.2 mm with no attritioning (Run 13-15 average).

	Density interval						
	1.3	1.4	1.5	1.6	1.7	1.8	Whole coal
Float yield	5.9%	29.8%	47.8%	57.5%	64.8%	69.9%	100.0%
Float ash	4.46%	8.77%	12.32%	14.60%	16.80%	18.72%	31.73%

Table C. 127: Overall washability for compressive breakage to a top size of 13.2 mm with 1 minute attritioning (Run 16).

	Density interval						
	1.3	1.4	1.5	1.6	1.7	1.8	Whole coal
Float yield	6.8%	29.3%	49.3%	58.0%	64.0%	69.7%	100.0%
Float ash	4.46%	8.09%	12.23%	14.33%	16.20%	18.39%	31.58%

Table C. 128: Overall washability for compressive breakage to a top size of 13.2 mm with 2 minutes attritioning (Run 17).

	Density interval						
	1.3	1.4	1.5	1.6	1.7	1.8	Whole coal
Float yield	5.2%	27.2%	45.3%	55.6%	63.1%	68.4%	100.0%
Float ash	4.46%	7.95%	11.99%	14.64%	16.97%	19.00%	32.56%

Table C. 129: Overall washability for compressive breakage to a top size of 13.2 mm with 5 minutes attritioning (Run 18).

	Density interval						
	1.3	1.4	1.5	1.6	1.7	1.8	Whole coal
Float yield	5.1%	28.2%	45.2%	54.3%	63.0%	68.5%	100.0%
Float ash	4.46%	8.42%	12.06%	14.43%	17.21%	19.29%	32.71%

Table C. 130: Overall washability for compressive breakage to a top size of 6.7 mm with no attritioning (Run 19-21 average).

	Density interval						
	1.3	1.4	1.5	1.6	1.7	1.8	Whole coal
Float yield	7.9%	25.8%	43.4%	52.9%	60.0%	65.9%	100.0%
Float ash	4.46%	7.39%	11.52%	14.05%	16.41%	18.82%	33.48%

Table C. 131: Overall washability for compressive breakage to a top size of 6.7 mm with 1 minute attritioning (Run 22).

	Density interval						
	1.3	1.4	1.5	1.6	1.7	1.8	Whole coal
Float yield	9.1%	28.7%	48.5%	59.0%	67.5%	73.5%	100.0%
Float ash	4.47%	7.37%	11.65%	14.21%	16.74%	18.91%	30.25%

Table C. 132: Overall washability for compressive breakage to a top size of 6.7 mm with 2 minutes attritioning (Run 23).

	Density interval						
	1.3	1.4	1.5	1.6	1.7	1.8	Whole coal
Float yield	11.9%	33.5%	50.2%	62.7%	70.2%	76.2%	100.0%
Float ash	4.47%	6.58%	10.54%	13.56%	15.79%	17.92%	28.34%

Table C. 133: Overall washability for compressive breakage to a top size of 6.7 mm with 5 minutes attritioning (Run 24).

	Density interval						
	1.3	1.4	1.5	1.6	1.7	1.8	Whole coal
Float yield	12.1%	31.3%	49.6%	60.3%	68.2%	73.8%	100.0%
Float ash	4.47%	7.02%	10.96%	13.62%	16.03%	18.07%	29.52%

Figure C. 87 presents the cumulative floats mass yield and the corresponding cumulative float ash yield for raw coal, whilst Figure C. 88 presents the ash curve for compressive breakage to a top size of 13.2 mm.

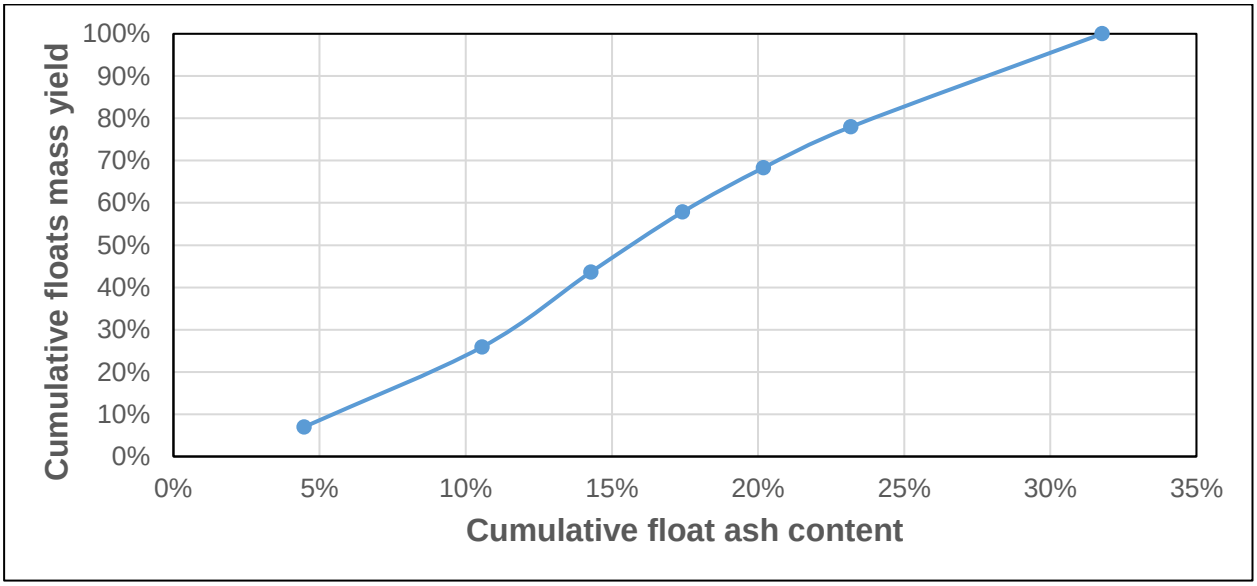

Figure C. 87: Ash curve for raw ROM coal.

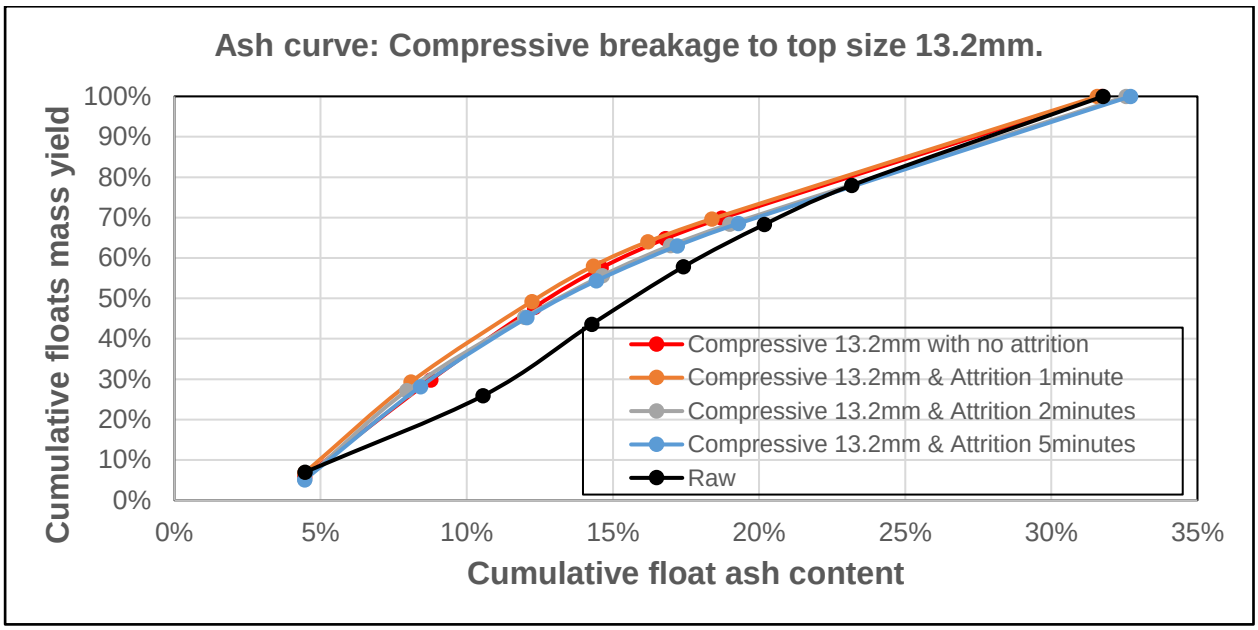

Figure C. 88: Ash curve for compressive breakage to a top size of 13.2 mm.

Liberation:

Liberation of material with a relative density of 1.4 and lower was investigated. Equation D- 16 to Equation D- 19 was used to calculate the data given in Table C. 134 to Table C. 150. The mass liberated refers to the mass of material with a relative density lower than 1.4, whilst the unliberated material refers to the material with a relative density higher than 1.4.

Table C. 134: Liberation curve for raw ROM coal.

Liberation curve (RD<1.4) (liberation is defined by RD lower than 1.4)						
Particle size	Fractional mass (%)	Cumulative fractional yield (%)	Mass liberated (g)	Mass unliberated (g)	% liberated	Cumulative liberation
0.00	0.00%	0.00%	0.00	0.00	0.00%	0.00%
0.50	3.82%	3.82%	234.16	270.91	46.36%	46.36%
1.00	3.75%	7.58%	229.61	134.62	63.04%	53.35%
2.00	4.24%	11.81%	259.50	135.80	65.65%	57.19%
4.75	4.20%	16.01%	257.00	343.50	42.80%	52.56%
6.70	2.72%	18.73%	166.40	217.30	43.37%	50.99%
9.50	1.18%	19.92%	72.50	326.40	18.17%	46.05%
13.20	0.78%	20.70%	47.90	342.00	12.29%	41.71%
19.00	1.18%	21.88%	72.10	616.70	10.47%	35.94%
26.50	0.94%	22.81%	57.30	598.50	8.74%	31.87%
37.50	0.00%	22.81%	0.00	541.50	0.00%	28.36%
53.00	3.08%	25.89%	188.30	547.40	25.59%	28.00%
75.00	0.00%	25.89%	0.00	462.40	0.00%	25.89%

Table C. 135: Liberation curve for impact breakage to a top size of 13.2 mm with no attritioning (Run 1-3 average).

Liberation curve (RD<1.4) (liberation is defined by RD lower than 1.4)						
Particle size	Fractional mass (%)	Cumulative fractional yield (%)	Mass liberated (g)	Mass unliberated (g)	% liberated	Cumulative liberation
0.00	0.00%	0.00%	0.00	0.00	0.00%	0.00%
0.50	4.58%	4.58%	283.29	334.16	45.88%	45.88%
1.00	5.59%	10.17%	345.53	229.92	60.05%	52.71%
2.00	4.77%	14.94%	295.00	314.33	48.41%	51.26%
4.75	5.46%	20.40%	337.53	673.83	33.37%	44.83%
6.70	2.00%	22.40%	123.90	416.57	22.92%	41.30%
9.50	2.17%	24.57%	134.27	631.70	17.53%	36.88%
13.20	2.99%	27.56%	184.83	1879.30	8.95%	27.56%

Table C. 136: Liberation curve for impact breakage to a top size of 13.2 mm with 1 minute attritioning (Run 4).

Liberation curve (RD<1.4) (liberation is defined by RD lower than 1.4)						
Particle size	Fractional mass (%)	Cumulative fractional yield (%)	Mass liberated (g)	Mass unliberated (g)	% liberated	Cumulative liberation
0.00	0.00%	0.00%	0.00	0.00	0.00%	0.00%
0.50	4.20%	4.20%	257.58	373.04	40.85%	40.85%
1.00	3.29%	7.49%	201.66	216.62	48.21%	43.78%
2.00	4.74%	12.23%	290.90	328.90	46.93%	44.95%
4.75	4.98%	17.21%	305.30	844.90	26.54%	37.44%
6.70	1.66%	18.87%	102.10	615.70	14.22%	32.73%
9.50	1.91%	20.78%	117.10	1001.80	10.47%	27.38%
13.20	1.41%	22.19%	86.20	1391.10	5.83%	22.19%

Table C. 137: Liberation curve for impact breakage to a top size of 13.2 mm with 2 minutes attritioning (Run 5).

Liberation curve (RD<1.4) (liberation is defined by RD lower than 1.4)						
Particle size	Fractional mass (%)	Cumulative fractional yield (%)	Mass liberated (g)	Mass unliberated (g)	% liberated	Cumulative liberation
0.00	0.00%	0.00%	0.00	0.00	0.00%	0.00%
0.50	4.77%	4.77%	286.62	330.91	46.41%	46.41%
1.00	4.22%	8.98%	253.59	181.89	58.23%	51.30%
2.00	6.04%	15.02%	363.30	284.20	56.11%	53.13%
4.75	6.81%	21.83%	409.40	649.30	38.67%	47.58%
6.70	2.49%	24.33%	150.00	458.90	24.63%	43.43%
9.50	3.14%	27.47%	189.10	675.00	21.88%	39.03%
13.20	3.11%	30.58%	187.00	1594.50	10.50%	30.58%

Table C. 138: Liberation curve for impact breakage to a top size of 13.2 mm with 5 minutes attritioning (Run 6).

Liberation curve (RD<1.4) (liberation is defined by RD lower than 1.4)						
Particle size	Fractional mass (%)	Cumulative fractional yield (%)	Mass liberated (g)	Mass unliberated (g)	% liberated	Cumulative liberation
0.00	0.00%	0.00%	0.00	0.00	0.00%	0.00%
0.50	4.28%	4.28%	257.58	373.04	40.85%	40.85%
1.00	3.66%	7.94%	220.14	216.62	50.40%	44.76%
2.00	7.17%	15.12%	431.30	359.20	54.56%	48.93%
4.75	6.57%	21.68%	394.80	761.50	34.14%	43.26%
6.70	1.97%	23.66%	118.60	508.30	18.92%	39.07%
9.50	2.26%	25.91%	135.70	735.00	15.59%	34.53%
13.20	2.16%	28.07%	129.80	1371.60	8.65%	28.07%

Table C. 139: Liberation curve for impact breakage to a top size of 6.7 mm with no attritioning (Run 7-9 average).

Liberation curve (RD<1.4) (liberation is defined by RD lower than 1.4)						
Particle size	Fractional mass (%)	Cumulative fractional yield (%)	Mass liberated (g)	Mass unliberated (g)	% liberated	Cumulative liberation
0.00	0.00%	0.00%	0.00	0.00	0.00%	0.00%
0.50	5.21%	5.21%	316.77	426.73	42.60%	42.60%
1.00	3.69%	8.89%	224.29	240.75	48.23%	44.77%
2.00	7.80%	16.69%	474.23	371.43	56.08%	49.42%
4.75	8.82%	25.51%	536.73	822.17	39.50%	45.47%
6.70	7.60%	33.11%	462.07	2207.90	17.31%	33.11%

Table C. 140: Liberation curve for impact breakage to a top size of 6.7 mm with 1 minute attritioning (Run 10).

Liberation curve (RD<1.4) (liberation is defined by RD lower than 1.4)						
Particle size	Fractional mass (%)	Cumulative fractional yield (%)	Mass liberated (g)	Mass unliberated (g)	% liberated	Cumulative liberation
0.00	0.00%	0.00%	0.00	0.00	0.00%	0.00%
0.50	14.04%	14.04%	908.43	260.50	77.71%	77.71%
1.00	7.57%	21.61%	490.00	178.37	73.31%	76.11%
2.00	6.98%	28.60%	451.90	464.80	49.30%	67.19%
4.75	11.88%	40.48%	768.90	1236.20	38.35%	55.04%
6.70	4.53%	45.01%	292.80	1418.40	17.11%	45.01%

Table C. 141: Liberation curve for impact breakage to a top size of 6.7 mm with 2 minutes attritioning (Run 11).

Liberation curve (RD<1.4) (liberation is defined by RD lower than 1.4)						
Particle size	Fractional mass (%)	Cumulative fractional yield (%)	Mass liberated (g)	Mass unliberated (g)	% liberated	Cumulative liberation
0.00	0.00%	0.00%	0.00	0.00	0.00%	0.00%
0.50	9.96%	9.96%	572.99	492.29	53.79%	53.79%
1.00	5.58%	15.54%	320.83	263.79	54.88%	54.17%
2.00	8.34%	23.88%	479.90	431.50	52.66%	53.63%
4.75	10.42%	34.30%	599.20	1051.90	36.29%	46.84%
6.70	4.70%	39.00%	270.40	1269.50	17.56%	39.00%

Table C. 142: Liberation curve for impact breakage to a top size of 6.7 mm with 5 minutes attritioning (Run 12).

Liberation curve (RD<1.4) (liberation is defined by RD lower than 1.4)						
Particle size	Fractional mass (%)	Cumulative fractional yield (%)	Mass liberated (g)	Mass unliberated (g)	% liberated	Cumulative liberation
0.00	0.00%	0.00%	0.00	0.00	0.00%	0.00%
0.50	14.85%	14.85%	908.43	260.50	77.71%	77.71%
1.00	7.95%	22.80%	486.02	178.37	73.15%	76.06%
2.00	6.91%	29.71%	423.00	435.20	49.29%	67.52%
4.75	9.11%	38.82%	557.40	1153.50	32.58%	53.94%
6.70	3.61%	42.43%	220.80	1494.00	12.88%	42.43%

Table C. 143: Liberation curve for compressive breakage to a top size of 13.2 mm with no attritioning (Run 13-15 average).

Liberation curve (RD<1.4) (liberation is defined by RD lower than 1.4)						
Particle size	Fractional mass (%)	Cumulative fractional yield (%)	Mass liberated (g)	Mass unliberated (g)	% liberated	Cumulative liberation
0.00	0.00%	0.00%	0.00	0.00	0.00%	0.00%
0.50	4.80%	4.80%	270.39	455.69	37.24%	37.24%
1.00	5.08%	9.89%	286.04	256.28	52.74%	43.87%
2.00	5.69%	15.58%	320.17	261.33	55.06%	47.39%
4.75	6.85%	22.42%	385.33	641.20	37.54%	43.87%
6.70	2.32%	24.75%	130.83	422.23	23.66%	40.61%
9.50	2.67%	27.42%	150.17	727.43	17.11%	35.82%
13.20	2.37%	29.79%	133.30	1187.33	10.09%	29.79%

Table C. 144: Liberation curve for compressive breakage to a top size of 13.2 mm with 1 minute attritioning (Run 16).

Liberation curve (RD<1.4) (liberation is defined by RD lower than 1.4)						
Particle size	Fractional mass (%)	Cumulative fractional yield (%)	Mass liberated (g)	Mass unliberated (g)	% liberated	Cumulative liberation
0.00	0.00%	0.00%	0.00	0.00	0.00%	0.00%
0.50	5.70%	5.70%	342.27	448.36	43.29%	43.29%
1.00	5.54%	11.24%	333.01	250.76	57.04%	49.13%
2.00	5.23%	16.47%	313.90	274.00	53.39%	50.41%
4.75	5.97%	22.44%	358.90	684.00	34.41%	44.86%
6.70	2.18%	24.62%	130.70	470.90	21.73%	41.00%
9.50	2.48%	27.10%	149.00	837.30	15.11%	35.44%
13.20	2.23%	29.33%	134.20	1279.70	9.49%	29.33%

Table C. 145: Liberation curve for compressive breakage to a top size of 13.2 mm with 2 minutes attritioning (Run 17).

Liberation curve (RD<1.4) (liberation is defined by RD lower than 1.4)						
Particle size	Fractional mass (%)	Cumulative fractional yield (%)	Mass liberated (g)	Mass unliberated (g)	% liberated	Cumulative liberation
0.00	0.00%	0.00%	0.00	0.00	0.00%	0.00%
0.50	7.01%	7.01%	441.45	538.99	45.03%	45.03%
1.00	5.09%	12.11%	320.54	254.22	55.77%	49.00%
2.00	4.50%	16.61%	283.40	292.40	49.22%	49.06%
4.75	5.00%	21.61%	314.70	715.10	30.56%	43.03%
6.70	1.60%	23.20%	100.50	501.30	16.70%	38.82%
9.50	2.10%	25.31%	132.30	901.60	12.80%	33.21%
13.20	1.88%	27.18%	118.10	1379.70	7.88%	27.18%

Table C. 146: Liberation curve for compressive breakage to a top size of 13.2 mm with 5 minutes attritioning (Run 18).

Liberation curve (RD<1.4) (liberation is defined by RD lower than 1.4)						
Particle size	Fractional mass (%)	Cumulative fractional yield (%)	Mass liberated (g)	Mass unliberated (g)	% liberated	Cumulative liberation
0.00	0.00%	0.00%	0.00	0.00	0.00%	0.00%
0.50	5.69%	5.69%	342.27	448.36	43.29%	43.29%
1.00	5.52%	11.21%	332.09	250.76	56.98%	49.10%
2.00	5.56%	16.78%	334.60	297.50	52.93%	50.31%
4.75	5.82%	22.60%	350.10	733.80	32.30%	43.99%
6.70	1.85%	24.46%	111.50	496.10	18.35%	39.78%
9.50	1.72%	26.18%	103.60	840.40	10.97%	33.92%
13.20	1.98%	28.16%	119.30	1252.80	8.69%	28.16%

Table C. 147: Liberation curve for compressive breakage to a top size of 6.7 mm with no attritioning (Run 19-21 average).

Liberation curve (RD<1.4) (liberation is defined by RD lower than 1.4)						
Particle size	Fractional mass (%)	Cumulative fractional yield (%)	Mass liberated (g)	Mass unliberated (g)	% liberated	Cumulative liberation
0.00	0.00%	0.00%	0.00	0.00	0.00%	0.00%
0.50	5.40%	5.40%	330.52	607.68	35.23%	35.23%
1.00	4.86%	10.26%	297.54	385.89	43.54%	38.73%
2.00	5.60%	15.86%	343.10	462.57	42.59%	40.01%
4.75	7.18%	23.05%	439.93	1421.30	23.64%	32.90%
6.70	2.78%	25.82%	170.03	1664.57	9.27%	25.82%

Table C. 148: Liberation curve for compressive breakage to a top size of 6.7 mm with 1 minute attritioning (Run 22).

Liberation curve (RD<1.4) (liberation is defined by RD lower than 1.4)						
Particle size	Fractional mass (%)	Cumulative fractional yield (%)	Mass liberated (g)	Mass unliberated (g)	% liberated	Cumulative liberation
0.00	0.00%	0.00%	0.00	0.00	0.00%	0.00%
0.50	6.16%	6.16%	368.72	562.50	39.60%	39.60%
1.00	4.84%	11.00%	290.14	345.25	45.66%	42.06%
2.00	6.33%	17.33%	378.90	494.30	43.39%	42.53%
4.75	8.33%	25.65%	498.70	1539.80	24.46%	34.31%
6.70	3.09%	28.74%	185.30	1326.20	12.26%	28.74%

Table C. 149: Liberation curve for compressive breakage to a top size of 6.7 mm with 2 minutes attritioning (Run 23).

Liberation curve (RD<1.4) (liberation is defined by RD lower than 1.4)						
Particle size	Fractional mass (%)	Cumulative fractional yield (%)	Mass liberated (g)	Mass unliberated (g)	% liberated	Cumulative liberation
0.00	0.00%	0.00%	0.00	0.00	0.00%	0.00%
0.50	8.15%	8.15%	499.02	547.26	47.69%	47.69%
1.00	6.74%	14.89%	412.77	321.45	56.22%	51.21%
2.00	6.45%	21.34%	395.30	443.10	47.15%	49.91%
4.75	9.49%	30.83%	581.00	1530.70	27.51%	39.91%
6.70	2.65%	33.48%	162.60	1231.50	11.66%	33.48%

Table C. 150: Liberation curve for compressive breakage to a top size of 6.7 mm with 5 minutes attritioning (Run 24).

Liberation curve (RD<1.4) (liberation is defined by RD lower than 1.4)						
Particle size	Fractional mass (%)	Cumulative fractional yield (%)	Mass liberated (g)	Mass unliberated (g)	% liberated	Cumulative liberation
0.00	0.00%	0.00%	0.00	0.00	0.00%	0.00%
0.50	6.17%	6.17%	368.72	562.50	39.60%	39.60%
1.00	4.83%	11.01%	288.84	345.25	45.55%	42.01%
2.00	6.57%	17.57%	392.30	422.40	48.15%	44.11%
4.75	10.23%	27.81%	611.40	1555.80	28.21%	36.53%
6.70	3.53%	31.33%	210.70	1216.30	14.77%	31.33%

The cumulative yield of liberated material (RD<1.4) was plotted against particle size, as given in Figure C. 89 for that of raw coal.

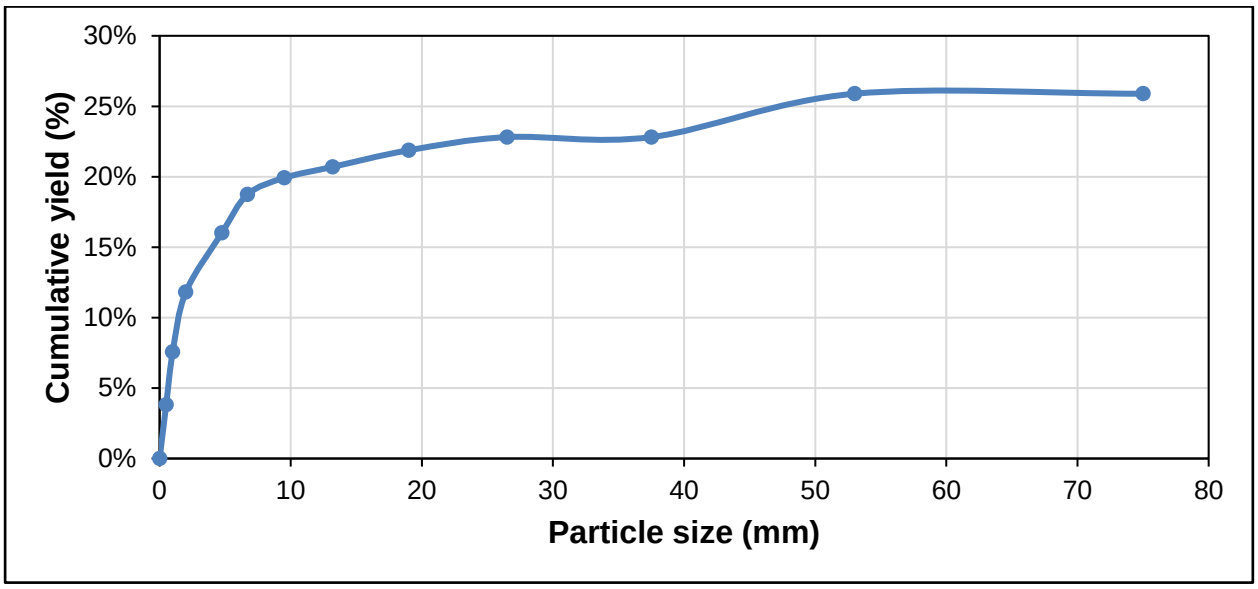

Figure C. 89: Liberation curve (RD<1.4) for raw ROM coal.

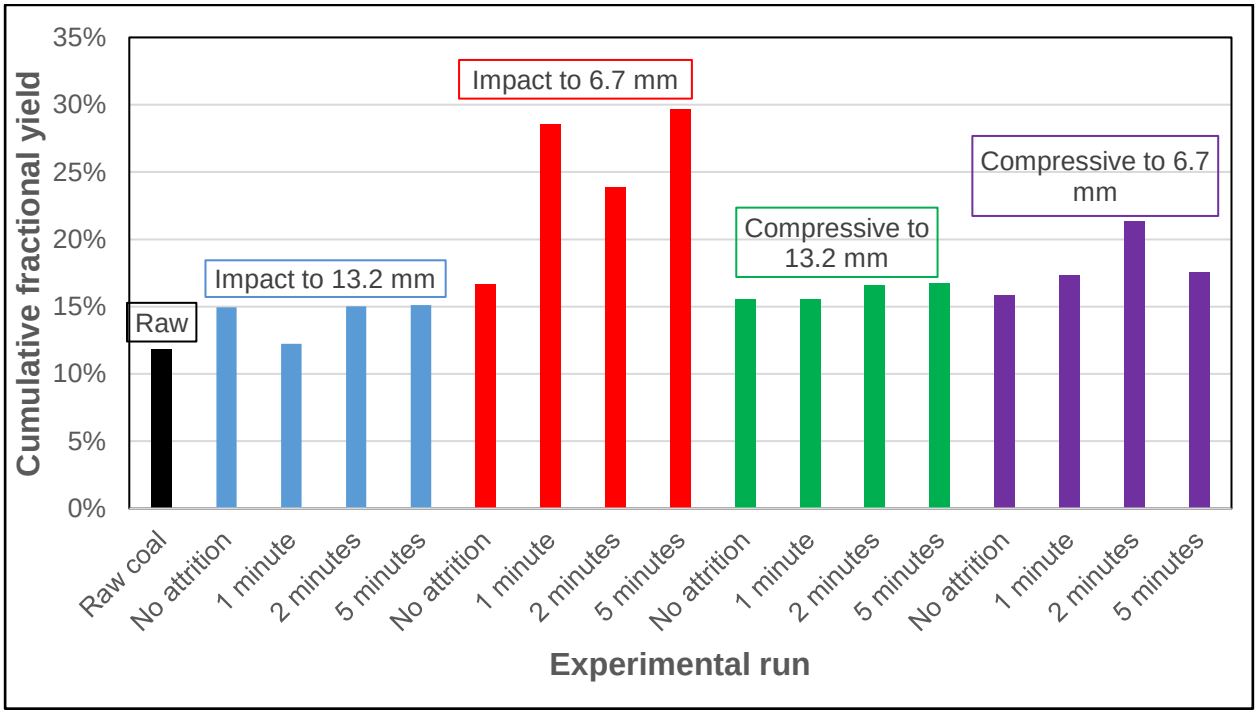

Figure C. 90: Cumulative fractional yield of liberated coal macerals (with RD<1.4) and within the particle size interval of 0-2 mm.

Hypothetical density wash:

A hypothetical ash yield of 10 % was specified. The overall cumulative yield and required overall hypothetical density for a specific target ash was projected using Excel's forecast function by using the cumulative float ash and cumulative float yield. The cumulative float yield for an overall hypothetical density at each particle size interval was also calculated using this method, as well as the cumulative float yield and float ash per particle size. The data is presented in Table C. 151 to Table C. 168.

Table C. 151: Overall hypothetical ash for raw ROM coal (continue on next page).

Overall									
Cumulative float ash	4.47%	10.56%	14.28%	17.42%	20.18%	23.17%		31.77%	Target ash	10%
Cumulative float yield	6.98%	25.89%	43.62%	57.83%	68.30%	77.97%		100.00%	Cumulative yield	24.2%
RD	1.3	1.4	1.5	1.6	1.7	1.8	Whole coal		Required RD	1.39
For 0-0.5 mm (for an overall hypothetical density, how much will the yield be at particle size 0-0.5mm?										
Cumulative float ash	4.35%	5.38%	6.69%	11.24%	11.87%	12.66%		19.35%		
Cumulative float yield	0.12%	46.37%	56.90%	80.15%	83.17%	85.84%		100.00%	Cumulative yield	42.1%
RD	1.3	1.4	1.5	1.6	1.7	1.8	Whole coal		Required RD	1.39
For 0.5-1 mm (for an overall hypothetical density, how much will the yield be at particle size 0.5-1mm?										
Cumulative float ash	4.35%	5.33%	6.04%	8.89%	9.39%	10.17%		15.35%		
Cumulative float yield	3.70%	63.03%	70.08%	84.87%	87.06%	89.58%		100.00%	Cumulative yield	57.6%
RD	1.3	1.4	1.5	1.6	1.7	1.8	Whole coal		Required RD	1.39
For 1-2 mm (for an overall hypothetical density, how much will the yield be at particle size 1-2mm?										
Cumulative float ash	4.47%	7.88%	9.47%	10.80%	11.75%	12.55%		18.79%		
Cumulative float yield	38.76%	65.58%	75.81%	82.02%	85.27%	87.44%		100.00%	Cumulative yield	63.1%
RD	1.3	1.4	1.5	1.6	1.7	1.8	Whole coal		Required RD	1.39
For 2-4.75 mm (for an overall hypothetical density, how much will the yield be at particle size 2-4.75mm?										
Cumulative float ash	4.47%	8.58%	11.93%	13.99%	15.57%	17.05%		25.75%		
Cumulative float yield	21.71%	42.81%	61.26%	70.95%	76.55%	80.73%		100.00%	Cumulative yield	40.9%
RD	1.3	1.4	1.5	1.6	1.7	1.8	Whole coal		Required RD	1.39
For 4.75-6.7 mm (for an overall hypothetical density, how much will the yield be at particle size 4.75-6.7mm?										
Cumulative float ash	4.47%	7.07%	10.85%	13.21%	14.80%	16.23%		24.46%		
Cumulative float yield	29.87%	43.45%	61.98%	72.52%	78.12%	82.11%		100.00%	Cumulative yield	42.2%
RD	1.3	1.4	1.5	1.6	1.7	1.8	Whole coal		Required RD	1.39
For 6.7-9.5 mm (for an overall hypothetical density, how much will the yield be at particle size 6.7-9.5mm?										
Cumulative float ash	4.47%	11.60%	16.55%	19.24%	21.20%	23.25%		31.87%		
Cumulative float yield	2.61%	18.13%	46.39%	62.37%	70.97%	77.88%		100.00%	Cumulative yield	16.7%
RD	1.3	1.4	1.5	1.6	1.7	1.8	Whole coal		Required RD	1.39
For 9.5-13.2 mm (for an overall hypothetical density, how much will the yield be at particle size 9.5-13.2mm?										
Cumulative float ash	4.47%	11.95%	17.14%	19.70%	23.13%	24.63%		36.41%		
Cumulative float yield	1.26%	12.28%	37.01%	49.92%	63.78%	68.66%		100.00%	Cumulative yield	11.3%
RD	1.3	1.4	1.5	1.6	1.7	1.8	Whole coal		Required RD	1.39

Table C. 152: Overall hypothetical ash for raw ROM coal (continued from previous page).

For 13.2-19 mm (for an overall hypothetical density, how much will the yield be at particle size 13.2-19mm?									
Cumulative float ash	4.47%	12.80%	17.76%	20.24%	22.18%	25.01%	37.47%		
Cumulative float yield	0.00%	10.48%	37.12%	50.62%	57.99%	66.52%	100.00%	Cumulative yield	9.5%
RD	1.3	1.4	1.5	1.6	1.7	1.8	Whole coal	Required RD	1.39
For 19-26.5 mm (for an overall hypothetical density, how much will the yield be at particle size 19-26.5mm?									
Cumulative float ash	4.47%	12.80%	17.54%	21.60%	23.55%	28.09%	37.57%		
Cumulative float yield	0.00%	8.76%	27.77%	48.46%	56.38%	72.23%	100.00%	Cumulative yield	8.0%
RD	1.3	1.4	1.5	1.6	1.7	1.8	Whole coal	Required RD	1.39
For 26.5-37.5 mm (for an overall hypothetical density, how much will the yield be at particle size 26.5-37.5 mm?									
Cumulative float ash	4.47%	12.72%	19.72%	24.81%	29.82%	31.91%	40.99%		
Cumulative float yield	0.00%	0.00%	9.72%	31.75%	59.89%	70.06%	100.00%	Cumulative yield	0.0%
RD	1.3	1.4	1.5	1.6	1.7	1.8	Whole coal	Required RD	1.39
For 37.5-53 mm (for an overall hypothetical density, how much will the yield be at particle size 37.5-53 mm?									
Cumulative float ash	4.47%	12.80%	16.48%	18.80%	18.80%	18.80%	31.77%		
Cumulative float yield	0.00%	25.62%	54.74%	70.13%	70.13%	70.13%	100.00%	Cumulative yield	23.3%
RD	1.3	1.4	1.5	1.6	1.7	1.8	Whole coal	Required RD	1.39
For 53-75 mm (for an overall hypothetical density, how much will the yield be at particle size 53-75 mm?									
Cumulative float ash	4.47%	12.72%	13.35%	14.48%	35.47%	40.34%	40.34%		
Cumulative float yield	0.00%	0.00%	0.00%	0.00%	44.64%	100.00%	100.00%	Cumulative yield	0.0%
RD	1.3	1.4	1.5	1.6	1.7	1.8	Whole coal	Required RD	1.39

Table C. 153: Overall hypothetical ash for impact breakage to a top size of 13.2 mm with no attrition (Run 1-3 average).

Overall									
Cumulative float ash	4.44%	8.19%	12.58%	14.59%	17.18%	19.03%	32.39%	Target ash	10%
Cumulative float yield	7.61%	27.54%	47.61%	55.73%	64.05%	68.90%	100.00%	Cumulative yield	35.8%
RD	1.3	1.4	1.5	1.6	1.7	1.8	Whole coal	Required RD	1.44
For 0-0.5 mm (for an overall hypothetical density, how much will the yield be at particle size 0-0.5mm?									
Cumulative float ash	4.35%	5.32%	7.40%	8.82%	10.46%	11.33%	20.80%		
Cumulative float yield	2.90%	45.85%	64.66%	71.47%	77.88%	80.48%	100.00%	Cumulative yield	53.6%
RD	1.3	1.4	1.5	1.6	1.7	1.8	Whole coal	Required RD	1.44
For 0.5-1 mm (for an overall hypothetical density, how much will the yield be at particle size 0.5-1mm?									
Cumulative float ash	4.35%	5.14%	6.42%	7.53%	8.80%	9.79%	16.73%		
Cumulative float yield	14.07%	60.04%	72.72%	78.20%	83.14%	86.14%	100.00%	Cumulative yield	65.3%
RD	1.3	1.4	1.5	1.6	1.7	1.8	Whole coal	Required RD	1.44
For 1-2 mm (for an overall hypothetical density, how much will the yield be at particle size 1-2mm?									
Cumulative float ash	4.47%	7.72%	11.19%	12.37%	13.83%	15.33%	23.51%		
Cumulative float yield	29.51%	48.38%	68.05%	73.53%	78.50%	82.56%	100.00%	Cumulative yield	56.5%
RD	1.3	1.4	1.5	1.6	1.7	1.8	Whole coal	Required RD	1.44
For 2-4.75 mm (for an overall hypothetical density, how much will the yield be at particle size 2-4.75mm?									
Cumulative float ash	4.47%	9.18%	13.26%	15.09%	17.17%	19.05%	29.82%		
Cumulative float yield	14.50%	33.33%	54.37%	62.69%	69.85%	75.05%	100.00%	Cumulative yield	42.0%
RD	1.3	1.4	1.5	1.6	1.7	1.8	Whole coal	Required RD	1.44
For 4.75-6.7 mm (for an overall hypothetical density, how much will the yield be at particle size 4.75-6.7mm?									
Cumulative float ash	4.47%	11.30%	15.48%	17.50%	20.03%	21.95%	34.20%		
Cumulative float yield	4.12%	22.88%	45.42%	55.03%	64.07%	69.57%	100.00%	Cumulative yield	32.2%
RD	1.3	1.4	1.5	1.6	1.7	1.8	Whole coal	Required RD	1.44
For 6.7-9.5 mm (for an overall hypothetical density, how much will the yield be at particle size 6.7-9.5mm?									
Cumulative float ash	4.47%	11.96%	16.49%	18.53%	21.15%	23.34%	35.73%		
Cumulative float yield	1.78%	17.51%	42.05%	52.14%	61.66%	68.12%	100.00%	Cumulative yield	27.6%
RD	1.3	1.4	1.5	1.6	1.7	1.8	Whole coal	Required RD	1.44
For 9.5-13.2 mm (for an overall hypothetical density, how much will the yield be at particle size 9.5-13.2mm?									
Cumulative float ash	4.47%	12.39%	17.44%	19.69%	23.20%	25.29%	42.39%		
Cumulative float yield	0.45%	8.96%	28.79%	37.60%	48.35%	53.68%	100.00%	Cumulative yield	17.1%
RD	1.3	1.4	1.5	1.6	1.7	1.8	Whole coal	Required RD	1.44

Table C. 154: Overall hypothetical ash for impact breakage to a top size of 13.2 mm with 1 minute attrition (Run 4).

Overall run 4									
Cumulative float ash	4.45%	8.76%	13.06%	15.57%	18.82%	21.49%	35.37%	Target ash	10%
Cumulative float yield	4.93%	22.18%	39.51%	48.54%	58.66%	65.70%	100.00%	Cumulative yield	27.2%
RD	1.3	1.4	1.5	1.6	1.7	1.8	Whole coal	Required RD	1.43
For 0-0.5 mm (for an overall hypothetical density, how much will the yield be at particle size 0-0.5mm?									
Cumulative float ash	4.35%	5.33%	7.51%	8.70%	11.37%	12.23%	23.49%		
Cumulative float yield	2.24%	40.86%	58.85%	64.01%	73.83%	76.36%	100.00%	Cumulative yield	46.1%
RD	1.3	1.4	1.5	1.6	1.7	1.8	Whole coal	Required RD	1.43
For 0.5-1 mm (for an overall hypothetical density, how much will the yield be at particle size 0.5-1mm?									
Cumulative float ash	4.35%	5.16%	6.74%	8.13%	10.26%	11.51%	21.65%		
Cumulative float yield	10.41%	48.24%	61.58%	67.60%	75.37%	79.03%	100.00%	Cumulative yield	52.1%
RD	1.3	1.4	1.5	1.6	1.7	1.8	Whole coal	Required RD	1.43
For 1-2 mm (for an overall hypothetical density, how much will the yield be at particle size 1-2mm?									
Cumulative float ash	4.47%	9.06%	11.34%	12.87%	15.28%	17.30%	26.46%		
Cumulative float yield	21.09%	46.93%	59.70%	66.14%	74.06%	79.60%	100.00%	Cumulative yield	50.6%
RD	1.3	1.4	1.5	1.6	1.7	1.8	Whole coal	Required RD	1.43
For 2-4.75 mm (for an overall hypothetical density, how much will the yield be at particle size 2-4.75mm?									
Cumulative float ash	4.47%	10.39%	14.09%	16.15%	19.15%	21.84%	34.23%		
Cumulative float yield	7.68%	26.52%	43.97%	52.29%	61.90%	69.32%	100.00%	Cumulative yield	31.6%
RD	1.3	1.4	1.5	1.6	1.7	1.8	Whole coal	Required RD	1.43
For 4.75-6.7 mm (for an overall hypothetical density, how much will the yield be at particle size 4.75-6.7mm?									
Cumulative float ash	4.47%	11.66%	16.27%	18.96%	22.22%	25.19%	38.50%		
Cumulative float yield	1.96%	14.26%	33.39%	44.49%	55.42%	64.05%	100.00%	Cumulative yield	19.8%
RD	1.3	1.4	1.5	1.6	1.7	1.8	Whole coal	Required RD	1.43
For 6.7-9.5 mm (for an overall hypothetical density, how much will the yield be at particle size 6.7-9.5mm?									
Cumulative float ash	4.47%	12.32%	17.12%	19.78%	23.04%	25.76%	40.71%		
Cumulative float yield	0.60%	10.47%	29.82%	40.73%	51.43%	58.99%	100.00%	Cumulative yield	16.1%
RD	1.3	1.4	1.5	1.6	1.7	1.8	Whole coal	Required RD	1.43
For 9.5-13.2 mm (for an overall hypothetical density, how much will the yield be at particle size 9.5-13.2mm?									
Cumulative float ash	4.47%	12.33%	17.88%	20.77%	24.44%	27.74%	43.39%		
Cumulative float yield	0.33%	5.81%	23.40%	34.15%	45.52%	54.61%	100.00%	Cumulative yield	10.9%
RD	1.3	1.4	1.5	1.6	1.7	1.8	Whole coal	Required RD	1.43

Table C. 155: Overall hypothetical ash for impact breakage to a top size of 13.2 mm with 2 minutes attrition (Run 5).

Overall									
Cumulative float ash	4.45%	8.93%	12.08%	14.85%	17.37%	19.21%	32.37%	Target ash	10%
Cumulative float yield	6.97%	30.58%	45.43%	56.15%	64.37%	69.21%	100.00%	Cumulative yield	35.6%
RD	1.3	1.4	1.5	1.6	1.7	1.8	Whole coal	Required RD	1.43
For 0-0.5 mm (for an overall hypothetical density, how much will the yield be at particle size 0-0.5mm?									
Cumulative float ash	4.35%	5.37%	7.15%	8.54%	10.47%	11.04%	22.25%		
Cumulative float yield	0.78%	46.40%	61.96%	68.19%	75.39%	77.04%	100.00%	Cumulative yield	51.7%
RD	1.3	1.4	1.5	1.6	1.7	1.8	Whole coal	Required RD	1.43
For 0.5-1 mm (for an overall hypothetical density, how much will the yield be at particle size 0.5-1mm?									
Cumulative float ash	4.35%	5.19%	6.28%	7.48%	8.93%	9.93%	18.77%		
Cumulative float yield	10.93%	58.23%	68.46%	74.00%	79.39%	82.30%	100.00%	Cumulative yield	61.7%
RD	1.3	1.4	1.5	1.6	1.7	1.8	Whole coal	Required RD	1.43
For 1-2 mm (for an overall hypothetical density, how much will the yield be at particle size 1-2mm?									
Cumulative float ash	4.47%	8.76%	10.43%	12.11%	13.65%	14.96%	23.30%		
Cumulative float yield	27.21%	56.08%	66.20%	73.63%	78.83%	82.36%	100.00%	Cumulative yield	59.5%
RD	1.3	1.4	1.5	1.6	1.7	1.8	Whole coal	Required RD	1.43
For 2-4.75 mm (for an overall hypothetical density, how much will the yield be at particle size 2-4.75mm?									
Cumulative float ash	4.47%	9.52%	12.23%	14.58%	16.89%	18.45%	29.54%		
Cumulative float yield	15.23%	38.69%	52.67%	62.61%	70.40%	74.66%	100.00%	Cumulative yield	43.4%
RD	1.3	1.4	1.5	1.6	1.7	1.8	Whole coal	Required RD	1.43
For 4.75-6.7 mm (for an overall hypothetical density, how much will the yield be at particle size 4.75-6.7mm?									
Cumulative float ash	4.47%	11.90%	15.03%	17.74%	20.34%	22.04%	35.35%		
Cumulative float yield	2.67%	24.63%	41.05%	53.02%	62.12%	66.86%	100.00%	Cumulative yield	30.2%
RD	1.3	1.4	1.5	1.6	1.7	1.8	Whole coal	Required RD	1.43
For 6.7-9.5 mm (for an overall hypothetical density, how much will the yield be at particle size 6.7-9.5mm?									
Cumulative float ash	4.47%	12.43%	15.77%	18.51%	21.13%	22.99%	35.34%		
Cumulative float yield	0.97%	21.87%	40.32%	53.27%	63.02%	68.52%	100.00%	Cumulative yield	28.1%
RD	1.3	1.4	1.5	1.6	1.7	1.8	Whole coal	Required RD	1.43
For 9.5-13.2 mm (for an overall hypothetical density, how much will the yield be at particle size 9.5-13.2mm?									
Cumulative float ash	4.47%	12.59%	16.86%	20.36%	23.29%	25.87%	41.71%		
Cumulative float yield	0.27%	10.50%	26.19%	39.89%	49.48%	56.43%	100.00%	Cumulative yield	15.8%
RD	1.3	1.4	1.5	1.6	1.7	1.8	Whole coal	Required RD	1.43

Table C. 156: Overall hypothetical ash for impact breakage to a top size of 13.2 mm with 5 minutes attrition (Run 6).

Overall									
Cumulative float ash	4.45%	8.71%	12.57%	14.92%	17.40%	19.30%	32.73%	Target ash	10%
Cumulative float yield	7.81%	28.05%	46.04%	55.35%	63.53%	68.50%	100.00%	Cumulative yield	34.1%
RD	1.3	1.4	1.5	1.6	1.7	1.8	Whole coal	Required RD	1.43
For 0-0.5 mm (for an overall hypothetical density, how much will the yield be at particle size 0-0.5mm?									
Cumulative float ash	4.35%	5.33%	7.50%	8.70%	11.37%	12.25%	23.52%		
Cumulative float yield	2.19%	40.84%	58.78%	63.93%	73.76%	76.34%	100.00%	Cumulative yield	46.8%
RD	1.3	1.4	1.5	1.6	1.7	1.8	Whole coal	Required RD	1.43
For 0.5-1 mm (for an overall hypothetical density, how much will the yield be at particle size 0.5-1mm?									
Cumulative float ash	4.35%	5.10%	6.57%	7.90%	9.93%	11.11%	20.93%		
Cumulative float yield	14.21%	50.48%	63.17%	68.97%	76.41%	79.86%	100.00%	Cumulative yield	54.7%
RD	1.3	1.4	1.5	1.6	1.7	1.8	Whole coal	Required RD	1.43
For 1-2 mm (for an overall hypothetical density, how much will the yield be at particle size 1-2mm?									
Cumulative float ash	4.47%	8.78%	10.49%	11.92%	13.46%	14.82%	24.69%		
Cumulative float yield	26.31%	54.52%	64.64%	70.72%	75.67%	79.16%	100.00%	Cumulative yield	57.9%
RD	1.3	1.4	1.5	1.6	1.7	1.8	Whole coal	Required RD	1.43
For 2-4.75 mm (for an overall hypothetical density, how much will the yield be at particle size 2-4.75mm?									
Cumulative float ash	4.47%	9.53%	12.92%	15.16%	17.26%	18.86%	30.97%		
Cumulative float yield	13.42%	34.11%	51.17%	60.79%	67.81%	72.07%	100.00%	Cumulative yield	39.8%
RD	1.3	1.4	1.5	1.6	1.7	1.8	Whole coal	Required RD	1.43
For 4.75-6.7 mm (for an overall hypothetical density, how much will the yield be at particle size 4.75-6.7mm?									
Cumulative float ash	4.47%	11.54%	15.95%	18.40%	20.87%	22.68%	35.84%		
Cumulative float yield	2.88%	18.89%	41.04%	52.64%	61.55%	66.73%	100.00%	Cumulative yield	26.3%
RD	1.3	1.4	1.5	1.6	1.7	1.8	Whole coal	Required RD	1.43
For 6.7-9.5 mm (for an overall hypothetical density, how much will the yield be at particle size 6.7-9.5mm?									
Cumulative float ash	4.47%	12.21%	16.70%	19.11%	22.01%	23.83%	36.52%		
Cumulative float yield	1.10%	15.60%	38.79%	50.59%	61.49%	66.94%	100.00%	Cumulative yield	23.3%
RD	1.3	1.4	1.5	1.6	1.7	1.8	Whole coal	Required RD	1.43
For 9.5-13.2 mm (for an overall hypothetical density, how much will the yield be at particle size 9.5-13.2mm?									
Cumulative float ash	4.47%	12.61%	17.55%	20.23%	22.91%	25.76%	42.11%		
Cumulative float yield	0.20%	8.61%	28.29%	39.38%	47.80%	55.17%	100.00%	Cumulative yield	15.2%
RD	1.3	1.4	1.5	1.6	1.7	1.8	Whole coal	Required RD	1.43

Table C. 157: Overall hypothetical ash for impact breakage to a top size of 6.7 mm with no attrition (Run 7-9 average).

Overall									
Cumulative float ash	4.45%	8.92%	11.99%	14.57%	16.71%	18.76%	30.52%	Target ash	10%
Cumulative float yield	8.36%	33.10%	48.93%	59.87%	67.09%	72.72%	100.00%	Cumulative yield	38.7%
RD	1.3	1.4	1.5	1.6	1.7	1.8	Whole coal	Required RD	1.44
For 0-0.5 mm (for an overall hypothetical density, how much will the yield be at particle size 0-0.5mm?									
Cumulative float ash	4.35%	5.34%	7.22%	9.78%	11.09%	12.50%	22.46%		
Cumulative float yield	1.72%	42.55%	57.77%	69.56%	74.71%	78.97%	100.00%	Cumulative yield	47.9%
RD	1.3	1.4	1.5	1.6	1.7	1.8	Whole coal	Required RD	1.44
For 0.5-1 mm (for an overall hypothetical density, how much will the yield be at particle size 0.5-1mm?									
Cumulative float ash	4.35%	5.17%	6.77%	8.83%	10.35%	11.98%	20.55%		
Cumulative float yield	10.20%	48.24%	61.83%	71.24%	77.12%	82.09%	100.00%	Cumulative yield	53.0%
RD	1.3	1.4	1.5	1.6	1.7	1.8	Whole coal	Required RD	1.44
For 1-2 mm (for an overall hypothetical density, how much will the yield be at particle size 1-2mm?									
Cumulative float ash	4.47%	8.88%	10.64%	12.24%	13.80%	15.32%	22.98%		
Cumulative float yield	26.40%	56.04%	66.91%	74.17%	79.50%	83.67%	100.00%	Cumulative yield	59.9%
RD	1.3	1.4	1.5	1.6	1.7	1.8	Whole coal	Required RD	1.44
For 2-4.75 mm (for an overall hypothetical density, how much will the yield be at particle size 2-4.75mm?									
Cumulative float ash	4.47%	9.80%	12.53%	14.79%	16.76%	18.56%	28.86%		
Cumulative float yield	14.23%	39.53%	54.57%	64.59%	71.40%	76.41%	100.00%	Cumulative yield	44.8%
RD	1.3	1.4	1.5	1.6	1.7	1.8	Whole coal	Required RD	1.44
For 4.75-6.7 mm (for an overall hypothetical density, how much will the yield be at particle size 4.75-6.7mm?									
Cumulative float ash	4.47%	12.23%	16.09%	18.95%	21.51%	23.96%	37.73%		
Cumulative float yield	1.18%	17.29%	35.66%	48.26%	57.10%	64.00%	100.00%	Cumulative yield	23.7%
RD	1.3	1.4	1.5	1.6	1.7	1.8	Whole coal	Required RD	1.44

Table C. 158: Overall hypothetical ash for impact breakage to a top size of 6.7 mm with 1 minute attritioning (Run 10).

Overall									
Cumulative float ash	4.45%	6.48%	9.09%	11.19%	13.04%	14.92%	26.59%	Target ash	10%
Cumulative float yield	17.30%	45.01%	57.06%	64.99%	70.54%	75.17%	100.00%	Cumulative yield	60.5%
RD	1.3	1.4	1.5	1.6	1.7	1.8	Whole coal	Required RD	1.54
For 0-0.5 mm (for an overall hypothetical density, how much will the yield be at particle size 0-0.5mm?									
Cumulative float ash	4.35%	5.31%	5.73%	6.55%	7.03%	7.55%	12.62%		
Cumulative float yield	5.70%	77.70%	82.57%	86.83%	88.77%	90.32%	100.00%	Cumulative yield	84.4%
RD	1.3	1.4	1.5	1.6	1.7	1.8	Whole coal	Required RD	1.54
For 0.5-1 mm (for an overall hypothetical density, how much will the yield be at particle size 0.5-1mm?									
Cumulative float ash	4.35%	5.15%	5.68%	6.53%	7.26%	8.11%	14.01%		
Cumulative float yield	16.63%	73.31%	79.01%	83.27%	86.07%	88.59%	100.00%	Cumulative yield	80.9%
RD	1.3	1.4	1.5	1.6	1.7	1.8	Whole coal	Required RD	1.54
For 1-2 mm (for an overall hypothetical density, how much will the yield be at particle size 1-2mm?									
Cumulative float ash	4.47%	6.89%	9.54%	11.50%	13.43%	15.38%	24.14%		
Cumulative float yield	35.00%	49.33%	62.17%	70.01%	76.15%	81.30%	100.00%	Cumulative yield	65.6%
RD	1.3	1.4	1.5	1.6	1.7	1.8	Whole coal	Required RD	1.54
For 2-4.75 mm (for an overall hypothetical density, how much will the yield be at particle size 2-4.75mm?									
Cumulative float ash	4.47%	7.40%	10.94%	13.29%	15.54%	17.64%	28.49%		
Cumulative float yield	24.85%	38.35%	53.84%	63.01%	70.14%	75.66%	100.00%	Cumulative yield	57.8%
RD	1.3	1.4	1.5	1.6	1.7	1.8	Whole coal	Required RD	1.54
For 4.75-6.7 mm (for an overall hypothetical density, how much will the yield be at particle size 4.75-6.7mm?									
Cumulative float ash	4.47%	9.32%	14.17%	17.34%	19.88%	22.61%	40.16%		
Cumulative float yield	7.15%	17.10%	32.05%	42.53%	49.45%	55.69%	100.00%	Cumulative yield	36.6%
RD	1.3	1.4	1.5	1.6	1.7	1.8	Whole coal	Required RD	1.54

Table C. 159: Overall hypothetical ash for impact breakage to a top size of 6.7 mm with 2 minutes attritioning (Run 11).

Overall									
Cumulative float ash	4.45%	7.32%	10.42%	12.93%	15.03%	16.58%	27.37%	Target ash	10%
Cumulative float yield	13.70%	39.01%	54.11%	64.67%	71.76%	76.10%	100.00%	Cumulative yield	52.1%
RD	1.3	1.4	1.5	1.6	1.7	1.8	Whole coal	Required RD	1.49
For 0-0.5 mm (for an overall hypothetical density, how much will the yield be at particle size 0-0.5mm?									
Cumulative float ash	4.35%	5.32%	6.34%	8.62%	9.80%	11.21%	19.98%		
Cumulative float yield	3.62%	53.78%	62.80%	73.22%	77.75%	81.97%	100.00%	Cumulative yield	61.6%
RD	1.3	1.4	1.5	1.6	1.7	1.8	Whole coal	Required RD	1.49
For 0.5-1 mm (for an overall hypothetical density, how much will the yield be at particle size 0.5-1mm?									
Cumulative float ash	4.35%	5.12%	6.19%	8.16%	9.51%	10.99%	19.41%		
Cumulative float yield	14.17%	54.92%	64.27%	73.23%	78.35%	82.78%	100.00%	Cumulative yield	63.0%
RD	1.3	1.4	1.5	1.6	1.7	1.8	Whole coal	Required RD	1.49
For 1-2 mm (for an overall hypothetical density, how much will the yield be at particle size 1-2mm?									
Cumulative float ash	4.47%	7.27%	9.64%	11.41%	13.05%	14.36%	23.37%		
Cumulative float yield	35.00%	52.68%	65.07%	72.46%	77.76%	81.17%	100.00%	Cumulative yield	63.4%
RD	1.3	1.4	1.5	1.6	1.7	1.8	Whole coal	Required RD	1.49
For 2-4.75 mm (for an overall hypothetical density, how much will the yield be at particle size 2-4.75mm?									
Cumulative float ash	4.47%	8.85%	12.45%	14.85%	17.12%	18.55%	28.56%		
Cumulative float yield	17.21%	36.31%	54.32%	64.98%	73.03%	77.07%	100.00%	Cumulative yield	51.9%
RD	1.3	1.4	1.5	1.6	1.7	1.8	Whole coal	Required RD	1.49
For 4.75-6.7 mm (for an overall hypothetical density, how much will the yield be at particle size 4.75-6.7mm?									
Cumulative float ash	4.47%	10.84%	15.56%	18.52%	21.24%	23.08%	36.60%		
Cumulative float yield	4.15%	17.56%	37.54%	50.58%	60.22%	65.45%	100.00%	Cumulative yield	34.8%
RD	1.3	1.4	1.5	1.6	1.7	1.8	Whole coal	Required RD	1.49

Table C. 160: Overall hypothetical ash for impact breakage to a top size of 6.7 mm with 5 minutes attritioning (Run 12).

Overall									
Cumulative float ash	4.44%	6.80%	10.03%	12.10%	14.25%	16.39%	26.04%	Target ash	10%
Cumulative float yield	12.74%	42.43%	57.72%	66.13%	73.02%	78.79%	100.00%	Cumulative yield	57.6%
RD	1.3	1.4	1.5	1.6	1.7	1.8	Whole coal	Required RD	1.50
For 0-0.5 mm (for an overall hypothetical density, how much will the yield be at particle size 0-0.5mm?									
Cumulative float ash	4.35%	5.31%	5.73%	6.54%	7.03%	7.54%	12.61%		
Cumulative float yield	5.71%	77.75%	82.62%	86.86%	88.80%	90.31%	100.00%	Cumulative yield	82.6%
RD	1.3	1.4	1.5	1.6	1.7	1.8	Whole coal	Required RD	1.50
For 0.5-1 mm (for an overall hypothetical density, how much will the yield be at particle size 0.5-1mm?									
Cumulative float ash	4.35%	5.16%	5.69%	6.54%	7.28%	8.12%	14.08%		
Cumulative float yield	16.13%	73.18%	78.89%	83.13%	85.99%	88.48%	100.00%	Cumulative yield	78.8%
RD	1.3	1.4	1.5	1.6	1.7	1.8	Whole coal	Required RD	1.50
For 1-2 mm (for an overall hypothetical density, how much will the yield be at particle size 1-2mm?									
Cumulative float ash	4.47%	7.56%	10.43%	12.17%	13.86%	15.89%	23.65%		
Cumulative float yield	31.00%	49.25%	64.50%	72.06%	77.69%	83.25%	100.00%	Cumulative yield	64.4%
RD	1.3	1.4	1.5	1.6	1.7	1.8	Whole coal	Required RD	1.50
For 2-4.75 mm (for an overall hypothetical density, how much will the yield be at particle size 2-4.75mm?									
Cumulative float ash	4.47%	8.52%	12.79%	15.19%	17.59%	19.88%	28.96%		
Cumulative float yield	16.73%	32.57%	52.66%	63.32%	71.83%	78.55%	100.00%	Cumulative yield	52.5%
RD	1.3	1.4	1.5	1.6	1.7	1.8	Whole coal	Required RD	1.50
For 4.75-6.7 mm (for an overall hypothetical density, how much will the yield be at particle size 4.75-6.7mm?									
Cumulative float ash	4.47%	10.80%	16.36%	18.97%	22.16%	25.23%	38.11%		
Cumulative float yield	3.10%	12.88%	34.21%	45.27%	56.12%	65.18%	100.00%	Cumulative yield	34.0%
RD	1.3	1.4	1.5	1.6	1.7	1.8	Whole coal	Required RD	1.50

Table C. 161: Overall hypothetical ash for compressive breakage to a top size of 13.2 mm with no attritioning (Run 13-15 average).

Overall									
Cumulative float ash	4.46%	8.77%	12.32%	14.60%	16.80%	18.72%	31.73%	Target ash	10%
Cumulative float yield	5.89%	29.78%	47.83%	57.53%	64.81%	69.88%	100.00%	Cumulative yield	36.0%
RD	1.3	1.4	1.5	1.6	1.7	1.8	Whole coal	Required RD	1.43
For 0-0.5 mm (for an overall hypothetical density, how much will the yield be at particle size 0-0.5mm?									
Cumulative float ash	4.35%	5.38%	7.83%	10.52%	12.03%	12.94%	22.77%		
Cumulative float yield	0.16%	37.24%	56.94%	69.90%	76.18%	79.05%	100.00%	Cumulative yield	44.1%
RD	1.3	1.4	1.5	1.6	1.7	1.8	Whole coal	Required RD	1.43
For 0.5-1 mm (for an overall hypothetical density, how much will the yield be at particle size 0.5-1mm?									
Cumulative float ash	4.35%	5.33%	6.75%	8.65%	10.00%	11.18%	18.96%		
Cumulative float yield	3.01%	52.70%	65.87%	75.00%	80.39%	84.02%	100.00%	Cumulative yield	57.3%
RD	1.3	1.4	1.5	1.6	1.7	1.8	Whole coal	Required RD	1.43
For 1-2 mm (for an overall hypothetical density, how much will the yield be at particle size 1-2mm?									
Cumulative float ash	4.47%	9.13%	10.96%	12.15%	13.51%	14.99%	24.32%		
Cumulative float yield	24.30%	55.08%	66.60%	71.93%	76.38%	80.25%	100.00%	Cumulative yield	59.1%
RD	1.3	1.4	1.5	1.6	1.7	1.8	Whole coal	Required RD	1.43
For 2-4.75 mm (for an overall hypothetical density, how much will the yield be at particle size 2-4.75mm?									
Cumulative float ash	4.47%	9.92%	12.95%	14.67%	16.64%	18.50%	30.15%		
Cumulative float yield	12.99%	37.55%	54.39%	61.95%	68.42%	73.36%	100.00%	Cumulative yield	43.4%
RD	1.3	1.4	1.5	1.6	1.7	1.8	Whole coal	Required RD	1.43
For 4.75-6.7 mm (for an overall hypothetical density, how much will the yield be at particle size 4.75-6.7mm?									
Cumulative float ash	4.47%	11.58%	15.42%	17.40%	19.67%	21.54%	35.09%		
Cumulative float yield	3.46%	23.63%	44.70%	53.87%	61.61%	66.70%	100.00%	Cumulative yield	30.9%
RD	1.3	1.4	1.5	1.6	1.7	1.8	Whole coal	Required RD	1.43
For 6.7-9.5 mm (for an overall hypothetical density, how much will the yield be at particle size 6.7-9.5mm?									
Cumulative float ash	4.47%	12.12%	16.42%	18.65%	21.15%	23.51%	36.93%		
Cumulative float yield	1.41%	17.12%	39.49%	49.94%	58.65%	65.32%	100.00%	Cumulative yield	24.9%
RD	1.3	1.4	1.5	1.6	1.7	1.8	Whole coal	Required RD	1.43
For 9.5-13.2 mm (for an overall hypothetical density, how much will the yield be at particle size 9.5-13.2mm?									
Cumulative float ash	4.47%	12.31%	17.13%	19.95%	22.86%	25.31%	41.50%		
Cumulative float yield	0.60%	10.09%	28.92%	40.37%	49.70%	56.13%	100.00%	Cumulative yield	16.6%
RD	1.3	1.4	1.5	1.6	1.7	1.8	Whole coal	Required RD	1.43

Table C. 162: Overall hypothetical ash for compressive breakage to a top size of 13.2 mm with 1 minute attritioning (Run 16).

Overall									
Cumulative float ash	4.46%	8.09%	12.23%	14.33%	16.20%	18.39%	31.58%	Target ash	10%
Cumulative float yield	6.84%	29.33%	49.26%	58.01%	64.03%	69.69%	100.00%	Cumulative yield	38.5%
RD	1.3	1.4	1.5	1.6	1.7	1.8	Whole coal	Required RD	1.45
For 0-0.5 mm (for an overall hypothetical density, how much will the yield be at particle size 0-0.5mm?									
Cumulative float ash	4.35%	5.38%	7.55%	9.27%	10.62%	11.94%	21.60%		
Cumulative float yield	0.15%	43.27%	62.43%	70.65%	75.89%	79.85%	100.00%	Cumulative yield	52.1%
RD	1.3	1.4	1.5	1.6	1.7	1.8	Whole coal	Required RD	1.45
For 0.5-1 mm (for an overall hypothetical density, how much will the yield be at particle size 0.5-1mm?									
Cumulative float ash	4.35%	5.33%	6.69%	7.98%	9.18%	10.27%	17.83%		
Cumulative float yield	2.88%	57.00%	70.47%	76.75%	81.48%	84.77%	100.00%	Cumulative yield	63.2%
RD	1.3	1.4	1.5	1.6	1.7	1.8	Whole coal	Required RD	1.45
For 1-2 mm (for an overall hypothetical density, how much will the yield be at particle size 1-2mm?									
Cumulative float ash	4.47%	7.66%	10.10%	11.50%	12.71%	14.41%	23.39%		
Cumulative float yield	32.96%	53.37%	66.94%	72.96%	76.84%	81.22%	100.00%	Cumulative yield	59.6%
RD	1.3	1.4	1.5	1.6	1.7	1.8	Whole coal	Required RD	1.45
For 2-4.75 mm (for an overall hypothetical density, how much will the yield be at particle size 2-4.75mm?									
Cumulative float ash	4.47%	9.12%	13.07%	14.91%	16.55%	18.61%	29.87%		
Cumulative float yield	15.22%	34.41%	54.87%	63.17%	68.65%	74.18%	100.00%	Cumulative yield	43.8%
RD	1.3	1.4	1.5	1.6	1.7	1.8	Whole coal	Required RD	1.45
For 4.75-6.7 mm (for an overall hypothetical density, how much will the yield be at particle size 4.75-6.7mm?									
Cumulative float ash	4.47%	11.27%	15.82%	17.83%	19.74%	21.80%	33.82%		
Cumulative float yield	3.99%	21.76%	47.11%	57.39%	64.37%	70.26%	100.00%	Cumulative yield	33.4%
RD	1.3	1.4	1.5	1.6	1.7	1.8	Whole coal	Required RD	1.45
For 6.7-9.5 mm (for an overall hypothetical density, how much will the yield be at particle size 6.7-9.5mm?									
Cumulative float ash	4.47%	12.23%	16.94%	19.21%	21.33%	23.41%	36.46%		
Cumulative float yield	1.04%	15.10%	40.68%	52.50%	60.35%	66.38%	100.00%	Cumulative yield	26.9%
RD	1.3	1.4	1.5	1.6	1.7	1.8	Whole coal	Required RD	1.45
For 9.5-13.2 mm (for an overall hypothetical density, how much will the yield be at particle size 9.5-13.2mm?									
Cumulative float ash	4.47%	12.43%	17.29%	19.59%	21.97%	25.35%	43.14%		
Cumulative float yield	0.42%	9.51%	28.54%	37.32%	43.91%	51.76%	100.00%	Cumulative yield	18.3%
RD	1.3	1.4	1.5	1.6	1.7	1.8	Whole coal	Required RD	1.45

Table C. 163: Overall hypothetical ash for compressive breakage to a top size of 13.2 mm with 2 minutes attritioning (Run 17).

Overall									
Cumulative float ash	4.46%	7.95%	11.99%	14.64%	16.97%	19.00%	32.56%	Target ash	10%
Cumulative float yield	5.23%	27.17%	45.31%	55.63%	63.08%	68.36%	100.00%	Cumulative yield	36.4%
RD	1.3	1.4	1.5	1.6	1.7	1.8	Whole coal	Required RD	1.45
For 0-0.5 mm (for an overall hypothetical density, how much will the yield be at particle size 0-0.5mm?									
Cumulative float ash	4.35%	5.38%	7.66%	9.04%	10.16%	11.13%	20.56%		
Cumulative float yield	0.19%	45.02%	66.47%	73.35%	77.78%	80.67%	100.00%	Cumulative yield	55.9%
RD	1.3	1.4	1.5	1.6	1.7	1.8	Whole coal	Required RD	1.45
For 0.5-1 mm (for an overall hypothetical density, how much will the yield be at particle size 0.5-1mm?									
Cumulative float ash	4.35%	5.35%	6.39%	7.82%	9.34%	10.62%	19.95%		
Cumulative float yield	1.97%	55.75%	65.28%	71.74%	77.33%	81.05%	100.00%	Cumulative yield	60.6%
RD	1.3	1.4	1.5	1.6	1.7	1.8	Whole coal	Required RD	1.45
For 1-2 mm (for an overall hypothetical density, how much will the yield be at particle size 1-2mm?									
Cumulative float ash	4.47%	8.25%	10.86%	12.49%	14.13%	15.65%	24.77%		
Cumulative float yield	26.91%	49.23%	63.79%	70.90%	76.37%	80.42%	100.00%	Cumulative yield	56.6%
RD	1.3	1.4	1.5	1.6	1.7	1.8	Whole coal	Required RD	1.45
For 2-4.75 mm (for an overall hypothetical density, how much will the yield be at particle size 2-4.75mm?									
Cumulative float ash	4.47%	9.45%	13.36%	15.52%	17.85%	19.87%	31.80%		
Cumulative float yield	12.28%	30.54%	49.36%	58.58%	66.34%	71.84%	100.00%	Cumulative yield	40.1%
RD	1.3	1.4	1.5	1.6	1.7	1.8	Whole coal	Required RD	1.45
For 4.75-6.7 mm (for an overall hypothetical density, how much will the yield be at particle size 4.75-6.7mm?									
Cumulative float ash	4.47%	11.09%	15.97%	18.55%	21.22%	23.51%	36.57%		
Cumulative float yield	3.45%	16.72%	38.56%	50.26%	59.67%	66.25%	100.00%	Cumulative yield	27.8%
RD	1.3	1.4	1.5	1.6	1.7	1.8	Whole coal	Required RD	1.45
For 6.7-9.5 mm (for an overall hypothetical density, how much will the yield be at particle size 6.7-9.5mm?									
Cumulative float ash	4.47%	12.17%	16.94%	19.66%	22.16%	24.28%	38.46%		
Cumulative float yield	0.97%	12.83%	34.83%	47.66%	56.60%	62.61%	100.00%	Cumulative yield	24.0%
RD	1.3	1.4	1.5	1.6	1.7	1.8	Whole coal	Required RD	1.45
For 9.5-13.2 mm (for an overall hypothetical density, how much will the yield be at particle size 9.5-13.2mm?									
Cumulative float ash	4.47%	12.54%	17.35%	20.90%	23.68%	26.28%	43.09%		
Cumulative float yield	0.25%	7.86%	23.87%	37.65%	46.51%	53.24%	100.00%	Cumulative yield	16.0%
RD	1.3	1.4	1.5	1.6	1.7	1.8	Whole coal	Required RD	1.45

Table C. 164: Overall hypothetical ash for compressive breakage to a top size of 13.2 mm with 5 minutes attritioning (Run 18).

Overall									
Cumulative float ash	4.46%	8.42%	12.06%	14.43%	17.21%	19.29%	32.71%	Target ash	10%
Cumulative float yield	5.09%	28.18%	45.22%	54.34%	63.02%	68.52%	100.00%	Cumulative yield	35.6%
RD	1.3	1.4	1.5	1.6	1.7	1.8	Whole coal	Required RD	1.44
For 0-0.5 mm (for an overall hypothetical density, how much will the yield be at particle size 0-0.5mm?									
Cumulative float ash	4.35%	5.38%	7.55%	9.27%	10.62%	11.94%	21.60%		
Cumulative float yield	0.15%	43.27%	62.43%	70.65%	75.89%	79.85%	100.00%	Cumulative yield	51.6%
RD	1.3	1.4	1.5	1.6	1.7	1.8	Whole coal	Required RD	1.44
For 0.5-1 mm (for an overall hypothetical density, how much will the yield be at particle size 0.5-1mm?									
Cumulative float ash	4.35%	5.34%	6.70%	7.98%	9.19%	10.28%	17.84%		
Cumulative float yield	2.78%	56.95%	70.44%	76.73%	81.46%	84.76%	100.00%	Cumulative yield	62.8%
RD	1.3	1.4	1.5	1.6	1.7	1.8	Whole coal	Required RD	1.44
For 1-2 mm (for an overall hypothetical density, how much will the yield be at particle size 1-2mm?									
Cumulative float ash	4.47%	9.60%	11.39%	12.77%	14.25%	15.90%	25.23%		
Cumulative float yield	20.34%	52.95%	64.35%	70.53%	75.48%	79.85%	100.00%	Cumulative yield	57.9%
RD	1.3	1.4	1.5	1.6	1.7	1.8	Whole coal	Required RD	1.44
For 2-4.75 mm (for an overall hypothetical density, how much will the yield be at particle size 2-4.75mm?									
Cumulative float ash	4.47%	9.87%	13.24%	15.37%	17.53%	19.86%	32.05%		
Cumulative float yield	11.37%	32.28%	49.08%	58.01%	65.00%	71.21%	100.00%	Cumulative yield	39.6%
RD	1.3	1.4	1.5	1.6	1.7	1.8	Whole coal	Required RD	1.44
For 4.75-6.7 mm (for an overall hypothetical density, how much will the yield be at particle size 4.75-6.7mm?									
Cumulative float ash	4.47%	11.28%	15.67%	18.08%	21.16%	23.43%	36.78%		
Cumulative float yield	3.36%	18.40%	38.38%	48.66%	59.15%	65.58%	100.00%	Cumulative yield	27.1%
RD	1.3	1.4	1.5	1.6	1.7	1.8	Whole coal	Required RD	1.44
For 6.7-9.5 mm (for an overall hypothetical density, how much will the yield be at particle size 6.7-9.5mm?									
Cumulative float ash	4.47%	11.94%	17.09%	19.41%	23.15%	25.57%	39.23%		
Cumulative float yield	1.15%	11.02%	32.68%	42.61%	55.54%	62.74%	100.00%	Cumulative yield	20.4%
RD	1.3	1.4	1.5	1.6	1.7	1.8	Whole coal	Required RD	1.44
For 9.5-13.2 mm (for an overall hypothetical density, how much will the yield be at particle size 9.5-13.2mm?									
Cumulative float ash	4.47%	12.43%	17.11%	20.25%	24.01%	26.19%	43.11%		
Cumulative float yield	0.39%	8.72%	24.36%	35.63%	47.33%	53.02%	100.00%	Cumulative yield	15.5%
RD	1.3	1.4	1.5	1.6	1.7	1.8	Whole coal	Required RD	1.44

Table C. 165: Overall hypothetical ash for compressive breakage to a top size of 6.7 mm with no attritioning (Run 19-21 average).

Overall									
Cumulative float ash	4.46%	7.39%	11.52%	14.05%	16.41%	18.82%	33.48%	Target ash	10%
Cumulative float yield	7.92%	25.81%	43.43%	52.86%	59.96%	65.89%	100.00%	Cumulative yield	37.0%
RD	1.3	1.4	1.5	1.6	1.7	1.8	Whole coal	Required RD	1.46
For 0-0.5 mm (for an overall hypothetical density, how much will the yield be at particle size 0-0.5mm?									
Cumulative float ash	4.35%	5.38%	8.10%	10.42%	11.95%	13.07%	23.43%		
Cumulative float yield	0.07%	35.18%	57.11%	68.21%	74.41%	77.87%	100.00%	Cumulative yield	49.1%
RD	1.3	1.4	1.5	1.6	1.7	1.8	Whole coal	Required RD	1.46
For 0.5-1 mm (for an overall hypothetical density, how much will the yield be at particle size 0.5-1mm?									
Cumulative float ash	4.35%	5.32%	7.29%	9.24%	10.74%	11.92%	22.35%		
Cumulative float yield	2.60%	43.51%	60.07%	69.02%	74.75%	78.25%	100.00%	Cumulative yield	54.0%
RD	1.3	1.4	1.5	1.6	1.7	1.8	Whole coal	Required RD	1.46
For 1-2 mm (for an overall hypothetical density, how much will the yield be at particle size 1-2mm?									
Cumulative float ash	4.47%	7.42%	10.56%	12.20%	14.16%	16.22%	28.00%		
Cumulative float yield	27.51%	42.55%	57.14%	63.45%	69.30%	74.39%	100.00%	Cumulative yield	51.8%
RD	1.3	1.4	1.5	1.6	1.7	1.8	Whole coal	Required RD	1.46
For 2-4.75 mm (for an overall hypothetical density, how much will the yield be at particle size 2-4.75mm?									
Cumulative float ash	4.47%	8.90%	13.74%	16.17%	18.63%	21.30%	34.81%		
Cumulative float yield	11.08%	23.64%	42.78%	52.35%	60.01%	66.98%	100.00%	Cumulative yield	35.8%
RD	1.3	1.4	1.5	1.6	1.7	1.8	Whole coal	Required RD	1.46
For 4.75-6.7 mm (for an overall hypothetical density, how much will the yield be at particle size 4.75-6.7mm?									
Cumulative float ash	4.47%	10.91%	16.44%	19.49%	22.48%	25.69%	43.84%		
Cumulative float yield	2.10%	9.25%	24.84%	34.86%	42.90%	50.32%	100.00%	Cumulative yield	19.1%
RD	1.3	1.4	1.5	1.6	1.7	1.8	Whole coal	Required RD	1.46

Table C. 166: Overall hypothetical ash for compressive breakage to a top size of 6.7 mm with 1 minute attritioning (Run 22).

Overall									
Cumulative float ash	4.47%	7.37%	11.65%	14.21%	16.74%	18.91%	30.25%	Target ash	10%
Cumulative float yield	9.06%	28.74%	48.48%	59.03%	67.50%	73.53%	100.00%	Cumulative yield	40.9%
RD	1.3	1.4	1.5	1.6	1.7	1.8	Whole coal	Required RD	1.46
For 0-0.5 mm (for an overall hypothetical density, how much will the yield be at particle size 0-0.5mm?									
Cumulative float ash	4.35%	5.39%	7.82%	9.82%	11.09%	12.25%	22.51%		
Cumulative float yield	0.00%	39.55%	60.32%	69.97%	74.98%	78.46%	100.00%	Cumulative yield	52.3%
RD	1.3	1.4	1.5	1.6	1.7	1.8	Whole coal	Required RD	1.46
For 0.5-1 mm (for an overall hypothetical density, how much will the yield be at particle size 0.5-1mm?									
Cumulative float ash	4.35%	5.36%	7.26%	9.03%	10.52%	11.68%	21.37%		
Cumulative float yield	1.32%	45.66%	62.36%	70.66%	76.42%	79.91%	100.00%	Cumulative yield	55.9%
RD	1.3	1.4	1.5	1.6	1.7	1.8	Whole coal	Required RD	1.46
For 1-2 mm (for an overall hypothetical density, how much will the yield be at particle size 1-2mm?									
Cumulative float ash	4.47%	7.61%	10.90%	12.93%	14.77%	16.68%	26.09%		
Cumulative float yield	27.04%	43.38%	59.57%	68.15%	74.19%	79.34%	100.00%	Cumulative yield	53.3%
RD	1.3	1.4	1.5	1.6	1.7	1.8	Whole coal	Required RD	1.46
For 2-4.75 mm (for an overall hypothetical density, how much will the yield be at particle size 2-4.75mm?									
Cumulative float ash	4.47%	8.66%	13.58%	16.36%	19.23%	21.64%	32.86%		
Cumulative float yield	12.17%	24.46%	44.10%	55.57%	65.39%	72.36%	100.00%	Cumulative yield	36.5%
RD	1.3	1.4	1.5	1.6	1.7	1.8	Whole coal	Required RD	1.46
For 4.75-6.7 mm (for an overall hypothetical density, how much will the yield be at particle size 4.75-6.7mm?									
Cumulative float ash	4.47%	10.55%	16.48%	19.18%	22.35%	24.98%	37.63%		
Cumulative float yield	3.33%	12.29%	34.84%	46.81%	58.11%	66.03%	100.00%	Cumulative yield	26.1%
RD	1.3	1.4	1.5	1.6	1.7	1.8	Whole coal	Required RD	1.46

Table C. 167: Overall hypothetical ash for compressive breakage to a top size of 6.7 mm with 2 minutes attritioning (Run 23).

Overall									
Cumulative float ash	4.47%	6.58%	10.54%	13.56%	15.79%	17.92%	28.34%	Target ash	10%
Cumulative float yield	11.85%	33.48%	50.24%	62.67%	70.21%	76.18%	100.00%	Cumulative yield	47.9%
RD	1.3	1.4	1.5	1.6	1.7	1.8	Whole coal	Required RD	1.49
For 0-0.5 mm (for an overall hypothetical density, how much will the yield be at particle size 0-0.5mm?									
Cumulative float ash	4.35%	5.39%	6.61%	9.38%	10.54%	12.08%	22.12%		
Cumulative float yield	0.03%	47.67%	57.68%	69.97%	74.42%	78.99%	100.00%	Cumulative yield	56.3%
RD	1.3	1.4	1.5	1.6	1.7	1.8	Whole coal	Required RD	1.49
For 0.5-1 mm (for an overall hypothetical density, how much will the yield be at particle size 0.5-1mm?									
Cumulative float ash	4.35%	5.37%	6.45%	8.74%	9.82%	10.69%	18.28%		
Cumulative float yield	1.00%	56.21%	66.31%	77.48%	81.90%	84.57%	100.00%	Cumulative yield	64.9%
RD	1.3	1.4	1.5	1.6	1.7	1.8	Whole coal	Required RD	1.49
For 1-2 mm (for an overall hypothetical density, how much will the yield be at particle size 1-2mm?									
Cumulative float ash	4.47%	6.73%	9.89%	11.83%	13.62%	15.53%	24.35%		
Cumulative float yield	34.38%	47.15%	62.34%	70.29%	76.06%	81.09%	100.00%	Cumulative yield	60.3%
RD	1.3	1.4	1.5	1.6	1.7	1.8	Whole coal	Required RD	1.49
For 2-4.75 mm (for an overall hypothetical density, how much will the yield be at particle size 2-4.75mm?									
Cumulative float ash	4.47%	7.50%	12.49%	15.64%	18.17%	20.54%	31.02%		
Cumulative float yield	17.51%	27.52%	46.54%	59.38%	68.05%	74.86%	100.00%	Cumulative yield	43.9%
RD	1.3	1.4	1.5	1.6	1.7	1.8	Whole coal	Required RD	1.49
For 4.75-6.7 mm (for an overall hypothetical density, how much will the yield be at particle size 4.75-6.7mm?									
Cumulative float ash	4.47%	9.72%	16.35%	19.62%	22.46%	25.01%	36.67%		
Cumulative float yield	4.31%	11.64%	34.53%	49.78%	60.63%	68.67%	100.00%	Cumulative yield	31.4%
RD	1.3	1.4	1.5	1.6	1.7	1.8	Whole coal	Required RD	1.49

Table C. 168: Overall hypothetical ash for compressive breakage to a top size of 6.7 mm with 5 minutes attritioning (Run 24).

Overall									
Cumulative float ash	4.47%	7.02%	10.96%	13.62%	16.03%	18.07%	29.52%	Target ash	10%
Cumulative float yield	12.06%	31.34%	49.63%	60.27%	68.21%	73.79%	100.00%	Cumulative yield	45.2%
RD	1.3	1.4	1.5	1.6	1.7	1.8	Whole coal	Required RD	1.48
For 0-0.5 mm (for an overall hypothetical density, how much will the yield be at particle size 0-0.5mm?									
Cumulative float ash	4.35%	5.39%	7.81%	9.82%	11.09%	12.24%	22.51%		
Cumulative float yield	0.02%	39.59%	60.30%	69.99%	74.99%	78.45%	100.00%	Cumulative yield	55.2%
RD	1.3	1.4	1.5	1.6	1.7	1.8	Whole coal	Required RD	1.48
For 0.5-1 mm (for an overall hypothetical density, how much will the yield be at particle size 0.5-1mm?									
Cumulative float ash	4.35%	5.36%	7.27%	9.04%	10.53%	11.69%	21.41%		
Cumulative float yield	1.13%	45.52%	62.30%	70.59%	76.34%	79.83%	100.00%	Cumulative yield	58.2%
RD	1.3	1.4	1.5	1.6	1.7	1.8	Whole coal	Required RD	1.48
For 1-2 mm (for an overall hypothetical density, how much will the yield be at particle size 1-2mm?									
Cumulative float ash	4.47%	7.10%	9.67%	11.67%	13.59%	15.23%	25.33%		
Cumulative float yield	32.94%	48.13%	60.45%	68.31%	74.32%	78.50%	100.00%	Cumulative yield	57.4%
RD	1.3	1.4	1.5	1.6	1.7	1.8	Whole coal	Required RD	1.48
For 2-4.75 mm (for an overall hypothetical density, how much will the yield be at particle size 2-4.75mm?									
Cumulative float ash	4.47%	7.85%	12.54%	15.38%	18.02%	20.36%	31.50%		
Cumulative float yield	16.79%	28.23%	46.68%	58.06%	66.86%	73.39%	100.00%	Cumulative yield	42.2%
RD	1.3	1.4	1.5	1.6	1.7	1.8	Whole coal	Required RD	1.48
For 4.75-6.7 mm (for an overall hypothetical density, how much will the yield be at particle size 4.75-6.7mm?									
Cumulative float ash	4.47%	9.59%	15.48%	18.55%	21.62%	24.10%	37.07%		
Cumulative float yield	5.69%	14.78%	35.33%	48.10%	58.73%	65.97%	100.00%	Cumulative yield	30.3%
RD	1.3	1.4	1.5	1.6	1.7	1.8	Whole coal	Required RD	1.48

The feed and product PSD was calculated using Equation D- 20 and Equation D- 21.

Table C. 169: Projected float yield and according particle size distributions for raw ROM coal.

Particle size	Cumulative float yield	Feed PSD	Product PSD
0-0.5mm	42.1%	8.26%	14.4%
0.5-1mm	57.6%	5.95%	14.2%
1-2mm	63.1%	6.45%	16.9%
2-4.75mm	40.9%	9.81%	16.6%
4.75-6.7mm	42.2%	6.26%	10.9%
6.7-9.5mm	16.7%	6.51%	4.5%
9.5-13.2mm	11.3%	6.35%	3.0%
13.2-19mm	9.5%	11.26%	4.4%
19-26.5mm	8.0%	10.73%	3.5%
26.5-37.5mm	0.0%	8.85%	0.0%
37.5-53mm	23.3%	12.02%	11.6%
53-75mm	0.0%	7.55%	0.0%

Table C. 170: Projected float yield and according particle size distributions for impact breakage to a top size of 13.2 mm with no attritioning (Run 1-3 average).

Particle size	Cumulative float yield	Feed PSD	Product PSD
0-0.5mm	53.6%	9.99%	14.9%
0.5-1mm	65.3%	9.31%	17.0%
1-2mm	56.5%	9.86%	15.5%
2-4.75mm	42.0%	16.35%	19.2%
4.75-6.7mm	32.2%	8.74%	7.9%
6.7-9.5mm	27.6%	12.39%	9.6%
9.5-13.2mm	17.1%	33.37%	16.0%

Table C. 171: Projected float yield and according particle size distributions for impact breakage to a top size of 13.2 mm with 1 minute attritioning (Run 4).

Particle size	Cumulative float yield	Feed PSD	Product PSD
0-0.5mm	46.1%	10.28%	17.4%
0.5-1mm	52.1%	6.82%	13.1%
1-2mm	50.6%	10.10%	18.8%
2-4.75mm	31.6%	18.74%	21.8%
4.75-6.7mm	19.8%	11.71%	8.5%
6.7-9.5mm	16.1%	18.24%	10.8%
9.5-13.2mm	10.9%	24.10%	9.7%

Table C. 172: Projected float yield and according particle size distributions for impact breakage to a top size of 13.2 mm with 2 minutes attritioning (Run 5).

Particle size	Cumulative float yield	Feed PSD	Product PSD
0-0.5mm	51.7%	10.28%	14.9%
0.5-1mm	61.7%	7.23%	12.5%
1-2mm	59.5%	10.77%	18.0%
2-4.75mm	43.4%	17.60%	21.5%
4.75-6.7mm	30.2%	10.11%	8.6%
6.7-9.5mm	28.1%	14.36%	11.3%
9.5-13.2mm	15.8%	29.64%	13.2%

Table C. 173: Projected float yield and according particle size distributions for impact breakage to a top size of 13.2 mm with 5 minutes attritioning (Run 6).

Particle size	Cumulative float yield	Feed PSD	Product PSD
0-0.5mm	46.8%	10.48%	14.4%
0.5-1mm	54.7%	7.25%	11.6%
1-2mm	57.9%	13.15%	22.4%
2-4.75mm	39.8%	19.23%	22.5%
4.75-6.7mm	26.3%	10.43%	8.0%
6.7-9.5mm	23.3%	14.49%	9.9%
9.5-13.2mm	15.2%	24.96%	11.1%

Table C. 174: Projected float yield and according particle size distributions for impact breakage to a top size of 6.7 mm with no attritioning (Run 7-9 average).

Particle size	Cumulative float yield	Feed PSD	Product PSD
0-0.5mm	47.9%	12.22%	15.1%
0.5-1mm	53.0%	7.65%	10.5%
1-2mm	59.9%	13.90%	21.5%
2-4.75mm	44.8%	22.34%	25.9%
4.75-6.7mm	23.7%	43.89%	27.0%

Table C. 175: Projected float yield and according particle size distributions for impact breakage to a top size of 6.7 mm with 1 minute attritioning (Run 10).

Particle size	Cumulative float yield	Feed PSD	Product PSD
0-0.5mm	84.4%	18.07%	25.2%
0.5-1mm	80.9%	10.34%	13.8%
1-2mm	65.6%	14.17%	15.4%
2-4.75mm	57.8%	30.98%	29.6%
4.75-6.7mm	36.6%	26.43%	16.0%

Table C. 176: Projected float yield and according particle size distributions for impact breakage to a top size of 6.7 mm with 2 minutes attritioning (Run 11).

Particle size	Cumulative float yield	Feed PSD	Product PSD
0-0.5mm	61.6%	18.52%	21.9%
0.5-1mm	63.0%	10.16%	12.3%
1-2mm	63.4%	15.83%	19.3%
2-4.75mm	51.9%	28.71%	28.6%
4.75-6.7mm	34.8%	26.78%	17.9%

Table C. 177: Projected float yield and according particle size distributions for impact breakage to a top size of 6.7 mm with 5 minutes attritioning (Run 12).

Particle size	Cumulative float yield	Feed PSD	Product PSD
0-0.5mm	82.6%	19.10%	27.4%
0.5-1mm	78.8%	10.85%	14.9%
1-2mm	64.4%	14.03%	15.7%
2-4.75mm	52.5%	27.98%	25.5%
4.75-6.7mm	34.0%	28.04%	16.6%

Table C. 178: Projected float yield and according particle size distributions for compressive breakage to a top size of 13.2 mm with no attritioning (Run 13-15 average).

Particle size	Cumulative float yield	Feed PSD	Product PSD
0-0.5mm	44.1%	12.89%	15.8%
0.5-1mm	57.3%	9.64%	15.3%
1-2mm	59.1%	10.33%	16.9%
2-4.75mm	43.4%	18.24%	22.0%
4.75-6.7mm	30.9%	9.82%	8.4%
6.7-9.5mm	24.9%	15.60%	10.8%
9.5-13.2mm	16.6%	23.48%	10.8%

Table C. 179: Projected float yield and according particle size distributions for compressive breakage to a top size of 13.2 mm with 1 minute attritioning (Run 16).

Particle size	Cumulative float yield	Feed PSD	Product PSD
0-0.5mm	52.1%	13.15%	17.8%
0.5-1mm	63.2%	9.72%	16.0%
1-2mm	59.6%	9.80%	15.2%
2-4.75mm	43.8%	17.35%	19.7%
4.75-6.7mm	33.4%	10.02%	8.7%
6.7-9.5mm	26.9%	16.42%	11.5%
9.5-13.2mm	18.3%	23.55%	11.2%

Table C. 180: Projected float yield and according particle size distributions for compressive breakage to a top size of 13.2 mm with 2 minutes attritioning (Run 17).

Particle size	Cumulative float yield	Feed PSD	Product PSD
0-0.5mm	55.9%	15.57%	23.9%
0.5-1mm	60.6%	9.13%	15.2%
1-2mm	56.6%	9.14%	14.2%
2-4.75mm	40.1%	16.37%	18.0%
4.75-6.7mm	27.8%	9.57%	7.3%
6.7-9.5mm	24.0%	16.45%	10.8%
9.5-13.2mm	16.0%	23.79%	10.5%

Table C. 181: Projected float yield and according particle size distributions for compressive breakage to a top size of 13.2 mm with 5 minutes attritioning (Run 18).

Particle size	Cumulative float yield	Feed PSD	Product PSD
0-0.5mm	51.6%	13.14%	19.1%
0.5-1mm	62.8%	9.71%	17.1%
1-2mm	57.9%	10.52%	17.1%
2-4.75mm	39.6%	18.02%	20.0%
4.75-6.7mm	27.1%	10.11%	7.7%
6.7-9.5mm	20.4%	15.69%	9.0%
9.5-13.2mm	15.5%	22.81%	9.9%

Table C. 182: Projected float yield and according particle size distributions for compressive breakage to a top size of 6.7 mm with no attritioning (Run 19-21 average).

Particle size	Cumulative float yield	Feed PSD	Product PSD
0-0.5mm	49.1%	15.32%	20.3%
0.5-1mm	54.0%	11.17%	16.3%
1-2mm	51.8%	13.16%	18.4%
2-4.75mm	35.8%	30.41%	29.4%
4.75-6.7mm	19.1%	29.95%	15.5%

Table C. 183: Projected float yield and according particle size distributions for compressive breakage to a top size of 6.7 mm with 1 minute attritioning (Run 22).

Particle size	Cumulative float yield	Feed PSD	Product PSD
0-0.5mm	52.3%	15.56%	19.9%
0.5-1mm	55.9%	10.60%	14.5%
1-2mm	53.3%	14.58%	19.0%
2-4.75mm	36.5%	34.02%	30.4%
4.75-6.7mm	26.1%	25.24%	16.1%

Table C. 184: Projected float yield and according particle size distributions for compressive breakage to a top size of 6.7 mm with 2 minutes attritioning (Run 23).

Particle size	Cumulative float yield	Feed PSD	Product PSD
0-0.5mm	56.3%	17.08%	20.1%
0.5-1mm	64.9%	11.99%	16.2%
1-2mm	60.3%	13.70%	17.2%
2-4.75mm	43.9%	34.48%	31.6%
4.75-6.7mm	31.4%	22.75%	14.9%

Table C. 185: Projected float yield and according particle size distributions for compressive breakage to a top size of 6.7 mm with 5 minutes attritioning (Run 24).

Particle size	Cumulative float yield	Feed PSD	Product PSD
0-0.5mm	55.2%	15.59%	19.1%
0.5-1mm	58.2%	10.61%	13.7%
1-2mm	57.4%	13.63%	17.3%
2-4.75mm	42.2%	36.27%	33.9%
4.75-6.7mm	30.3%	23.89%	16.0%

Table C. 186: Cumulative feed PSD and float PSD for raw ROM coal.

Particle size (mm)	Cumulative feed PSD	Cumulative float PSD
0	0%	0%
0.5	8.26%	14.4%
1	14.21%	28.6%
2	20.66%	45.4%
4.75	30.47%	62.0%
6.7	36.73%	73.0%
9.5	43.24%	77.5%
13.2	49.59%	80.4%
19	60.85%	84.9%
26.5	71.58%	88.4%
37.5	80.43%	88.4%
53	92.45%	100.0%
75	100.00%	100.0%

Table C. 187: Cumulative feed PSD and float PSD for impact breakage to a top size of 13.2 mm with no attritioning (Run 1-3 average).

Particle size (mm)	Cumulative feed PSD	Cumulative float PSD
0	0%	0%
0.5	9.99%	14.9%
1	19.30%	31.9%
2	29.15%	47.5%
4.75	45.50%	66.6%
6.7	54.24%	74.5%
9.5	66.63%	84.0%
13.2	100.00%	100.0%

Table C. 188: Cumulative feed PSD and float PSD for impact breakage to a top size of 13.2 mm with 1 minute attritioning (Run 4).

Particle size (mm)	Cumulative feed PSD	Cumulative float PSD
0	0%	0%
0.5	10.28%	17.4%
1	17.10%	30.5%
2	27.20%	49.3%
4.75	45.94%	71.0%
6.7	57.66%	79.6%
9.5	75.90%	90.3%
13.2	100.00%	100.0%

Table C. 189: Cumulative feed PSD and float PSD for impact breakage to a top size of 13.2 mm with 2 minutes attritioning (Run 5).

Particle size (mm)	Cumulative feed PSD	Cumulative float PSD
0	0%	0%
0.5	10.28%	14.9%
1	17.51%	27.5%
2	28.29%	45.5%
4.75	45.89%	66.9%
6.7	56.00%	75.5%
9.5	70.36%	86.8%
13.2	100.00%	100.0%

Table C. 190: Cumulative feed PSD and float PSD for impact breakage to a top size of 13.2 mm with 5 minutes attritioning (Run 6).

Particle size (mm)	Cumulative feed PSD	Cumulative float PSD
0	0%	0%
0.5	10.48%	14.4%
1	17.73%	26.1%
2	30.88%	48.4%
4.75	50.12%	70.9%
6.7	60.55%	78.9%
9.5	75.04%	88.9%
13.2	100.00%	100.0%

Table C. 191: Cumulative feed PSD and float PSD for impact breakage to a top size of 6.7 mm with no attritioning (Run 7-9 average).

Particle size (mm)	Cumulative feed PSD	Cumulative float PSD
0	0%	0%
0.5	12.22%	15.1%
1	19.87%	25.6%
2	33.77%	47.2%
4.75	56.11%	73.0%
6.7	100.00%	100.0%

Table C. 192: Cumulative feed PSD and float PSD for impact breakage to a top size of 6.7 mm with 1 minute attritioning (Run 10).

Particle size (mm)	Cumulative feed PSD	Cumulative float PSD
0	0%	0%
0.5	18.07%	25.2%
1	28.41%	39.0%
2	42.58%	54.4%
4.75	73.57%	84.0%
6.7	100.00%	100.0%

Table C. 193: Cumulative feed PSD and float PSD for impact breakage to a top size of 6.7 mm with 2 minutes attritioning (Run 11).

Particle size (mm)	Cumulative feed PSD	Cumulative float PSD
0	0%	0%
0.5	18.52%	21.9%
1	28.69%	34.2%
2	44.52%	53.5%
4.75	73.22%	82.1%
6.7	100.00%	100.0%

Table C. 194: Cumulative feed PSD and float PSD for impact breakage to a top size of 6.7 mm with 5 minutes attritioning (Run 12).

Particle size (mm)	Cumulative feed PSD	Cumulative float PSD
0	0%	0%
0.5	19.10%	27.4%
1	29.96%	42.3%
2	43.99%	57.9%
4.75	71.96%	83.4%
6.7	100.00%	100.0%

Table C. 195: Cumulative feed PSD and float PSD for compressive breakage to a top size of 13.2 mm with no attritioning (Run 13-15 average).

Particle size (mm)	Cumulative feed PSD	Cumulative float PSD
0	0%	0%
0.5	12.89%	15.8%
1	22.53%	31.1%
2	32.86%	48.0%
4.75	51.10%	70.0%
6.7	60.92%	78.4%
9.5	76.52%	89.2%
13.2	100.00%	100.0%

Table C. 196: Cumulative feed PSD and float PSD for compressive breakage to a top size of 13.2 mm with 1 minute attritioning (Run 16).

Particle size (mm)	Cumulative feed PSD	Cumulative float PSD
0	0%	0%
0.5	13.15%	17.8%
1	22.87%	33.7%
2	32.67%	48.9%
4.75	50.01%	68.7%
6.7	60.03%	77.4%
9.5	76.45%	88.8%
13.2	100.00%	100.0%

Table C. 197: Cumulative feed PSD and float PSD for compressive breakage to a top size of 13.2 mm with 2 minutes attritioning (Run 17).

Particle size (mm)	Cumulative feed PSD	Cumulative float PSD
0	0%	0%
0.5	15.57%	23.9%
1	24.69%	39.1%
2	33.83%	53.4%
4.75	50.19%	71.4%
6.7	59.76%	78.7%
9.5	76.21%	89.5%
13.2	100.00%	100.0%

Table C. 198: Cumulative feed PSD and float PSD for compressive breakage to a top size of 13.2 mm with 5 minutes attritioning (Run 18).

Particle size (mm)	Cumulative feed PSD	Cumulative float PSD
0	0%	0%
0.5	13.14%	19.1%
1	22.85%	36.2%
2	33.37%	53.3%
4.75	51.39%	73.4%
6.7	61.50%	81.1%
9.5	77.19%	90.1%
13.2	100.00%	100.0%

Table C. 199: Cumulative feed PSD and float PSD for compressive breakage to a top size of 6.7 mm with no attritioning (Run 19-21 average).

Particle size (mm)	Cumulative feed PSD	Cumulative float PSD
0	0%	0%
0.5	15.32%	20.3%
1	26.49%	36.7%
2	39.65%	55.1%
4.75	70.05%	84.5%
6.7	100.00%	100.0%

Table C. 200: Cumulative feed PSD and float PSD for compressive breakage to a top size of 6.7 mm with 1 minute attritioning (Run 22).

Particle size (mm)	Cumulative feed PSD	Cumulative float PSD
0	0%	0%
0.5	15.56%	19.9%
1	26.16%	34.4%
2	40.74%	53.4%
4.75	74.76%	83.9%
6.7	100.00%	100.0%

Table C. 201: Cumulative feed PSD and float PSD for compressive breakage to a top size of 6.7 mm with 2 minutes attritioning (Run 23).

Particle size (mm)	Cumulative feed PSD	Cumulative float PSD
0	0%	0%
0.5	17.08%	20.1%
1	29.07%	36.3%
2	42.76%	53.5%
4.75	77.25%	85.1%
6.7	100.00%	100.0%

Table C. 202: Cumulative feed PSD and float PSD for compressive breakage to a top size of 6.7 mm with 5 minutes attritioning (Run 24).

Particle size (mm)	Cumulative feed PSD	Cumulative float PSD
0	0%	0%
0.5	15.59%	19.1%
1	26.21%	32.8%
2	39.84%	50.1%
4.75	76.11%	84.0%
6.7	100.00%	100.0%

The cumulative feed PSD and the cumulative float PSD was illustrated by using the following graphs:

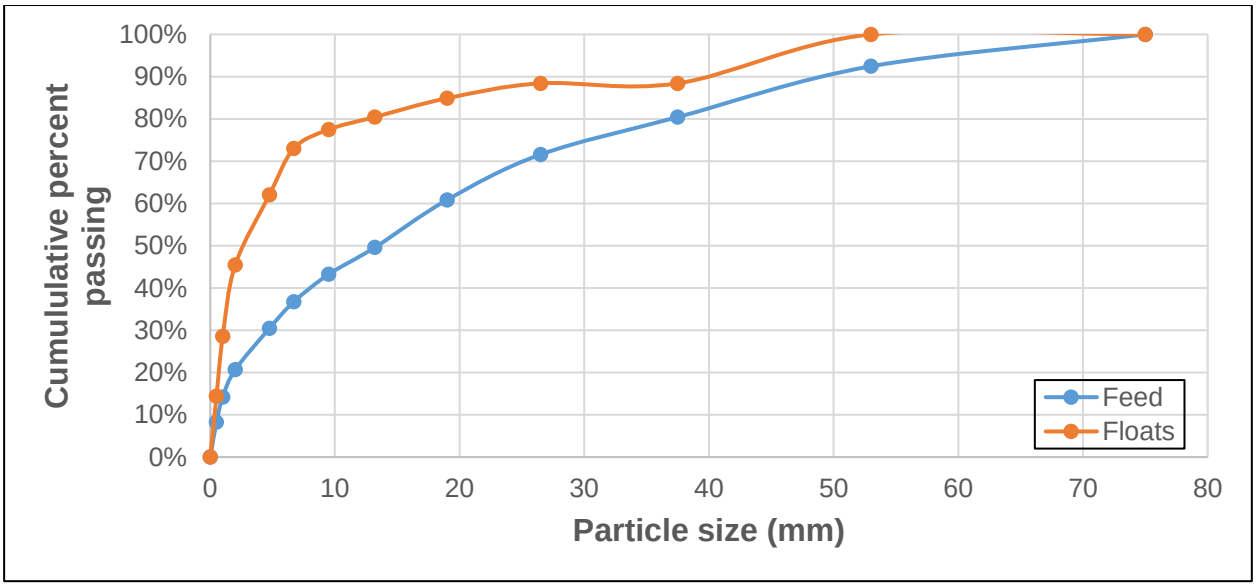

Figure C. 91: Hypothetical density wash curve for raw ROM coal.

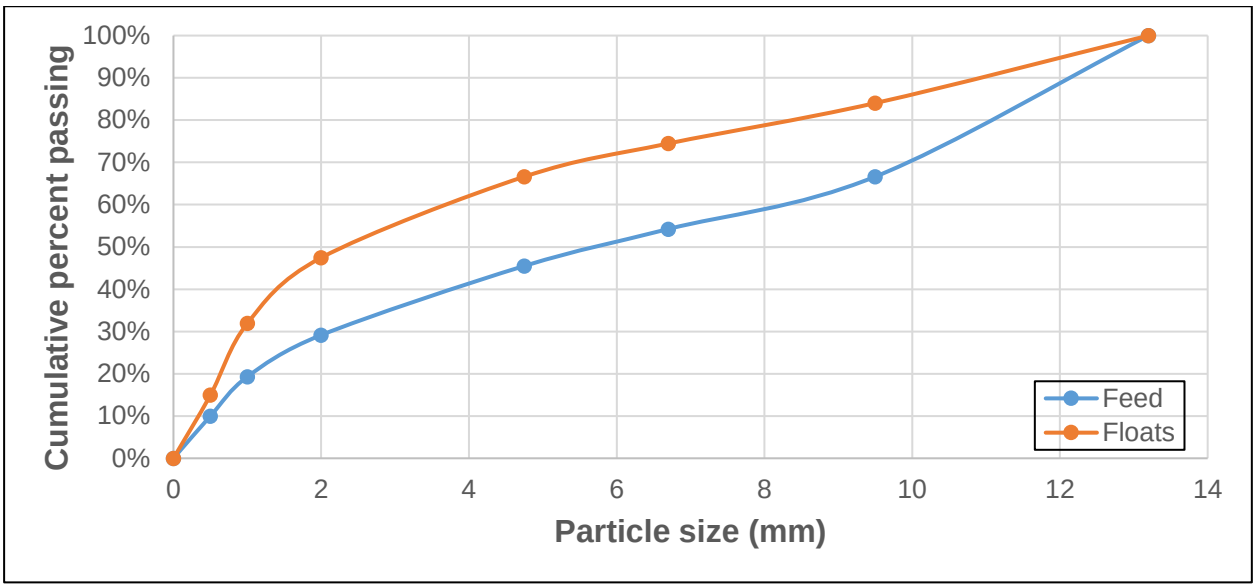

Figure C. 92: Hypothetical density wash curve for impact breakage to a top size of 13.2 mm with no attritioning (Run 1-3 average).

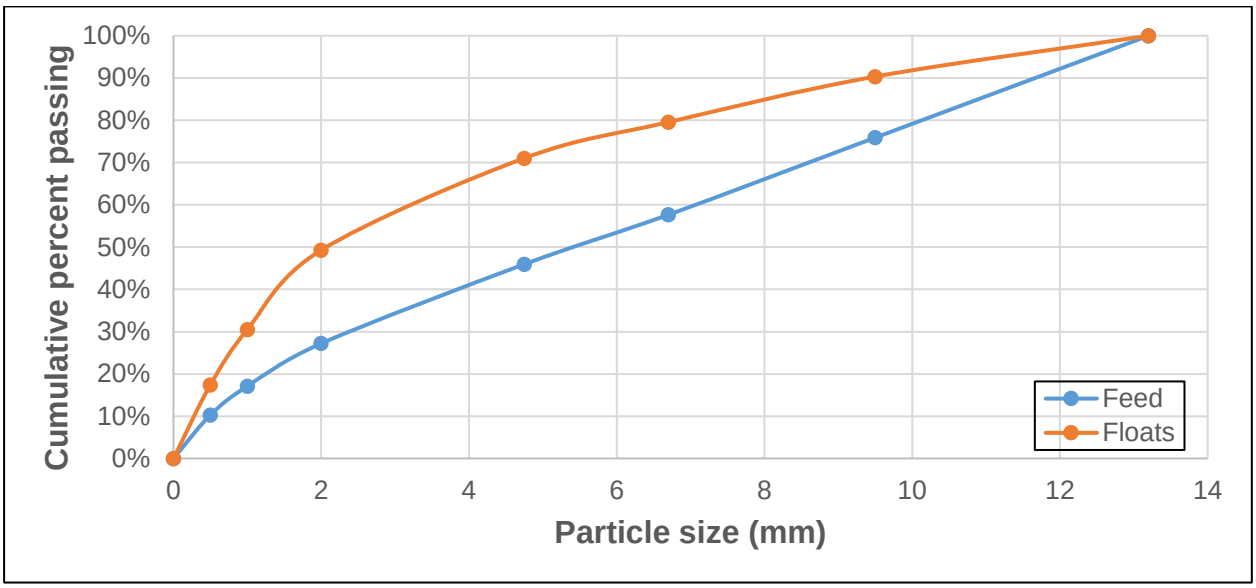

Figure C. 93: Hypothetical density wash curve for impact breakage to a top size of 13.2 mm with 1 minute attritioning (Run 4).

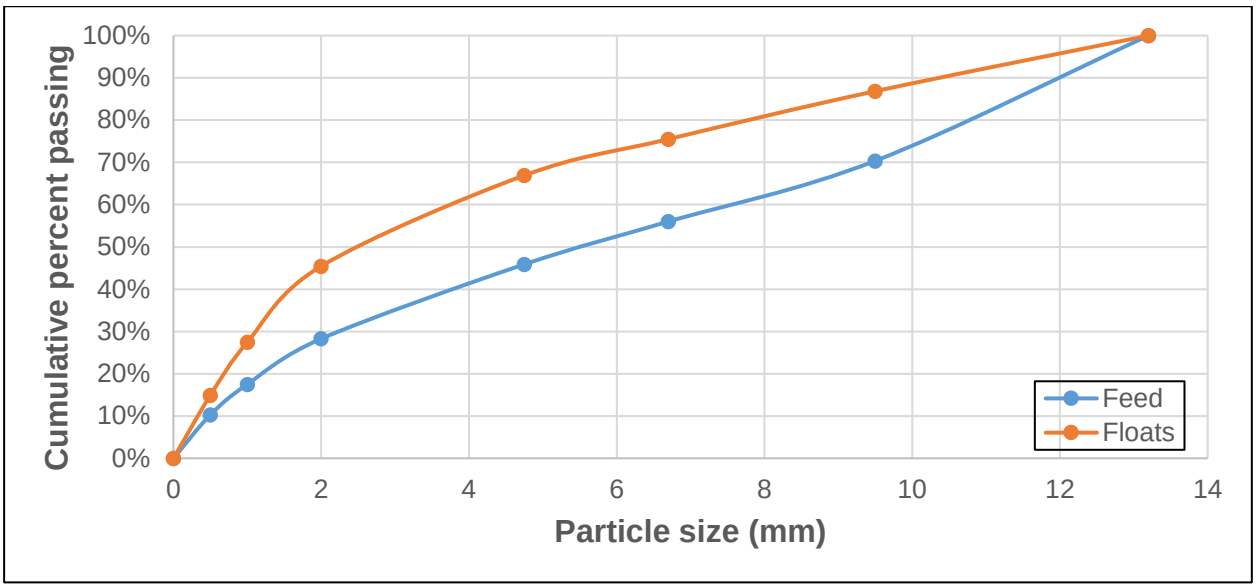

Figure C. 94: Hypothetical density wash curve for impact breakage to a top size of 13.2 mm with 2 minutes attritioning (Run 5).

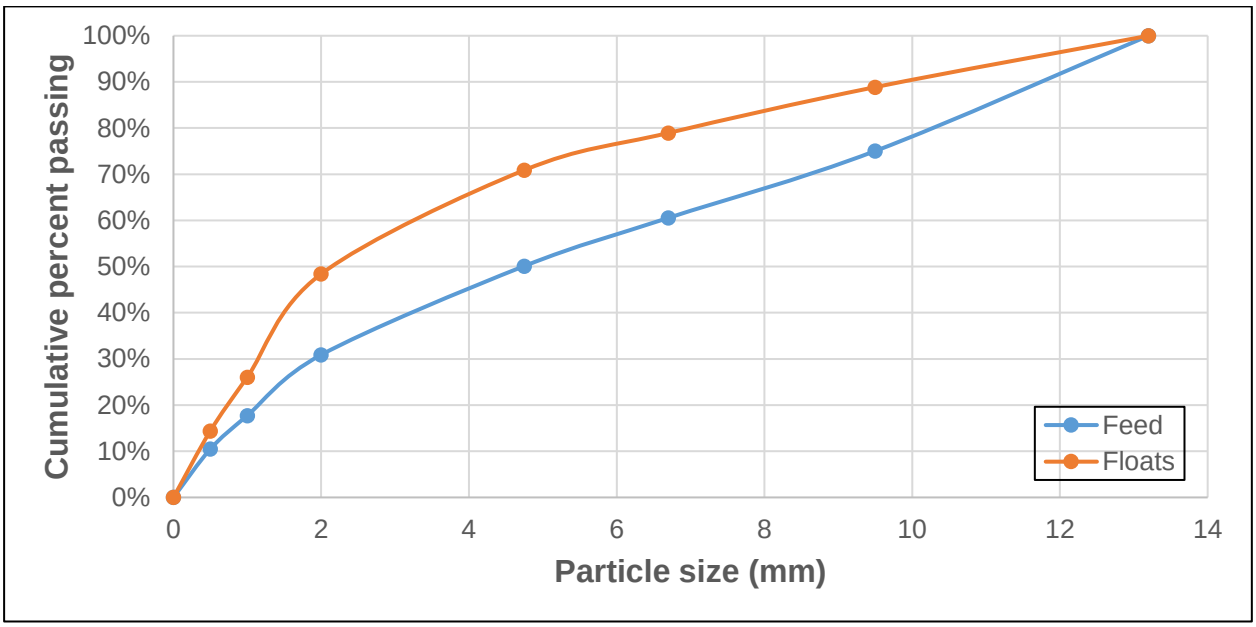

Figure C. 95: Hypothetical density wash curve for impact breakage to a top size of 13.2 mm with 5 minutes attritioning (Run 6).

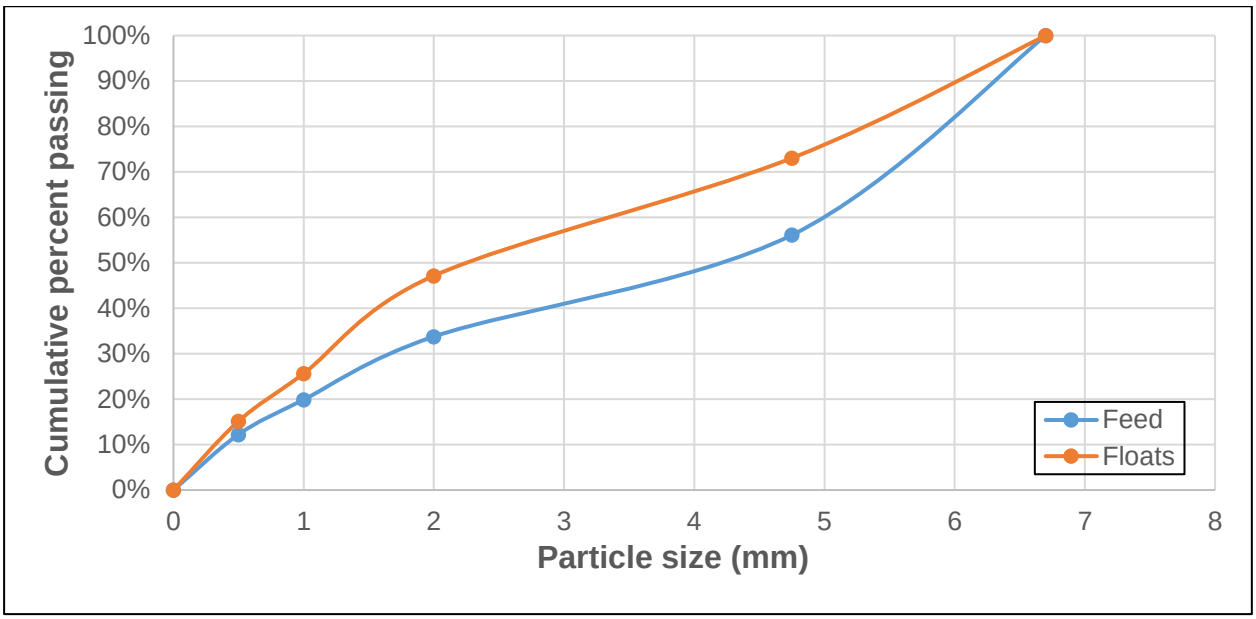

Figure C. 96: Hypothetical density wash curve for impact breakage to a top size of 6.7 mm with no attritioning (Run 7-9 average).

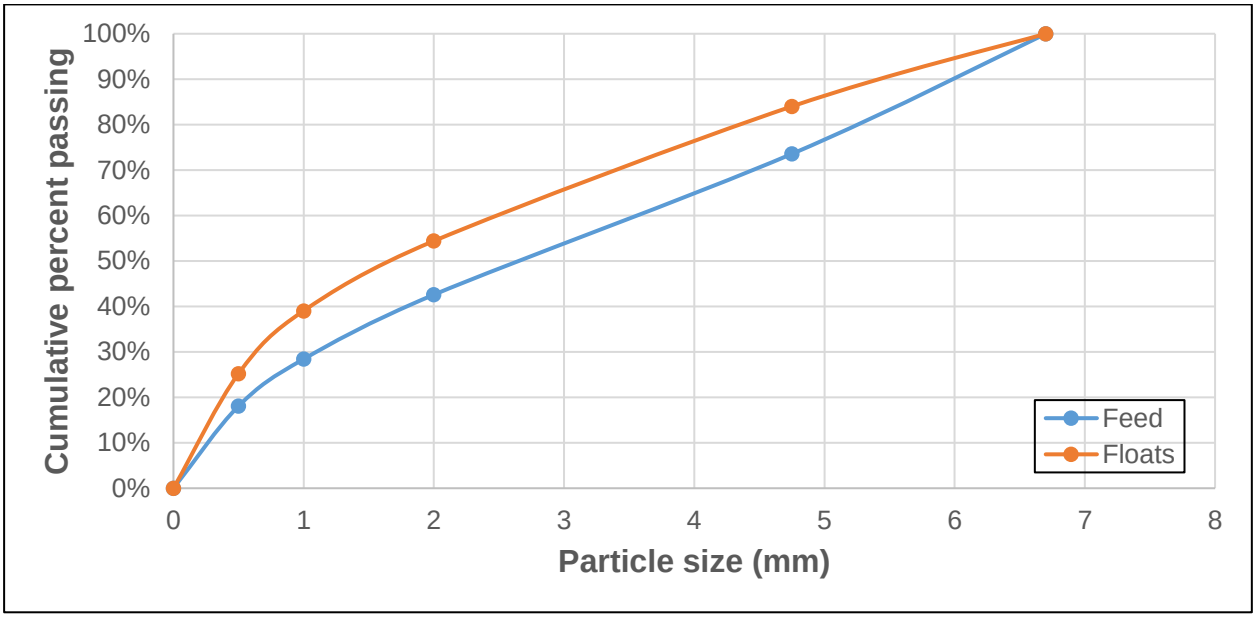

Figure C. 97: Hypothetical density wash curve for impact breakage to a top size of 6.7 mm with 1 minute attritioning (Run10).

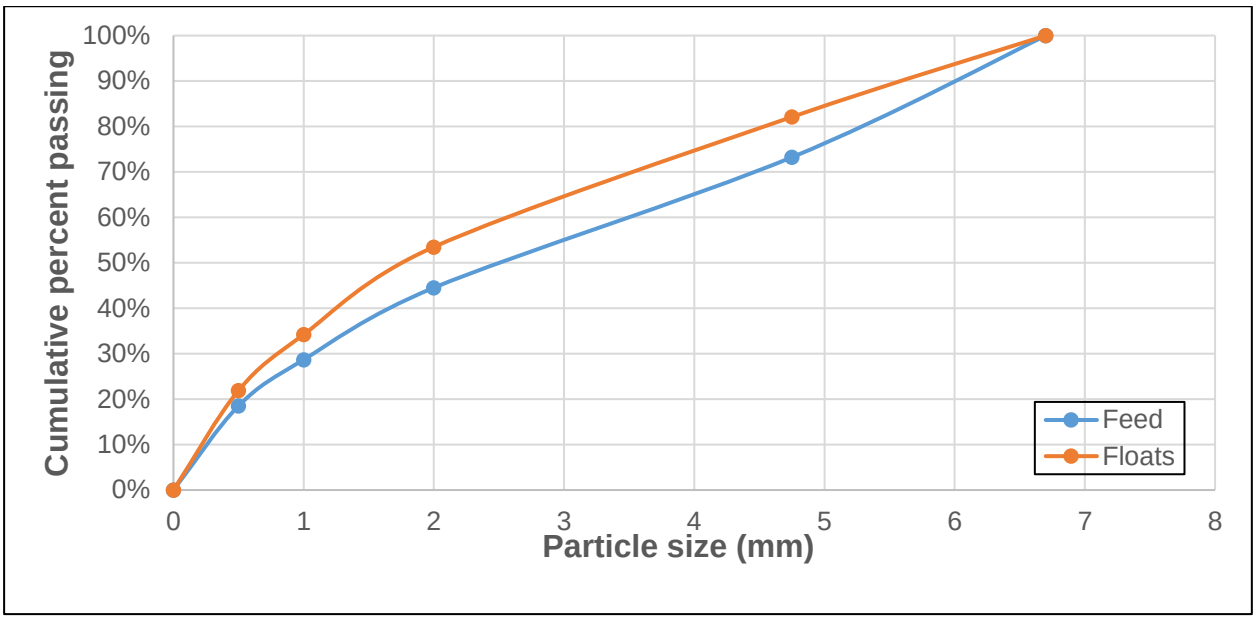

Figure C. 98: Hypothetical density wash curve for impact breakage to a top size of 6.7 mm with 2 minutes attritioning (Run 11).

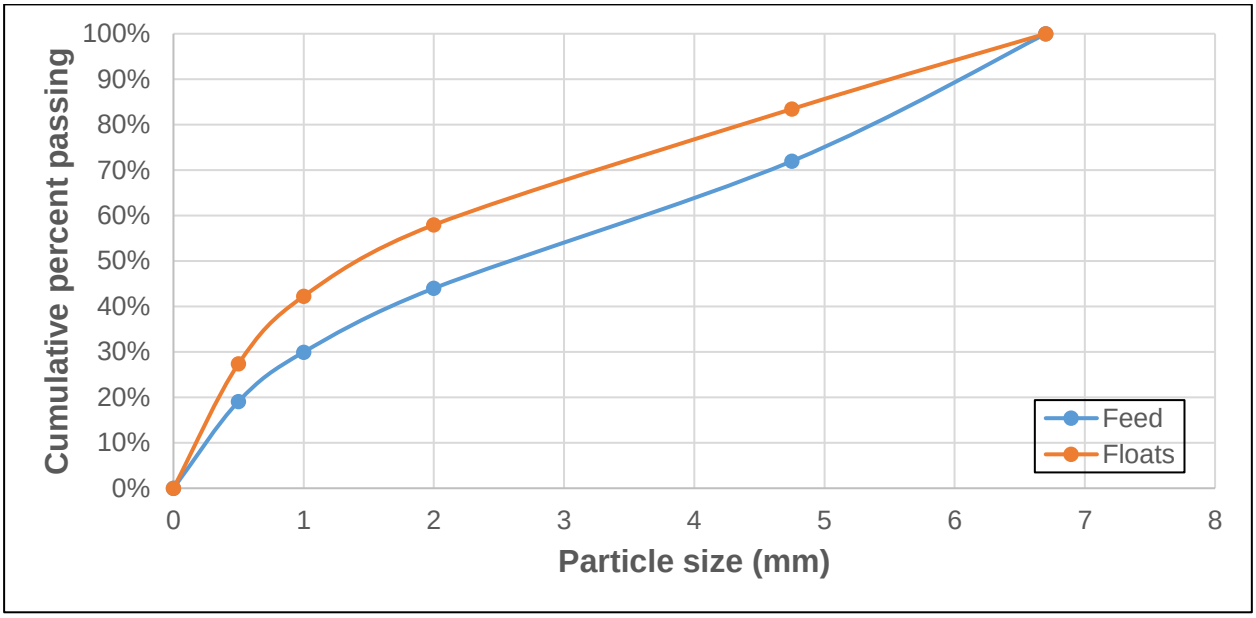

Figure C. 99: Hypothetical density wash curve for impact breakage to a top size of 6.7 mm with 5 minutes attritioning (Run 12).

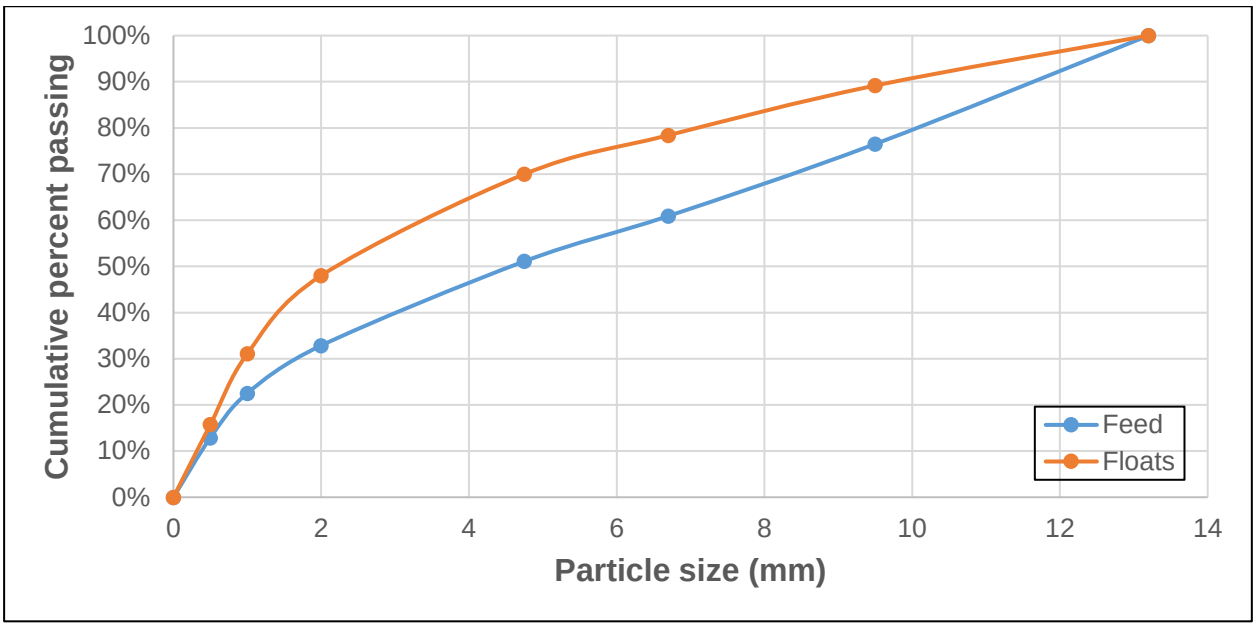

Figure C. 100: Hypothetical density wash curve for compressive breakage to a top size of 13.2 mm with no attritioning (Run 13-15 average).

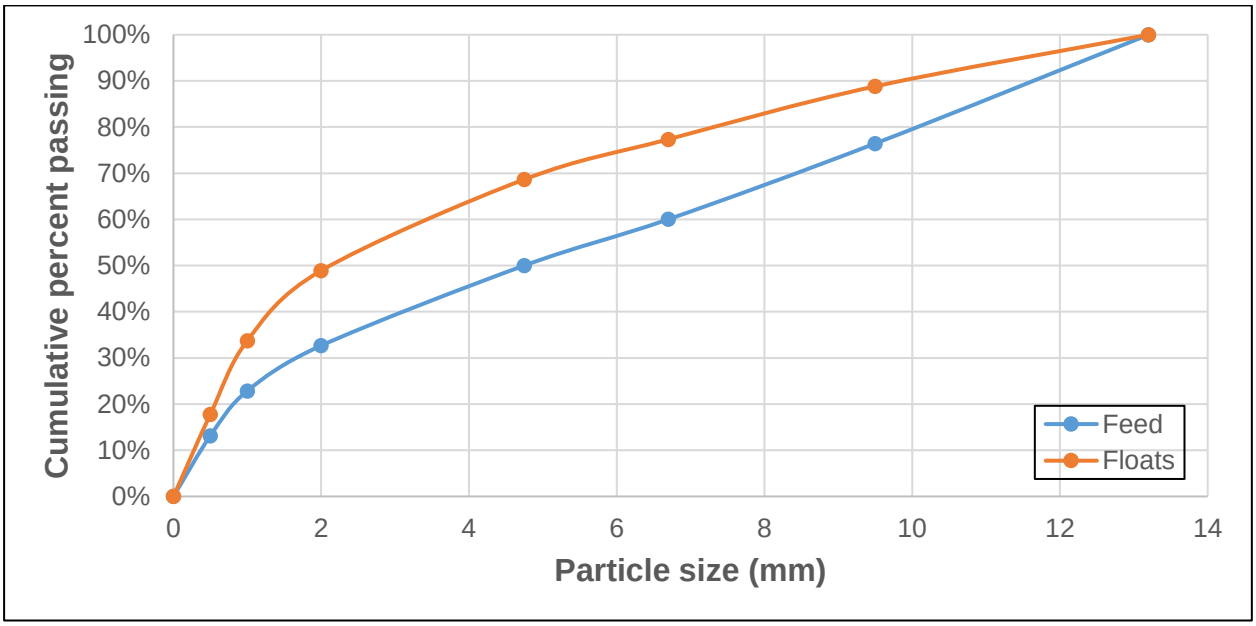

Figure C. 101: Hypothetical density wash curve for compressive breakage to a top size of 13.2 mm with 1 minute attritioning (Run 16).

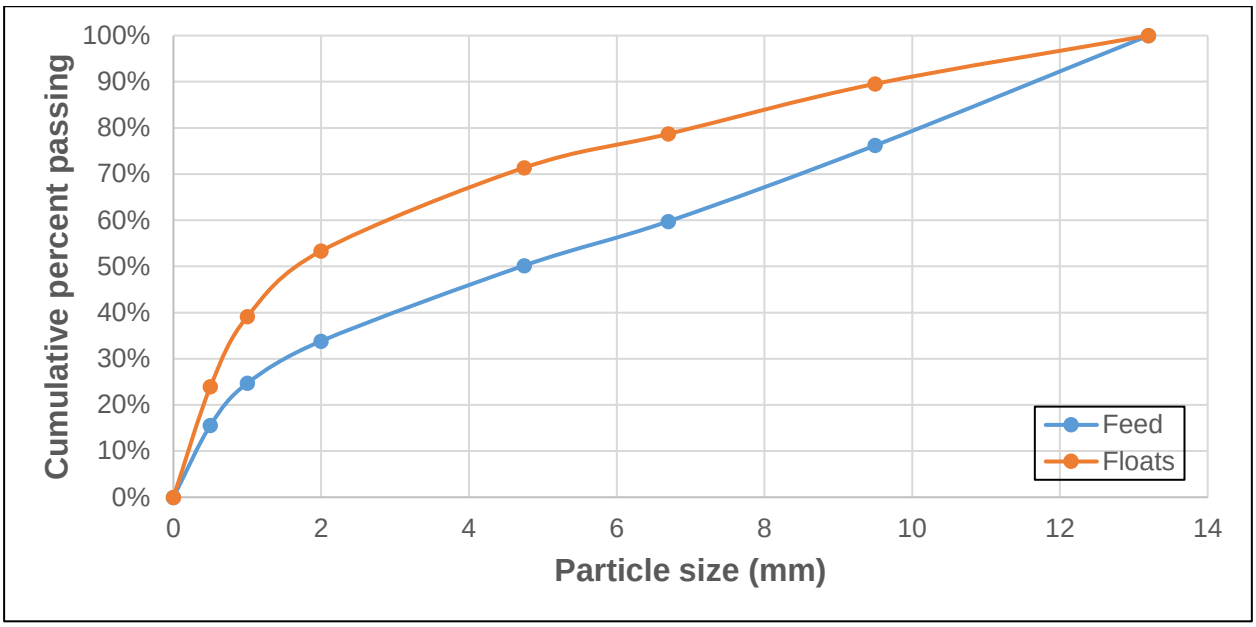

Figure C. 102: Hypothetical density wash curve for compressive breakage to a top size of 13.2 mm with 2 minutes attritioning (Run 17).

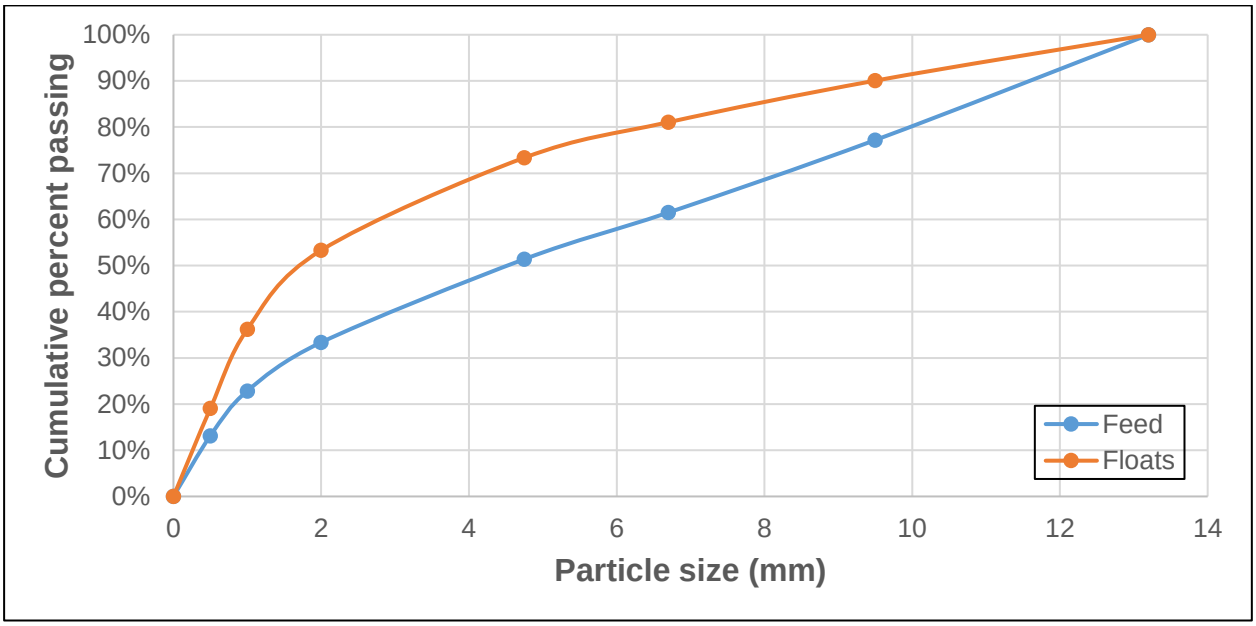

Figure C. 103: Hypothetical density wash curve for compressive breakage to a top size of 13.2 mm with 5 minutes attritioning (Run 18).

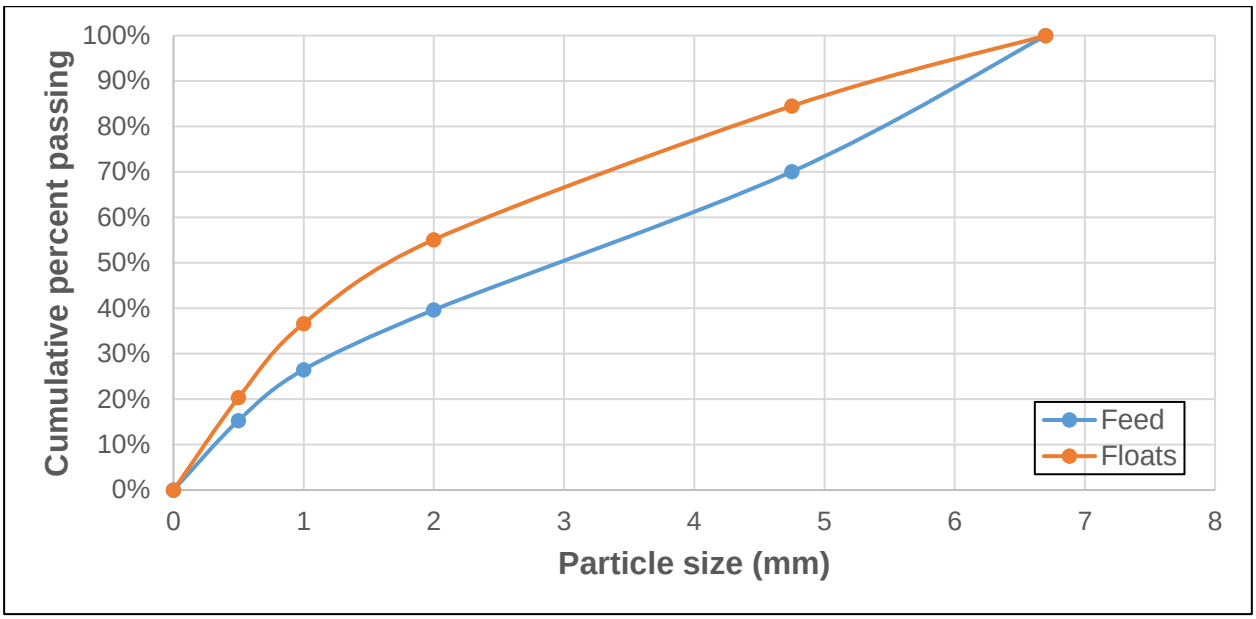

Figure C. 104: Hypothetical density wash curve for compressive breakage to a top size of 6.7 mm with no attritioning (Run 19-21 average).

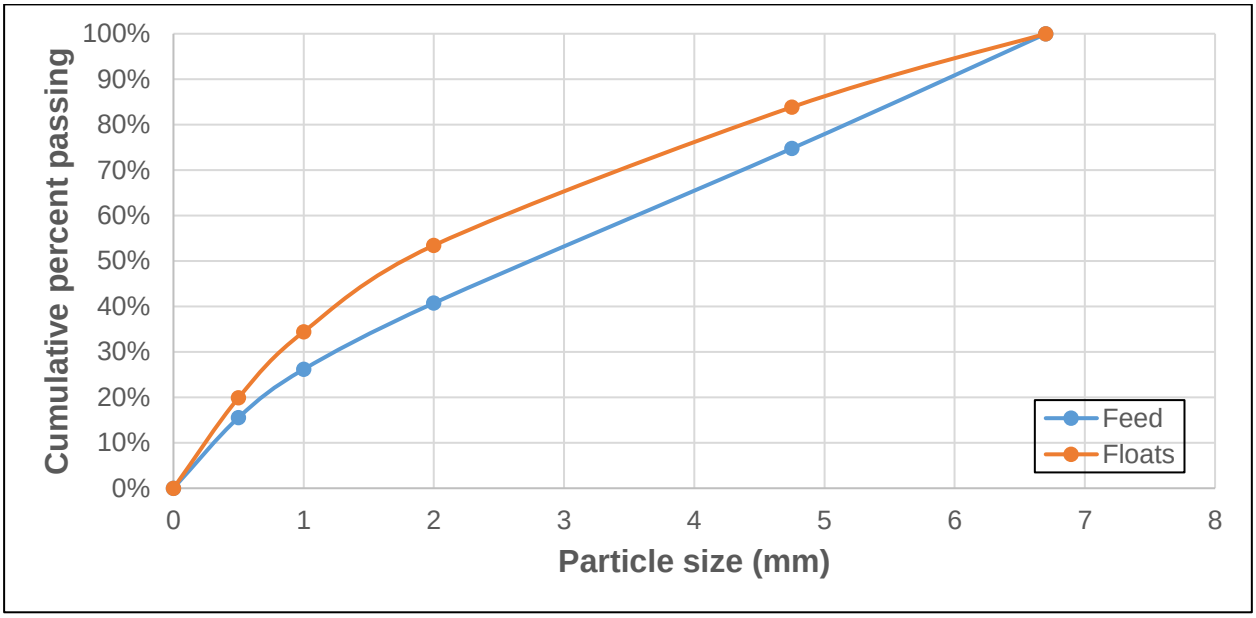

Figure C. 105: Hypothetical density wash curve for compressive breakage to a top size of 6.7 mm with 1 minute attritioning (Run 22).

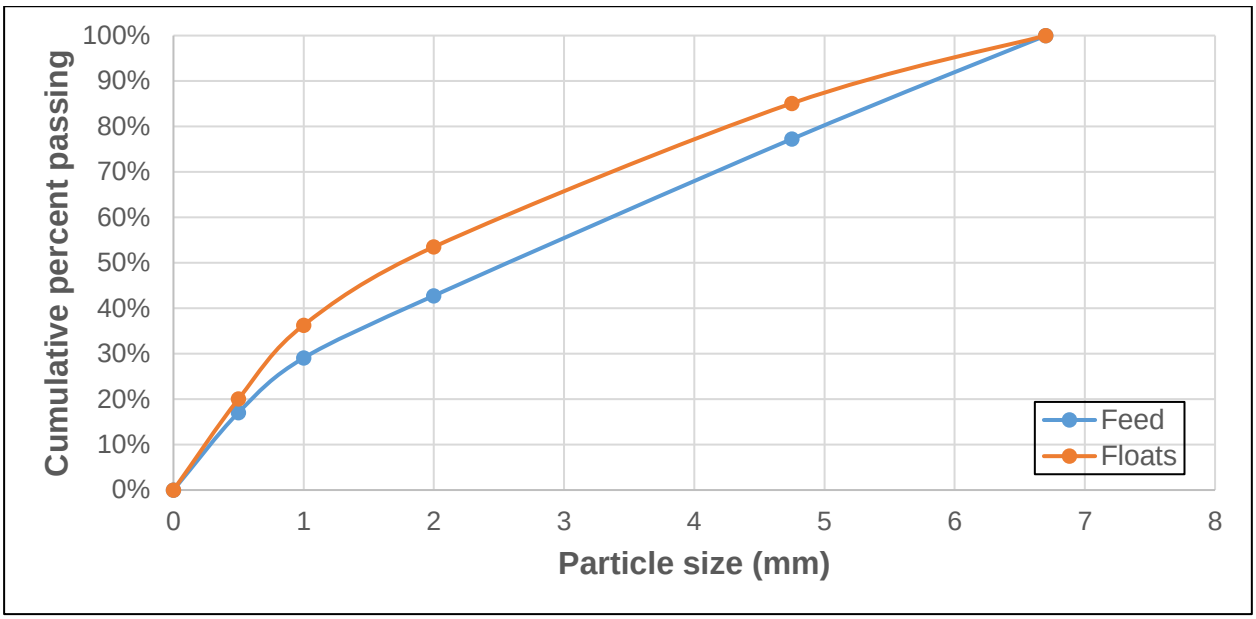

Figure C. 106: Hypothetical density wash curve for compressive breakage to a top size of 6.7 mm with 2 minutes attritioning (Run 23).

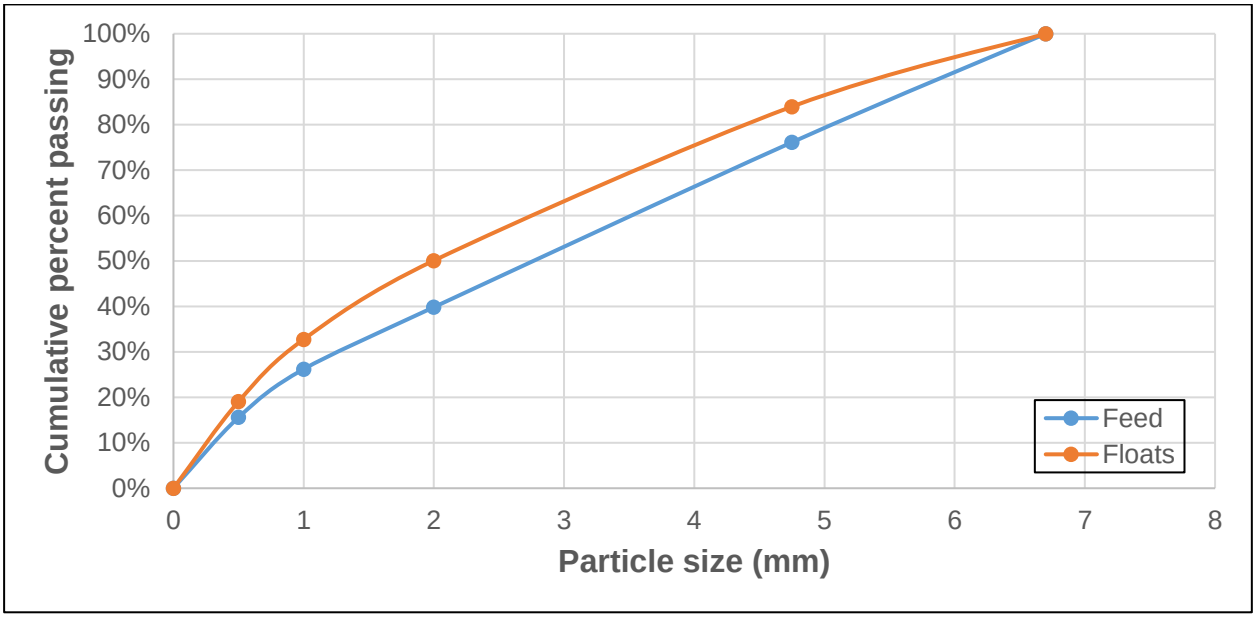

Figure C. 107: Hypothetical density wash curve for compressive breakage to a top size of 6.7 mm with 5 minutes attritioning (Run 24).

Standard deviation:

Standard deviations were calculated by using Equation 4.2.

Table C. 203: Standard deviation on fractional mass yield for impact breakage to top size of 13.2 mm with no attrition (Runs 1-3).

Particle size	F1.3	1.3-1.4	1.4-1.5	1.5-1.6	1.6-1.7	1.7-1.8	S1.8
9.5-13.2 mm	0.18	0.40	2.74	1.54	1.31	0.38	2.15
6.7-9.5 mm	0.16	0.02	0.98	1.10	0.18	0.13	0.04
4.75-6.7 mm	0.24	0.45	0.57	0.57	0.16	0.10	0.16
2-4.75 mm	1.41	0.85	1.45	0.73	0.21	0.06	0.25
1-2 mm	1.64	0.79	1.41	0.24	0.10	0.07	0.24
0.5-1 mm	0.71	1.58	0.56	0.24	0.15	0.12	0.31
0-0.5 mm	0.27	0.80	0.45	0.19	0.15	0.03	0.28

Table C. 204: Standard deviation on fractional mass yield for impact breakage to top size of 6.7 mm with no attrition (Runs 7-9).

Particle size	F1.3	1.3-1.4	1.4-1.5	1.5-1.6	1.6-1.7	1.7-1.8	S1.8
4.75-6.7 mm	0.09	2.49	1.88	1.03	0.23	0.78	0.74
2-4.75 mm	1.23	1.49	1.18	0.57	0.20	0.29	0.52
1-2 mm	0.48	1.65	0.80	0.25	0.07	0.15	0.37
0.5-1 mm	0.32	0.21	0.29	0.14	0.05	0.06	0.31
0-0.5 mm	0.17	1.70	0.66	0.75	0.41	0.20	1.46

Table C. 205: Standard deviation on fractional mass yield for compressive breakage to top size of 13.2 mm with no attrition (Runs 13-15).

Particle size	F1.3	1.3-1.4	1.4-1.5	1.5-1.6	1.6-1.7	1.7-1.8	S1.8
9.5-13.2 mm	0.10	0.89	0.47	0.14	0.34	0.12	0.61
6.7-9.5 mm	0.05	0.18	0.31	0.26	0.10	0.37	1.12
4.75-6.7 mm	0.04	0.09	0.24	0.04	0.01	0.04	0.80
2-4.75 mm	0.56	0.62	0.27	0.06	0.03	0.01	0.92
1-2 mm	0.56	0.95	0.14	0.04	0.02	0.04	0.38
0.5-1 mm	0.09	0.84	0.25	0.31	0.08	0.09	0.15
0-0.5 mm	0.01	0.95	0.81	0.70	0.20	0.08	0.49

Table C. 206: Standard deviation on fractional mass yield for compressive breakage to top size of 6.7 mm with no attrition (Runs 19-21).

Particle size	F1.3	1.3-1.4	1.4-1.5	1.5-1.6	1.6-1.7	1.7-1.8	S1.8
4.75-6.7 mm	0.05	0.26	0.34	0.57	0.61	0.35	2.41
2-4.75 mm	0.20	0.73	0.42	0.19	0.18	0.31	1.30
1-2 mm	0.33	0.20	0.11	0.09	0.04	0.09	0.22
0.5-1 mm	0.10	0.38	0.52	0.06	0.03	0.08	0.10
0-0.5 mm	0.00	0.65	0.94	0.11	0.03	0.16	0.31

Experimental error:

Experimental errors were calculated by using Equation 4.3.

Table C. 207: Experimental error on fractional mass yield for impact breakage to top size of 13.2 mm with no attrition (Run 1-3).

Particle size	F1.3	1.3-1.4	1.4-1.5	1.5-1.6	1.6-1.7	1.7-1.8	S1.8
9.5-13.2 mm	0.20	0.45	3.10	1.75	1.49	0.43	2.43
6.7-9.5 mm	0.18	0.03	1.11	1.24	0.20	0.14	0.05
4.75-6.7 mm	0.27	0.51	0.64	0.64	0.19	0.11	0.18
2-4.75 mm	1.59	0.97	1.64	0.82	0.24	0.07	0.28
1-2 mm	1.85	0.90	1.59	0.28	0.11	0.07	0.27
0.5-1 mm	0.80	1.79	0.63	0.27	0.17	0.14	0.35
0-0.5 mm	0.31	0.90	0.51	0.21	0.17	0.03	0.32

Table C. 208: Experimental error on fractional mass yield for impact breakage to top size of 6.7 mm with no attrition (Run 7-9).

Particle size	F1.3	1.3-1.4	1.4-1.5	1.5-1.6	1.6-1.7	1.7-1.8	S1.8
4.75-6.7 mm	0.10	2.82	2.12	1.17	0.26	0.89	0.84
2-4.75 mm	1.39	1.69	1.33	0.64	0.23	0.33	0.59
1-2 mm	0.55	1.87	0.90	0.28	0.07	0.17	0.42
0.5-1 mm	0.36	0.24	0.33	0.16	0.06	0.06	0.35
0-0.5 mm	0.20	1.92	0.75	0.85	0.47	0.23	1.66

Table C. 209: Experimental error on fractional mass yield for compressive breakage to top size of 13.2 mm with no attrition (Run 13-15).

Particle size	F1.3	1.3-1.4	1.4-1.5	1.5-1.6	1.6-1.7	1.7-1.8	S1.8
9.5-13.2 mm	0.11	1.01	0.53	0.15	0.38	0.13	0.70
6.7-9.5 mm	0.05	0.20	0.35	0.30	0.11	0.41	1.27
4.75-6.7 mm	0.04	0.10	0.27	0.05	0.01	0.05	0.90
2-4.75 mm	0.63	0.70	0.30	0.07	0.04	0.02	1.04
1-2 mm	0.63	1.08	0.16	0.05	0.03	0.04	0.43
0.5-1 mm	0.10	0.95	0.28	0.35	0.09	0.11	0.17
0-0.5 mm	0.01	1.07	0.91	0.80	0.23	0.09	0.55

Table C. 210: Experimental error on fractional mass yield for compressive breakage to top size of 6.7 mm with no attrition (Run 19-21).

Particle size	F1.3	1.3-1.4	1.4-1.5	1.5-1.6	1.6-1.7	1.7-1.8	S1.8
4.75-6.7 mm	0.06	0.29	0.38	0.65	0.69	0.40	2.73
2-4.75 mm	0.23	0.83	0.48	0.21	0.20	0.35	1.47
1-2 mm	0.37	0.22	0.13	0.10	0.04	0.11	0.25
0.5-1 mm	0.11	0.43	0.59	0.07	0.04	0.09	0.12
0-0.5 mm	0.00	0.74	1.07	0.13	0.04	0.18	0.35

Table C. 211: Repeatability and experimental error on fractional mass yield of attritioning.

Particle size (mm)	Average	Standard deviation	Error
4.75-6.7	25.24%	1.86	2.11
2-4.75	30.04%	1.20	1.35
1-2	15.40%	0.39	0.45
0.5-1	12.57%	0.38	0.43
0-0.5	16.76%	1.71	1.93

Table C. 212: Averages for proximate, calorific value and swelling index analysis results expressed on a dry basis (average of 0.0-1.0 mm and 1.0-13.2 mm results).

Sample Name	Ash (%)	Volatile matter (%)	Fixed Carbon (%)	Calorific value (MJ/kg)	Total sulphur (%)	Free swelling index
F1.3	4.41	21.03	74.56	34.09	1.21	8.25
1.3-1.4	9.10	19.66	71.24	32.24	1.06	6.50
1.4-1.5	16.08	18.28	65.64	29.37	1.11	4.75
1.5-1.6	24.71	17.24	58.06	25.68	1.14	1.25
1.6-1.7	32.12	16.08	51.80	22.77	1.18	0.00
1.7-1.8	40.76	15.17	44.08	19.39	1.21	0.00
S1.8	61.05	18.90	20.05	9.92	2.97	0.00

Table C. 213: Averages for proximate, calorific value and swelling index analysis results expressed on an air dry basis.

Sample	Inherent moisture %	Ash %	Volatile matter %	Fixed Carbon %	Calorific value (MJ/kg)	Total sulphur %	Free swelling index
F1.3	1.35	4.35	20.75	73.55	34.09	1.21	8.25
1.3-1.4	1.60	8.95	19.35	70.10	32.24	1.06	6.50
1.4-1.5	1.80	15.80	17.95	64.45	29.37	1.11	4.75
1.5-1.6	1.90	24.25	16.90	56.95	25.68	1.14	1.25
1.6-1.7	2.30	31.40	15.70	50.60	22.77	1.18	0.00
1.7-1.8	2.30	39.85	14.80	43.05	19.39	1.21	0.00
S1.8	3.05	59.20	18.25	19.50	9.92	2.97	0.00

Table C. 214: Standard deviation for proximate, calorific value and swelling index analysis results expressed on an air dry basis.

Sample	Inherent moisture	Ash	Volatile matter	Fixed Carbon	Calorific value	Total sulphur	Free swelling index
F1.3	0.21	0.07	2.62	2.33	0.13	0.33	1.06
1.3-1.4	0.00	5.16	3.04	2.12	2.21	0.23	3.54
1.4-1.5	0.28	5.09	2.47	2.33	1.74	0.29	3.18
1.5-1.6	0.85	3.46	2.26	0.35	0.88	0.45	0.35
1.6-1.7	0.99	4.95	2.26	1.70	1.17	0.54	0.00
1.7-1.8	1.13	5.30	2.69	1.48	1.43	0.49	0.00
S1.8	1.77	2.69	7.85	6.93	1.02	1.80	0.00

Table C. 215: Experimental errors for proximate, calorific value and swelling index analysis results expressed on an air dry basis.

Sample	Inherent moisture	Ash	Volatile matter	Fixed Carbon	Calorific value	Total sulphur	Free swelling index
F1.3	0.29	0.10	3.63	3.23	0.18	0.45	1.47
1.3-1.4	0.00	7.15	4.21	2.94	3.07	0.31	4.90
1.4-1.5	0.39	7.06	3.43	3.23	2.41	0.40	4.41
1.5-1.6	1.18	4.80	3.14	0.49	1.23	0.63	0.49
1.6-1.7	1.37	6.86	3.14	2.35	1.63	0.74	0.00
1.7-1.8	1.57	7.35	3.72	2.06	1.98	0.69	0.00
S1.8	2.45	3.72	10.88	9.60	1.41	2.49	0.00

Table C. 216: Repeatability limits for proximate, calorific value and swelling index analysis results expressed on an air dry basis.

Sample	Inherent moisture	Ash	Volatile matter	Fixed Carbon	Calorific value	Total sulphur	Free swelling index
F1.3	0.59	0.20	7.33	6.53	0.36	0.91	2.97
S1.3F1.4	0.00	14.45	8.51	5.94	6.20	0.63	9.90
S1.4F1.5	0.79	14.26	6.93	6.53	4.87	0.81	8.91
S1.5F1.6	2.38	9.70	6.34	0.99	2.47	1.27	0.99
S1.6F1.7	2.77	13.86	6.34	4.75	3.29	1.50	0.00
S1.7F1.8	3.17	14.85	7.52	4.16	4.00	1.39	0.00
S1.8	4.95	7.52	21.98	19.40	2.85	5.03	0.00

Table C. 217: Absolute difference between values for proximate, calorific value and swelling index analysis results expressed on an air dry basis.

Sample	Inherent moisture	Ash	Volatile matter	Fixed Carbon	Calorific value	Total sulphur	Free swelling index
F1.3	0.30	0.10	3.70	3.30	0.18	0.46	1.50
S1.3F1.4	0.00	7.30	4.30	3.00	3.13	0.32	5.00
S1.4F1.5	0.40	7.20	3.50	3.30	2.46	0.41	4.50
S1.5F1.6	1.20	4.90	3.20	0.50	1.25	0.64	0.50
S1.6F1.7	1.40	7.00	3.20	2.40	1.66	0.76	0.00
S1.7F1.8	1.60	7.50	3.80	2.10	2.02	0.70	0.00
S1.8	2.50	3.80	11.10	9.80	1.44	2.54	0.00

Table C. 218: Accuracy check for proximate, calorific value and swelling index analysis results expressed on an air dry basis (*Outside accepted limits according to SANS 5725-6:2009).

Sample	Inherent moisture	Ash	Volatile matter	Fixed Carbon	Calorific value	Total sulphur	Free swelling index
F1.3	1.35	4.35	20.75	73.55	34.09	1.21	8.25
S1.3F1.4	1.60*	8.95	19.35	70.10	32.24	1.06	6.50
S1.4F1.5	1.80	15.80	17.95	64.45	29.37	1.11	4.75
S1.5F1.6	1.90	24.25	16.90	56.95	25.68	1.14	1.25
S1.6F1.7	2.30	31.40	15.70	50.60	22.77	1.18	0.00*
S1.7F1.8	2.30	39.85	14.80	43.05	19.39	1.21	0.00*
S1.8	3.05	59.20	18.25	19.50	9.92	2.97	0.00*

APPENDIX D: CALCULATIONS

Conversion of coal properties (proximate analysis, CV and FSI) results on air dry basis to a dry basis (SACPS, 2015:68):

$$Property\ on\ dry\ basis = \frac{property\ on\ air\ dry\ basis * 100}{100 - inherent\ moisture\ \%} \quad \textbf{D- 1}$$

Percentage yield increase:

$$Percentage\ yield\ increase \quad \textbf{D- 2}$$
$$= \frac{Cumulative\ yield\ of\ raw\ coal - cumulative\ yield\ of\ any\ given\ run}{Cumulative\ yield\ of\ raw\ coal}$$
$$\times 100$$

Initial mass at a specific particle size interval:

$$Initial\ mass\ at\ specific\ particle\ size\ interval \quad \textbf{D- 3}$$
$$= sample\ and\ sieve\ mass\ at\ that\ specific\ size\ interval$$
$$- sieve\ mass$$

For particle sizes smaller than 4.75 mm, the sample was split into a quarter to do PSD. The mass in each particle size was converted to be as for the total sample according to:

$$Initial\ mass\ at\ a\ specific\ particle\ size$$
$$= \frac{Sample\ with\ sieve\ mass\ at\ specific\ particle\ size\ after\ riffler\ splitter - sieve\ mass}{Total\ mass\ after\ riffler\ splitter}$$
$$\times (Total\ mass\ of\ sample\ and\ sieve\ before\ riffler\ splitter\ for\ 0 - 4.75\ mm\ particles$$
$$- sieve\ mass)$$

D- 4

Final mass at a specific particle size interval:

$$Final\ PSD\ mass\ at\ a\ specific\ size\ interval \quad \textbf{D- 5}$$
$$= Sum\ of\ final\ masses\ at\ all\ RD\ intervals\ for\ that\ specific\ size\ interval$$

Mass after rotary splitter, that is the mass of 0.0-1.0 mm particles used for float-sink analysis using organic liquids:

$$\begin{aligned} &Mass\ of\ 0-1\ mm\ particles \\ &=\sum(sample\ mass\ and\ sieve\ mass\ at\ each\ RD\ interval\ for\ size\ 0 \\ &-0.5mm-sieve\ mass) \\ &+\sum(sample\ mass\ and\ sieve\ mass\ at\ each\ RD\ interval\ for\ size\ 0.5 \\ &-1.0mm-sieve\ mass) \end{aligned} \quad \textbf{D- 6}$$

$$\begin{aligned} &Mass\ \%\ of\ 0-1mm\ particles \\ &=Mass\ of\ 0-1\ mm\ particles \\ &-(0-1mm\ sample\ mass\ and\ sieve\ mass\ before\ rotary\ splitter \\ &-sieve\ mass)\times 100 \end{aligned} \quad \textbf{D- 7}$$

Mass loss:

$$Mass\ loss\ \% = 1-\frac{Final\ or\ intermediate\ mass}{Initial\ mass}\times 100 \quad \textbf{D- 8}$$

Normalized mass percentage:

$$\begin{aligned} &Normalized\ mass\ \%\ for\ specific\ size\ interval \\ &=\frac{Mass\ at\ specific\ size\ interval}{Total\ mass\ of\ whole\ sample} \end{aligned} \quad \textbf{D- 9}$$

Final mass after float-sink analysis and particle size distribution:

$$\begin{aligned} &Final\ mass\ at\ a\ specific\ particle\ size\ interval\ for\ a\ RD\ interval \\ &=Sample\ mass\ with\ sieve\ for\ specific\ particle\ size \\ &-sieve\ mass \end{aligned} \quad \textbf{D- 10}$$

Fractional mass yield after float-sink analysis and particle size distribution:

$$\begin{aligned} &Fractional\ mass\ yield \\ &=\frac{Mass\ at\ a\ specific\ particle\ size\ interval\ at\ a\ specific\ RD}{Total\ mass\ of\ whole\ sample} \end{aligned} \quad \textbf{D- 11}$$

The cumulative float yield was calculated by cumulatively adding the total fractional mass yield at each RD interval to give a total cumulative float yield of 100% at S1.8.

Particle size per density, and density per particle size:

The *particle size per density* was calculated for each RD interval by cumulatively adding the mass percentage at each particle size interval for a specific RD interval as a fraction of the total mass at that specific RD interval. Thus the total mass fraction at that specific RD interval added up to 1. The *density per particle size*, or float yield, was calculated similar. The density per particle size for each particle size interval was calculated by cumulatively adding the mass at each RD interval for a specific particle size interval as a fraction of the total mass at that specific particle size interval. Thus the total mass fraction at that specific size interval will add up to 1.

Float ash per particle size:

$$Float\ ash\ per\ particle\ size = \frac{\frac{Final\ mass\ at\ specific\ particle\ size\ at\ specific\ RD}{Total\ mass\ at\ specific\ particle\ size} \times Ash\%\ at\ RD\ interval}{Mass\ fraction\ of\ total\ per\ particle\ size\ at\ RD} \quad \textbf{D- 12}$$

$$\begin{aligned} Ash\%\ at\ RD\ interval = {} & (Ash\ \%\ at\ RD\ interval\ for\ 0 \\ & - 1mm\ size \times mass\ fraction\ of\ 0 - 1mm\ size\ at\ RD) \\ & + (Ash\ \%\ at\ RD\ interval\ for\ 1 \\ & - 13.2mm\ size \times mass\ fraction\ of\ 1 \\ & - 13.2mm\ size\ at\ RD) \end{aligned} \quad \textbf{D- 13}$$

Overall washability:

$$Float\ yield\ at\ specific\ RD\ interval = \frac{Total\ mass\ at\ specific\ RD\ interval}{Total\ mass\ of\ whole\ sample} \quad \textbf{D- 14}$$

The float yield was multiplied by the ash yield% at the corresponding RD interval and cumulatively added. The float ash was determined according to:

$$Float\ ash = \frac{Cumulative\ (Float\ yield\ at\ specific\ RD\ interval \times ash\ \%\ at\ specific\ RD\ interval)}{float\ yield} \quad \textbf{D- 15}$$

Liberation curve (liberation is defined by RD lower than 1.4):

$$Mass\ liberated = Final\ mass\ at\ F1.3\ for\ specific\ particle\ size + Final\ mass\ at\ RD1.3 - 1.4\ for\ specific\ particle\ size \quad \textbf{D- 16}$$

$$Mass\ unliberated = \sum Final\ mass\ at\ RD\ intervals\ (excluding\ F1.3\ and\ 1.3 - 1.4)\ for\ specific\ particle\ size \quad \textbf{D- 17}$$

$$Fractional\ mass\ \%\ at\ specific\ particle\ size = \frac{Mass\ liberated}{Total\ mass\ of\ whole\ sample} \quad \textbf{D- 18}$$

$$\%\ liberated = \frac{Mass\ liberated\ \%}{(Mass\ liberated\ \% + mass\ unliberated\ \%)} \quad \textbf{D- 19}$$

Hypothetical density wash:

The overall cumulative yield and required overall hypothetical density for a specific target ash was projected using Excel's forecast function by using the cumulative float ash and cumulative float yield. The cumulative float yield for an overall hypothetical density at each particle size interval was also calculated using this method, as well as the cumulative float yield and float ash per particle size.

The feed PSD at each particle size interval was calculated by:

$$Feed\ PSD\% = \frac{Total\ mass\%\ for\ specific\ particle\ size\ interval}{Total\ mass\%\ which\ is\ 100} \quad \textbf{D- 20}$$

The product PSD was estimated by:

$$Product\ PSD\% = \frac{Cumulative\ float\ yield\ at\ specific\ PSD\ interval \times Feed\ PSD\%\ for\ specific\ PSD\ interval}{\sum Cumulative\ float\ yield \times Feed\ PSD\%\ for\ all\ PSD\ intervals}$$

D- 21